USAAEFA PROJECT NO. 68-25

A FLIGHT RESEARCH INVESTIGATION OF AUTOROTATIONAL PERFORMANCE AND HEIGHT-VELOCITY TESTING OF A SINGLE MAIN ROTOR SINGLE ENGINE HELICOPTER

FINAL REPORT

KENNETH R. FERRELL
PROJECT OFFICER

JOHN J. SHAPLEY
PROJECT PILOT

ALAN C. FREDERICKSON
PROJECT ENGINEER

ROBERT A. KYKER
PROJECT MATHEMATICIAN

MARCH 1976

Approved for public release; distribution unlimited.

UNITED STATES ARMY AVIATION ENGINEERING FLIGHT ACTIVITY
EDWARDS AIR FORCE BASE, CALIFORNIA 93523

DISCLAIMER NOTICE

The findings of this report are not to be construed as an official Department of the Army position unless so designated by other authorized documents.

DISPOSITION INSTRUCTIONS

Destroy this report when it is no longer needed. Do not return it to the originator.

TRADE NAMES

The use of trade names in this report does not constitute an official endorsement or approval of the use of the commercial hardware and software.

DISCLAIMER NOTICE

THIS DOCUMENT IS BEST QUALITY PRACTICABLE. THE COPY FURNISHED TO DDC CONTAINED A SIGNIFICANT NUMBER OF PAGES WHICH DO NOT REPRODUCE LEGIBLY.

UNCLASSIFIED
SECURITY CLASSIFICATION OF THIS PAGE *(When Data Entered)*

REPORT DOCUMENTATION PAGE

READ INSTRUCTIONS BEFORE COMPLETING FORM

1. REPORT NUMBER: USAAEFA PROJECT NO. 68-25	2. GOVT ACCESSION NO.
3 RECIPIENT'S CATALOG NUMBER	
4. TITLE (and Subtitle): A FLIGHT RESEARCH INVESTIGATION OF AUTOROTATIONAL PERFORMANCE AND HEIGHT-VELOCITY TESTING OF A SINGLE MAIN ROTOR SINGLE ENGINE HELICOPTER	5. TYPE OF REPORT & PERIOD COVERED: FINAL REPORT May 68 - Mar 69.
	6. PERFORMING ORG. REPORT NUMBER: USAAEFA PROJECT NO. 68-25
7. AUTHOR(s): KENNETH R. FERRELL, ROBERT A. KYKER, ALAN C. FREDERICKSON, JOHN J. SHAPLEY	8 CONTRACT OR GRANT NUMBER(s)
9. PERFORMING ORGANIZATION NAME AND ADDRESS: US ARMY AVIATION ENGINEERING FLIGHT ACTIVITY EDWARDS AIR FORCE BASE, CALIFORNIA 93523	10. PROGRAM ELEMENT, PROJECT, TASK AREA & WORK UNIT NUMBERS
11. CONTROLLING OFFICE NAME AND ADDRESS: US ARMY AVIATION ENGINEERING FLIGHT ACTIVITY EDWARDS AIR FORCE BASE, CALIFORNIA 93523	12. REPORT DATE: March 1976 13. NUMBER OF PAGES: 384
14 MONITORING AGENCY NAME & ADDRESS *(If different from Controlling Office)*	15 SECURITY CLASS. *(of this report)*: UNCLASSIFIED 15a DECLASSIFICATION/DOWNGRADING SCHEDULE: N/A

16 DISTRIBUTION STATEMENT *(of this Report)*

Approved for public release; distribution unlimited.

17 DISTRIBUTION STATEMENT *(of the abstract entered in Block 20, If different from Report)*

18 SUPPLEMENTARY NOTES

19 KEY WORDS *(Continue on reverse side if necessary and identify by block number)*

Flight research investigation
UH-1C helicopter
Autorotational performance
Height-velocity tests
Pilot technique
Rotor performance
Aircraft capability

20 ABSTRACT *(Continue on reverse side if necessary and identify by block number)*

Autorotational performance and height-velocity (H-V) testing were conducted to examine the effects of pilot technique and operating variables on rotor performance and aircraft capability during these maneuvers. Various testing methods were compared and ways to provide the operators with more meaningful information were considered. The testing was conducted by the United States Army Aviation Engineering Flight Activity at Edwards Air Force Base, California, as well as at a sea-level site near Shafter, California, and at high-altitude sites in the vicinity

DD FORM 1 JAN 73 1473 EDITION OF 1 NOV 65 IS OBSOLETE

UNCLASSIFIED
SECURITY CLASSIFICATION OF THIS PAGE *(When Data Entered)*

of Bishop, California. The testing was accomplished with a UH-1C helicopter, USA S/N 63-8684. Test results show that separating the H-V maneuver into entry, dive, flare, and landing phases during tests at a safe height above the ground provided the best evaluation of both aircraft behavior and pilot requirements. The H-V diagram was then developed using a selected technique or criteria in a much safer manner and with reduced flight time. An improved methodology was developed which utilized theory and preliminary flight data to produce H-V diagrams with a reduced testing hazard. A data presentation requirement was developed and a demonstration outline is shown.

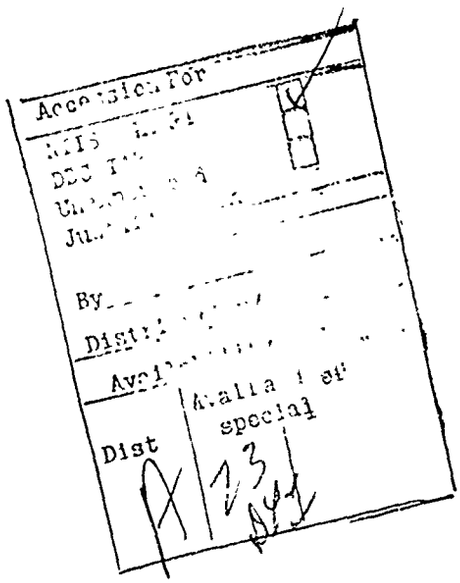

TABLE OF CONTENTS

INTRODUCTION

BACKGROUND

1. Autorotational performance and height-velocity (H-V) testing are normally conducted to obtain data for operators' manuals. The H-V portion is presented as an emergency procedure. Historically, a large number of accidents have occurred during autorotational and H-V testing by the United States Army Aviation Engineering Flight Activity (USAAEFA), other test agencies, and aircraft manufacturers. Data compiled by the United States Army Agency for Aviation Safety (USAAAVS) (ref 1, app A) reveal that throughout the Army, autorotational landing accidents are common in operational and training units. Practice autorotations are conducted at conditions which should produce safe autorotational landings. However, during the period 1 July 1969 to 31 December 1971, practice autorotations resulted in 486 accidents and incidents, which cost $7,143,800; 2 fatalities; and 43 injuries. Including actual emergency autorotations in the same time period, there were a total of 1195 accidents and incidents, costing $74,837,000, which resulted in 82 fatalities and 606 injuries. Further investigation shows that the demonstration requirements of military specification MIL-H-8501A (ref 2) do not adequately define control power, control margins, rotor speed decay, or response to power failure. In addition, the data presented to the operators in many handbooks do not reflect adequate description and discussion of the special test conditions and limitations and thus are unrealistic or misleading for operational use. Although considerable work had been done to investigate autorotational performance (refs 3 through 6), there was still a great deal unknown, and a further research effort was necessary. The United States Army Aviation Systems Command* directed (ref 7) that USAAEFA develop a flight program (ref 8) to study the H-V maneuver and provide data concerning effects of pilot technique, aircraft performance, and the influence of operating variables.

TEST OBJECTIVES

2. The overall objectives were to investigate the H-V maneuver, to establish an improved test methodology, and provide operators with more meaningful pilot information. Secondary goals were to examine demonstration requirements and provide data concerning design requirements. Specific objectives were as follows:

a. Determination of normal pilot reaction time to an unannounced engine failure in the absence of an engine failure warning system.

b. Evaluate the effect of pilot reaction time, aircraft response, and displacement of critical controls on altitude loss, and time required to achieve steady-state autorotational flight following a simulated engine failure.

*Since redesignated the Army Aviation Research and Development Command

c. Determine adequate autorotation entry test criteria for future tests on single-engine helicopters.

d. Determine the effect of airspeed and rotor speed on rate of descent and glide distance, as well as evaluate the effects of maneuvering flight on descent performance in autorotational flight.

e. Establish test criteria for determining effective flare airspeed requirements for future tests.

f. Determine the time and altitude required to effect a power recovery from autorotational flight and establish standard test techniques for making this determination for future tests.

g. Determine the amount of lift available from the rotational energy stored in the rotor system at various gross weight, rotor speed, and airspeed conditions.

h. Reassess H-V test techniques utilized in past government qualification of single-engine rotary wing vehicles.

i. Recommend effective handbook presentation methods for all the above data for the operators' manuals.

DESCRIPTION

3. The tests were conducted with a UH-1C helicopter (SN 63-8684) which is a single-main-rotor Army utility aircraft. A detailed description of the aircraft is presented in reference 9, appendix A, and in appendix B. Table 1 compares the UH-1C with some other helicopters of similar configuration.

Table 1. Comparison of Single-Main-Rotor Helicopters.

Helicopter Model	Maximum Gross Weight (lb)	Maximum Engine Power (shp)	Rotor Inertia ($slug/ft^2$)	Cruise True Airspeed (kt)
TH-55A	1670	160	132	75
OH-6A	2400	252	208	125
OH-58A	3000	317	607	110
UH-1C	9500	1100	2800	125
AH-1G	9500	1100	2800	140
CH-34	13,300	1425	4568	134
CH-3C	22,050	2500	8950	130
CH-53A	42,000	5700	24,276	159

The UH-1C is categorized as a medium-weight, high-rotor-inertia vehicle. The flying qualities of the UH-1 series helicopters are well documented and are generally considered to be satisfactory, with an absence of any large or unacceptable deviations from MIL-H-8501A.

TEST SCOPE

4. The intended scope encompassed a complete study of single-rotor helicopter autorotation and H-V performance. All primary design variables were to be examined in detail and data generated which would have general applicability toward test, design, and demonstration requirements.

5. Variations in pilot technique were used to assess pilot capabilities and investigate performance limits of the test aircraft. Autorotational entries from hover, forward flight, climbs, and descent were tested. Entries from vertical climb and descent were not evaluated. Tests were not conducted to evaluate the effects of surface wind and air turbulence. The aircraft power available limited the test gross weight to a maximum of 8500 pounds. Tests were conducted at field elevations of 425, 4120, and 9500 feet. The density altitude range tested was from 840 to 11,650 feet with respective temperatures of 11 and 9°C. Colder temperatures were not available and thus the data may not reflect compressibility effects. The longitudinal and lateral centers of gravity (cg) were near the center of allowable travel for all tests.

TEST METHODOLOGY

6. The H-V maneuver was divided into the segments shown in figure A.

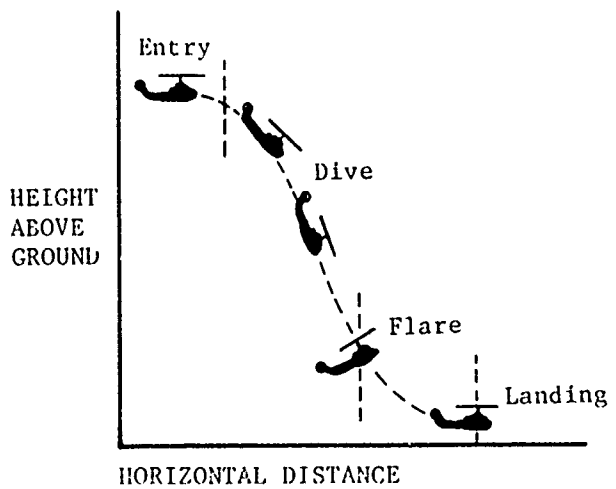

Figure A. Height-Velocity Maneuver

Where each segment is identified as follows:

a. Entry - Power reduction, any imposed control movement delay to simulate pilot recognition and reaction time, arrestment of angular motion or rotor speed decay, and recovery from resulting attitudes.

b. Dive - Longitudinal cyclic pushover to achieve a desired dive angle and acceleration to a flare airspeed (for altitudes requiring less than maximum H-V performance, there may be a deceleration to reduce rate of descent to a pilot-tolerable value prior to the flare).

c. Flare - Combined longitudinal cyclic and collective control application to increase the angle of attack, increase and control rotor speed and decrease downward and/or forward velocity.

d. Landing - Leveling of aircraft through cyclic application or use of collective and cyclic application to level aircraft, arrest sink rate and make a touchdown.

Each segment was tested separately to minimize the pilot workload and allow isolation of the particular variables being investigated. In the interests of safety, each test was conducted at a sufficient altitude to allow a power recovery. This method reduced the number of landings and minimized the hazards inherent to an actual autorotational touchdown.

7. For the various entry conditions, the throttle was rapidly closed to simulate a sudden engine failure and the controls maintained fixed for a selected delay time. Aircraft behavior was recorded and pilot comments made as to recognition signals, severity of reaction, and necessary recovery action. On subsequent entries, the severity of the entry condition and/or the delay time was increased until an aircraft or pilot limitation was reached.

8. Following each entry, the effectiveness of the pushover was evaluated by measuring the aircraft reaction to forward longitudinal cyclic inputs to attain nose-down attitudes and rates of change of attitude. The aircraft was dived with varied rates of longitudinal control application to increasing dive angles to determine the acceleration characteristics. An incremental buildup was used, and the tests were terminated when the pilot considered that a faster pushover rate or more nose-down attitude was unsafe or was considerably beyond a normal maneuver.

9. Flare effectiveness tests were conducted by initiating flares at various airspeeds from both steady-state and accelerating autorotations. Both cyclic and collective applications were used. Flare rate and magnitude of flare were both evaluated. At the conclusion of the flare, forward cyclic was used to level the aircraft prior to power recovery.

10. Landing tests were conducted from a hover and at low forward airspeeds (zero to 40 knots true airspeed) (KTAS) and at heights near the ground (less than

100 feet). Starting from hover conditions the helicopter was stabilized at the desired height and after the power reduction, rotor energy was used to cushion the landing. Delay time was increased on successive points, and for a given delay time the effect of different collective application, rates, and magnitudes were evaluated. Hover height was increased until the maximum tolerable touchdown sink airspeed was approached. For low-airspeed tests the helicopter was stabilized in level flight, power was rapidly reduced, and landings were made with various delay times and pilot techniques. Different height and airspeed combinations were tested until a critical cutoff point was reached. Following the individual H-V segment tests, the results were used to define a total maneuver in terms of pilot requirements and associated performance. Complete H-V profiles were then flown.

11. The height and distance traveled during a given maneuver were recorded photographically with a Fairchild Flight Analyzer (FFA). A limitation of this device is that it provides only two-dimensional data and has a restricted field of view. To provide accurate values, the maneuver must be conducted in a plane normal to the camera line of sight and at a constant distance. The pilot must track along a runway center line and perform the maneuver within the camera view. The minimum power recovery height varies with the aircraft and engine response and must be sufficient to allow an autorotational landing should the engine power not be regained. Figure B illustrates the allowable airspace for a typical test arrangement.

12. The airspace dimensions shown in figure B are for a camera offset distance of 1500 feet, which was the maximum that was practical for the UH-1C aircraft. A greater offset will increase the airspace available; however, the photographic image of the aircraft will be reduced in size, thus decreasing data accuracy.

13. At the start of the program it was difficult for the pilot to perform certain maneuvers within the boundaries outlined in figure B. For example, it was uncomfortable to flare the aircraft at a low airspeed while reducing the rotor speed to a low value at 500 feet above the ground. The maneuvers were demanding with respect to use of cockpit indicators and there was little opportunity for outside reference. As experience was gained, the task became easier. The pilot had to take particular care not to concentrate on a particular test condition for too long a time since allowances had to be made for a recovery to prevent ground contact.

14. Aircraft performance, stability and control, position, and motion data were recorded on board the aircraft through the use of visual indicators, photopanel, and oscillograph recorders. A detailed instrumentation listing is presented in appendix C.

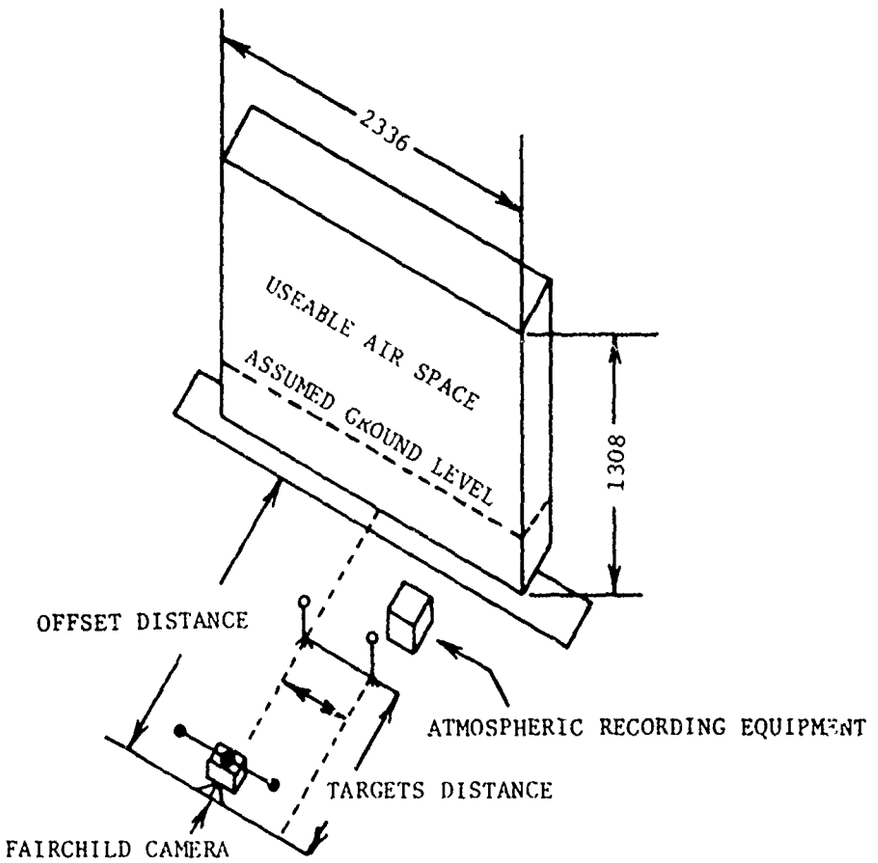

Figure B. Fairchild Camera Arrangement

RESULTS AND DISCUSSION

GENERAL

15. The results and discussion are presented in the sequence necessary to make a successful landing after a power loss. The sequence is power reduction, dive, flare, and landing. Following the individual phases is a description of an improved test methodology and suggested demonstration requirements. Each major section considers pilot requirements and opinions and aircraft characteristics, as well as force and energy considerations. In summary, the results and discussion show that a majority of the objectives were achieved. The conclusions and recommendations provide guidance for additional testing, definition of human factors items, and suggested aircraft design goals.

ENTRY TO AUTOROTATION

General

16. The entry to autorotation is the phase during which the aircraft is transitioning from a powered flight condition to a controlled autorotational condition. Typical aircraft operating conditions for stabilized level flight are shown in figures 1 through 3, appendix F. The entry is composed of a power reduction, a delay in corrective control input, and a recovery action by the pilot. The exact nature of the power reduction directly affects both the pilot requirements and the aircraft response. The delay in pilot corrective action and the aircraft response determines the recovery requirements. A controls-fixed test technique was used to best show the aircraft response and allow pilot assessment of the relative importance of the various recognition signals. The characteristic aircraft reaction will vary with gross weight, cg, airspeed, and power. The recovery portion of the entry involves the pilot action necessary to correct for the aircraft motion generated during the pilot delay phase. Entry tests were conducted from flight regimes of hover, takeoff and acceleration, climb, level flight, and powered descent. Various types of power reductions and different pilot delay times were investigated.

Power Reduction

17. The transient nature of the power reduction can vary greatly and directly influences the aircraft response. Common causes of power loss such as fuel starvation, fuel control malfunctions, engine deterioration, or damage from an external source must all be considered when estimating the expected aircraft response and necessary pilot reaction. A graphical representation of some different types of power reduction is shown in figure C.

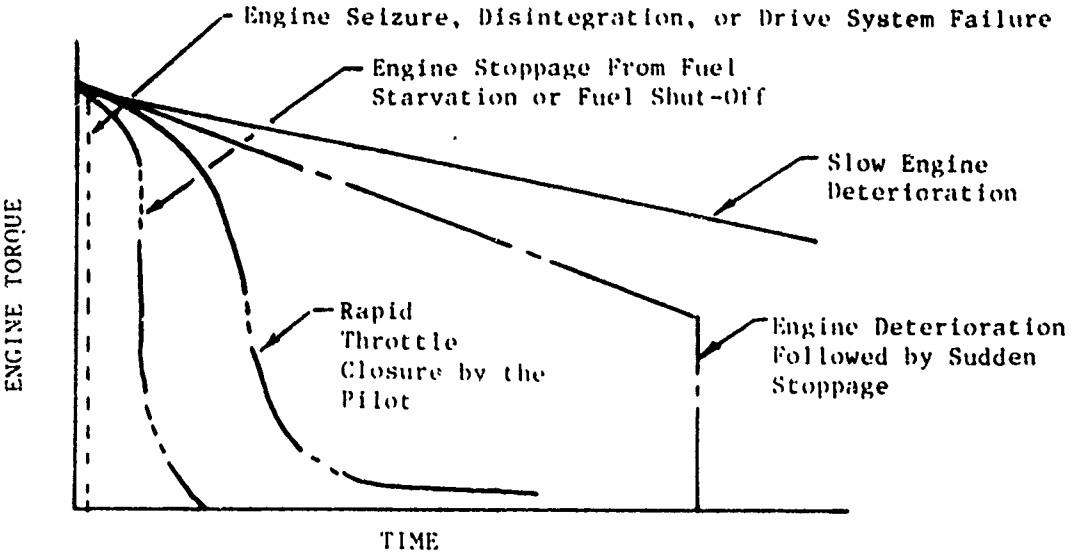

Figure C. Engine Torque Reduction With Type of Power Failure.

18. During the test program, power was usually reduced by the pilot closing the throttle as shown in figures 4 through 7, appendix F. With this procedure, it was noted that engine output torque would not go to zero, but would decrease to approximately 5 psi (60 shp) and remain constant during the autorotation and landing. A similar characteristic had been reported in reference 10, appendix A. Analysis showed that both the residual power and the nature of the power reduction significantly affected the aircraft response.

19. Engine failure modes have not been adequately defined for all power plants in the Army inventory. The most severe case of power reduction (engine seizure) was not simulated but could be expected to cause the greatest aircraft response and require corrective pilot action in the shortest time. At the same time, the pilot should receive the strongest cues as to the occurrence of a power failure. A fuel shutoff was accomplished and provided essentially the same aircraft response or pilot cues as when a rapid throttle closure was used. A slow power reduction causes the mildest aircraft response. However, pilot cues are not strong and engine deterioration may be detectable only from a warning system or from monitoring of the cockpit instruments. When the pilot is aware that a gradual power loss is occurring, an immediate partial powered landing can be made. He should be prepared for total power failure during the landing and when possible should minimize power required by landing with forward airspeed.

20. The handling qualities requirements (ref 2, app A) specify that with a 2-second delay from power reduction to movement of the collective pitch control, the rotor speed will not fall below a safe minimum transient value. It is also required that the attitude change during the 2-second delay must not exceed 10 degrees about any axis at airspeeds above best climb airspeed or 20 degrees of yaw at airspeeds below best climb airspeed. The initial tests quickly established that those requirements are unrealistic in some areas and are inadequate demonstration criteria in all cases. Immediate action by the pilot on cyclic and directional controls prevents an aircraft response which would otherwise be expected in an operational situation where the pilot is busy with other tasks and delays in reaction time for all controls will occur. Qualitative tests were conducted which suggested that the demonstration requirements should be based on what the pilot could sense and what he could do in terms of corrective action. These qualitative tests also indicated that the above factors had a different significance for the various flight regimes and operating conditions. It is, of course, mandatory that an acceptable corrective action be within the capability of the aircraft in terms of control power and structural integrity.

21. The engine failure cues that may be made available to the pilot include audio, visual, and kinesthetic signals. In aircraft where the pilot is near an engine or transmission, audio cues may be valuable. However, experience in several aircraft has indicated that audio cues from the aircraft are generally unreliable and that they have too much lag to be of real use to the pilot. Visual cues are separated into instrument indications and external sight pictures. Engine instruments have inherent lag and to be useful require that the pilot be observing them at the instant of power failure. Engine instrument cues are also of limited value because they give the pilot no information concerning the proper corrective action. For this, he must view a sight picture, observe attitude instruments, or assess the aircraft motion. The tests revealed that in most flight conditions more rapid, more reliable, and stronger cues are available from the aircraft reaction to power reduction. Exceptions include partial-power descent and situations where the pilot is intensely concentrating on a maneuver or task. Since the pilot's attention could be in any direction at any given instant, the engine visual failure devices must be displayed so as to always be in the pilot's field of vision. In addition, there should be an audio warning signal. The engine warning system should be activated by the parameter that most quickly indicates an engine failure and also one which will not reflect a normal power reduction.

22. The tests were first conducted keeping all controls fixed for 1 second after the power reduction. The delay time was then incrementally increased to the maximum that was considered safe. This technique quickly revealed the areas that were critical with respect to particular pilot responses. For a kinesthetic cue to be developed there must be a perceptible change in the aircraft operating condition. Thus, an aircraft which has minimal response to a power reduction will not indicate to the pilot that an emergency has occurred, and that there is a need for immediate corrective action. Primary pilot cues generated by aircraft motion are angular accelerations, angular rates, attitude changes, and linear accelerations along the flight path or aircraft axes. Secondary kinesthetic cues are aircraft vibration and control force feedback.

23. The power reduction tests were accomplished with three test pilots of varying experience. Qualitative judgments were made by each pilot as to the predominant recognition cue. In certain areas, the results were inconclusive; however, in critical areas such as high aircraft response requiring immediate pilot reaction, there was good agreement as to both the pilot cue and the required corrective action. Also, each pilot seemed to readily respond to the critical parameter regardless of which aircraft axis or which flight control was involved. On this basis the tests indicated that the most important recognition element was the magnitude and direction of the cue. It could not be determined whether the pilot responded primarily to the absolute magnitude of the cue, or the magnitude relative to the other cues.

24. The cues available to the pilot can be considered in short and long-term phases. The short-term phase consists of the initial accelerations and rates generated by the unbalance in forces and moments as the engine torque is removed from the rotor shaft. The long-term phase is the resultant rates and attitudes caused by the initial response and inherent stability characteristics. In some cases, it may not be possible for the pilot to differentiate between the two phases.

25. With controls fixed, the aircraft response to a rapid power reduction is similar to a step-type control input in that for a short term the force imbalance is essentially constant. Previous stability and control data (ref 11, app A) show that for a step control input maximum accelerations are generally reached within 0.5 second and the maximum rates occur within 1.5 seconds after the input. Similar response characteristics are evident in figures 4 through 7, appendix F.

26. Pilot response to the aircraft reaction was examined during the buildup in delay times of 1 second, 2 seconds, and maximum. These tests indicated that, with the exception of hover, the maximum short-term rates or accelerations were not important to the pilot.

27. In hover, the pilot instinctively reacted to the rapid directional changes that follow power reduction. The time delay was approximately 0.3 second, which was essentially his minimum reaction time. The angular accelerations, rates, and attitudes had not increased to any significant degree, and appeared to be too low for primary recognition cues. However, the yaw angular acceleration generated a lateral acceleration at the pilot station which increased rapidly. Previous testing (refs 12 and 13, app A) had demonstrated that pilots were very sensitive to side force and could recognize changes as low as 0.05g (1.6 feet per second per second) (ft/sec^2). The lateral acceleration is a more desirable demonstration criteria for recognition of engine failure than angular yaw acceleration or rate because of the variance in pilot displacement from the cg in different aircraft.

28. At low airspeeds such as those shown in figure 5, appendix F, the aircraft response to power reduction is considerably less than in hover, and the pilot could safely delay for more than 3 seconds. The pilot recovery was initially for the yaw, closely followed by lateral input for roll recovery. Roll and yaw accelerations had essentially reached a constant value by the time recovery was initiated. The only significant attitude change occurring was in yaw.

29. At an intermediate airspeed of 60 KTAS, as shown in figure 6, appendix F, the aircraft reaction to power reduction was minimal and the pilot was given very weak cues. The allowable pilot delay was more than 5 seconds, and recovery was necessary primarily because of low rotor speed. The short-term maximum rates and accelerations had occurred prior to 2 seconds. At recovery, the roll rate had stabilized at essentially 4 degrees per second (deg/sec), and the yaw rate was 7 deg/sec. Roll and yaw attitudes were 20 and 27 degrees, respectively, at recovery.

30. The aircraft response in the high-speed flight regime is shown in figure 7, appendix F. The maximum delay time was 4.5 seconds for an airspeed of 111 KTAS. The characteristic motion at high speed was an immediate left yaw acceleration closely followed by a left roll acceleration. Roll and yaw rates were to the left throughout the power reduction phase. Roll and yaw attitudes increased rapidly and reached maximums of 40 and 30 degrees at recovery. Motion in pitch was very small. However, the visual sensation in the cockpit was one of roll and pitch rather than roll and yaw. This apparent discrepancy between the qualitative and quantitative data can be resolved by considering the difference between the references for the instruments and the pilot. To the pilot, pitch-down is when the aircraft turns toward the ground. To the instrument, pitch is motion about the lateral axis of the aircraft. An additional factor is the pilot's higher sensitivity to pitch attitude than to roll or yaw attitudes. Thus, when the aircraft has rolled left, a left yaw rotates the aircraft toward the ground, and the pilot senses that it is pitching nose down.

31. During climb or level flight at heavy gross weight, the delay time became more critical. There was a sensation of "falling through" or "slowing down" as power decreased. In addition, the rotor speed decay rate was more noticeable. Comparison of data at 50 KTAS for level flight at 7000 and 8400 pounds and climbs at indicated torques of 29 and 35 psi shows that the aircraft short-term angular motions are essentially the same in each case. However, there was considerable difference in the normal acceleration characteristic, as shown in figure D.

For the lightweight level flight condition the change in normal acceleration was barely perceptible and was of no immediate concern to the pilot. At the heavyweight level flight condition the minimum normal acceleration reached was lower and there was an acceleration downward when recovery was necessary. During a low powered climb at light weight, the torque was less than for the level flight heavyweight condition; the change in normal acceleration and pilot concern was also decreased. A power reduction during a high power climb at light weight generated the most change in normal acceleration and caused the greatest pilot concern as well as a decrease in acceptable delay time. The change was on the order of 3.5 ft/sec^2 and was a strong, unmistakable pilot cue that power had been reduced and that the flight path was changing.

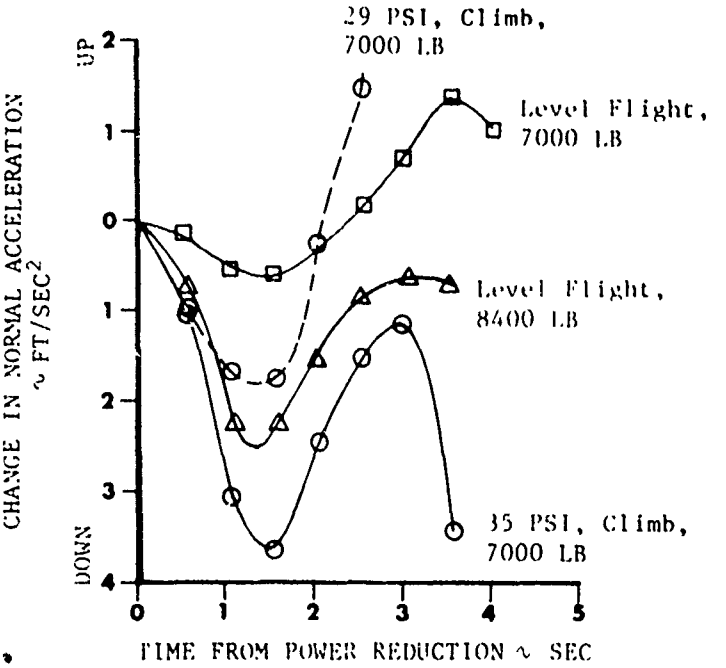

Figure D. Normal Acceleration Characteristics During Power Reduction.

32. The short-term aircraft response to power reduction was qualitatively judged to be the same for all altitudes tested. However, the overall pilot assessment was that there was a small degradation in lateral-directional stability occurring as altitude was increased. This judgment was substantiated by analysis of the attitude data from density altitudes of 1110 and 11,120 feet. The altitude effect became more noticeable with increased delay time and as the entry airspeed became higher. Typical results of the angular motions are summarized in figure 8, appendix F.

Forces, Energies, and Powers

33. At power reduction, the removal of driving torque from the rotor creates a force imbalance as the controls are held fixed and rotor speed decreases. Angular motions and decelerations alter the flight path and operating conditions with elapsed time. The primary forces considered are thrust, drag, and gravity. The energy state is described by the aircraft kinetic energy, aircraft potential energy, and the kinetic energy of the rotor. During the tests it was found that rotational energy of the fuselage was insignificant when compared to the other energy states. The rotor-induced power, rotor profile power, tail rotor power, and aircraft parasite power terms are determined from classical calculation procedures. As the pilot makes control inputs to effect the recovery, he is controlling the forces to direct the aircraft along the desired flight path, control the energy losses, and minimize the power required.

34. The existence of residual engine power was noted during previous tests (ref 10, app A) and confirmed during this program. The measured engine power was 60 shp at flight-idle during autorotation. The residual power will affect the rate of descent, transfer of energy between energy states, or rate of total energy loss, the importance of which varies with the flight situation. An approximation of rate-of-descent change ($\Delta R/D$) attributable to the residual power is obtained from steady-state power analysis:

$$\Delta R/D = \frac{\Delta shp \times 33,000}{GW}$$

Where:

Δshp = Residual power

GW = Gross weight

The residual power decreases rate of descent by 283 ft/min for the UH-1C at a gross weight of 7000 pounds.

35. Main rotor and tail rotor thrust changes occur within 0.5 second after the power reduction begins. The rate of thrust decrease and the magnitude of the decrease is highest in the hover and lessens with increased airspeeds. The drag force changes very little until the characteristic right sideslip is introduced, at which time there is a significant increase due to the difference in the effective flat plate area of the front and side fuselage profiles.

36. During the power reduction there is a total energy loss which is caused by the decrease in main rotor kinetic energy. The magnitude of the loss follows rotor speed decay characteristics shown in figures 4 through 7, appendix F and is summarized in figure E. (The area under the curve is a measure of total speed loss as a function of time).
The greater rotor speed loss with altitude slightly lowers the low hover point on the H-V diagram.

37. The power to the main rotor could not be instantaneously reduced, and this undoubtedly influenced the total aircraft response as previously discussed. The induced power is essentially constant until the collective pitch is decreased during the recovery. In forward flight, the rotor profile power increased initially as the angle of attack increased and the rotor flapped aft, changing the rotor inflow angle; then it decreased in a linear manner until the collective was lowered.

Flight Path Changes

38. Typical height changes during controls-fixed power reductions are summarized in figure 9, appendix F. During the power reduction with collective fixed, the rotor kinetic energy is dissipated to compensate for the engine shp available while

Avg. Gross WT = 7000 LB
Skid Height = 10 FT
Entry Rotor Speed = 324 RPM

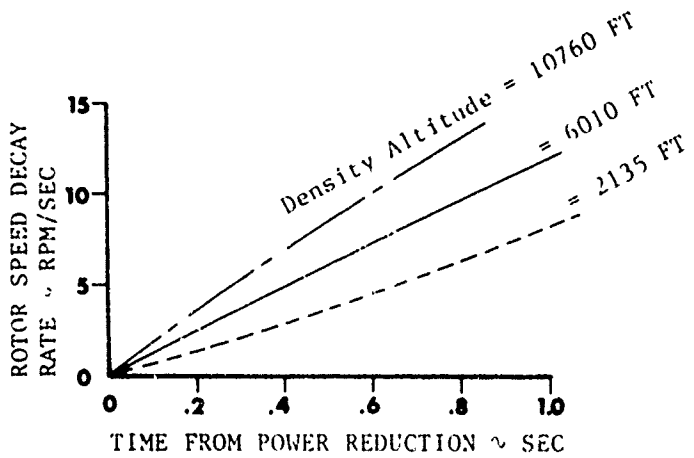

Note: Power Reduced by Rapidly Reducing Throttle to Flight Idle

Figure E. Rotor Speed Loss During Power Reduction From Hover.

rotor profile power and induced power remain relatively constant. Depending on the flight condition, thrust output stays fairly constant with fixed collective, which minimizes the height loss. For a given time delay, height loss is greatest for a hover and decreases with forward airspeed. At airspeeds above 80 KTAS, there is a tendency to climb slightly, especially during recovery, primarily due to the higher inflow velocity effect on thrust when the rotor flaps aft. During entry from a stabilized climb, the aircraft continues on the upward flight path for several seconds before a downward displacement begins.

Recovery

39. The recovery is the action necessary to control aircraft motions generated by the power reduction and aggravated by delay time. In the power reduction phase, pilot judgment was used to define a tolerance limit in terms of a maximum allowable delay time. This tolerance limit was based on the pilot's concern for a given cue or a set of circumstances. The first recovery motion defines the critical axis or control. Control inputs to correct for other motions were usually made as an instinctive action. The maximum delay tolerable to the pilot was less than maximum delay in terms of aircraft capability, which is determined by the most extreme attitude from which the aircraft can be recovered with the maximum control power available. The difference in the two limits represents a margin available to the pilot who inadvertently delays longer than was considered reasonable during these tests.

40. Pertinent information concerning the aircraft motions during entry and at recovery is presented in figures 10 through 12, appendix F. In hover, the power reduction generates a yaw, which gives the pilot a very strong cue. With a high pilot awareness, the delay time is essentially the pilot reaction time. Figure 4 shows such a recovery where yaw rate was stopped at 7 deg/sec within 1.0 second and there was little attitude change. Right pedal input was just under 2 inches, which left a margin of 2.6 inches (37 percent). A delay on the order of 2 seconds would place the directional control near the right limit. Conditions which increase the hover power required will create more yaw, make the recovery time more critical, and increase the necessary pilot effort.

41. As airspeed is increased from hover to 20 KTAS, the yaw control requirement decreases and lateral control inputs become important to the recovery. Above 20 KTAS, lateral control inputs are generally the most critical recovery item. For intermediate airspeeds near the minimum power-required point, aircraft motion during the entry and at recovery is very small, and the delay time can approach 6 seconds. With increasing airspeeds above 80 KTAS, the increasing roll rate tends to cause the pilot to recover sooner. At 120 KTAS the delay time was 4 seconds and the lateral control input was 5.6 inches, which left a margin of 8.9 percent. The decreasing delay time and lower bank angles at higher airspeeds suggest the pilot is using roll rate or acceleration as a cue. A detailed discussion of typical recovery characteristics at high airspeed/high torque conditions is presented in reference 14, appendix A.

42. A summary of the recovery information is shown in figure F. Basing recovery on a minimum rotor speed is unsatisfactory. The audio warning is activated at 305 rpm (±5 rpm) and the minimum steady-state autorotation rotor speed is 294 rpm. At hover and an airspeed below 15 KTAS, the rotor speed decay does not provide warning soon enough, whereas at airspeeds above 15 KTAS, the rotor speed limit is too conservative. Recovery on the basis of pilot tolerance leaves considerable control margin except at the critical high airspeeds. Above 100 KTAS there is less than 10 percent control margin during the recovery. However, the UH-1C has increased control response with increased airspeed, as shown in reference 10, appendix A, and thus a constant percentage control margin imposes an unrealistic requirement at some conditions.

DIVE

General

43. The dive phase of an autorotation is the interval between completion of the entry phase and the start of the flare. The maneuver typically consists of a longitudinal cyclic pushover to a nose-down attitude, followed by acceleration to a desired flare airspeed. Given enough altitude, a steady-state autorotation at the flare airspeed could be established and then a flare performed at any selected time. In a maximum performance case, the flare airspeed is reached at flare height above the ground with little or no time spent in a steady-state descent.

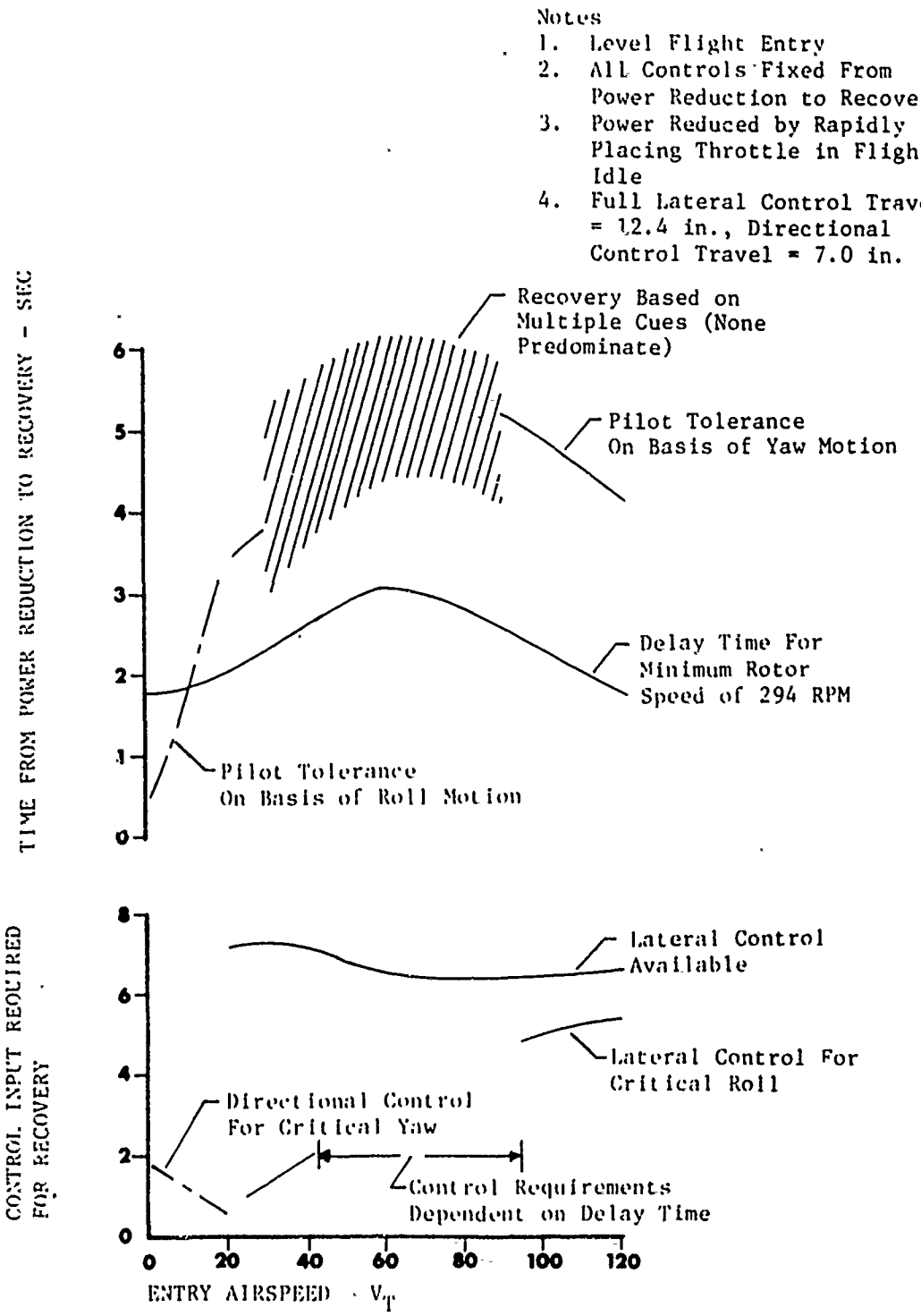

Figure F. Summary of Delay Times and Control Requirements for Recovery.

44. The entry airspeed and flight conditions dictate the required control inputs for the dive. The critical case for the dive occurs at low airspeeds and during climbing conditions. At low speeds the dive angle is greatest, which requires the most pilot effort, and the angle must be selected precisely to minimize height loss. In high powered climb the pilot task is made difficult by the aircraft response, change in normal acceleration, and the large change in flight path angle. The complexity of the dive phase decreases with entry airspeed to the point where no pushover is necessary when the initial velocity is already greater than the desired flare airspeed.

Pushover

Level Flight:

45. After the power reduction and the recovery, a pushover is accomplished to achieve a nose-down attitude for acceleration to flare airspeed. The magnitude and rate of initial cyclic input are largely determined by knowledge of aircraft response characteristics and the airspeed gain that will be needed. Summaries of aircraft performance during the pushover and some characteristics at selected conditions are shown in figures 13 through 19, appendix F.

46. A generalized longitudinal stick input for a pushover from a low-speed entry for the UH-1C helicopter is shown in figure G. The collective pitch is lowered in conjunction with the longitudinal control motion. Required lateral and directional control inputs are made as the aircraft responds to the pushover. As the cyclic control is moved forward the aircraft responds with a nose-down pitch, at which time the pilot is provided cues to guide his following actions. The pitch acceleration reaches a maximum at T_1, and the pilot responds by ceasing the forward control input. At this time, the pitch rate and attitude are becoming more nose down, and aft cyclic is necessary to bring these motions under control. The aft cyclic input is continued at a constant rate until the pitch rate reaches maximum at T_2. There is then a characteristic slowing of the aft control input. However, the attitude is still becoming more nose down, and longitudinal control is used to stabilize on an attitude that will produce desired airspeed.

47. The considerable scatter in the pushover data shown in figure 13, appendix F, illustrates the pilot's difficulty in judging the amount and rate of forward longitudinal control required. At this point in time, the pilot has only his knowledge of flight conditions and expected aircraft response to guide his actions. The forward control input decreased from about 3 inches at 10 KTAS to zero at flare airspeed. After the initial input, the aircraft generated cues which were then used to determine the need for further control inputs. The pitch rate and attitude data contained in figure 13-1 is much more consistent than was the control input data. This demonstrates the response to the cues and the pilot's ability to obtain this repeatable profile for a wide range of flight conditions. The maximum pilot acceptable pitch rates and attitudes of 18 deg/sec and 33 degrees, respectively, occurred at the low-speed entry at 11 KTAS. Maximum values then decreased with higher forward airspeeds. These tolerance limits are consistent with test results cited in references 15 through 18, appendix A. The minimum normal acceleration

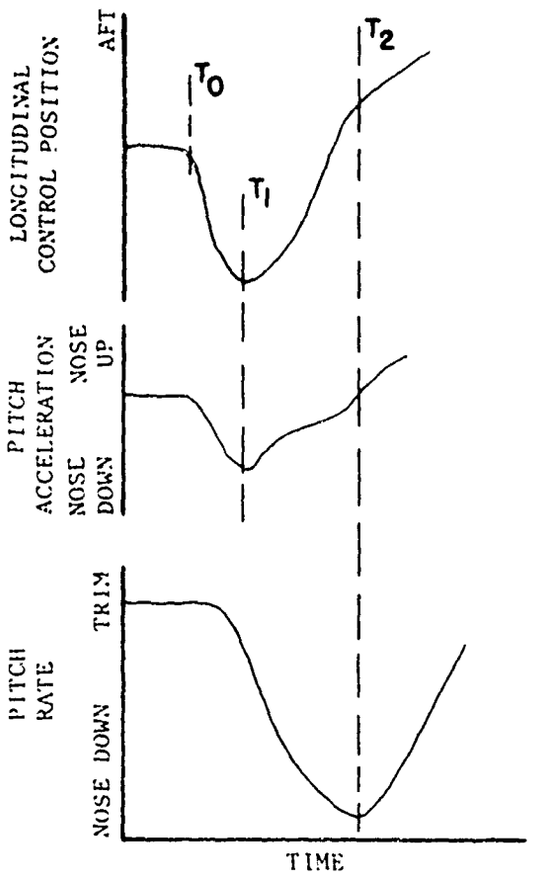

Figure G. Typical Pushover Maneuver.

usually occurred 1 second after the forward control input, with the exact timing depending on the control input in each case. This normal acceleration was an important pilot cue, and the minimum tended to be near 0.5g, regardless of the pushover airspeed. Pushovers from level flight showed no significant trends with gross weight or density altitude. The pilot adjusted control inputs to obtain similar performance at a given airspeed for all conditions tested.

48. The effect of varying the rate of pushover is obtained from the comparisons shown in figures 14 and 17, appendix F. The "normal" pushover is similar to those previously discussed and represents a desirable maneuver from the pilot's viewpoint. The "steep" pushover produces extreme attitudes and is beyond reasonable pilot tolerance limits. The steep pushover generates considerably higher pitching motions. However, the time duration is small, and the normal acceleration is essentially the same for both maneuvers. In addition, when the aft cyclic correction is made, the input is larger and more rapid for the steep pushover, which tends to negate the larger initial forward cyclic input.

49. During a pushover from a level flight entry, the forward cyclic and decreased collective pitch input rapidly slows the rotor speed decay while introducing an increased rate of descent. The maximum downward vertical acceleration occurs just after the highest pitch acceleration is reached. Characteristically, the airspeed increase is noted approximately 1 second after the pushover. Induced power required decreases rapidly when the collective pitch is lowered; however, profile power decreases as the aircraft pitches down and reaches a minimum during the acceleration. A pushover requires 2 to 3 seconds, and while the angular motions are significant, there is little time for the flight path to change. Thus, the height loss during the pushover was largely determined by the conditions at the start of the maneuver. At 16 KTAS, the height loss was 35 feet, decreasing as pushover speed neared flare airspeed.

Climb:

50. Pilot input for pushover following a power reduction during climb is complicated by the longitudinal instability between 40 and 60 KTAS, caused by the stall of the horizontal stabilizer (ref 11, app A). Also, the transition from climb to autorotation constitutes a greater trim change and a greater change in stability and control characteristics. These considerations are reflected in the greater variation in longitudinal control inputs during climb pushovers, as shown in a comparison of figures 13 and 15, appendix F. The normal pilot input during pushover generated 25 to 30 percent higher pitch accelerations and rates than were found during pushovers from level flight. The pitch attitudes were also consistently 10 to 15 degrees more nose down.

51. As was the case for level flight pushovers, after the initial cyclic input the normal acceleration was the critical parameter used by the pilot to determine the longitudinal control inputs. At low speed and low rates of climb, the normal acceleration characteristics during a climb pushover are much the same as in level flight. However, increasing rates of climb produce considerably lower normal acceleration values during the pushover. The power required is higher during the climb, which causes an increase in rotor speed decay rate of about 10 rpm per second.

52. The critical dependence of normal acceleration on longitudinal control input is shown in figure 17, appendix F, which compares three pushover time histories at a 48-KTAS entry airspeed and a 35-ft/sec climb rate. A different type of control input is used in each case. With no forward input, normal acceleration decreases to 0.5g, and with a moderate input of 1.3 inches, drops to 0.3g. The largest forward cyclic input of 2.1 inches yields a minimum normal acceleration of 0.06g. Controllability is decreased at low values of normal acceleration and pilot control of the aircraft may be adversely affected at values this low. The ease with which uncomfortably low g values can be reached increases pilot concern during the pushover from climbing entries.

53. The greater collective pitch control decrease and the more nose-down pitching motions for a pushover from climb cause higher vertical and longitudinal

accelerations. However, the effect of these accelerations is opposed by the upward flight path during the entry and at the start of the pushover. The resultant net height loss during pushover from climb entry was usually less than 15 feet, as opposed to 35 feet for level flight.

Acceleration

Level Flight:

54. The acceleration phase of the dive begins when the pushover is completed and is concluded when the aircraft is at conditions suitable for an effective flare. Sixty KTAS was the target airspeed chosen for this analysis and is near the airspeed for minimum rate of descent in steady-state autorotation. Figure H shows a representative time history sequence of events in a low-speed entry and dive.

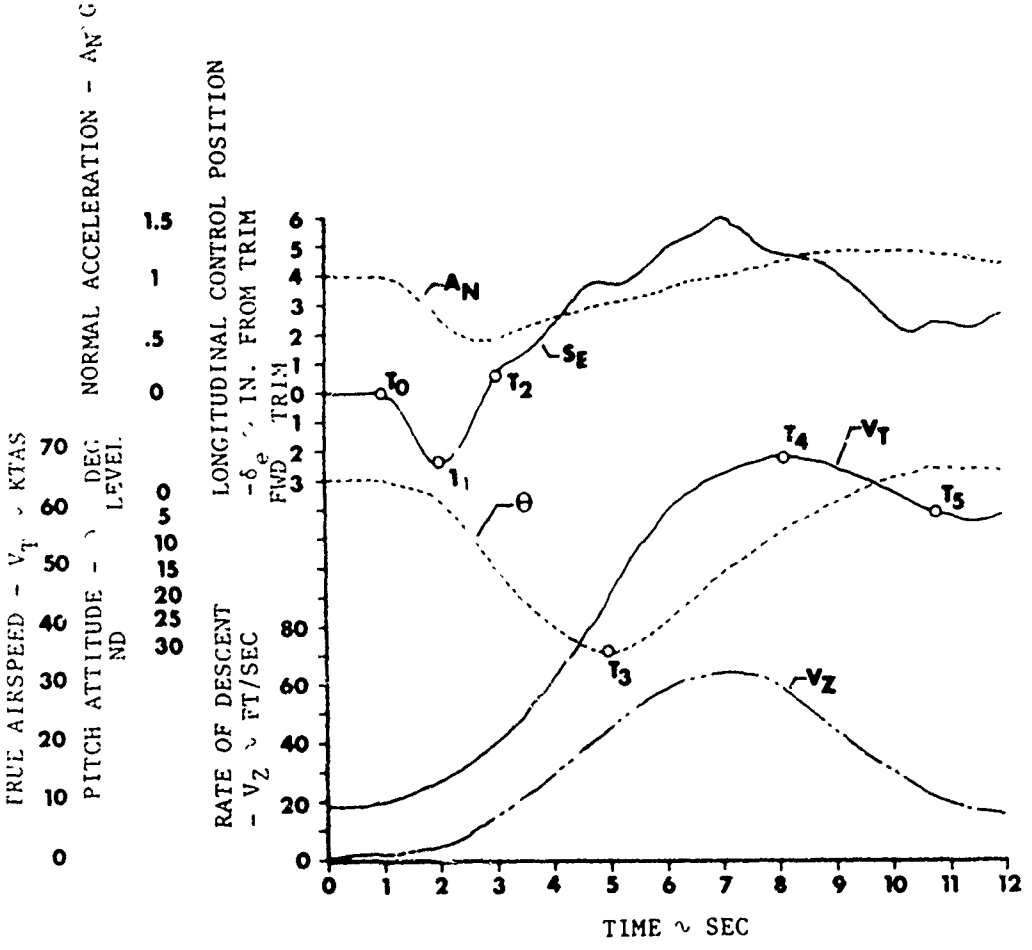

Figure H. Typical Dive Characteristics.

Cardinal points in the maneuver are noted by subscripted times (T_i) which will be identified in the discussion. The maximum nose-down pitch attitudes are reached at T_3. The larger values occur at the lower airspeeds where the pushover inputs and desired airspeed gains are greatest. The maximum longitudinal acceleration accompanies the maximum pitch attitude. The 60-KTAS target airspeed is reached at about this time. There was a characteristic overshoot with a maximum airspeed being attained at T_4. Normal acceleration was usually passing through unity between times T_3 and T_4. The pilot cue then was to apply aft longitudinal control and maintain a load factor of slightly greater than 1, which in turn stabilized the airspeed and reduced rate of descent.

55. During the pushover, the aircraft is pitching nose down and accelerating along the flight path. The pilot must judge the airspeed gain and determine when the aim airspeed will be reached. The maximum nose-down attitude was reached 1 or 2 seconds prior to the maximum airspeed. Maximum pitch-down attitudes from figure 13-2, appendix F, show an essentially linear variation from 32 degrees for an 11-knot entry to 2 degrees at an entry airspeed of 70 KTAS. As the aircraft reaches 60 KTAS the normal acceleration is below 1g, the pitch attitude is nose down, and the rate of descent is high and still increasing.

56. The maximum airspeeds that occurred when the pilot had to dive to gain airspeed define T_4, and are shown in figure 13-5, appendix F. The maximum airspeeds reached are determined by the pilot judgment of control required during pushover, acceleration along the flight path, and timing for stabilizing at the aim airspeed. The maximum airspeed reached during the acceleration generally exceeded the target flare airspeed by 8 KTAS. The rate of descent and flight path angle at maximum airspeed are shown in figure 13-5. At entries below 50 KTAS, the rates of descent and flight path angles were generally between 50 and 60 ft/sec and 25 to 30 degrees, respectively. The rate of descent drops off sharply for the higher entry airspeeds because of the smaller airspeed changes and the more shallow pushovers. Correspondingly, flight path angle is less steep for the higher airspeed entries.

57. After reaching the maximum airspeed, the aircraft is decelerated as the pilot stabilizes on the target airspeed. There was usually an overcorrection and the airspeed decreased below 60 KTAS, which is defined as T_5. At this point, the normal acceleration is positive, pitch attitude is nose up, and the aircraft is decelerating. The time interval between the initial 60 KTAS and T_5 is usually 4 or 5 seconds, which is nearly half the time spent in the total dive maneuver. In this time span, the pilot is transitioning the aircraft from a dynamic acceleration to a steady-state autorotation condition. Comparison of figures 13-5 and 13-6, appendix F, shows the most significant changes to occur for entry airspeeds below 50 KTAS. During the deceleration and stabilizing of airspeed, the rate of descent is reduced by about 30 ft/sec, and the flight path angle is decreased by 30 degrees. The great differences in flight path angle and rate of descent indicate that the aircraft is in a poor position to initiate flare at T_4, but in a good position at T_5, even though the airspeed has decreased. Figure 1 illustrates the flight path and airspeed relations for various entry airspeeds.

Entry True Airspeed ~ KTAS	Flight Path Angle at 60 KTAS Accelerating	Rate of Descent at 60 KTAS Stabilized
11	16	26
35	14	22
48	15	26
60	13	22

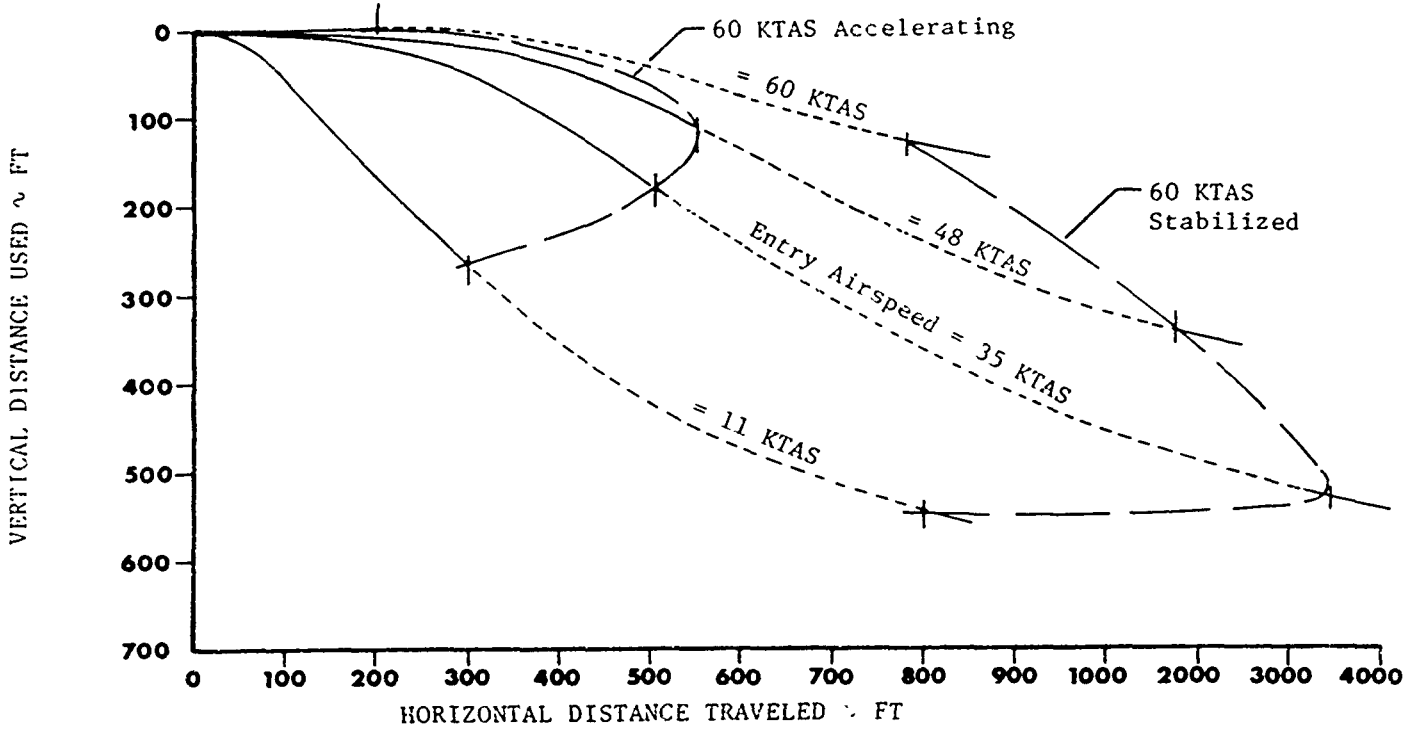

Figure I. Flight Profile for Dive.

The pilot consistently achieved similar flight conditions at the end of the dive regardless of the entry airspeeds. A steeper pushover should reduce the height loss to reach 60 KTAS; however, this may cause the airspeed to exceed the aim by a greater value. In such an instance the rate of descent will then be higher, which complicates the deceleration and may result in more total altitude required for a dive. The importance of the interval from 60 KTAS acceleration to 60 KTAS stabilized can be seen in figure J, which shows altitude loss from entry to various conditions. Approximately half the total height loss in the dive occurs during this deceleration.

58. Rotor speed is decreasing at the time of pushover and the decay rate is slowed by the downward collective control input. Minimum rotor speed was generally reached at the most nose-down attitude. Rotor speed characteristics are summarized in figure 13-9, appendix F. During the aircraft deceleration (T_4 to T_5), rotor speed increases; however, the rate of increase is about 20 percent lower than the maximum loss rate during entry and pushover. Thus, the duration of the deceleration phase determines the rotor energy at the start of the flare and influences the flare performance.

59. During the acceleration, the potential energy is converted to aircraft kinetic energy. After pushover, aircraft kinetic energy rises from that at entry conditions to a maximum at the highest airspeed, with the greatest rate of increase occurring near the time of maximum pitch-down attitude and longitudinal acceleration. The largest kinetic energies and maximum rates of change during the dive are shown

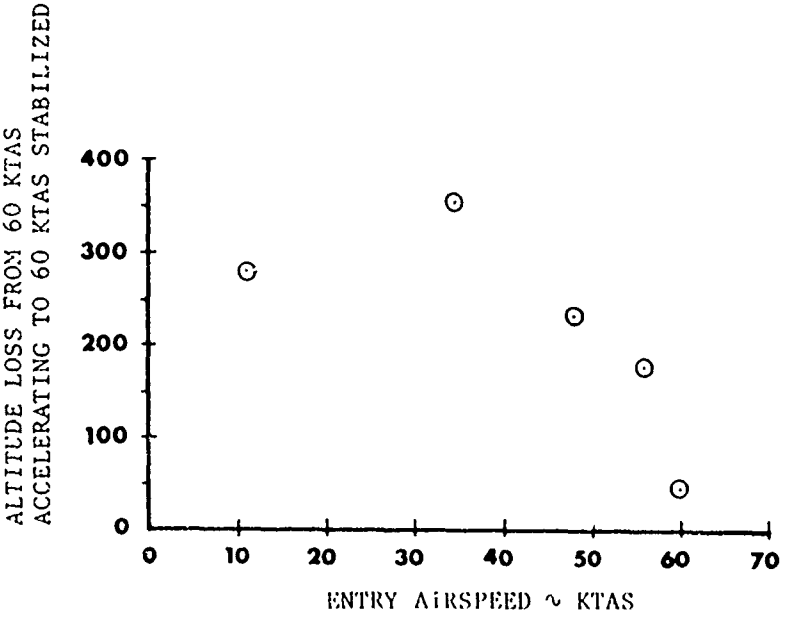

Figure J. Deceleration Characteristics.

in figure 13-8, appendix F. As soon as entry occurs and the aircraft starts losing altitude, potential energy decreases. The maximum descent rate accompanies the greatest rate of potential energy loss, and these values are also shown in figure 13-8.

60. Rate of kinetic energy gain and rate of potential energy loss drop off sharply past the 50-KTAS entry airspeeds corresponding to the more shallow dives from these conditions. The total aircraft energy, to include potential, kinetic, and rotor, begins to decrease at entry. The rate of total energy loss has local maximums during the entry and dive; one occurs just after power failure and prior to T_0, and another during the dive in the vicinity of T_4. These energy loss rate maximums are shown in figure 13-10, appendix F.

Climb:

61 The pilot input for a pushover during a climb entry is shown in figure 15, appendix F, and typically there is a wide variation in both amount and rate of forward longitudinal control input. As in level flight, the pitch rate, pitch attitude, and normal acceleration data were more consistent than were the initial control input data. The maximum pitch attitudes were 10 degrees more nose down for the acceleration after a pushover from climb. Also, the minimum normal acceleration reached was approximately 0.1g less, and the longitudinal acceleration was greater. Those conditions made it more difficult for the pilot to judge airspeed gain, and there was a tendency to exceed the target airspeed by 5 KTAS more than for the level flight entry case. A higher airspeed produces a higher rate of descent, so that a longer deceleration is needed to give the same conditions at the start of the flare. Conditions at the maximum airspeed are presented in figure 15-4, and show a higher rate of descent and a steeper flight path angle.

62. Main rotor performance during pushover and dive is shown in figure 15-9, appendix F. Total rotor speed change and rate of decay are more severe from the higher power climbing conditions than for level flight at similar airspeeds. The rotor speed loss ranges from 90 to 40 rpm, compared with 70 to 30 rpm in level flight entries. Rates of rotor speed gain during the dive are more comparable, as the diving portions are very similar.

63. Maximum kinetic energies and kinetic and potential energy rates of change are shown in figure 15-8, appendix F. Maximum kinetic energy rate of increase occurs somewhat sooner than in level flight entry dives, and the values tend to be larger. Maximum potential energy loss rates are slightly higher than for dives from level flight entry.

FLARE

General

64. The flare is defined as the transition maneuver required to proceed from the dive condition to one from which a safe landing can be made. This maneuver is complicated by the many pilot judgments which must be made and the critical

dependence upon the magnitude, timing, and sequence of the control inputs. Pilot apprehension is a factor because of ground proximity and rate of closure. The flare effectiveness is considered in terms of forces generated and energy relationships that transpire during the flare maneuver and will be influenced by the flare airspeed and rotor characteristics, as well as the magnitude and rapidity of the control inputs. The minimum flare airspeed is selected on the basis of some established aircraft performance or pilot suitability criteria.

65. As the longitudinal control is moved aft to effect a nose-up attitude, the increased angle of attack causes the rotor to accelerate. The thrust vector is increased and is tilted aft, which decreases forward speed and rate of descent. During the flare the aircraft energy is converted to rotor energy, which will be used during the landing maneuver. During the cyclic flare collective control application may be necessary to prevent rotor overspeed or to slow the vertical descent rate. A collective application is usually without cyclic input from a steady-state descent condition when the forward speed at flare termination is not a primary concern. The collective pitch application causes a thrust increase and a loss in rotor speed. The increased thrust slows rate of descent and decreases the flight path angle. Some aft cyclic may be used to prevent excessive rotor speed loss or to decrease forward speed.

Cyclic Flare

66. The aircraft operating conditions during a steady-state descent have been previously published in references 6, 10, and 11, appendix A, and for this test are summarized in figures 20 and 21, appendix F. Cyclic flare performance is summarized in figure 22. Cyclic flares from steady-state and dive conditions are shown in figures 23 through 33.

67. Tests were conducted to evaluate aircraft performance and obtain pilot opinion concerning flare techniques, flare rates, and flare attitudes. The aircraft stability and control characteristics influenced the pilot's judgment of control input. The characteristic shape of the longitudinal control input for a cyclic flare is illustrated in figure K.

At low and moderate speeds there was a tendency to apply excessive aft cyclic, which then required a forward control adjustment to a position forward of the initial trim point, as shown by V_1 and V_2, figure K. For the higher airspeeds, V_3 and V_4, the pilot could better judge the correct control input needed for the desired result.

68. At the start of the flare, the pilot has only his knowledge of the expected aircraft response to guide the amount of control input needed at different airspeeds. The aft cyclic control input, T_0 to T_1, was generally made at a rate of about 5 inches per second. The aft control input was continued until the maximum pitch acceleration was reached at T_1. For all flare airspeeds the maximum pitch accelerations were on the order of 15 deg/sec^2. The control input was then maintained until the pitch rate reached a maximum at T_2. The time interval between T_1 and T_2 varies with pitch controllability characteristics and is thus longest at

intermediate flare airspeeds and decreases at the high and low-speed extremes. After the maximum pitch rate was reached, the cyclic control was moved forward to attain the desired pitch attitude. The maximum acceptable pitch attitude at different flare airspeeds is shown in figure 22-3, appendix F. For airspeeds below 45 KTAS there was very little to be gained from the flare and the pilot used shallow flare angles. As the flare performance increased progressively with higher flare airspeeds, the pilot increased flare attitude to a maximum of about 30 degrees nose-up. Higher angles were possible but they were uncomfortable and restricted forward visibility.

69. Flares at 35 KTAS and below were found to vary considerably from those at higher airspeeds. This unusual condition is represented by V_1 in figure K. At T_1, the angular pitch accelerations were typical and would appear to be satisfactory. However, there was a downward acceleration and lack of flight path change, which so strongly influenced the pilot that he quickly moved the stick forward to level the aircraft. Normal acceleration forces generated during flares at different airspeeds are summarized in figure L.

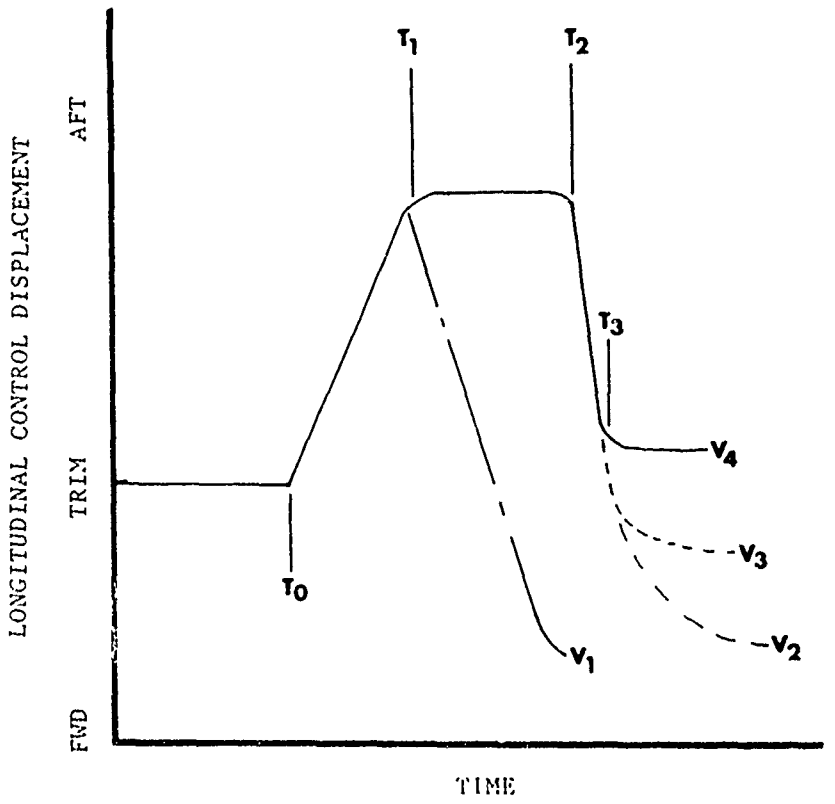

Figure K. Longitudinal Control Input for a Cyclic Flare.

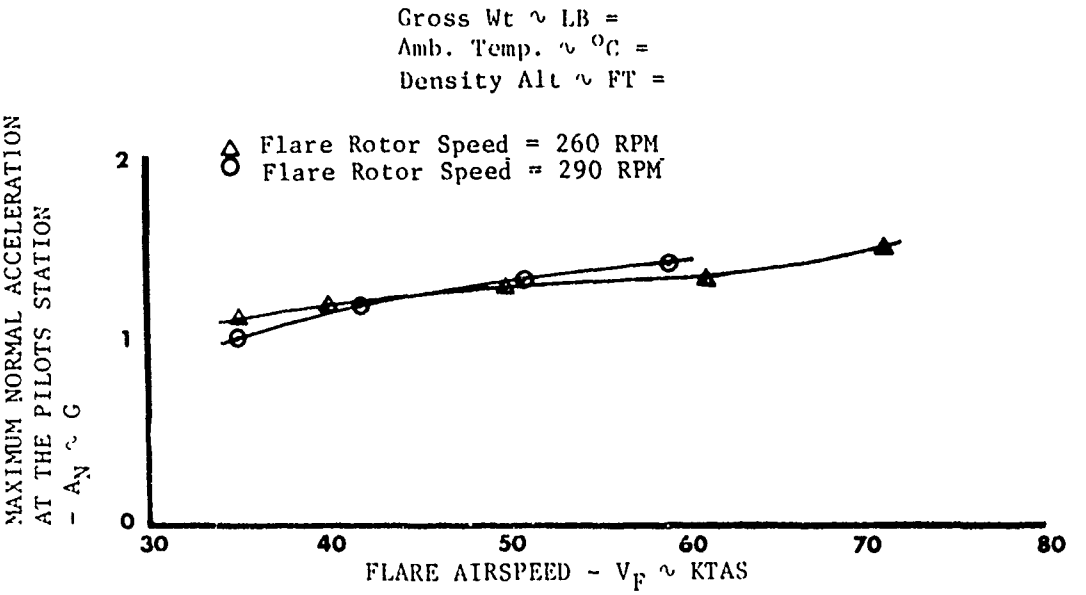

Figure L. Normal Accelerations from Cyclic Flares.

70. The maximum aft control input of 5 inches at the 45-KTAS condition did not violate a 10-percent aft control margin. The left lateral and left directional control requirements during the flare were small and were of no particular concern. During the flare, there was a tendency to yaw right.

71. The pitch attitude becomes progressively more nose up as airspeed is decreased from 50 KTAS during steady-state descent, the descent angle steepens, and the rate of descent becomes greater. Descent angles during steady-state autorotations are shown in figure M.

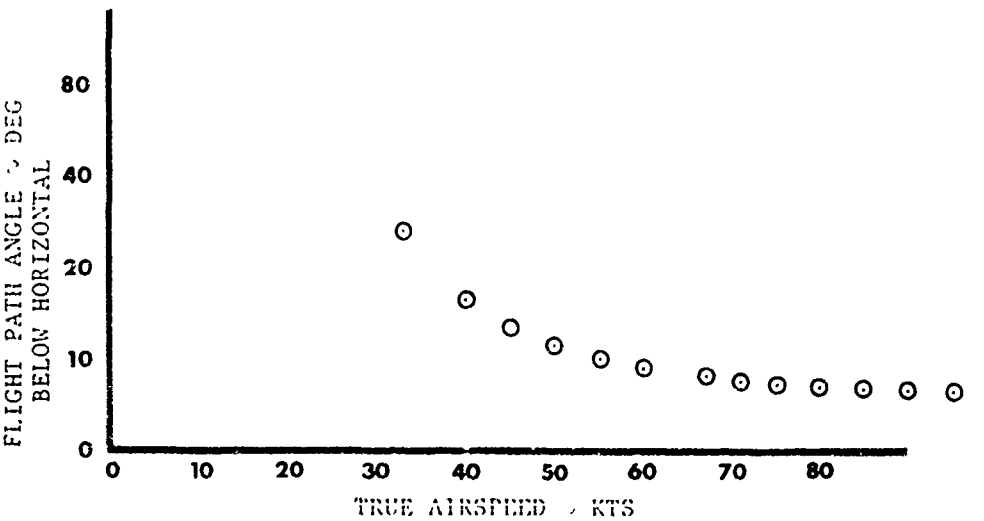

Figure M. Flight Path Angle in Steady State Autorotation.

The flare effectiveness, flight path angle, and ground proximity determine the acceptable pitch attitude. The acceptable pitch attitude became more nose-up as the flare airspeed increased. However, the resultant angle-of-attack change tends to be about 20 degrees for all the flare conditions. Thrust changes occur immediately after the aft cyclic input and at flare airspeeds above 40 KTAS, build to a maximum as the pilot is stabilizing on the desired pitch attitude.

72. There is generally a decrease in rotor speed during the entry and dive which can be as large as 60 rpm, depending upon the initial delay time and duration of the deceleration phase of the dive. Thus, the rotor speed at flare could be well below the steady-state minimum of 294 rpm.

73. Tests were conducted at rotor speeds of 260 and 290 rpm, and are summarized in figure 22, appendix F. In general, the performance is better at the high rotor speed for flare airspeeds below 40 KTAS. Above 40 KTAS, the performance is similar for both rotor speeds and becomes progressively better with increased airspeed. The decelerating horizontal and vertical forces follow the main rotor thrust trends. The cyclic flare effectively decreases the forward motion and also slows the rate of descent. At low speed there is little thrust increase from the flare; however, tilting the thrust vector aft introduces an aft force, which slows forward speed even though there is little vertical deceleration. At higher speeds, the horizontal deceleration is more pronounced because of the combined effects of aft tilt and increased thrust.

74. The energy change during the flare is one of exchanging aircraft kinetic and potential energy losses for an increase in the main rotor energy. The total aircraft energy changes during the flare can be expressed as

$$\Delta E_{system} = \Delta KE_{AC} + \Delta PE + \Delta KE_{MR} \qquad (1)$$

Where:

ΔKE_{AC} = Change in aircraft kinetic energy

ΔPE = Change in aircraft potential energy

ΔKE_{MR} = Change in main rotor kinetic energy

The first two terms on the right side of the equation are negative, since the aircraft is losing speed and altitude. The change in potential energy depends on the initial rate of descent and the decrease that occurs during the flare. The kinetic energy of the rotor increases when a gain in rotor speed occurs. Energy changes are summarized in figure 22-9, appendix F. For the low-speed flares, there is little effect from the flare and the aircraft continues to descend with no signficant change in flight path or rotor energy. The efficiency of the flare is defined as the energy conversion ratio, as calculated from equation 2.

$$\eta = \frac{\Delta KE_{MR}}{\Delta KE_{AC} + \Delta PE} \qquad (2)$$

Where:

η = Flare efficiency

The improved efficiency with increasing airspeed is summarized in figure N.

The low efficiency at low airspeeds is caused by the large amount of energy needed to overcome the increased rotor power required. When the flare efficiency is low, it is very important that the pilot utilize the energy in the best manner. Although there is more efficiency at high speeds, the total energy which must be dissipated is also much higher. This energy loss can be accomplished through a combination of the higher flare angle and increased time for which the flare is maintained. Additional details of the characteristics during deceleration from high-speed conditions are presented in the landing discussion (para 94). The gain in rotor kinetic energy was essentially zero at 35 KTAS and increased to 200 shp per second at 50 KTAS. At flare airspeeds above 50 KTAS, the pilot tended to decrease the flare angle and duration such that there was little additional gain in effectiveness. The energy terms summed as in equation 1 are shown graphically in figure O.

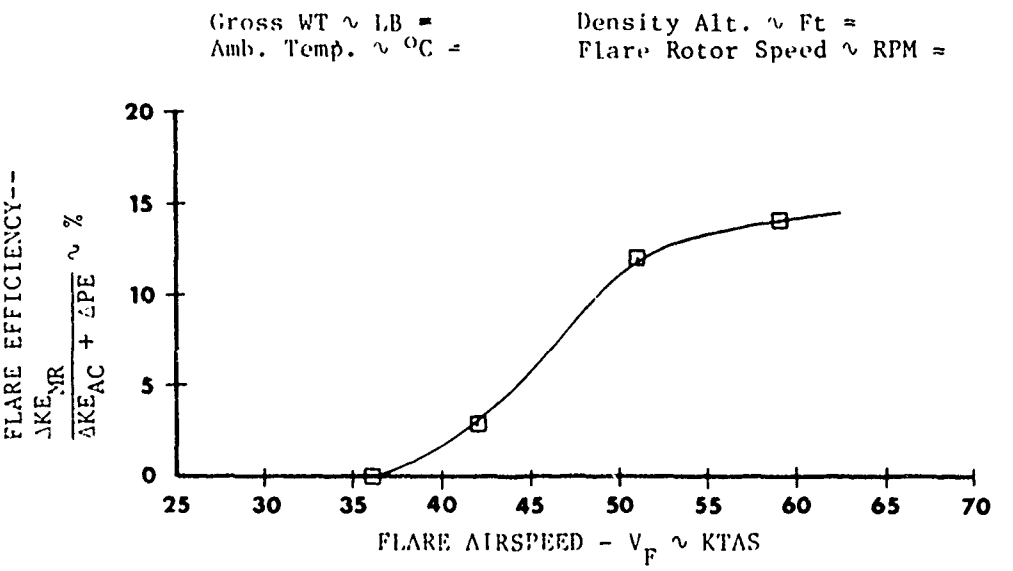

Figure N. Flare Efficiency.

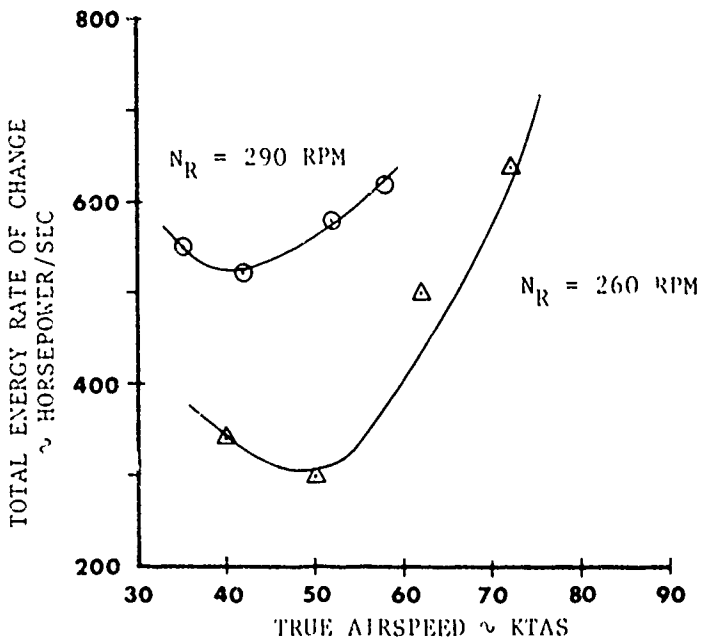

Figure O. Total Energy Changes During Cyclic Flare.

75. The total energy rate of change is greater at the higher rotor speed, and an effective flare can be accomplished at a lower airspeed. At flare airspeeds below the minimum effective the rotor is not accelerating, the aircraft is not being slowed, and the total energy change is primarily a loss in potential energy over which the pilot has no control. Flare airspeed increases to 70 KTAS are progressively more desirable. At airspeeds above 70 KTAS, the flare performance available is greater than that needed for normal situations.

76. The height loss during the flare from 50 KTAS was 20 feet for 260 rpm and 60 feet for a rotor speed of 290 rpm. The greater height loss is attributed to the higher rate of descent at flare entry for the 290-rpm condition. At flare airspeeds above the minimum effective airspeed, the loss was essentially a constant for the technique used. However, there was sufficient performance available for the pilot to control height loss by adjusting the technique and accepting the different rotor energy and kinetic energy characteristcs that will result.

Altitude Effects

77. Typical time histories of the flare characteristics at a density altitude of 9400 feet are presented in figures 29 and 30, appendix F. Comparison with a density altitude of 870 feet in figures 23 and 24 shows no apparent change in the pilot cues and the flare was accomplished in the same manner. The angular

pitch acceleration and rate developed appears to be slightly lower at the high altitude. The rotor acceleration and thrust development are also slower at high altitude. A higher true airspeed is required to produce an effective flare, which necessitates a greater altitude loss during the dive. Results at two altitudes are compared in figure P.

78. Figure P reflects a change in the flare characteristics with flare airspeed. At the high altitude, the longer time required for the flare and the less effective decelerations result in more height loss during the flare. The time difference of 1 second corresponds to about 30 feet at an airspeed of 60 KTAS. The pilot must account for the added height loss by starting the flare higher above the ground or by executing a more rapid flare as the density altitude increases.

Gross Weight Effects

79. Increasing gross weight from 6890 to 8125 pounds required no change in the cyclic flare technique so far as the pilot was concerned. Comparison of figures 26 and 28, appendix F, shows angular pitch response to be essentially the same for both weights. At the heavier weight the rotor speed tended to increase more rapidly. The induced power required was approximately 100 shp higher and the normal acceleration was reduced by 7 ft/sec^2. Thus, for a given flare technique and performance, increased gross weight requires a higher flare airspeed or a longer flare duration.

Rate of Cyclic Flare

80. The cyclic flare can be accomplished at any rate desired by the pilot. During these tests the majority were conducted at a "normal" rate which was based on

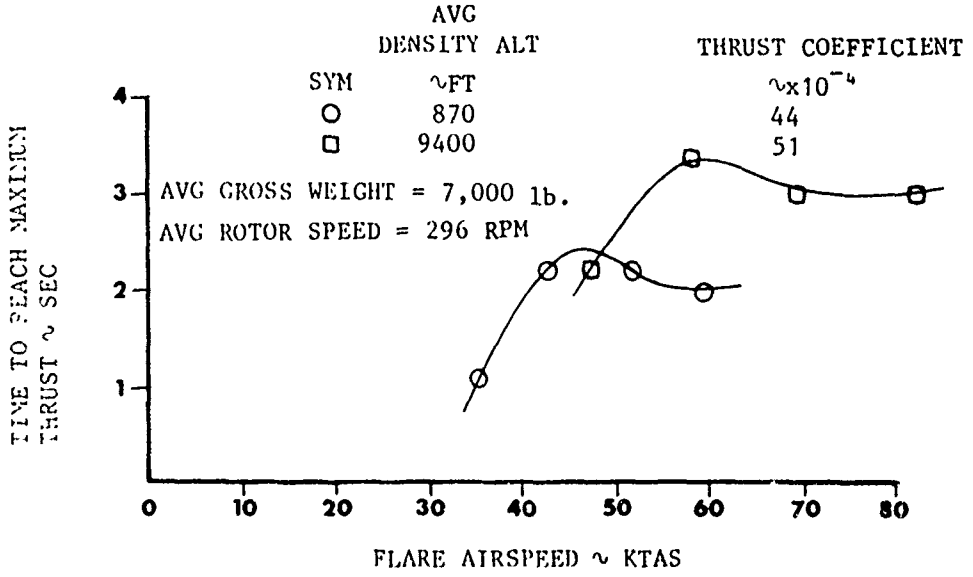

Figure P. Comparison of Thrust Characteristics with Density Altitude Change

pilot familiarity with the aircraft and his judgment as to what the performance requirements were for the flare condition. Aft cyclic control inputs up to 2 inches per second produced flares that were considered slow, control inputs of 2.5 to 5.5 inches per second were normal, and inputs higher than 5 inches per second generated rapid flares. Characteristic performance changes that occur with rate of cyclic flare can be obtained from figure 33, appendix F.

81. With a rapid flare the aircraft pitches much more quickly and the cyclic input must be adjusted rapidly to prevent excessive rates from being generated. This can be accomplished so that the flare attitude increases to a desired maximum in 4 seconds. Rotor speed also increases much more rapidly with a sharp flare and caution must be used to prevent exceeding the limit. The thrust increase is more rapid and reaches a higher value than for a given cyclic input at a slower rate. The change in the flare effectiveness is illustrated by figure Q. The benefits of a rapid flare are essentially nil at lower airspeed and progressively increase with higher airspeed.

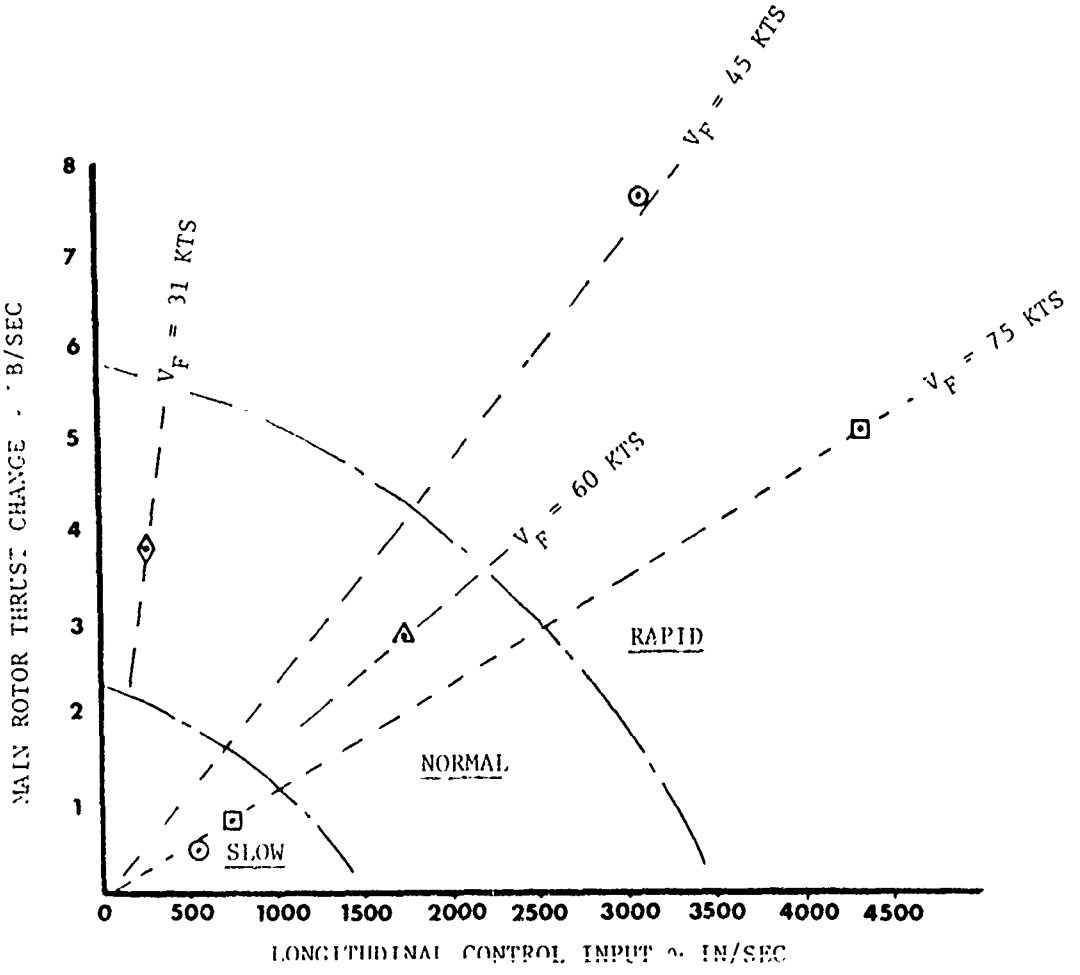

Figure Q. Thrust Characteristics with Rate of Cyclic Flare.

82. The greater thrust and pitch attitude with a rapid flare significantly decreases the airspeed and rate of descent. The energy exchange is more effective with a larger decrease in aircraft kinetic energy and a smaller loss in potential energy while providing more rotor energy to use during the landing phase.

Flare from Accelerating Autorotation

83. Typical flares from a diving condition at low and medium flare airspeeds are shown in figures 31 and 32, appendix F. Table 2 compares conditions at the start of the flare from accelerating and steady-state autorotations.

The most significant differences to the pilot are the much higher rates of descent and the extreme nose-down attitudes. The angle of attack and power required are important with respect to rotor performance in the flare.

84. The control inputs, aircraft response, and pilot comments suggest that no alternate pilot considerations are necessary for the two maneuvers. Although the aircraft is considerably more nose down, the change in attitude and angle of attack is essentially the same. Flares from dives introduce considerably more roll and yaw response with an accompanying increase in pilot workload. At 60 KTAS, the flare from the accelerating autorotation generated a rotor speed increase of 13 rpm/sec as compared to 8 rpm/sec for the steady-state case. The thrust characteristics follow the rotor speed trends, with about 25 percent more thrust being realized when flaring from a dive. The acceleration components in the horizontal and vertical axes were also larger than during a flare from steady state.

Table 2. Comparison of Aircraft Conditions at Flare From a Dive and From Steady State.[1]

Flare Condition	True Airspeed (kt)	Pitch Attitude (deg)	Angle of Attack (deg)	Rate of Descent (ft/sec)
Dive	39	-14	20	36
	48	-15	21	46
	60	-18	11	45
Steady state	35	4	41	40
	42	1	23	27
	59	Zero	15	26

[1]Average rotor speed: N_R; 300 rpm.

85. At the start of the flare, fixing airspeed and rotor speed establishes the kinetic energy conditions. Potential energy is determined by the height above the ground, which was not a constant for the flight data shown in appendix F. However, in a dive, the flare produces a larger gain in rotor energy while at the same time the higher descent rate is causing a more rapid loss of potential energy. The result is that the energy exchange from aircraft to rotor is more effective when flaring from a dive, although the total energy characteristics are essentially the same.

86. The main rotor-induced power characteristics are similar, although when flaring from a dive the magnitude is about 25 percent higher. Profile power characteristics are considerably different. A more rapid increase in profile power with aft control input is caused by the higher rotor speed gains.

87. The effect of the cyclic flare on rate of descent and forward airspeed is essentially the same whether starting from steady state or a dive. Thus, for a given airspeed the higher initial rate of descent results in a higher rate of descent at the conclusion of the flare maneuver. Also, for a given time increment the height loss will be correspondingly greater. At 60 KTAS the vertical distances are 140 and 80 feet, respectively, for dive and steady-state flares.

Collective Applications

88. The collective flare is generally made from steady-state descent conditions such as are shown in figure 20, appendix F. The collective application is particularly important at airspeeds below the minimum airspeed where an effective cyclic flare cannot be used to increase rotor speed. In this airspeed range, the rotor energy is all that the pilot has available to decelerate the aircraft and cushion the landing. The characteristic collective input was the same for all test conditions and is illustrated in figure R.

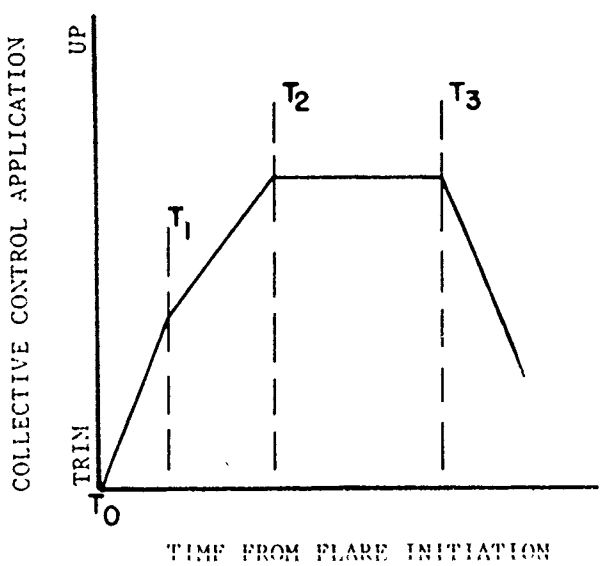

Figure R. Typical Control Input for Collective Flare.

89. The initial rate of collective input ($T_0 - T_1$) was maintained until the normal accelerations had peaked at about 1.5g. The collective was then input at a rate of 1 to 1.5 inches per second until the normal acceleration had begun to decrease. Also, during the second phase ($T_1 - T_2$) the rotor decay rate had stabilized at a value of about 20 rpm/sec; the rate of descent and the descent angle were decreasing rapidly. The maximum collective control position was held until the normal acceleration had returned to nearly 1, at which time it was apparent the flare was no longer effective and the collective was lowered.

90. The thrust increase during the flare was about 700 pounds per inch of collective application and there was little airspeed effect for the range of 40 to 70 KTAS. The horizontal and vertical decelerations were about 3 and 15 ft/sec^2, respectively. The flare maneuver typically reduced the rate of descent 30 ft/sec and decreased airspeed by about 5 knots.

91. Aircraft kinetic energy is decreased at the expense of the rotor kinetic energy loss. The efficiency of the flare is defined by

$$\text{Efficiency} = \frac{\text{Aircraft kinetic energy}}{\text{Rotor kinetic energy + potential energy}}$$

The rotor energy was converted with an efficiency of approximately 25 percent.

92. In steady-state autorotation, rate of descent at flare initiation is highest at low airspeeds and reaches a minimum at 50 KTAS. At this or higher airspeeds, the rate of descent could be stopped with a collective flare height loss of about 60 feet. Significant increases in height lost during the flare were encountered when the flare airspeed was below 50 KTAS.

LANDING

General

93. The nature of the landing is primarily dictated by the entry conditions. The three general types of landings to be considered are those from low hover; low-speed, low-altitude; and high-speed, low-altitude. When landing from a hover, there is only rotor energy to dissipate the potential energy of the aircraft. In low-speed, low-altitude flight, the kinetic and potential energy of the aircraft can be used to varying degrees depending on the height-airspeed combination. As airspeed is increased toward a minimum effective flare airspeed, a greater amount of flare can be used. When above the minimum effective flare airspeed, the excess aircraft kinetic energy can be used to build rotor speed and maintain height while slowing to a desirable touchdown speed. Each landing must be accomplished within the gear limits and with sufficient rotor speed to prevent excessive main rotor flapping which may allow the rotor blade to strike the tail boom.

Hover Landing

94. The hover landing data shown in figures 37 through 40, appendix E, were obtained from power reductions in a stabilized hover. The rapid yaw acceleration with power reduction provided the pilot with an immediate, unmistakable cue and, thus, the only delay was essentially the pilot reaction time. Approximately 2 inches of directional pedals were required to control the yawing motion. There was also a need for about 1 inch of aft and right cyclic during the power reduction and landing.

95. From power reduction to landing, the rotor speed decreases rapidly. At hover height below 10 feet, the pilot has no option but to input collective as required prior to ground contact. The constant collective application of approximately 1.6 inches per second shown in figure 37, appendix F, was sufficient to counter a downward acceleration of 2.5 ft/sec^2 and maintain a 3-ft/sec rate of descent. The results show that the pilot could make very good judgments concerning the rate of descent, ground proximity, and amount of control required to make a safe landing.

96. Increasing height above the ground or increasing gross weight adds to the potential energy which the rotor must dissipate. However, the rotor energy available is fixed for a given rotor speed and, thus, the pilot judgment of collective usage becomes more critical. For maximum safety margin, the rotor speed should be the highest allowable so as to have the greatest rotor energy available when hovering near the ground. Tests were conducted at a 5-foot skid height while increasing the gross weight. The collective was applied so that full input was reached at ground contact. The increased gross weight caused a higher rate of descent after the power reduction, and the pilot had to input the collective more rapidly. This, in turn, generated more thrust so that over a certain weight range the average rate of descent from power reduction to touchdown was essentially the same. At a certain gross weight the total rotor capability is being used and the pilot cannot prevent an increase of rate of descent with added gross weight. The tests were conducted at density altitudes of 2940 and 7000 feet, and there was no difference in the resulting performance. As rate of descent at touchdown became greater than 2 ft/sec, there was an ever-present concern that a hard landing had occurred. As the height above the ground is increased, a technique change is necessary. Up to a given height, a constant-rate collective input will keep touchdown rate of descent within limits. Additional height then dictates that the collective input be delayed and rotor energy be conserved until the aircraft is near the ground. The initial tests were conducted using a technique of maintaining a contant collective position until near the ground, and then applying full collective prior to ground contact. The pilot tended to apply the collective when rate of descent was 7 ft/sec or greater.

97. Improved hover landing performance can be obtained by altering the technique as shown in figures 39 and 40, appendix F. Lowering the collective decreases thrust and increases the rate of descent. At the same time, rotor energy is conserved

so that it may be used just prior to touchdown. However, this technique is very critical with respect to height or rate of descent and is considerably beyond that expected during an actual emergency. The largest, most rapid collective input of 7.5 in./sec is shown in figure 40. The thrust increase of 4500 pounds caused a vertical acceleration of 0.35g and decreased rate of descent by 5 ft/sec.

Low-speed, Low-Altitude Landings

98. Low-speed, low-altitude landings are defined as those accomplished from the area A-B-C-D shown in figure S (excluding hover). When the power reduction occurs outside the avoid area, the dive and flare determine the conditions from which the landing will be made. Forward speed and rate of descent should be relatively low, and rotor speed should be in the upper ranges. For a power reduction within the area A-B-C-D, pilot recognition and action are critical, since there is a rapid rotor speed decay and rate-of-descent increase immediately after the power reduction.

In this area there is not sufficient height above the ground to dive and gain airspeed, nor is there adequate airspeed to accomplish an effective cyclic flare. Figures 41 and 42, appendix F, show low-speed approaches and landings. During the approach, the technique was to maintain the highest thrust without bleeding rotor speed and decrease forward speed. As the aircraft nears the ground the collective is input in the same manner as during a hover landing.

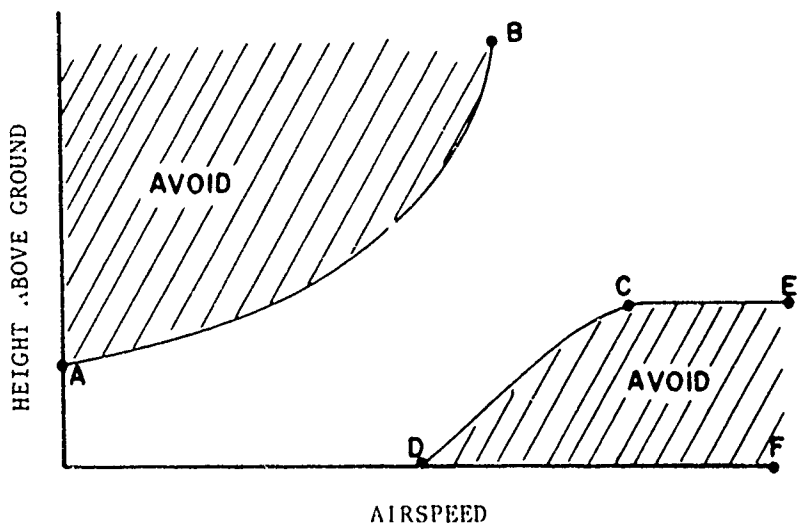

Figure S. Landing Envelope.

99. During the landing shown in figure 41, appendix F, the thrust reached a maximum before the full-up collective position was reached and then decreased as the rotor speed decayed. The longitudinal control was moved aft 1 second prior to touchdown, which increased thrust and rapidly decreased forward speed from 17 to 5 KTAS.

100. The collective application during landing rapidly decreased the rotor speed while effectively reducing forward speed and rate of descent. The rotor energy was used more efficiently than during the hover landing or during flares at altitude. The improvement is apparently caused by the ground effect. which was not present during the flare tests.

High-Speed, Low-Altitude Landings

101. The high-speed avoid area shown as C-D-E-F, figure S, is defined by the entry characteristics and the aircraft geometry. During the entry, the aircraft motions may cause a flight path change and height loss as the controls are held fixed. Additional height may be lost as the recovery is accomplished. At high speed, the aircraft must be slowed prior to landing, which requires that sufficient altitude be available to maneuver. Figure T illustrates the UH-1C helicopter and ground clearance requirement for typical deceleration or obstacle avoidance maneuvers.

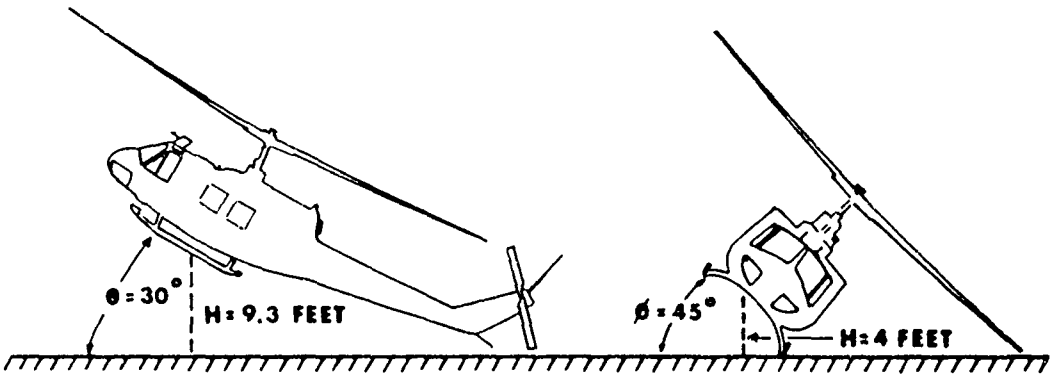

Figure T. UH-1C Ground Clearance Requirements for Maneuvering

Thus, the height of the avoid area at C-E is the sum of the three items discussed. For the UH-1C, an entry at 111 KTAS with a 2-second delay produces a height loss of 55 feet (fig. 1, app F). A 30-degree flare requires 9 feet, which establishes the minimum avoid area at 64 feet.

102. The high-speed touchdown, point D, figure S, is determined by the landing gear capability in terms of drag loads since there is no height available for recovery and/or flare. The rotor thrust and rate of descent at touchdown establishes the normal force experienced by the landing gear. Landing terrain and type of landing gear determines the coefficient of friction. From these, landing gear loads, decelerating forces, and sliding distances can then be calculated.

103. In the event of a power reduction occurring within the avoid area, rapid pilot recognition with little delay time minimizes the height loss, facilitates recovery, and may allow a safe landing maneuver. In such a case, collective control can be used to gain height at a sacrifice of rotor speed. The airspeed is then decreased with a cyclic flare, which restores rotor speed and allows the low-speed, low-altitude area to be entered with a relatively low rate of descent. From this point, a landing is accomplished as previously described.

HEIGHT-VELOCITY DIAGRAMS

General

104. The H-V diagram will depend on the aircraft flight characteristics, technique, and constraints, as well as the landing terrain. The flight condition will determine whether a dive and/or a flare will be required. The maneuver can be considered in terms of three general cases, as shown in figure U.

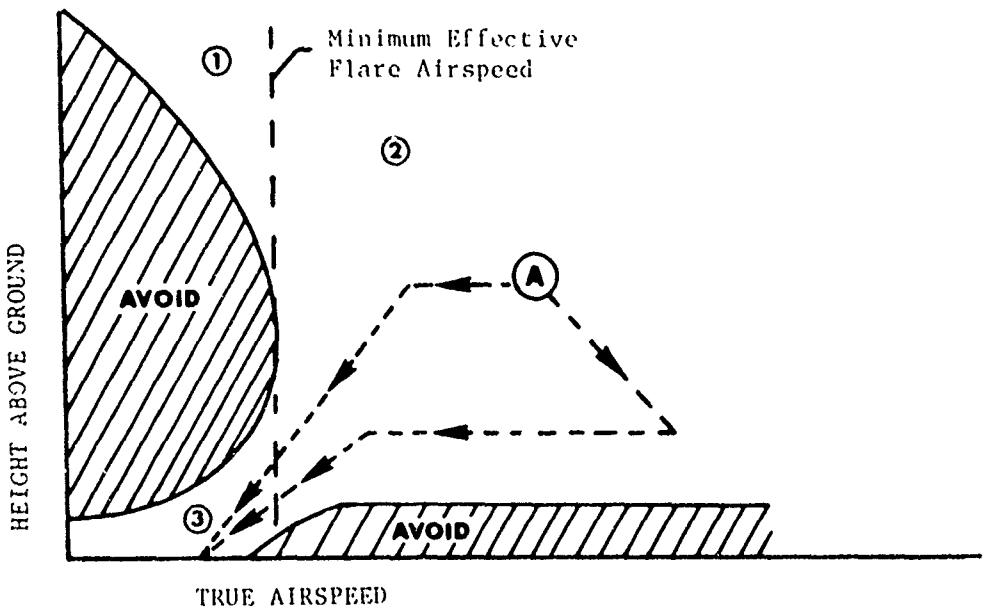

Figure U. Height-Velocity Diagram.

From area 1, the aircraft must be dived to reach the minimum effective flare airspeed. The intent is to minimize rotor energy losses while exchanging potential energy for aircraft kinetic energy. In area 2, there is sufficient airspeed for an effective flare, and a dive is not necessary. The potential energy must be dissipated while maintaining airspeed and rotor speed. The low airspeed in area 3 prevents an effective flare, and rotor energy must be used to overcome the aircraft potential energy and descend to a landing.

105. The criticality of the pilot actions is primarily dependent upon proximity to the avoid areas. When close to the curve the pilot must closely adhere to the technique and conditions on which the curve is based. When at a reasonable distance from the curve, the pilot has a great many options on how to arrive at a safe landing condition. For example, from point A, figure U, the pilot could:

a. Maintain altitude while decelerating and gaining rotor speed, then maintain flight path to the ground, using pitch attitude and collective pitch to control airspeed and keep rate of descent within limits.

b. Dive to gain airspeed and lose altitude; then use a steep cyclic flare to decrease airspeed, build rotor speed, and maintain height; descend in a landing attitude with collective pitch controlling rate of descent.

The major difference in the two cases is that in the second, the potential energy is converted to kinetic energy and conserved for a period of time, whereas, in the first case, the energy is dissipated from the outset.

Experimental Height-Velocity Tests

106. The experimental H-V diagram shown in figure 43, appendix F, was developed at the high-altitude test site (9500-foot elevation). Prior to the test, the pilot technique, aircraft limits, and test conditions were specified for the various flight regimes shown in figure U. To determine the curve at each airspeed, the procedure was to decrease height in suitable increments so that the pilot could assess the performance margin at each test condition. For each series, the entry airspeed was held constant so the pilot would not have to contend with different entry characteristics on successive points. Figure V illustrates a typical sequence of test points. The test at any given entry airspeed was terminated when the pilot judged that the performance margin had decreased to the point where exceptional techniques were required or there was not allowance for a small variance in pilot performance.

107. In a practical case, the number of points required to establish the curve at a given airspeed will vary with characteristics of the test vehicle, the performance margin, and the experience of the personnel conducting the test. A well-behaved aircraft allows the pilot to more quickly and more confidently choose the height increments to arrive at the final point with fewer test points. When the desired curve is near the limits of pilot ability or aircraft capability, the height increments must be small, more test points will be required, and the degree of risk increases rapidly. Experienced test personnel can assess the nature of a given maneuver and quickly estimate the margin or predict the performance on successive points.

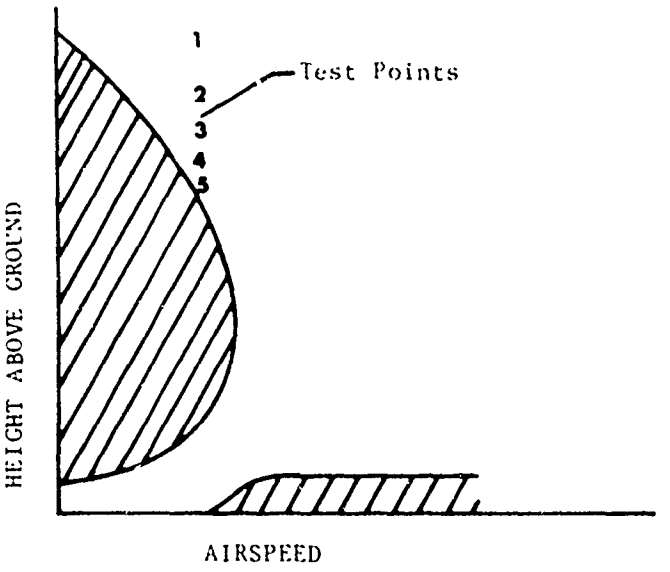

Figure V. Test Point Sequence for Determination of Height-Velocity Diagram.

108. All points flown to determine the H-V diagram are presented on figure 43, appendix F. The pilot judgment of each point is annotated. As expected, in a test of this nature there is considerable scatter in the data which cannot be totally accounted for in an engineering analysis. Thus, the pilot comment is the best single indicator of relative merit of each test point, and is used to locate the curve. The H-V diagram for the AH-1G helicopter is compared to UH-1C data in figure 43. The two aircraft have the same rotor system and should have similar performance capabilities. The results are from independent tests and, in both cases, the pilots used maximum performance capability and pilot suitability to arrive at the recommended H-V diagram. The close agreement indicates each pilot's ability to independently judge all factors during the tests and agree on a realistic H-V diagram for operational aviators.

109. Power reduction and landing maneuvers during the H-V tests are illustrated in figures 44 through 48, appendix F. The low-airspeed case depicted in figure 45 shows all the elements required to land after a power reduction; *ie*, entry, pushover, dive, flare, and landing. Idealized longitudinal control inputs for each phase have previously been shown. These are assembled as a single unit in figure W and compared to the pilot actions which occurred during the experimental H-V tests.

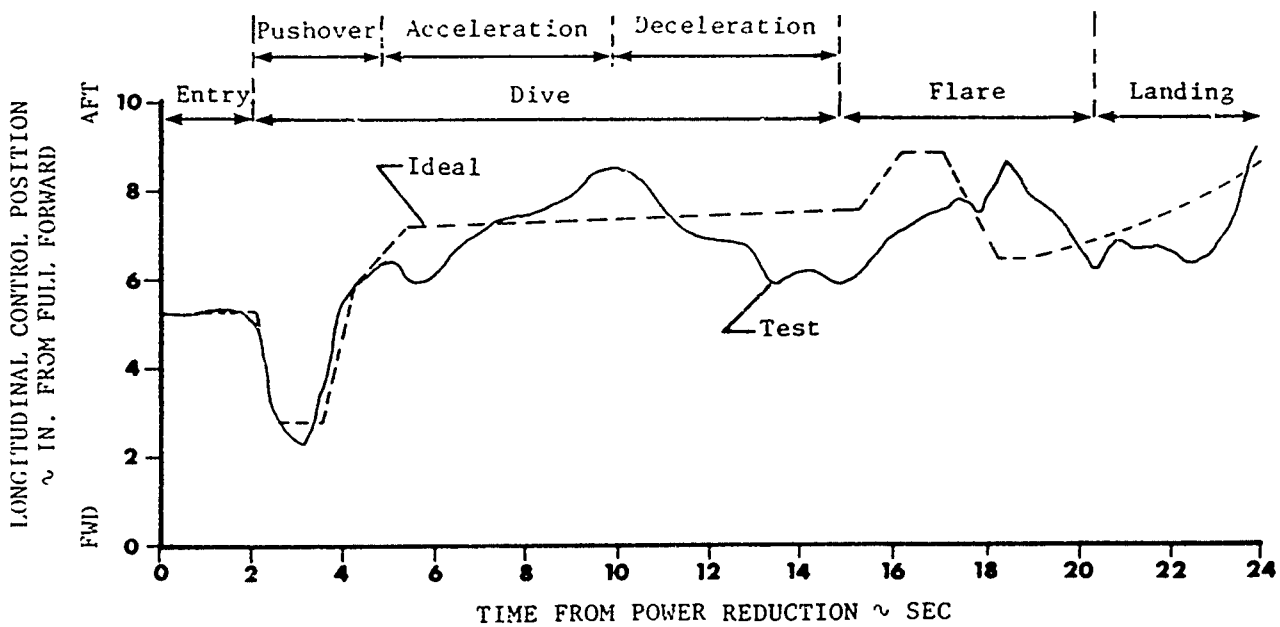

Figure W. Comparison of Ideal Pilot Inputs with Test Results.

Table 3. Comparison of Performance From Total Autorotation and Individual Tests.

Phase	Height Loss (ft)	
	Individual Tests	Total Autorotation
Entry (10 KTAS)	Zero	10
Pushover	120	40
Drive	400	500
Flare	80	90
Landing	20	20
Totals	620	660

110. Viewing the total autorotation as the sum of its parts, a comparison can be made of the performance obtained from tests of each phase with that resulting during a total nameuver. Results are presented in table 3.

In most cases, the performance for each portion of the total autorotation compares favorably with the individual tests, and the height required for the total autorotation is greater by only 40 feet. The most significant variation occurs in the pushover and dive portions. This is caused by the difficultv in separating the two portions during a total autorotation. However, the sum of the two compares favorably. Analysis of the individual parameters shows a performance loss may be caused by the pilot introducing additional decision points. At each decision point the response to the input was evaluated, and then further action was taken. A good example of this is the characteristic "double cyclic flare" shown in figure W, during the time interval from 17 to 18 seconds. During this time interval, the aircraft state is being assessed and decisions are being made as to when and how much aft cyclic can or need be applied to obtain the necessary performance.

111. Another aspect of comparing the performance from the two sources is the lateral motion. The individual test maneuvers are conducted quickly, and there is not sufficient time for lateral motions to develop. While in the total autorotation, the motion is cumulative and becomes more significant as time lapses. The lateral motions require bank angles that increase rate of descent and load factors which influence rotor speed. The maneuvers produce energy losses that reduce aircraft capability and add to the pilot workoad, which in turn can further detract from the overall performance.

112. During the H-V tests, a continual assessment was made concerning the pilot technique to be used. Aircraft performance, pilot difficulty, and safety margin were primary considerations. Pilot tolerance levels concerning pilot actions and cues had been obtained during the tests of each phase of the autorotation and landing maneuver. The complete technique which evolved is considerably removed from a maximum performance technique in certain areas. Notable examples are dive and flare rates and attitudes. In the H-V tests, the pilot chose lower pitch rates and the desirable attitudes were about 5 degrees less than those which were acceptable during the dive and flare tests. These changes add to the height required, but decrease the pilot effort and improve the safety margin for a given point on the H-V diagram.

113. The greatest variation was found in the deceleration portion of the dive. Maximum performance is obtained by the most rapid acceleration to flare airspeed, followed immediately by a large rapid cyclic flare. At the time of flare, the rate of descent will be on the order of 4000 ft/min. It was found during the H-V tests that the maximum performance flare was difficult for the pilot to accomplish accurately and repeatably. This introduces a high risk, and is undesirable from an operational viewpoint. In addition, at the outset the pilot is apprehensive about flaring with the high rate of descent, and considerable practice and training is needed before he can be at ease with the maneuver. Also, a flare from the dive at a high rate of descent dictates that the flare be started at a greater height above the ground, since more altitude is needed to reduce the rate of descent. A more realistic method was to maintain the flare airspeed and decrease rate of descent to something near the steady-state rate of descent which he is accustomed to experiencing. This deceleration requires 2 to 3 seconds and adds 100 to 200 feet to the H-V diagram. Using the deceleration technique builds a safety margin into the diagram, since maximum performance is available should the pilot be near the ground and need to flare immediately after reaching flare airspeed.

114. As the tests were being conducted, it became apparent that at a particular time in the maneuver it was very important that the pilot accomplish a certain action. Some actions were known while others were found during the data analysis. To accomplish the proper action at the proper time, the pilot must be observing the critical items. This is best illustrated by listing the order of priority for each phase of autorotation for entries from the high hover point to the knee of the diagram.

a. Entry:

(1) Attitude control on the critical axis.

(2) Reduction of collective pitch.

b. Dive:

(1) Pushover to nose-low attitude.

(2) Observe height above ground.

(3) Monitor airspeed until flare airspeed is reached.

(4) Observe height above ground.

(5) Control rotor speed to prevent overspeed.

(6) Maintain flare airspeed until flare is required.

c. Flare:

(1) Pitch up to accomplish a cyclic flare at recommended height above ground.

(2) Observe rotor speed and height above ground during flare.

(3) Apply collective pitch to prevent rotor overspeed, or decrease rate of descent when near the ground.

d. Landing:

(1) Assume a landing attitude.

(2) Apply collective pitch to cushion aircraft onto the ground.

The listing of priorities is meant to ensure that the pilot observes the most important items first. For example, rotor speed is of little concern during the entry. This is because rotor speed depends primarily on the collective pitch and secondly on losses caused by angle of attack and sideslip. The most important single item is pitch attitude, which is the pilot's way of controlling thrust, energy, and power-required relationships.

Evaluation of Pilot Technique

115. The H-V determination used techniques which produced good performance and, in the pilot's judgment, contained a margin for reasonable variation in technique with different pilots. However, for the H-V diagram to be a useful part of the operator's manual, the expected capabilities of all Army aviators must be included. It was considered that standardization instructor pilots (SIP's) from the United States Army Aviation School were the best judges of the desires and capabilities of the operational pilot. Two SIP's were invited to participate in the flight program. They provided quantitative data and qualitative comments concerning the H-V test methods.

116. Following a demonstration of the test technique, the flight tests were conducted and results are shown in figures 49 and 50, appendix F. Table 4 presents some of the more significant results and compares these with those obtained during the H-V tests.

Table 4. Comparison of SIP and H-V Test Techniques.

Condition	SIP		Test	
Entry true airspeed (kt)	8	18	11	18
Maximum nose-down pitch attitude (deg)	20	14	32	22
Maximum true airspeed in dive (kt)	44	49	70	49
Minimum rotor speed (rpm)	255	305	255	270
Maximum nose-up pitch attitude in flare (deg)	16	20	25	26
Maximum rotor speed in flare (rpm)	291	327	314	323
Collective input (in.)	9.6	8.5	9	7.7
Rotor speed at touchdown (rpm)	245	253	304	248

All pilots tended to dive the aircraft more as entry airspeed decreased. The most significant difference in the techniques is seen in the pitch rates and attitudes during the dive and the flare portions. The higher values tend to minimize power required and facilitate the energy exchanges during these critical times.

117. The test technique reflects an imposed 2-second delay on all controls, while the SIP's used no intentional delay. The delay on the collective control is the primary cause for the much greater rotor speed loss shown at the test 18-KTAS entry condition. This loss in main rotor kinetic energy is overcome by the steeper flare, which builds considerably more rotor speed during the flare. Additional subtle differences are the timing of the control inputs and the flight profile.

118. The SIP technique was primarily concerned with rate of descent and attitude. The flare is slow and steepens as the ground is neared and airspeed decreases. Collective is added gradually during the flare, flight path changes are less abrupt, and in comparison with the test technique, more rotor speed is dissipated during the final portions of the descent and landings. The SIP technique

leaves the pilot fewer options during the final phases and commits the aircraft to a landing at an earlier time. This results primarily because, with the gradual deceleration, the aircraft passes through minimum effective flare airspeed with a low rate of energy exchange, whereas with the test technique, the energy exchange is higher at the critical airspeed point.

119. The SIP's could repeat their flight profiles with a high degree of accuracy, and could make low forward speed landings. They were most accustomed to autorotations from entry airspeeds above 40 KTAS and at first, for lower airspeeds, were reluctant to assume extreme nose-down attitudes. Their technique changed rapidly after the demonstration and in the final data summarized in table 4, approached the test technique. They were particularly concerned with pilot ability to accurately judge the flare attitude and height, as well as the likelihood of the tail rotor contacting the ground. Similar tests with other SIP's were repeated in subsequent programs with similar results. Additional information can be obtained from references 15, 16, and 17, appendix A.

120. The tests with the SIP's were conducted from an altitude considered safe by the test pilot, and in all cases there was a performance margin. The technique used by the SIP's did not sufficiently change the performance to the point of invalidating the curves generated by the test technique.

IMPROVED TEST METHODOLOGY

General

121. An improved test methodology should reduce flight hazards to personnel and equipment and reduce flight time and cost, as well as produce larger-quantity, better-quality data. A purely experimental method has proven to be unsatisfactory because of flight safety aspects and the excessive flight effort needed to gather the data. Entirely theoretical approaches are inadequate and should a satisfactory one be developed, there would still be the credibility factor. The ideal method is one which uses the best features of both theory and flight test results. The total methodology consists of preparation, analysis, and flight test. The magnitude, timing, and interrelation of these phases will be dictated by the individual program circumstances. This section of the report summarizes the test results and analysis and develops recommended procedures for H-V testing.

Test Preparation

122. Test preparation includes conventional program planning and documentation, analysis of aircraft design and flight characteristics, and predictions of aircraft performance on the basis of theory or previous test results. Program planning is detailed in reference 16, appendix A. The aircraft physical characteristics are reviewed for specific items which may need special attention during the test. Types of control systems may influence pilot technique or impose control limitations. Engine response may have a bearing on power recovery

procedures. Rotor inertia is important with respect to rotor decay and thus, delay times and flight limits. Type of landing gear can determine landing technique or requirements for the test site.

123. The nature of the performance prediction is dependent upon the development status of the test vehicle. For an experimental aircraft, a great deal of theory and wind tunnel data will have to be used. With a prototype aircraft, limited qualiiative flight experience and quantitative test data are usually available. Fully developed aircraft generally have the basic characteristics defined for conventional flight regimes and the task is one of extrapolation into unusual flight conditions. The magnitude of the prediction effort can vary greatly; however, emphasis must be placed on items which will most strongly influence flight safety. The predictions are in terms of parameters that can be verified by analysis of flight data. It must also be remembered that a successful prediction technique is one of continual updating on the basis of information gained in each test effort.

124. Stability and control data are used to calculate the expected angular motion after a power reduction and to assess the recovery capability. The difference between control positions in powered flight and in a steady-state descent provide insight to the imbalance that will be generated by the power reduction. Figures 51 and 52, appendix F, show typical trim changes and longitudinal controllability characteristics of the UH-1C helicopter as documented in reference 11, appendix A. A comparison of the test results in table 5 and the calculated response shows the test situation to be generally less critical than the calculated values would indicate.

The lower test values are most probably caused by the slow engine torque reduction and the residual power which, in effect, gives something less than a step change in the aircraft force balance.

Table 5. Comparison of Test and Calculated Aircraft Response to Power Reduction.[1]

Axis	Angular Acceleration (deg/sec^2)		Angular Rate (deg/sec)		Attitude (deg)	
	Calculated	Test	Calculated	Test	Calculated	Test
Pitch	4.5	2	3.75	0.5	1.3	0.25
Roll	9	6	4.5	3	2.5	1
Yaw	16	10	8	8	3.5	4

[1]True airspeed.

125. In the low-speed, low-altitude flight regime aircraft energy exchanges are very limited and thus, conservation of rotor energy is of primary importance. For other areas minimum rotor speeds may have flying qualities or structural load implications. The expected rotor speed decay is calculated as shown in reference 19, appendix A. A delay time equal to that required for rotor speed to decay to the minimum steady-state value is a reasonable limitation for the initial tests. The importance of rotor speed decay is evaluated during the flight tests and the limitation is adjusted accordingly.

126. Control positions and control power data are used to determine motions or attitudes from which a recovery can be accomplished. A desirable percentage of control margin is selected and is subtracted from the total control available to obtain the extreme that will be reached during the recovery. The difference between the recovery limit and the power-on control position can be used to obtain the control available to the pilot. The delay time is then limited so that the motions generated during the entry are not larger than can be corrected with the control available.

127. Engine acceleration information from calibrations or flight tests can be used in conjunction with steady-state descent performance to estimate power recovery height above the ground, *ie*,

Recovery height = Rate of descent x engine acceleration time

The initial calculation does not include height required to overcome momentum and must be adjusted as information is gained concerning rotor acceleration, thrust response, and flight path changes. Details concerning aircraft and test site preparation are presented in reference 16, appendix A.

Analytical Methods

128. The minimum flight program is obtained by predicting performance and then conducting confirmatory tests. The inadequacies of theory are overcome by basing the calculations on actual performance of the test vehicle. An ideal analytical method would be one that predicts all aspects of the power reduction, autorotation, and landing. This would include aircraft angular motions and the effect of, or requirement for, pilot input. Mathematical models were developed which used the flight test data in an empirical fashion. These models are described in appendix E. Of particular interest in using the models is the fact that the effects of individual flight variables can be isolated. Technique can be maintained constant while changing altitude, gross weight, initial airspeed, etc. The technique can also be systematically varied while keeping the other parameters constant.

Three-Dimensional Model Usage:

129. The three-dimensional model was designed to make predictions for H-V curves in either of two ways. A total autorotational maneuver could be optimized or it could be broken into segments which are individually optimized. In either case, the analytical techniques would be similar.

130. The mathematical model is initially run at some sample flight condition (airspeed, rotor speed, climb, acceleration, attitude, engine power, etc.). The engine power is then diminished at a predetermined rate to simulate any mode of engine failure. The aircraft is then stabilized as rapidly as possible using the appropriate controls. The maximum allowable delay time is determined by fixing all controls and noting at what time 90 percent of available control was needed to effect a recovery. This constitutes the entry segment. Technique for stabilizing attitude is largely trial and error, using the available flight test data as a starting point. The desired result is to stabilize the aircraft with the least altitude loss.

131. The next flight segment (pushover and acceleration) is intended to attain flare airspeed with the smallest height loss. Again, technique is largely trial and error and is heavily dependent on initial velocity and accelerations. Establishing optimum technique is an arduous task because of the many ways flare airspeed can be attained. Because optimum performance is sought, steady-state descent will not be included in the dive portion. In fact, the flare should begin somewhat prior to reaching flare airspeed so that aircraft acceleration will carry it just to the flare airspeed.

132. The cyclic flare is intended to slow the aircraft's forward speed, increase rotor speed, and also slow vertical descent. Once the flare has been accomplished, the aircraft will be outside the avoid area where a safe landing is assured and modeling is not necessary.

133. As developed, the three-dimensional model is not of sufficient accuracy to predict a satisfactory H-V diagram. The reasons for the inaccuracies, as well as difficulties encountered while using the model, are discussed in appendix E. However, it can be used to provide information on selected items such as flare performance. Since a cyclic flare is basically a two-dimensional maneuver with only one control input, it is especially adaptable to partial correlation. Partial correlation is not, however, an entirely adequate modeling technique as it relies too heavily on flight test data which are not appropriate to the point being flown. Once the correlation equations and coefficients are established, the flying of the model should be completely independent of prior flights. The data presented in appendix E show the effects of airspeed variance on flare performance using partial correlation and an identical pilot technique. The 50-KTAS test case agrees well with the calculated performance. The calculated curve shows the expected results with airspeed changes and the trends are similar to the results presented in figure 21, appendix F. The requirement to change technique with airspeed is well illustrated by the rotor speed loss with flare at low airspeeds and the excessive pitching that would result at airspeeds above 60 KTAS.

Two-Dimensional Model Usage:

134. The inability of the three-dimensional model to predict usable H-V diagrams led to the development of the two-dimensional model described in appendix E. The parameters required for the flight path input option are the power provided by the engine at the rotor hub and a time-dependent flight profile for a total autorotational maneuver. The output is the rotor speed, thrust, and pitch attitude that would be required to effect such a flight profile.

135. The modification of existing flight profiles can be most easily done by proportionately "shrinking" time and vertical and horizontal distance. This method is not applicable in the high-speed region, since the technique could vary too greatly with height above ground. For example, the pilot could climb if he was very low, or maintain altitude if he was moderately low and wanted only to decrease airspeed or build rotor inertia. However, the technique of "shrinking" the flight path for those points above the knee of the H-V diagram is valid because of the relatively constant shape of the flight path from entry in that area.

136. Test points obtained while experimentally developing the H-V diagram were used as base-line data to predict performance with other techniques. The method used was to establish a flight path for autorotations at different heights above the ground and then allow the model to predict pitch attitude, rotor speed, and main rotor thrust. Results are shown in appendix E. From predictions such as these it is possible to establish a particular limit and then obtain the resultant performance. Another approach is to set a required performance value and then consider the necessary aircraft motions required. It should be noted that possible flight paths produce consistent realistic sets of data, whereas impossible flight paths produce random data which are clearly unrealistic. Thus, an optimum can be inferred from the model predictions. An experimental H-V diagram compares favorably with several H-V curves generated by the two-dimensional model shown in figure AA, appendix E. It should be noted that as the entry airspeed increases from a hover, the nose-down pitch attitude in dive becomes less important with respect to the performance that can be obtained.

137. The flight test portion of an H-V program should concern itself with obtaining smooth, efficient flight profiles at various airspeeds and at an altitude that will allow power recovery. These flight profiles would then lend themselves to modification for input to the two-dimensional model.

Flight Tests

138. The predictive flight tests provide data concerning the man/machine relationship and document the aircraft response to control applications, operating conditions, and atmospheric variables without performing H-V touchdowns. Each phase of the autorotation and landing maneuver must be examined prior to accomplishing H-V landings to ensure understanding of the pilot requirements and aircraft performance limitations. Care must be used to obtain data at the extremes of the flight envelope or operating conditions as well as to the limits of expected pilot performance. The data may be qualitative or quantitative, depending upon the scope of the program and the depth of analysis needed. The tests should be conducted in a manner which will produce data suitable for comparison with any predicted results or to further analytical efforts. Table 6 shows an outline of the complete test matrix which may be necessary.

139. The first test in each area is conducted at the conditions expected to be least critical with respect to flight safety. The build-up parameters are then increased in degree of criticality while observing the change in the limiting parameters. Qualitative pilot comments and analysis are used to update the limitations and test conditions. Generally, test results will permit elimination of many items initially listed in table 6.

Table 6. Flight Tests for Autorotation and Landing Performance.

Test	Flight Regime	Gross Weight	Rotor Speed	Airspeed	Altitude	Buildup Parameter	Expected Limitation
Power reduction and recovery	Level flight, climb, descent	Minimum and maximum	Minimum and maximum	Zero to V_{max}	Sea level to operational limits	Delay time	Angular rates or attitudes, control required to recover
Pushover	Level flight, climb	Minimum and maximum	At minimum reached during power reduction and delay	Zero to V_{flare}	Sea level to operational limits	Forward cyclic input	Forward control margin, pitch-down rate of attitude
Acceleration	From pushover conditions	From pushover conditions	Minimum and maximum	From pushover to V_{flare} - 10 kt; V_{flare}; V_{flare} + 10 kt	Sea level to operational limits	Aim airspeed	NONE
Deceleration	From acceleration conditions	From acceleration conditions	Minimum and maximum	From acceleration airspeed to 3000 to 2000 ft/min R/D	Sea level to operational limits	Deceleration time	NONE
Cyclic flare	From steady-state autorotation	Minimum and maximum	Minimum and maximum	$V_{min\ R/D}$, ±20 kt in 10 kt increments	Sea level to operational limits	Rate and amount of aft control input	Aft control margin, pitch rate or pitch attitude, rotor speed
Cyclic flare	From deceleration	From deceleration	Minimum and maximum	From acceleration and deceleration airspeed and R/D conditions	Sea level to operational limits	Same as steady state	Same as steady state
Landing	Hover	Minimum and maximum	Minimum and maximum	Zero	Sea level to nighest field elevation available	Hover height	Collective control available, minimum rotor speed, landing gear strength
Landing	Level flight, climb-out	Minimum and maximum	Minimum and maximum	20, 40, V_{flare}	Sea level to highest field elevation available	Height above ground, increments added to maximum hover height	Same as hover landing

140. The autorotation and landing maneuver is extremely dependent upon pilot technique and thus, the pilot's comments are of particular importance. These comments should establish a pilot tolerance in terms of how long he will delay recovery, what motions or attitudes are acceptable, what control motions are acceptable, and how these items correlate with the aircraft capability. The test pilot must make a judgment as to how his performance compares with training criteria and what is expected of field aviators. A most desirable approach is to obtain data on how operational pilots conduct an autorotational maneuver. From these varied judgments and data, a technique is established which will generate H-V curves that are realistic and usable by the operational pilot.

141. After the predictive testing and modeling have been completed, the autorotation and landing performance with the recommended technique should be demonstrated for the aircraft operating and flight envelope by accomplishing actual H-V landings from entry points along the predicted curve.

DEMONSTRATION REQUIREMENTS

General

142. Those who conduct the tests must demonstrate the aircraft capabilities or recommended performance to the procuring or user agency. The demonstration should provide all necessary information concerning structural integrity, safety of flight, or envelope limitations in terms of adequate control margins and suitable pilot techniques. All possible aspects of operating conditions, mission requirements, and pilot proficiency should be considered. The demonstration should be a combined engineering review and flight presentation. The engineering portion includes experimental results, calculations, or theoretical analysis. Documentation should be available to support the technical methods used in the engineering effort. The flight demonstration should not include any further investigative testing and should be devoted to areas which provide maximum information with minimum risk.

Demonstration Conditions and Procedures

143. The terms and definitions of the demonstration must be fully documented and clearly understood by all participants. The demonstration must consider the expected aircraft operating environment and mission requirements, including landing terrain, surface wind, gross weight, altitude, rotor speed, and cg location. The demonstration should be at the most critical conditions possible while maintaining a safety margin for the demonstration aircraft and personnel. The touchdown gear loads and forward speed must be specified. Pilot technique should be reviewed for items which are unusual or contrary to normal practice. The demonstration pilots should have sufficient experience to assess theoretical or experimental information in terms of operational missions or situations which were not specifically tested. Qualitative pilot comments are necessary to evaluate suitability in terms of expected pilot proficiency. The aircraft motions and pilot inputs should be quantitatively recorded.

Aircraft Limitations

144. Since an engine failure can occur at any operating condition or during any pilot activity, the aircraft flight envelope and limitations must be clearly specified. The reason for each limit must be stated and supported with quantitative data. Minimum rotor speeds during entry and the associated structural loads must be considered. Control input needed to recover should be assessed in terms of aircraft control moments and angular motions. Degraded control response during low load factor may be a consideration during pushovers. Rotor acceleration during the flare, maximum allowable rotor speed, and any thrust limits must be thoroughly discussed. Rotor/fuselage clearance may also be a factor. Stability augmentation systems and their input to aircraft motions during an engine failure should be fully documented. The pilot technique should consider any devices which limit control input.

Flight Demonstrations

145. Prior to flight demonstrations, all conditions, procedures, and limitations must be reviewed to ensure adequate flight safety margins. The demonstration points will be at the most critical corners of the envelope. The minimum demonstration points will be from high hover, low hover, minimum flare airspeed, the envelope maximum airspeed, and at maximum power climb at best-climb airspeed. The demonstration aircraft should be at the specified mission configuration and atmospheric and operating conditions.

146. The aircraft response to engine failure should be demonstrated. This includes identification of critical axis and primary cues. The allowable delay time should be evaluated in terms of flight regime or operating conditions. In no case should it be necessary to move the critical control sooner than 0.5 second after the power reduction. The recovery should not violate a 10-percent control margin on the critical control. There should be no control requirements which are not in natural response to aircraft motions nor should there be undue pilot concern with rates or attitudes during the recovery.

147. The dive, flare, and landing techniques should be demonstrated. During the pushover, the longitudinal control should not be within 10 percent of the forward limit for the most critical cg location. In addition, for pilot comfort the change in vertical acceleration at the pilot station should not exceed 0.5g. The flare should not place the longitudinal control within 10 percent of aft limit for a most forward cg location, and a similar forward control margin should exist when the aircraft is leveled prior to landing. The maximum collective application should leave a 10-percent margin and at touchdown the minimum rotor speed should not be less than the allowable transient limit.

Presentation

148. The data presentation should consist of a handling qualities section and a performance section. The handling qualities section should outline the cues for various types of engine failure and the expected aircraft response to the power

reduction. Recovery, dive, flare, and landing techniques must be presented in detail for all conditions and flight regimes. Any technique variations with operating conditions or landing terrain should be carefully noted. The performance should show the areas from which a landing can be accomplished and the particular conditions or limitations associated with the performance shown. Performance is presented in terms of atmospheric conditions, gross weight, and configuration. A typical listing of the various considerations should accompany the performance curve as follows.

a. Operating limitations:

(1) Gross weight - Not more than ____ pounds.

(2) Density altitude - Not more than ____ feet.

(3) Landing surface - Vegetation ____, bearing ratio ____, coefficient of friction not more than ____.

(4) Surface wind - ____ knots (headwind component).

(5) Rotor speed - Not less than ____ rpm at power reduction.

(6) Touchdown rate of descent (entry from knee and above) - ____ feet per second or ____ percent gear limit.

(7) Forward airspeed at touchdown - Not to exceed ____ knots.

(8) Sliding distance (entry from knee and above) - Not to exceed ____ feet for ____ airspeed for a specified surface.

b. Pilot technique:

(1) Delay time - ____ seconds on all flight controls.

(2) Dive pitch attitude - Not to exceed ____ degrees.

(3) Rate of control input - Not to exceed ____ inches per second.

(4) Control margin - Not to violate 10 percent remaining.

(5) Flare attitude - Not less than ____ degrees.

(6) Recommended deceleration and flare airspeed - Not less than ____ knots.

(7) Probability of safe landing - ____ percent, based on 0.5 second deviation of time delay or airspeed and 5 degrees attitude variation.

149. The "known risk" method assumes that there is a degree of risk associated with operating the aircraft in any flight condition. Thus, a mission or flight maneuver can be assessed in terms of pilot requirements and aircraft capabilities. Figure X gives a graphical representation of a "known risk" H-V diagram.

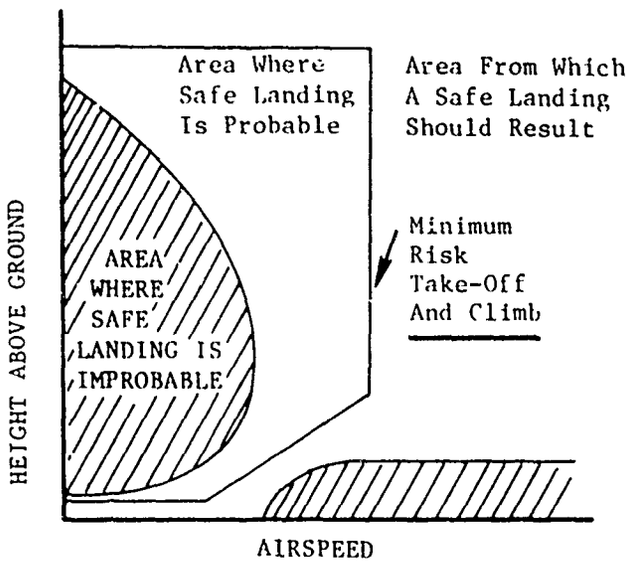

Figure X. Probability Performance Presentation.

The inner curve represents the maximum performance that can be obtained under ideal conditions with optimum pilot technique. This performance is not repeatable, and is calculated or estimated rather than demonstrated. The 90-percent risk area represents a performance area that is repeatable by a test pilot in a controlled environment with a certain amount of margin for technique variation. This is equivalent to the maximum performance that is attained during conventional H-V engineering flight tests. The 50-percent risk area is a performance area which can be easily and consistently demonstrated under controlled conditions. This is the area where experienced pilots should perform after the technique has been demonstrated. This may also be the highest risk area that operational pilots can realistically be expected to master without specialized and very detailed training. On the basis of present training and proficiency levels, the 25-percent risk area may be the performance area which is most common to the operational pilot. Their training and experience has primarily been limited to performing power-off landings from steady-state descents. This, in effect, gives them experience in the safest portion of the H-V curve and provides little insight to the more critical conditions. The pilot technique, limitations, or conditions must be specified for each of the risk levels presented.

150. The "probability" presentation in figure Y shows three areas and the expected performance from engine failure in each.

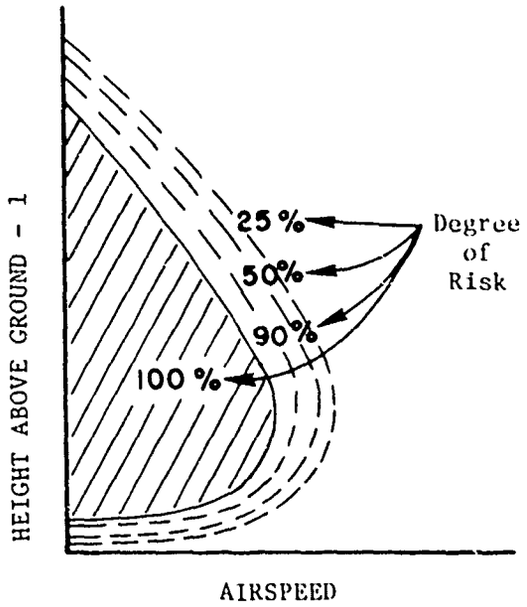

Figure Y. Known Risk Performance Presentation.

The size of the shaded area can be chosen to encompass any desired level of performance. Within the shaded area are various degrees of risk where some pilots under certain circumstances could make a safe landing. Extreme care must be taken to ensure that the area is not so small as to demand unrealistic performance or so large that credibility is lost. The area where a safe landing is probable is bounded by the low-speed shaded area and the minimum-risk takeoff and climb-out profile. The technique and probability must accompany the performance presentation.

151. The final portion of the presentation is a recommended training program. The training program should outline the flight training needed to achieve the performance demonstrated or that required for any recommended performance level.

CONCLUSIONS

GENERAL

152. Separating the H-V maneuver into the various phases best allows evaluation of aircraft behavior and performance in terms of pilot cues, technique requirements, and pilot tolerances. General aircraft responses are readily apparent and pilot response or desires are well defined. Modeling techniques were partially successful and formed a valuable part of an improved methodology. Improved data presentations can be developed to more fully inform the pilot as to the performance available, the associated risk, and the necessary pilot actions.

ENTRY TO AUTOROTATION

153. During entry the pilot recognition of power loss and proper control input is most critical at the extremes of the envelope. Specific characteristics noted during the entry phase include:

a. The aircraft response, pilot cues, and allowable delay time will vary significantly with the nature of the power reduction (para 18).

b. Power reduction by rapidly moving the throttle to flight idle may not provide the pilot with the most severe case of engine failure (para 20).

c. Engine failure characteristics are not sufficiently documented to allow testing or calculations for all expected aircraft response (para 20).

d. Qualitative pilot opinion and quantitative reaction of various pilots is in close agreement in areas where delay time is critical (para 27).

e. Recognition of engine failure in hover is most rapid and positive when lateral accelerations at the pilot station are above 0.05g (para 27).

f. The maximum allowable pilot delay time at a particular flight condition is determined by the aircraft response about a particular axis (paras 27 through 31).

g. For the UH-1C, recovery on the basis of pilot tolerance leaves considerable control margin except at the critical high airspeed (para 43).

h. The low rotor speed warning in the UH-1C is far too slow to adequately warn the pilot that the engine has failed (para 43).

DIVE

154. The dive portion is of particular importance because it constitutes the greatest altitude loss during an H-V maneuver and is in an area with which the pilot is least familiar. Significant conclusions revealed by the evaluation are as follows:

a. The pilot judgment of pushover requirement is most difficult in the critical low-speed flight regime (para 45).

b. Maximum pilot tolerances during pushover were 18 deg/sec for pitch rate and 32 degrees nose down for pitch attitude (para 48).

c. Termination of pushover was based on approximately 0.5g normal acceleration (para 48).

d. During the acceleration airspeed must be closely monitored to prevent exceeding the target flare airspeed (para 57).

FLARE

155. Judgment of flare height and the amount of flare required in conjunction with timing of cyclic and collective controls generates a situation which is most conducive to pilot error. The flare tests produce the following conclusions:

a. Flare attitudes in excess of 30 degrees nose up were uncomfortable and restricted forward visibility (para 69).

b. Cyclic flare effectiveness decreases with lower airspeeds and at airspeeds below the minimum effective (35 KTAS for the UH-1C) generates a downward acceleration (para 70).

c. Flare effectiveness decreased with higher density altitude and the flare must be accomplished higher above the ground (para 79).

d. Increasing gross weight from 7000 to 8000 pounds requires a higher flare airspeed or a longer flare duration (para 80).

e. Increasing the rate of flare improves the flare effectiveness, with the gain being proportional to the flare airspeed (para 82).

f. Technique for flares from accelerating and steady-state autorotations was essentially the same (para 85).

g. A given flare from accelerating autorotation produces a greater rotor speed and thrust gain than when accomplished from a steady-state autorotation (para 85).

LANDING

156. In the landing phase, the pilot has the fewest options and the touchdown rate of descent is mostly dependent on judicious application of collective pitch. Notable items during the landing phase are as follows:

a. Hover autorotation touchdowns in excess of 2 ft/sec were uncomfortable and created concern as to whether a hard landing had occurred (para 97).

b. During a hover landing, a more rapid collective input increased thrust generated and more quickly slowed rate of descent (para 98).

HEIGHT-VELOCITY TESTING

157. Testing each individual phase separately provides data which allow the total H-V maneuvers to be accomplished more safely, more quickly, and in a manner which will yield more informative H-V diagrams. The H-V tests led to the following conclusions:

a. Safe conduct of experimental H-V diagrams is most dependent on the ability to assess the criticality of each condition (para 107).

b. As test points near the maximum performance H-V diagram, the testing effort and degree of risk increase very rapidly (para 108).

c. When accomplishing a power reduction, autorotation, and landing as a continuous maneuver, the pilot task is considerably more difficult than when performing each phase individually (paras 110 through 114).

d. Summation of height required for the various phases compares favorably with results from a total maneuver (para 111).

e. Obtaining maximum performance requires techniques that are beyond normal pilot desires and for which special training must be provided (paras 113, 114, 119, and 120).

f. Sequencing pilot actions for each phase of the H-V maneuvers provides the pilot with greatest safety and minimum pilot workload (para 115).

TEST METHODOLOGY

158. The maximum benefit of H-V testing with a minimum of risk and flight operation is obtained with a methodology which stresses analytical techniques prior

to the flight tests and concludes with a comprehensive demonstration and presentation effort. Observations drawn from test results include:

a. Using stability and control data to predict aircraft reaction to power reduction produced calculated results that are more severe than those obtained during the entry tests (para 125).

b. The three-dimensional model is not of sufficient accuracy to predict a satisfactory H-V diagram (para 134).

c. Using empirical data, the two-dimensional model predicts H-V diagrams which agree well with flight test results (para 137).

d. An H-V maneuver can easily be separated into the various phases and each examined in turn to determine flight characteristics, aircraft performance, pilot techniques, and a predicted H-V diagram with a minimum of flight hazard (para 139).

e. A demonstration of the recommended power loss emergency procedure is necessary for the user to adequately understand the many variables which influence any specified performance (para 143).

f. Recommended H-V diagrams should be accompanied by a detailed listing of all conditions needed to achieve the specified performance (para 143).

g. Presenting some indication of performance levels and pilot requirements allows the pilot to realistically assess the risk associated with a particular operating condition (paras 150 and 151).

RECOMMENDATIONS

159. Engine failure modes should be defined for all helicopter models in the Army inventory (para 20).

160. All entry tests should be conducted in a progressive manner which will provide information concerning the most critical aircraft response to power reduction (para 23).

161. Pilot training should be oriented to provide the operator with the expertise necessary to cope with the most critical aircraft response (paras 24, 28, 30 and 31).

162. The maximum pilot delay time used in determining the H-V diagram should be defined in terms of the critical control parameter (para 21).

163. The maximum pilot delay time should be limited to generation of a 0.5g lateral acceleration or rates and attitudes which require less than 90 percent of the control remaining to make a recovery, or prevent exceeding the minimum transient rotor speed (paras 28, 30 and 31).

164. An engine failure warning device should sense the quickest indicator of engine failure and the pilot should be presented with a visual display and an aural warning (para 22).

165. Minimum flare effective airspeed should be clearly defined and the operator's manual should reflect that flares at lower airspeeds will significantly decrease the performance available (paras 69 and 70).

166. The detrimental effects of increasing gross weight or density altitude on flare should be presented in the operator's manual (paras 79 and 80).

167. Landing gear capability to withstand horizontal loads should be determined and used as a criteria for landing speeds in various types of terrain (para 103).

168. The improved H-V testing methodology should be applied to all future efforts (para 122).

169. Appropriate military specifications should be revised to reflect the results of this investigation (paras 144, 147, 148, and 149).

APPENDIX A. REFERENCES

1. Study, USAAAVS, "Autorotation Report," to be published.

2. Military Specification, MIL-H-8501A, *Helicopter Flying and Ground Handling Qualities; General Requirements For*, 7 September 1961, with Amendment 1, 3 April 1962.

3. Engineering Report, Hiller Aircraft Company, No. 64-37, *Recommended Revision to Civil Aeronautics Regulation 6, Concerning Height-Velocity Autorotation Requirements*, April 1964.

4. Paper, Kidwell, J. C., "Height-Velocity Curves and Their Effect on Operational Capability," presented at the American Helicopter Society/US Army Symposium, 14-16 November 1967, Fort Monroe, Virginia.

5. Aircraft Development Service Report, Federal Aviation Administration, No. ADS-84, *An Evaluation of the Height-Velocity Diagram of a Heavyweight, High Rotor Inertia, Single-Engine Helicopter*, November 1966.

6. Final Report, USAASTA, Project No. 68-04, *Special Study of Autorotation Procedures*, April 1968.

7. Letter, AVSCOM, AMSAV-E(ERS), 10 April 1968, Subject: Advanced Methodology Program to Establish Autorotational Entry and Power-Off Landing Criteria for Single-Engine Rotary Wing Vehicles, AVSCOM Test Directive No. 68-25.

8. Test Plan, USAASTA, Project No. 68-25, *Engineering Study of the Autorotational Flight and Landing Characteristics of the UH-1C Helicopter*, August 1968.

9. Technical Manual, TM 55-1520-220-10, *Operator's Manual, Army Model UH-1C Helicopter*, November 1968.

10. Final Report, USAASTA, Project No. 70-23, *Investigation of Engine Rigging, Airspeed and Rotor RPM Effects on Steady-State Autorotational Performance*, December 1970.

11. Final Report, USAAVNTA, US Army Test and Evaluation Command, Project No. 4-4-0108-03, *Engineering Flight Test of the UH-1B Helicopter Equipped with the 540 Rotor System, Phase D*, December 1966.

12. Final Report, USAA[illegible]TA, Project No. 68-22, *Rotary Wing Vehicle External Stores Jettison Envelope F[illegible] Established Requirements*, August 1970.

13. Final Report, USAASTA, Project No. 71-30, *Study, Pilot Perceived Jettison Envelope*, June 1973.

14. Final Report, USAASTA, Project No. 70-25, *Engineering Flight Test, AH-1G (Hueycobra) Helicopter, Autorotational Entry Characteristics*, April 1971.

15. Final Report, USAASTA, Project No. 68-37, *Army Preliminary Evaluation of the AH-1G Tractor Tail Rotor Modification*, June 1969.

16. Final Report, USAASTA, Project No. 72-73, *Guidelines for Height-Velocity Testing of Single-Engine, Skid Gear Helicopters*, October 1973.

17. Final Report, USAASTA, Project No. 69-13, *Height-Velocity Test, AH-1G Helicopter*, February 1971.

18. Final Report, USAASTA, Project No. 69-16, *Height-Velocity Test, OH-58A Helicopter*, June 1971.

19. Technical Note, USAASTA, No. 24, *Quick Methods for Estimating Rotor Speed Decay After Throttle Chop*, December 1972.

20. Technical Note, USAASTA, No. 14, *Data Reduction Procedure for Oscillograph and Photopanel Acquisition Systems as Derived in the Height-Velocity Study, Project 68-25*, 8 May 1970.

21. Technical Note, USAASTA, No. 34A, *An Investigation of Errors between Oscillograph and Fairchild Data Sources*, December 1971.

22. Textbook, A. Gessow and G. C. Myers Jr, *Aerodynamics of the Helicopter*, Macmillan Company, New York, 1952.

23. Report, Bell Helicopter Company, No. 299-099-557, *An Energy Method for Prediction of Helicopter Maneuverability*, December 1971.

24. Technical Note, USAASTA, No. 17, *Redevelopment of the Thrust-Power Relations Used in the Hoffman Model: the AMAD Model*, 17 July 1970.

APPENDIX B. AIRCRAFT DESCRIPTION

GENERAL

1. The UH-1C/540 rotor helicopter is a general utility helicopter suitable for a variety of missions. Several armament kits may be installed.

2. The test helicopter, USA S/N 63-8684, was a standard UH-1B modified by incorporating the 540 rotor and related systems.

MAIN ROTOR SYSTEM

3. The 540 "door-hinge" rotor system is a two-bladed semirigid system with a flex-beam hub. The flex-beam hub is a broad, thin steel plate by which the rotor system is given high in-plane stiffness, but soft flapping restraint. Rotor centrifugal loads are transmitted to the flex-beam by a multiwound wire torsion-tension strap. Control inputs about the feathering axis are imparted through a pitch horn located at the hub trailing edge. The feathering axis bearing resembles a door-hinge concept. A conventional stabilizer bar is used. Torque is transmitted to the rotor through a splined trunnion which also provides the teetering movement. Both the trunnion and feathering hinge bearings, as well as all other rotor head bearings, are teflon and require no lubrication. No collective counterweights are used.

FLIGHT CONTROLS

4. The primary flight controls include the cyclic control stick, collective control stick, and directional control pedals. All flight controls are mechanical and are hydraulically boosted. Force trim is provided for the cyclic stick to provide force gradients in the boosted systems.

5. The elevator is an inverted airfoil giving a nose-up pitching moment at forward speed. The angle of incidence of the elevator is variable through an interconnection to the longitudinal cyclic stick. The vertical fin is cambered to give a nose-left yawing moment at forward speed. This yawing moment reduces the amount of left pedal required to balance rotor torque at high speed.

AIRCRAFT DIMENSIONS AND DESIGN INFORMATION

Overall Dimensions

Aircraft length (rotor turning)	52 ft, 8.84 in.
Fuselage length	36 ft, 6.35 in.
Maximum fuselage width (horizontal stabilizer)	9 ft, 4.0 in.
Minimum rotor ground clearance	5 ft, 10.5 in.

Main Rotor

Rotor diameter	44 ft, zero in.
Chord	27 in.
Airfoil	Special 0009 1/3% symmetrical
Twist	-10 deg
Disc area	1520 ft^2
Blade area	49.5 ft^2 per blade
Solidity ratio	0.0651
Rotor inertia	2800 slug-ft^2
Preconing angle	2.75 deg
Collective pitch travel (25 percent radius)	Zero to 20 deg
Longitudinal cyclic travel (hub yoke)	±14 deg
Lateral cyclic travel (hub yoke)	±10 deg

Aircraft Weights and Moments of Inertia

Detail specification empty weight (FY 64)	4842 lb
Design gross weight	6600 lb
Moment of inertia, 6800 lb, cg at FS 131.50, BL .06, WL 61.20	
I_X	2738.47 slug-ft^2
I_Y	9037.80 slug-ft^2
I_Z	7348.39 slug-ft^2

Datum Reference Line

Fuselage station	7.6 in. aft of tip of nose bubble protrusion
Buttline	Aircraft center line
Water line	Base of skids

FLIGHT LIMITS

Center of Gravity

Forward cg	FS 125 at 8150 lb. Varies linearly to FS 126.7 at 9500 lb
Aft cg	FS 138 at 7000 lb. Varies linearly to FS 132.0 at 9500 lb

Airspeed

Below 7500-lb gross weight	140 KCAS from sea level to 3000 ft H_D. Decrease 3 KCAS per 1000 ft above 3000 ft H_D
8500-lb gross weight	130 KCAS from sea level to 3000 ft H_D. Decrease 3 KCAS per 1000 ft above 3000 ft H_D
9500-lb gross weight	125 KCAS from sea level to 3000 ft H_D. Decrease 3 KCAS per 1000 ft H_D

Rotor Speed

Power on	294 rpm 324 rpm
Power off	294 rpm 339 rpm

Maneuvering Flight Load Factors

At 6600 lb gross weight + 3.0	-0.5
At 9500 lb gross weight + 2.08	-0.35

Main Transmission Power Limit

At 314 rpm	1100 shp

APPENDIX C. INSTRUMENTATION

GENERAL

1. The test aircraft was instrumented to sense the operating conditions and motions during steady-state and dynamic autrorotational maneuvers. Linear acceleration sensors were installed at the aircraft cg and at the pilot station for a comparison of angular motion effects on the pilot sensory cues. A swiveling pitot-static airspeed sensor was mounted on a boom extending 96 inches from the nose of the aircraft. Angle-of-attack and angle-of-sideslip vanes were also mounted on the boom. The airborne data were recorded on a 50-channel Consolidated Electronics Corporation oscillograph. Selected test variables were displayed on instruments mounted in the pilot and engineer instrument panels. Ground station equipment was used to measure atmospheric conditions near the runway and the aircraft flight profile was photographically recorded by a Fairchild Flight Analyzer.

AIRBORNE INSTRUMENTATION

2. Data obtained from instruments mounted in the engineer instrument panel were primarily used to monitor test progress and ensure data validity. The information on the pilot panel was used to accurately establish the desired conditions and provide real time engineering data. The following parameters were displayed.

Engineer Panel

Standard system airspeed
Standard system altitude
Ambient air temperature
Engine torque
Fuel-used totalizer
Oscillograph correlation counter
Photopan ' counter
Vertical accelerometer with "maximum value recording needle"
Engine speed
Rotor speed

Oscillograph

Engineer event marker
Pilot event marker
Camera blip
Voltage monitor
Collective stick position

Longitudinal stick position
Pitch attitude
Pitch rate
Angle of attack
Longitudinal acceleration (cg)
Lateral acceleration (cg)
Normal acceleration (cg)
Left gear deflection
Right gear deflection
Lateral stick position
Pedal position
Roll attitude
Roll rate
Yaw attitude
Yaw rate
Angle of sideslip
Rotor blip
Touchdown velocity
Throttle position
Lift link
Pilot lateral acceleration
Pilot vertical acceleration
Rotor speed
Yaw angular acceleration
Roll angular acceleration
Pitch angular acceleration

Pilot Panel

System airspeed (boom)
System altitude (boom)
Radar altimeter
Rotor speed
Collective stick position
Landing gear load indicator with "maximum value recording needle"
Engine tachometer
Exhaust gas temperature

Photopanel

Standard system airspeed
Standard system altitude
System airspeed (boom)
System altitude (boom)
Outside air temperature
Torquemeter
Rotor speed

Gas generator
Exhaust gas temperature
Fuel-used totalizer
Stop watch
Engineer event
Pilot event
Oscillograph correlation counter
Landing gear load indicator

GROUND EQUIPMENT

3. The pressure and atmospheric temperature conditions were recorded at a ground station. Wind speed and direction were measured at 5 feet above ground level. The flight profile recorded by a Fairchild camera shows only height and distance and does not include lateral motion of the helicopter.

APPENDIX D. TERMINOLOGY

The following list defines terminology used in this report.

Symbol	Definition	Units	Equation
a	Angle of attack of aircraft	deg or rad	
a_r	Calculated angle of attack of rotor tip path plane	deg or rad	
β	Angle of sideslip of aircraft; positive right, negative left	deg or rad	
δ_a	Lateral control position	inches	
δ_c	Collective control position	inches	
δ_e	Longitudinal control position	inches	
δ_r	Directional control position	inches	
θ	Pitch attitude: positive nose up, negative nose down	deg or rad	
θ_t	Blade twist	deg or rad	
λ	Inflow ratio	–	$(V \sin a_r - \nu_i)/\Omega R$
μ	Advance (or tip speed ratio)	–	$(V \cos a_r)/\Omega R$
ν_i	Induced velocity	ft/sec	
ρ	Air density	slug-ft^3	
σ	Rotor solidity	–	$bc/\pi R$
ϕ	Roll attitude: positive right, negative left from level	deg or rad	
ψ	Yaw attitude: positive right, negative left from original heading	deg or rad	
Ω	Main rotor speed	radian/sec	

Abbreviation	Definition	Units	Equation
A	Acceleration	ft/sec^2	
A_{disc}	Area of disc or effective disc area	ft^2	πR^2 or $\pi R^2 B^2$
AS	Airspeed	KTAS	
a	Slope of rotor blade lift curve	–	
B	Tip loss factor	..	
b	Number of blades	–	
c	Blade chord	feet	
C_D	Drag coefficient	–	$F_D/(1/2\rho A_{disc}V^2)$
C_P	Power coefficient	–	$(P_i + P_o)(\rho A_{disc}V_{tip}^3)$
C_T	Thrust coefficient	–	$F_{MR}/(A_{disc}\rho V_{tip}^2)$
D	Distance traveled	feet	
F	Force	pounds	
g	Acceleration of gravity	$32.2\ ft/sec^2$	
I	Moments of inertia of rotor	$slug\text{-}ft^2$	
I_{xx}, I_{yy}, I_{zz}	Moments of inertia of aircraft less rotor	$slug\text{-}ft^2$	
KE	Kinetic energy	ft-lb	$KE_{MR} = 0.51\Omega^2$ and $KE_{AC} = 0.5MV$
m	Mass of aircraft	slugs	
N_R	Main rotor speed	rpm (refer to Ω)	
P_i	Induced power: power required to produce thrust	HP or ft-lb/sec	$F_{MR}v_i$

Abbreviation	Definition	Units	Equation
P_o	Profile power: power required to drag rotor blades through the air	HP or ft-lb/sec	
P_p	Parasite power: power required to overcome aircraft drag	HP or ft-lb/sec	$F_D V$
P_{Sft}	Engine power available at main rotor hub after transmission and accessory losses	HP or ft-lb/sec	
PE	Potential energy	ft-lb	mgh
Q	Torque	ft-lb	
R	Blade radius	feet	
S	Fusclage wetted area	ft^2	
T	Thrust	pounds	
TILT-X	Longitudinal tilt of the thrust vector in the shaft axis: positive aft, negative forward	radians	
TILT-Y	Lateral tilt of the thrust vector in the shaft axis: positive right, negative left	radians	
V	Velocity	ft/sec	
V_{tip}	Blade tip speed	ft/sec	ΩR
W	Aircraft gross weight	pounds	

Subscript	Definition
D	Drag
p, s, or g	Principal, shaft, or ground reference system
x, y, or z	Longitudinal, lateral, or vertical

Subscript	Definition
MR	Main rotor
N	Normal
TR	Tail rotor

APPENDIX E. DATA ANALYSIS

BASICS OF AUTOROTATIONAL FLIGHT MANEUVERS

General

1. Autorotational flight maneuvers, including each phase, can be described in terms of energy and power. The following explanation represents a helpful summary to aid in understanding of autorotational flight.

Powered Flight

2. In powered flight, shaft horsepower is supplied to the main and tail rotors to compensate for rotor power required (induced power (P_i) and profile power (P_o)), fuselage parasite drag power (P_p), and changes in the energy state of the aircraft. Increasing the shaft horsepower above that required for steady level flight will cause the aircraft to climb (increase potential energy (PE)) or increase airspeed (kinetic energy (KE)). In equation form, the power relationship becomes:

$$P_{Sft} = P_R + P_P + \frac{dE_T}{dt} \qquad (1)$$

Where:

P_{Sft} = Engine power available at rotor

P_R = Rotor power required = $P_i + P_o$

$\frac{dE_T}{dt}$ = Time rate of change of total aircraft energy

Total energy is made up of potential energy, aircraft kinetic energy, and rotor rotational energy (KE_{MR}):

$$P_{Sft} = \quad P_{Sft} = P_o + P_i + P_p + \frac{dKE_{AC}}{dt} + \frac{dKE_{MR}}{dt} + \frac{dPE}{dt} \qquad (2)$$

A more detailed development of equation 2 can be found in reference 24, appendix A, and in the data processing section of this appendix. The basic assumptions in the above relationship are that (1) tail rotor power required (P_i and P_o) and tail rotor moment of inertia are negligible compared to the main rotor variables and (2) fuselage rotational energy and rates of change of energy are also negligible (test data indicated that power from fuselage rotational energy

was less than 10 shp at all times). For the purposes of this discussion, including these variables does not contribute to understanding autorotational flight.

3. In conceptual form, the power relationship becomes a system which absorbs power (P_{Sft}), loses power to the environment (P_{LOST}), and has a measurable energy state as shown in figure A.

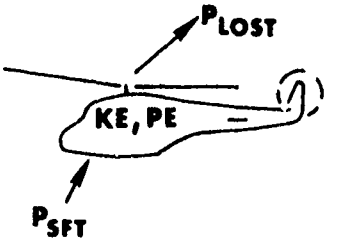

Figure A. Power and Energy Relationships.

4. When the power absorbed equals power lost, the sum total of the energy states remains constant. The power lost to the environment is due to the inefficiency of the system in producing thrust (P_i), dragging the blades through the air (P_o), and dragging the aircraft through the air (P_p). Power lost is not retrievable, which becomes very important and will be discussed later.

Autorotational Flight

5. In autorotational flight P_{Sft} becomes zero when engine shp is lost. The power balance relationship then requires the aircraft total energy to decrease at a rate equivalent to the power lost to the environment:

$$\frac{dE_T}{dt} = -P_{LOST} \qquad (3)$$

Recognizing that E_T is the sum of the aircraft's kinetic, rotational, and potential energies, equation 3 can be used to explain four phases of autorotational flight performance.

Entry:

6. During entry, P_{Sft} decreases at a rate dependent on the type of engine failure. Thrust and attitude do not change appreciably during the short entry interval and there is not a significant force imbalance to cause the aircraft to accelerate (or decelerate). Therefore, kinetic and potential energies remain relatively constant. The rotor kinetic energy, KE_{MR}, decreases and tends to compensate for the

difference between P_{Sft} and power lost. When thrust changes significantly, due either to rotor speed decay or aircraft attitude change, the force imbalance will cause acceleration. These accelerations produce changes in the aircraft kinetic and potential energy levels. These changes, in most cases, are negative and thus reduce the need for rotor speed decay to be the sole compensator for the power deficiency.

Instead of

$$\frac{dKE_{MR}}{dt} = -P_{LOST}$$

KE and PE decrease also, and the rotor speed decay decreases.

$$\frac{dKE_{MR}}{dt} + \frac{dPE}{dt} + \frac{dKE_{AC}}{dt} + -P_{LOST}$$

Dive:

. The dive phase of the autorotation maneuver follows the same analogy as the entry phase. In this case, however, the collective pitch is decreased, which causes a thrust loss. This creates a force imbalance which accelerates the aircraft. At the same time (for most dive maneuvers), a forward longitudinal cyclic input rotates the thrust vector forward, and the aircraft pitches downward. The nose-down pitch and forward flapping (cyclic input) combine to increase the horizontal thrust component and decrease the vertical thrust component. This results in an increase in both forward (A_X) and downward (A_Z) accelerations. The amount of cyclic input and the amount of pitch-down attitude allowed in the dive dictate the accelerations. As the aircraft begins to accelerate, the kinetic and potential energy levels change and these power sources become significant. As the aircraft speed increases, kinetic energy absorbs power similar to the powered flight case. However, the negative rate of change of potential energy is generally greater than the positive rate of change of kinetic energy (especially for the high-altitude, low-airspeed entries) so that the net result is negative, and the amount of power needed from the rotor is reduced. Also, as the aircraft is pitched nose down, the angle of attack on the rotor changes and the $P_i + P_o$ are reduced, which reduces the P_{LOST} term. The combination of power from potential energy and reduction of P_{LOST} allows the rotor speed to stabilize or, depending on flight conditions, to increase.

8. Therefore, in the dive phase, potential energy is exchanged to provide for the rotor power required. As the rate of descent increases, the rotor speed decay rate goes to zero and rotor speed becomes stabilized. At this point, if the aircraft has not reached the desired flare airspeed, a higher rate of descent is required to further increase kinetic energy. When the steady-state dive is attained, power required by the main rotor plus the fuselage parasite drag power will equal the power gain from potential energy change.

Flare:

9. In the flare phase of autorotation, a more complex exchange of energy occurs. As before, there is a decrease in the total energy level of the system due to the P_{LOST} term. From the dive attitude, aft cyclic is applied, and the aircraft is pitched nose-up. The increased angle of attack increases rotor inflow and rotor speed begins to build (assuming an effective flare airspeed has been reached and no collective pitch is applied). As rotor speed and the inflow increase, main rotor thrust increases (increasing $P_i + P_o$), providing a vertical force imbalance which decreases the forward speed. This loss of forward and vertical velocities lowers the kinetic energy of the aircraft, producing negative $\frac{dKE_{AC}}{dt}$ which supplies the power to increase rpm and to overcome the increasing $P_i + P_o$ terms. Depending on the rate of cyclic application and airspeed, the exchange of kinetic energy into rotor rotational energy can be such that an overspeed condition could exist In a flare, the principle source of power comes from the decreasing kinetic energy. The more the aircraft is pitched, causing thrust to be greater, the greater will be the rate of change in the aircraft kinetic energy, especially for high-speed flares. The excess loss of kinetic energy must then cause an increase in rotor energy (rotor overspeed) or potential energy (climb). When the flare conditions are such that loss of aircraft kinetic energy causes an excess of rotational energy, it becomes necessary to increase collective pitch, which increases $P_i + P_o$ and absorbs the excess P_{KE}. However, the increased collective pitch also increases thrust, which could decrease rate of descent too fast or even cause a climb condition. This may not be desirable, especially if the entry was from the high-altitude low-speed portion of the H-V curve. Also, increasing collective pitch at this time limits the amount of collective that will be available during the landing. If the flare is initiated before the proper flare airspeed is reached, then the inflow will not be enough to build the thrust to a level where the deceleration creates the power necessary to overcome the rotor power required and build rotor speed.

Landing:

10. The landing phase is much simpler. It consists of an exchange of rotor rotational energy to dissipate any rate of descent left after the flare, and to overcome power required. Once the forward speed has been decreased to the desired landing airspeed and rotor speed has been increased, the aircraft is leveled and collective applied. This action causes thrust to increase significantly in the vertical direction, decreasing the rate of descent to within the landing gear limits. Since thrust is directed almost completely in the vertical direction, there will not be any further deceleration of forward horizontal speed (other than that caused by drag). Therefore, the flare must have dissipated any forward horizontal velocity to within the gear limits. Once the landing phase is initiated, it will not be possible to further decrease forward airspeed. As collective is applied, the only source of energy available to compensate for the increased $P_i + P_o$ is the rotor rotational energy, as KE_{AC} and PE are negligible. This causes rotor speed to decrease. What is critical here is that there are no other energy sources available to supply power

once the landing phase is initiated. When rotor speed has decreased below some minimum control becomes difficult and the thrust generated drops considerably below gross weight. Also critical is the collective control margin left after the flare phase. If there is not enough collective left, rate of descent cannot be properly dissipated. Therefore, if the aircraft is not ready for landing and touchdown after the flare phase, a crash can be expected.

Summary

11. Several generalizations are possible through this simple analogy of autorotational flight. First, is the importance of the total energy and power-lost variables. It takes a certain amount of time to lose altitude and effect a landing. During that time period, the P_i, P_o and P_p variables are dissipating energy to the environment. If the autorotation is flown with a less than optimum technique, the energy level at flare initiation will be less than would have been possible. The greater the total energy of the aircraft at flare initiation, the greater will be the error margin for the flare and landing phases.

12. The total energy lost term, or more specifically, the time integral of power lost in relation to the total energy available at the start of the maneuver is what enables the helicopter to land safely (with little remaining energy) after an autorotational descent. Integrating equation 3 over the entry time of the autorotation, the total energy remaining at touchdown ($E_{T_{TD}}$) is defined as:

$$E_{T_D} = E_{T_O} - \int_{t=0}^{TD} P_{LOST}\, dt \tag{4}$$

Where:

E_{TO} is the total energy of the system at the start of the maneuver.

Equation 4 can be further broken down into autorotational phases:

$$E_{T_{TD}} = E_{T_O} - \int_{t=0}^{entry} P_{LOST}\, dt - \int_{entry}^{dive} P_{LOST}\, dt - \int_{dive}^{flare} P_{LOST}\, dt - \int_{flare}^{TD} P_{LOST}\, dt \tag{5}$$

Optimal technique includes the minimizing of the integral through the dive phase. This assures adequate time and power to allow a significant error margin during the flare. Because a low energy touchdown is desirable and because the landing phase has a relatively narrow window of acceptable technique, the bulk of the excess power must be dissipated during the flare. Therefore, from a purely energy viewpoint, an inefficient flare is desirable (after assuring adequate rotor speed).

13. As the entry condition approaches the H-V curve E_{T_G} generally decreases. To effect a safe landing (minimal $E_{T_{TD}}$) the pilot must dissipate as little of the total energy as possible to P_i and P_o during the autorotation phases of entry and dive so that he has some margin during flare and landing.

14. It should be noted that the exchange of energy during each phase is not equally efficient for all entry conditions. For instance, at high hover, E_{T_O} consists entirely of potential and rotor kinetic energies. During the entry and dive, not much can be done except to pitch the aircraft over, minimize $P_i + P_o$, and "fall" to increase rate of descent. The power available from KE_{AC} is minimal as initial airspeed is so low. Contrast that with the high-speed, low-altitude portion of the curve. There the objective is to decrease the high KE_{AC} and depending on technique, not increase PE. However, rapidly pitching the aircraft nose-up and increasing the inflow to the rotor will create a potential rotor overspeed situation. Collective application will increase $P_i + P_o$, thus dissipating the excess $P_{KE_{AC}}$, but there are limits to how much collective can be applied. Additionally, thrust will increase rapidly and a climb condition may result. Therefore, the pilot wants to have a higher P_{LOST}. In any event, he must be certain to have adequate collective control remaining to effect a landing.

REFERENCE AXES

General

15. Precise definition of all reference axes used is essential to data processing and to the proper interpretation of data. It is rare that instrumentation systems can be installed on an aircraft such that no correction is required to make the data produced meaningful in relation to the aircraft. Knowledge of the exact location and orientation of the instruments allows transformation of all data to a common reference system. Similarly, during analysis it is often more useful to consider a given set of data in a particular reference system.

16. The reference systems used in this program include the principal, gravity, inertial, and shaft axis systems, as well as several instrument reference systems. Figure B illustrates the various reference systems.

Principal Axis System

17. The principal (or body) axis system is located at the aircraft cg. It is a right-hand orthogonal system with the X axis positive forward, Y axis positive to the right, and the Z axis positive downward. The X-Y plane is parallel to the water lines of the aircraft.

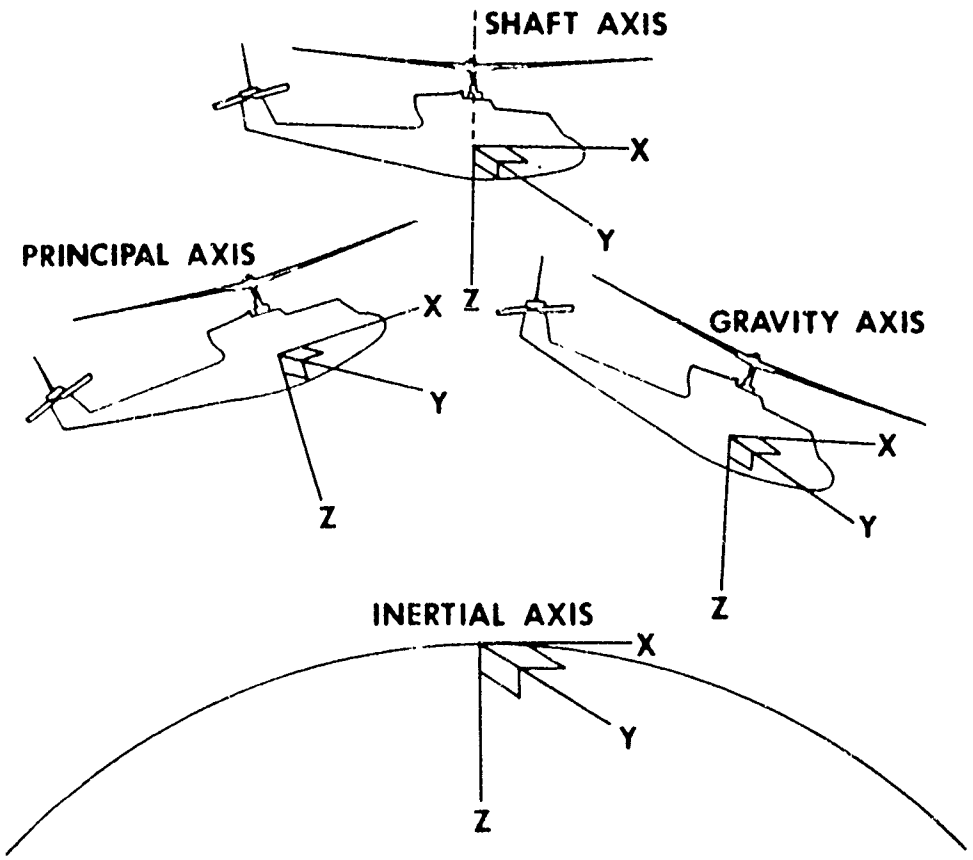

Figure B. Reference Axes.

Inertial Axis System

18. The inertial (or ground) axis system is referenced to a fixed point on the ground. It is a right-hand orthogonal system with the Z axis positive downward along a radius of the earth. The X axis is positive forward along the heading of the aircraft at time zero. The Y axis is positive to the right.

Gravity Axis System

19. If the inertial reference system is allowed to translate such that its origin is fixed at the aircraft cg, it becomes the gravity axis system. Unlike the stationary inertial system, the gravity system accelerates with the aircraft. However, regardless of aircraft motion, the axes remain parallel to those of the inertial system.

Shaft Axis System

20. The shaft axis system's origin is located at the aircraft cg. The three axes are mutually perpendicular, with the Z axis positive downward and oriented parallel to the rotor shaft. The X axis is positive forward and the Y axis positive right.

Instrument Reference Systems

21. Because each instrument is located and oriented in a different manner, each instrument axis system must be corrected to one of the standard systems.

Transformations

22. The orientation of one orthogonal reference system with respect to another can be defined by the use of three Euler angles. In this program, the instrumentation dictated that the Euler angles reference yaw, pitch, and roll, in that order. Yaw is measured positive right about the Z axis, pitch is measured positive up about the yaw rotated Y axis, and roll is positive right about the yaw and pitch rotated X axis (fig. C).

23. All transformations from one right-hand orthogonal system to another are similar in format. Following is an example of a transformation from the gravity axis system to the principal axis system.

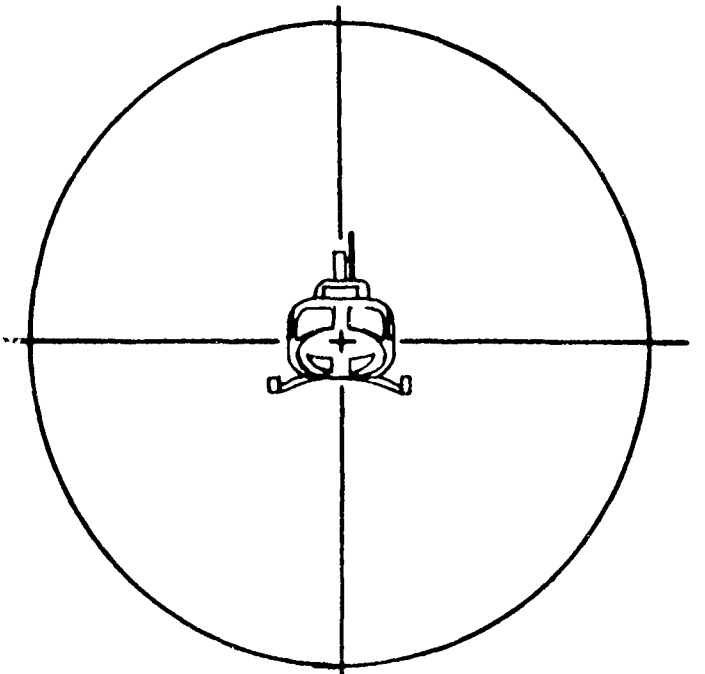

A. ALIGNED WITH GRAVITY AXES

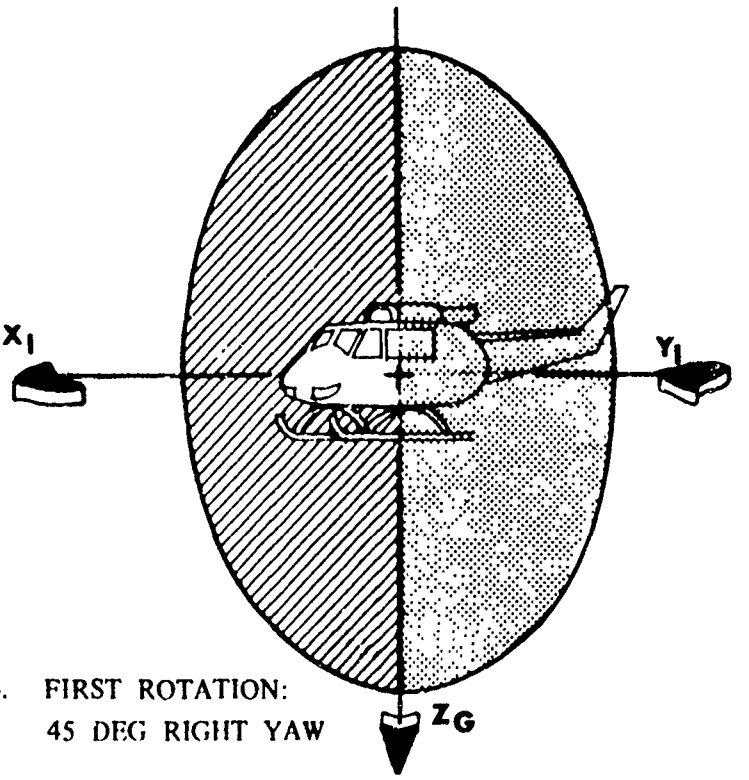

B. FIRST ROTATION:
45 DEG RIGHT YAW

Figure C. Axis Transformation.

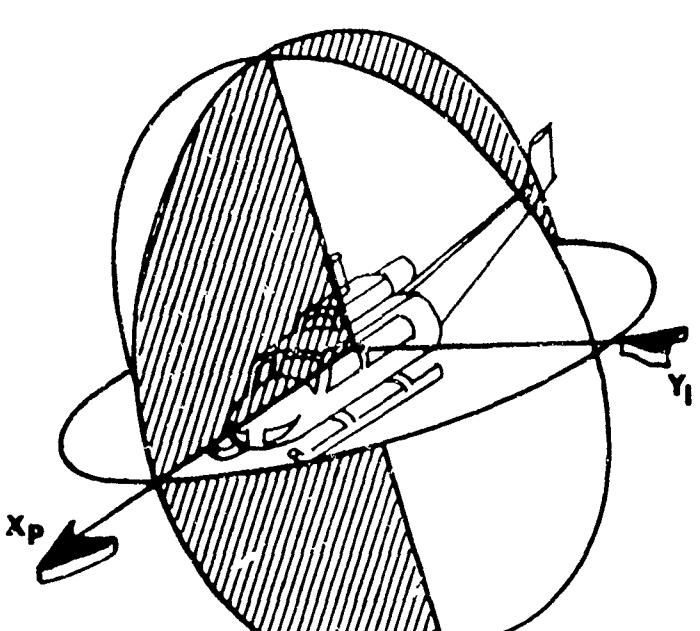

C. SECOND ROTATION:
45 DEG RIGHT YAW, 15 DEG PITCH DOWN

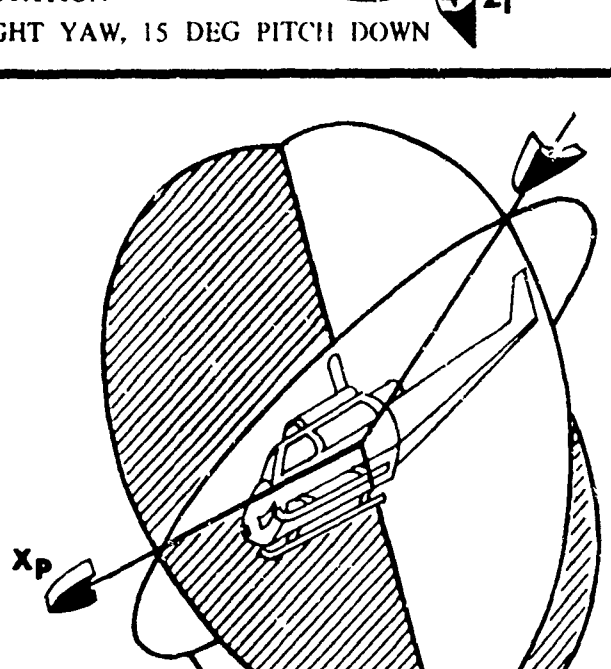

D. THIRD ROTATION:
45 DEG RIGHT YAW,
15 DEG PITCH DOWN,
45 DEG RIGHT ROLL

Figure C. Axis Transformation.

First rotation, yaw about Z_G axis

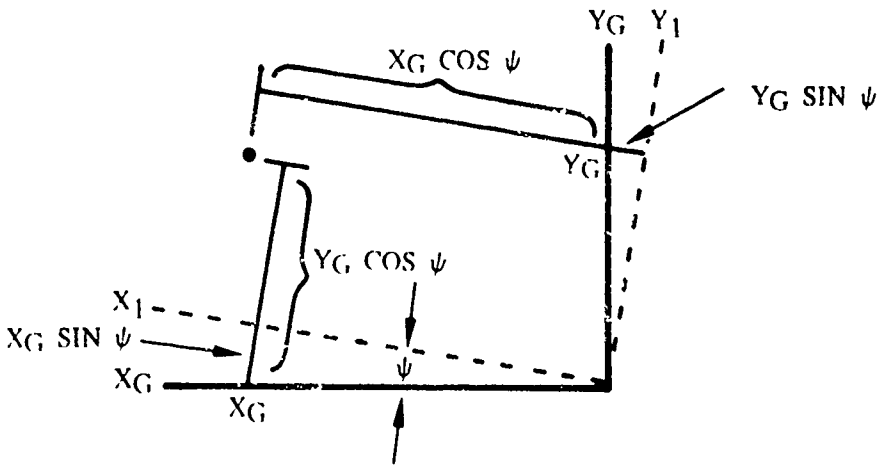

Figure D. Yaw Transformation.

$$\begin{bmatrix} X_1 \\ Y_1 \\ Z_1 \end{bmatrix} = \begin{bmatrix} \cos\psi & \sin\psi & 0 \\ -\sin\psi & \cos\psi & 0 \\ 0 & 0 & 1 \end{bmatrix} \begin{bmatrix} X_G \\ Y_G \\ Z_G \end{bmatrix} \quad (6)$$

Second rotation: pitch about Y_1 axis

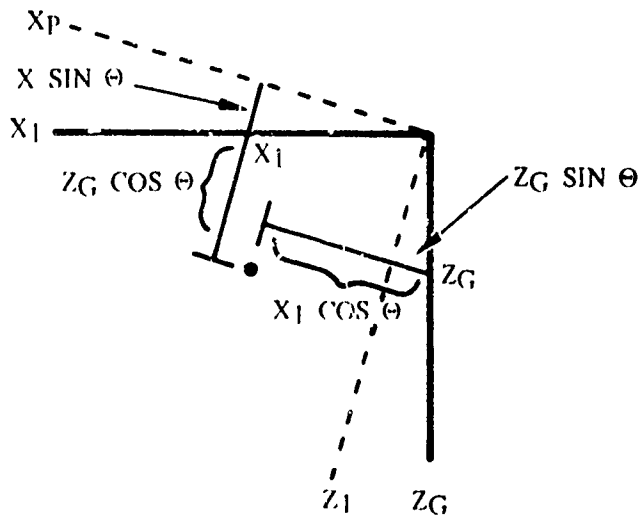

Figure E. Pitch Transformation.

$$\begin{bmatrix} X_P \\ Y_1 \\ Z_1 \end{bmatrix} = \begin{bmatrix} \cos\theta & 0 & -\sin\theta \\ 0 & 1 & 0 \\ \sin\theta & 0 & \cos\theta \end{bmatrix} \begin{bmatrix} X_1 \\ Y_1 \\ Z_G \end{bmatrix} \tag{7}$$

Third rotation: roll about X_p axis

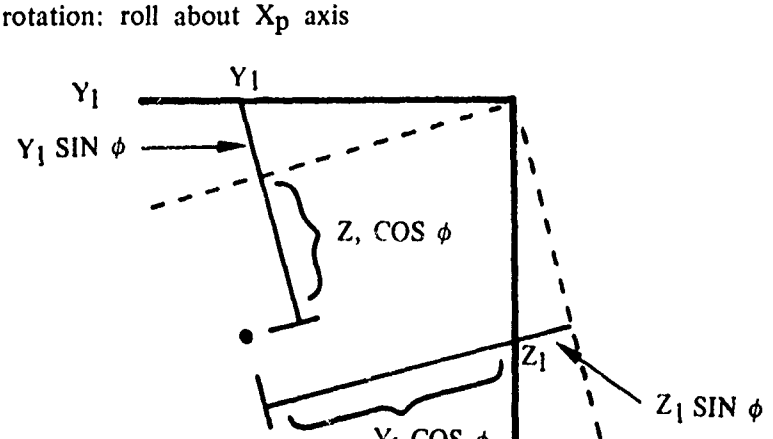

Figure F. Roll Transformation.

$$\begin{bmatrix} X_P \\ Y_P \\ Z_P \end{bmatrix} = \begin{bmatrix} 1 & 0 & 0 \\ 0 & \cos\phi & \sin\phi \\ 0 & -\sin\phi & \cos\phi \end{bmatrix} \begin{bmatrix} X_P \\ Y_1 \\ Z_1 \end{bmatrix} \tag{8}$$

Combining equations 6, 7, and 8:

$$\begin{bmatrix} X_P \\ Y_P \\ Z_P \end{bmatrix} = \begin{bmatrix} (\cos\theta\ \cos\psi) & (\cos\theta\ \cos\psi) & (-\sin\theta) \\ (\sin\phi\ \sin\theta\ \sin\psi - \cos\phi\ \sin\psi) & (\sin\phi\ \sin\theta\ \sin\psi + \cos\phi\ \cos\psi) & (\sin\phi\ \cos\theta) \\ (\cos\phi\ \cos\theta\ \cos\psi + \sin\phi\ \sin\theta) & (\cos\phi\ \cos\theta\ \cos\psi - \sin\phi\ \sin\psi) & (\cos\phi\ \cos\theta) \end{bmatrix} \begin{bmatrix} X_G \\ Y_G \\ Z_G \end{bmatrix} \tag{9}$$

DATA PROCESSING AND ANALYSIS

General

24. The data processing and anlysis consisted mainly of a validation phase and a calculation phase. A flow chart of the total data processing is shown in figure G.

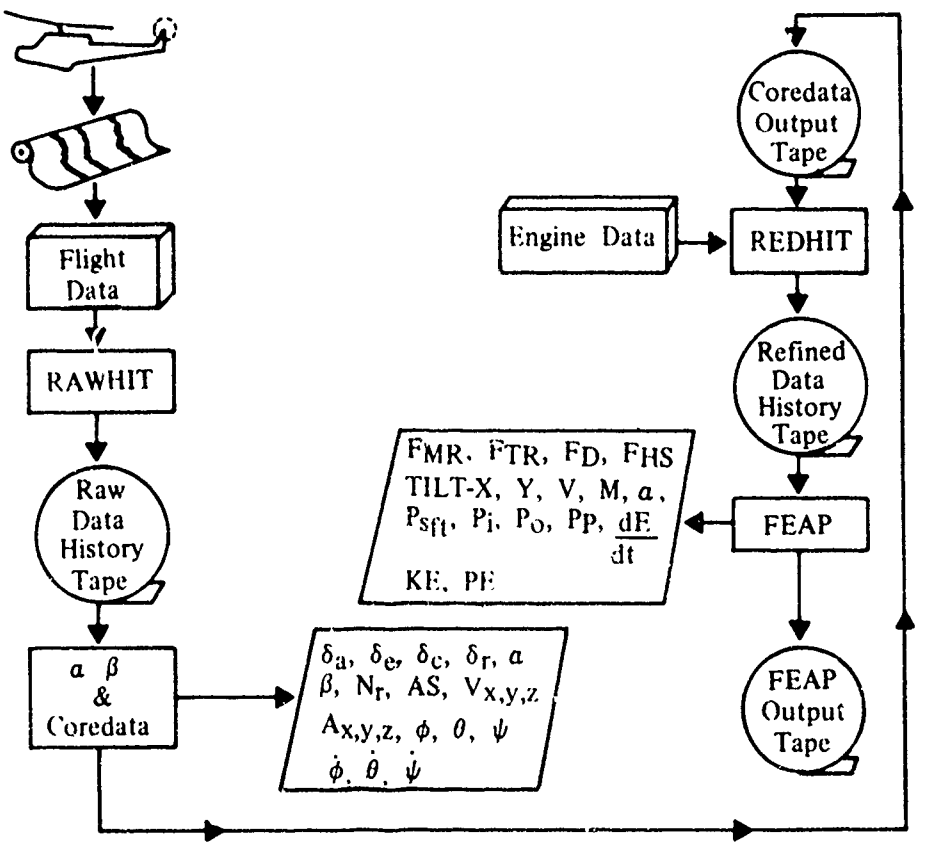

Figure G. Data Processing Flow Chart.

25. The data from all sources were read manually and punched onto computer cards. Programs were developed to cross-check the data from different sources and reduce it to engineering units. The reduced data were then used to calculate force, energy, and power terms, as well as several aerodynamic nondimensional terms.

Data Validation and Initial Calculations

26. The data reading accuracy was found to be very critical because of the considerable manipulation of data in subsequent programs. A study was conducted to determine the maximum attainable reading accuracy versus the minimum accuracy the data analysis could tolerate (refs 20 and 21, app A). After the data were read and punched onto cards, the information was put on magnetic tape with the raw data history tape program (RAWHIT).

27. Angle of attack and sideslip were input to the alpha-beta program which aligns all the data and provides the proper format for the computerized reduction of data (COREDATA) program. It also adds the effect of any wind that may be present.

28. The validation process in COREDATA allows for the correction of instrument biases, identification of instrument malfunction or reading errors, and determination of data smoothing suitability. Tolerance limits are established which reject data which are unsuitable for further processing.

29. The basis for the validation procedure is that for a given parameter, similar values should be obtained from different recording sources. Comparisons are made between the attitude versus angular rate data, wind-corrected true airspeed versus accelerometer data, and angles of attack and sideslip versus accelerometer and angular rate data. When significant differences in the data are encountered, the data are corrected, identified as unsuitable for further processing, or identified as a source of possible inaccuracies in the statistical analysis. A COREDATA process flow chart is shown in figure H.

30. The time evaluation allows corrections to be made for any time or sequencing errors in the recording systems. Accurate time is required since the data are differentiated and integrated with respect to time in later sections. The curve fit section also synchronizes the data from the different recording sources and allows for different reading densities from the recording systems. The derivative section provides angular rate and acceleration data from the rate gyro data. It also provides rate of change of attitude data. The final step in the data preparation is to process the data through the Euler check section. The rates of change of attitude are transformed through Euler angles to obtain components along the body axes of the aircraft. These body axes components are then compared individually with the rate gyro readings. The comparison reveals time lags between the attitude and rate gyros, existence of any misalignment, and data reading errors.

31. The Bias I section calculates body axis airspeed components from airspeed data and linear acceleration components at the cg from accelerometer data. The accelerations are calculated assuming that no preflight bias exists in the data. The information is then used in the Bias II section where the unbiased accelerations are integrated by Simpson's Rule and compared with the components of airspeed. From this comparison, the preflight bias (average difference between airspeed and velocity components) is determined and then used in the acceleration section to

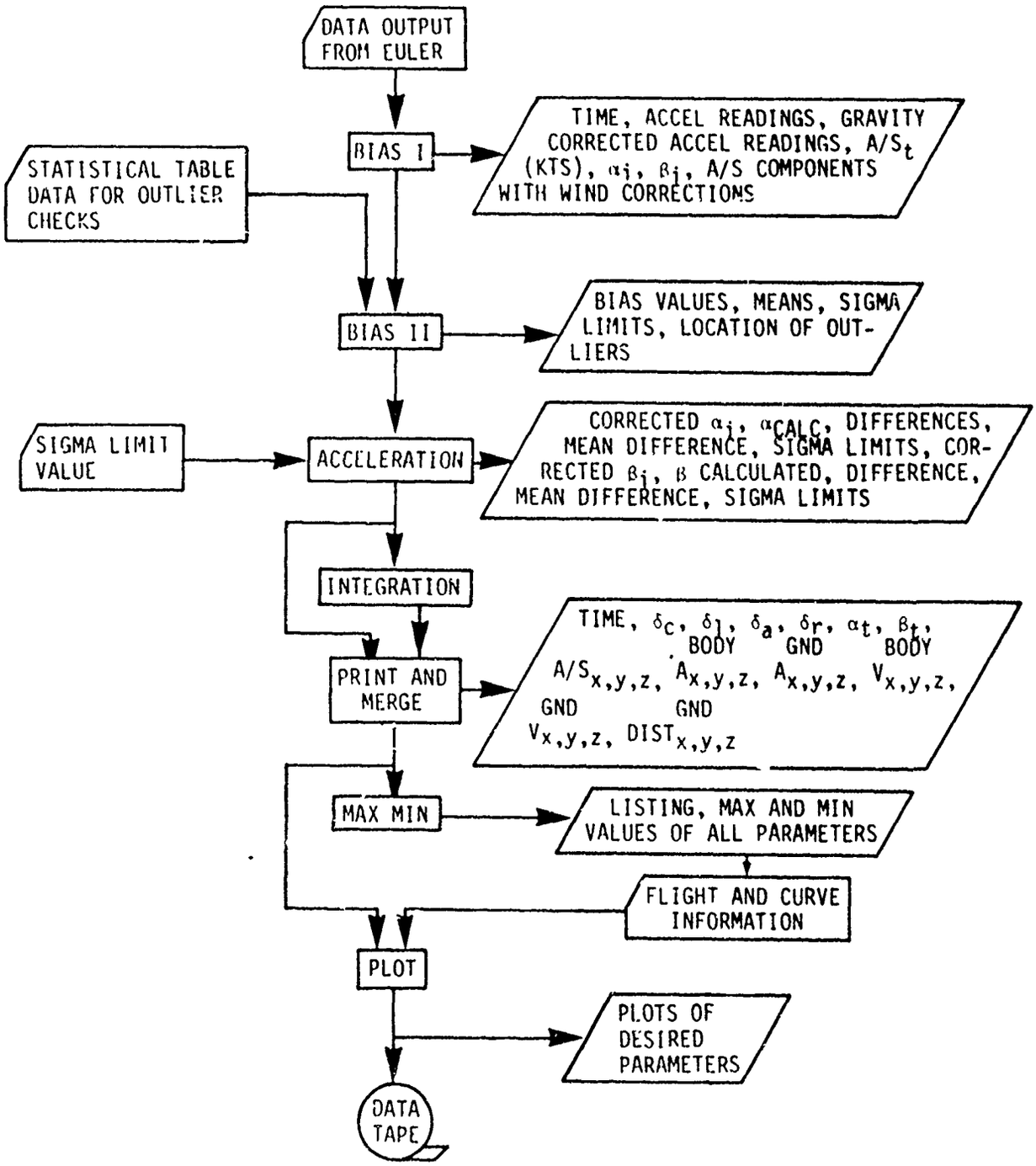

Figure H. COREDATA Flow Chart.

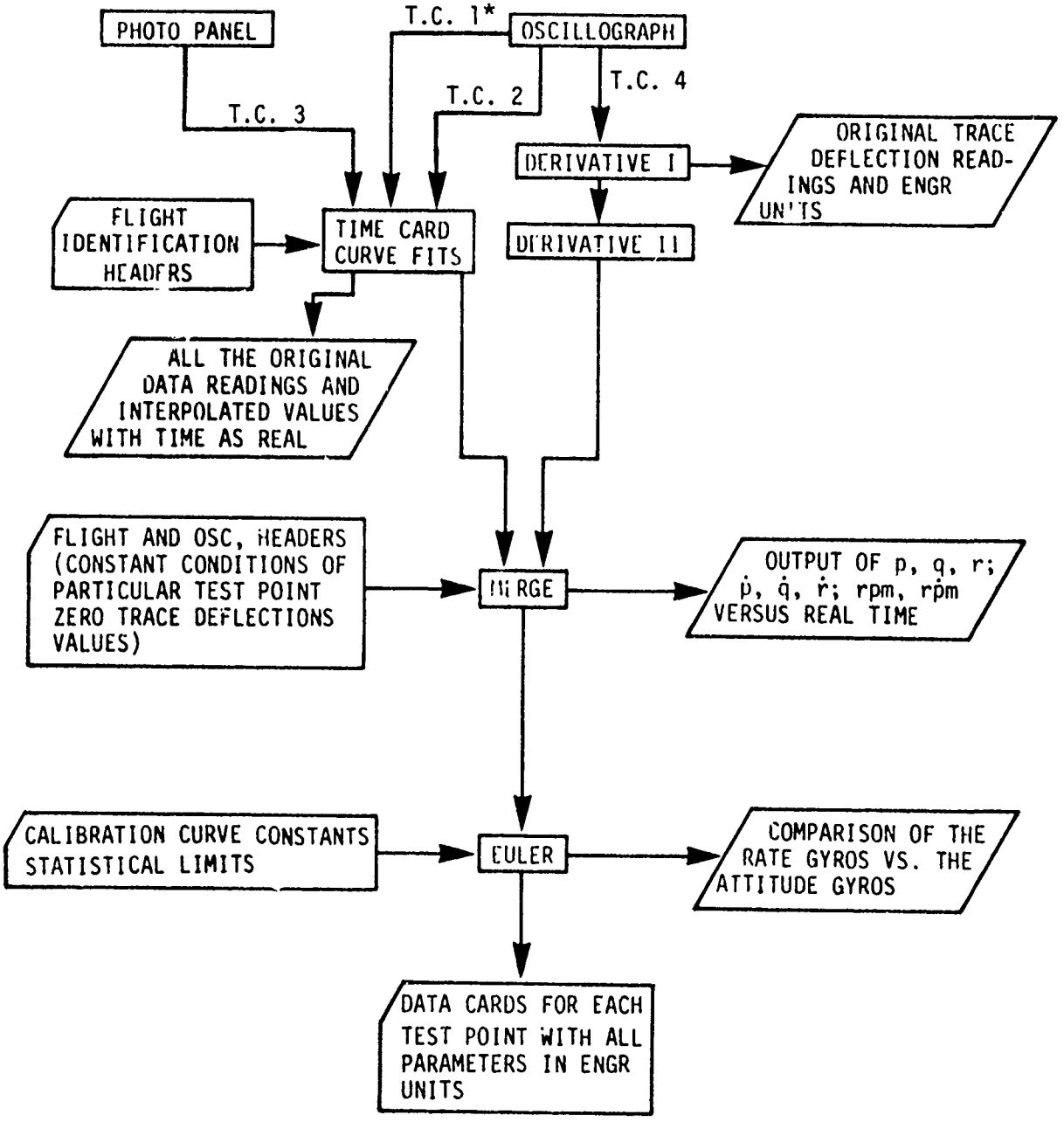

*T.C. signifies a specific deck of time cards.

Figure H. COREDATA Flow Chart.

more accurately calculate the linear acceleration of the aircraft cg. The acceleration section also provides a direct check on the angles of attack and sideslip by comparing the recorded values with those calculated from the angular rates and integrated acceleration data.

32. The output of the acceleration section is then input to the integration section, which uses a spline function technique to integrate the acceleration data. A wind correction analysis corrects the airspeed reading to true ground and aircraft velocities at time zero. Using these velocity components as initial velocities and initial zero distances, the integration section calculates the components of velocity in the aircraft body axes and ground axes and the ground distances traveled.

33. The tape output of COREDATA and engine data is placed in the refined data history tape program (REDHIT), which provides an output for additional calculations.

Force, Energy, and Power Calculations

34. Once the data have been processed through REDHIT, it is ready for input into the force, energy, and power program (FEAP). FEAP calculates forces, energies, and powers using three-dimensional force analysis, momentum theory, and energy-power relationships.

Force Calculations

35. Force equations were derived using standard $\Sigma F = mA$ and $\Sigma M = I\Omega$ equations. Figure I shows force and moment balance diagrams.

36. Resultant drag force (F_D) is coincident with relative wind. Because angle of attack (α) is measured only within the X-Z plane of the aircraft, a new term must be introduced where:

$$\Phi = \tan^{-1} (\cos\beta \tan\alpha)$$

37. Force balance equations:

$$ma_{xp} = F_{MR_{xp}} + W_{xp} - F_D \cos\Phi \cos\beta \quad (10)$$

$$ma_{yp} = F_{MR_{yp}} + W_{yp} - F_D \cos\Phi \sin\beta + F_{TR} \quad (11)$$

$$ma_{zp} = F_{MR_{zp}} + W_{zp} - F_D \sin\Phi + F_{HS} \quad (12)$$

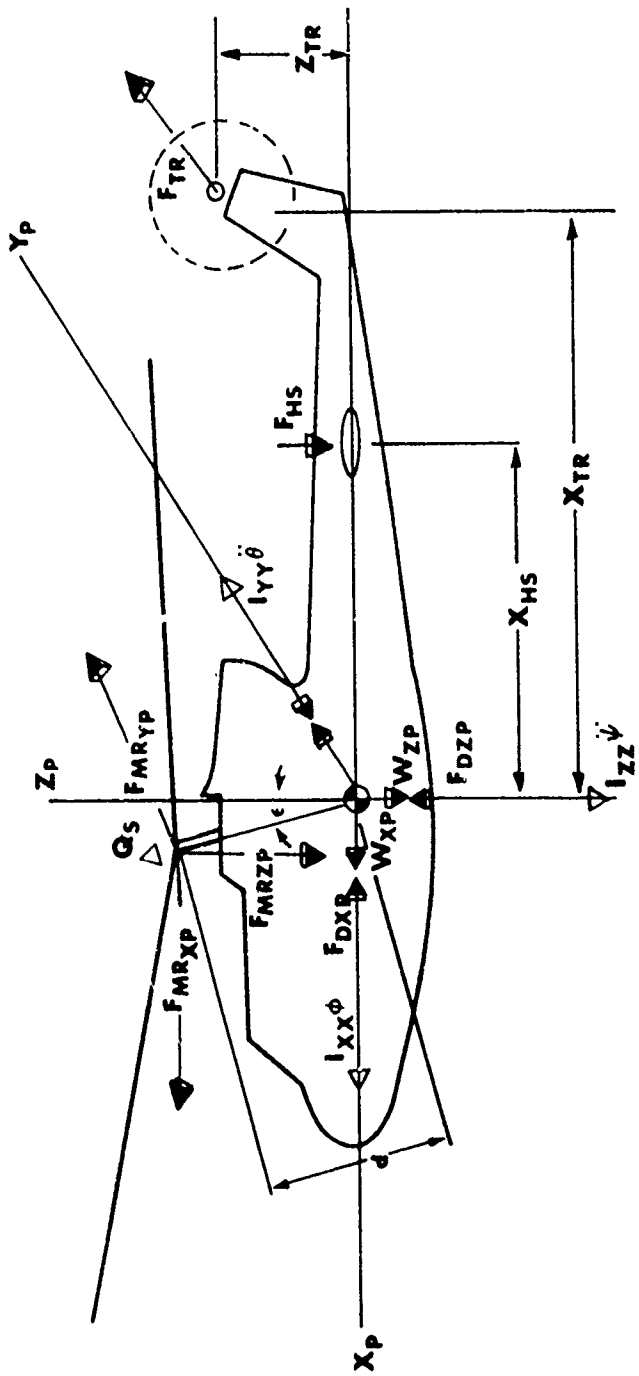

Figure I. Force and Moment Balance Diagram.

38. Moment balance equations:

$$I_{xx}\ddot{\phi} = F_{MR_{yp}}\, d\cos\varepsilon + F_{TR}\, Z_{TR} - Q_s \sin\varepsilon \tag{13}$$

$$I_{yy}\ddot{\theta} = F_{MR_{xp}}\, d\cos\varepsilon - F_{MR_{zp}}\, d\sin\varepsilon + F_{HS}\, x_{HS} \tag{14}$$

$$I_{zz}\ddot{\psi} = F_{MR_{yp}}\, d\sin\varepsilon - F_{TR}\, x_{TR} + Q_s \cos\varepsilon \tag{15}$$

39. In matrix form, equations 10 through 15 yield:

$$\begin{bmatrix} ma_{xp} - W_{xp} \\ ma_{yp} - W_{yp} \\ ma_{zp} - W_{zp} \\ I_{xx}\ddot{\phi} + Q_s \sin\varepsilon \\ I_{yy}\ddot{\theta} \\ I_{zz}\ddot{\psi} - Q_s \cos\varepsilon \end{bmatrix} = \begin{bmatrix} 1 & 0 & 0 & 0 & -\cos\phi\cos\beta & 0 & F_{MR_{xp}} \\ 0 & 1 & 0 & 1 & -\cos\phi\sin\beta & 0 & F_{MR_{yp}} \\ 0 & 0 & 1 & 0 & -\sin\phi & 1 & F_{MR_{zp}} \\ 0 & d\cos\varepsilon & 0 & Z_{TR} & 0 & 0 & F_{TR} \\ -d\cos\varepsilon & 0 & -d\sin\varepsilon & 0 & 0 & x_{HS} & F_D \\ 0 & d\sin\varepsilon & 0 & -x_{TR} & 0 & 0 & F_{HS} \end{bmatrix}$$

40. Substituting

$$A_1 = d\sin\varepsilon \qquad A_6 = I_{xx}\ddot{\phi} + Q_s \sin\varepsilon$$

$$A_2 = d\cos\varepsilon \qquad A_7 = I_{yy}\ddot{\theta}$$

$$A_3 = ma_{xp} - W_{xp} \qquad A_8 = -\cos\phi\cos\beta$$

$$A_4 = I_{zz}\ddot{\psi} - Q_s \cos\varepsilon \qquad A_9 = -\sin\phi$$

$$A_5 = ma_{zp} - W_{zp}$$

into equation 16 yields

$$\begin{bmatrix} A_3 \\ ma_y - W_y \\ A_5 \\ A_6 \\ A_7 \\ A_4 \end{bmatrix} = \begin{bmatrix} 1 & 0 & 0 & 0 & A_8 & 0 & F_{MR_{xp}} \\ 0 & 0 & 0 & 1 & -\cos\phi \sin\beta & 0 & F_{MR_{yp}} \\ 0 & 0 & 1 & 0 & A_9 & 1 & F_{MR_{zp}} \\ 0 & A_2 & 0 & Z_{TR} & 0 & 0 & F_{TR} \\ -A_2 & 0 & -A_1 & 0 & 0 & x_{HS} & F_D \\ 0 & A_1 & 0 & -x_{TR} & 0 & 0 & F_{HS} \end{bmatrix} \quad (17)$$

P_{Set} = Power available at the rotor hub

$(P_i + P_o + P_p)$ = Power required for equilibrium flight.

Solving for the six unknown forces,

$$F_{TR} = (A_1 A_6/2 - A_4)/(x_{TR} + A_1 {}_{TR}/A_2) \quad (18)$$

$$F_{MR_{yp}} = (A_6 - Z_{TR} F_{TR})/A_2 \quad (19)$$

$$F_{MR_{xp}} = A_3 - A_8 F_D \quad (20)$$

$$F_{MR_{zp}} = A_5 - A_9 F_D - F_{HS} \quad (21)$$

$$F_{HS} = (A_7 - A_2 F_{MF_{xp}} + A_1 A_5 - A_1 A_9 F_D)/(A_1 + x_{HS}) \quad (22)$$

$$F_D = (W_{yp} - ma_{yp} + F_{MR_{yp}} + F_{TR})/(\cos\phi \sin\beta) \quad (23)$$

41. The equation for F_D is unavoidably sensitive to small errors in sideslip (β). Therefore, the following general aerodynamic drag relation was used:

$$F_D = \rho/2 \left[(C_{D_{xp}} S_{xp} V_{xp}^2)^2 + (C_{D_{yp}} S_{yp} V_{yp}^2)^2 + (C_{D_{zp}} S_{zp} V_{zp}^2)^2 \right]^{1/2} \quad (24)$$

Energy Calculations

42. Potential, kinetic, and rotor energies are calculated in FEAP. The equations used are as follows:

$$PE = mgh \tag{25}$$

$$KE_{AC} = 1/2\ (mV^2) \tag{26}$$

$$KE_{MR} = 1/2\ (I\Omega^2) \tag{27}$$

$$E_T = PE + KE_{AC} + KE_{MR} \tag{28}$$

Potential energy was calculated such that PE = 0 at the end of the point. Aircraft body rotational energy was neglected due to its relatively small magnitude.

Power Calculations

43. The basic equation used to calculate power reflects the relationship between rate of change of energy and power required.

$$P_{Sft} - (P_i + P_o + P_p) = \frac{dKE_{AC}}{dt} + \frac{dPE}{dt} + \frac{dKE_{MR}}{dt} + P_{BODY} \tag{29}$$

Where:

P_{Sft} = Power available at the rotor hub

$(P_i + P_o + P_p)$ = Power required for equilibrium flight

$\frac{dKE_{AC}}{dt} + \frac{dPE}{dt} + \frac{dKE_{MR}}{dt} + P_{BODY}$ = excess power (power deficiency if negative)

44. Engine power (P_{eng}) is calculated using the measured values of torque and N_2 speed. Transmission and accessory losses are assumed to be a constant 20 shp. Tail rotor power is calculated as a function of F_{TR}, λ_{TR}, μ_{TR}, and σ_{TR} (ref 22, app A).

$$P_{Sft} = P_{eng} - 20HP - P_{TR} \tag{30}$$

$$P_p = F_D V \tag{31}$$

$$P_i = F_{MR} v_i \tag{32}$$

$$\frac{dKE_{AC}}{dt} = \text{slope of kinetic energy curve} \tag{33}$$

$$\frac{dPE}{dt} = \text{slope of potential energy curve} \tag{34}$$

$$\frac{dKE_{MR}}{dt} = \text{slope of rotor energy curve} \tag{35}$$

$$P_{BODY} = I_{xx}\dot{\phi}\ddot{\phi} + I_{yy}\dot{\theta}\ddot{\theta} + I_{zz}\dot{\psi}\ddot{\psi} \tag{36}$$

45. The only remaining unknown in equation 20 is P_O, which can be determined by subtraction.

Other Calculations

46. Longitudinal and lateral angular displacement of main rotor thrust (TILT-X and TILT-Y) are calculated by comparing $F_{MR_{XS}}$, $F_{MR_{YS}}$, and $F_{MR_{ZS}}$. TILT-X is positive when the thrust vector is tilted backward, and TILT-Y is positive when thrust vector is tilted to the right.

$$\text{TILT-X} = \tan^{-1}\left(F_{MR_{xs}}/F_{MR_{zs}}\right) \tag{37}$$

$$\text{TILT-Y} = \tan^{-1}\left(-F_{MR_{ys}}/F_{MR_{zs}}\right) \tag{38}$$

47. Induced velocity (v_i) is calculated using the equation from reference 19, appendix A.

$$v_i = F_{MR}/2\rho V' A_{disc} \tag{39}$$

where V' is the resultant velocity at the rotor (vector sum of induced velocity and translational velocity).

$$V' = \left[(V\sin\alpha_r - v_i)^2 + (V\cos\alpha_r)^2\right]^{1/2} \tag{40}$$

Equation 40 can be reduced to the form:

$$\left(\frac{V'}{V}\right)^2 = \frac{v_i^2}{V^2} - 2\left(\frac{v_i}{V}\right)\sin\alpha_r + 1 \tag{41}$$

Making the substitution $\overline{v_i} = \frac{v_i}{V}$:

$$\left(\frac{V'}{V}\right)^2 = \overline{v}_i^2 - 2\,\overline{v}_i\,\sin\alpha_r + 1 \tag{42}$$

A term $\overline{T}$ is created where:

$$\overline{T} = F_{MR}/2\rho V^2 A_{disc} \tag{43}$$

Dividing by equation 39, and squaring both sides:

$$\overline{T}^2 = \left(\frac{V'}{V}\right)^2 \overline{v}_i^2 \tag{44}$$

Substituting equation 42 into equation 44,

$$\overline{T}^2 = \overline{v}_i^4 - 2\overline{v}_i^3\,\sin\alpha_r + \overline{v}_i^2 \tag{45}$$

Equation 45 is solved for v_i using the Newton-Raphson method, and multiplying by V to obtain v_i.

48. Inflow ratio (λ) and advance ratio (μ) are calculated using the equations,

$$\lambda = (V\,\sin\alpha_r - v_i)/\Omega R \tag{46}$$

$$\mu = V\,\cos\alpha_r/\Omega R \tag{47}$$

MODEL AND RELATED PROGRAMS

General

49. At the outset of this program, it was considered necessary to attempt development of a mathematical model to predict autorotational performance. However, rather than rely on a purely theoretical basis for the model, it was concluded that the use of empirical flight test data would be more practical. Toward this end, two additional programs were developed: the correlation coefficient program (CORCOF), and correlation and regression analysis program (CORA). A flow chart is shown in figure J.

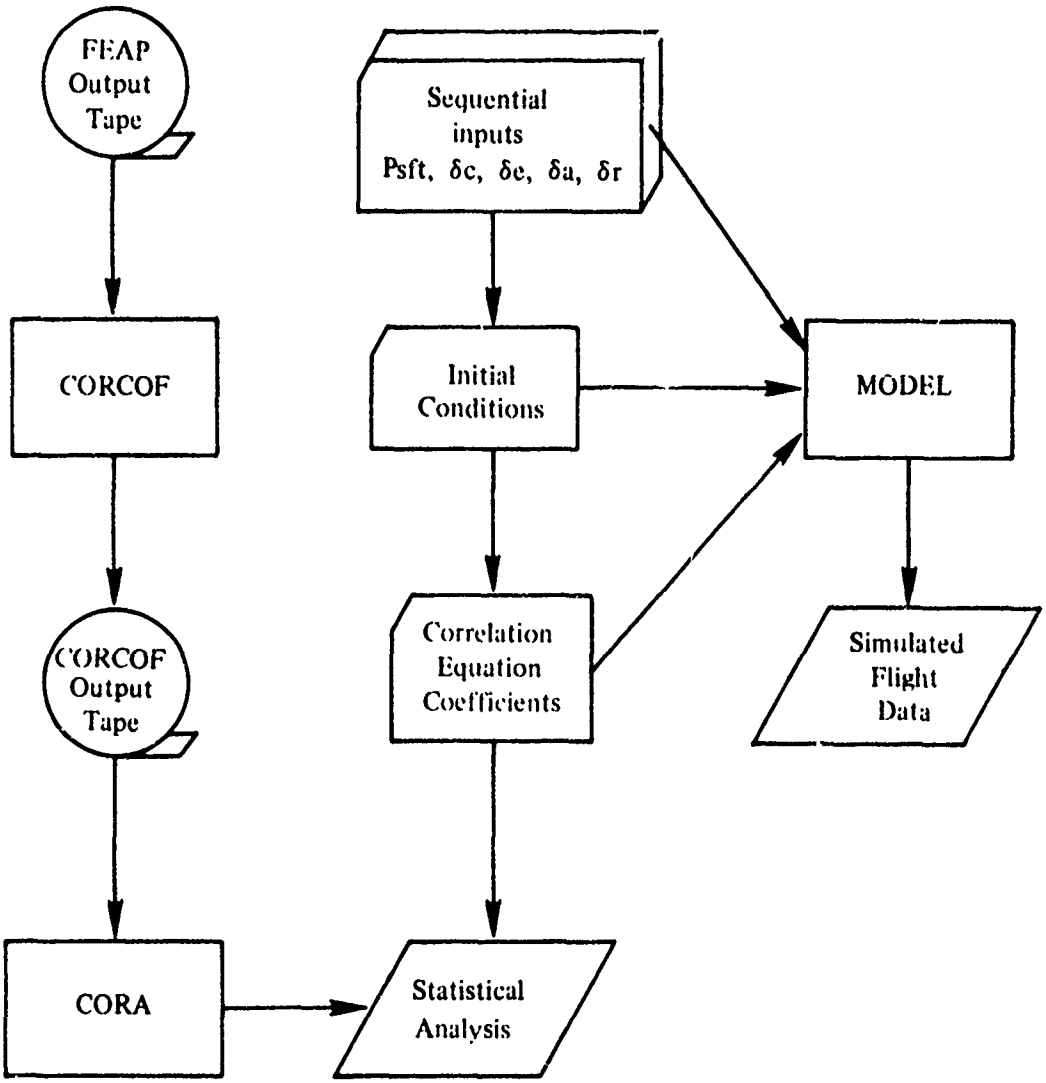

FIGURE J. FLOW CHART OF MODEL AND RELATED PROGRAMS

CORCOF and CORCOF Subroutines

50. Input to CORCOF is provided by the FEAP output tape. CORCOF reads and stores values for TILT-X, TILT-Y, and F_{HS}, and calculates the values for $C_{T_{MR}}$, $C_{T_{TR}}$, $C_{P_{MR}}$, and $C_{P_{TR}}$. It prints the values for λ_{MR}, λ_{TR}, μ_{MR}, and μ_{TR} calculated in FEAP, as well as the thrust and power coefficients. There are six CORCOF subroutines corresponding to the parameters $C_{T_{MR}}$, $C_{T_{TR}}$, F_{HS}, TILT-Y, TILT-X, and $C_{P_{MR}}$. It is the purpose of these subroutines to set up their respective parameters ($Y_k = C_{T_{MR}}$, $C_{T_{MR}}$, etc.) in the form.

$$Y_k = A_0 + \sum_{i=1}^{n} A_i X_i \tag{48}$$

Where X_i is a function of various independent nondimensional terms, as well as control position. As an example, an equation for $C_{T_{MR}}$ will be examined.

$$Y_1 = C_{T_{MR}} \tag{49}$$

$$X_1 = \sigma a \delta_c B_{MR} \tag{50}$$

$$X_2 = \sigma a \mu^2 \delta_c B_{MR} \tag{51}$$

$$X_3 = \sigma a \theta_t B_{MR} \tag{52}$$

$$X_4 = \sigma a \theta_t \mu B_{MR} \tag{53}$$

$$X_5 = \sigma a \lambda B_{MR} \tag{54}$$

This equation then takes the form:

$$C_{T_{MR}} = A_0 + A_1 (\sigma a \delta_c B_{MR}) + A_2 (\sigma a \mu^2 \delta_c B_{MR}) + A_3 (\sigma a \theta_t B_{MR}) + A_4 (\sigma a \theta_t \mu B_{MR}) + A_5 (\sigma a \lambda B_{MR}) \tag{55}$$

Other equations are functions of the following variables:

$$C_{T_{TR}} = f_2 (\lambda_{TR}, \mu_{TR}^2, \delta_r) \quad (56)$$

$$F_{HS} = f_3(\alpha_{HS}, \alpha_{HS}^2, \rho, AS), \text{ where } \alpha_{HS} = g(\delta_e, AS_{HS_{x,z}}) \quad (57)$$

$$\text{TILT-Y} = f_4 (\delta_C, \delta_a, \delta_e, B_{MR}, \mu_{MR}, \mu_{MR}^2, \mu_{MR}^3, I, \lambda_{MR}, \theta_t, \rho, I_R) \quad (58)$$

$$\text{TILT-X} = f_5 (\mu_{MR}, \mu_{MR}^2, \mu_{MR}^3, \lambda_{MR}, \delta_c, \delta_e, \theta_t, B_{MR}) \quad (59)$$

$$C_{P_{MR}} = f_6 (C_{T_{MR}}^{3/2}, \mu_{MR}, \lambda_{MR}) \quad (60)$$

As can be seen, these equations represent an empirical development of the theoretical relationship between the parameter in question and measurable quantities such as μ, λ, and δ. In some cases the user has a choice of two or more subroutines for a given parameter. The only unknowns in equation 48 are the A_i coefficients. These are produced by the CORA program.

CORA Program

51. CORA provides the statistical analysis required to calculate the A_i coefficients. It is a USAAEFA adaptation of the Air Force Flight Test Center Weighted Regression and Analysis Program (WRAP).

52. Given the X_i and Y values from CORCOF for n + 1 time points, the equations can be solved for all A_i terms. However, since there are more than n + 1 time points available, and because consistent values for A_i are not obtainable with the data used, a statistical approach was used to fit the A_i terms to the flight data. A statistical multiple correlation and regression technique combines the data and calculates a single set of A_i coefficients for each equation. Correlation coefficients are also calculated to indicate how well the equations fit the data and thus, the relative confidence that may be placed in the results. At the discretion of the operator, a value for Y is calculated using the A_i coefficients in the correlation equations for each time point. These values can be compared to the values generated in FEAP and CORCOF. Typical comparisons are shown in figures K through P. The difference, or residual, can then be printed and/or plotted for inspection.

53. It is reasonable to expect that one CORCOF option may be better suited to particular flight segments (flares, dives, etc.) while another option might be better suited to other flight segments. It should also be reasonable to expect that optimum results would be obtained by correlating data for each flight segment separately.

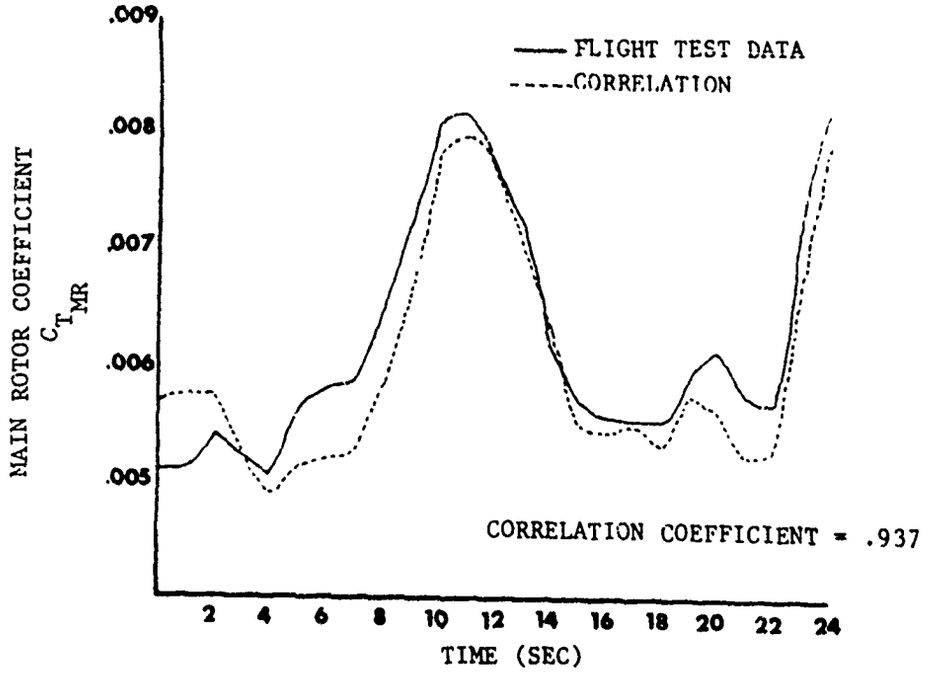

Figure K. Main Rotor Thrust Correlation.

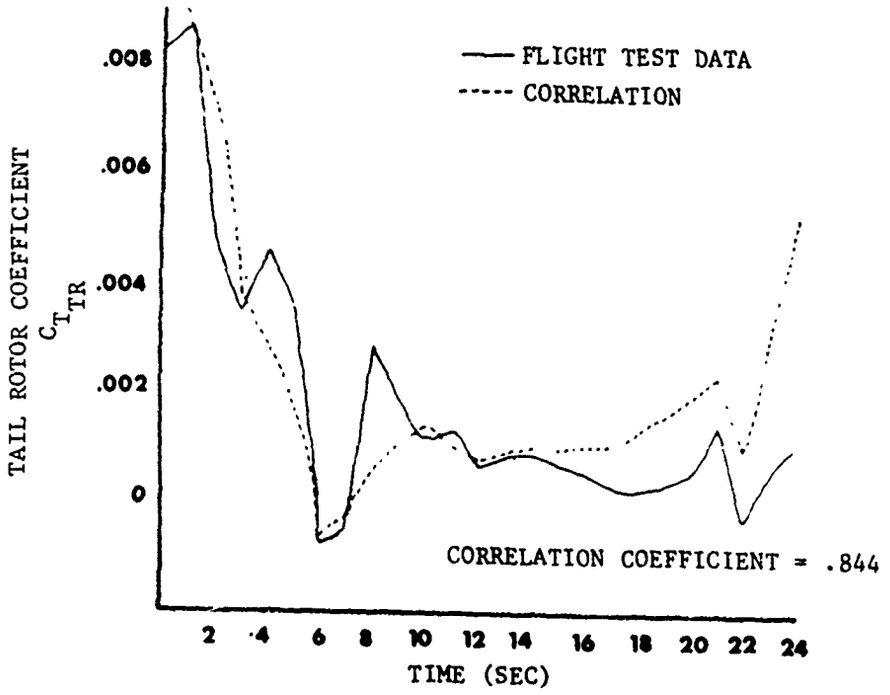

Figure L. Main Rotor Thrust Correlation.

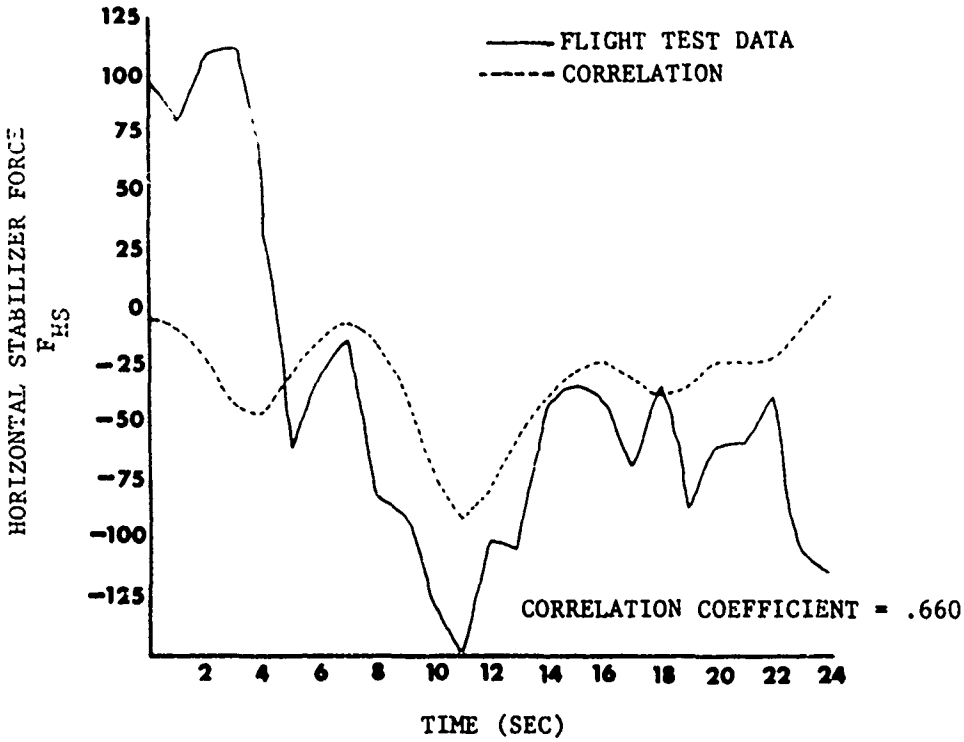

Figure M. Horizontal Stabilizer Force Correlation.

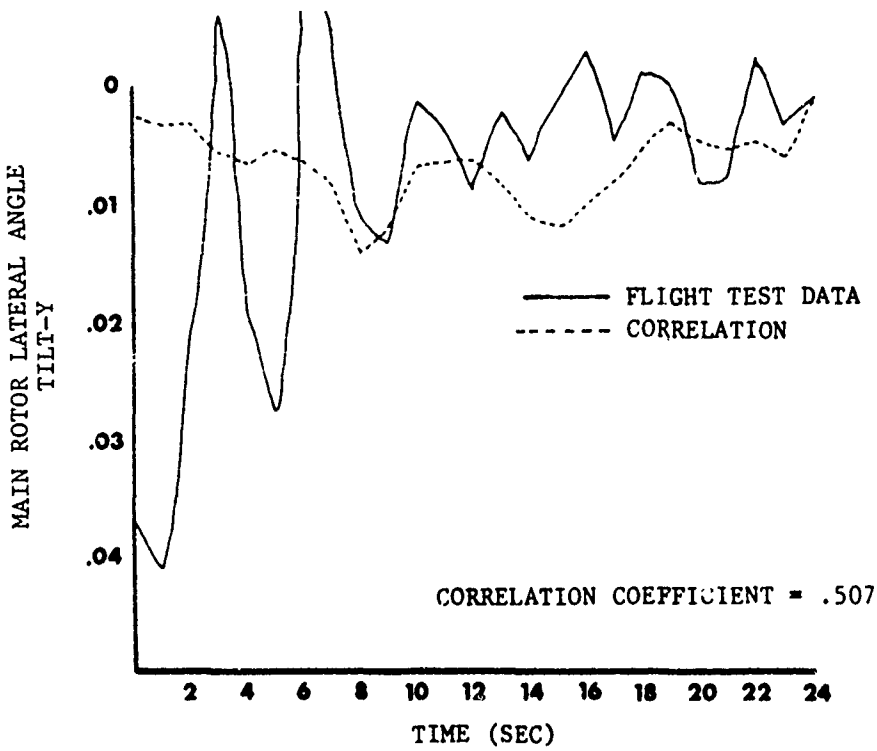

Figure N. Main Rotor Lateral Angle Correlation.

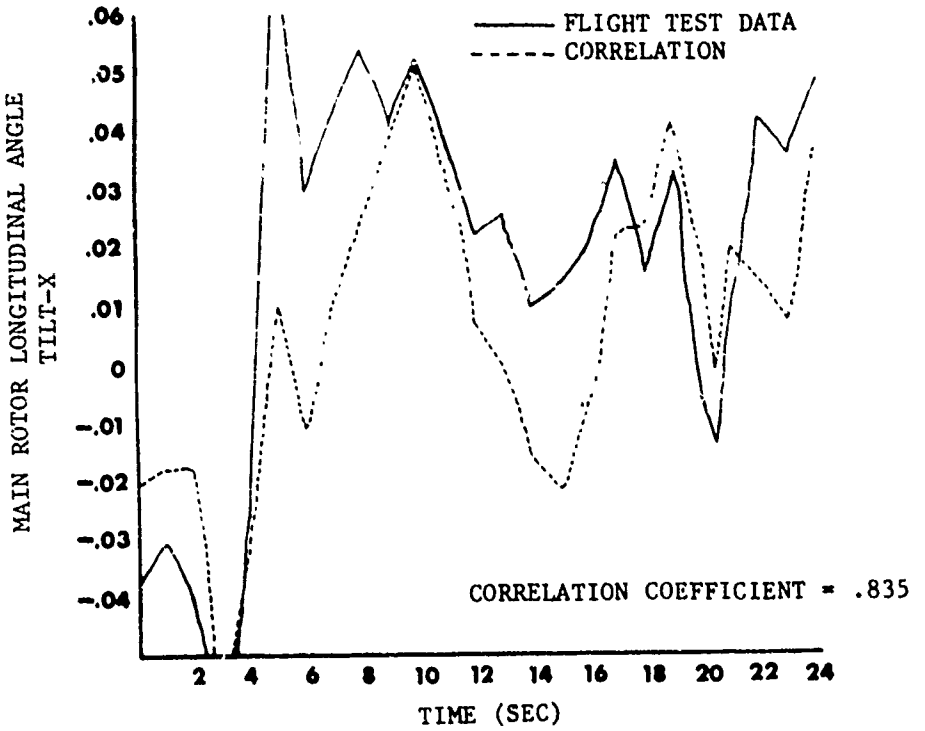

Figure O. Main Rotor Longitudinal Angle Correlation.

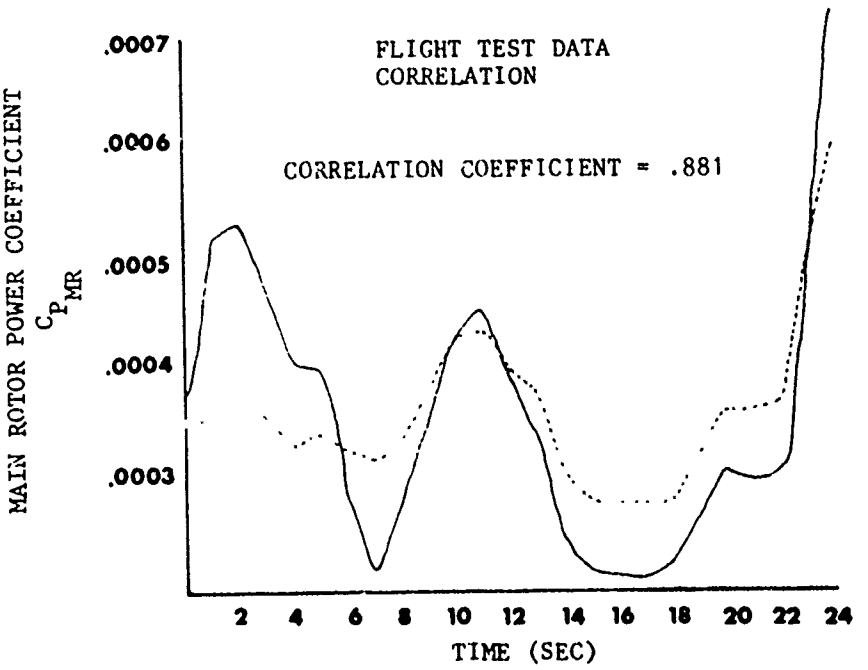

Figure P. Main Rotor Power Correlation.

Model

54. The primary function of the mathematical model is to predict aircraft performance, given initial conditions and subsequent control and power changes.

55. The method used is basically the inverse of the data processing to this point. Coefficients from the correlation equations are used to predict the six parameters in the CORCOF subroutines. These in turn are used to calculate powers and component forces, which are put in force and power balance equations. The resulting linear and angular accelerations are manipulated to determine velocities, distances, and attitudes. This procedure is looped for each time increment until the end of the flight. The flow is shown in figure Q.

56. The flight constants required are as follows:

a. Gross weight.

b. Density altitude (sigma).

c. I_{XX}, I_{yy}, I_{ZZ}.

d. X_{HS}, X_{TR}, Z_{TR} (fig. I).

e. ϵ (angle shaft axis makes with Zp axis).

f. I.

g. C_{D_X}, C_{D_y}, C_{D_Z}.

h. S_{xp}, S_{yp}, S_{zp}.

i. Wind velocity, wind direction, and aircraft heading.

j. Time increment for inputs.

57. Time zero values required are shown below:

a. Height above ground.

b. AS.

c. α.

d. β.

e. ϕ, θ, ψ.

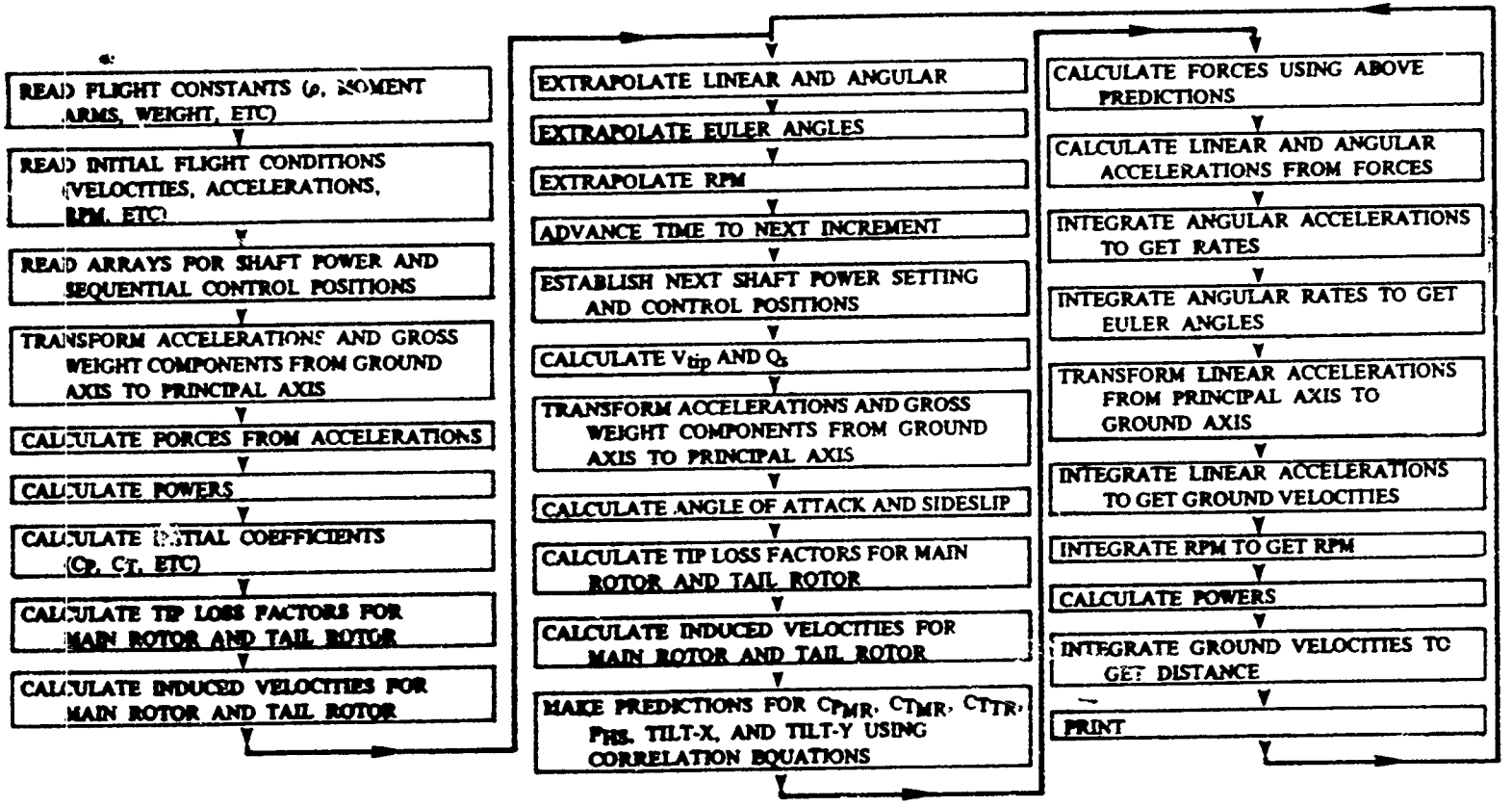

Figure Q. Height Velocity Mathematical Model Chart.

f. $\dot{\phi}$, $\dot{\theta}$, $\dot{\psi}$.

g. $\ddot{\phi}$, $\ddot{\theta}$, $\ddot{\psi}$.

h. N_r, $\dot{N}_r$.

i. A_{xg}, A_{yg}, A_{zg}.

j. $C_{T_{MR}}$, $C_{T_{MR}}$, $C_{P_{MR}}$, $C_{P_{TR}}$, TILT-X, TILT-Y, F_{HS}

k. P_{Sft}.

l. $(P_i + P_o)$.

58. Values required for each time increment are as follows:

a. δ_c, δ_e, δ_a, δ_r.

b. P_{Sft}.

59. Values output by the model are listed below:

a. ϕ, θ, ψ.

b. $\dot{\phi}$, $\dot{\theta}$, $\dot{\psi}$.

c. $\ddot{\phi}$, $\ddot{\theta}$, $\ddot{\psi}$.

d. Q_s.

e. $C_{T_{MR}}$, $C_{P_{MR}}$, $C_{T_{TR}}$, F_{HS}, TILT-X, TILT-Y.

f. $\nu_{i_{MR}}$, $\nu_{i_{TR}}$.

g. B_{MR}, B_{TR}.

h. λ_{MR}, λ_{TR}, μ_{MR}, μ_{TR}.

i. α, β.

j. AS.

k. N_r, $\dot{N}_r$.

l. F_{MR}, F_{TR}, F_D.

m. A_{xp}, A_{yp}, A_{zp}, A_{xg}, A_{yg}, A_{zg}.

n. V_{xg}, V_{yg}, V_{zg}.

o. X_g, Y_g, Z_g, and ground height.

Model Results

60. The accuracy of the model is clearly dependent on its ability to make good predictions of $C_{T_{MR}}$, $C_{T_{TR}}$, $C_{P_{MR}}$, F_{HS}, TILT-X, and TILT-Y, using the A_i coefficients from CORA. The suitability of the A_i coefficient can be measured by the correlation coefficient generated for each parameter in CORA. A chart showing correlation coefficient ranges for all flights is shown in table 1 (1.0 is maximum correlation).

Table 1.

Parameter	Correlation Coefficient	
	Range	(Mean)
$C_{T_{MR}}$	.710 to .983	(.896)
$C_{T_{TR}}$	.732 to .965	(.819)
$C_{P_{MR}}$	.792 to .964	(.850)
F_{HS}	.147 to .660	(.326)
TILT-X	.474 to .892	(.699)
TILT-Y	.291 to .814	(.658)

61. Generally speaking, $C_{T_{MR}}$, and $C_{P_{MR}}$ are performance parameters and $C_{T_{TR}}$, F_{HS}, TILT-X and TILT-Y are attitude parameters. From table 1, it could be expected that performance values (velocity, rotor speed, distance, etc.) would be reasonably accurate, while attitude values (yaw, pitch, roll, and angular rates) would show considerable error.

62. It should be noted that the predictions represented in figures K through P are obtained using variables calculated from flight test data in FEAP or COREDATA. In the model, these variables (μ, λ, etc.) are calculated using model-generated data. Therefore, errors in one parameter will eventually affect the other parameters, and their effect will continue to be cumulative. For example, an error in TILT-X will change aircraft attitude, which, in turn, will affect μ and λ, as well as changing the magnitude and direction of the force vectors.

63. As part of the model check-out procedure, model flights were made to duplicate flights actually flown. These were originally done using only one or two correlation equations and reading the other parameters from FEAP or CORCOF. Additional correlation equations were added one at a time. Good accuracy was maintained using $C_{T_{MR}}$, $C_{T_{TR}}$, and $C_{P_{MR}}$ together. Figure R shows predictions for flares using correlation equations for $C_{T_{MR}}$, $C_{T_{TR}}$, and $C_{P_{MR}}$. However, inclusion of each successive equation lessened accuracy to the point where the model output was of little value.

64. The reasons for poor correlation on F_{HS}, TILT-X, and TILT-Y are indeterminate. However, the two most obvious possibilities are inadequate test instrumentation and/or correlation on wrong or incomplete variables.

65. Considerable research and experimentation was spent on arriving at suitable correlation equations. A decision was made early in the program not to attempt any sophisticated rotor dynamics analysis. An inclusion of this sort of analysis may (or may not) have increased accuracy for TILT-X and TILT-Y.

66. The test instrumentation was, at best, minimal for data generation of the required accuracy. Correlation was made on data which had been smoothed several times, integrated, and generally manipulated to a great extent. Each operation may have introduced additional error.

67. The model would give excellent results if accurate and reliable predictions could be made for the six driving parameters. This was demonstrated in the check-out phase of the model. However, the major problem of predicting the six parameters remains.

68. Because the errors were mainly in attitude control, it was felt that it would be appropriate to experiment with a simpler two-dimensional model in which aircraft attitude is an input parameter.

SIMPLIFIED TWO-DIMENSIONAL HELICOPTER PERFORMANCE MODEL

General

69. Two-dimensional helicopter performance simulation has been used at USAAEFA since 1968. In the past, insufficient documentation and outdated programming limited their application to H-V testing. However, performance modeling can provide useful analytical information, and was recently updated to provide simplified input and operation.

70. The general theory behind this modeling concept was to obtain flight path and power data from flight test, and to modify basic momentum theory to predict the actual flight path. The simplified model is mathematically valid for any flight condition from vertical to forward flight. The analysis can also be extended to the same conditions in lateral flight. The elimination of one degree of freedom and simplification of the force balance model significantly reduces the complexity of the three-dimensional model previously discussed. Also, all flight parameters except profile power are directly calculated by basic momentum theory rather than the correlation equations previously described.

Force Balance

71. To determine the forces acting on the helicopter, Newton's Second Law is used to sum the exterior forces acting at the hub to obtain the linear acceleration of the hub. In general, the unbalanced forces acting along each axis cause an acceleration of the mass in the direction of the axial force imbalance; or,

$$\Sigma F_i = ma_i \tag{61}$$

Where:

i = A specific axis of a two-dimensional orthogonal reference system

(i = 1 implies the X or horizontal earth axes, and i = 2 implies the Z or vertical earth axis.)

Then,

F_{MR} = Thrust output of the rotor.

θ = Pitch attitudes (positive, nose up).

γ = Flight path angle (positive for positive rate of sink) (positive V_y).

V_X = Forward horizontal velocity of the aircraft.

V_Z = Vertical velocity of the aircraft (positive downward).

V = Inertial velocity of the aircraft (ground velocity).

F_D = Drag caused by the flat plate area of all nonlifting surfaces on the helicopter.

α_r = Angle of attack to the rotor disc (positive when inflow is from below the rotor).

72. It should be noticed that drag as shown in figure R is applied at the hub, producing no moment about the hub. In actuality, drag acts at the cg, producing a moment about the hub. In this derivation, it is assumed that the drag moment about the hub is cancelled by an equal and opposite aerodynamic moment of the rotor. When making this assumption, the force balance does not account for angular motion of the aircraft about the hub. Therefore, the angular rotation of the aircraft is negligible in comparison with the linear motion.

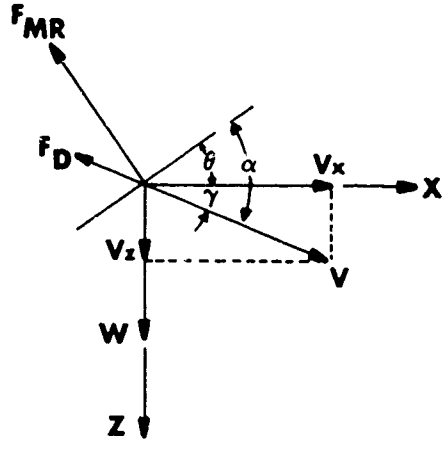

Figure R. Force and Drag Balance.

73. Summing forces along the X axis by reference to figure S,

$$ma_x = -F_{MR} \sin\theta - F_D \cos\gamma \tag{62}$$

Where:

$$m = Wgt/g$$

Summing forces along the Z axis,

$$ma_z = W - F_{MR} \cos\theta - F_D \sin\gamma \tag{63}$$

From figure R, figure S can be drawn to determine V', which is the inflow velocity at the rotor as defined in the momentum equation.

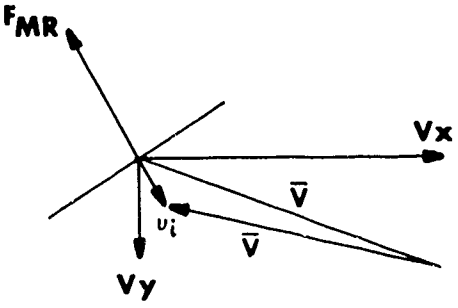

Figure S. Main Rotor Force and Velocity.

In vector notation,

$$\bar{V}' = \bar{V} + \bar{v}_i \tag{64}$$

Summing components along the thrust axis and the projection of the X axis in the rotor disc plane,

$$(V')^2 = V^2 \cos^2\alpha_r + (V\sin\alpha_r - v_i)^2 \tag{65}$$

Then,

$$V' = V^2 \cos^2\alpha_r + (V \sin\alpha_r - v_i)^2 \tag{66}$$

Power Energy Equation

74. The two-dimensional model calculates thrust by first determining the amount of induced power (P_i) available at each new point from the general power energy equation defined by equation 67. The resulting expression for P_i is as follows:

$$P_i = P_{Sft} - P_o - P_p - \frac{dKE}{dt} - \frac{dPE}{dt} - \frac{dKE_{MR}}{dt} \qquad (67)$$

Each term may be calculated from the model input or flight path motion except for main rotor profile power (P_o). One general expression for profile power (ref 19, app A) is derived in terms of the mean blade drag coefficient (C_{D_o}) as shown in equation 68.

$$P_o = C_{D_o} * \frac{\sigma}{8} \rho A_{disc} V_{tip}^3 * (1 = 4.6\mu^2) \qquad (68)$$

Blade drag coefficient (C_{D_o}) is known to be variable with blade angle and flight conditions, and must be determined empirically. For the UH-1C simulation, C_{D_o} was calculated from the FEAP program from both autorotation and level flight data. For simplicity, the results were determined as a function of thrust coefficient (C_T) and rotor inflow ratio (λ) and shown in figures T and U. In forward level flight the relationship was also a function of airspeed or advance ratio (μ). At airspeeds below the airspeed for minimum power (V), the variation with λ was nonlinear, as shown by figure T. This indicates that the ($1 + 4.6\mu^2$) correction is not effective in linearizing the C_{D_o} term in low-speed flight, either due to the increased power acquired by the induced down load on the fuselage or due to the nonlinear variation of C_{D_o} with blade angle of attack. In the future, an induced power correction factor such as described in reference 23, appendix A, should be used to improve the low-speed C_{D_o} data. However, figure U indicates that the variation of C_{D_o} with λ is nearly linear for a constant C_T at high forward flight airspeeds. Figure U also shows that there were no trends of C_{D_o} from the available data for the values of λ between -.02 and .018. Therefore, a mean value of C_{D_o} of 0.12 was used in the model when operating in this range of λ. The primary factor affecting C_{D_o} in this region seemed to be the vertical speed, but time did not permit the additional correlation effort. Additional effort is required to determine the optimum parameter to replace in the C_{D_o} correlation. In higher autorotational descents ($\lambda > .018$), the C_{D_o} variation with C_T and λ was again evident, as shown in figure U. These empirical data are utilized by the model to compute profile power for any particular flight condition. The use of these empirical data forces the model to perform similarly to the actual helicopter from which the data were obtained.

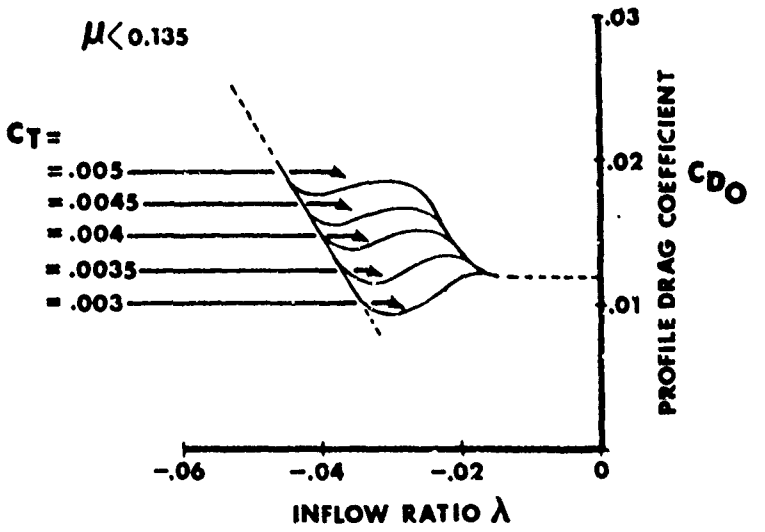

Figure T. Low Speed Blade Drag Coefficient.

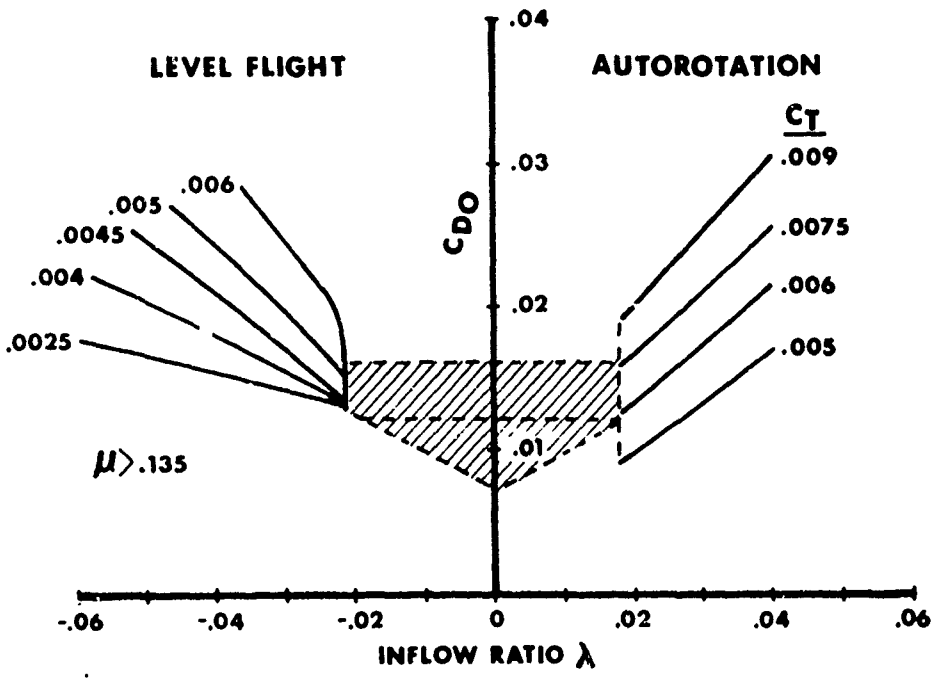

Figure U. High Speed and Autorotation Blade Drag Coefficient.

75. The model can then calculate the main rotor thrust by iterating on induced velocity (ν_i) simultaneously on two basic momentum theory equations derived in the data processing and analysis section of this appendix. These equations are expressed in terms of main rotor thrust, as shown below:

$$F_{MR} = P_i/\nu_i \tag{69}$$

$$F_{MR} = 2A_{disc}\, V'\nu_i\rho \tag{70}$$

Where V' is defined by equation 66.

Once the thrust is calculated for each new point, the flight path is integrated in the ground axes from the acceleration obtained from the simplified force balance in figure R. The computation for each new point requires an iterative solution of both thrust and C_{D_O}. Convergence normally occurs rapidly. However, some flight conditions, particularly at high descent rates and high deceleration, can cause extended calculations on the order of 30 seconds of computer time per point.

Model Input

76. The two-dimensional model is flown by inputting aircraft characteristics, initial conditions, and the engine power, rotor speed, and thrust vector at incremental time points. In figure V, the input was read from an actual flight path for the UH-1C helicopter. The model then calculated the thrust and integrated the flight path. The model is shown to be reasonably accurate. In addition to any error in the model techniques, variation of the model calculations from the flight path can be due to inaccuracies of initial velocities, lateral excursion from the x-z plane, and prevailing winds. The lateral excursion error would tend to cause the type of variation shown in figure V.

Flight Path Input

77. The two-dimensional model was also reorganized to permit input of a selected flight path. The experimental H-V profiles were first input to the model in the form of flight path time histories as shown in figures X through A-A. Additional flight profiles were also input to show the varying performance requirements at varying initial altitudes. The aircraft thrust vector and rotor speed for each flight path were calculated by the force balance and energy power equations previously discussed. In all simulations shown, decreasing entry height required increasing pushover and flare rates and attitudes. The reduced time spent in the dive and the lower rotor energy is readily apparent. The value of pilot judgment is clearly illustrated by the shape and grouping of the curves. In figure W, the test entry at a 650-foot hover was considered the minimum for a realistic technique. The simulations at 700 and 800 feet are very close to the test case in terms of attitudes,

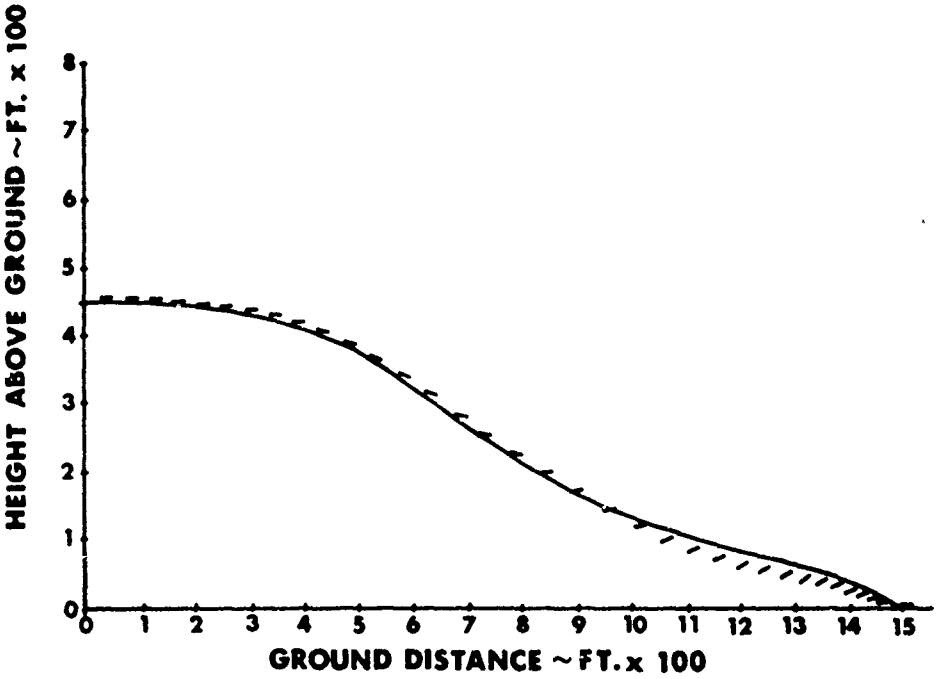

Figure V. Autorotational Landing Flight Path.

rotor energy, and time spent in the dive. However, lowering the entry height to 550 feet causes a discontinuity in the rotor speed curves. Further reductions in initial altitude clearly show that the maximum rotor speed that can be attained in the flare is very low, and the pushover attitudes rapidly exceed normal pilot tolerances. The importance of pitch attitude in the different flight path phases can be obtained by comparing the simulations at different airspeeds. For entry airspeeds on the back side of the power curve, increasing the H-V performance requires rapidly increasing nose-down attitudes as the initial height lessens. Flare attitudes remain relatively constant. For higher entry airspeeds the pushover attitude does not change results as significantly as does the flare attitude. The simulations at different entry airspeeds (figs. X, Y, and Z) were then used to construct the H-V diagrams shown in figure A-A. A family of calculated H-V curves were obtained by selecting a maximum pitch attitude during dive and flare. This is a reasonable approach, as an optimum H-V curve is largely a function of the pilot's ability to obtain the required pitch attitudes.

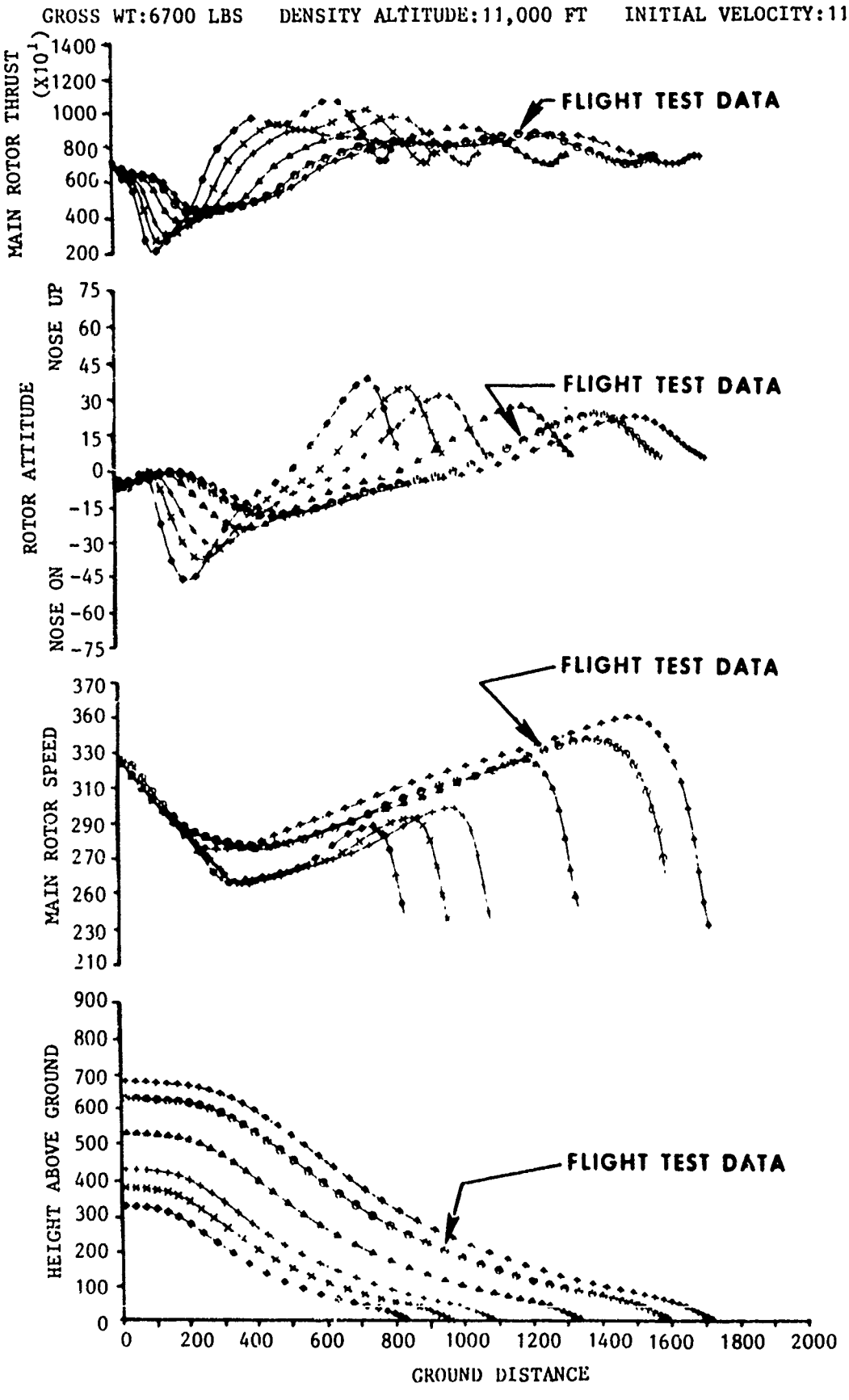

Figure W. Comparison of 2-Dimensional Model Predictions with Flight Test Data.

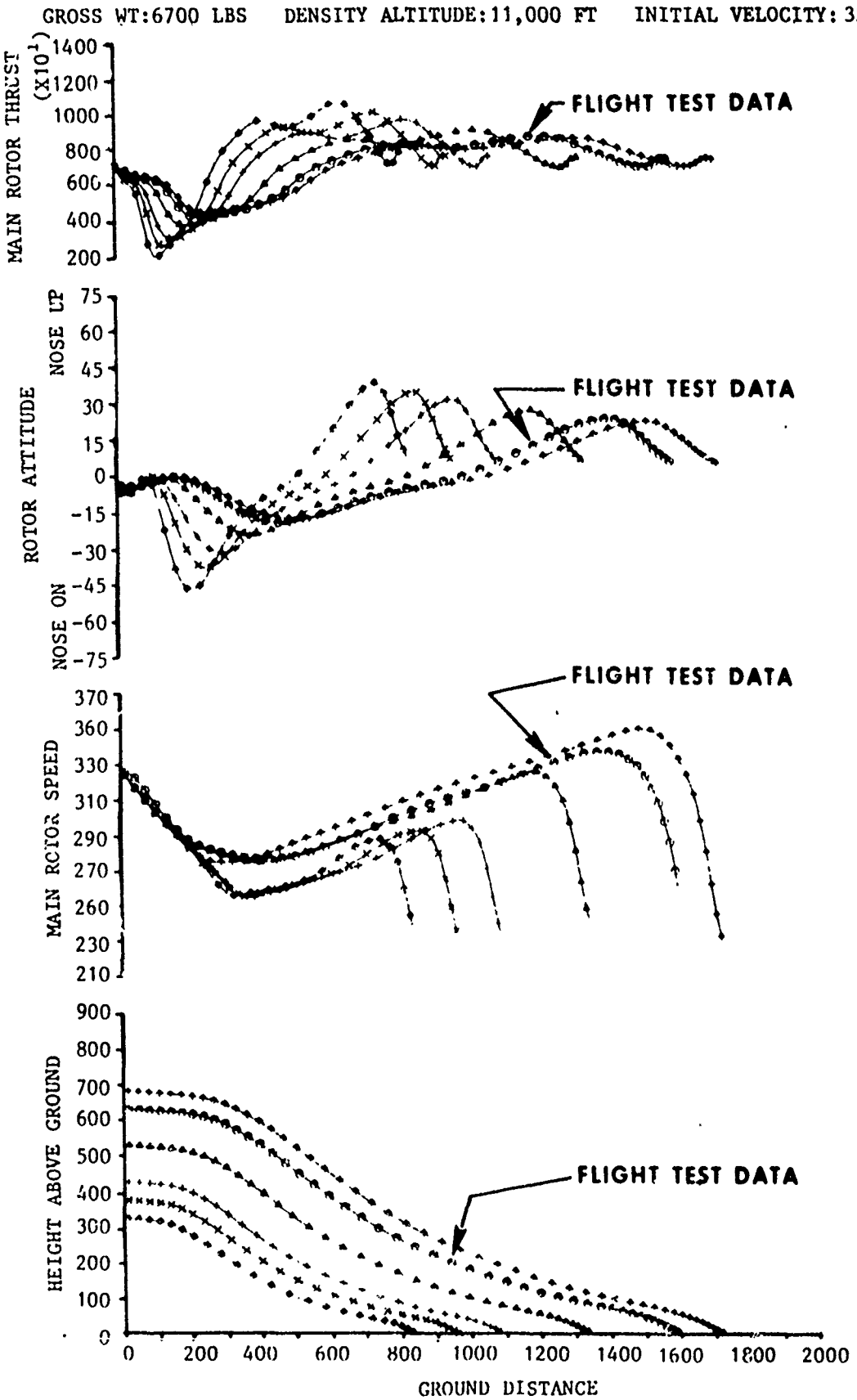

Figure X. Comparison of 2-Dimensional Model Predictions with Flight Test Data.

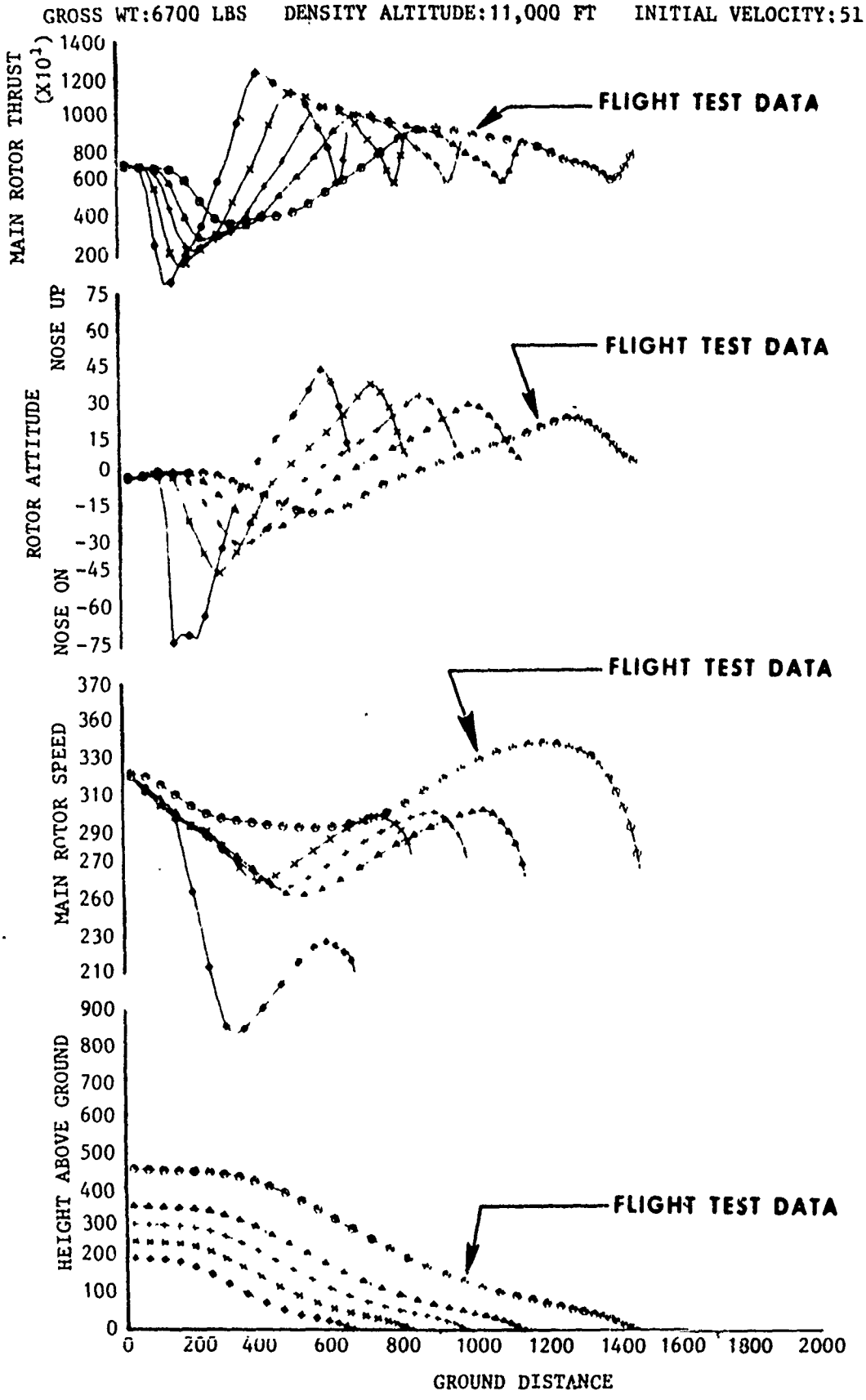

Figure Y. Comparison of 2-Dimensional Model Predictions with Flight Test Data.

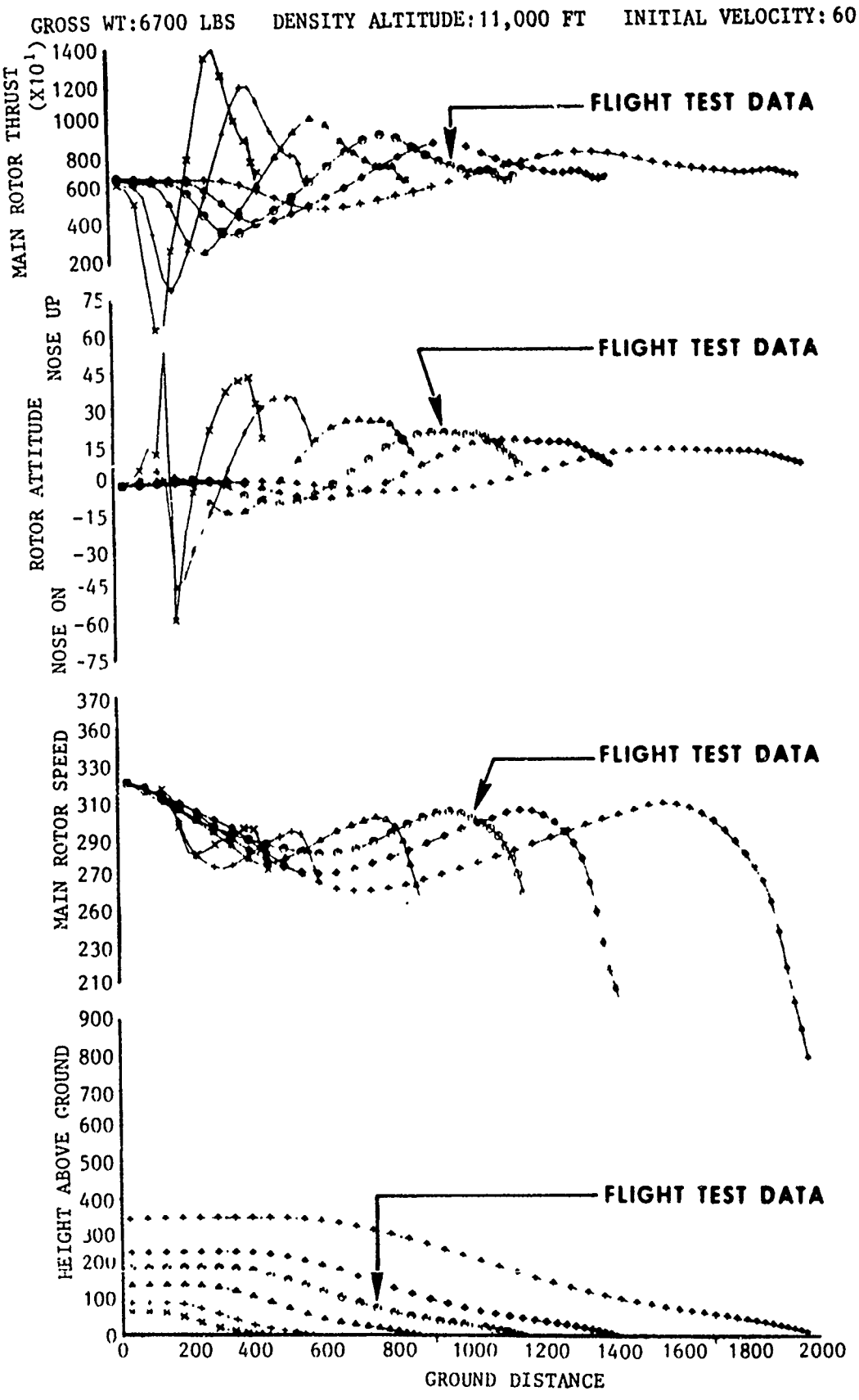

Figure Z. Comparison of 2-Dimensional Model Predictions with Flight Test Data.

FIGURE A-2
HEIGHT-VELOCITY DIAGRAMS FROM
TWO-DIMENSIONAL MODEL

NOTE:
1. Solid symbols denote test data.
2. Negative θ represents pushover and positive θ is the required flare attitude.
3. A_Z is the maximum vertical acceleration, generated during the flare.

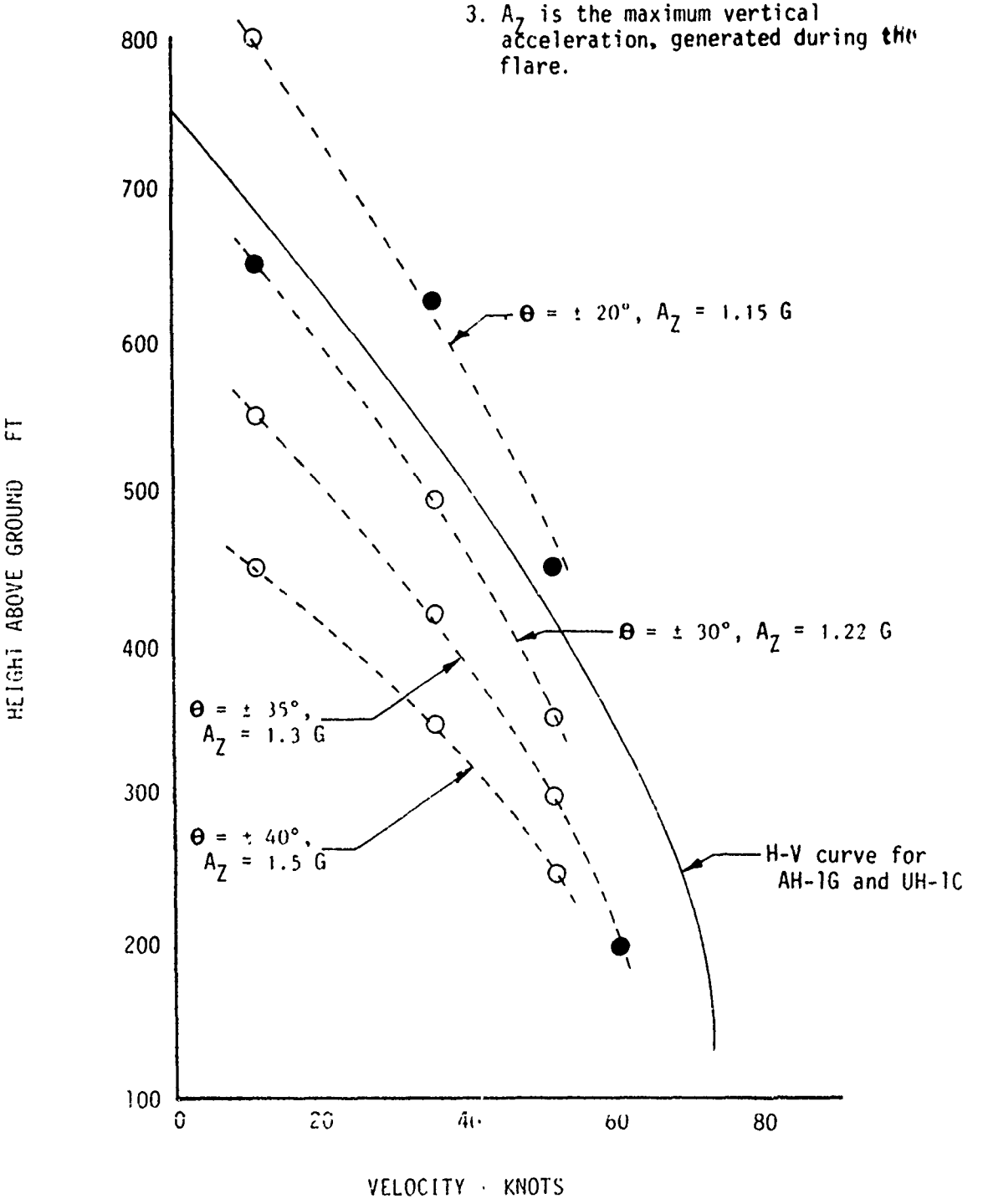

APPENDIX F. TEST DATA

INDEX

Flares

Landings

FIGURE 1-1

OPERATING CONDITIONS DURING LEVEL FLIGHT OF A LIGHT GROSS WEIGHT UH-1C

ROTOR SPEED = 324 RPM
GROSS WT = 6790 LB
THRUST COEFF = 0.00359
TOTAL LONGITUDINAL CONTROL TRAVEL = 12.7 IN.
TOTAL LATERAL CONTROL TRAVEL = 12.8 IN.
TOTAL DIRECTIONAL CONTROL TRAVEL = 7.0 IN.
TOTAL COLLECTIVE CONTROL TRAVEL = 10.4 IN.

USA TR 63-2054
DENSITY ALT = 1110 FT
AMB. TEMP = 15° C

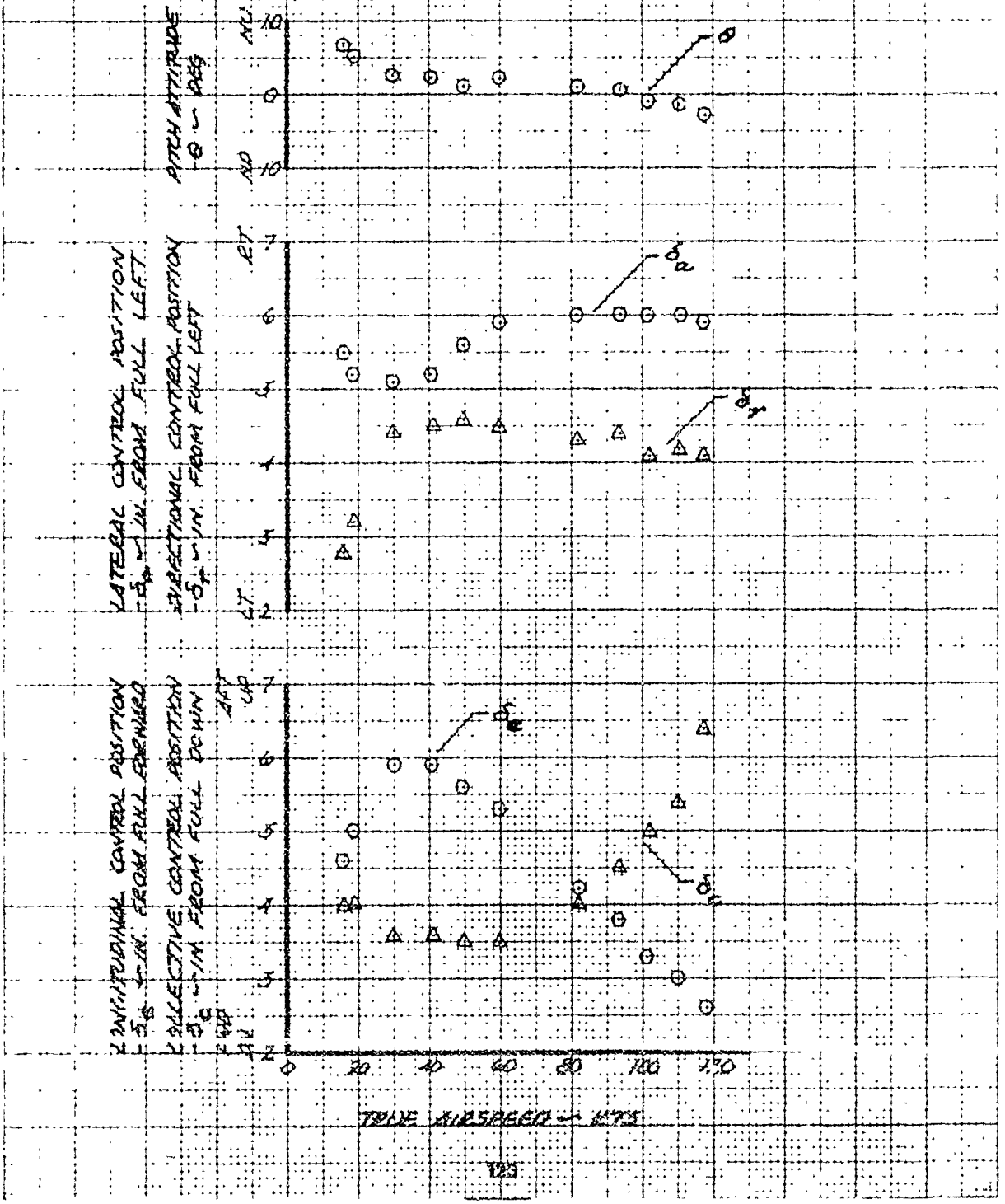

FIGURE 1-2

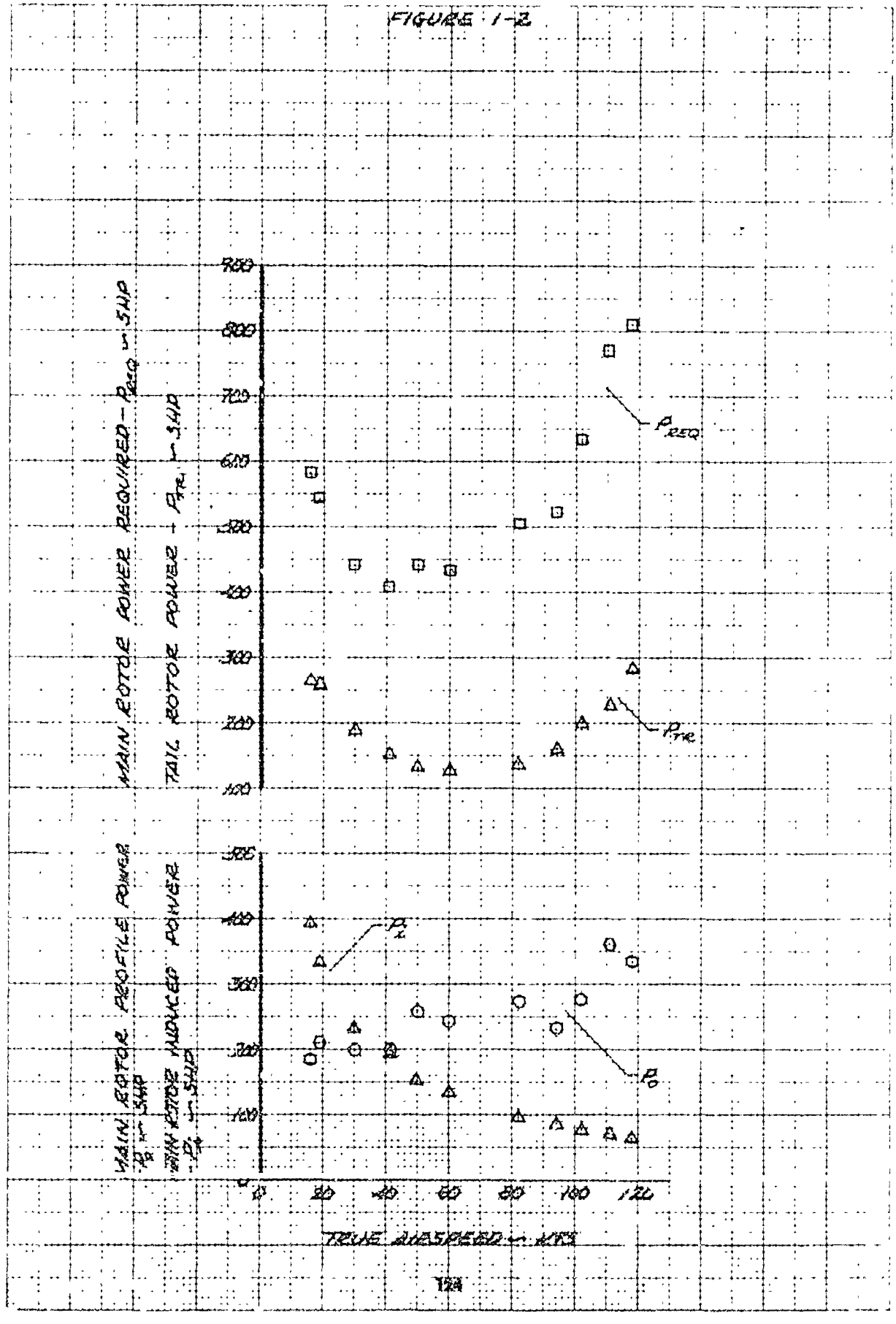
MAIN ROTOR POWER REQUIRED – P_{REQ} – SHP
TAIL ROTOR POWER – P_{TR} – SHP
MAIN ROTOR PROFILE POWER – P_o – SHP
MAIN ROTOR INDUCED POWER – P_i – SHP
P_{REQ}
P_{TR}
P_i
P_o
TRUE AIRSPEED – KTS

FIGURE 4-3

PARASITE POWER - P_p — SHP
TOTAL DRAG - D_T — LB
AIRSPEED - KNOTS TAS
TRUE AIRSPEED — KTAS

FIGURE 2-1

OPERATING CONVENTIONS DURING LEVEL FLIGHT AT A HEAVY GROSS WEIGHT

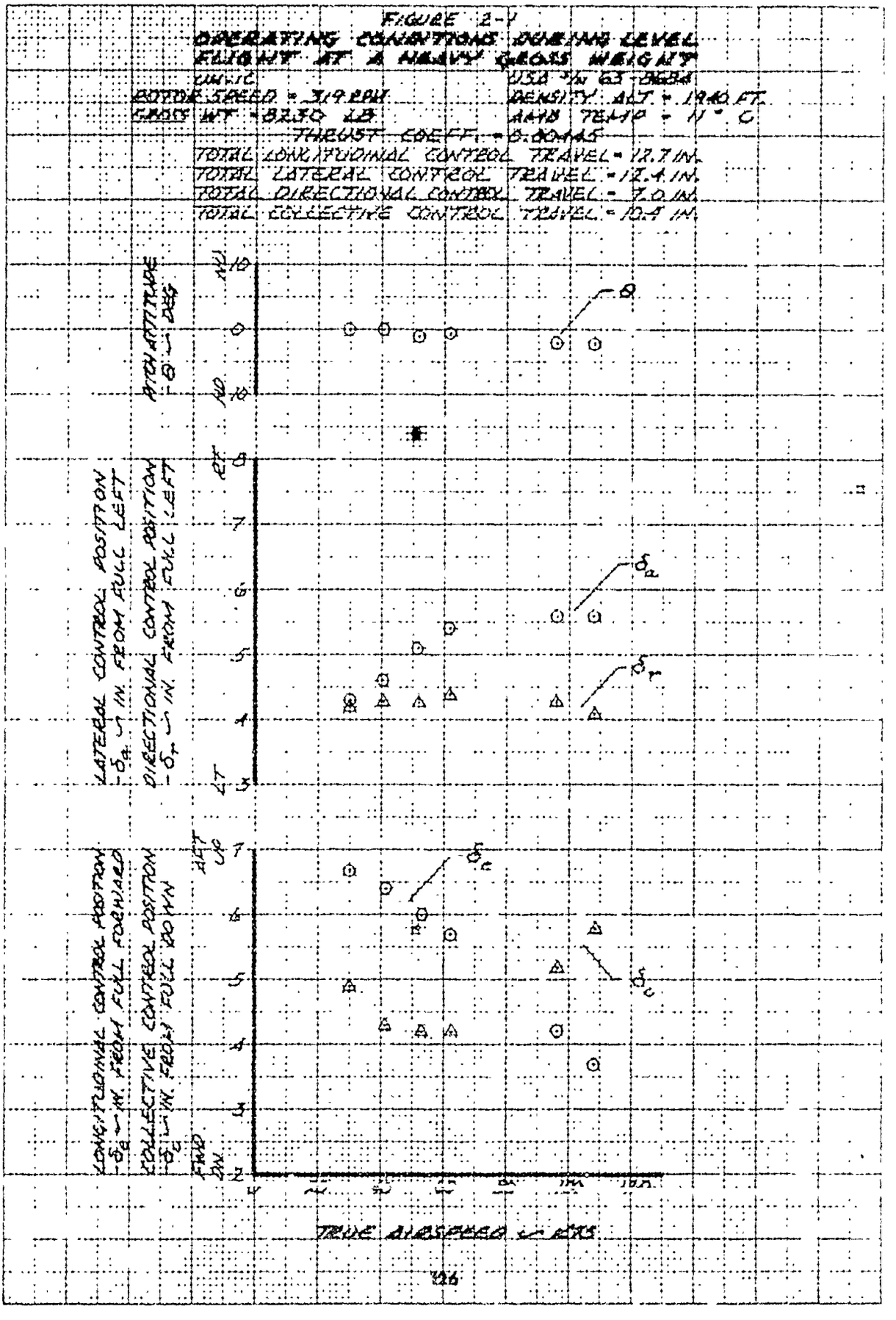

FIGURE 2-2

MAIN ROTOR PROFILE POWER
MAIN ROTOR INDUCED POWER
TAIL ROTOR POWER
MAIN ROTOR POWER REQUIRED - P_{REQ} — SHP
TAIL ROTOR POWER - P_{TR} — SHP
P_{REQ}
P_{TR}
P_I
P_O
TRUE AIRSPEED — KTS

FIGURE 2-5

PARASITE POWER - P_p — SHP
TOTAL DRAG - F_D — LB
KINETIC ENERGY
KE_{ss} — FT-LB
F_D
KE_{ss}
TRUE AIRSPEED — KTS

FIGURE 3-1

OPERATING CONDITIONS DURING REWARD CLIMB
UH-1C
USA 64-13684
ROTOR SPEED = 323 RPM
GROSS WT = 6920 LB
IND. TORQUE = 29 PSI
DENSITY ALT = 1020 FT
AMB. TEMP = 15 °C
THRUST COEFF = 0.00357
TOTAL LONGITUDINAL CONTROL TRAVEL = 12.7 IN.
TOTAL LATERAL CONTROL TRAVEL = 12.4 IN.
TOTAL DIRECTIONAL CONTROL TRAVEL = 7.0 IN.
TOTAL COLLECTIVE CONTROL TRAVEL = 10.2 IN.
RATE OF CLIMB - V_z - FT/MIN
PITCH ATTITUDE - θ - DEG
LATERAL CONTROL POSITION - δ_a - IN. FROM FULL LEFT
DIRECTIONAL CONTROL POSITION - δ_r - IN. FROM FULL LEFT
LONGITUDINAL CONTROL POSITION - δ_e - IN. FROM FULL FORWARD
COLLECTIVE CONTROL POSITION - δ_c - IN. FROM FULL DOWN
TRUE AIRSPEED - KTS

FIGURE 3-2
MAIN ROTOR POWER AVAILABLE - P_{AVAIL} - SHP
MAIN ROTOR POWER REQUIRED - P_{REQ} - SHP
TAIL ROTOR POWER - P_{TR} - SHP
MAIN ROTOR PROFILE POWER - P_o - SHP
MAIN ROTOR INDUCED POWER - P_i - SHP
PARASITE POWER - P_p - SHP
TOTAL DRAG - D_T - LB
AIRCRAFT KINETIC ENERGY - KE_{AC} - FT-LB x 10^-6
P_{AVAIL}
P_{REQ}
P_{TR}
P_o
P_i
P_p
D_T
KE_{AC}
0
20
40
60
80
100
120
TRUE AIRSPEED - KTS

FIGURE A-1

RAPID POWER REDUCTION FLOW DURING LANDING

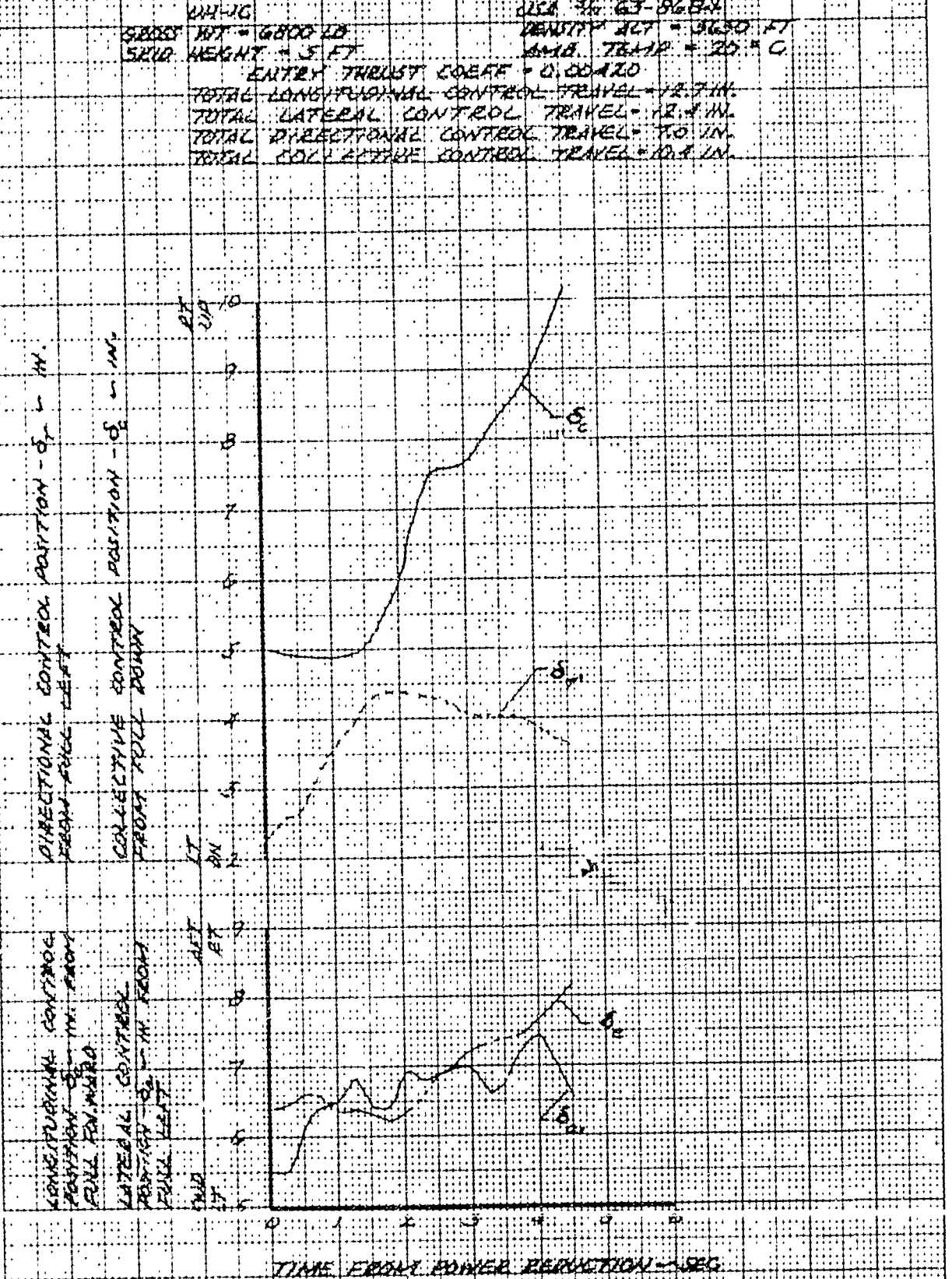

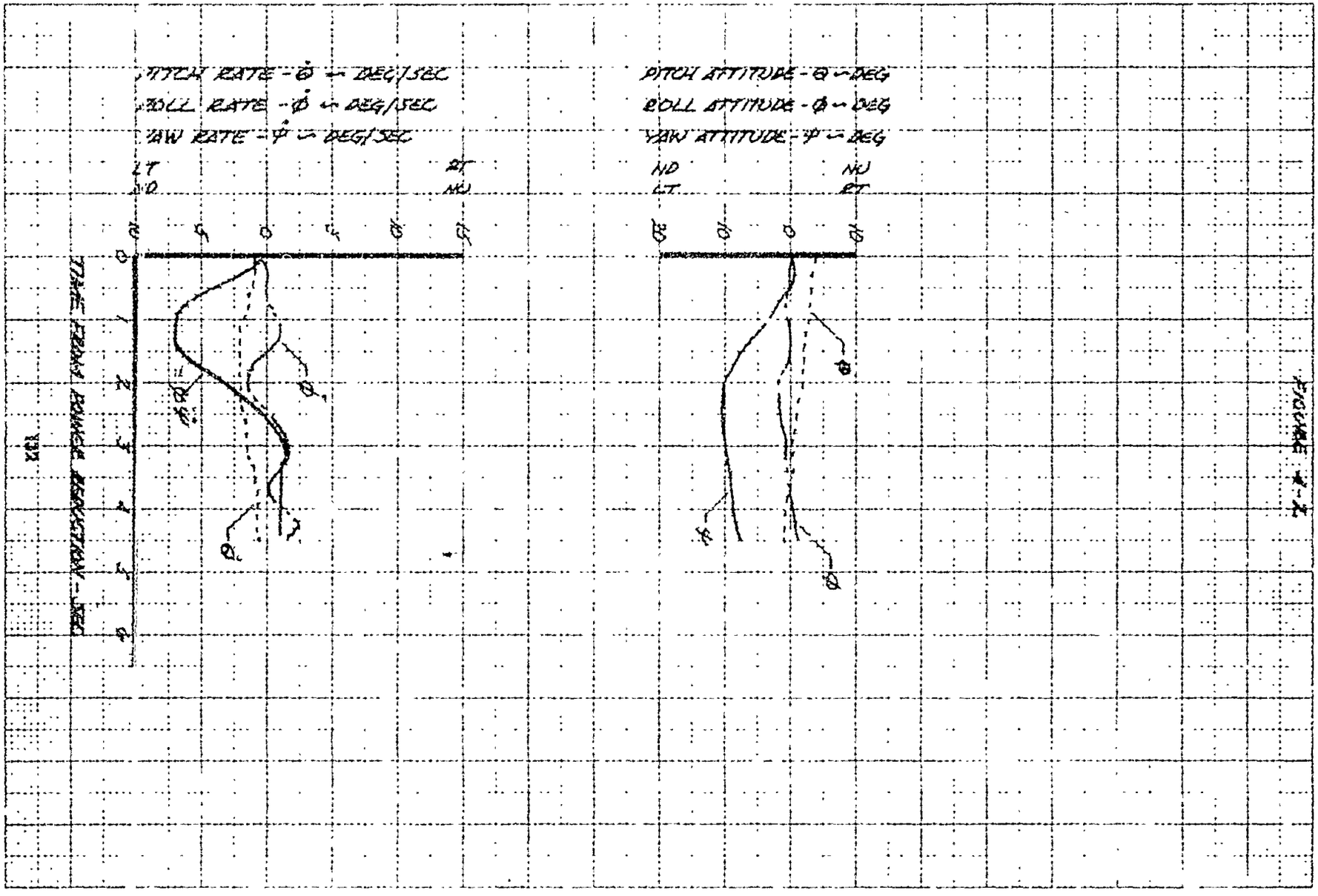
PITCH RATE - $\dot{\theta}$ ~ DEG/SEC
ROLL RATE - $\dot{\phi}$ ~ DEG/SEC
YAW RATE - $\dot{\psi}$ ~ DEG/SEC
PITCH ATTITUDE - θ ~ DEG
ROLL ATTITUDE - ϕ ~ DEG
YAW ATTITUDE - ψ ~ DEG
LT
RT
TIME FROM POWER DESCENT - SEC

FIGURE 4-2

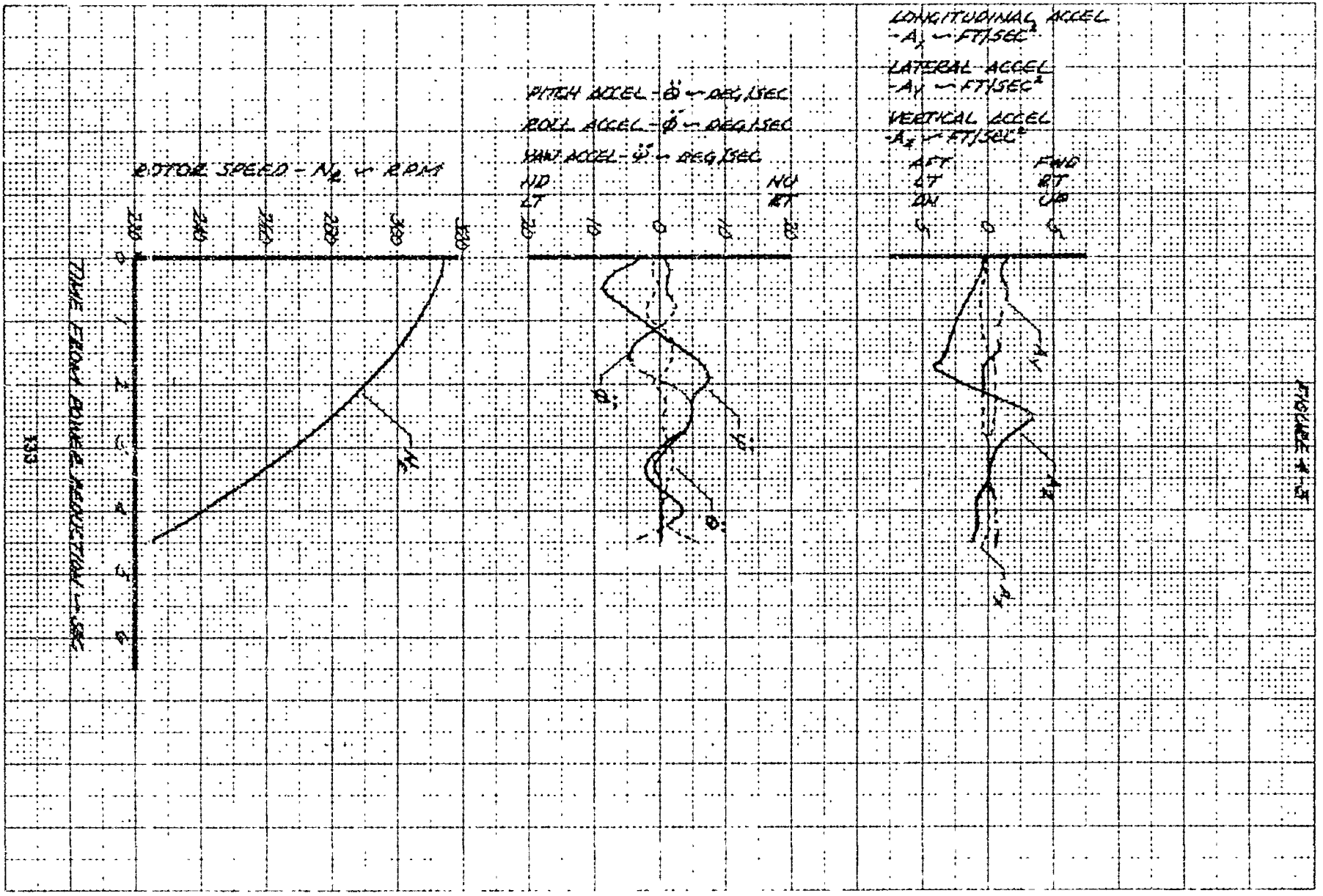
ROTOR SPEED - N_R - RPM
240
280
320
360
400
TIME FROM BOMB RELEASE - SEC
PITCH ACCEL - $\ddot{\theta}$ - DEG/SEC
ROLL ACCEL - $\ddot{\phi}$ - DEG/SEC
YAW ACCEL - $\ddot{\psi}$ - DEG/SEC
NU
RT
LONGITUDINAL ACCEL - A_x - FT/SEC^2
LATERAL ACCEL - A_y - FT/SEC^2
VERTICAL ACCEL - A_z - FT/SEC^2
AFT
FWD
RT
DN
A_x
A_y
A_z

FIGURE 4-31

FIGURE 4-4

MAIN ROTOR THRUST - T_{MR} - LB
TAIL ROTOR THRUST - T_{TR} - LB
10000
9000
8000
7000
6000
400
300
200
100
0
T_{TR}
T_{MR}
MAIN ROTOR INDUCED POWER - P_i - SHP
MAIN ROTOR PROFILE POWER - P_o - SHP
600
500
400
300
200
100
0
P_i
P_o
0
1
2
3
4
5
6
TIME FROM POWER REDUCTION - SEC

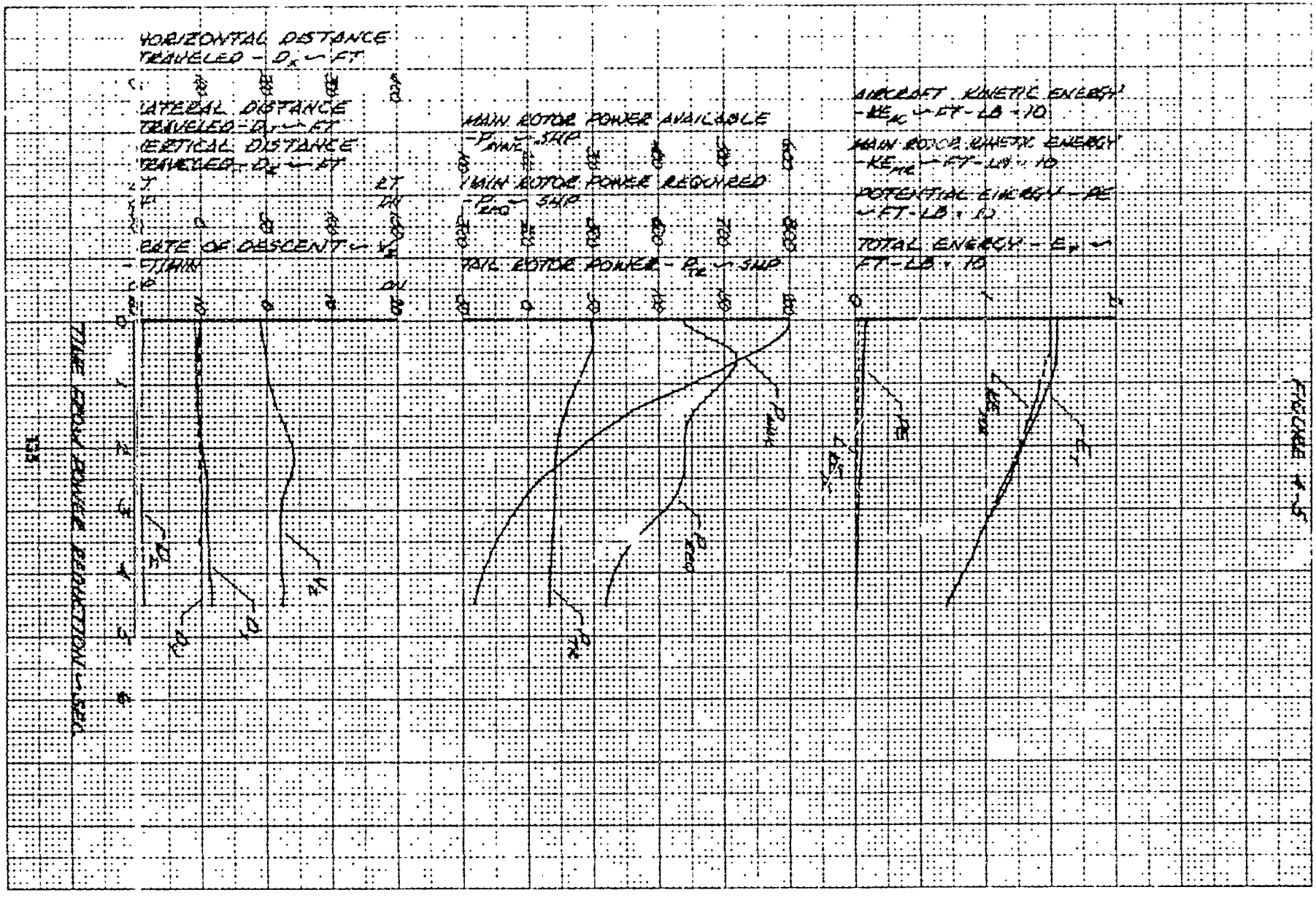
HORIZONTAL DISTANCE TRAVELED - D_x - FT
LATERAL DISTANCE TRAVELED - D_y - FT
VERTICAL DISTANCE TRAVELED - D_z - FT
RATE OF DESCENT - V_z - FPM
TIME FROM POWER REDUCTION - SEC
MAIN ROTOR POWER AVAILABLE - P_{AVAIL} - SHP
MAIN ROTOR POWER REQUIRED - P_{REQ} - SHP
TAIL ROTOR POWER - P_{TR} - SHP
AIRCRAFT KINETIC ENERGY - KE_{AC} - FT-LB x 10
MAIN ROTOR KINETIC ENERGY - KE_{MR} - FT-LB x 10
POTENTIAL ENERGY - PE - FT-LB x 10
TOTAL ENERGY - E_T - FT-LB x 10

FIGURE 4-5

FIGURE 4-6

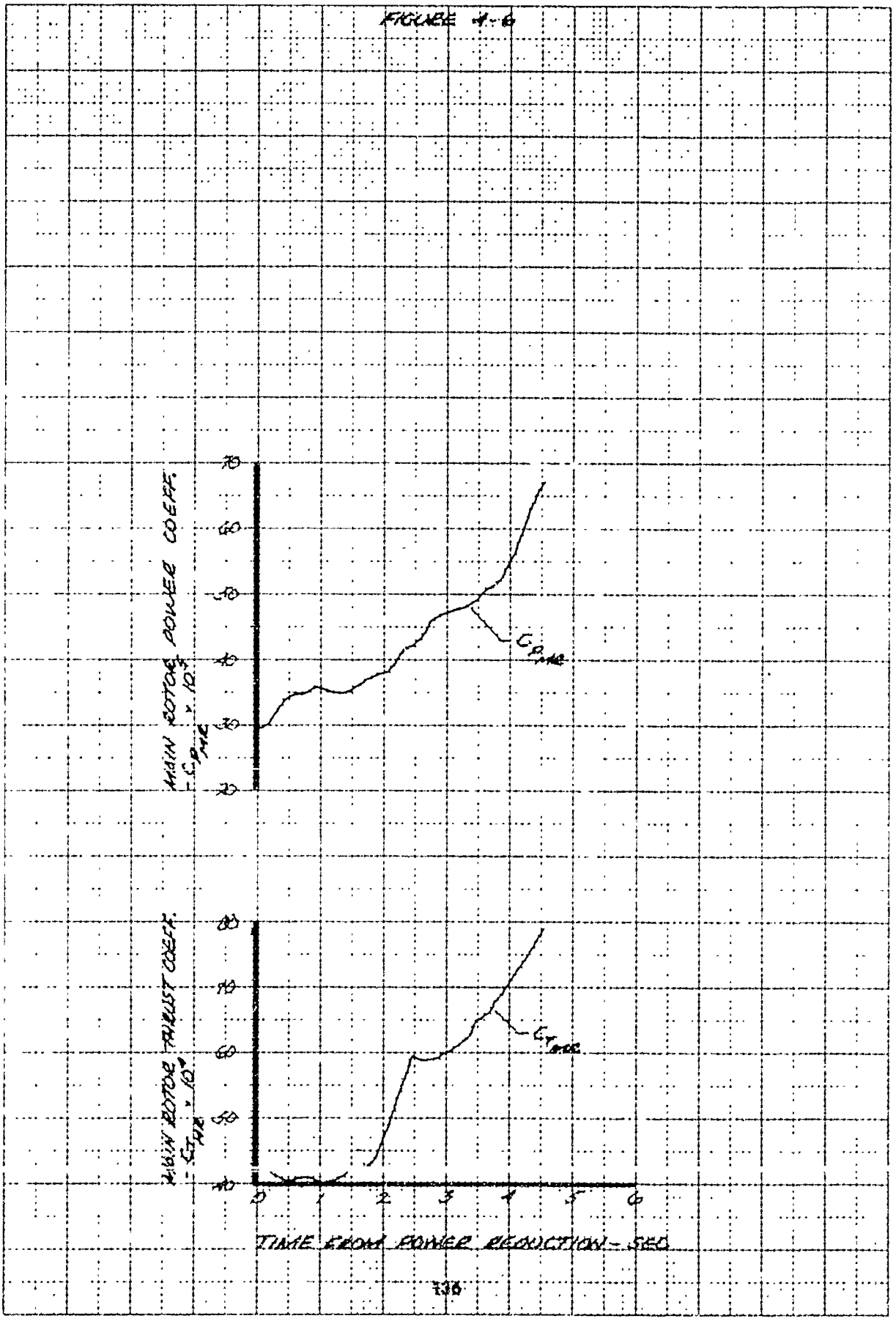
MAIN ROTOR POWER COEFF. - $C_{P_{MR}} \times 10^3$
70
60
50
40
30
20
$C_{P_{MR}}$
MAIN ROTOR THRUST COEFF. - $C_{T_{MR}} \times 10^3$
80
70
60
50
40
$C_{T_{MR}}$
0
1
2
3
4
5
6
TIME FROM POWER REDUCTION - SEC

FIGURE 5-1

RADIO POWER REDUCTION MANEUVER
SLOW SPEED FORWARD FLIGHT
CAP-TO
GROSS WT = 6750 LB
ENTRY WEIGHT = 19 LBS
ENTRY THRUST COEF = 0.00374
TOTAL LONGITUDINAL CONTROL TRAVEL = 12.7 IN.
TOTAL LATERAL CONTROL TRAVEL = 12.4 IN.
TOTAL DIRECTIONAL CONTROL TRAVEL = 4.6 IN.
TOTAL COLLECTIVE CONTROL TRAVEL = 10.4 IN.
ANGLE OF ATTACK OR SIDESLIP - DEG
TIME FROM POWER REDUCTION - SEC

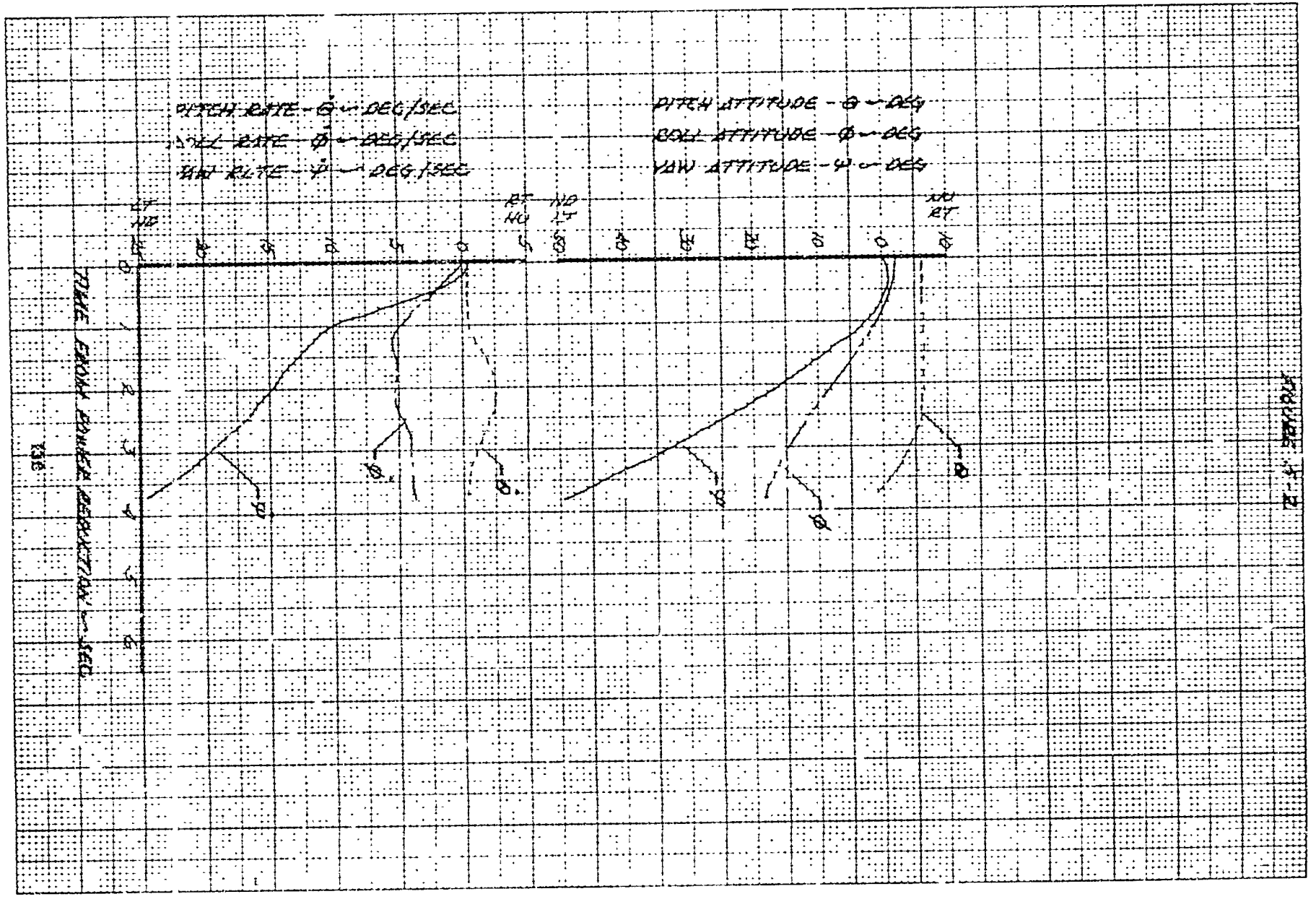
PITCH RATE - $\dot{\theta}$ - DEG/SEC
ROLL RATE - $\dot{\phi}$ - DEG/SEC
YAW RATE - $\dot{\psi}$ - DEG/SEC
PITCH ATTITUDE - θ - DEG
ROLL ATTITUDE - ϕ - DEG
YAW ATTITUDE - ψ - DEG
AT 140 KN
AT 100 KN
AT 40 KN
ϕ_x
ϕ_c
ψ
θ
ϕ
TIME FROM ENGINE FAILURE - SEC
136

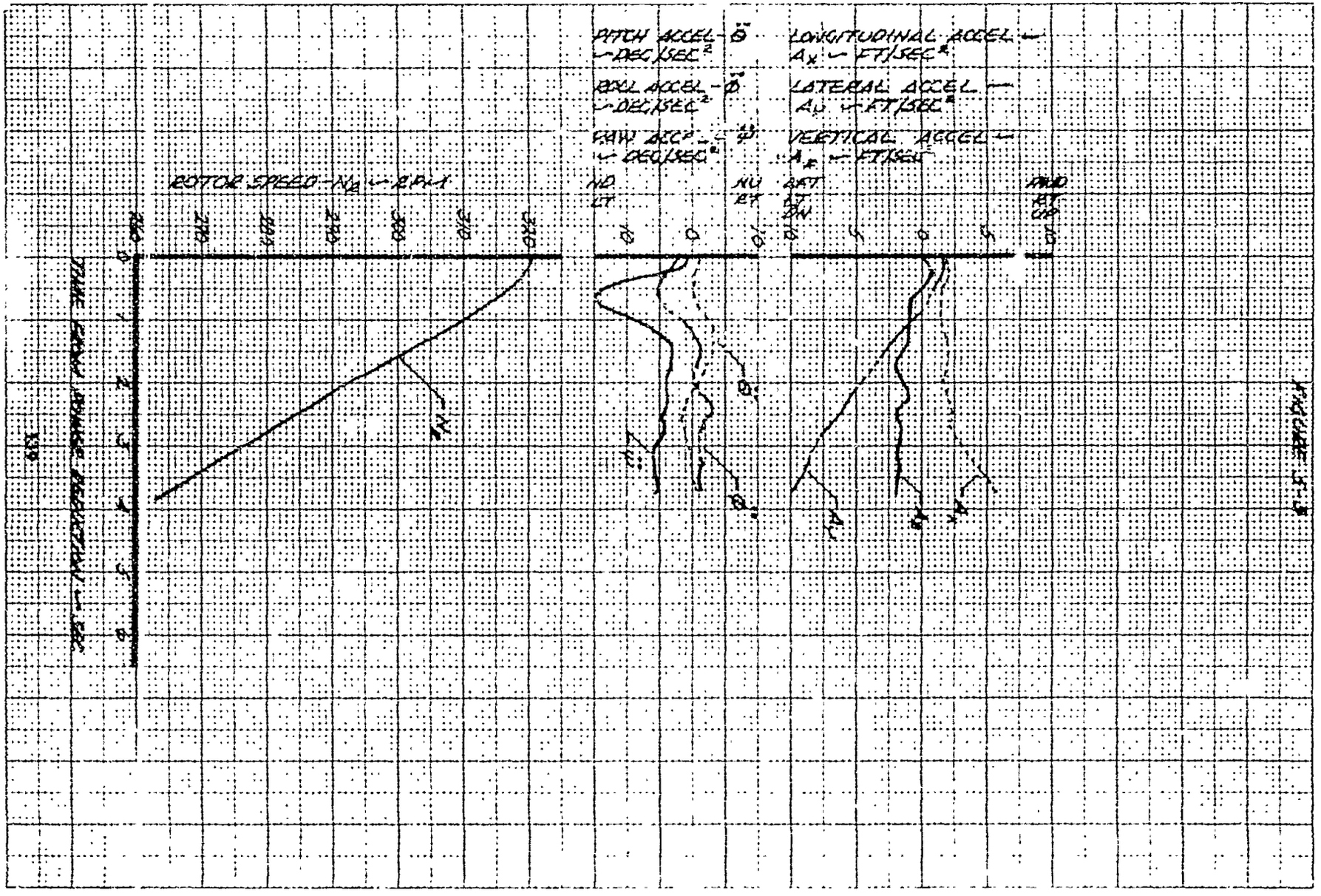
PITCH ACCEL - $\ddot{\theta}$ - DEG/SEC^2
ROLL ACCEL - $\ddot{\phi}$ - DEG/SEC^2
YAW ACC^N - $\ddot{\psi}$ - DEG/SEC^2
ROTOR SPEED - N_R - RPM
NO LT
NO RT
TIME FROM RELEASE - SEC
LONGITUDINAL ACCEL - A_X - FT/SEC^2
LATERAL ACCEL - A_Y - FT/SEC^2
VERTICAL ACCEL - A_Z - FT/SEC^2
AFT
LT
DN
AFT
OUT

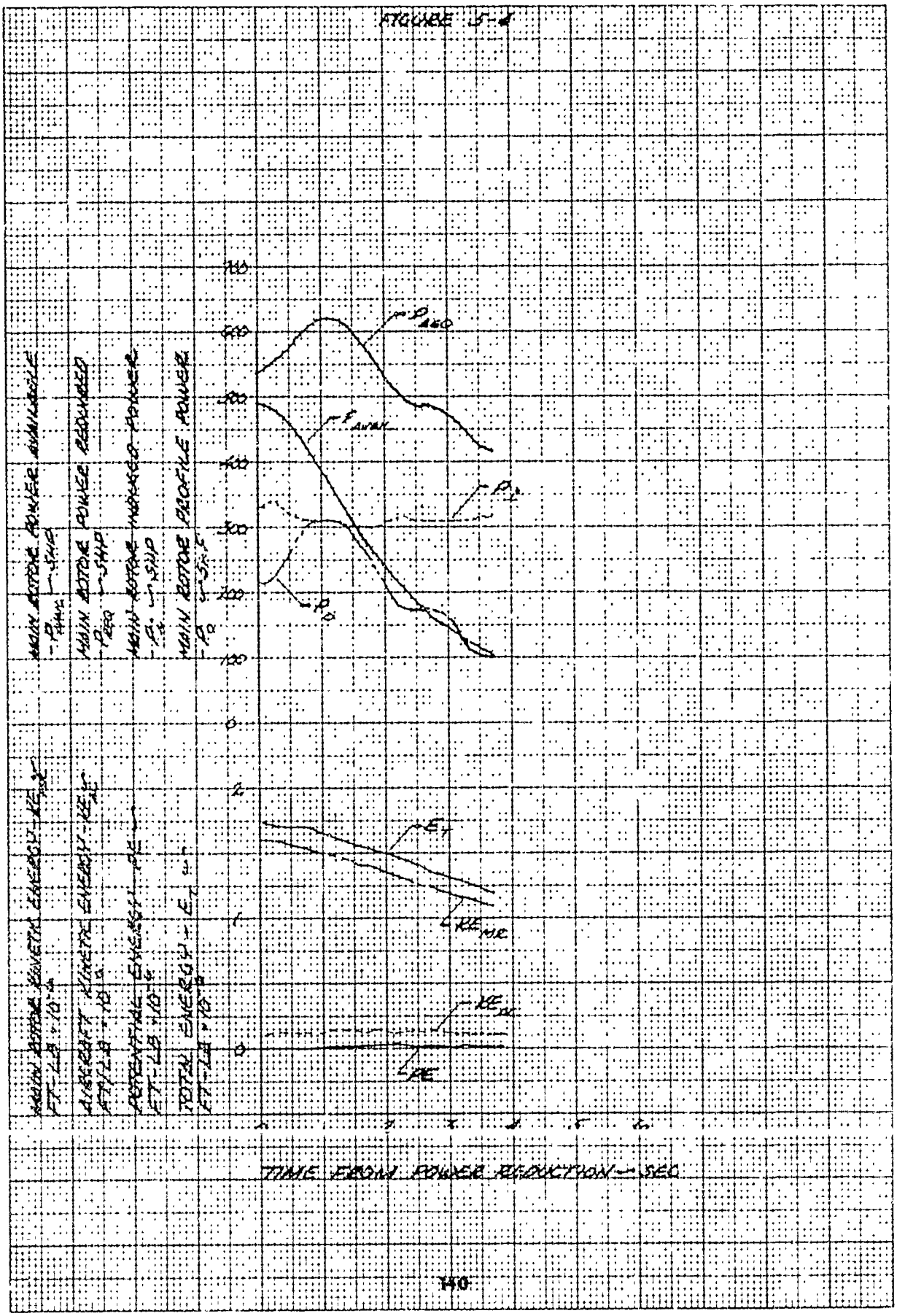
FIGURE 5-4
MAIN ROTOR POWER AVAILABLE
MAIN ROTOR POWER REQUIRED
MAIN ROTOR HARNESS POWER
MAIN ROTOR PROFILE POWER
ET-28 x 10⁻⁴
ET-28 x 10⁻⁴
ET-28 x 10⁻⁴
ET-28 x 10⁻⁴
TIME FROM POWER REDUCTION — SEC

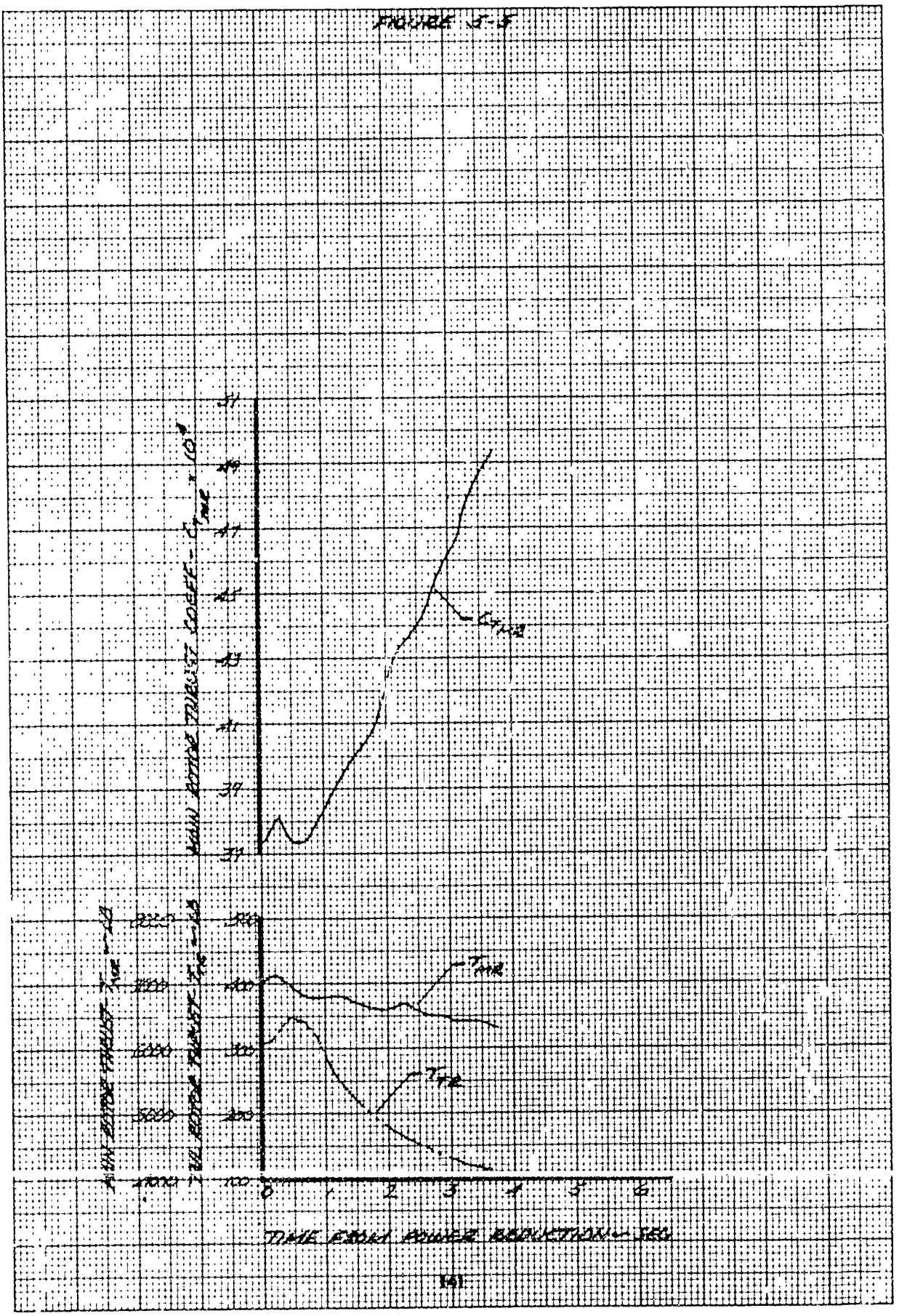
FIGURE 5-5
MAIN ROTOR THRUST COEFF - $C_{T_{MR}} \times 10^3$
MAIN ROTOR THRUST - T_{MR} - LB
TAIL ROTOR THRUST - T_{TR} - LB
TIME FROM POWER REDUCTION - SEC
T_{MR}
T_{TR}
$C_{T_{MR}}$

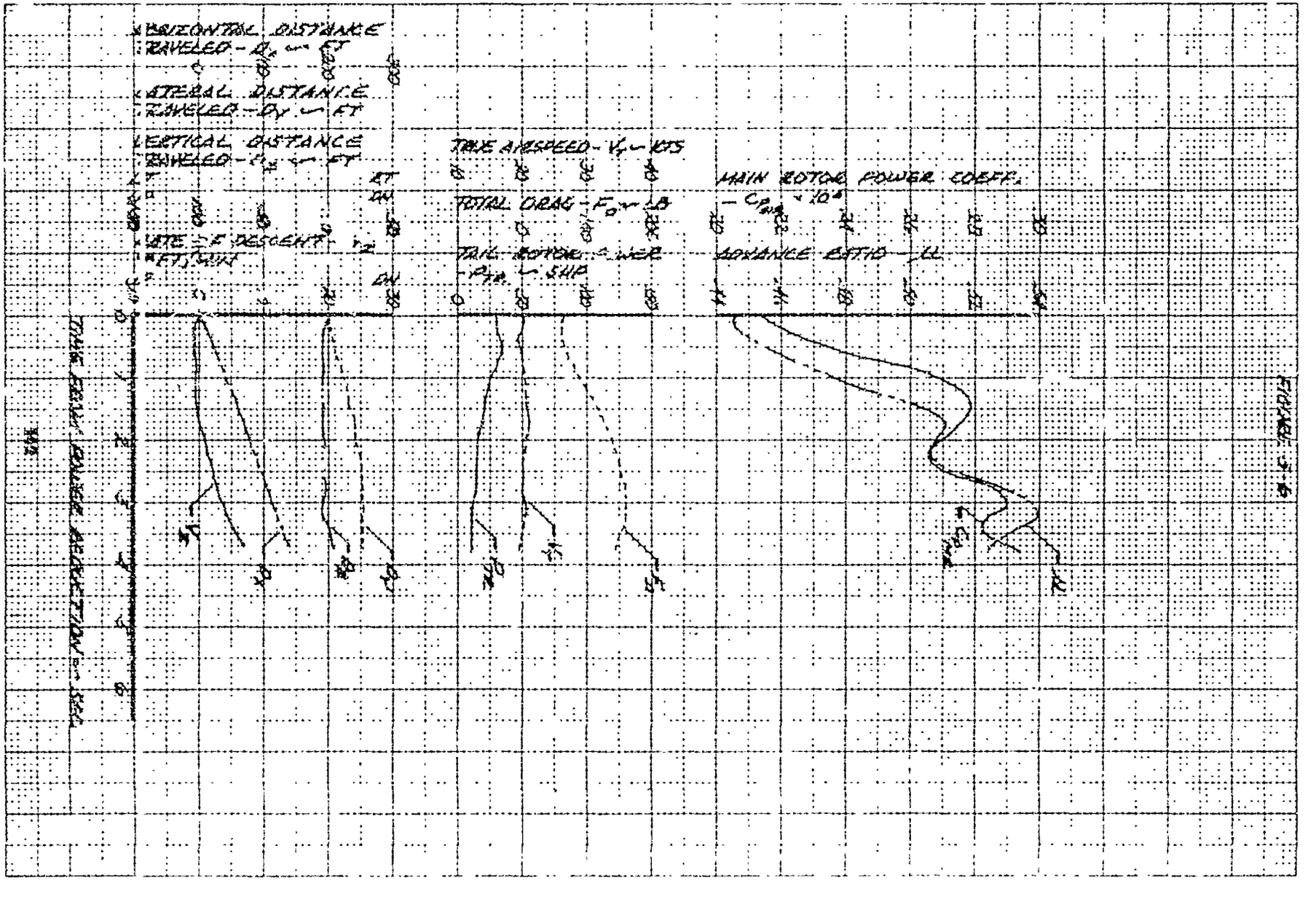
HORIZONTAL DISTANCE TRAVELED - D_x - FT
LATERAL DISTANCE TRAVELED - D_y - FT
VERTICAL DISTANCE TRAVELED - D_z - FT
RATE OF DESCENT - $\dot{h}$ FT/MIN
TRUE AIRSPEED - V_t - KTS
TOTAL DRAG - F_D - LB
TAIL ROTOR POWER - P_{TR} - SHP
MAIN ROTOR POWER COEFF. - $C_{P_{MR}} \times 10^6$
ADVANCE RATIO - μ
TOTAL FLIGHT TIME FROM RELEASE TO IMPACT - SEC

FIGURE 3-6

FIGURE 6-1

RAPID POWER REDUCTION DURING MEDIUM SPEED FORWARD FLIGHT

UH-1E

USA S/N 63-8684

GROSS WT = 6750 LB
ENTRY AIRSPEED = 60 KTS
ENTRY THRUST COEFF = 0.00361
DENSITY ALT = 1110 FT
AMB TEMP = 15° C

TOTAL LONGITUDINAL CONTROL TRAVEL = 12.7 IN.
TOTAL LATERAL CONTROL TRAVEL = 12.4 IN.
TOTAL DIRECTIONAL CONTROL TRAVEL = 7.0 IN.
TOTAL COLLECTIVE CONTROL TRAVEL = 10.4 IN.

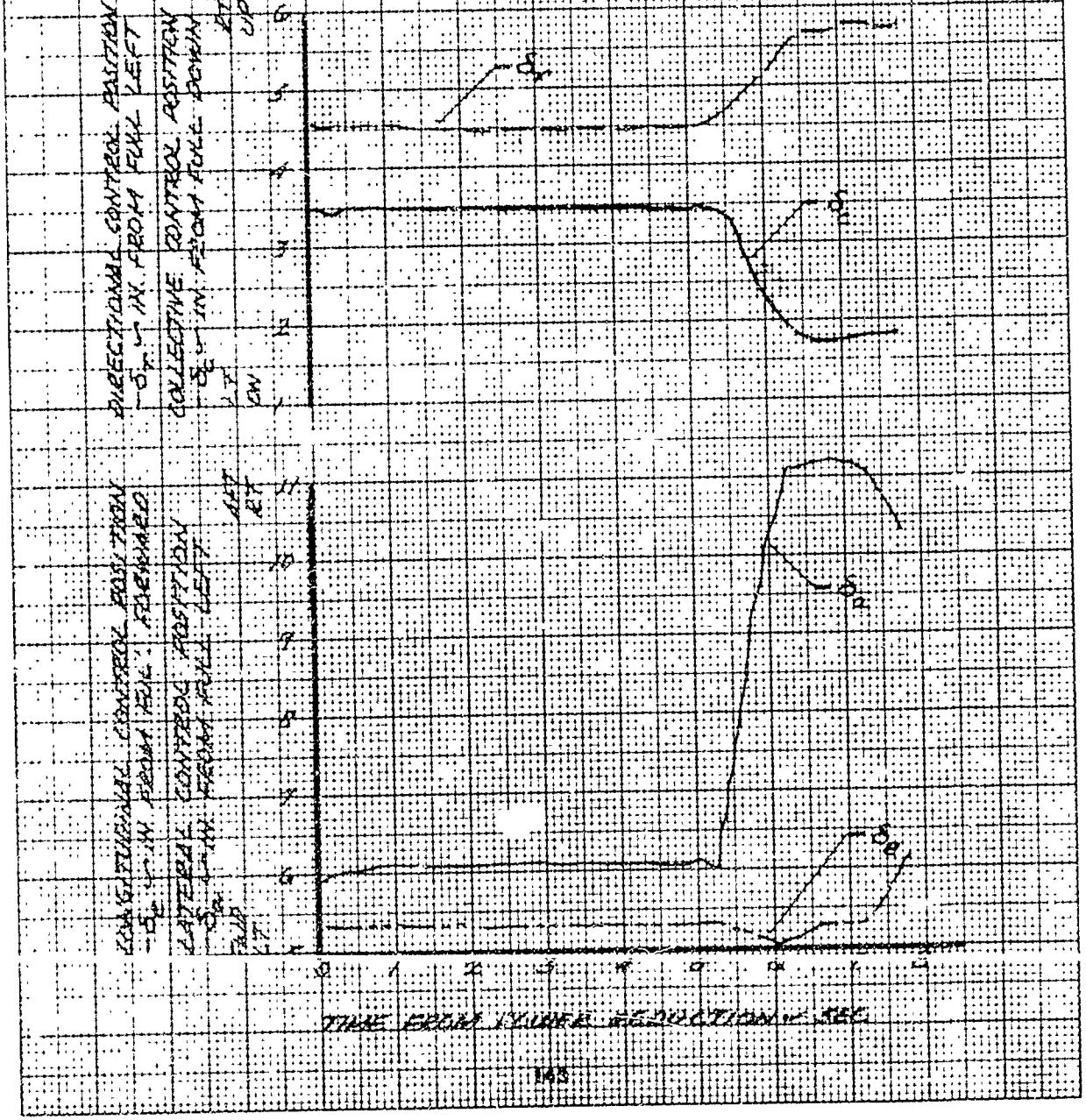

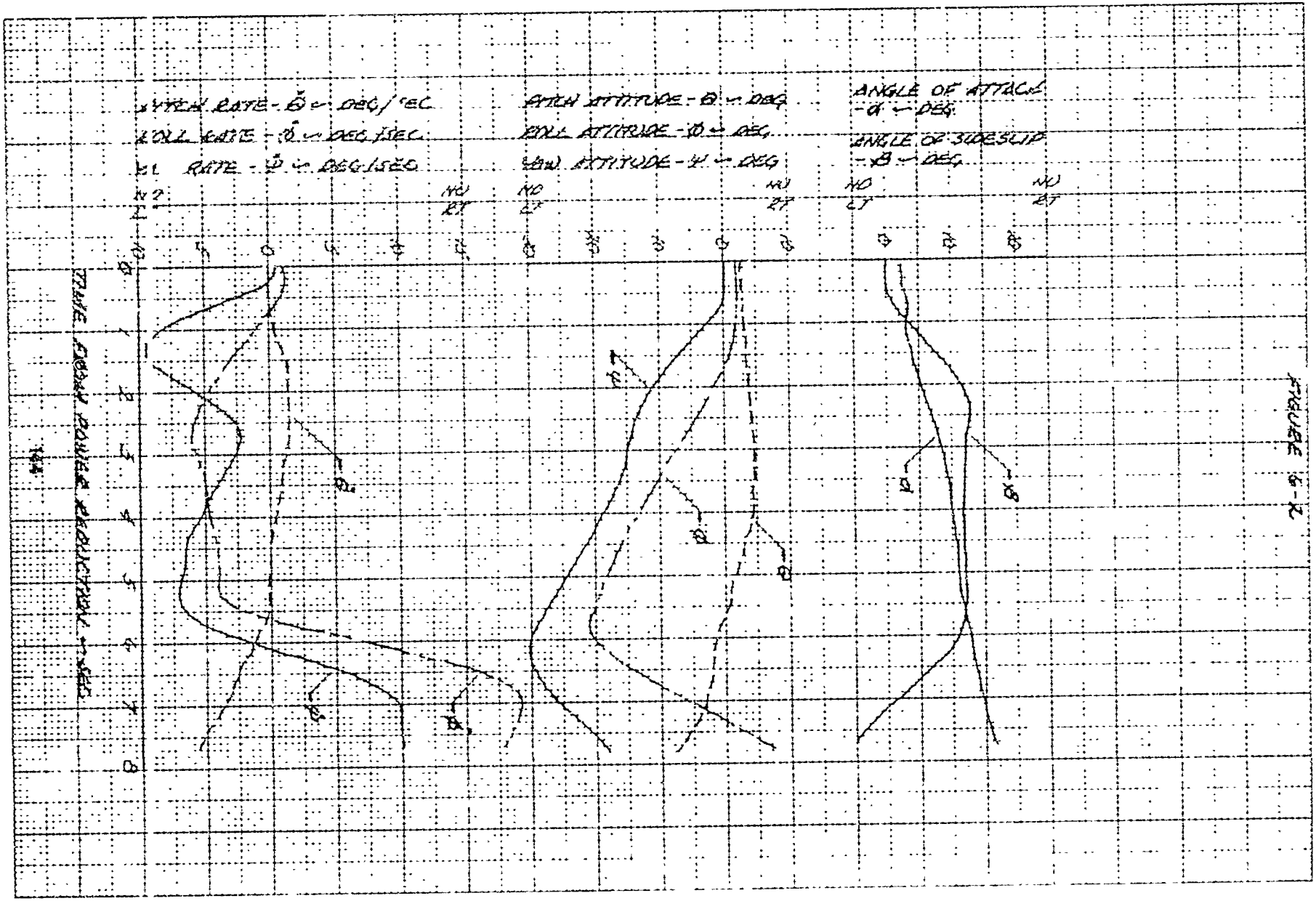
YAW RATE - $\dot{\psi}$ - DEG/SEC
ROLL RATE - $\dot{\phi}$ - DEG/SEC
PITCH RATE - $\dot{\theta}$ - DEG/SEC
PITCH ATTITUDE - θ - DEG
ROLL ATTITUDE - ϕ - DEG
YAW ATTITUDE - ψ - DEG
ANGLE OF ATTACK - α - DEG
ANGLE OF SIDESLIP - β - DEG
NO. 27
NO. 27
NO. 27
NO. 27
TIME FROM POWER REDUCTION - SEC

FIGURE 6-12

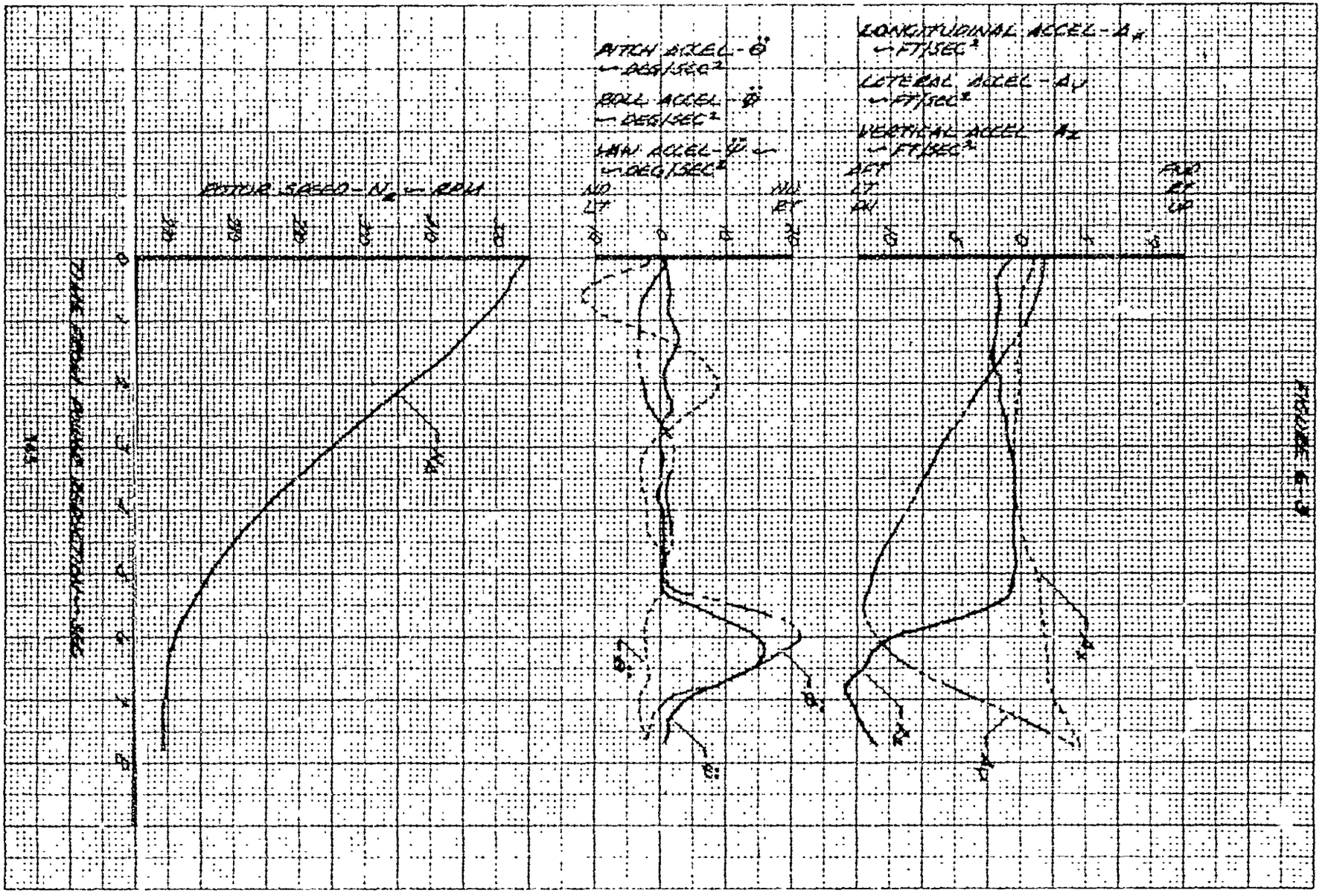
ROTOR SPEED - N_R — RPM
PITCH ACCEL - $\ddot{\theta}$
← DEG/SEC²
ROLL ACCEL - $\ddot{\phi}$
← DEG/SEC²
YAW ACCEL - $\ddot{\psi}$ ←
← DEG/SEC²
NO LT
NO RT
LONGITUDINAL ACCEL - $\dot{u}$
← FT/SEC²
LATERAL ACCEL - $\dot{v}$
← FT/SEC²
VERTICAL ACCEL - $\dot{w}$
← FT/SEC²
AFT LT
AFT RT
FWD LT
FWD RT
TIME FROM ARMING SEQUENCE - SEC

FIGURE 6-9

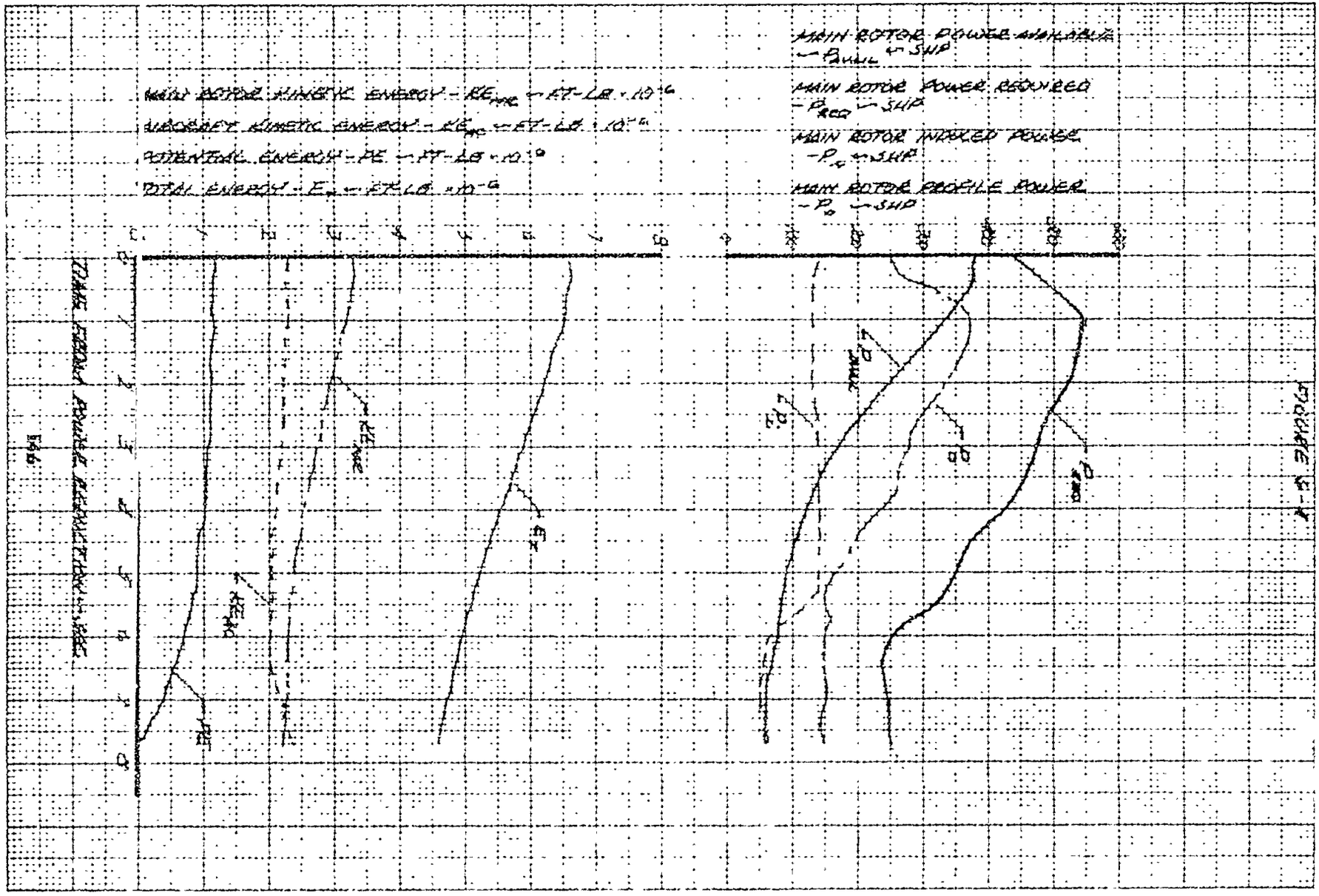
MAIN ROTOR KINETIC ENERGY - KE_{MR} - FT-LB × 10⁻⁶
HUBCRAFT KINETIC ENERGY - KE_{HC} - FT-LB × 10⁻⁶
POTENTIAL ENERGY - PE - FT-LB × 10⁻⁶
TOTAL ENERGY - E_T - FT-LB × 10⁻⁶
MAIN ROTOR POWER AVAILABLE - P_{AVAIL} - SHP
MAIN ROTOR POWER REQUIRED - P_{REQ} - SHP
MAIN ROTOR INDUCED POWER - P_i - SHP
MAIN ROTOR PROFILE POWER - P_o - SHP
ΔP_{SHAFT}
$\Delta P_{E.E.}$
P_o
P_{REQ}
KE_{MR}
KE_{HC}
E_T
PE
TOTAL ENERGY AND POWER REQUIREMENTS - KNEE
FIGURE E-4

FIGURE 6-5

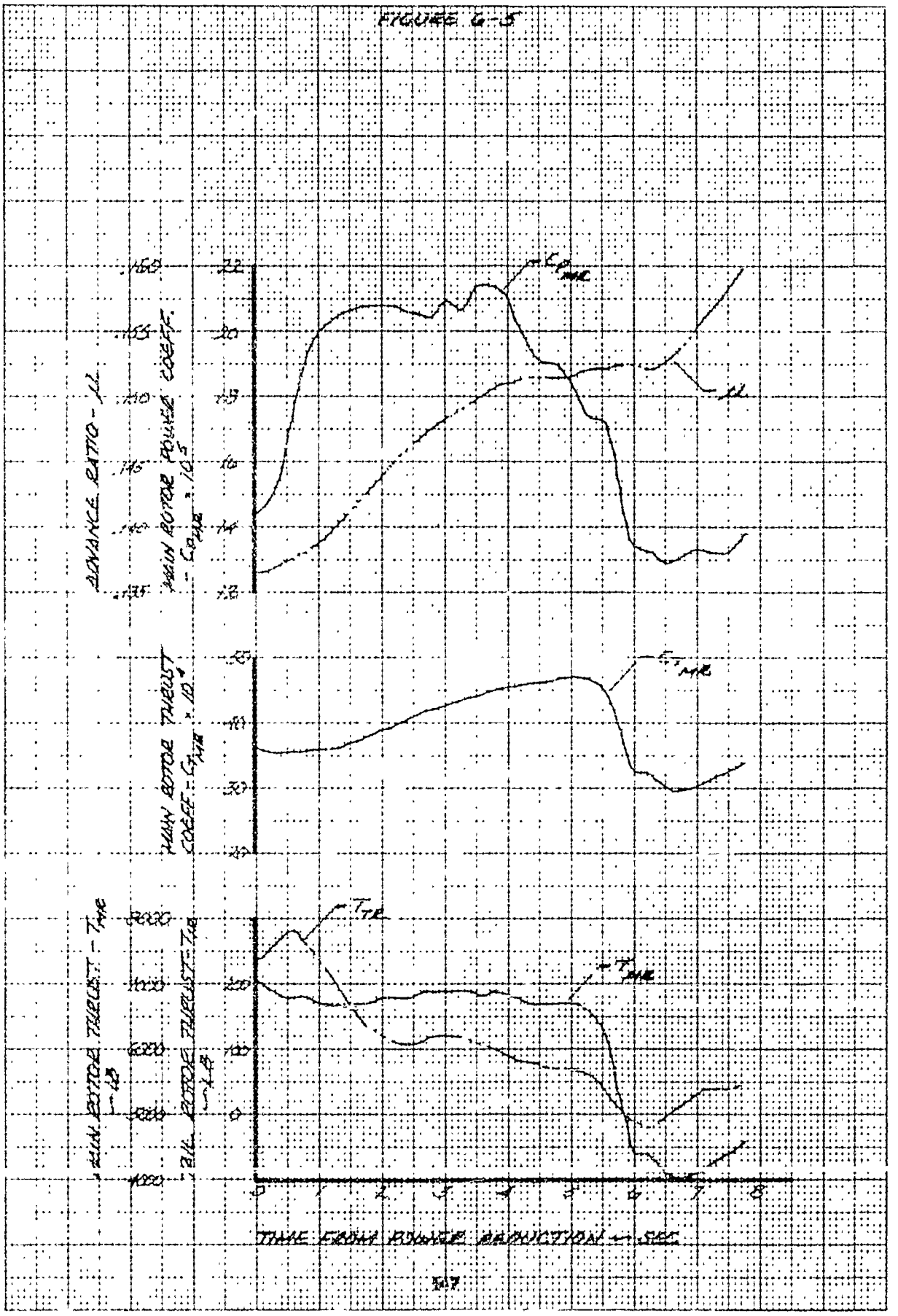
ADVANCE RATIO - μ
MAIN ROTOR POWER COEFF. - $C_{P_{MR}} \times 10^5$
MAIN ROTOR THRUST COEFF. - $C_{T_{MR}} \times 10^4$
MAIN ROTOR THRUST - T_{MR} - LB
TAIL ROTOR THRUST - T_{TR} - LB
$C_{P_{MR}}$
$C_{T_{MR}}$
T_{TR}
T_{MR}
μ
TIME FROM ROUTE REDUCTION - SEC

FIGURE 6-6

RELATIVE DISTANCE TRAVELED - D_R in FT
LATERAL DISTANCE TRAVELED - D_y in FT
VERTICAL DISTANCE TRAVELED - D_z in FT
TRUE AIRSPEED - V_T in KTS
TOTAL DRAG - F_D in LB
TAIL ROTOR POWER - P_{TR} in SHP
RATE OF DESCENT - V_z in FT/SEC
TIME FROM POWER REDUCTION - SEC
F_D
V_T
P_{TR}
D_z
D_x
D_y
V_z

FIGURE X-1

RAPID POWER REDUCTION DURING HIGH SPEED FORWARD FLIGHT

GROSS WT = 1793 LB
ENTRY AIRSPEED = 1M 1.10
DENSITY ALT = 1100 FT
RAM TEMP = 28 °C
ENTRY THRUST COEFF = 0.00355
TOTAL LONGITUDINAL CONTROL TRAVEL = 11.7 IN.
TOTAL LATERAL CONTROL TRAVEL = 11.4 IN.
TOTAL DIRECTIONAL CONTROL TRAVEL = 7.0 IN.
TOTAL COLLECTIVE CONTROL TRAVEL = 10.4 IN.

δ_L — LONGITUDINAL CONTROL POSITION, IN. FROM FULL FORWARD
δ_A — LATERAL CONTROL POSITION, IN. FROM FULL LEFT
δ_R — DIRECTIONAL CONTROL POSITION, IN. FROM FULL LEFT
δ_C — COLLECTIVE CONTROL POSITION, IN. FROM FULL DOWN

TIME FROM START OF POWER REDUCTION — SEC

FIGURE 7-2

PITCH ATTITUDE - θ - DEG
ROLL ATTITUDE - φ - DEG
YAW ATTITUDE - ψ - DEG
ANGLE OF ATTACK - α - DEG
ANGLE OF SIDESLIP - β - DEG
PITCH RATE - q - DEG/SEC
ROLL RATE - p - DEG/SEC
YAW RATE - r - DEG/SEC
TIME FROM ROUND RELEASE - SEC

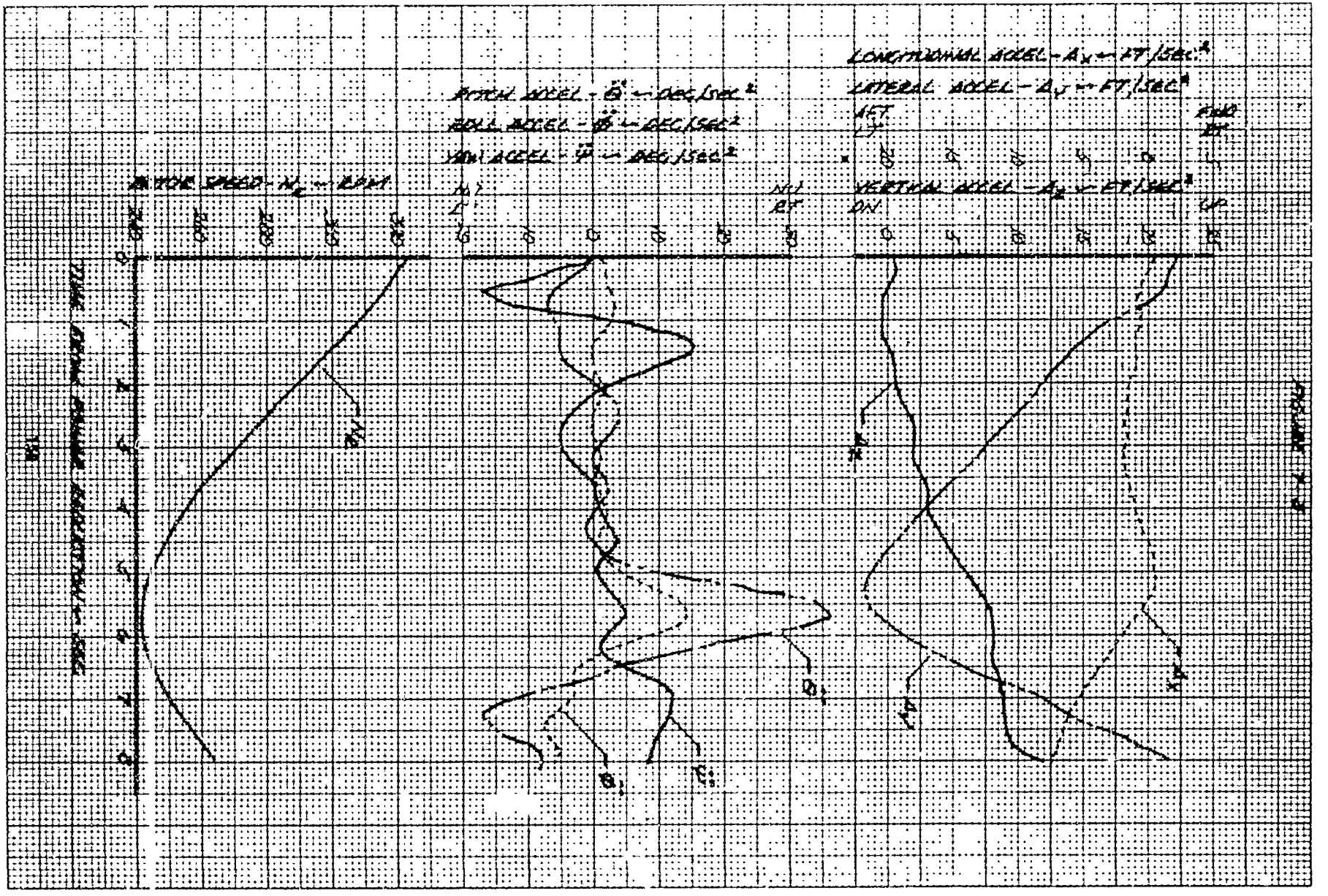
LONGITUDINAL ACCEL - A_x - FT/SEC.²
LATERAL ACCEL - A_y - FT/SEC.²
VERTICAL ACCEL - A_z - FT/SEC.²
ROLL ACCEL - $\ddot{\phi}$ - DEG/SEC²
YAW ACCEL - $\ddot{\psi}$ - DEG/SEC²
TIME FROM SPECIFIED INSTANT - SEC.

FIGURE 7-4

MEAN ATOMIC KINETIC ENERGY - KEV
INCIDENT KINETIC ENERGY - KEV
EQUILIBRIUM ENERGY - KEV
TOTAL ENERGY - KEV
TIME AFTER SOURCE REGULATION - SEC
E_T
KE_{at}
KE_{eq}
PE

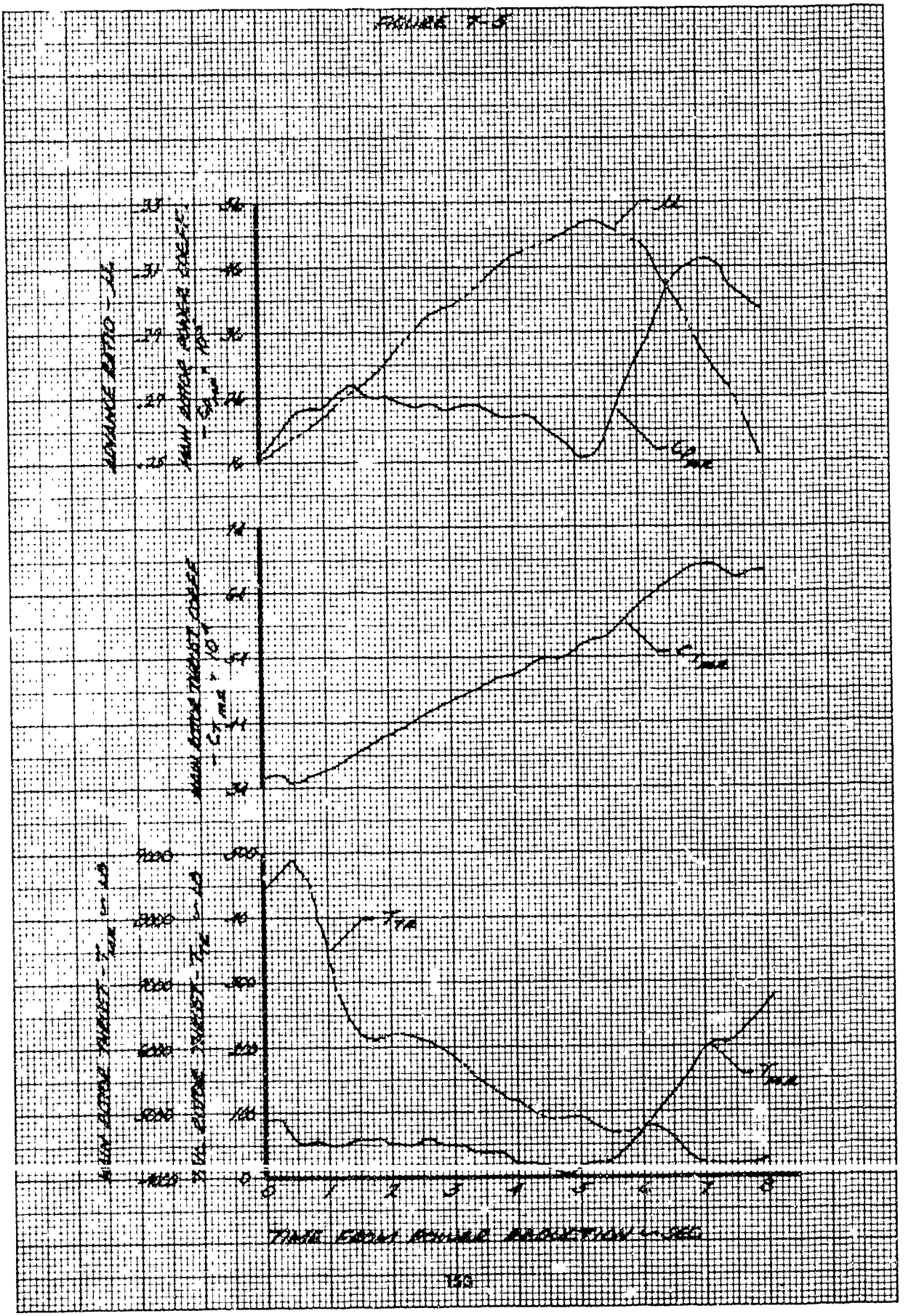
FIGURE 7-5
TIME FROM INITIAL ACCELERATION - SEC
153

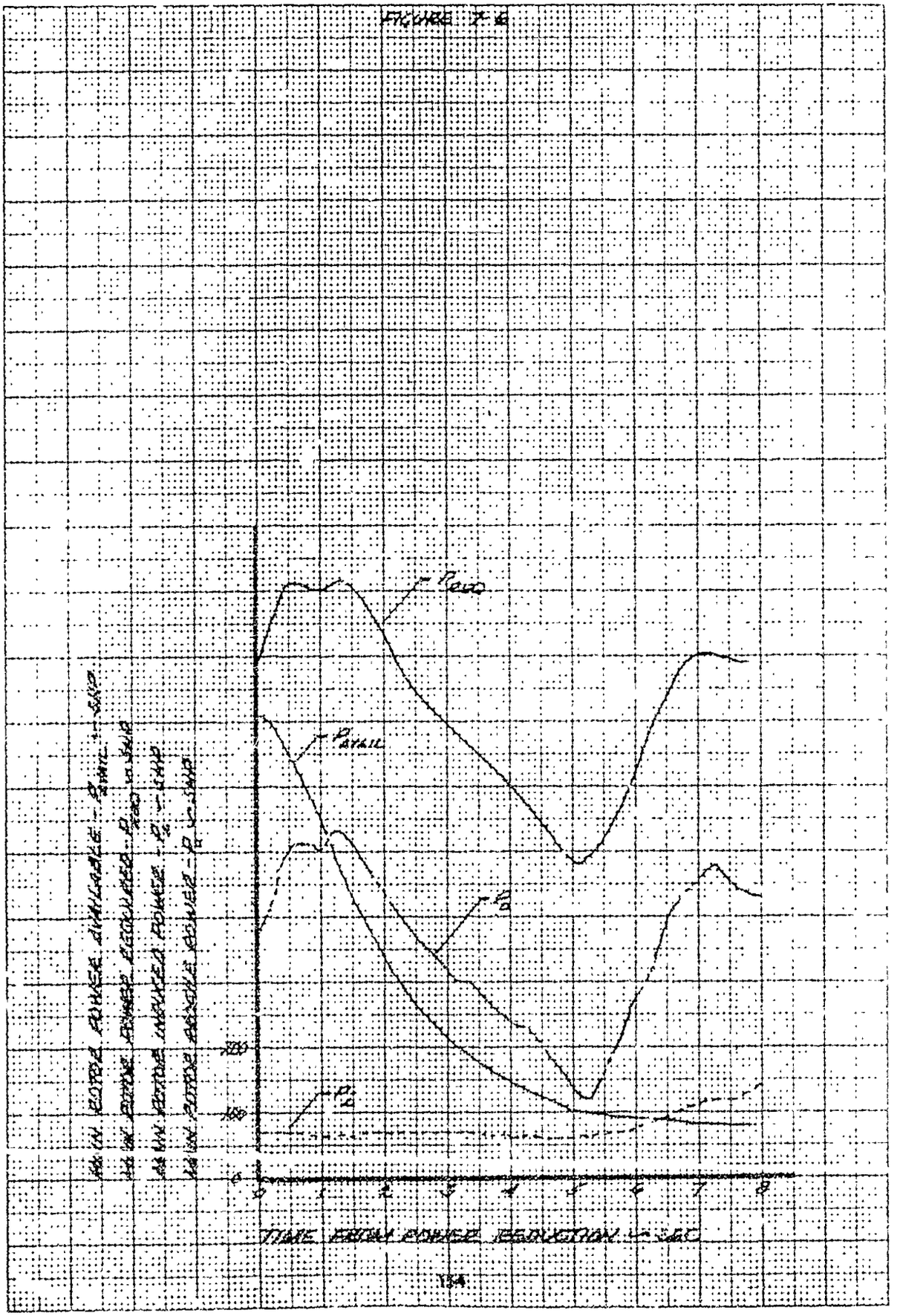
FIGURE 7-6
TIME FROM POWER REDUCTION, t, SEC

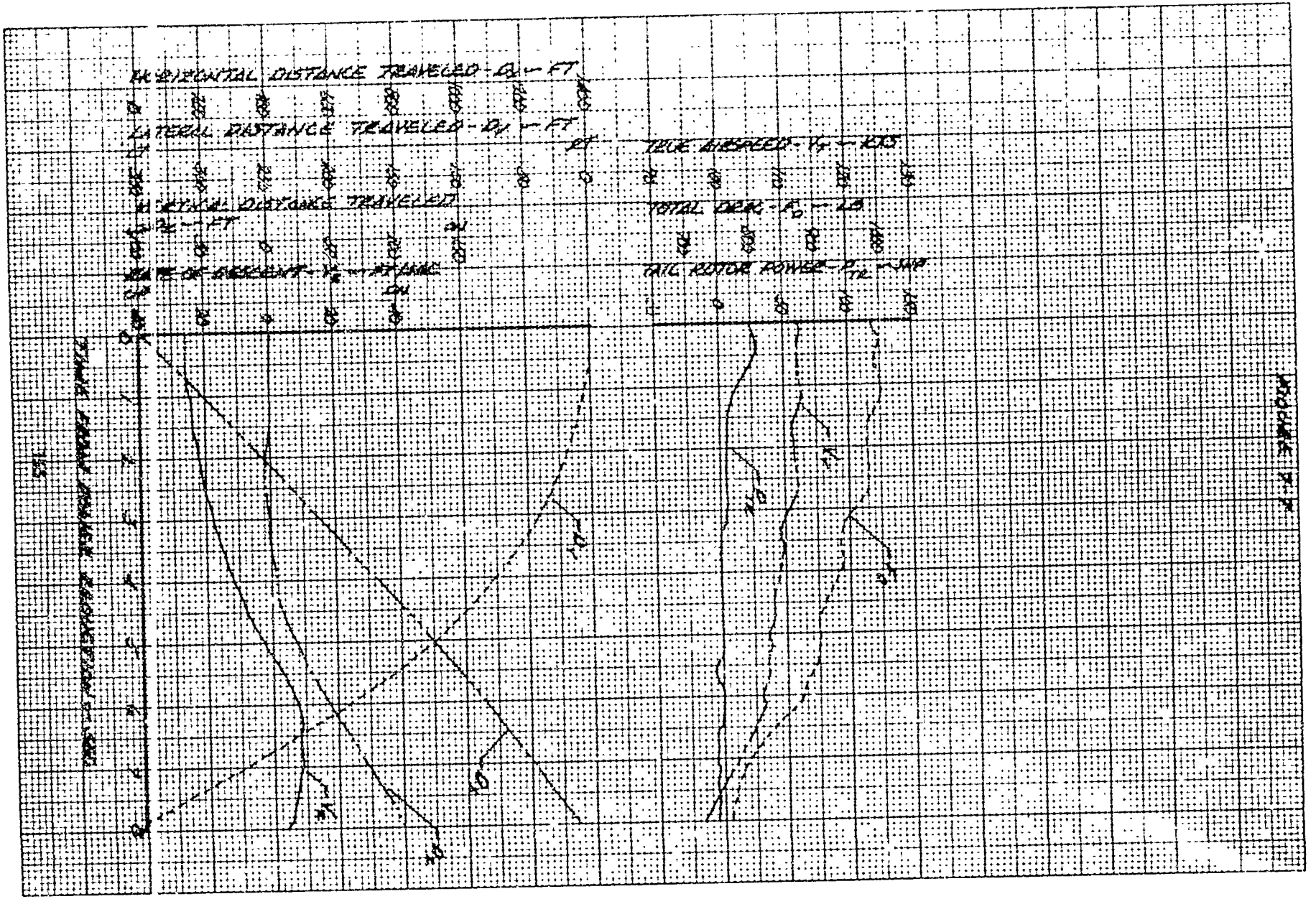
VERTICAL DISTANCE TRAVELED - d_v - FT
LATERAL DISTANCE TRAVELED - d_H - FT
TRUE AIRSPEED - V_T - KTS
TOTAL DRAG - A_D - LB
TOTAL DISTANCE TRAVELED - d_T - FT
RATE OF DESCENT - $\frac{dh}{dt}$ - FT/MIN
RATIO ROTOR POWER - P_{TR} - HP
FIGURE A-14

FIG. NO. B-1

ALTITUDE EFFECTS ON AIRCRAFT ATTITUDE FOLLOWING A RAPID THROTTLE CLOSURE

USA S/N 63-8864

CONF-10

PITCH	SYM ROLL	YAW	DENSITY ALT-FT	AMB TEMP °C	GROSS WT-1000 LBS	BOTTOM SPEED KNOTS
○	□	△	11110	13	67.90	327
●	■	▲	11120	12	70.00	324

NOTE: ALL CONTROLS FIXED DURING POWER REDUCTION

A RELATIVELY ATTITUDE TRACE SECONDS AFTER POWER REDUCTION

FIGURE 9-1

WEIGHT CHANGES FOLLOWING
A BLEND THROTTLE CLOSURE

OH-6C

USA 36-43-5683

SYM	ENTRY AIRSPEED KCAS	ALTITUDE FT-LB	DENSITY ALT FT	AMB TEMP °C	ENGINE SPEED RPM
△	60	6780	7110	13	321
○	65	8500	9140	11	319
▲	119	6800	7110	13	321
□	60	6780	7110	13	323
◇	60	6740	7020	13	323

NOTE:
ALL CONTROLS FIXED
DURING POWER REDUCTION

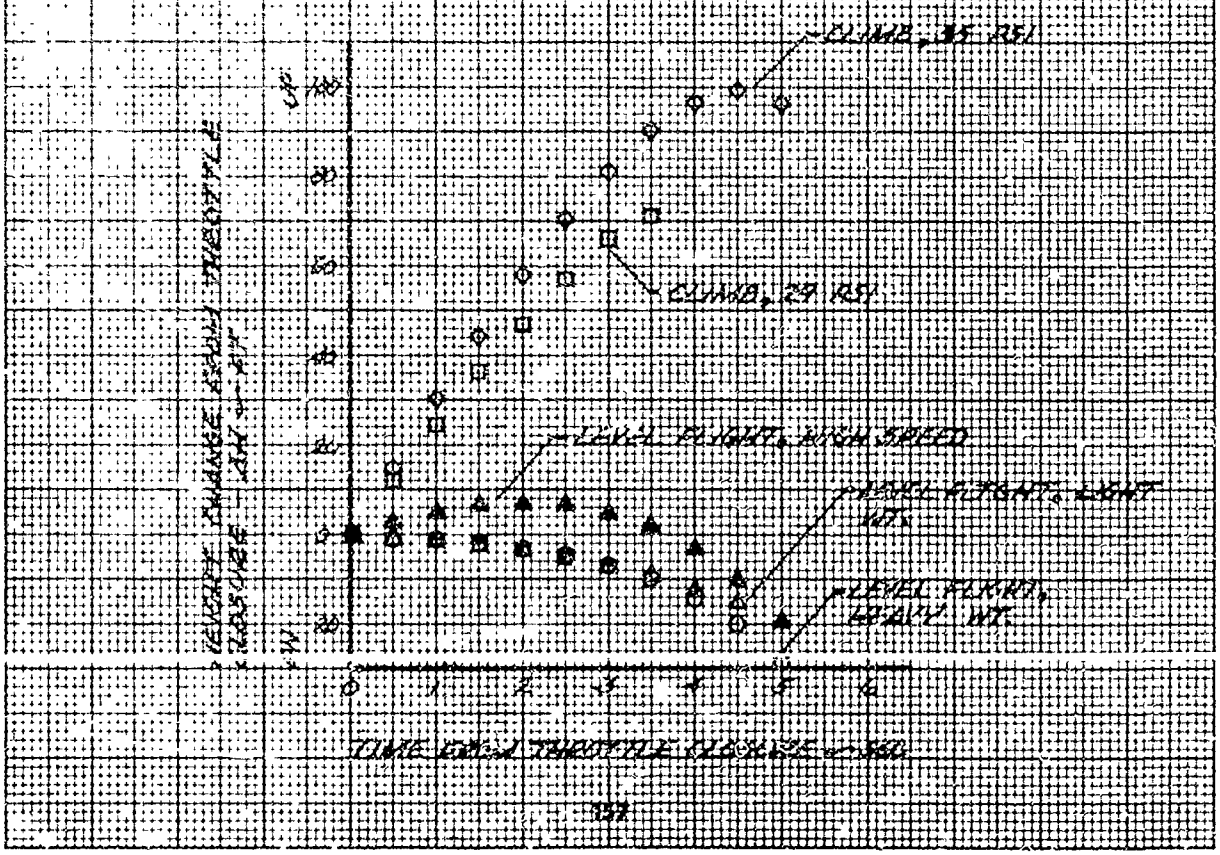

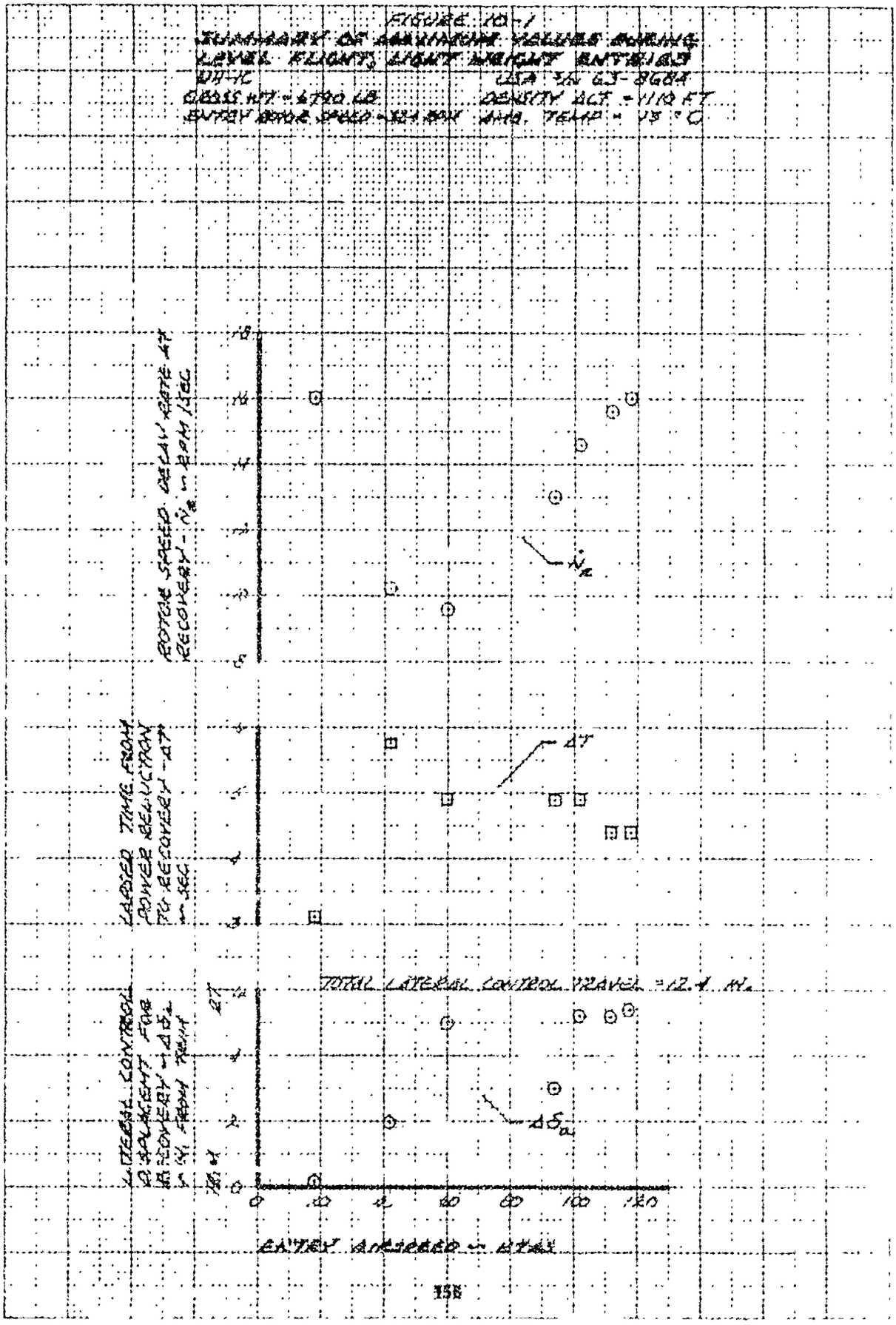
FIGURE 10-1
SUMMARY OF MAXIMUM VALUES DURING LEVEL FLIGHT, LIGHT WEIGHT ENTRIES
DH-1C
CASE 24 63-8684
GROSS WT = 6700 LB
DENSITY ALT = 1110 FT
ENTRY AIRSPEED = 324 KIAS AMB. TEMP = 95 °C
ROTOR SPEED DECAY RATE AT RECOVERY - $\dot{N}_R$ = RPM/SEC
LADDED TIME FROM POWER RECOVERY TO RECOVERY - ΔT = SEC
LATERAL CONTROL TO SATISFY ϕ_{max} = 45° IN RECOVERY - $\Delta\delta_a$ = % FROM TRIM
$\dot{N}_R$
ΔT
$\Delta\delta_a$
TOTAL LATERAL CONTROL TRAVEL = 42.4 IN.
0
20
40
60
80
100
120
ENTRY AIRSPEED = KIAS

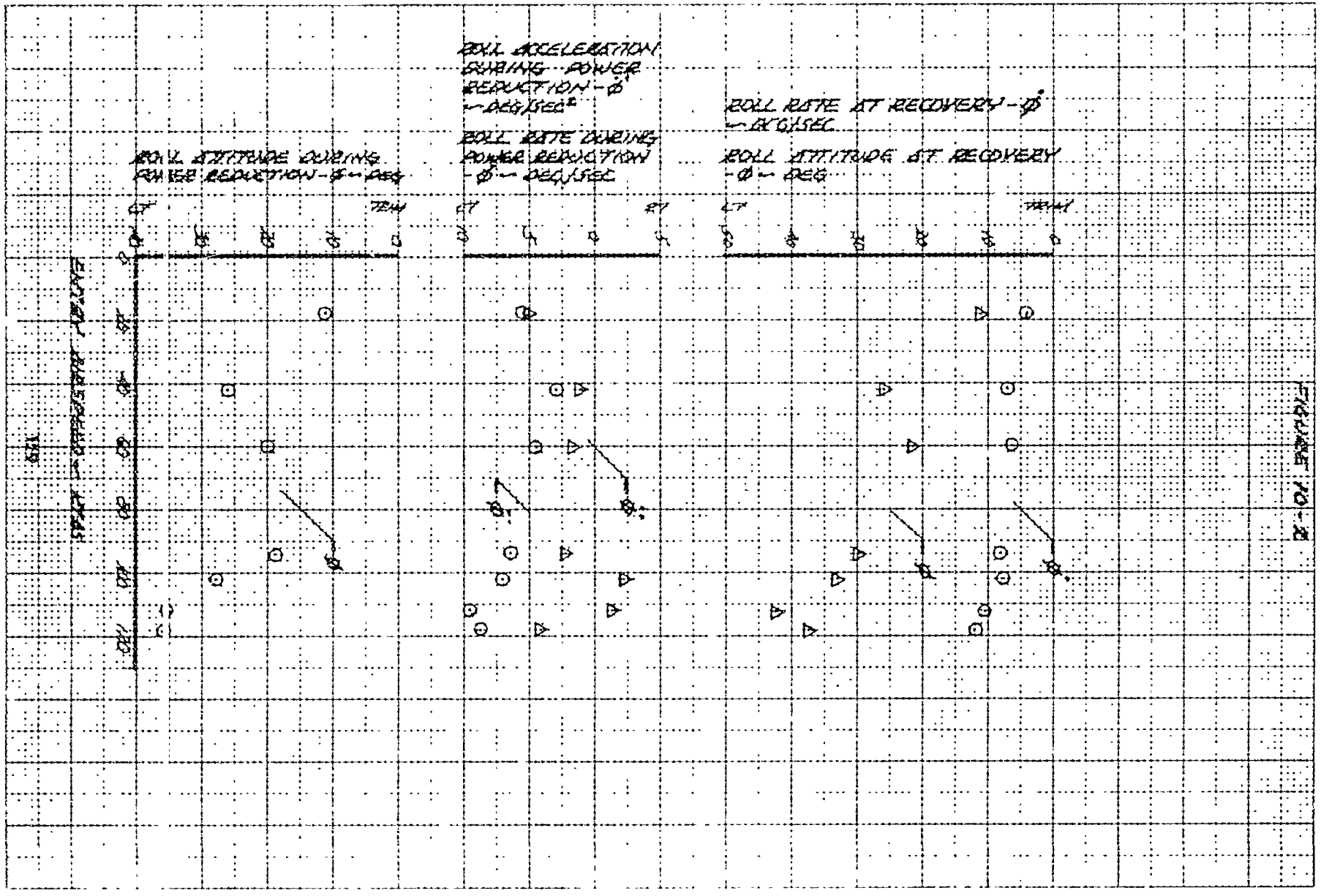
ROLL ACCELERATION DURING POWER REDUCTION - Ø̈ - DEG/SEC²
ROLL RATE DURING POWER REDUCTION - Ø̇ - DEG/SEC
ROLL RATE AT RECOVERY - Ø̇ - DEG/SEC
ROLL ATTITUDE DURING POWER REDUCTION - Ø - DEG
ROLL ATTITUDE AT RECOVERY - Ø - DEG
TIME
TIME
TIME
EARTH - RELATIVE ALTITUDE - FEET
FIGURE NO. 28

FIGURE VI-1

SUMMARY OF MAXIMUM AVAILABLE MANEUVER CAPABILITY, LATERAL CONTROL ENTIRELY

OH-1C

GROSS WT = 2870 LB

ENTRY ROTOR SPEED = 370 RPM

USA 3/4 GT-65-84

DENSITY ALT = 1940 FT.

AMB TEMP = 11° C

ROTOR SPEED DECAY RATE AT RECOVERY = $\dot{N}_R$ = POSITIVE

$\dot{N}_R$

$-\Delta T$

TOTAL LATERAL CONTROL TRAVEL = 12.4 IN.

$-A\xi_a$

ENTRY AIRSPEED - KIAS

0 20 40 60 80 100 120

0 2 4 6 8 10 12 14 16

ΔT = TIME FROM INITIATION OF RECOVERY MANEUVER TO RECOVERY = SEC

$A\xi_a$ = LATERAL CONTROL DISPLACEMENT FROM RECOVERY = IN.

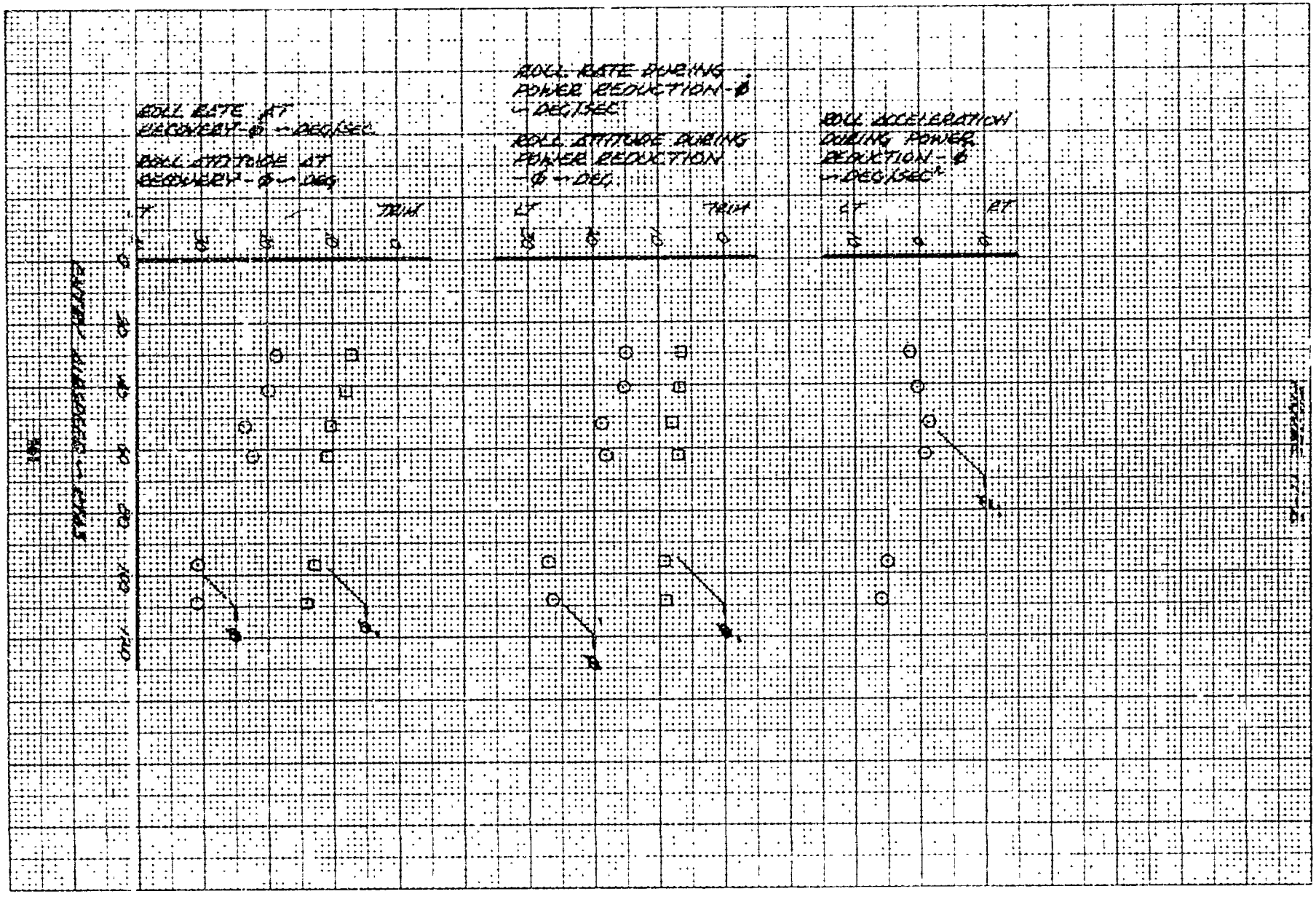
ROLL RATE AT RECOVERY - Φ → DEG/SEC
ROLL ATTITUDE AT RECOVERY - Φ → DEG
TRIM
ROLL RATE DURING POWER REDUCTION - Φ̇ → DEG/SEC
ROLL ATTITUDE DURING POWER REDUCTION - Φ → DEG
TRIM
ROLL ACCELERATION DURING POWER REDUCTION - Φ̈ → DEG/SEC²
AIRSPEED → KNOTS

FIGURE 12 - 1

SUMMARY OF MAXIMUM VALUES DURING LIGHT WEIGHT CLIMB ENTRIES

DH-1C
GROSS WT = 6820 LB
ENTRY ROTOR SPEED = 323 RPM
INDICATED ENGINE TORQUE = 70 PSI

CSA "A" 63-8684
DENSITY ALT = 1000 FT
OAT TEMP = 15 °C

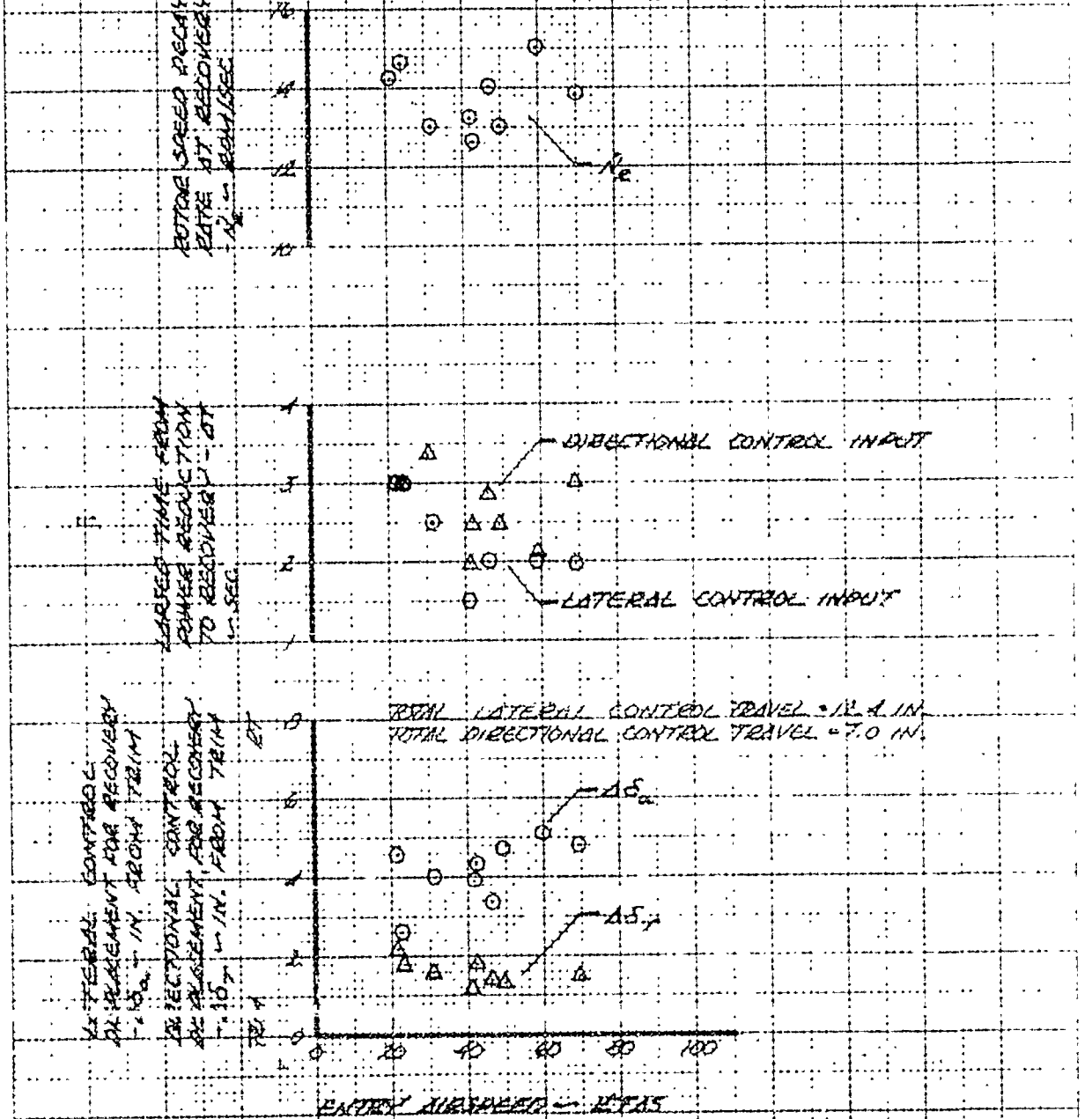

FIGURE 12-2
MINIMUM DURING POWER REDUCTION
MINIMUM DURING RECOVERY
ENTRY ALTITUDE - KFEET

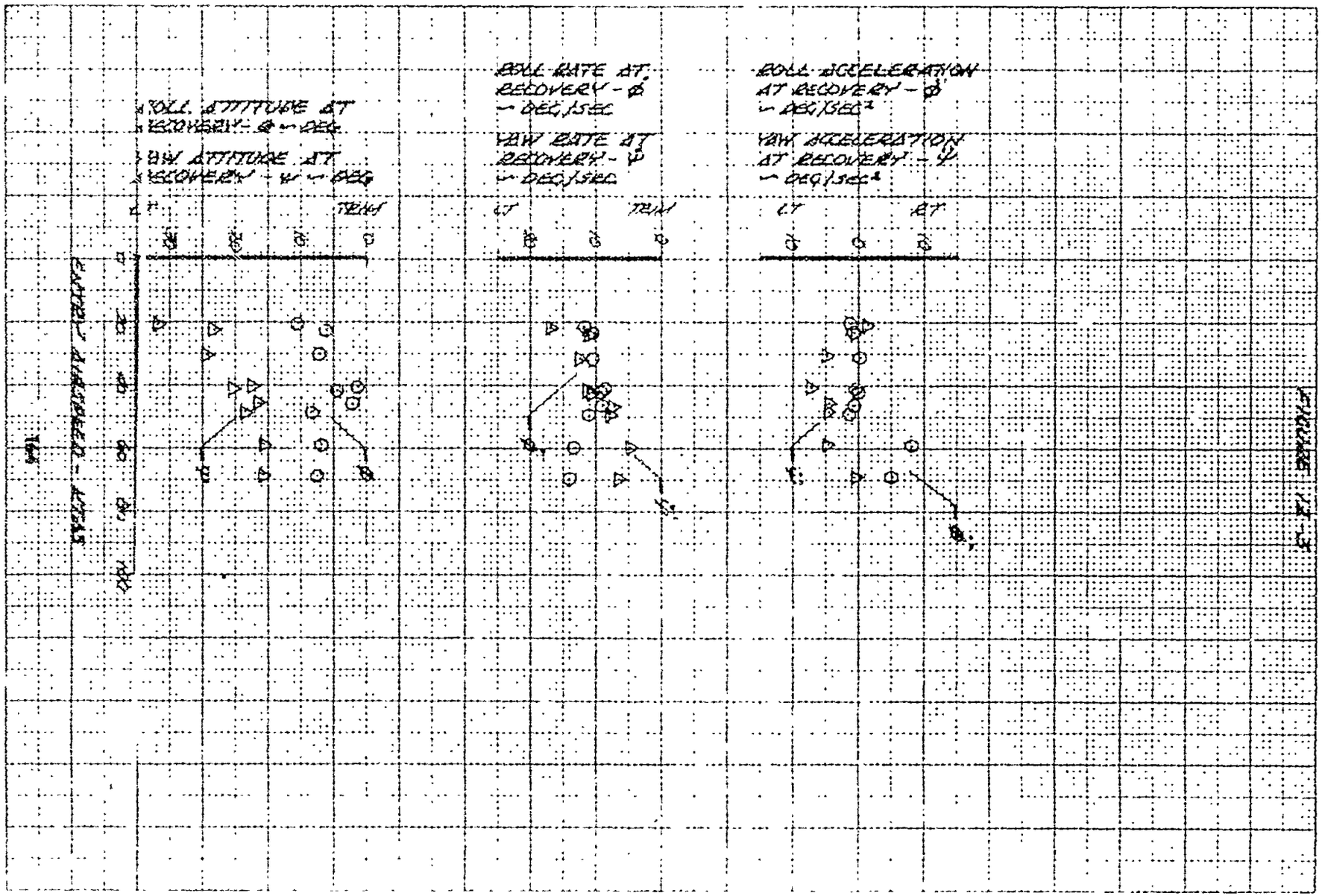
ROLL ATTITUDE AT RECOVERY - Φ - DEG
YAW ATTITUDE AT RECOVERY - Ψ - DEG
ROLL RATE AT RECOVERY - Φ̇ - DEG/SEC
YAW RATE AT RECOVERY - Ψ̇ - DEG/SEC
ROLL ACCELERATION AT RECOVERY - Φ̈ - DEG/SEC²
YAW ACCELERATION AT RECOVERY - Ψ̈ - DEG/SEC²
LAUNCH
LAUNCH
LAUNCH
EARTH-FIXED AZIMUTH

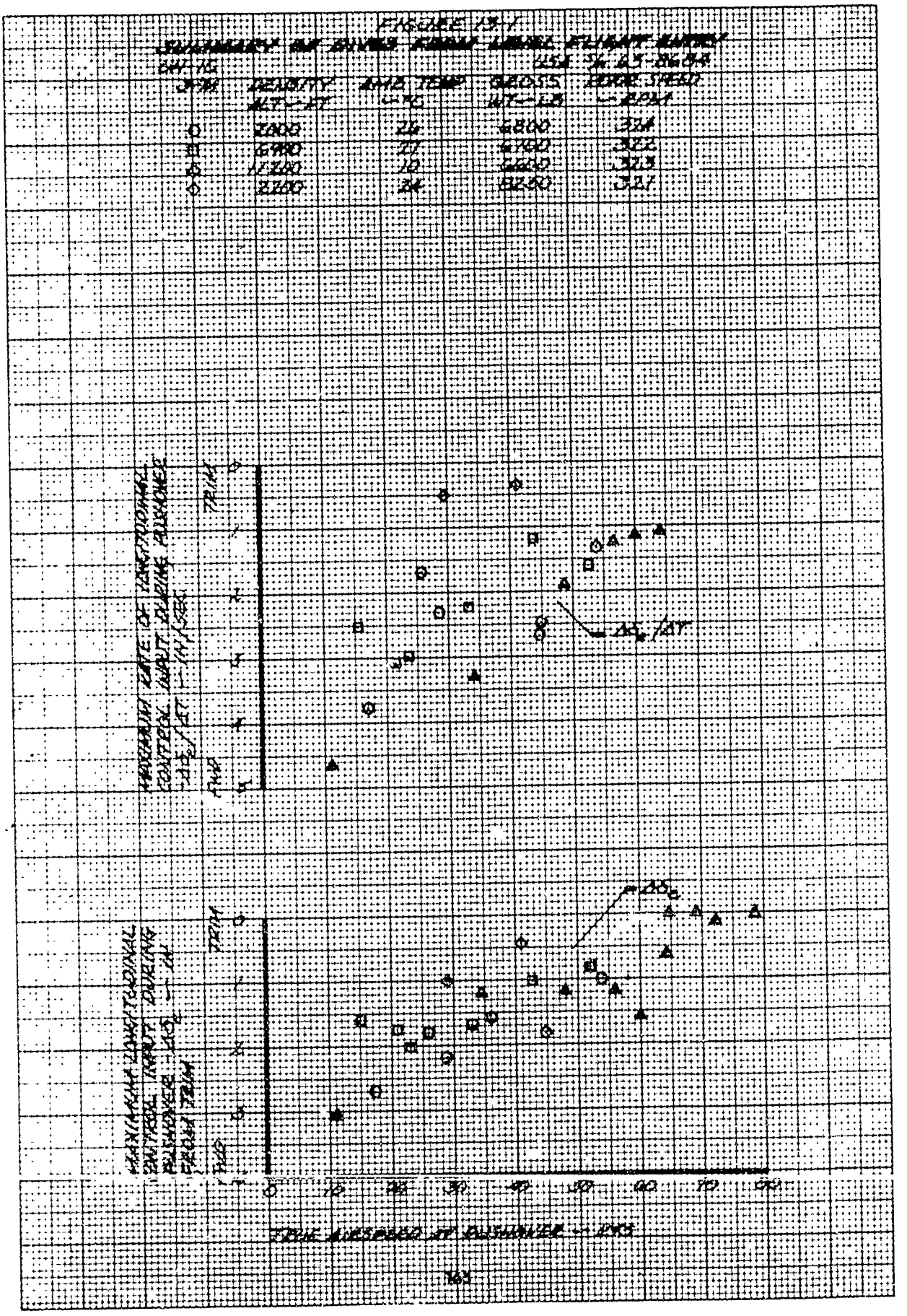

FIGURE 13-2

MINIMUM PITCH ATTITUDE DURING ACCELERATION
θ — DEG
MAXIMUM PITCH RATE DURING PUSHOVER, $\dot{\theta}$
— DEG/SEC
MAXIMUM PITCH ACCELERATION DURING PUSHOVER, $\ddot{\theta}$
— DEG/SEC²
TRUE AIRSPEED AT PUSHOVER — KTS

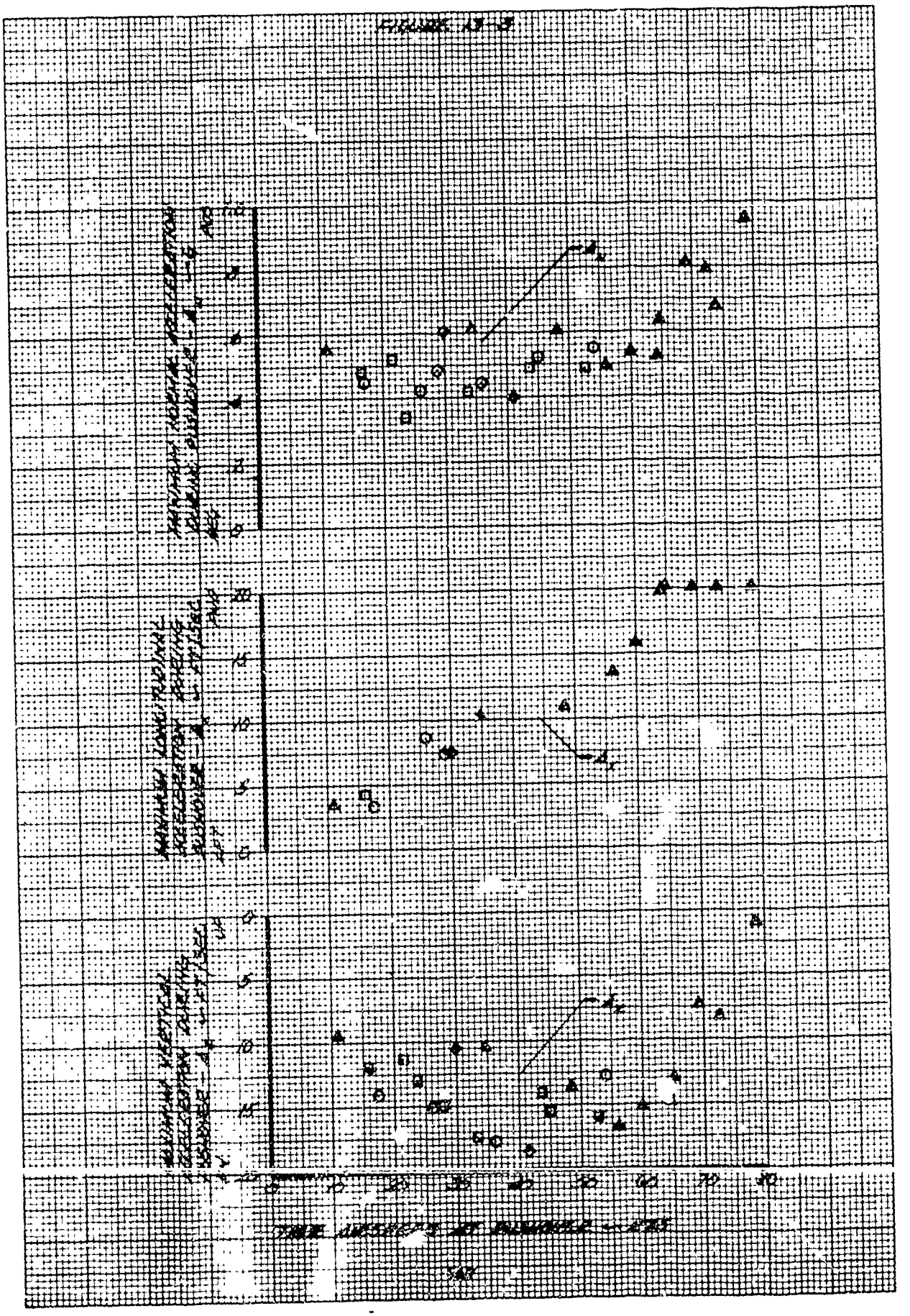

FIGURE 15-A

MAXIMUM INDUCED POWER
DURING ACCELERATION
= P_x - SHP
MAXIMUM AVAILABLE POWER
DURING ACCELERATION
= SHP
P_x
TIME REQUIRED TO ACCELERATE - SEC

FIGURE XV-4

RATE OF DESCENT AT MAXIMUM ANGLE OF BANK WITH MAXIMUM ALLOWABLE BANKING ACCELERATION = $\frac{1}{2}$ g = 16.1 FT/SEC²

MAXIMUM ALLOWABLE BANKING ACCELERATION = $\frac{1}{4}$ g = 8.05 FT/SEC²

$\frac{1}{2}$ g

$\frac{1}{4}$ g

TRUE AIRSPEED AT ALTITUDE — KTS

FIGURE 13.6

FLIGHT PATH ANGLE AT 60 KTS DURING DECELERATION
γ_{60}
RATE OF DESCENT AT 60 KTS DURING DECELERATION
$V_{z_{60}}$
HEADWIND GRADIENT REQUIRED TO KEEP DURING DECELERATION
ΔH_{60}
TRUE AIRSPEED AT RUNWAY — KTS

FIGURE 17
FLIGHT PATH ANGLE AT STABILIZED 160 KT DESCENT - γ, DEG
RATE OF DESCENT AT STABILIZED 160 KT DESCENT - K_z, FT/SEC
HEIGHT LOST FROM ALTITUDE TO STABILIZED 160 KT DESCENT ΔH, FT
K_z
ΔH
TRUE AIRSPEED AT ALTITUDE, KTS

FIGURES 13-8

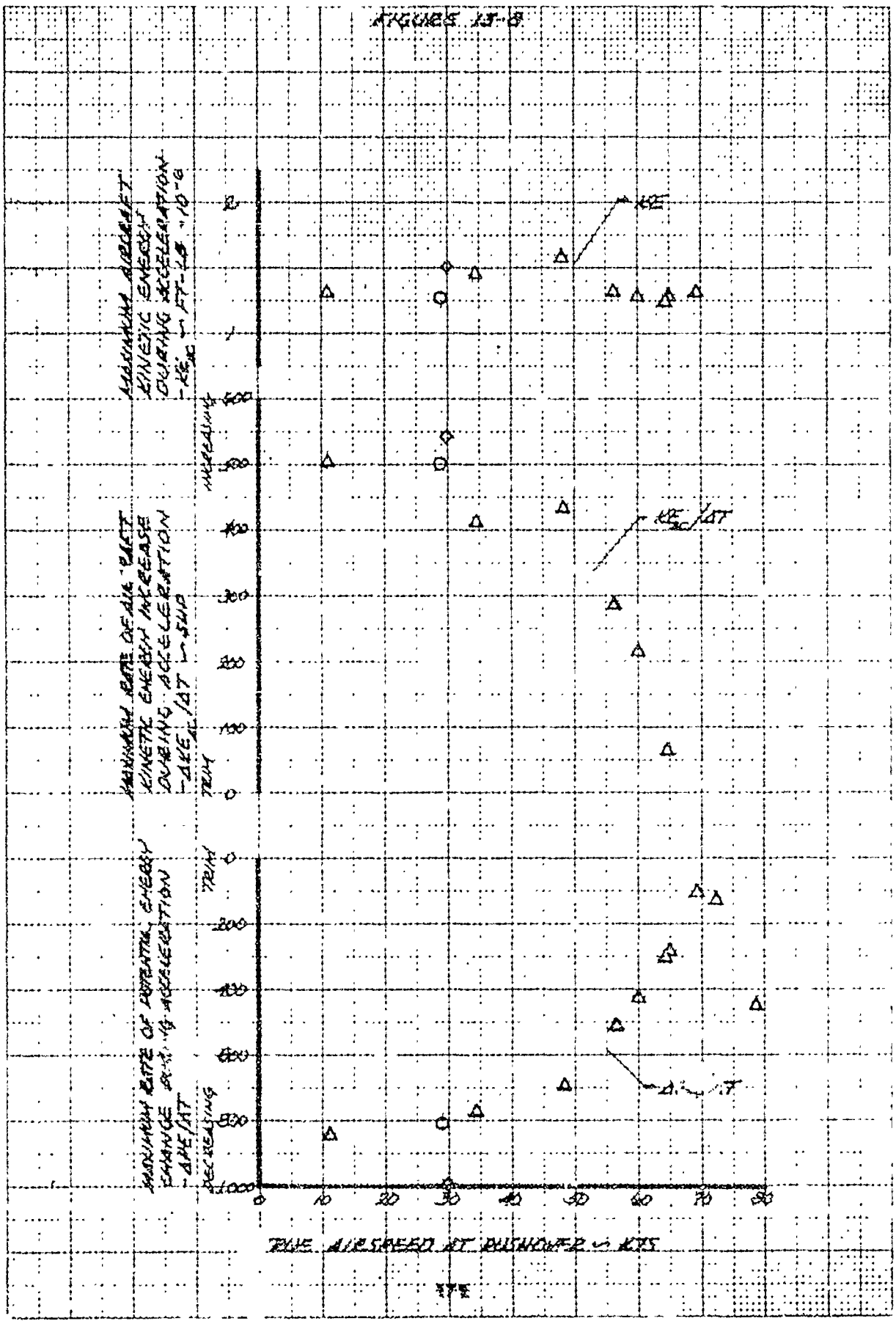
MAXIMUM RATE OF CHANGE OF POTENTIAL ENERGY
ENERGY RATE OF POTENTIAL ENERGY
CHANGE dH/dt, vs ACCELERATION
-ΔKE/ΔT
MAXIMUM RATE OF CHANGE OF KINETIC ENERGY
KINETIC ENERGY INCREASE
DURING ACCELERATION
-ΔKE/ΔT
MAXIMUM ALLOWABLE
KINETIC ENERGY
CHANGE ACCELERATION
-KE/ΔT
INCREASING
DECREASING
TRUE AIRSPEED AT PUSHOVER - KTS

173

FIGURE 17-10

MAXIMUM RATE OF TOTAL ENERGY LOSS DURING ENTRY AND ASCENT-AEROBRAKE - SHO

MAXIMUM RATE OF TOTAL ENERGY LOSS DURING ASCENT-AEROBRAKE - SHO

TRUE AIRSPEED AT AEROBRAKE - KFPS

FIGURE H-1

COMPARISON OF PUSHOVER RATES FROM MEDIUM SPEED FLIGHT

USA 62-8634

UH-1C

ROTOR SPEED = 322 RPM

GROSS WT = 7000 LB

DENSITY ALT = 700 FT

AMB TEMP = 20 °C

PUSHOVER AIRSPEED = 54 KTAS

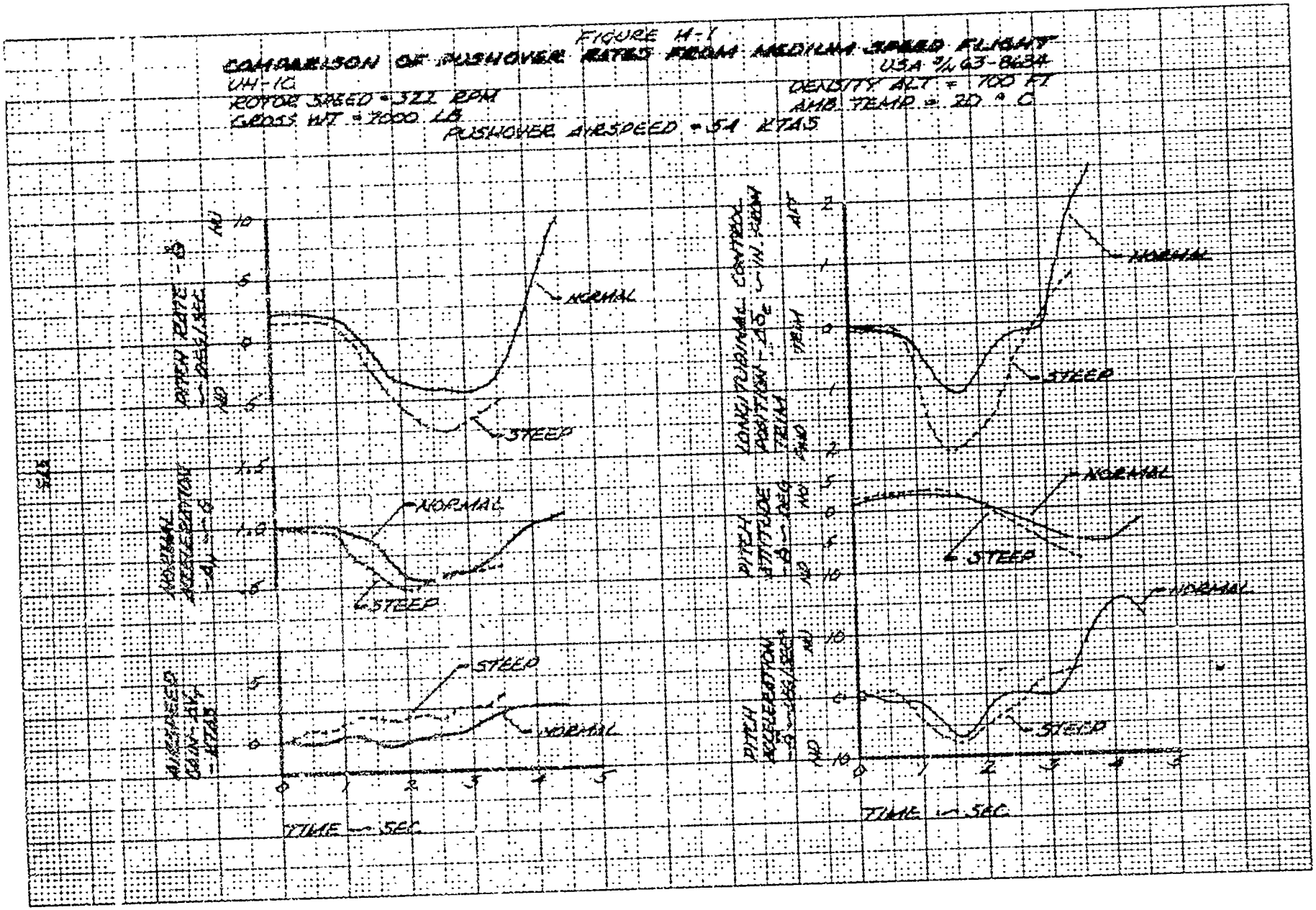

FIGURE 16-2

COMPARISON OF PUSHOVER RATES FROM LOW SPEED FLIGHT

CONFIG
ROTOR SPEED = 323 RPM
GROSS WT = 6800 LBS
PUSHOVER AIRSPEED = 120 KTAS

USA 9/W CG = 86.8
DENSITY ALT = 1200 FT
AMB. TEMP = 20°C

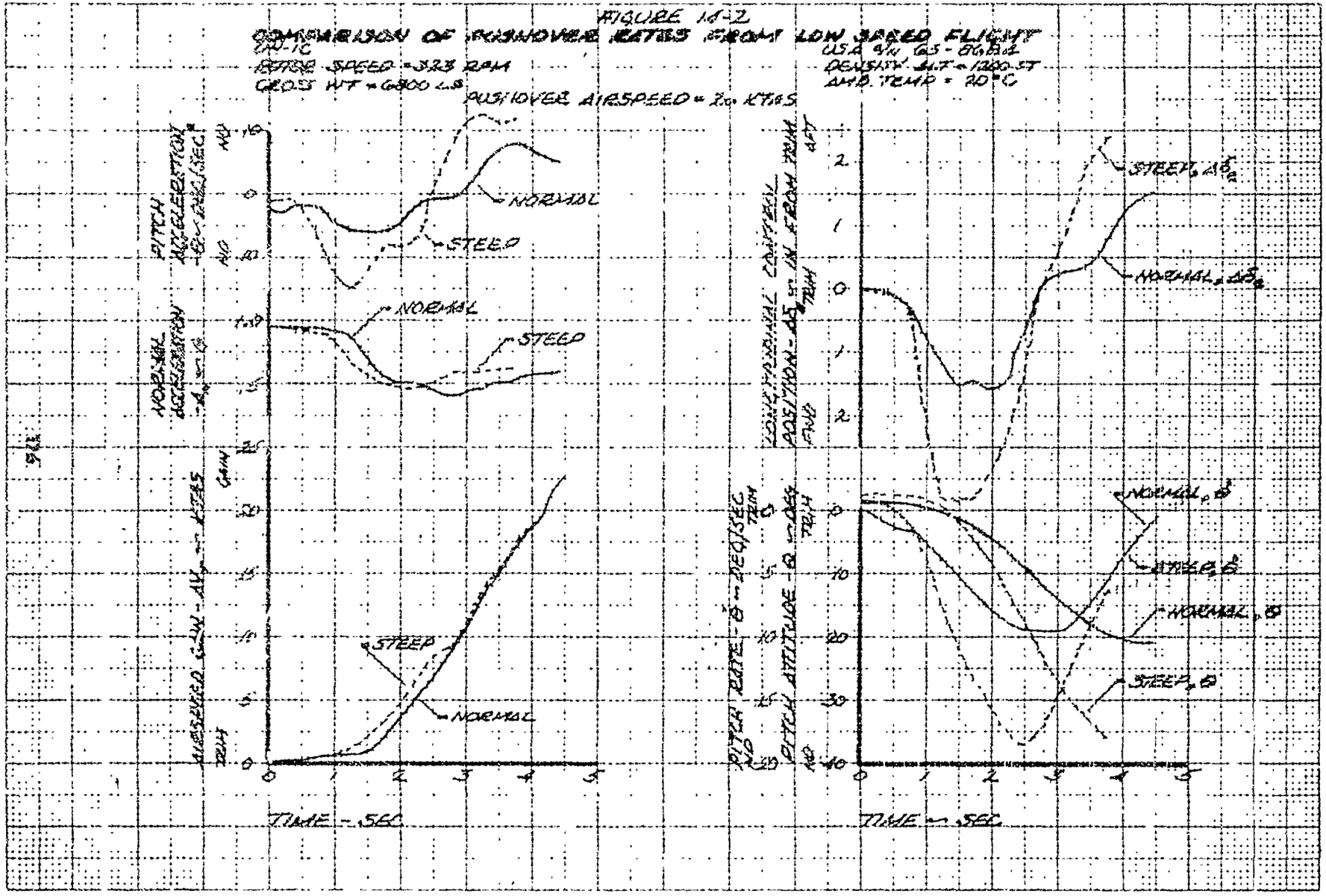

FIGURE 5-1

SUMMARY OF SWISS FARM CLIMB RATES

SYM	ALTITUDE MSL-FT	AMB TEMP °C	GROSS WT-LB	ENGINE POWER
○	10000	19	6600	32/
△	11000	10	6500	32/0
◇	12000	24	6500	32/

FIGURE 15-2

MAXIMUM PITCH ATTITUDE DURING ACCELERATION
MAXIMUM PITCH RATE DURING PULLOVER - θ̇
MAXIMUM PITCH ACCELERATION DURING PULLOVER - θ̈
TIME ASSESSED AT PULLOVER — KTS

FIGURE 27-1

MAXIMUM HEADWIND ACCELERATION DURING PUSHOVER - A_x FT/SEC²
MAXIMUM LONGITUDINAL ACCELERATION - A_x FT/SEC²
MINIMUM TAILWIND ACCELERATION DURING PUSHOVER - A_x FT/SEC²
TRUE AIRSPEED AT PUSHOVER — KTS

FIGURE 15-4

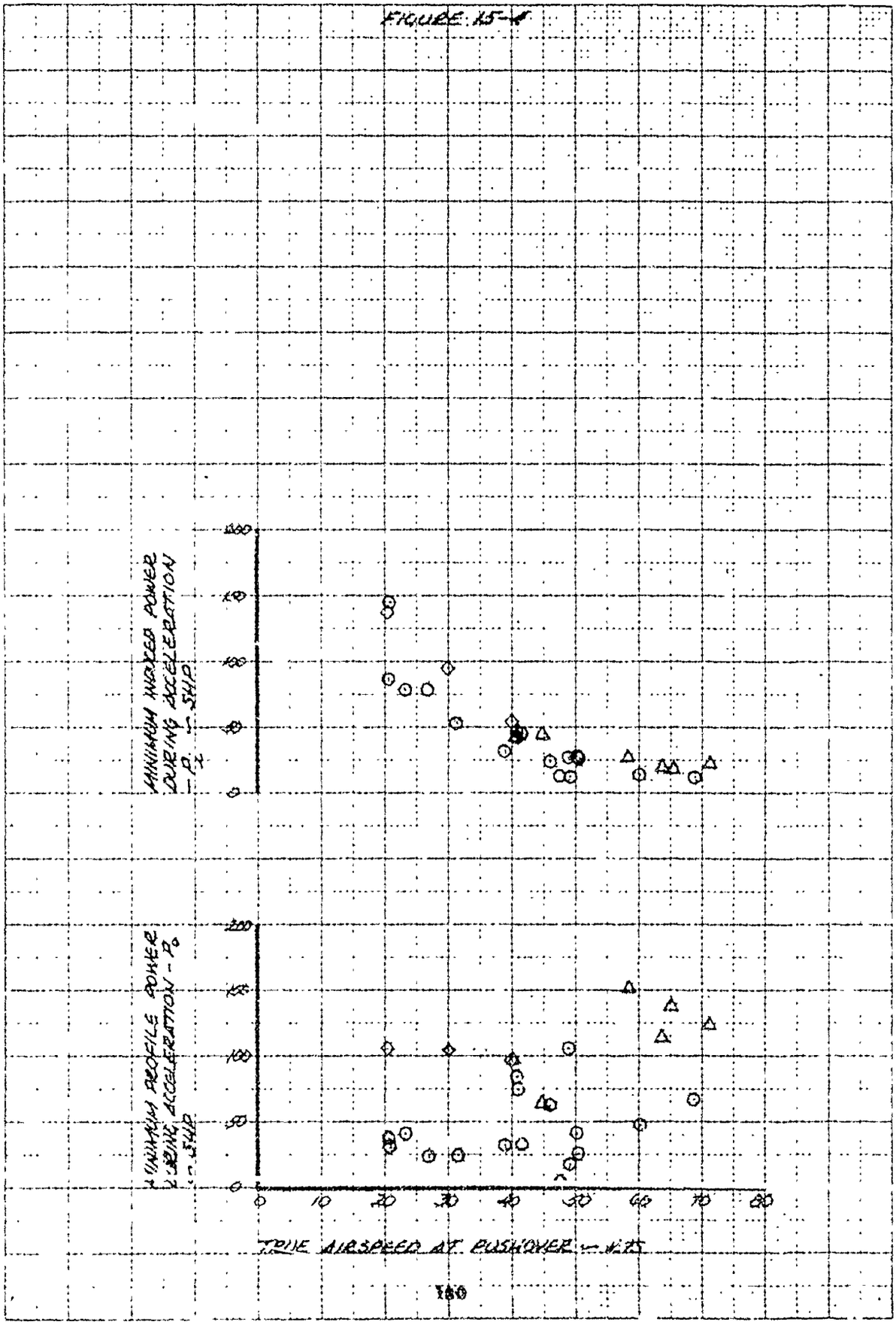
MINIMUM HOVER POWER DURING ACCELERATION - SHP
MINIMUM PROFILE POWER DURING ACCELERATION - SHP
TRUE AIRSPEED AT PUSHOVER - KTS

FIGURE 45-5

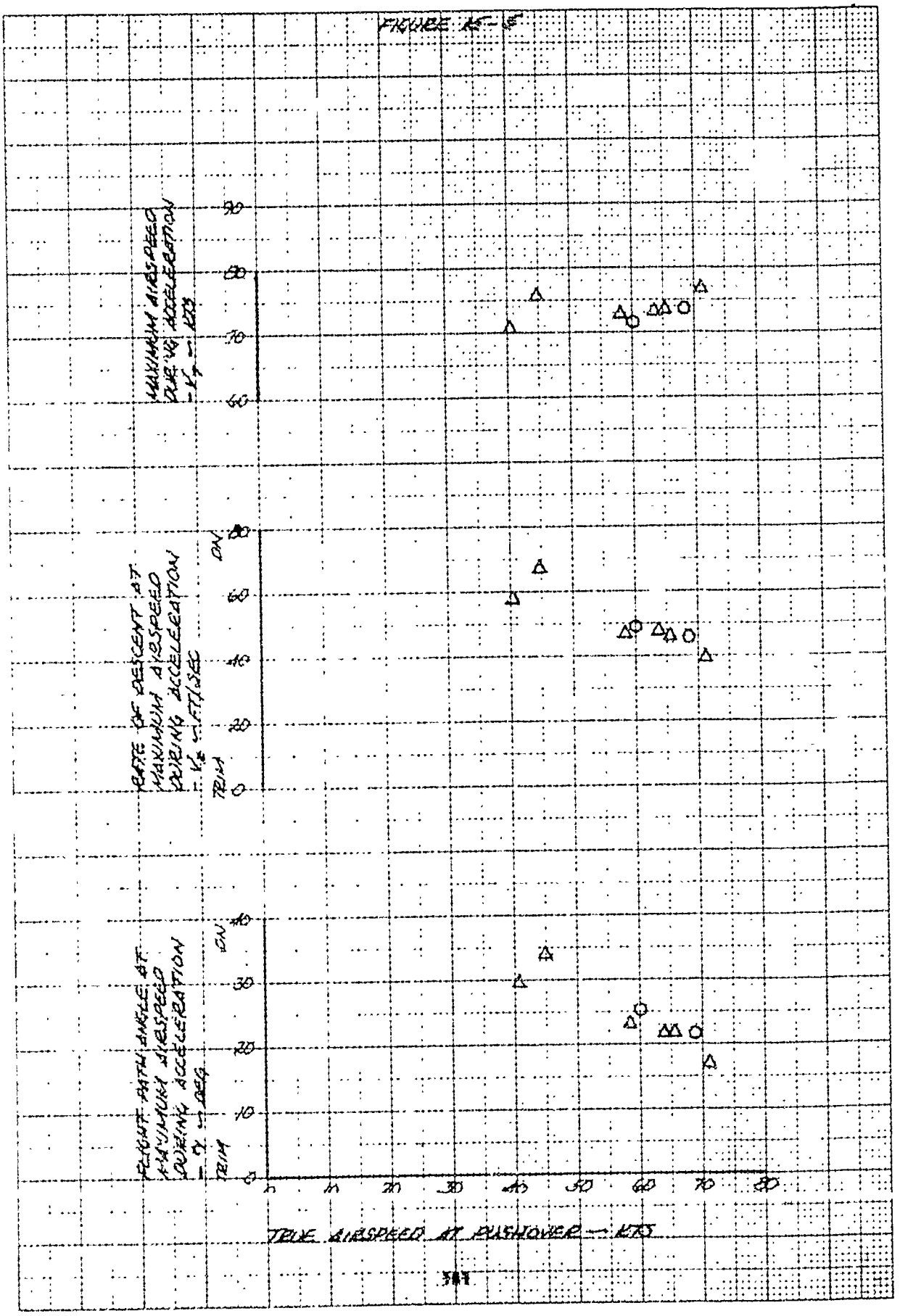
RATE OF DESCENT AT MAXIMUM AIRSPEED DURING ACCELERATION – V_y – FT/SEC
ON
TRIM
MAXIMUM AIRSPEED DURING ACCELERATION – KTS
FLIGHT PATH ANGLE AT MAXIMUM AIRSPEED DURING ACCELERATION – γ – DEG
ON
TRIM
TRUE AIRSPEED AT PUSHOVER – KTS

FIGURE A5-6

KEHART (USN) FLIGHT
RUSHOVER TO 60 KTS
PUSHOVER ACCELERATION
-1.4 - 1.7
RATE OF DESCENT AT 60 KTS
PUSHOVER ACCELERATION
-1.7 - 2.1
FLIGHT PATH ANGLE AT 60 KTS
PUSHOVER ACCELERATION -1.7 - 2.1
LEVEL
TRUE AIRSPEED AT PUSHOVER - KTS

FIGURE 15-7

FLIGHT PATH ANGLE
AT STABILIZED 60
KT. DESCENT - γ
DEGS
LEVEL
CAV
30
20
10
0
RATE OF DESCENT
AT STABILIZED 60
KT. DESCENT - Ḣ
FEET/SEC
LEVEL
CAV
60
40
20
0
HEIGHT LOSS FROM PUSHOVER TO
STABILIZED 60 KT DESCENT
- Δh - FT
LEVEL
CAV
100
200
300
400
500
TRUE AIRSPEED AT PUSHOVER - KTAS

FIGURE 15-7

RATE OF DESCENT AT STABILIZED 60 KT DESCENT - FT/SEC
FLIGHT PATH ANGLE AT STABILIZED 60 KT DESCENT - DEG
HEIGHT LOSS FROM PULLOUT TO STABILIZED 60 KT DESCENT - FT
LEVEL
TRUE AIRSPEED AT PULLOUT - KTS

FIGURE 15-9

MAXIMUM BOTTOM SPEED GAIN, MAXIMUM ROTOR SPEED
DECAY RATE DURING PUSHOVER
ENTRY AND PUSHOVER
KNOTS/SEC
KNOTS/SEC
GROUND SPEED LOST DURING
TRUE AIRSPEED AT PUSHOVER - KTS

FIGURE 45-10

MAXIMUM RATE OF TOTAL ENERGY CHANGE DURING ENTRY AND PULLOUT
-DE-/DT. -- SLUG
MAXIMUM RATE OF TOTAL ENERGY LOSS DURING DECELERATION
-DE/DT. -- SLUG
0
10
20
30
40
50
60
100
200
300
400
500
600

FIGURE No. 1

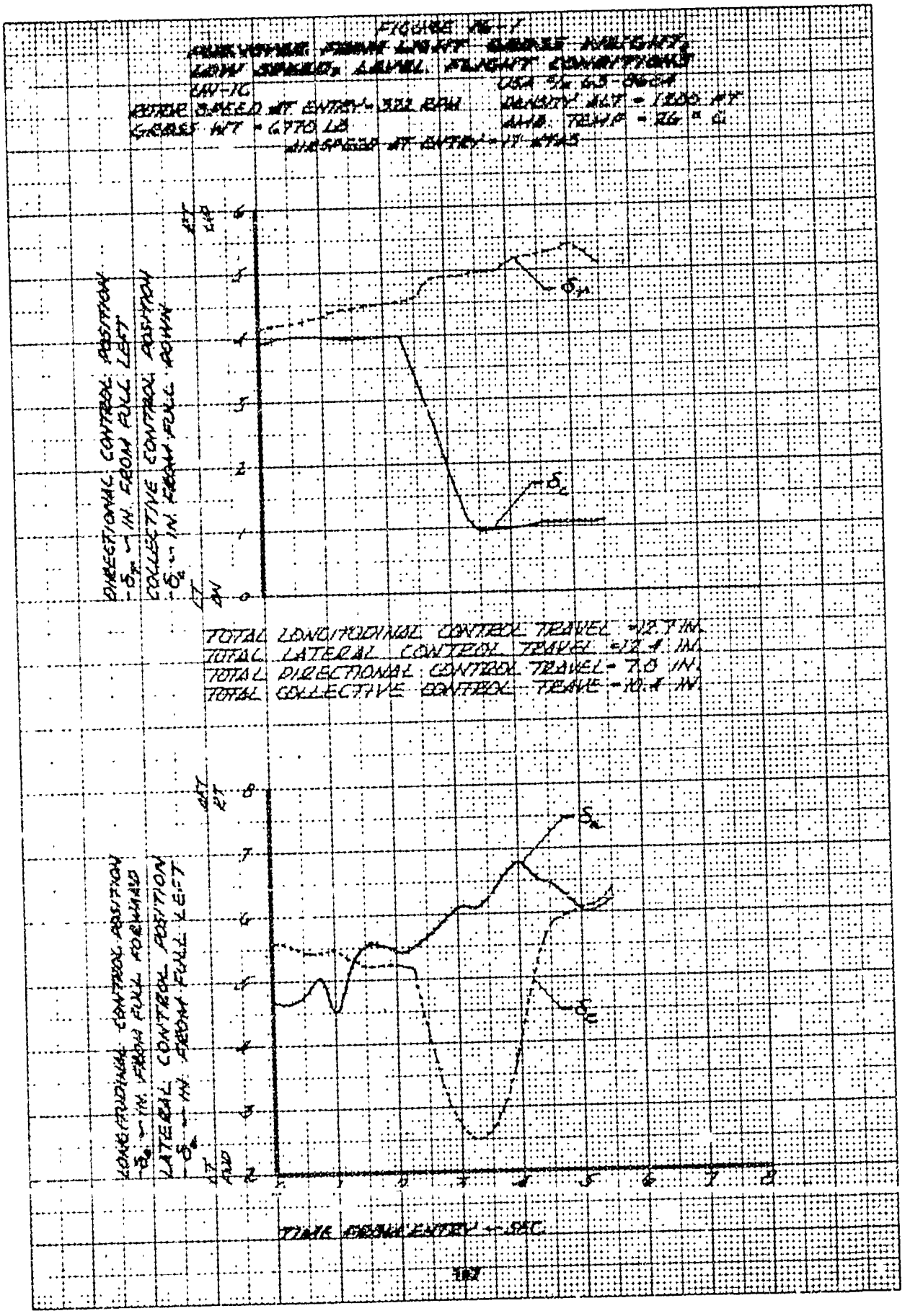
LAV-1C
ENTRY SPEED AT ENTRY = 332 KEAS
GROSS WT = 6770 LB
LONGITUDINAL CONTROL POSITION
-δe — IN. FROM FULL FORWARD
LATERAL CONTROL POSITION
-δa — IN. FROM FULL LEFT
DIRECTIONAL CONTROL POSITION
-δr — IN. FROM FULL LEFT
COLLECTIVE CONTROL POSITION
-δc — IN. FROM FULL DOWN
TOTAL LONGITUDINAL CONTROL TRAVEL = 12.7 IN.
TOTAL LATERAL CONTROL TRAVEL = 12.4 IN.
TOTAL DIRECTIONAL CONTROL TRAVEL = 7.0 IN.
TOTAL COLLECTIVE CONTROL TRAVEL = 10.4 IN.
TIME FROM ENTRY — SEC

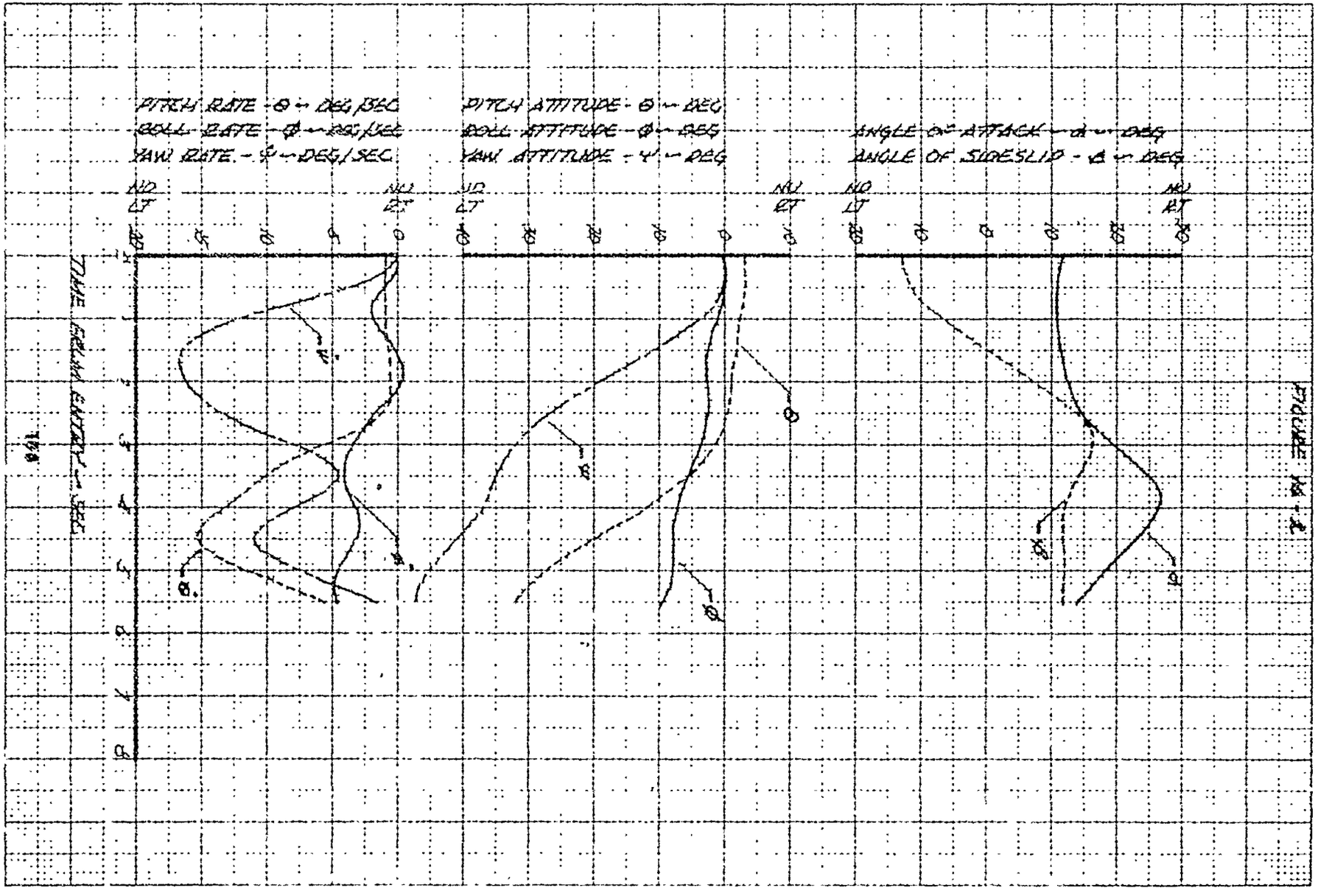
PITCH RATE - Θ̇ - DEG/SEC
ROLL RATE - Φ̇ - DEG/SEC
YAW RATE - Ψ̇ - DEG/SEC
PITCH ATTITUDE - Θ - DEG
ROLL ATTITUDE - Φ - DEG
YAW ATTITUDE - Ψ - DEG
ANGLE OF ATTACK - α - DEG
ANGLE OF SIDESLIP - β - DEG
MD LT
MU RT
TIME FROM LIFTOFF - SEC

FIGURE XX - 2

FIGURE 46 - 3

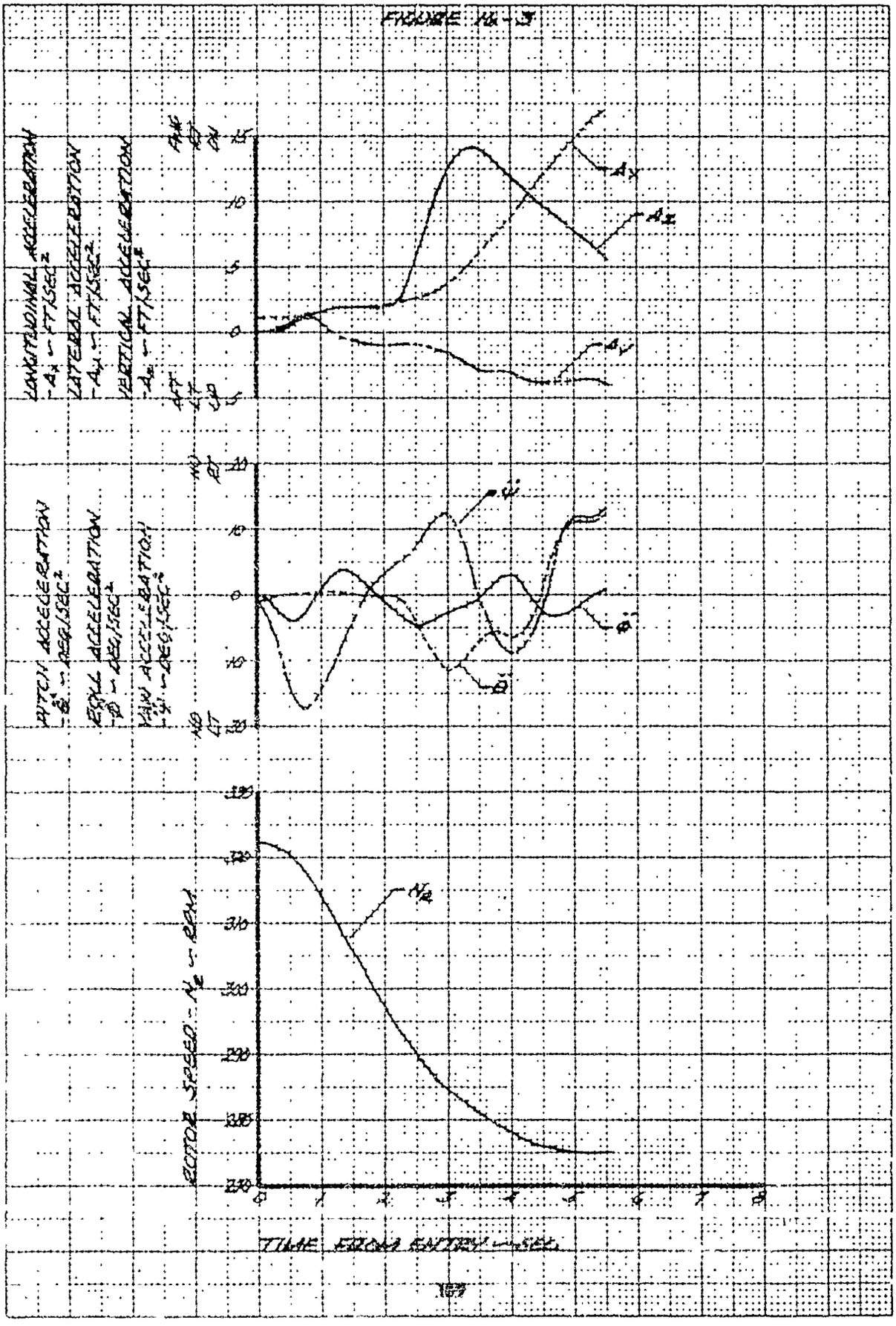
LONGITUDINAL ACCELERATION
- A_x -- FT/SEC²
LATERAL ACCELERATION
- A_y -- FT/SEC²
VERTICAL ACCELERATION
- A_z -- FT/SEC²
PITCH ACCELERATION
- $\dot{q}$ -- DEG/SEC²
ROLL ACCELERATION
- $\dot{p}$ -- DEG/SEC²
YAW ACCELERATION
- $\dot{r}$ -- DEG/SEC²
ROTOR SPEED - N_R -- RPM
TIME FROM ENTRY -- SEC
A_x
A_z
A_y
$\dot{q}$
$\dot{p}$
$\dot{r}$
N_R

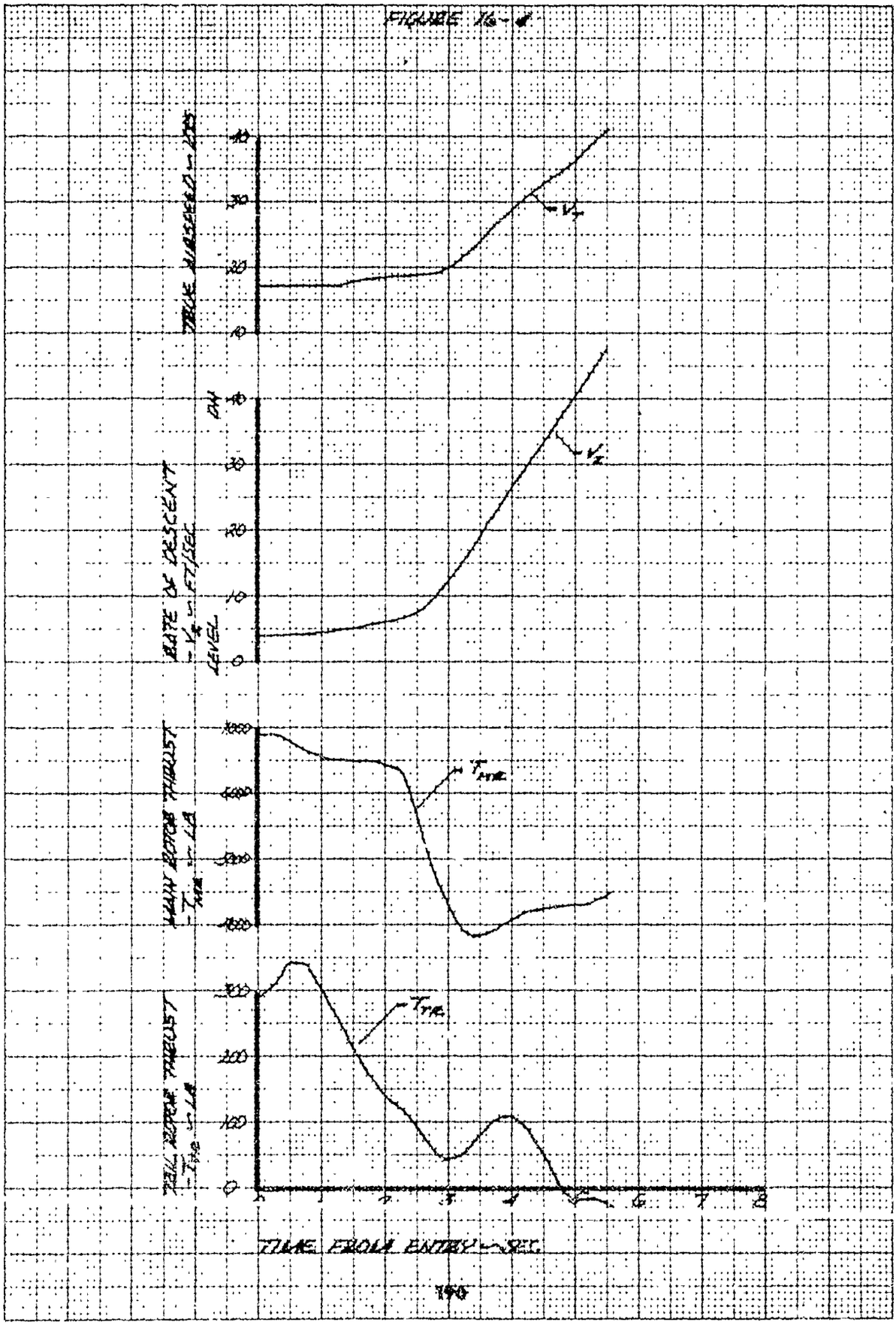
FIGURE 16-4
TRUE AIRSPEED — KNS
RATE OF DESCENT
$-V_z$ — FT/SEC
ALT LEVEL
MAIN ROTOR THRUST
$-T_{MR}$ — LB
TAIL ROTOR THRUST
$-T_{TR}$ — LB
V_T
V_z
T_{MR}
T_{TR}
TIME FROM ENTRY — SEC

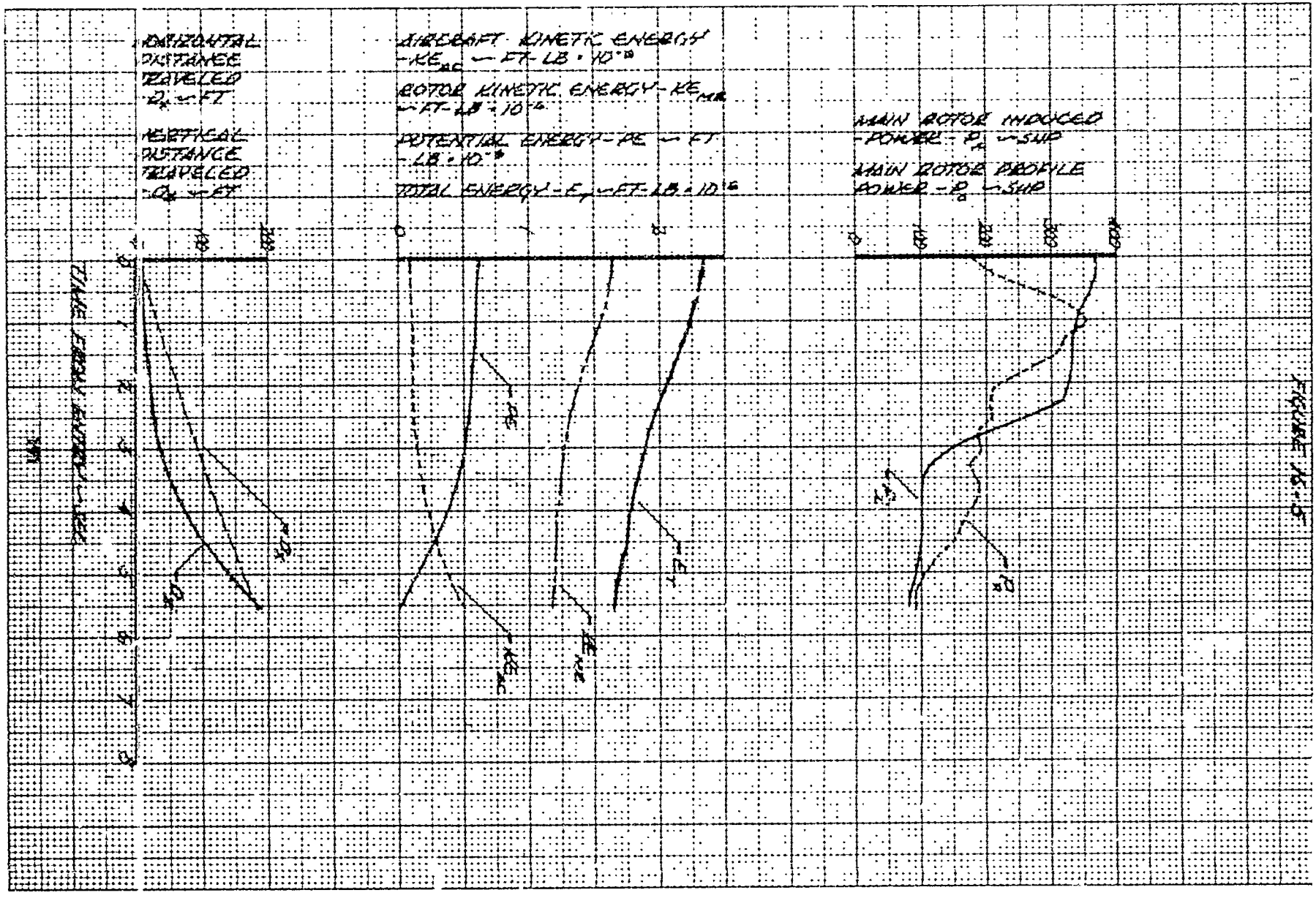
HORIZONTAL DISTANCE TRAVELED - D_x - FT
VERTICAL DISTANCE TRAVELED - D_y - FT
AIRCRAFT KINETIC ENERGY - KE_{AC} - FT-LB · 10^{-3}
ROTOR KINETIC ENERGY - KE_{MR} - FT-LB · 10^{-4}
POTENTIAL ENERGY - PE - FT-LB · 10^{-3}
TOTAL ENERGY - E_T - FT-LB · 10^{-6}
MAIN ROTOR INDUCED POWER - P_i - SHP
MAIN ROTOR PROFILE POWER - P_o - SHP
TIME FROM ENTRY - SEC
KE_{AC}
PE
KE_{MR}
E_T
D_x
D_y
P_i
P_o

FIGURE 15-5

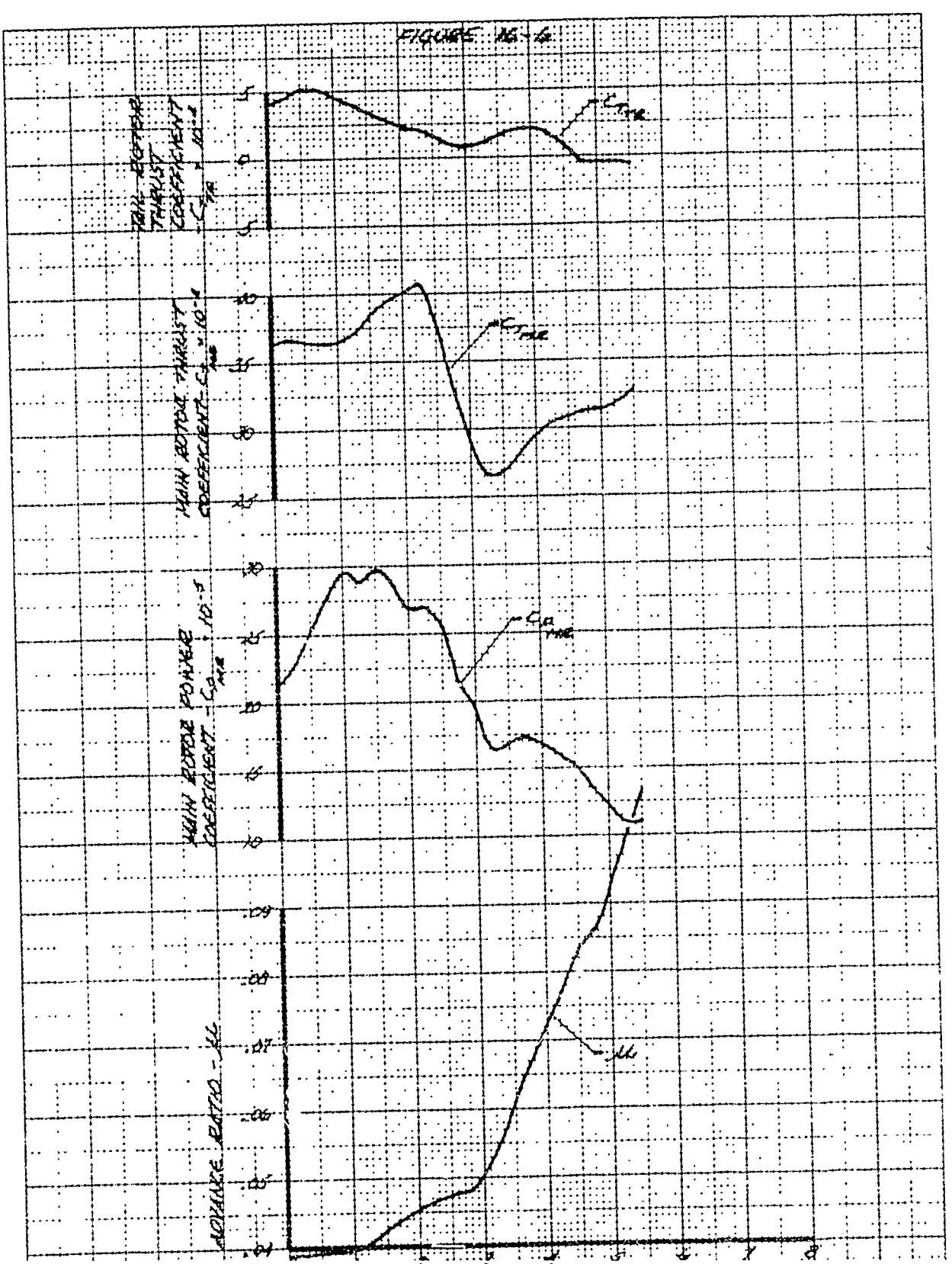
FIGURE 16-6
TAIL ROTOR THRUST COEFFICIENT - $C_{T_{TR}} \cdot 10^{-4}$
MAIN ROTOR THRUST COEFFICIENT - $C_{T_{MR}} \cdot 10^{-4}$
MAIN ROTOR POWER COEFFICIENT - $C_{Q_{MR}} \cdot 10^{-5}$
ADVANCE RATIO - μ
TIME FROM EARTH - SEC

FIGURE 17-1

COMPARISON OF MANEUVERS FROM CLIMB ENTRY

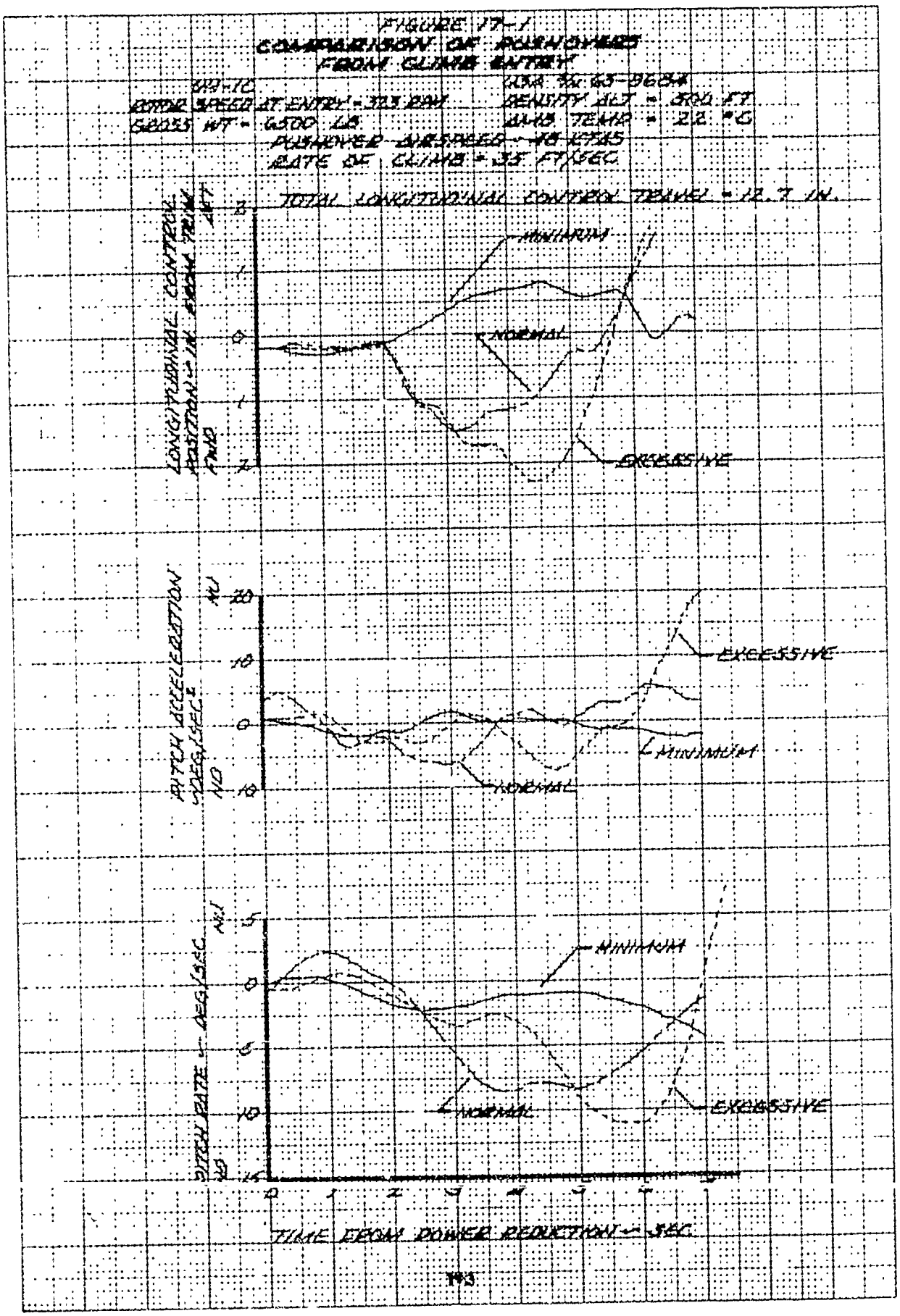

FIGURE IV-2

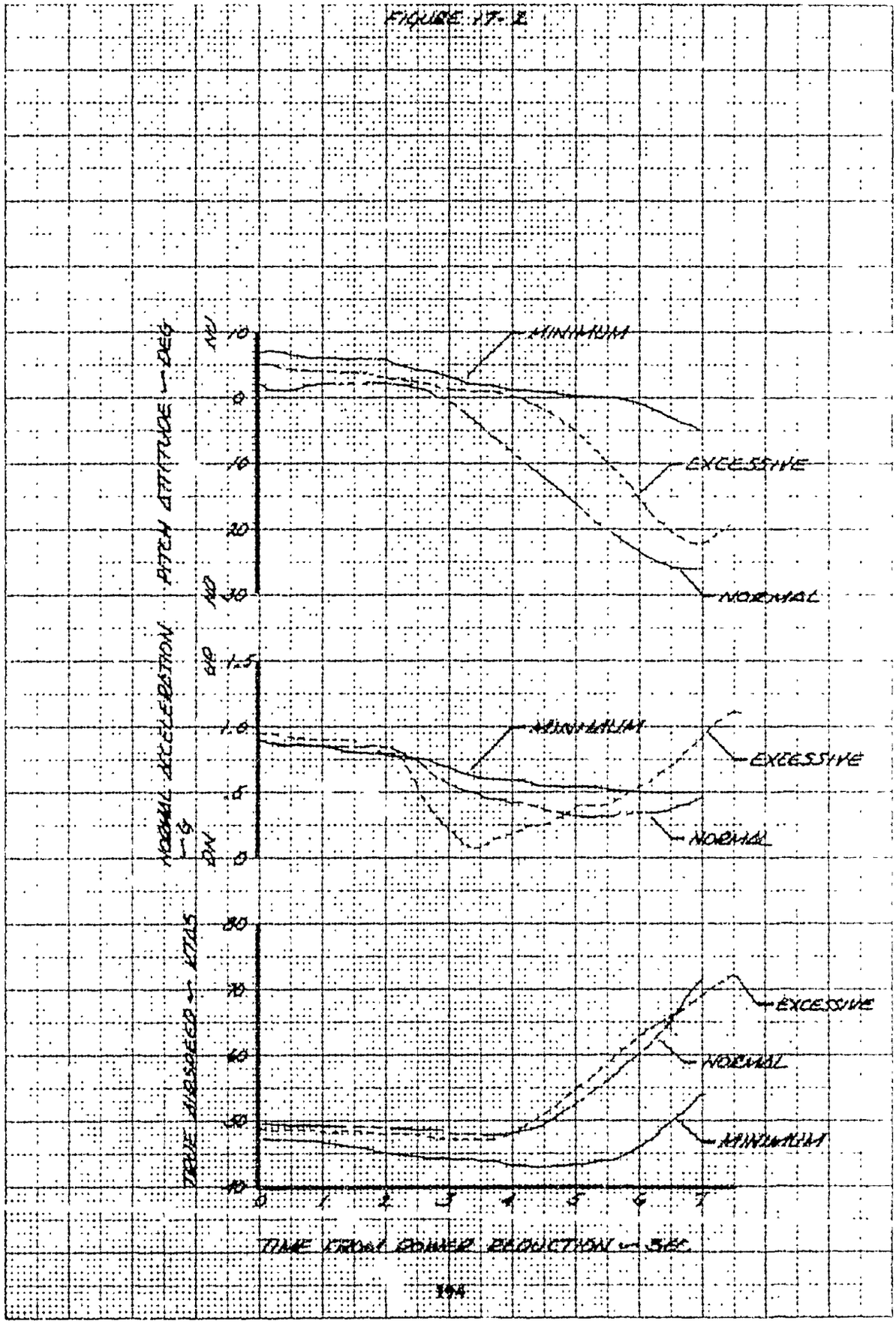
PITCH ATTITUDE — DEG
NORMAL ACCELERATION — G's
TRUE AIRSPEED — KTAS
TIME FROM POWER REDUCTION — SEC
MINIMUM
EXCESSIVE
NORMAL
MINIMUM
EXCESSIVE
NORMAL
EXCESSIVE
NORMAL
MINIMUM

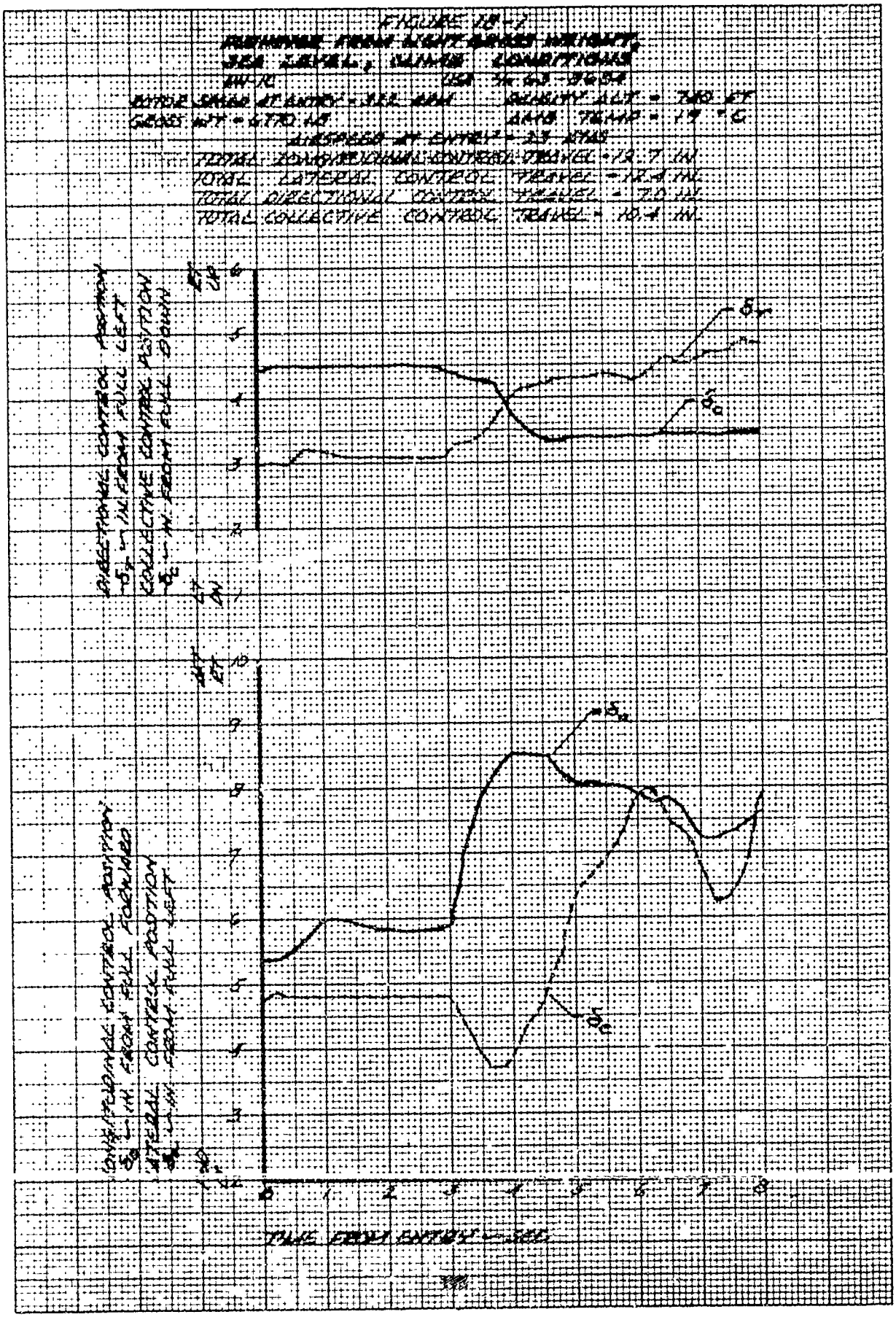
δ_r
δ_a
δ_e
δ_c
TIME FROM ENTRY — SEC

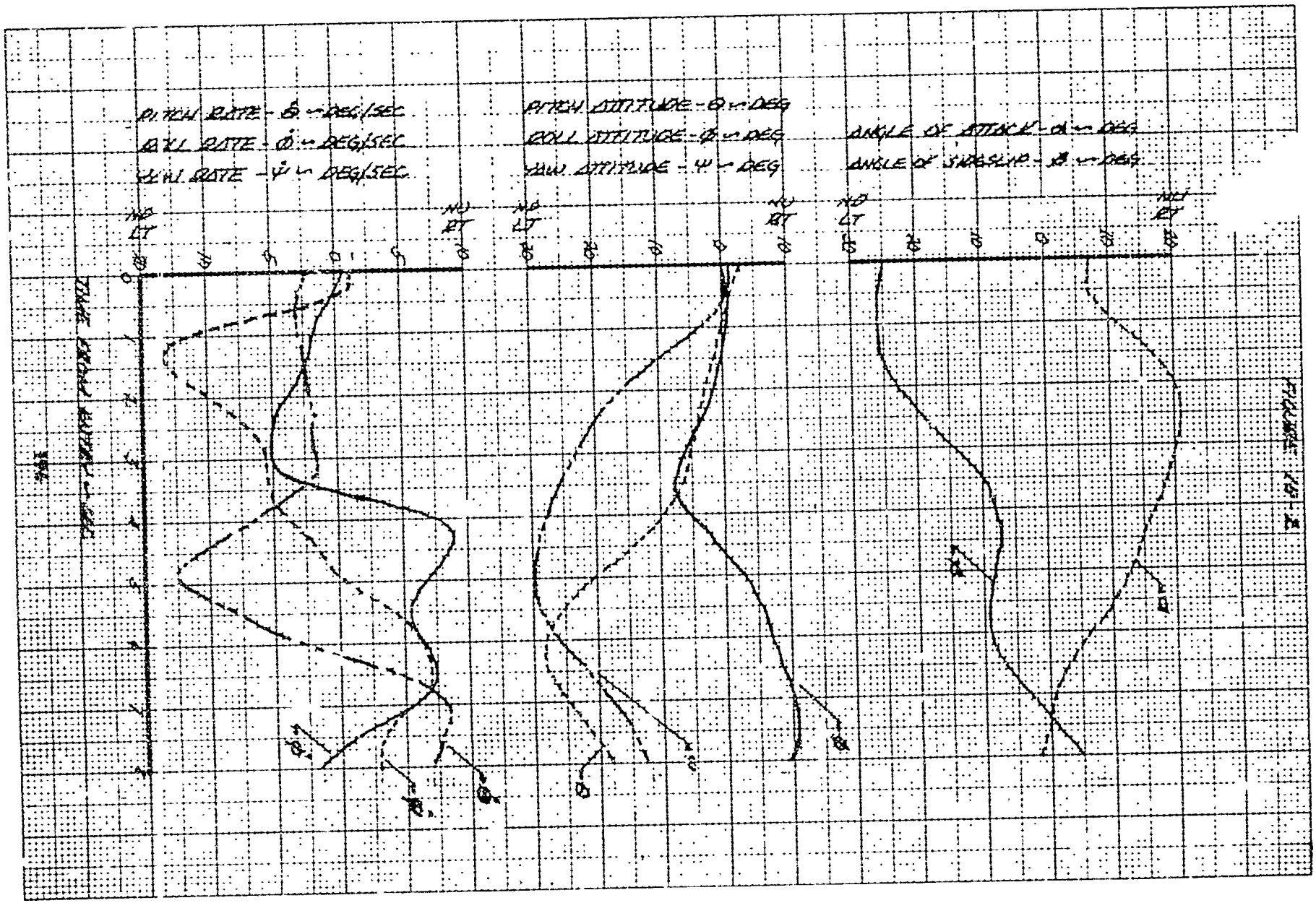
PITCH RATE - $\dot{\theta}$ - DEG/SEC
ROLL RATE - $\dot{\phi}$ - DEG/SEC
YAW RATE - $\dot{\psi}$ - DEG/SEC
PITCH ATTITUDE - θ - DEG
ROLL ATTITUDE - ϕ - DEG
YAW ATTITUDE - ψ - DEG
ANGLE OF ATTACK - α - DEG
ANGLE OF SIDESLIP - β - DEG
TIME FROM LIFTOFF - SEC

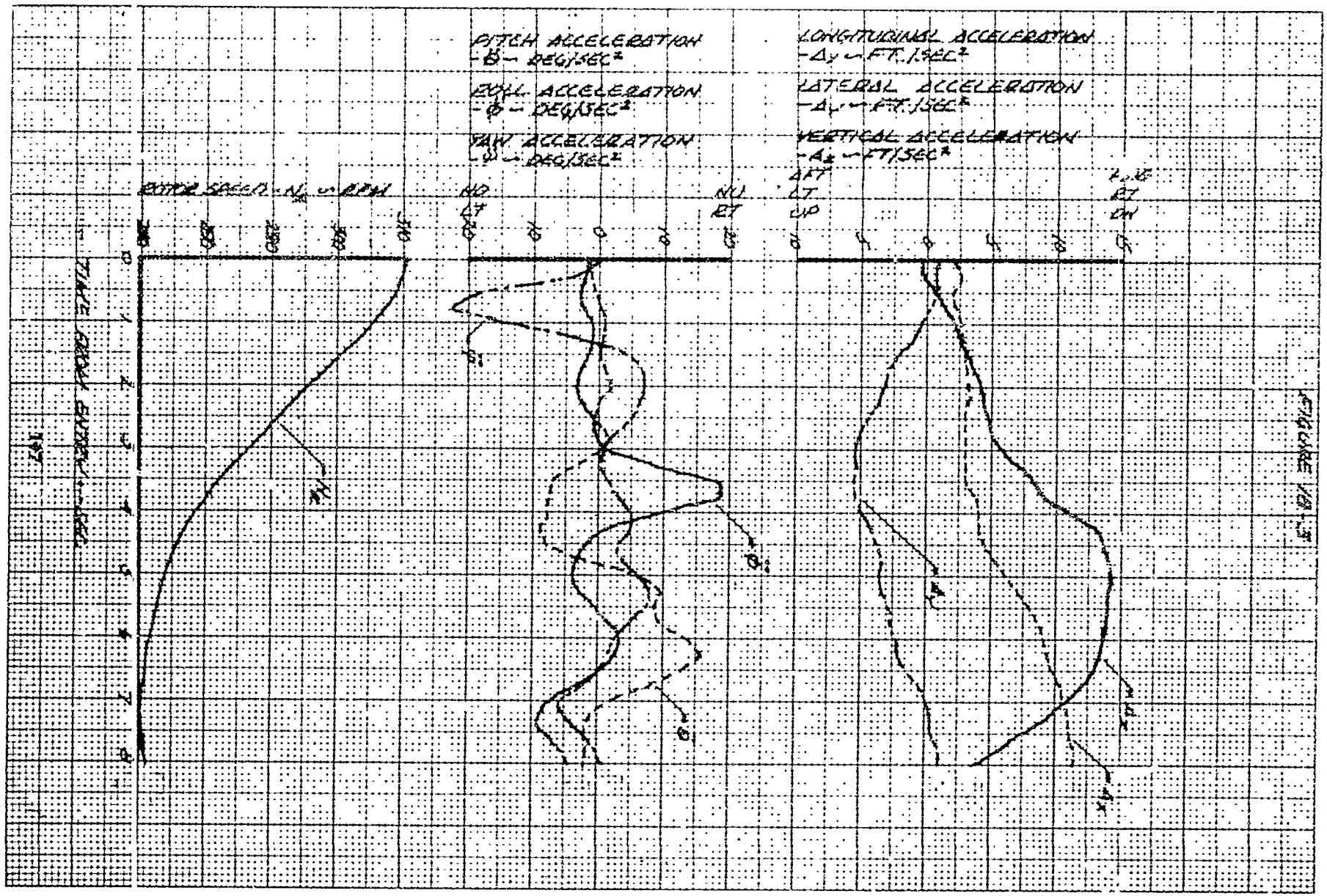
PITCH ACCELERATION
-θ̈ - DEG/SEC²
ROLL ACCELERATION
-φ̈ - DEG/SEC²
YAW ACCELERATION
-ψ̈ - DEG/SEC²
LONGITUDINAL ACCELERATION
-Ax - FT/SEC²
LATERAL ACCELERATION
-Ay - FT/SEC²
VERTICAL ACCELERATION
-Az - FT/SEC²
TIME FROM LAUNCH - SEC

FIGURE 19-4

TRUE AIRSPEED - V_T - KNOTS
RATE OF DESCENT - V_Z - FT/SEC
MAIN ROTOR THRUST - T_{MR} - LB
TAIL ROTOR THRUST - T_{TR} - LB
V_T
V_Z
T_{MR}
T_{TR}
TIME FROM ENTRY - SEC

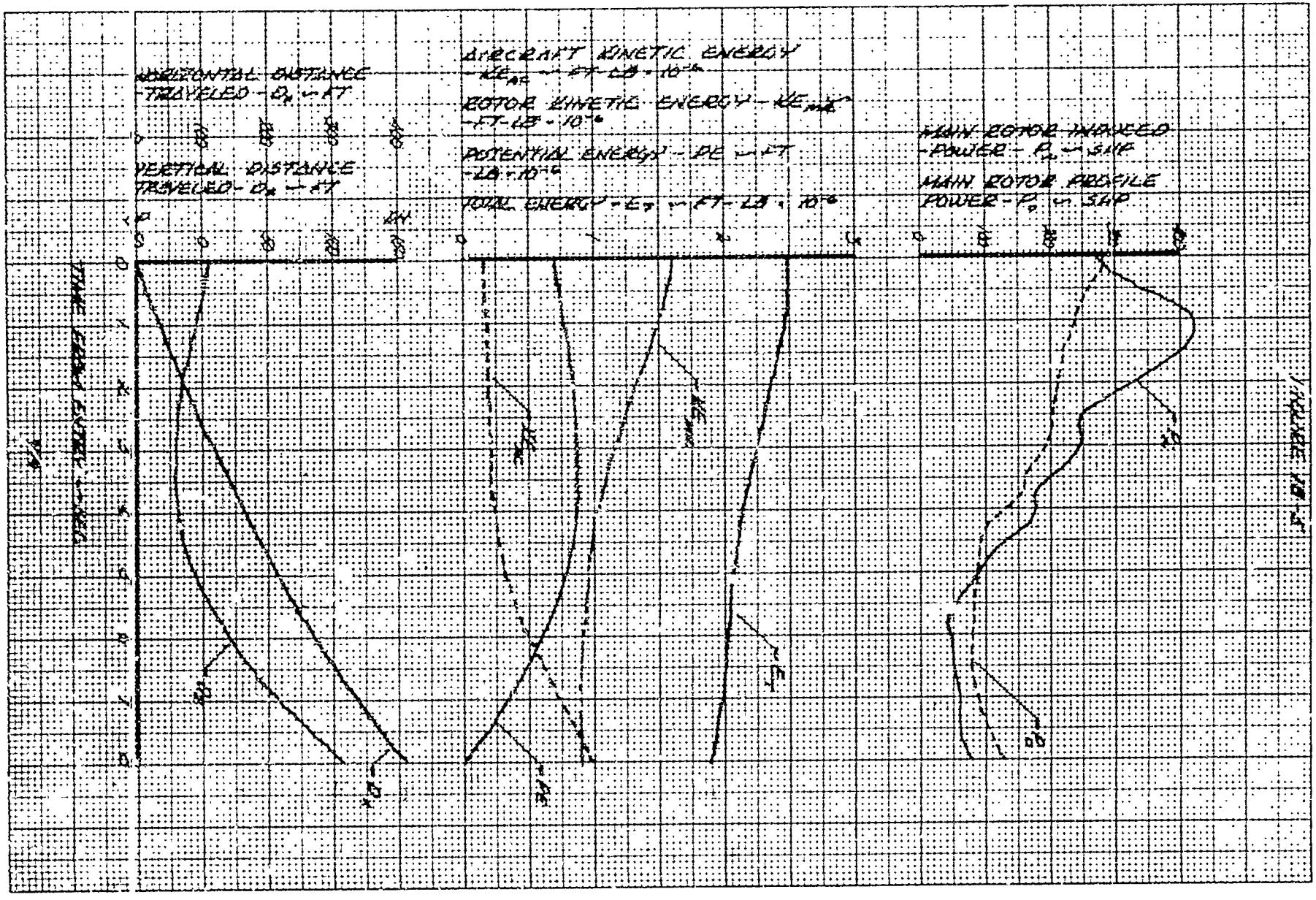
HORIZONTAL DISTANCE TRAVELED - D_x - FT
VERTICAL DISTANCE TRAVELED - D_y - FT
TIME FROM ENTRY - SEC
AIRCRAFT KINETIC ENERGY - KE_{AC} - FT-LB - 10^{-6}
ROTOR KINETIC ENERGY - KE_{ROT} - FT-LB - 10^{-6}
POTENTIAL ENERGY - PE - FT-LB - 10^{-6}
TOTAL ENERGY - E_T - FT-LB - 10^{-6}
MAIN ROTOR INDUCED POWER - P_i - SHP
MAIN ROTOR PROFILE POWER - P_o - SHP
FIGURE 18 - 5

FIGURE 18-6

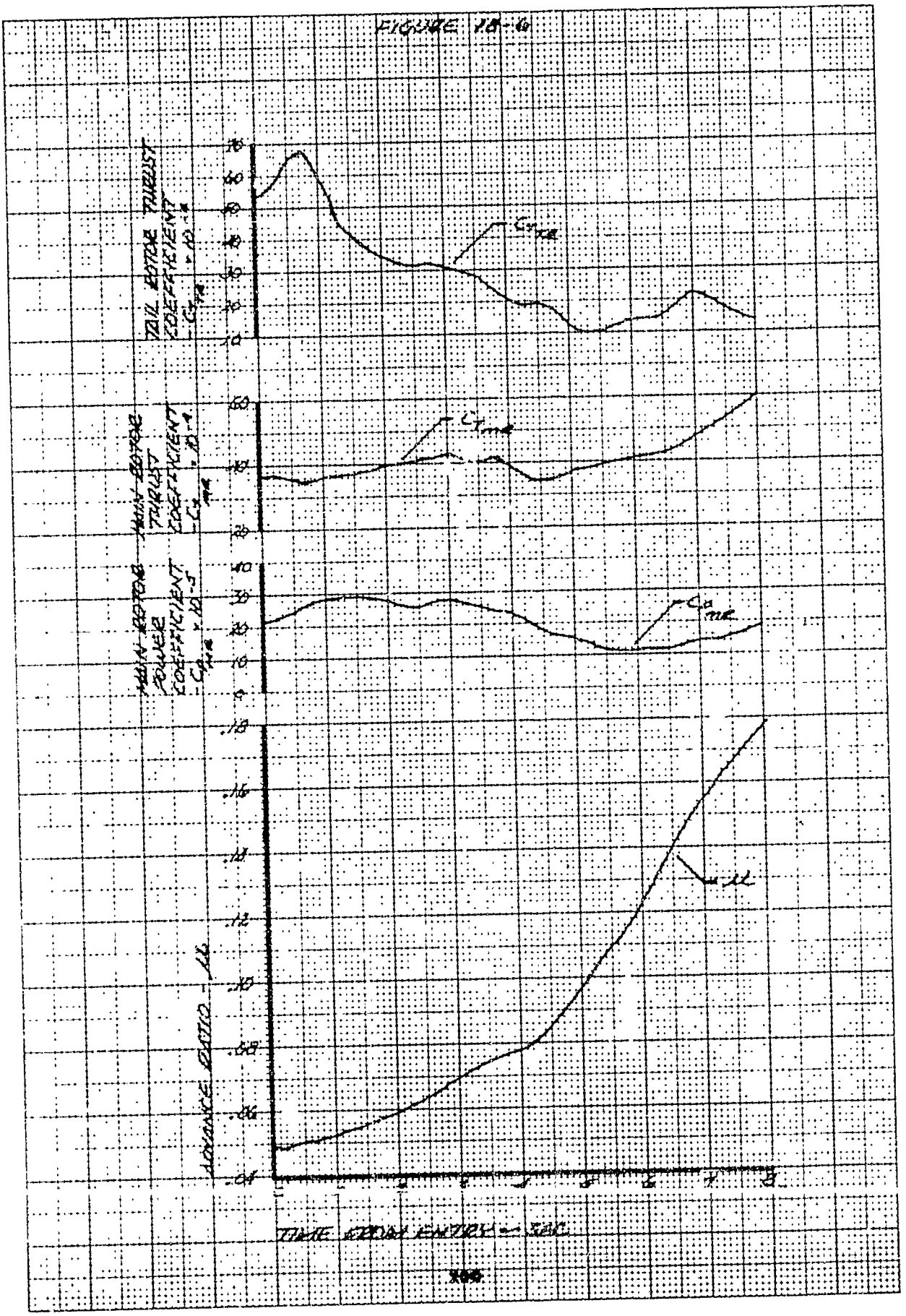
TAIL BOTTOM THRUST COEFFICIENT
MAIN BOTTOM THRUST COEFFICIENT
MAIN BOTTOM POWER COEFFICIENT
ADVANCE RATIO - J
TIME FROM ENTRY - SEC

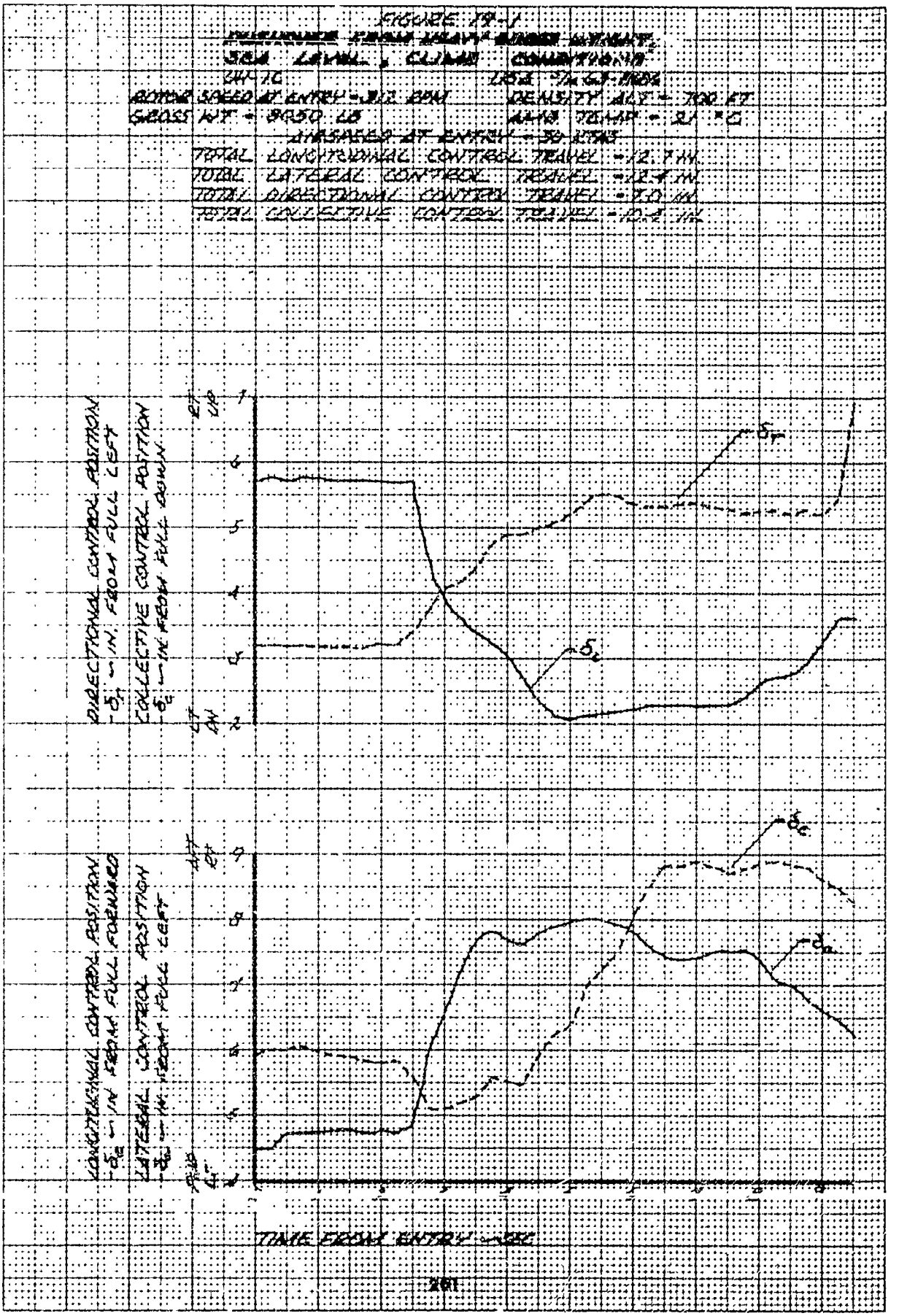
FIGURE 19-1
TOTAL LEVEL, CLEAN CONFIGURATION
ROTOR SPEED AT ENTRY = 312 RPM
GROSS WT = 9250 LB
DIRECTIONAL CONTROL POSITION
δ_r — IN. FROM FULL LEFT
COLLECTIVE CONTROL POSITION
δ_c — IN. FROM FULL DOWN
LONGITUDINAL CONTROL POSITION
δ_e — IN. FROM FULL FORWARD
LATERAL CONTROL POSITION
δ_a — IN. FROM FULL LEFT
TIME FROM ENTRY — SEC

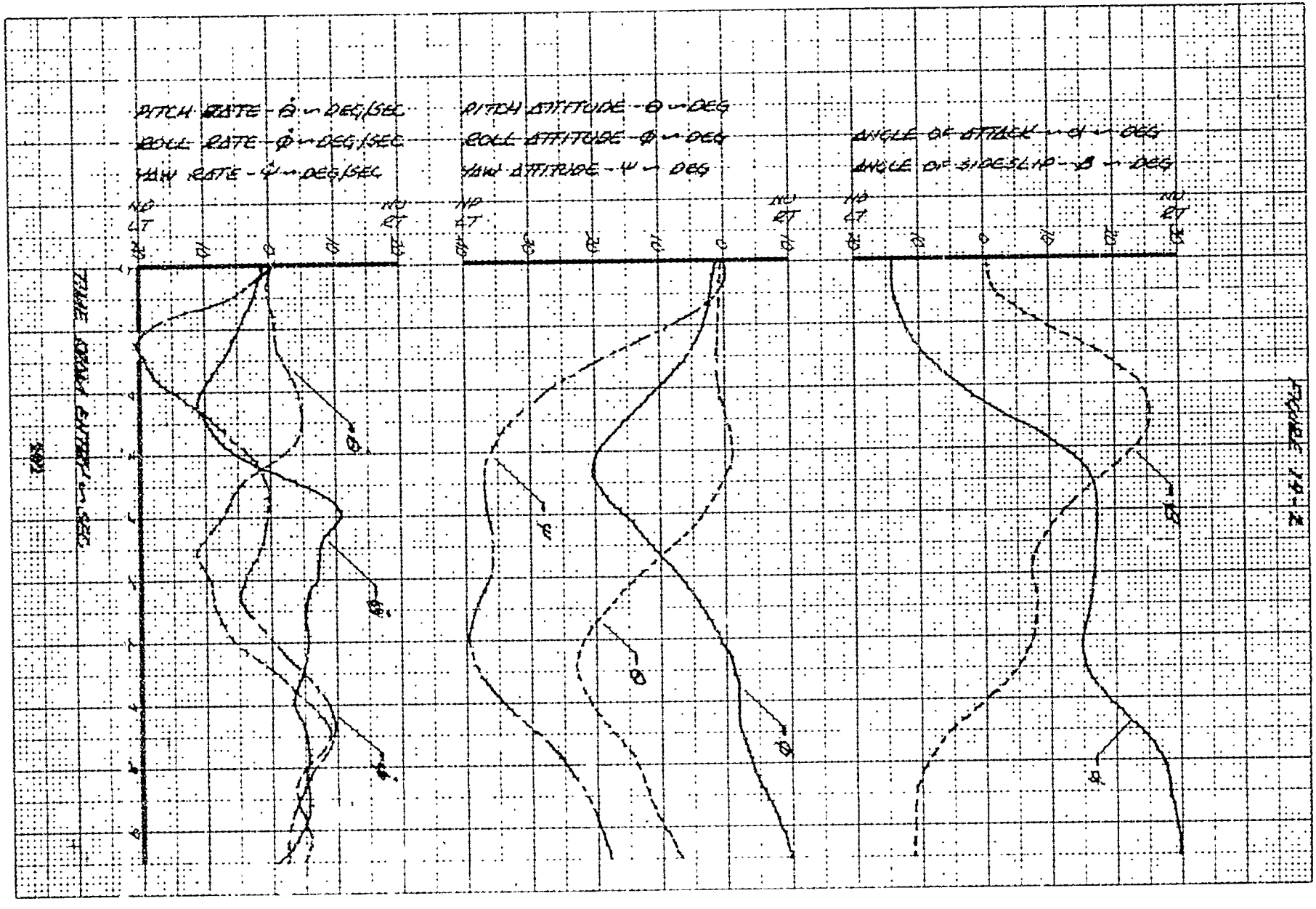
PITCH RATE - $\dot{\theta}$ - DEG/SEC
ROLL RATE - $\dot{\phi}$ - DEG/SEC
YAW RATE - $\dot{\psi}$ - DEG/SEC
PITCH ATTITUDE - θ - DEG
ROLL ATTITUDE - ϕ - DEG
YAW ATTITUDE - ψ - DEG
ANGLE OF ATTACK - α - DEG
ANGLE OF SIDESLIP - β - DEG
TIME FROM ENTRY - SEC
FIGURE 14-2

FIGURE 19-5

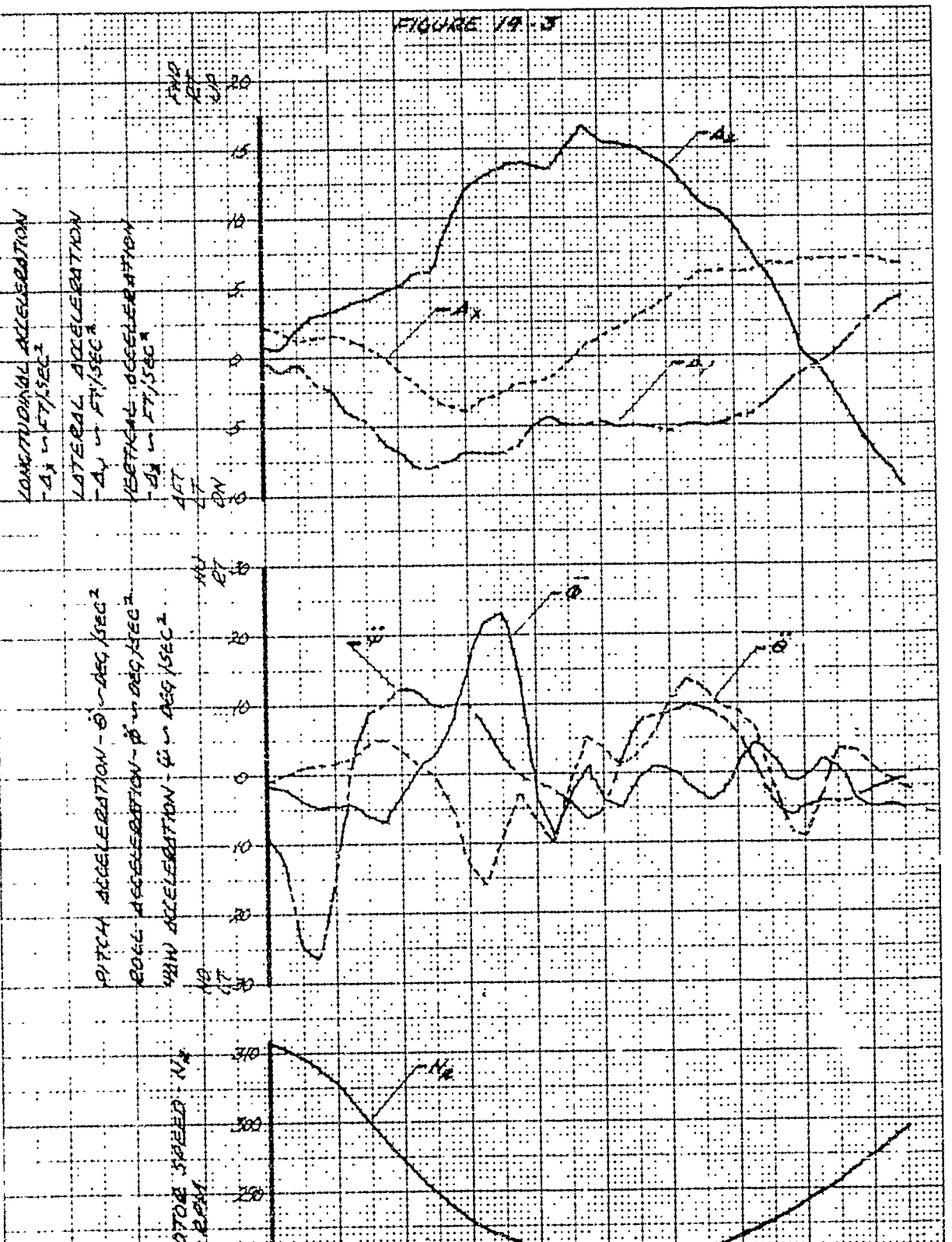
LONGITUDINAL ACCELERATION
$-A_x$ — FT/SEC²
LATERAL ACCELERATION
$-A_y$ — FT/SEC²
VERTICAL ACCELERATION
$-A_z$ — FT/SEC²
PITCH ACCELERATION - $\ddot{\theta}$ — DEG/SEC²
ROLL ACCELERATION - $\ddot{\phi}$ — DEG/SEC²
YAW ACCELERATION - $\ddot{\psi}$ — DEG/SEC²
ZOOTOB SPEED: N_z
— RPM
FWD
AFT
UP
DN
LEFT
RIGHT
TIME FROM ENTRY

FIGURE 19.4

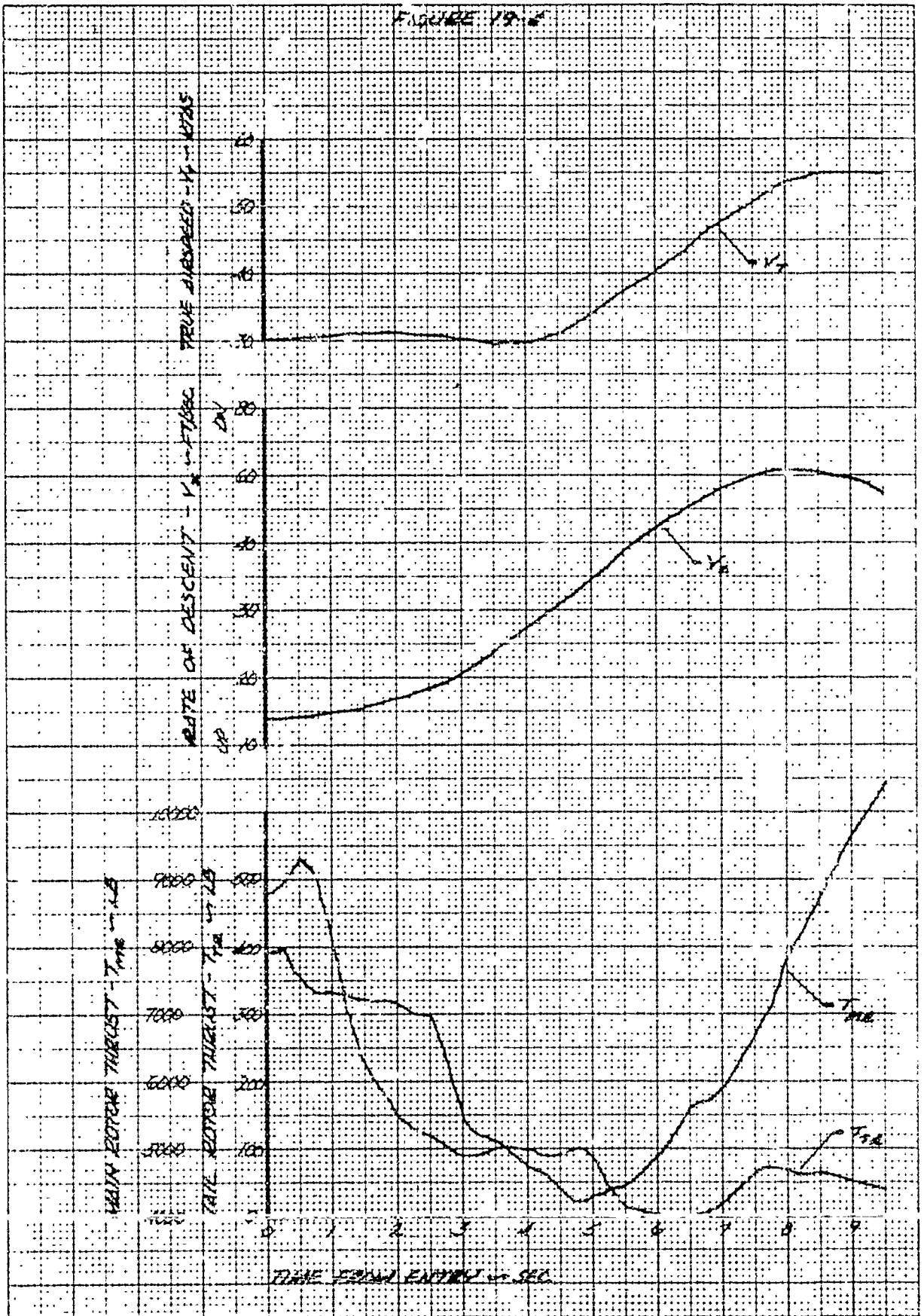
MAIN ENGINE THRUST - T_{ME} - LB
TAIL ENGINE THRUST - T_{TE} - LB
RATE OF DESCENT - V_R - FT/SEC
TRUE AIRSPEED - V_T - KNOTS
TIME FROM ENTRY - SEC
V_T
V_R
T_{ME}
T_{TE}

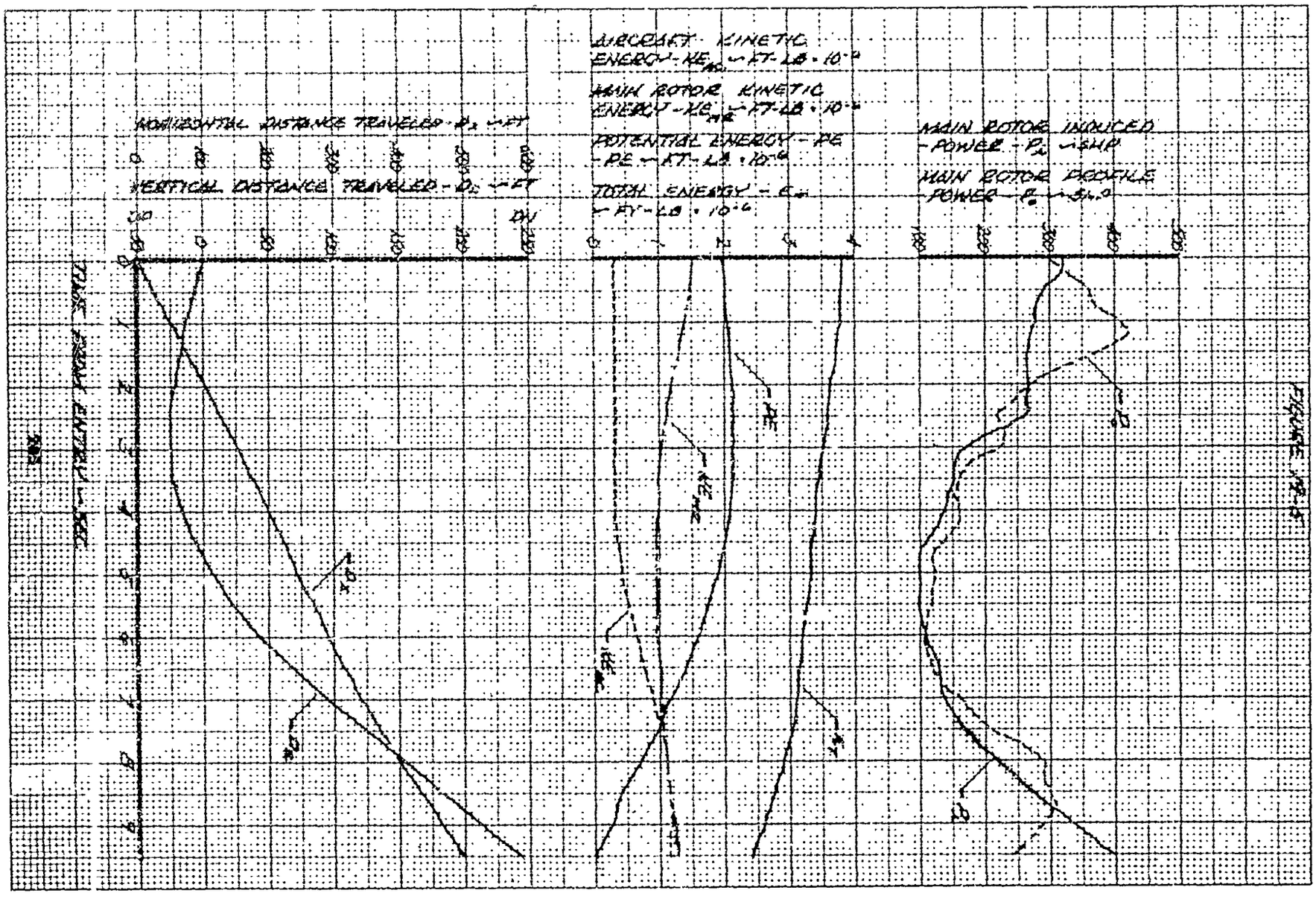
HORIZONTAL DISTANCE TRAVELED - D_x - FT
VERTICAL DISTANCE TRAVELED - D_z - FT
AIRCRAFT KINETIC ENERGY - KE_{AC} - FT-LB · 10^{-6}
MAIN ROTOR KINETIC ENERGY - KE_{MR} - FT-LB · 10^{-6}
POTENTIAL ENERGY - PE - PE - FT-LB · 10^{-6}
TOTAL ENERGY - E - FT-LB · 10^{-6}
MAIN ROTOR INDUCED POWER - P_i - SHP
MAIN ROTOR PROFILE POWER - P_o - SHP
TIME FROM ENTRY - SEC
PE
KE_{MR}
E
KE_{AC}
P_i
P_o

FIGURE 48-4

FIGURE 19-6

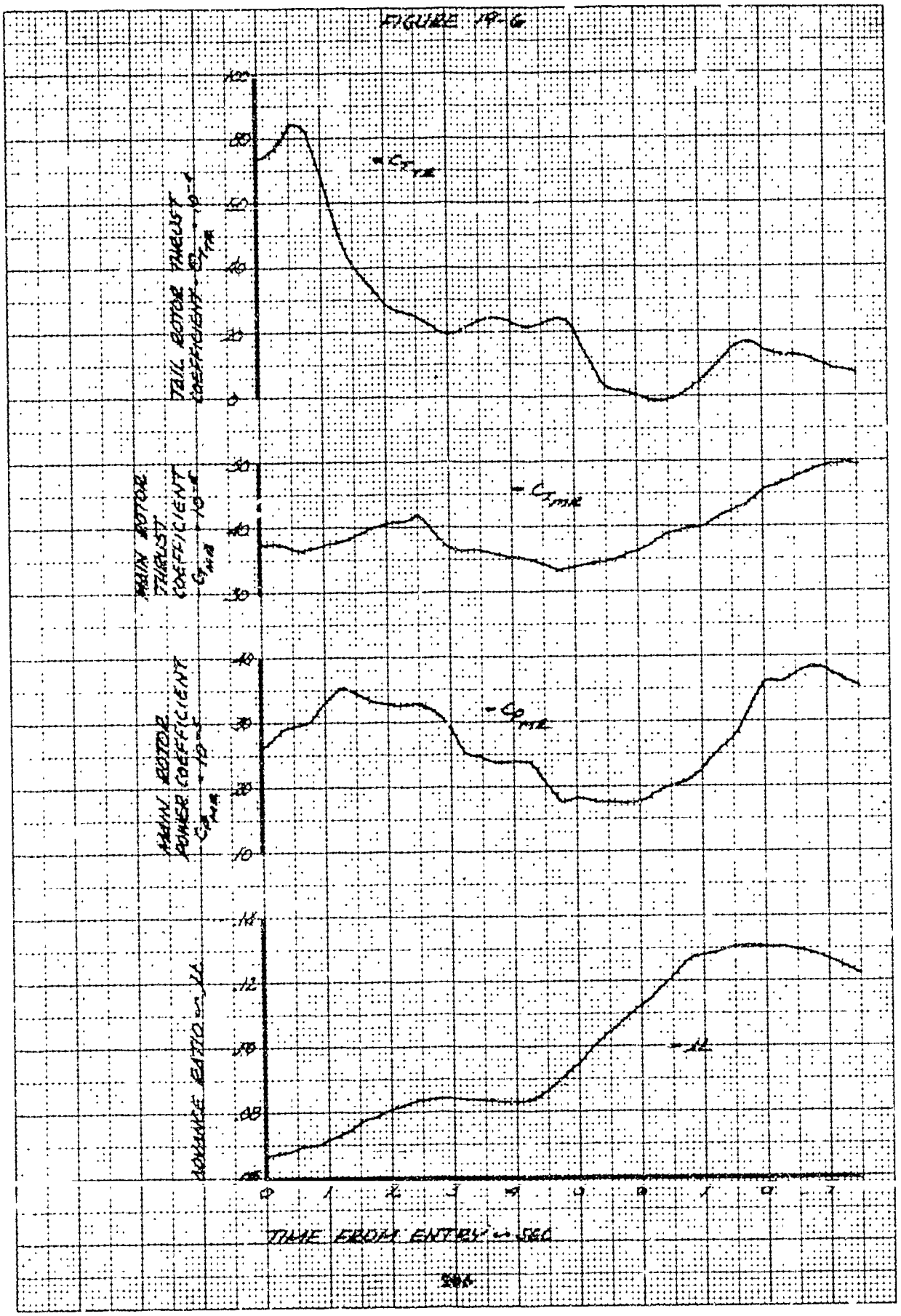
TAIL ROTOR THRUST COEFFICIENT $C_{T_{TR}}$
MAIN ROTOR THRUST COEFFICIENT $C_{T_{MR}}$
MAIN ROTOR POWER COEFFICIENT $C_{P_{MR}}$
ADVANCE RATIO = μ
$-C_{T_{TR}}$
$-C_{T_{MR}}$
$-C_{P_{MR}}$
$-\mu$
TIME FROM ENTRY - SEC

FIGURE 20-1

OPERATING CONDITIONS IN STEADY STATE DESCENT

UH-1C

USA S/N 63-8684

ROTOR SPEED = 300 RPM

DENSITY ALT = 8700 FT

GROSS WT = 6890 LB

AMB TEMP = 23° C

THRUST COEFF = 0.004110

TOTAL LONGITUDINAL CONTROL TRAVEL = 12.7 IN.

TOTAL LATERAL CONTROL TRAVEL = 12.4 IN.

TOTAL DIRECTIONAL CONTROL TRAVEL = 7.0 IN.

TOTAL COLLECTIVE CONTROL TRAVEL = 10.4 IN.

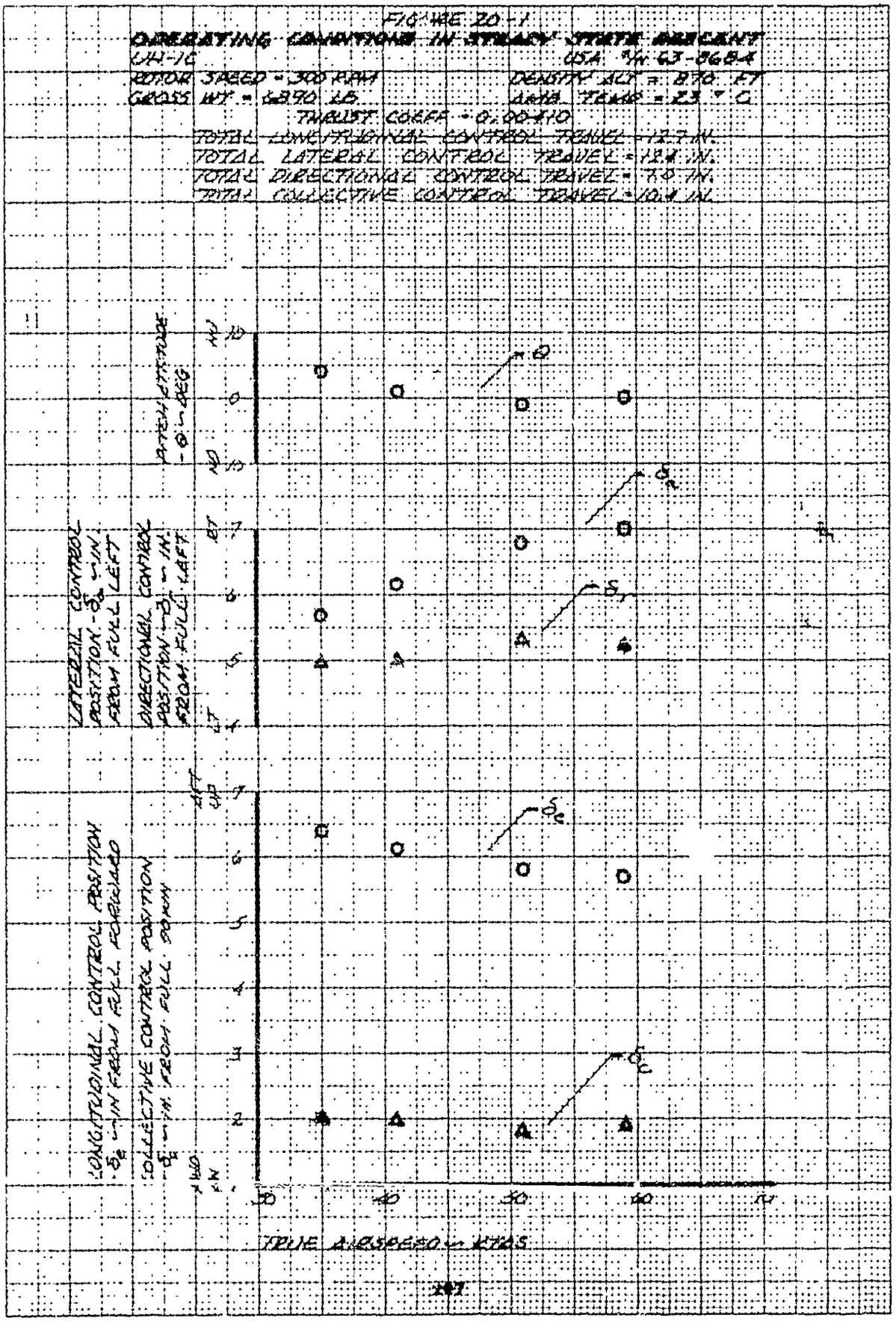

FIGURE 20-2

INCREASING ANGLE OF ATTACK
INCREASING ANGLE OF ATTACK
INCREASING ANGLE OF ATTACK
INCREASING ANGLE OF ATTACK
TRUE AIRSPEED — KNOTS

FIGURE 20-3

400
300
200
100
0
DRUG - K_D
K_D
40
30
20
10
0
RATE PER CLEARANCE - K_R
K_R
30
40
50
60
70

FIGURE 21-1

CONCEPTUAL COMPARISON IN STEADY-STATE DESCENT
USA 56 63-8684
ROTOR SPEED = 350 RPM
GROSS WT = 6250 LB
DENSITY ALT = 870 FT
OAT = 23 °C
THRUST COEFF = 0.00530
TOTAL LONGITUDINAL CONTROL TRAVEL = 12.7 IN.
TOTAL LATERAL CONTROL TRAVEL = 12.4 IN.
TOTAL DIRECTIONAL CONTROL TRAVEL = 7.0 IN.
TOTAL COLLECTIVE CONTROL TRAVEL = 10.4 IN.
LATERAL CONTROL POSITION - δa = IN. FROM FULL LEFT
DIRECTIONAL CONTROL POSITION - δr = IN. FROM FULL LEFT
COLLECTIVE CONTROL POSITION - δc = IN. FROM FULL DOWN
PITCH ATTITUDE - θ - DEG
NU
AFT
LEFT
UP
RIGHT
DOWN
TRUE AIRSPEED - KTAS
δa
δr
δc
δe

FIGURE II-2

MAIN BOTTLE MINIMUM POWER
P_{b_1} = 5HP
MAIN BOMB FACTOR POWER
P_{b_0} = 5HP
AUXILIARY POWER P_{a_1} = 5HP
0
100
200
300
400
P_{b_0}
P_{a_1}
P_{b_1}

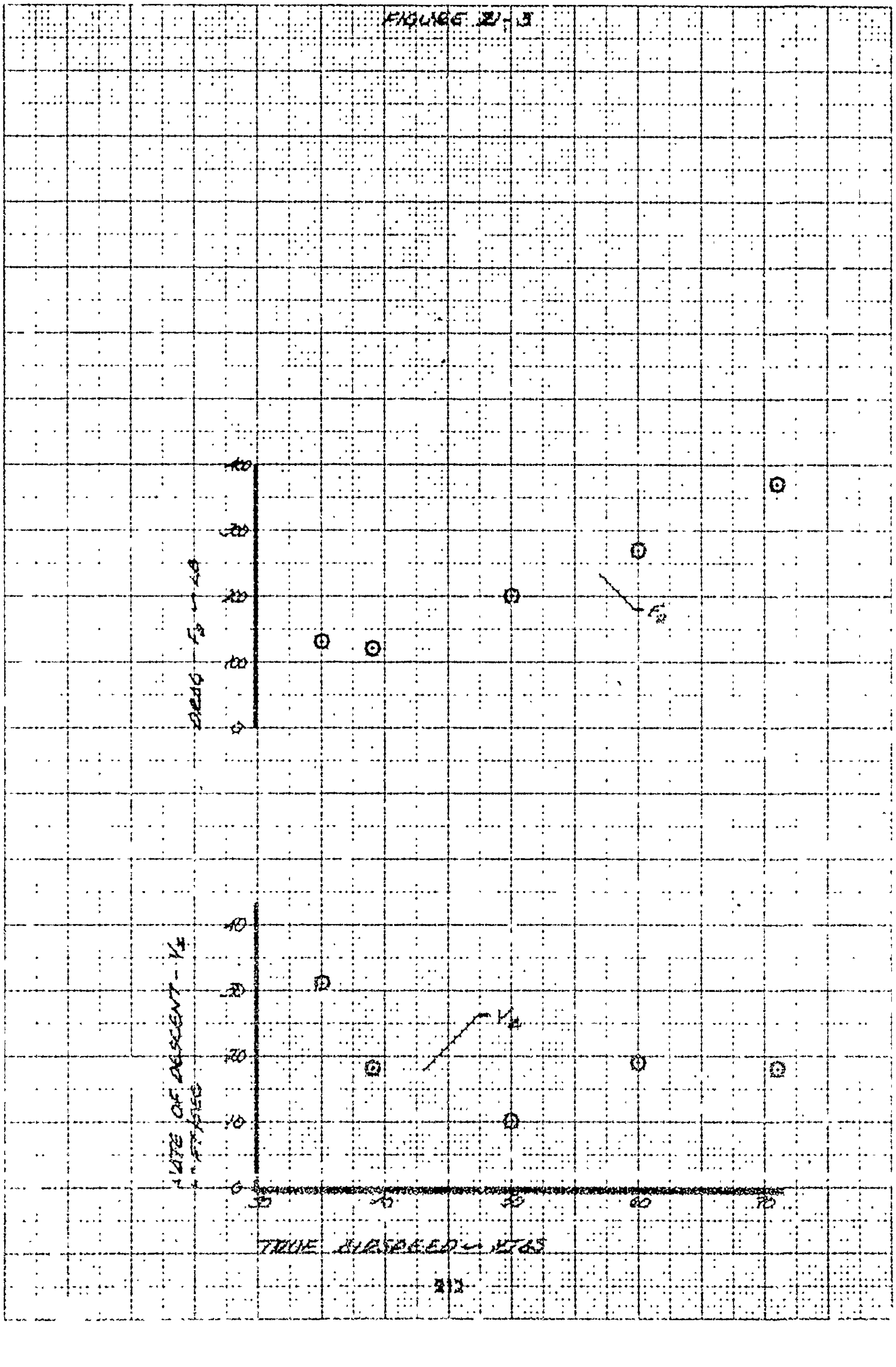
FIGURE IV-3
DRAG - F_D - LB
400
300
200
100
0
F_D
RATE OF DESCENT - V_z - FT/SEC
40
30
20
10
0
V_z
30
40
50
60
70
TRUE AIRSPEED - KTAS

FIGURE 22-1

CYCLIC FLARE PERFORMANCE

UH-1C USA S/N 65-10604

02033 WT = 6890 LB DENSITY ALT = SL

AMB. TEMP = 23 °C

SYM	AVG ROTOR SPEED AT FLARE - RPM	THRUST COEF AT FLARE
○	260	0.05550
◇	300	0.05410

MAST AFT LONGITUDINAL CONTROL POSITION DURING FLARE - δ_a - IN. FROM FULL FORWARD

LONGITUDINAL CONTROL MAST TILT DURING FLARE - δ_a - IN. FROM TRIM

AFT

AFT

FWD

FWD

MAXIMUM LONGITUDINAL CONTROL TRAVEL - 12.7 IN.

30 40 50 60 70

FLARE AIRSPEED - KNAS

FIGURE 22-2

SYM
AND ABOVE SPEED AT FLARE – RPM
260
300
MINIMUM ANGLE OF ATTACK DURING FLARE – α_{min} – DEG
ANGLE OF ATTACK CHANGE DURING FLARE – DEG
LESS FROM TRIM
TRIM
50
40
30
20
10
0
50
40
30
20
10
30
40
50
60
70
FLARE DISTANCE – FEET

FIGURE 22-3

SYM AVG ROTOR SPEED AT FLARE - RPM

200

300

ACCELERATION -ft - sec/sec²

MAXIMUM AVAILABLE RATE -ft - sec/sec

AVG MAXIMUM AVAILABLE ALTITUDE -ft - sec

FLARE ALTITUDE - FEET

FIGURE 22-4

SYM
AVG. ROTOR SPEED AT FLARE - RPM
260
300
MAXIMUM VERTICAL ACCELERATION - Δn_z
MAXIMUM HORIZONTAL ACCELERATION - Δx in FT/SEC²
MAXIMUM VERTICAL ACCELERATION - Δn_z in FT/SEC²
2.0
1.5
1.0
.5
ZERO
4
10
15
20
25
15
10
5
0
30
40
50
60
70

FIGURE 22-7

MAIN ROTOR SPEED AT FLARE = RPM
300
MAXIMUM MAIN ROTOR THRUST DURING FLARE
MAIN ROTOR THRUST INCREASE DURING FLARE
FLARE ALTITUDE = FEET

FIGURE 2.6

MAXIMUM RATE OF ROTOR SPEED INCREASE DURING FLARE - Δ Ω/Δt in RPM/SEC
ROTOR SPEED INCREASE DURING FLARE - ΔΩ in RPM
FLARE DISPLACEMENT - ΔZ in FT
MAX ROTOR SPEED IN FLARE - Ω in RPM
260
300
5
10
15
20
25
30

FIGURE 22-7

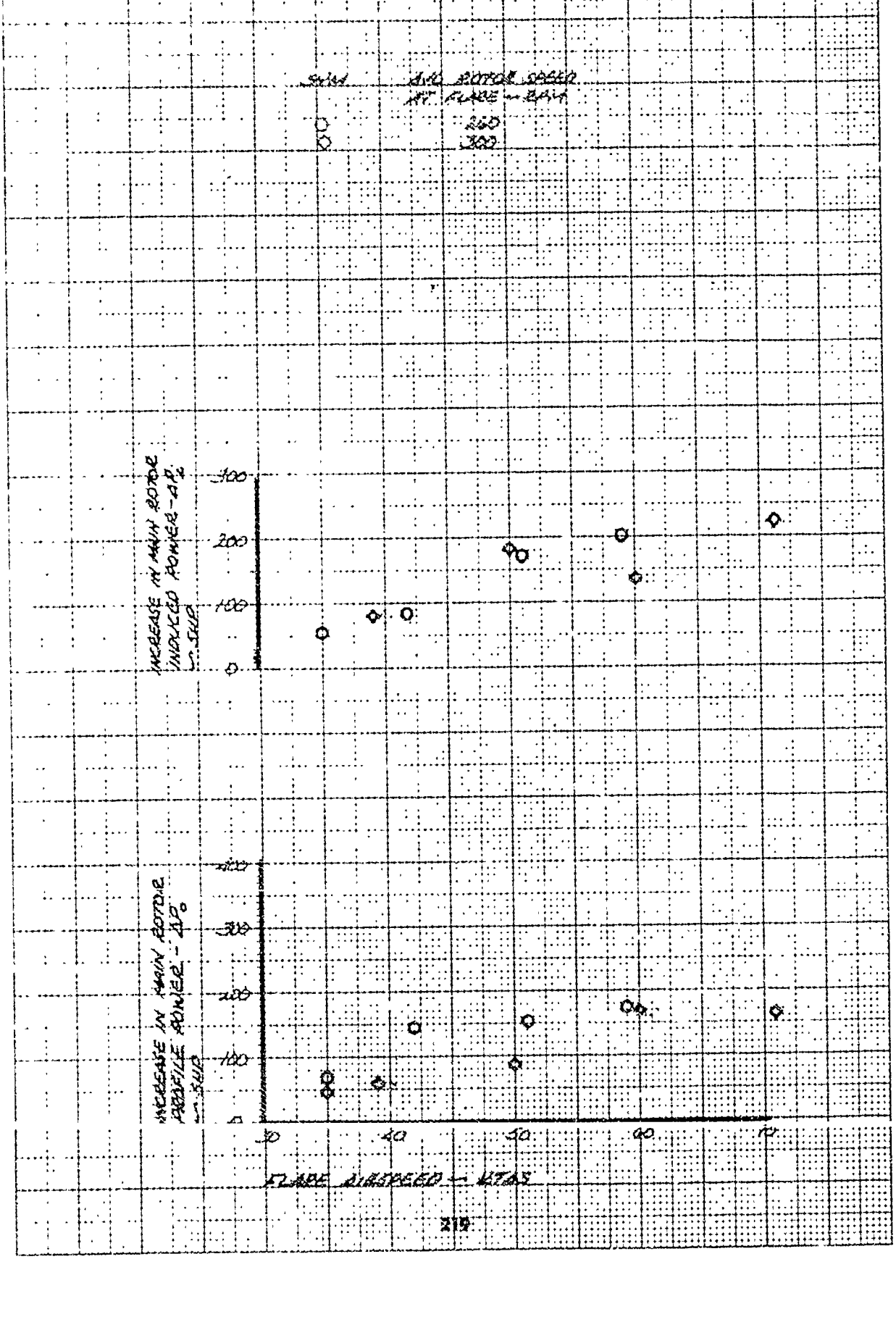
SHP
MAIN ROTOR SPEED AT FLARE = 294
260
300
INCREASE IN MAIN ROTOR INDUCED POWER - HP
SHP
100
200
100
INCREASE IN MAIN ROTOR PROFILE POWER - HP
SHP
100
200
300
400
10
40
50
60
70
FLARE AIRSPEED - KTAS

FIGURE 22-5

AND ROTOR SPEED AT FLARE - RPM
260
300
DECREASE IN FORWARD SPEED - KNOTS/SEC
DECREASE IN RATE OF DESCENT - FT/SEC
HORIZONTAL DISTANCE TRAVELED - FEET
HEIGHT LOST - FEET
FLARE AIRSPEED - KNOTS

FIGURE 22-9

MAXIMUM ABSOLUTE RATE OF CHANGE IN AIRCRAFT TOTAL ENERGY DURING FLARE - JET AIRPLANE

FLARE ALTITUDE - FEET

FIGURE 223-1

CYCLIC SCARE FROM LOW LEVEL STEADY STATE AUTOROTATION

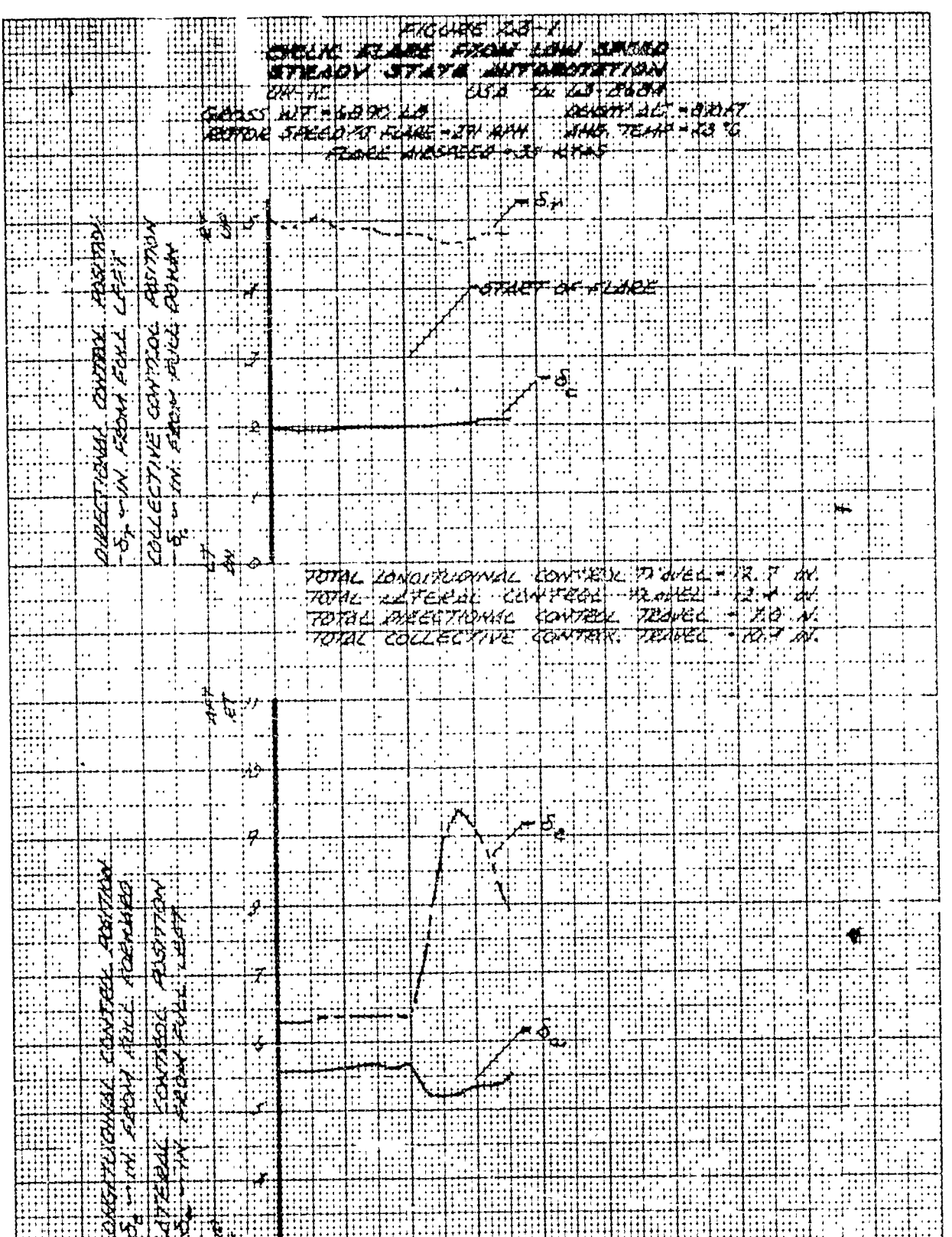

FIGURE 2.3-2
TIME - SEC

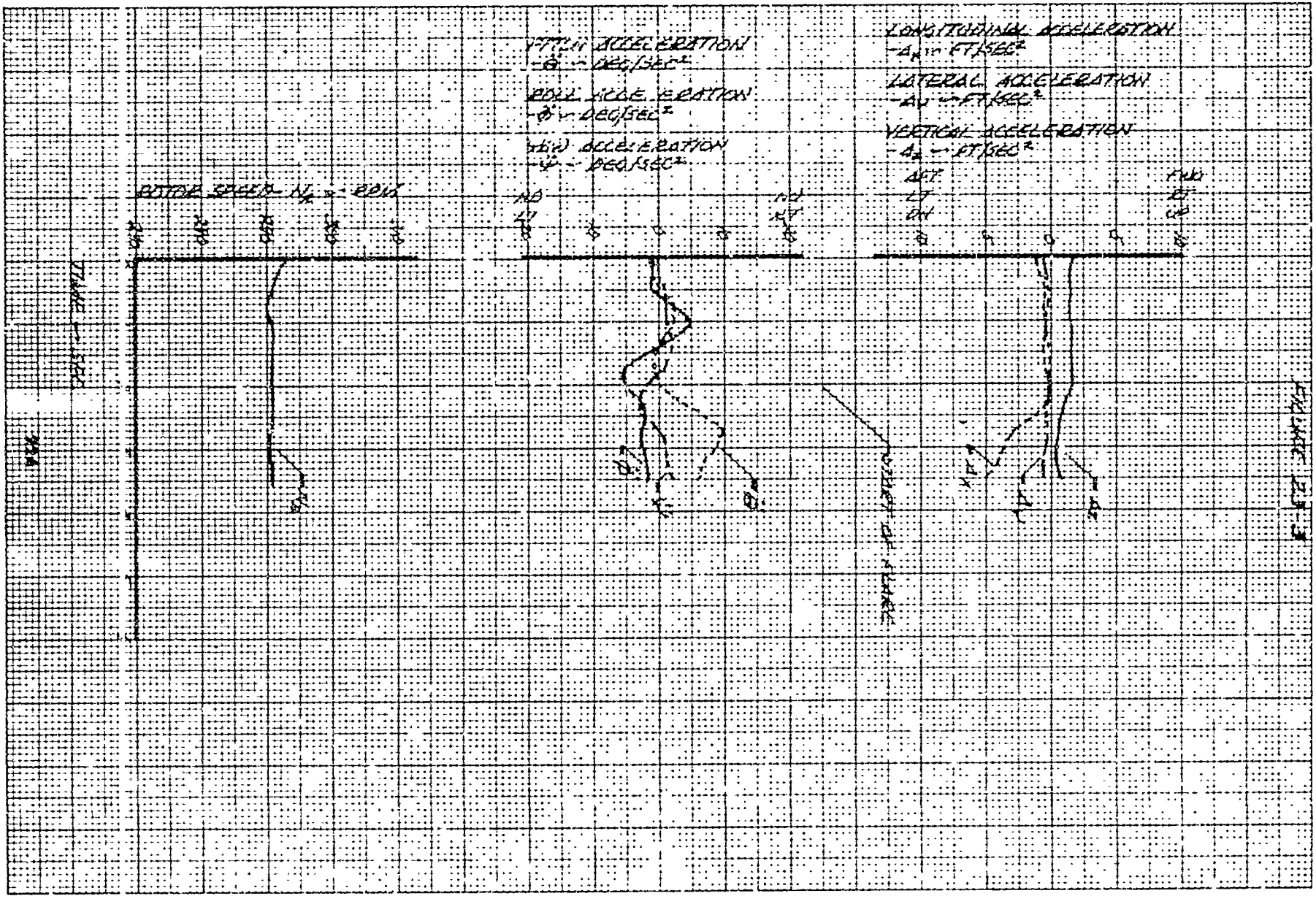
ROTOR SPEED - N_R = - RPM
TIME - SEC
PITCH ACCELERATION
$-\dot{\theta}$ - DEG/SEC^2
ROLL ACCELERATION
$-\dot{\phi}$ - DEG/SEC^2
YAW ACCELERATION
$-\dot{\psi}$ - DEG/SEC^2
LONGITUDINAL ACCELERATION
$-A_x$ - FT/SEC^2
LATERAL ACCELERATION
$-A_y$ - FT/SEC^2
VERTICAL ACCELERATION
$-A_z$ - FT/SEC^2
NUMBER OF FLIGHT
FLIGHT REF. E-3

FIGURE 2.3-4
START OF FLARE
RATE OF DESCENT
MAIN ENGINE THRUST
TIME - SEC

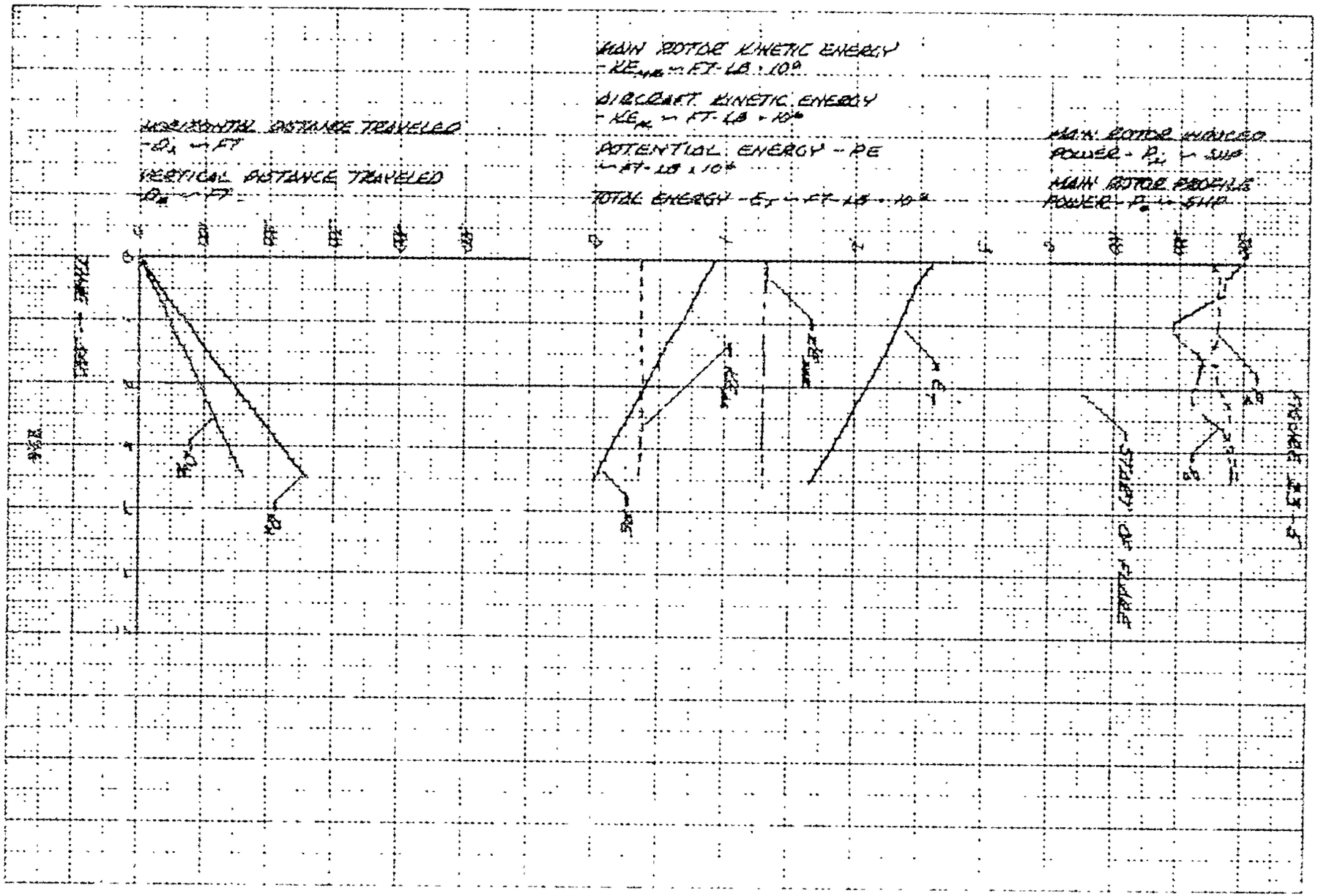
HORIZONTAL DISTANCE TRAVELED
- D_x - FT
VERTICAL DISTANCE TRAVELED
- D_z - FT
MAIN ROTOR KINETIC ENERGY
- KE_{MR} - FT-LB x 10^6
AIRCRAFT KINETIC ENERGY
- KE_{AC} - FT-LB x 10^6
POTENTIAL ENERGY - PE
- FT-LB x 10^6
TOTAL ENERGY - E_T - FT-LB x 10^6
MAIN ROTOR INDICATED POWER - P_{IMR} - SHP
MAIN ROTOR PROFILE POWER - P_{PMR} - SHP
STEADY CRUISE FLIGHT

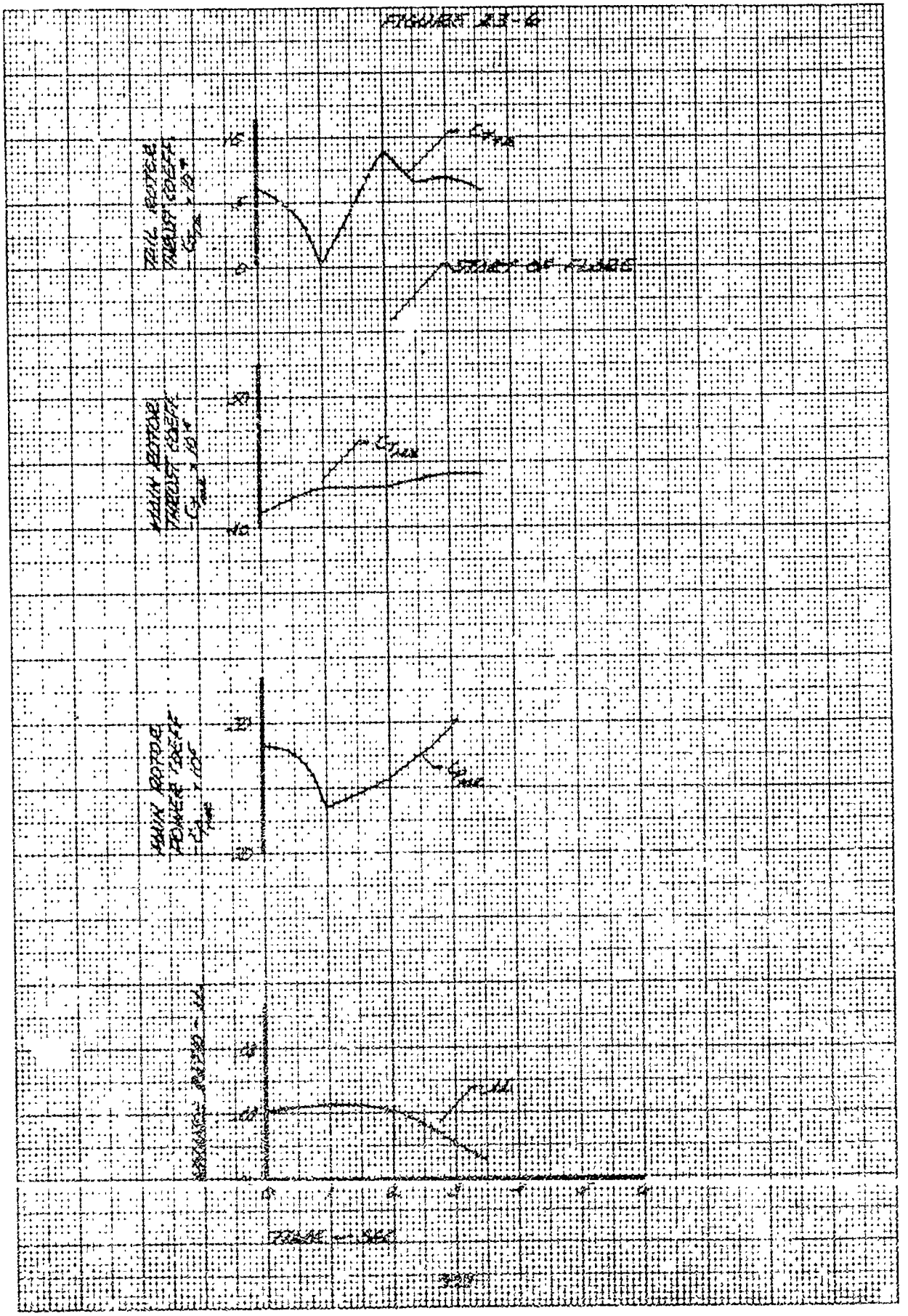
TAIL ROTOR
MAIN ROTOR
MAIN ROTOR
TIME - SEC

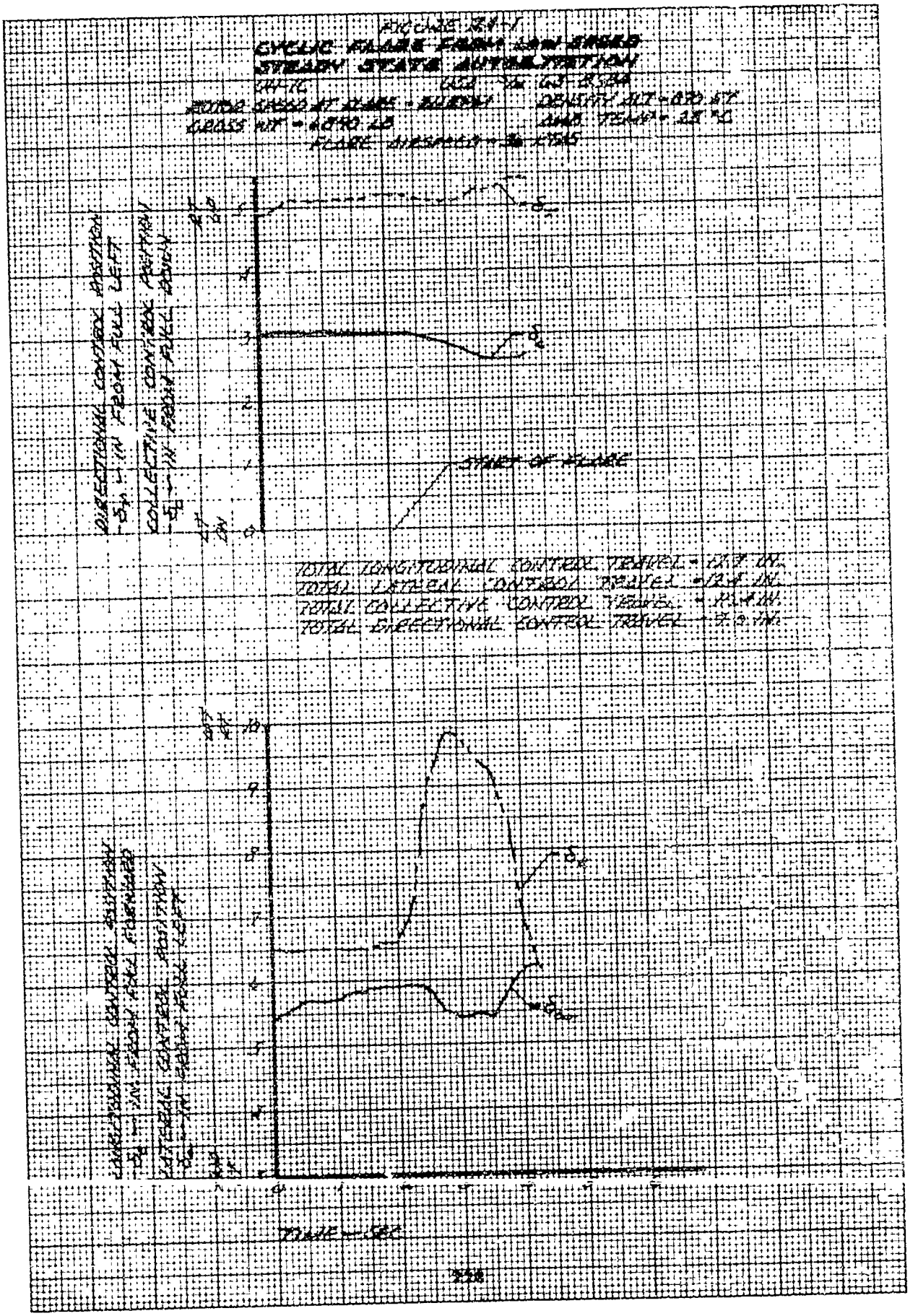
FIGURE X-11
CYCLIC FLARE FROM LOW SPEED
STEADY STATE AUTOROTATION
TIME—SEC

FIGURE 24-2
START OF FLARE
TIME — SEC

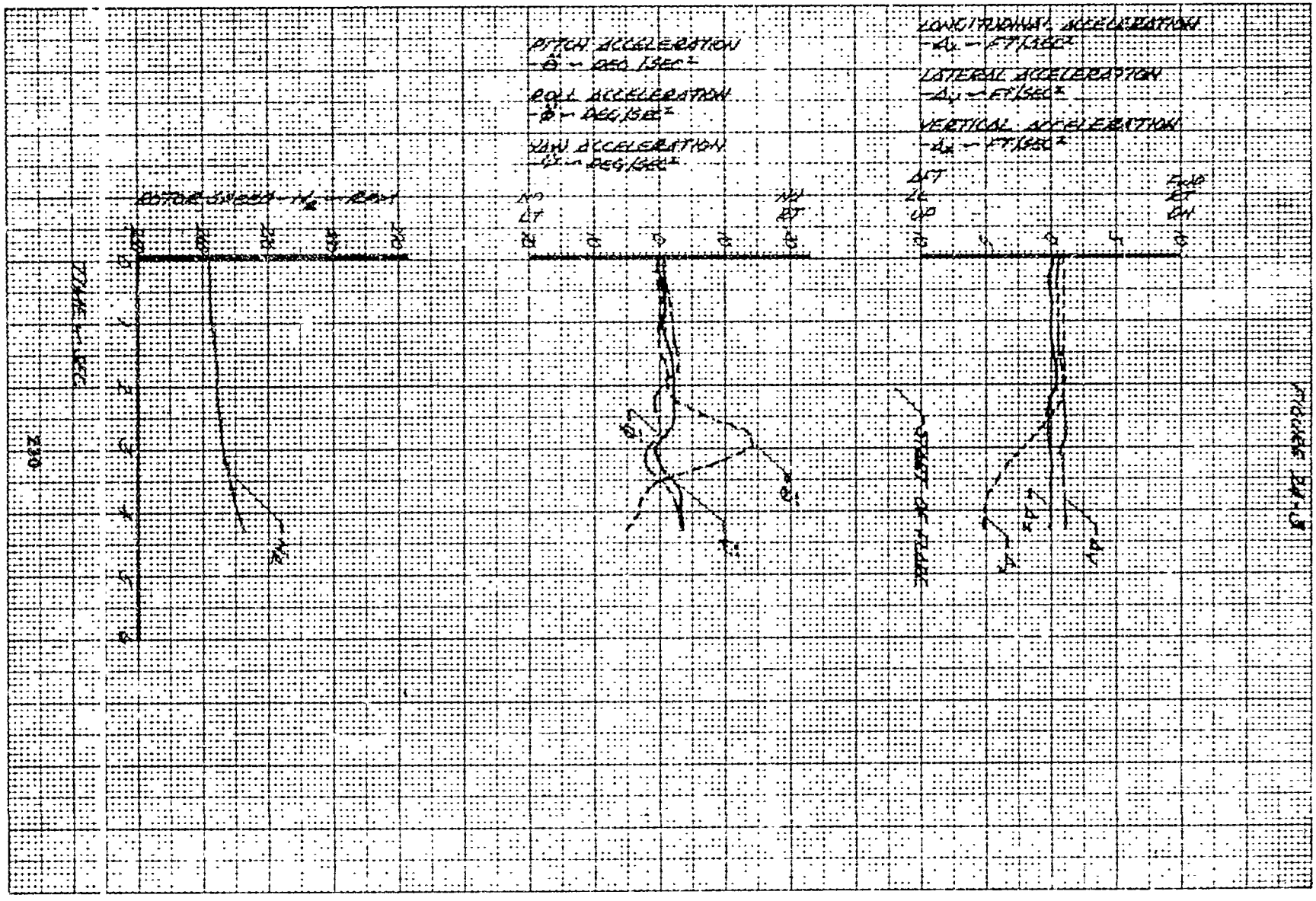
PITCH ACCELERATION
ROLL ACCELERATION
YAW ACCELERATION
LONGITUDINAL ACCELERATION
LATERAL ACCELERATION
VERTICAL ACCELERATION
TIME - SEC

FIGURE 24-4

FIGURE 24-5
MAIN ROTOR KINETIC ENERGY
MAIN ROTOR KINETIC ENERGY
POWER-ON - 1440
MAIN ROTOR KINETIC ENERGY
POWER-OFF - 1440
AUXILIARY ROTOR KINETIC ENERGY
HELICOPTER POTENTIAL ENERGY
TOTAL ENERGY
START OF FLARE
TIME - SEC

FIGURE 24-16

MAIN ROTOR THRUST COEFF. $C_{T_{MR}}$ x10²
TAIL ROTOR THRUST COEFF. $C_{T_{TR}}$ x10²
MAIN ROTOR POWER COEFF. $C_{P_{MR}}$ x10²
ADVANCE RATIO - μ
$C_{T_{TR}}$
$C_{T_{MR}}$
$C_{P_{MR}}$
-μ
TIME — SEC

FIGURE 25-1

CYCLIC FLARE FROM ARBITRARY
TRIMMED STEADY STATE CONDITION

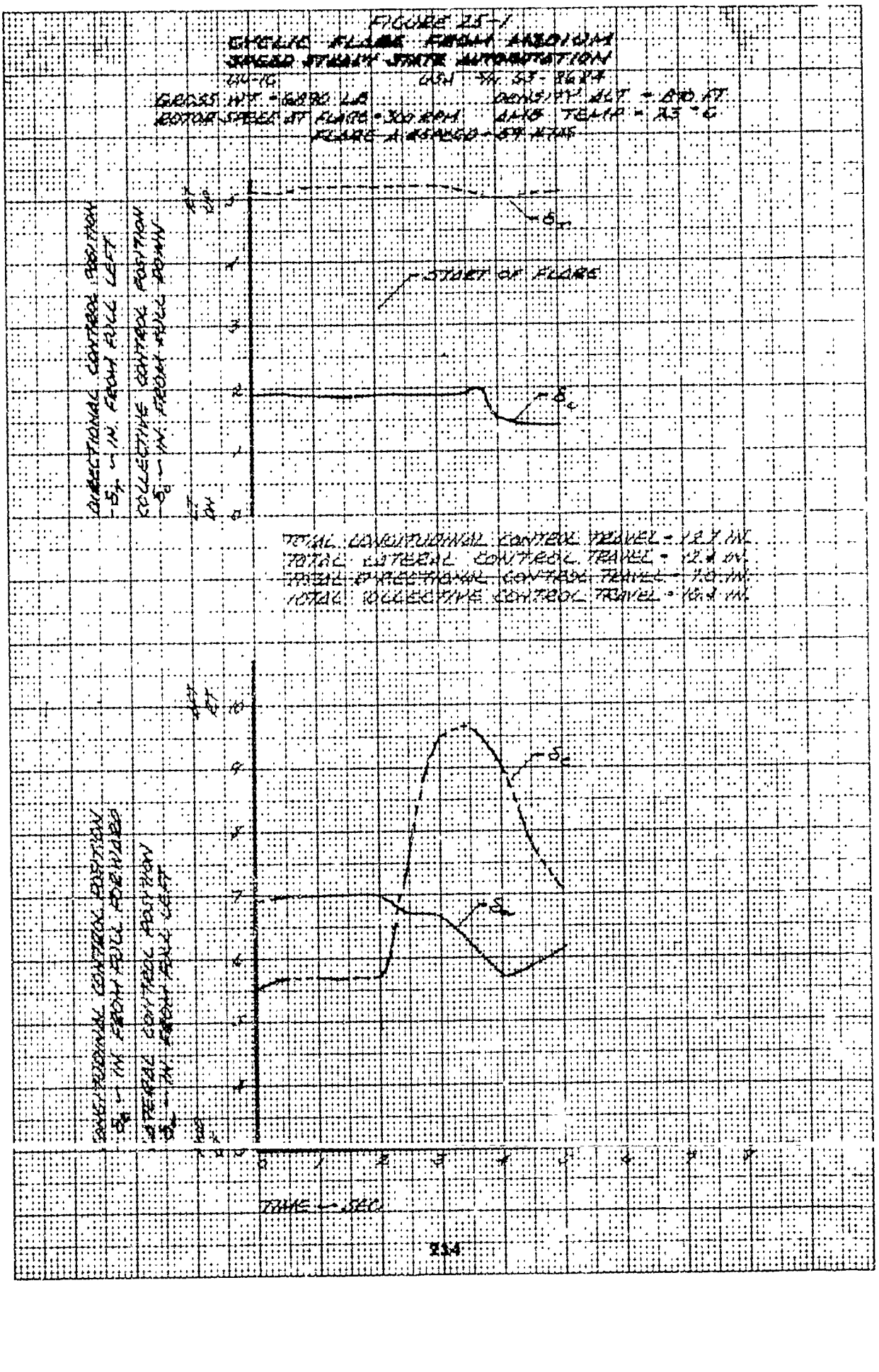

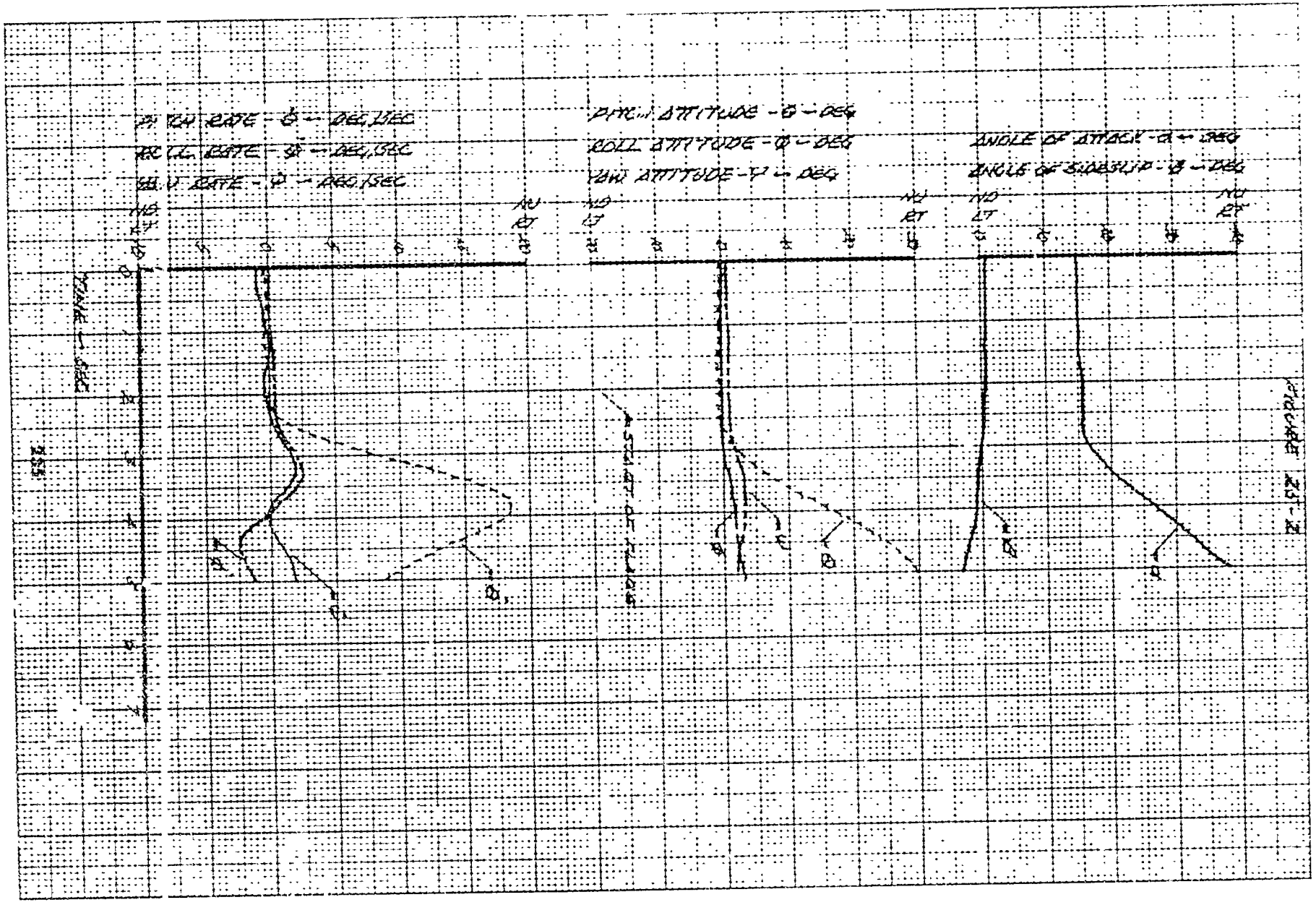
PITCH RATE - q - DEG/SEC
ROLL RATE - p - DEG/SEC
YAW RATE - r - DEG/SEC
PITCH ATTITUDE - θ - DEG
ROLL ATTITUDE - φ - DEG
YAW ATTITUDE - ψ - DEG
ANGLE OF ATTACK - α - DEG
ANGLE OF SIDESLIP - β - DEG
MACH - DEG
ALTITUDE - 1000 FT
MACH
ALTITUDE - 1000 FT

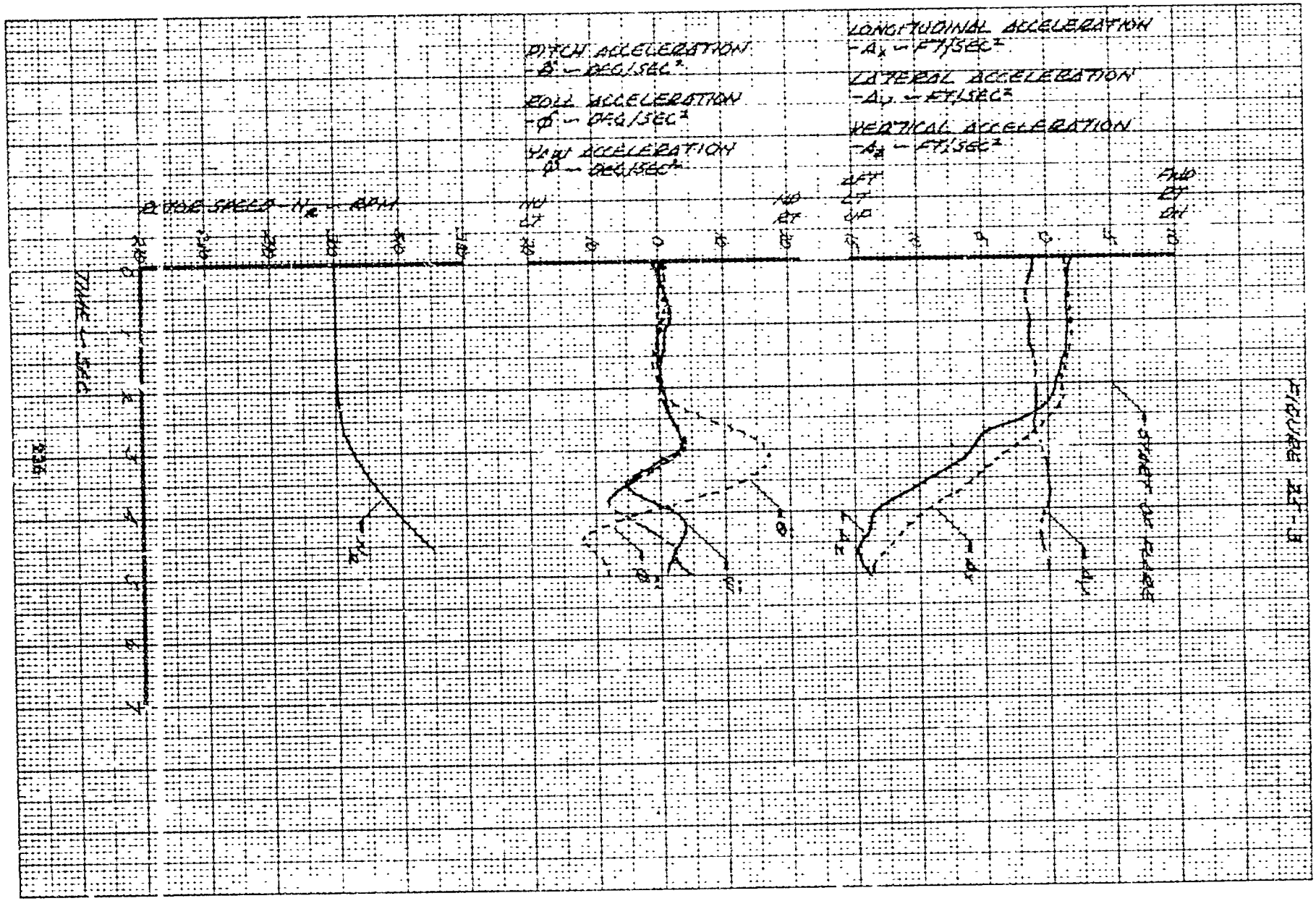
PITCH ACCELERATION
$-\dot{q}$ – DEG/SEC²
ROLL ACCELERATION
$-\dot{p}$ – DEG/SEC²
YAW ACCELERATION
$-\dot{r}$ – DEG/SEC²
LONGITUDINAL ACCELERATION
$-A_x$ – FT/SEC²
LATERAL ACCELERATION
$-A_y$ – FT/SEC²
VERTICAL ACCELERATION
$-A_z$ – FT/SEC²
TIME – SEC
OTHER AIRCRAFT

FIGURE 23-4

RATE OF DESCENT
FT/SEC
FLARE AIRSPEED
KTS
ANGULAR VELOCITY
DEG/SEC
ANGULAR ACCELERATION
DEG/SEC²
START OF FLARE
TIME - SEC

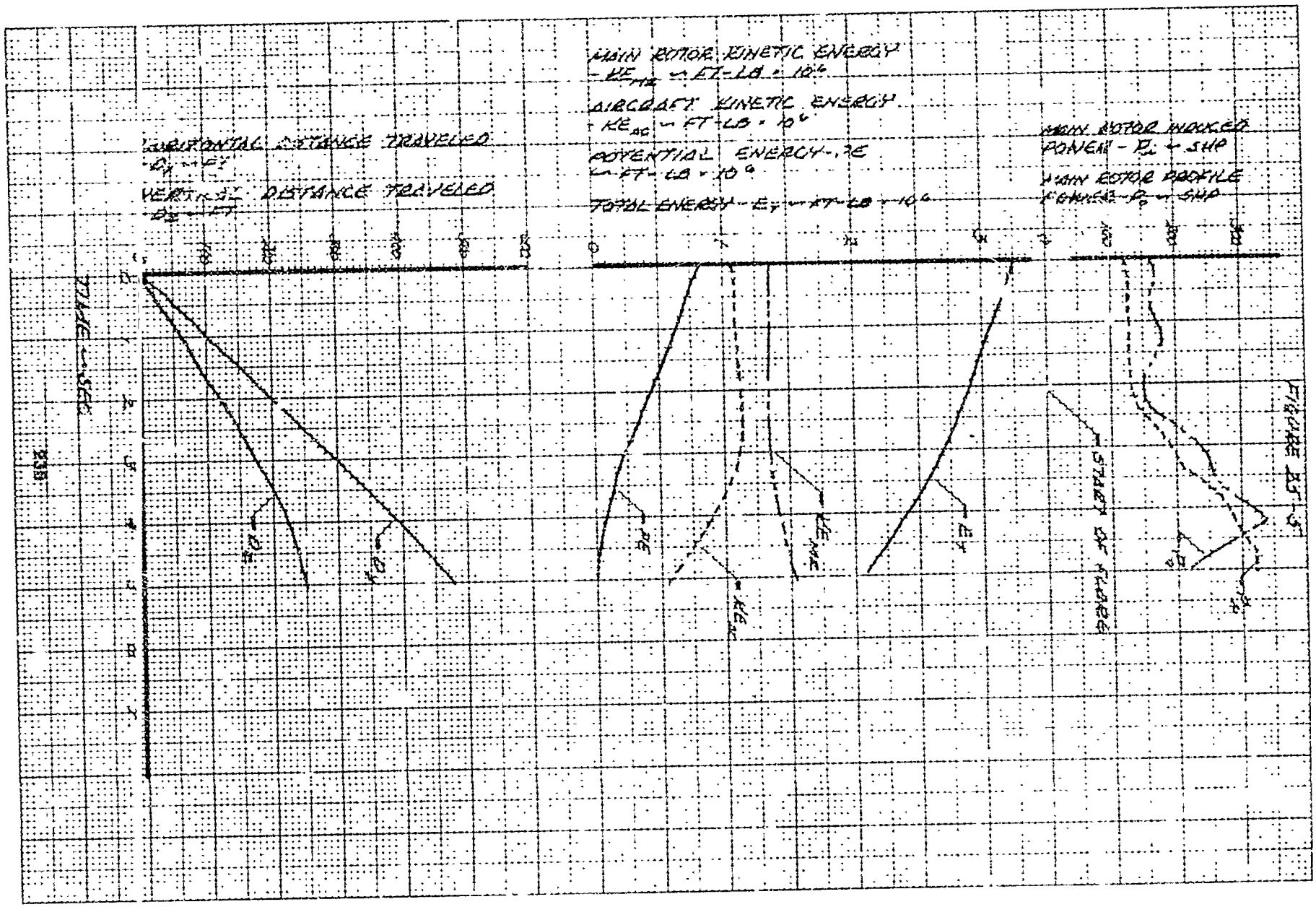
HORIZONTAL DISTANCE TRAVELED
D_H - FT
VERTICAL DISTANCE TRAVELED
D_V - FT
MAIN ROTOR KINETIC ENERGY
KE_{MR} - FT-LB - 10^6
AIRCRAFT KINETIC ENERGY
KE_{AC} - FT-LB - 10^6
POTENTIAL ENERGY - PE
FT-LB - 10^6
TOTAL ENERGY - E_T - FT-LB - 10^6
MAIN ROTOR MASKED POWER - P_M - SHP
MAIN ROTOR PROFILE POWER - P_P - SHP
TIME - SEC
START OF FLARE
D_{H_F}
D_{V_F}
PE
KE_{AC}
KE_{MR}
E_T
P_M
P_P

FIGURE B3-3

FIGURE 20-6

TAIL ROTOR THRUST COEFF.
MAIN ROTOR THRUST COEFF.
MAIN ROTOR POWER COEFF.
START OF FLARE
TIME - SEC

TIME - SEC

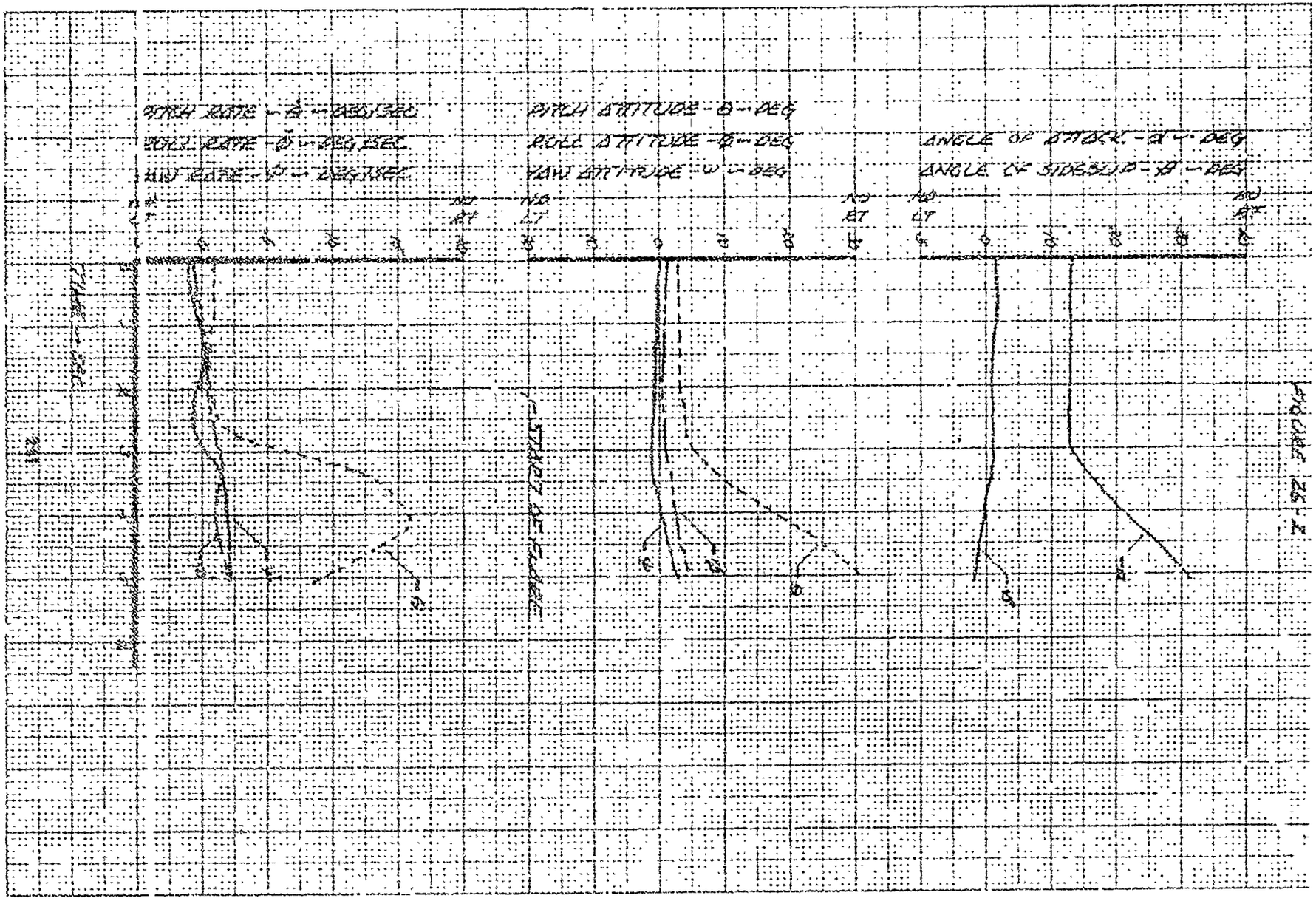
PITCH ATTITUDE - θ - DEG
ROLL ATTITUDE - Φ - DEG
YAW ATTITUDE - ψ - DEG
ANGLE OF ATTACK - α - DEG
ANGLE OF SIDESLIP - β - DEG
TIME - SEC
START OF MANEUVER
FIGURE 25-2

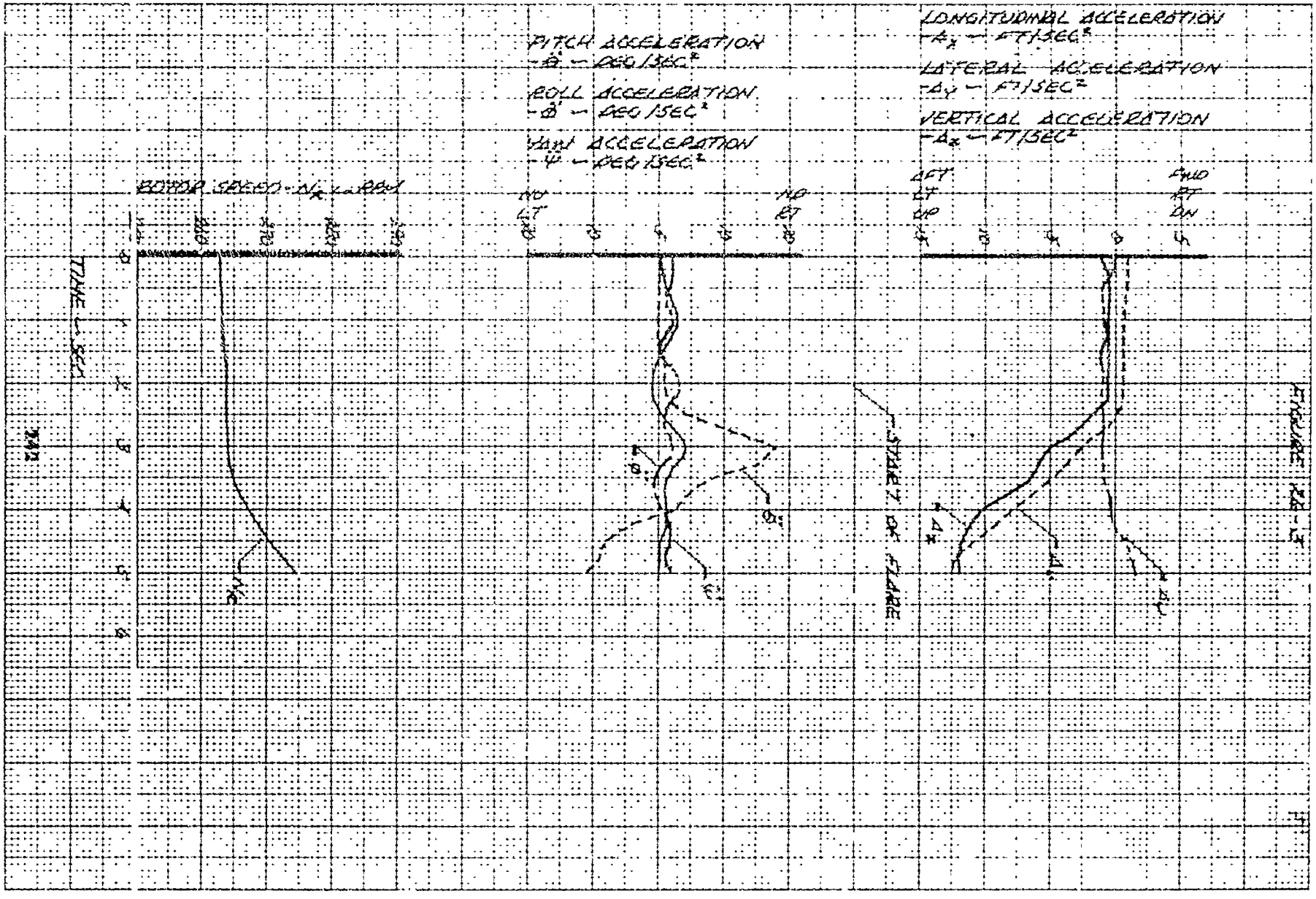
PITCH ACCELERATION
$-\ddot{\theta}$ – DEG/SEC²
ROLL ACCELERATION
$-\ddot{\phi}$ – DEG/SEC²
YAW ACCELERATION
$-\ddot{\psi}$ – DEG/SEC²
NO LT
NO RT
LONGITUDINAL ACCELERATION
$-A_x$ – FT/SEC²
LATERAL ACCELERATION
$-A_y$ – FT/SEC²
VERTICAL ACCELERATION
$-A_z$ – FT/SEC²
AFT
LT
AND
FT
AND
DN
ROTOR SPEED – Ω_R RPM
TIME – SEC
START OF FLARE
$\ddot{\theta}$
$\ddot{\phi}$
$\ddot{\psi}$
A_x
A_y
A_z

FIGURE 24-4

FLARE AIRSPEED
V_F - KTAS
RATE OF DESCENT
$\dot{h}$ - FT/SEC
START OF FLARE
V_F
$\dot{h}$
MAIN ROTOR THRUST
T_{MR} - LB
T_{MR}
TAIL ROTOR THRUST
T_{TR} - LB
T_{TR}
TIME - SEC

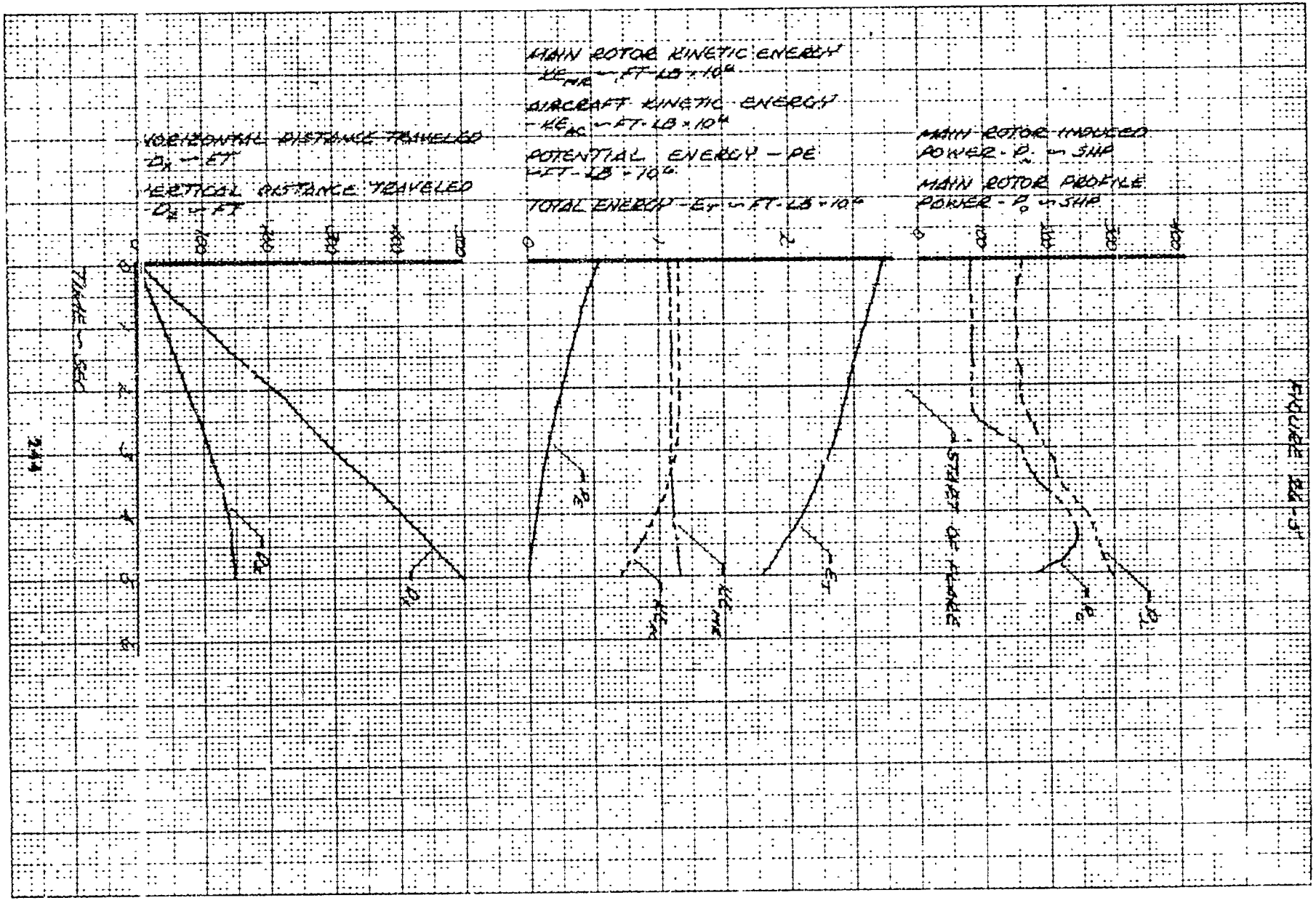
HORIZONTAL DISTANCE TRAVELED
D_x – FT
VERTICAL DISTANCE TRAVELED
D_z – FT
TIME – SEC
MAIN ROTOR KINETIC ENERGY
KE_{MR} – FT-LB × 10^4
AIRCRAFT KINETIC ENERGY
KE_{AC} – FT-LB × 10^4
POTENTIAL ENERGY – PE
FT-LB × 10^4
TOTAL ENERGY – E_T – FT-LB × 10^4
MAIN ROTOR INDUCED POWER – P_i – SHP
MAIN ROTOR PROFILE POWER – P_o – SHP
START OF HOVER

FIGURE 22 - 37

FIGURE 26-6

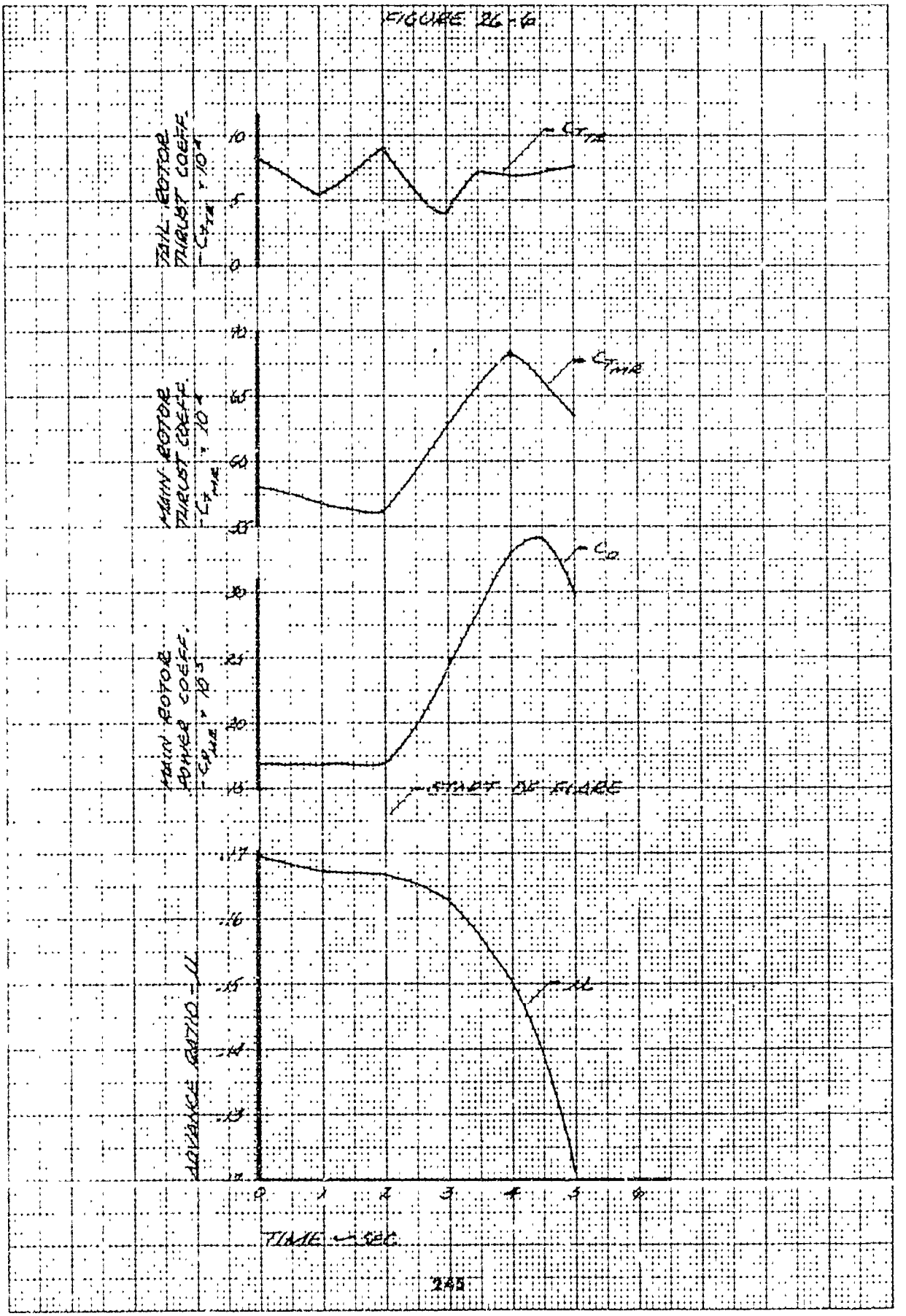
TAIL ROTOR THRUST COEFF. $C_{T_{TR}} \times 10^4$
MAIN ROTOR THRUST COEFF. $C_{T_{MR}} \times 10^4$
MAIN ROTOR POWER COEFF. $C_{P_{MR}} \times 10^3$
ADVANCE RATIO μ
$C_{T_{TR}}$
$C_{T_{MR}}$
C_Q
START OF FLARE
μ
TIME — SEC.

FIGURE 27-1

CYCLIC FLARE FROM MEDIUM SPEED STEADY STATE AUTOROTATION

CH-7C USN S/N 53-4634

GROSS WT = 8300 LB DENSITY ALT = 2200 FT

ROTOR SPEED AT FLARE = 296 RPM OAT TEMP = 24 °C

FLARE INITIATED AT 175 KIAS

TOTAL LONGITUDINAL CONTROL TRAVEL = 12.7 IN.

TOTAL LATERAL CONTROL TRAVEL = 12.2 IN.

TOTAL DIRECTIONAL CONTROL TRAVEL = 7.0 IN.

TOTAL COLLECTIVE CONTROL TRAVEL = 10.4 IN.

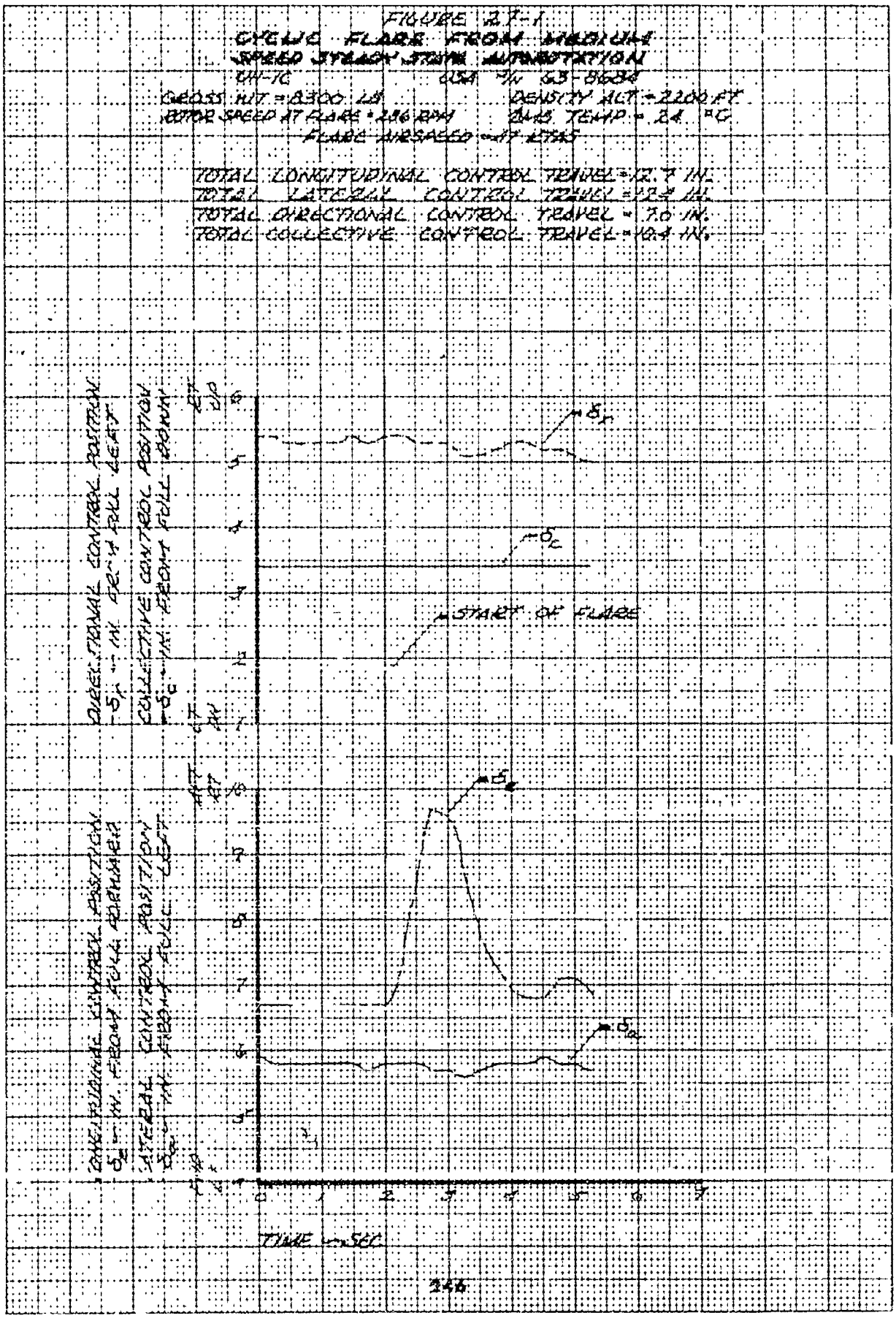

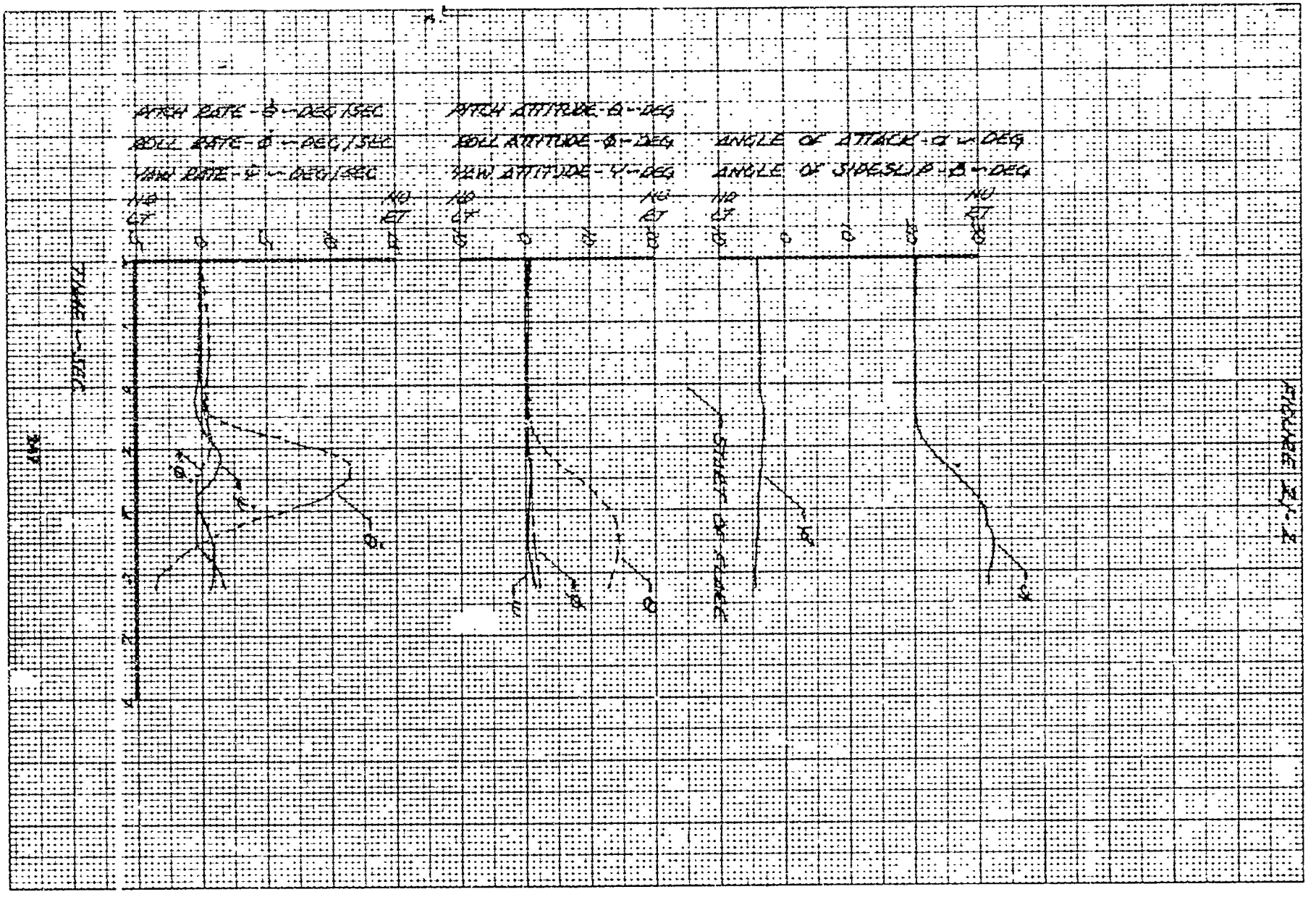
PITCH RATE - $\dot{\theta}$ - DEG/SEC
ROLL RATE - $\dot{\phi}$ - DEG/SEC
YAW RATE - $\dot{\psi}$ - DEG/SEC
PITCH ATTITUDE - θ - DEG
ROLL ATTITUDE - ϕ - DEG
YAW ATTITUDE - ψ - DEG
ANGLE OF ATTACK - α - DEG
ANGLE OF SIDESLIP - β - DEG
NO
LIFT
TIME - SEC
STORE SEPARATION

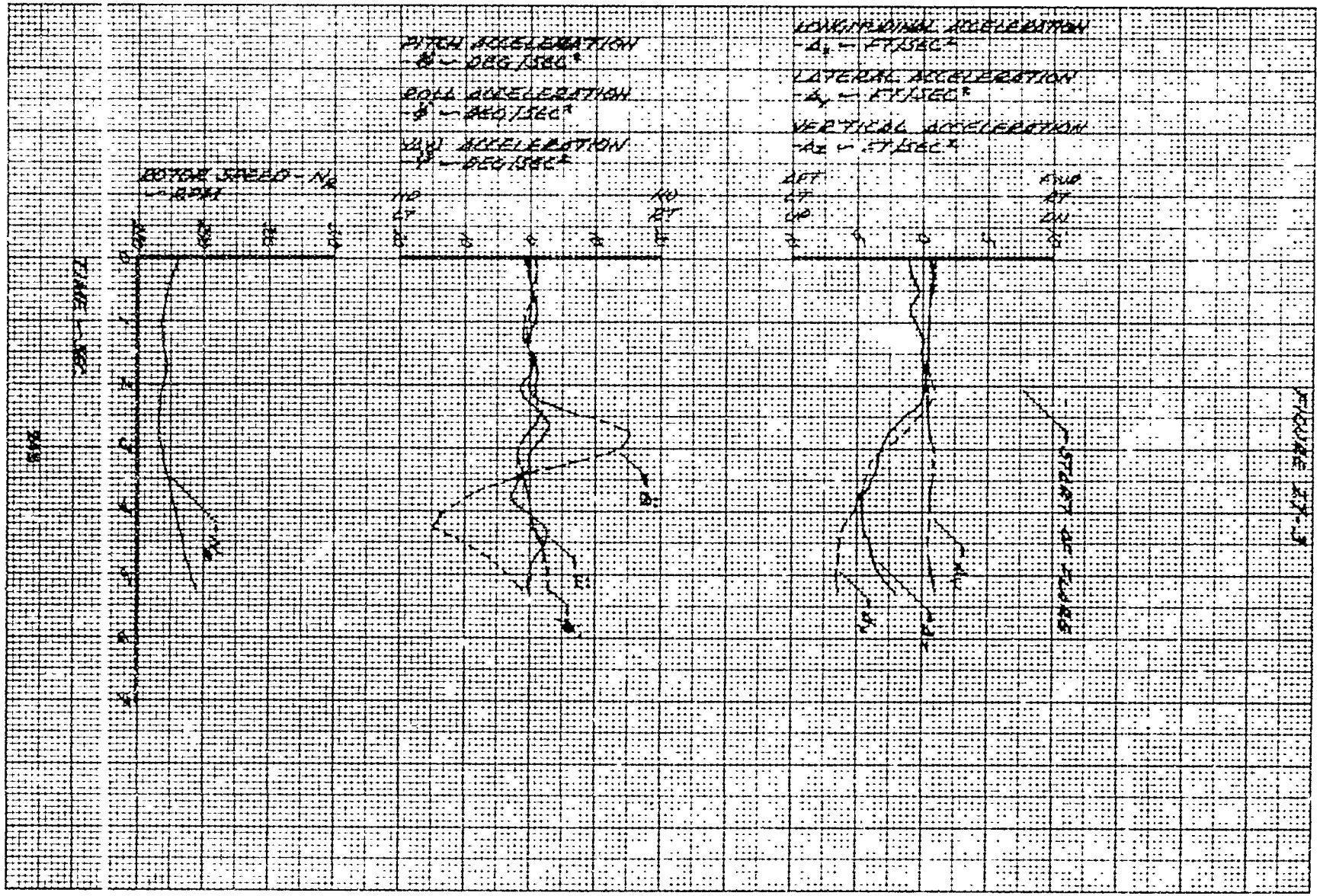
PITCH ACCELERATION
ROLL ACCELERATION
YAW ACCELERATION
LONGITUDINAL ACCELERATION
LATERAL ACCELERATION
VERTICAL ACCELERATION
TIME - SEC
START OF FLARE

FIGURE 27-4

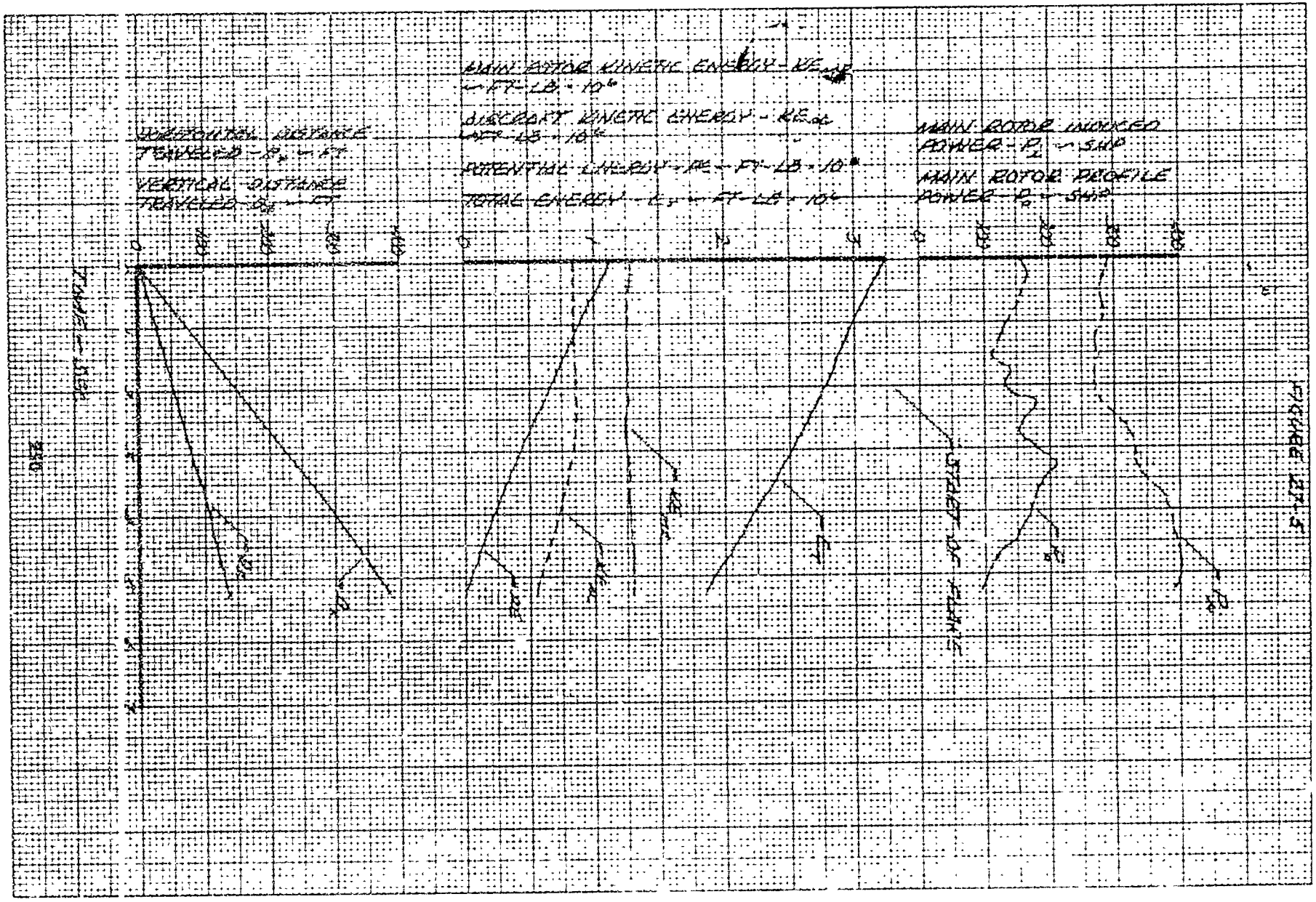
HORIZONTAL DISTANCE TRAVELED - X_a - FT
VERTICAL DISTANCE TRAVELED - S_a - FT
TIME - SEC
MAIN ROTOR KINETIC ENERGY - KE_{MR} - FT-LB - 10^6
AIRCRAFT KINETIC ENERGY - KE_{AC} - FT-LB - 10^6
POTENTIAL ENERGY - PE - FT-LB - 10^6
TOTAL ENERGY - E_T - FT-LB - 10^6
MAIN ROTOR INDUCED POWER - P_i - SHP
MAIN ROTOR PROFILE POWER - P_o - SHP
FIGURE 11-5

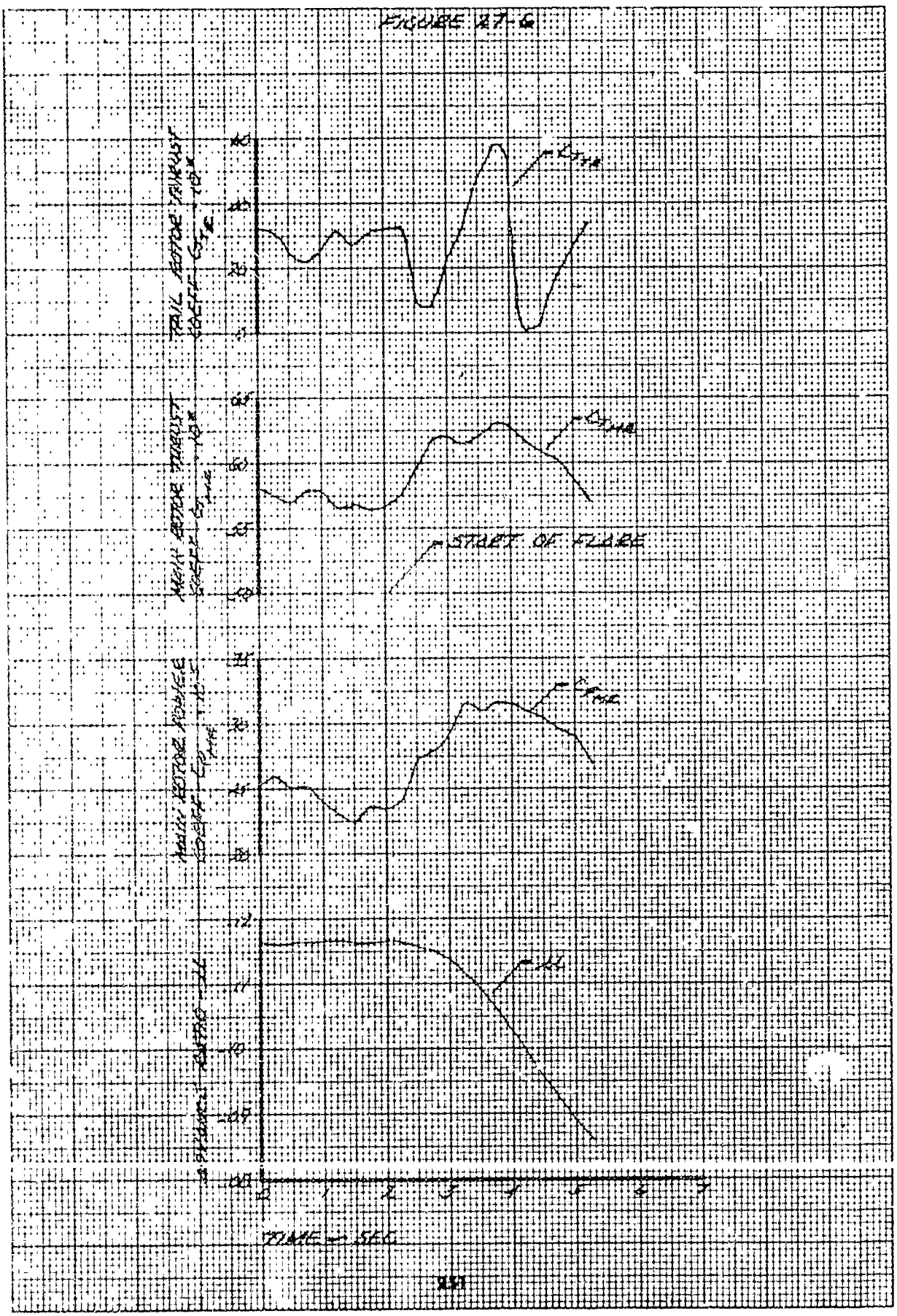
FIGURE 27-6
MAIN ENGINE THRUST
MAIN ENGINE POWER
TAIL ROTOR THRUST
START OF FLARE
TIME - SEC

FIGURE 2.5-1
CYCLIC FLARE FROM MEDIUM
SIZED STEADY STATE AMMONIA/AIR
GROSS WT = 3.55 LB
DENSITY ALT = 2200 FT
MAIN TEMP = 24 °C
TOTAL LONGITUDINAL CONTROL TRAVEL = 12.7 mm.
TOTAL LATERAL CONTROL TRAVEL = 12.7 mm.
TOTAL DIRECTIONAL CONTROL TRAVEL = 7.0 mm.
TOTAL COLLECTIVE CONTROL TRAVEL = 12.7 mm.
DIRECTIONAL CONTROL POSITION
δ_r - IN. FROM ZERO TO LEFT
COLLECTIVE CONTROL POSITION
δ_c - IN. FROM ZERO TO DOWN
δ_{r_T}
δ_c
δ_{r_R}
TIME - SEC
552

TIME – SEC

FIGURE 28-3

234

EFFECT OF FLAPS
TIME - SEC

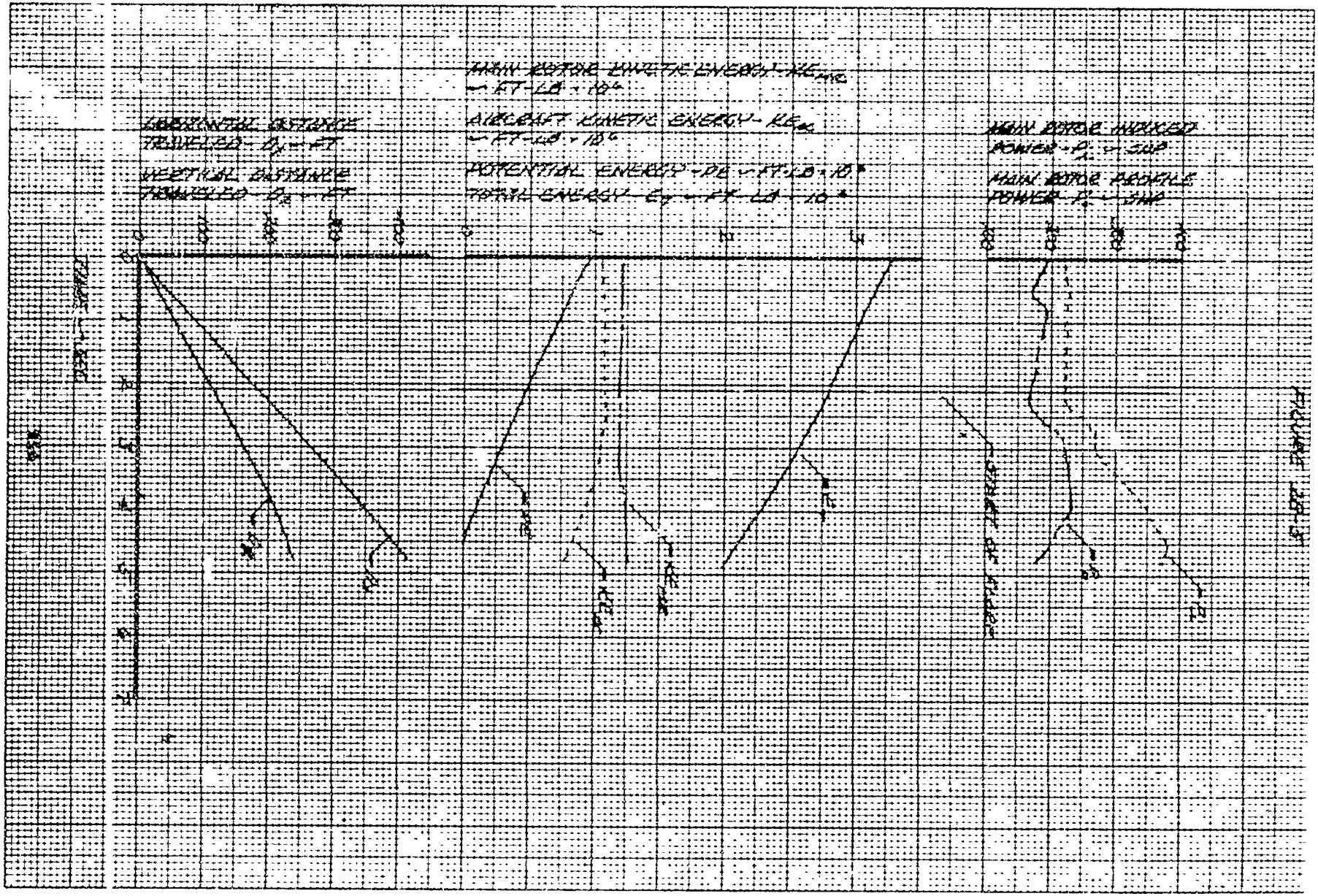
HORIZONTAL DISTANCE TRAVELED - D_x = FT
VERTICAL DISTANCE TRAVELED - D_y = FT
MAIN ROTOR KINETIC ENERGY - KE_{mr} = FT-LB × 10^6
AIRCRAFT KINETIC ENERGY - KE_{ac} = FT-LB × 10^6
POTENTIAL ENERGY - PE = FT-LB × 10^6
TOTAL ENERGY - E_T = FT-LB × 10^6
MAIN ROTOR INDICATED POWER - P_i = SHP
MAIN ROTOR PROFILE POWER - P_o = SHP
FIGURE 4-10

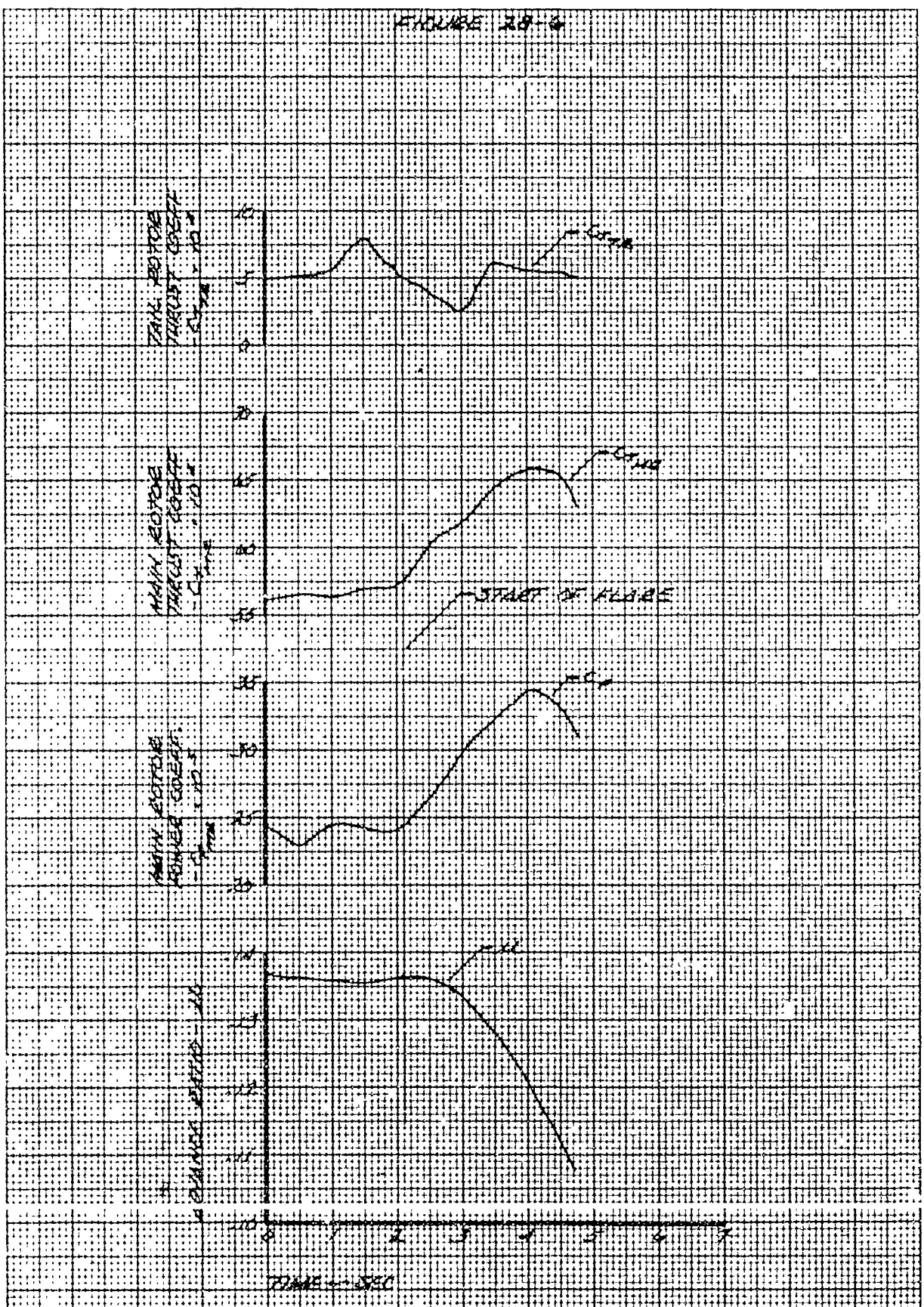
FIGURE 28-4
TAIL ROTOR THRUST COEFF.
MAIN ROTOR THRUST COEFF.
MAIN ROTOR POWER COEFF.
ROLL ANGLE
TIME - SEC

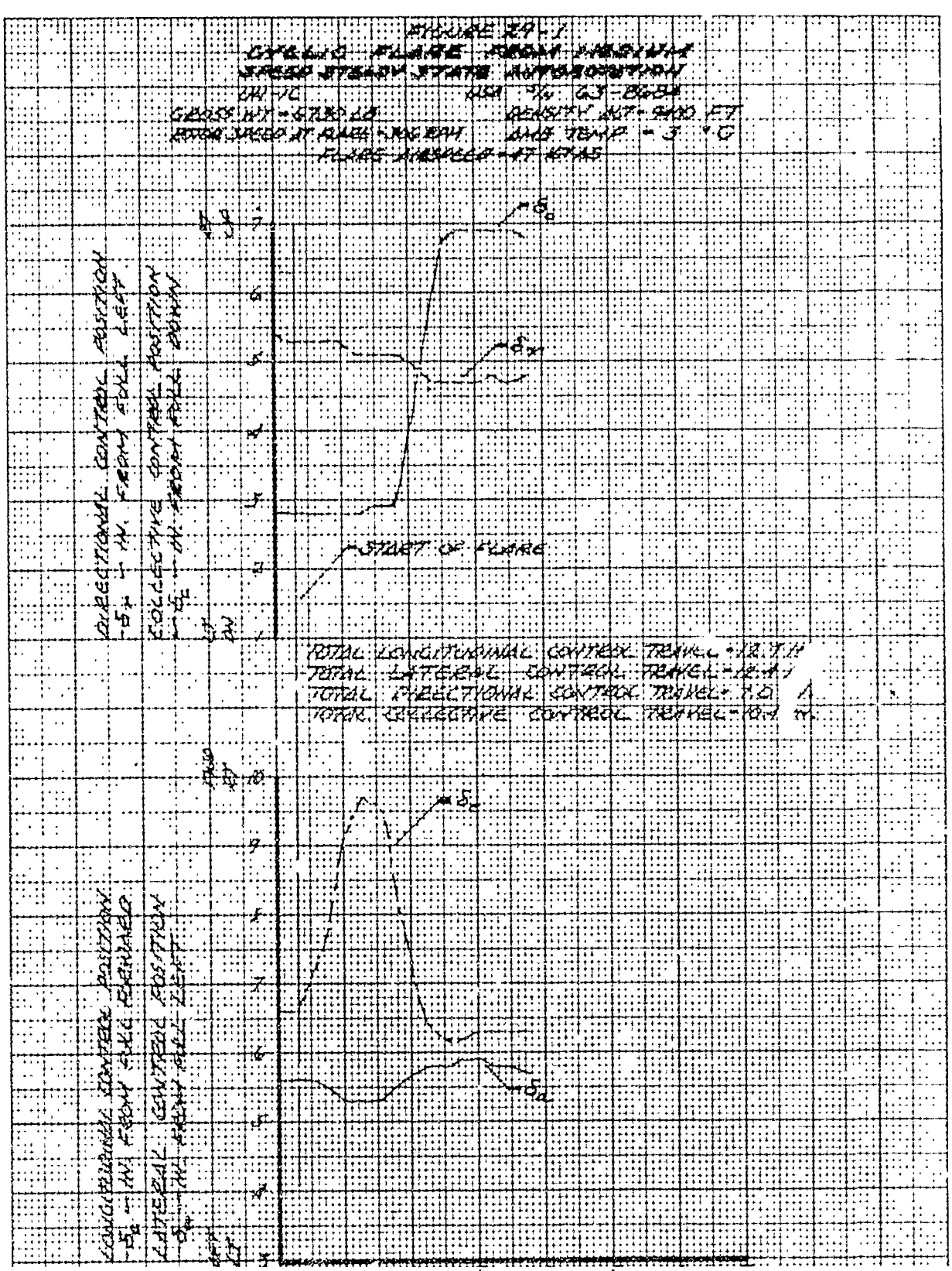
FIGURE 29-1
CYCLED FLARE FROM MACH 2.7
ALTITUDE
TOTAL LONGITUDINAL CONTROL TRAVEL = 12.7 in
TOTAL LATERAL CONTROL TRAVEL = 12.4 in
TOTAL DIRECTIONAL CONTROL TRAVEL = 7.0 in
TOTAL COLLECTIVE CONTROL TRAVEL = 0.4 in
START OF FLARE
TIME - SEC

FIGURE 22-2

START OF FLARE
TIME - SEC.
0
1
2
3
4
5
6
7
10
20
30
40
50
60
70
80
90
100
110
120
130
140
150
160
170
180
190
200
210
220
230
240
250
260
270
280
290
300
310
320
330
340
350
360

FIGURE 29-3
START OF MANEUVER
a_x
a_y
a_z
θ
ψ
ϕ
N_z
TIME — SEC

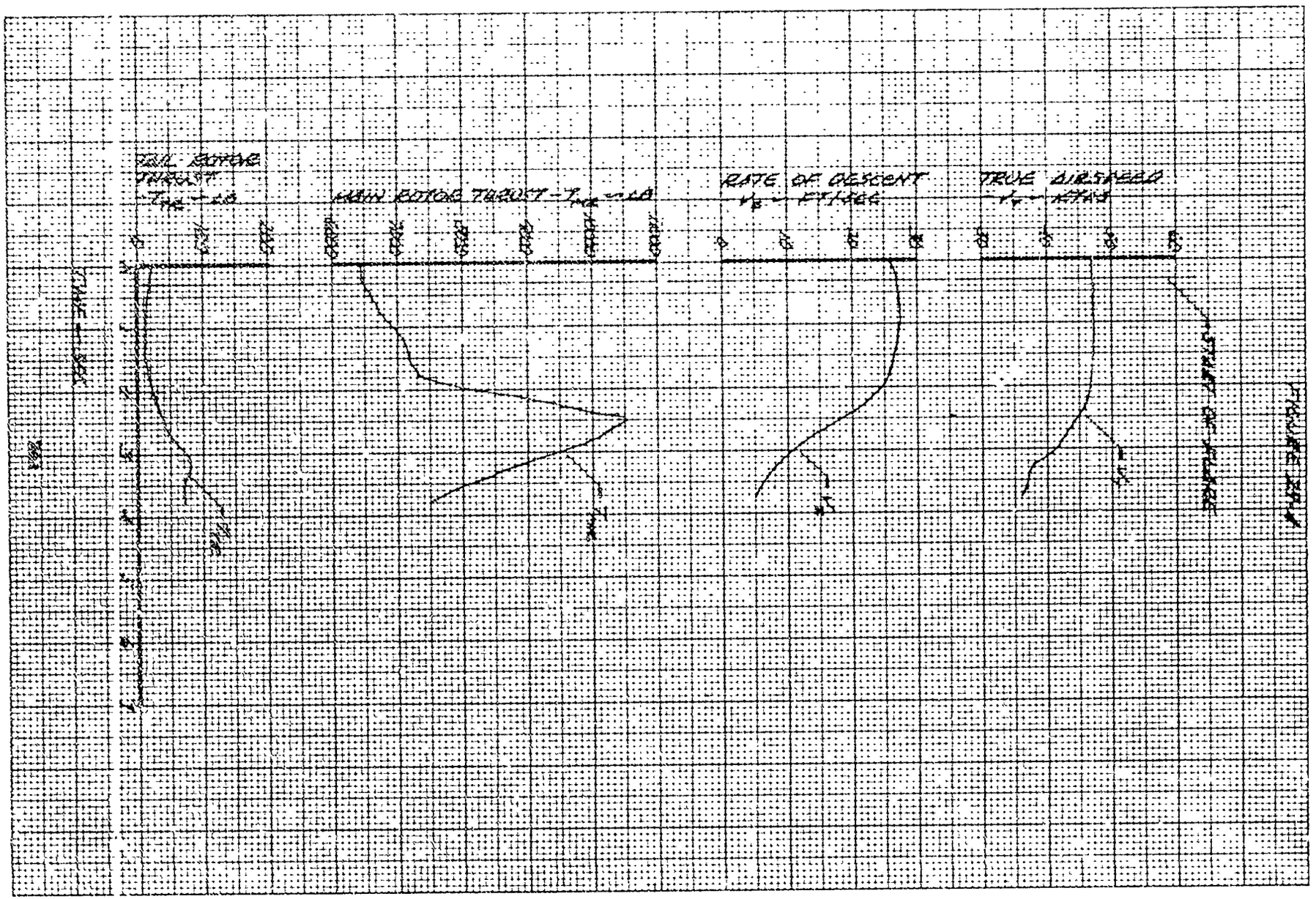
TAIL ROTOR THRUST
MAIN ROTOR THRUST
RATE OF DESCENT
TRUE AIRSPEED

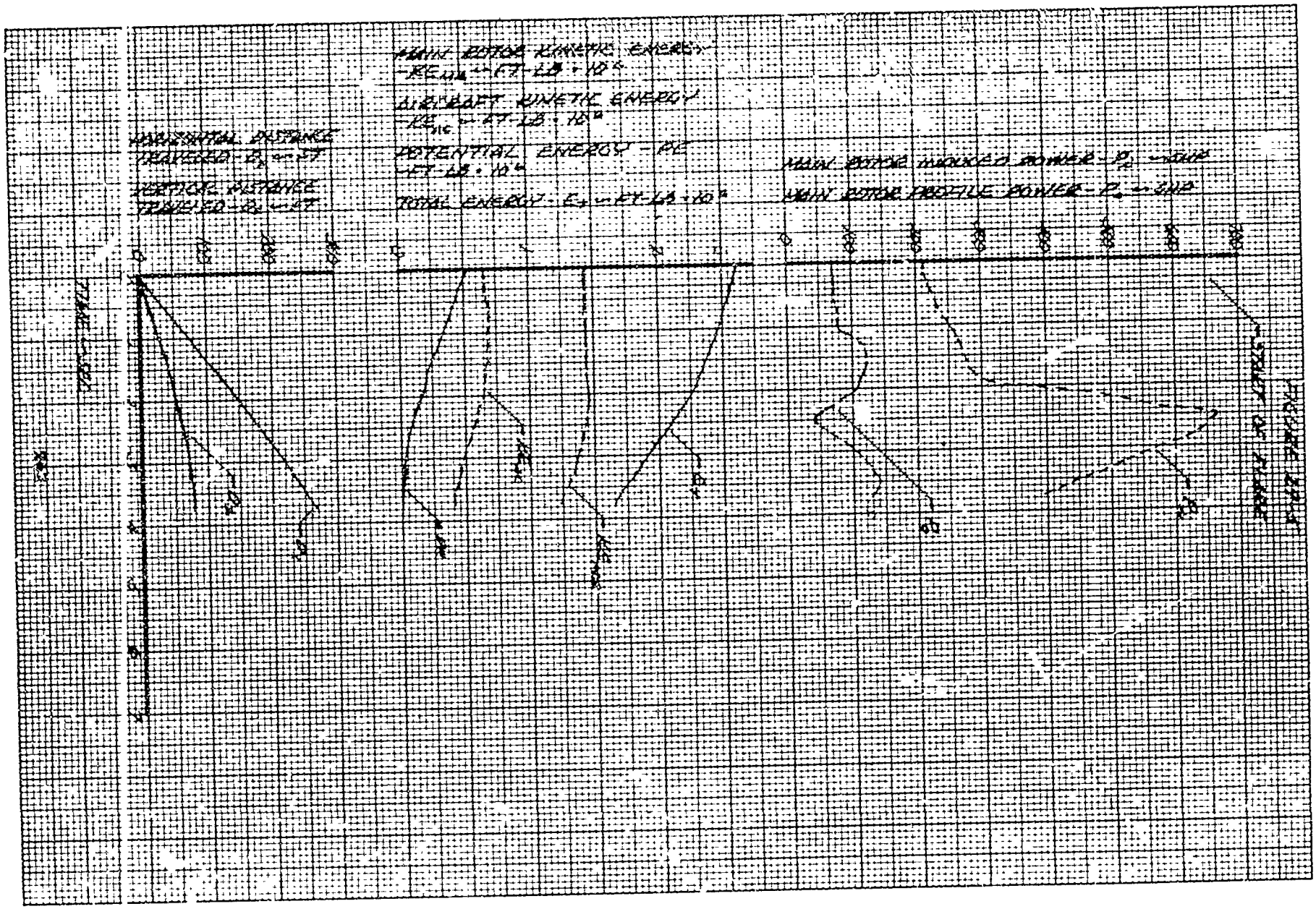
MAIN ROTOR KINETIC ENERGY
AIRCRAFT KINETIC ENERGY
POTENTIAL ENERGY - PE
TOTAL ENERGY - E
HORIZONTAL DISTANCE
VERTICAL DISTANCE
MAIN ROTOR INDUCED POWER - P
MAIN ROTOR PROFILE POWER - P
TIME

FIGURE 22-6
TAIL ROTOR THRUST COEFF. $C_{T_{TR}}$ 10^2
MAIN ROTOR THRUST COEFF. $C_{T_{MR}}$ 10^2
MAIN ROTOR POWER COEFF. $C_{P_{MR}}$ 10^4
$C_{T_{TR}}$
$C_{T_{MR}}$
$C_{P_{MR}}$
TIME - SEC

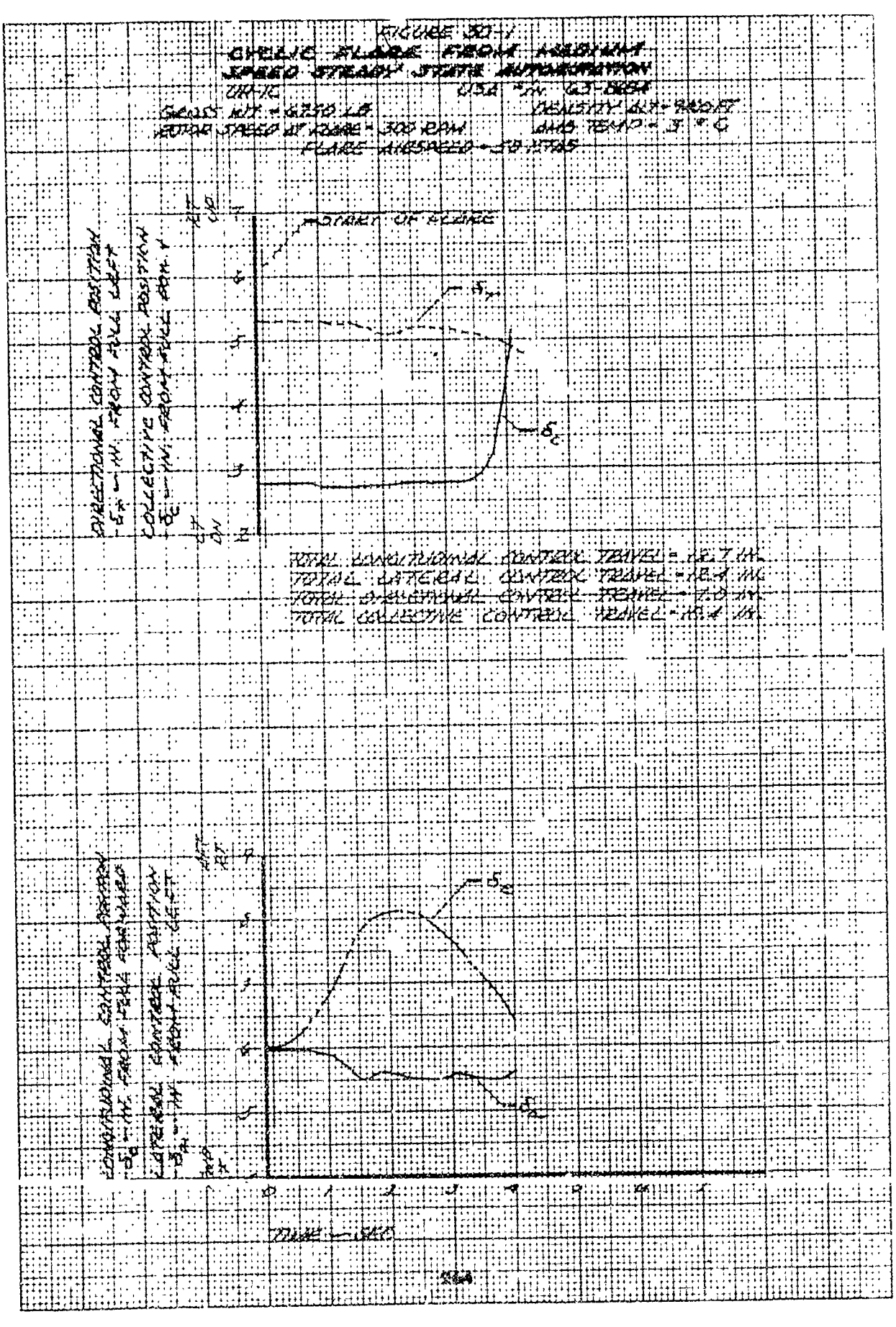
FIGURE 30-1
CYCLIC FLARE FROM MODERATE SPEED STEADY STATE AUTOROTATION
ZRP-1C
USA "ZRP" C.G. DATA
GROSS WT = 6250 LB
ROTOR SPEED AT FLARE = 300 RPM
DENSITY ALT = SEA LEVEL
OAT = 5 °C
FLARE AIRSPEED = 50 KTAS
MOMENT OF FLARE
δ_{ped}
δ_c
LONGITUDINAL CONTROL POSITION
δ_e — IN. FROM FULL LEFT
COLLECTIVE CONTROL POSITION
δ_c — IN. FROM FULL DOWN
TOTAL LONGITUDINAL CONTROL TRAVEL = 12.7 IN.
TOTAL LATERAL CONTROL TRAVEL = 12.7 IN.
TOTAL DIRECTIONAL CONTROL TRAVEL = 7.0 IN.
TOTAL COLLECTIVE CONTROL TRAVEL = 11.4 IN.
DIRECTIONAL CONTROL POSITION
δ_p — IN. FROM FULL LEFT
LATERAL CONTROL POSITION
δ_a — IN. FROM FULL LEFT
δ_{lat}
TIME — SEC

FIGURE 30-2

PITCH ATTITUDE - θ
DEG
ROLL ATTITUDE - φ
DEG
YAW ATTITUDE - ψ
DEG
PITCH RATE - θ̇
DEG/SEC
ROLL RATE - φ̇
DEG/SEC
YAW RATE - ψ̇
DEG/SEC
ANGLE OF ATTACK - α - DEG
ANGLE OF SIDESLIP - β - DEG
START OF FLARE
α
β
θ
φ
ψ
TIME - SEC

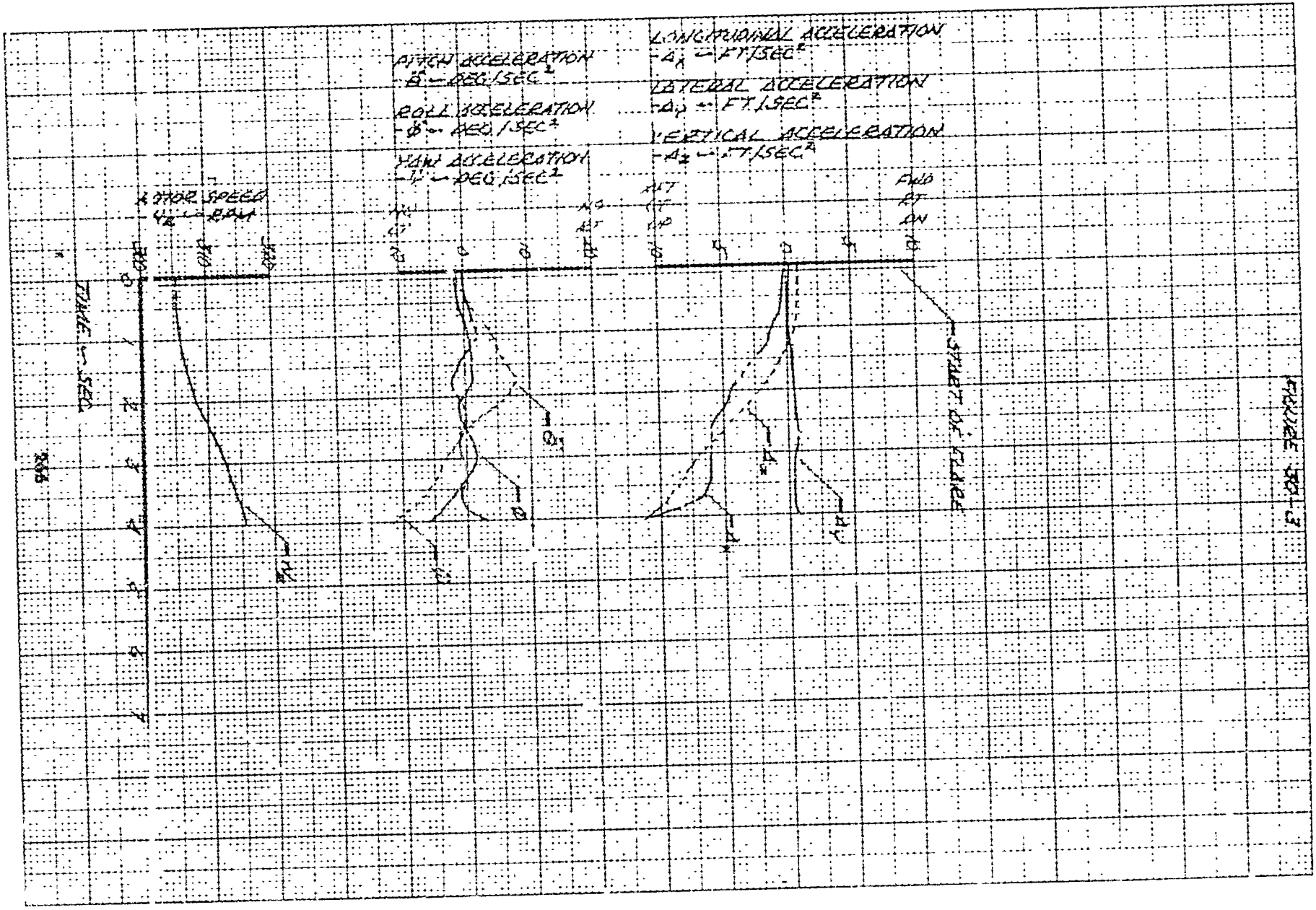
PITCH ACCELERATION
$\ddot{\theta}$ — DEG/SEC²
ROLL ACCELERATION
$\ddot{\phi}$ — DEG/SEC²
YAW ACCELERATION
$\ddot{\psi}$ — DEG/SEC²
LONGITUDINAL ACCELERATION
$-A_x$ — FT/SEC²
LATERAL ACCELERATION
$-A_y$ — FT/SEC²
VERTICAL ACCELERATION
$-A_z$ — FT/SEC²
FWD AT AFT
AFT
FWD AT FWD
STABILITY AXIS FLIGHT PATH
TIME — SEC
356

FIGURE 30-a

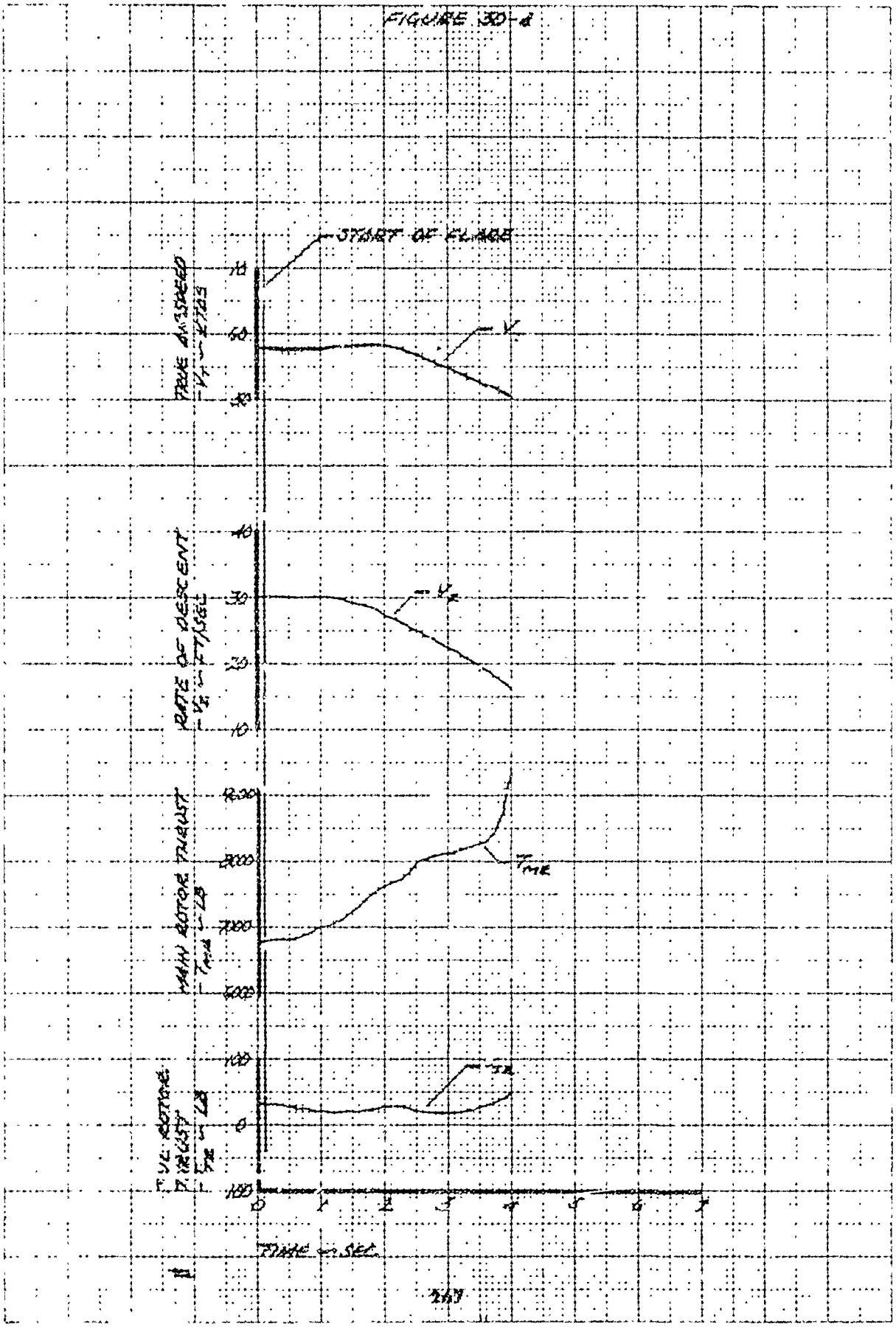
START OF FLARE
TRUE AIRSPEED
V_T — KTAS
V_T
RATE OF DESCENT
V_Z — FT/SEC
V_Z
MAIN ROTOR THRUST
T_{MR} — LB
T_{MR}
VC ROTOR THRUST
T_{VR} — LB
T_{VR}
TIME — SEC.

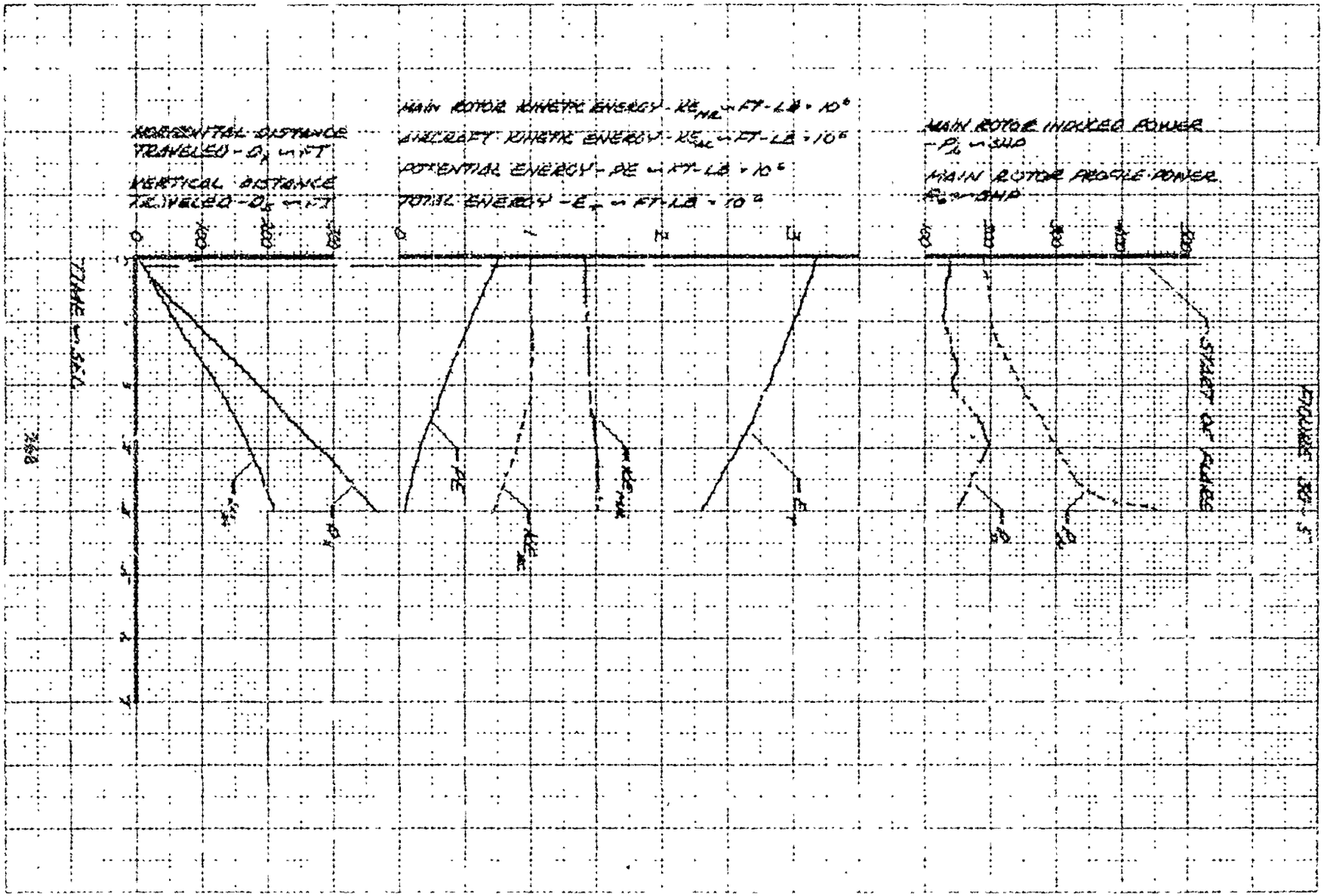
HORIZONTAL DISTANCE TRAVELED - D_x - FT
VERTICAL DISTANCE TRAVELED - D_y - FT
MAIN ROTOR KINETIC ENERGY - KE_{MR} - FT-LB × 10^6
AIRCRAFT KINETIC ENERGY - KE_{AC} - FT-LB × 10^6
POTENTIAL ENERGY - PE - FT-LB × 10^6
TOTAL ENERGY - E_T - FT-LB × 10^6
MAIN ROTOR INDICATED POWER - P_{IR} - SHP
MAIN ROTOR PROFILE POWER - P_o - SHP
TIME - SEC
START OF FLARE
FIGURE 18

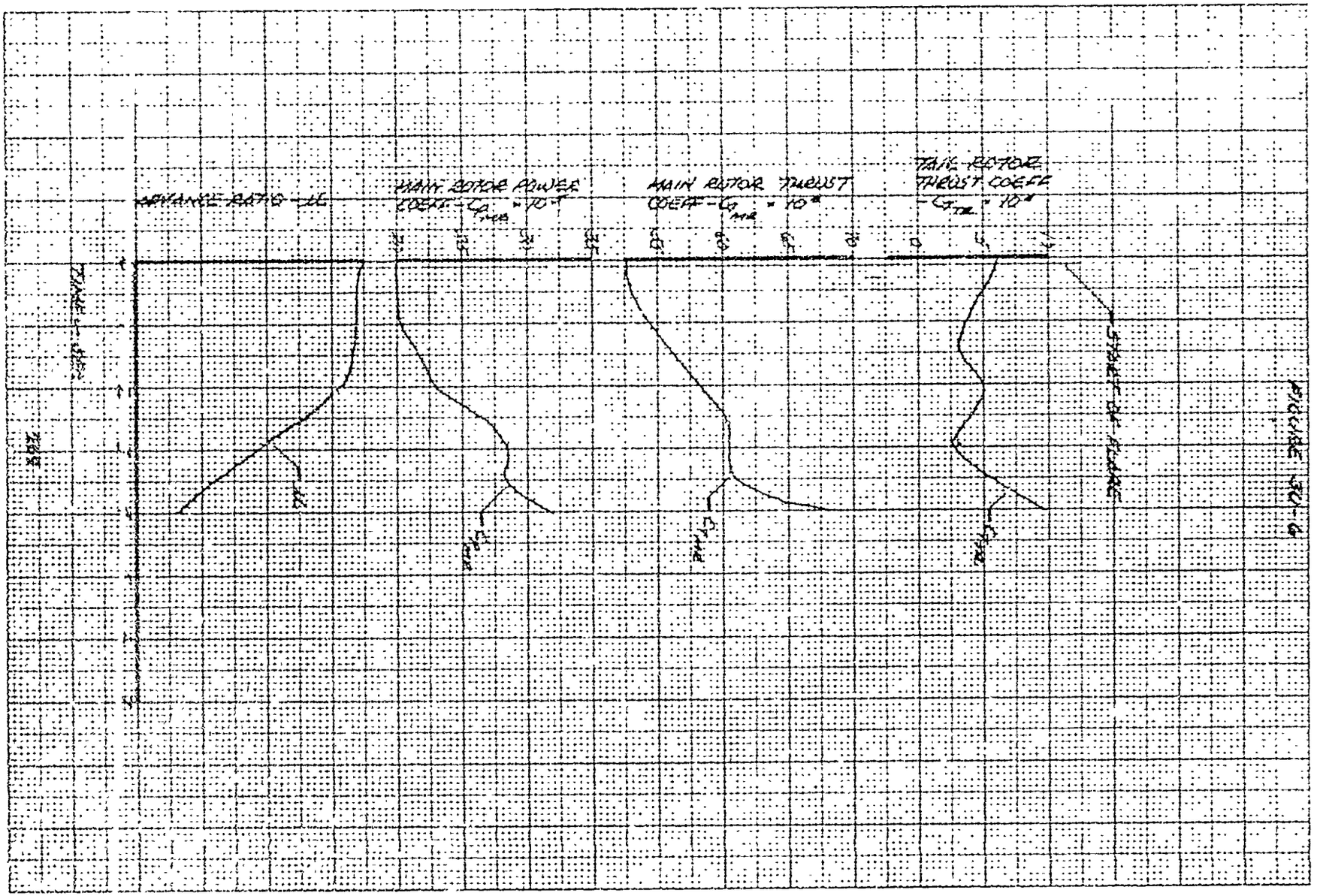
ADVANCE RATIO - μ
MAIN ROTOR POWER COEFF - $C_{P_{MR}} \times 10^{-4}$
MAIN ROTOR THRUST COEFF - $C_{T_{MR}} \times 10^{-4}$
TAIL ROTOR THRUST COEFF - $C_{T_{TR}} \times 10^{-4}$
POWER - HP
STABILITY BOUNDARY
FIGURE 3(A)-6

FIGURE IV-1

CYCLIC FLARE FROM LOW SPEED ACCELERATING AUTOROTATION

UH-1C

GROSS WT = 6690 LB
ROTOR SPEED AT FLARE = 300 RPM

DENSITY ALT = 2000 FT
AMB TEMP = 17 °C

FLARE AIRSPEED = 35 KTAS

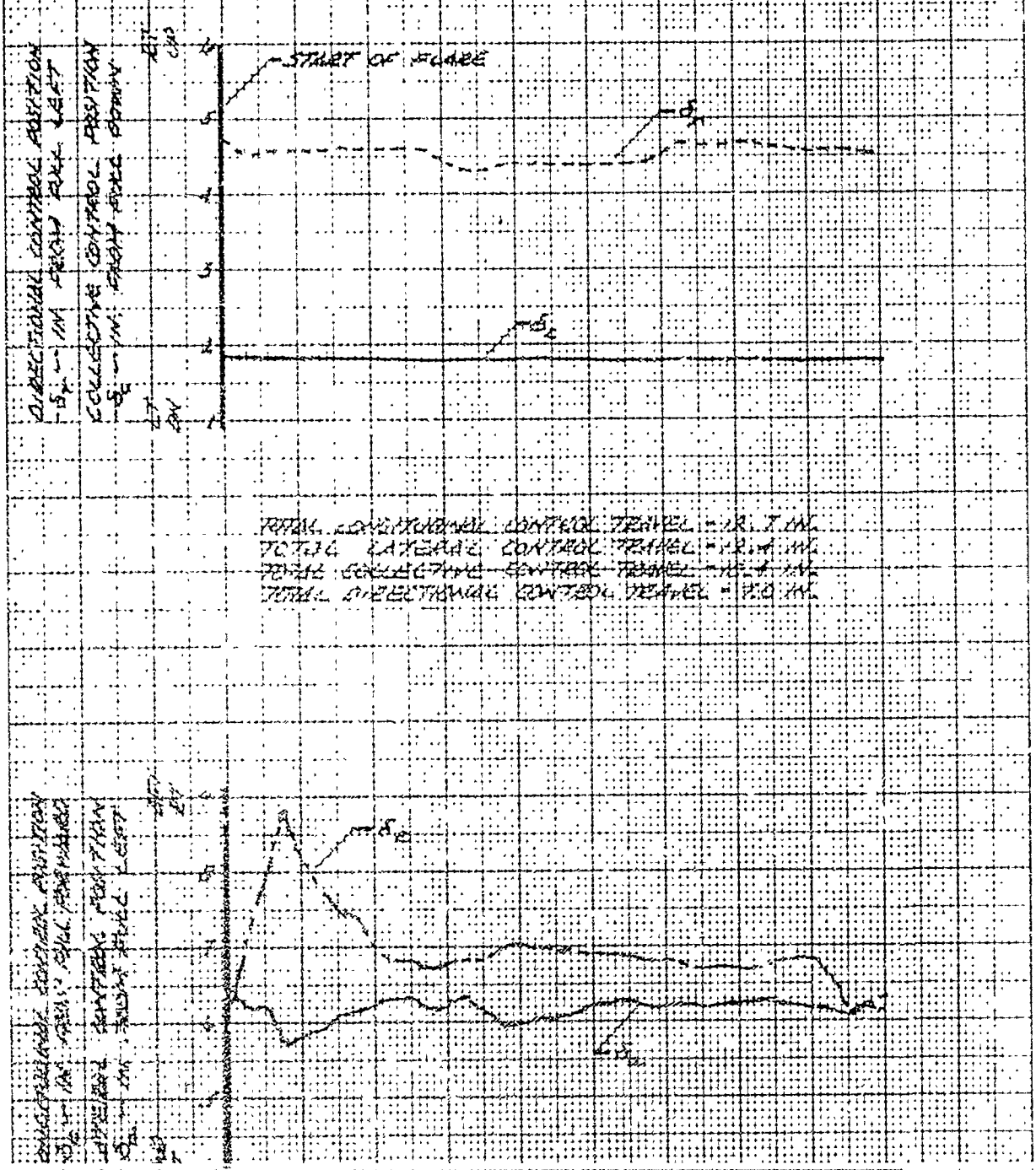

FIGURE 31-2

PITCH RATE - q - DEG/SEC
ROLL RATE - p - DEG/SEC
YAW RATE - r - DEG/SEC
PITCH ATTITUDE - θ - DEG
ROLL ATTITUDE - φ - DEG
YAW ATTITUDE - ψ - DEG
ANGLE OF ATTACK - α - DEG
ANGLE OF SIDESLIP - β - DEG
START OF FLARE
TIME - SEC

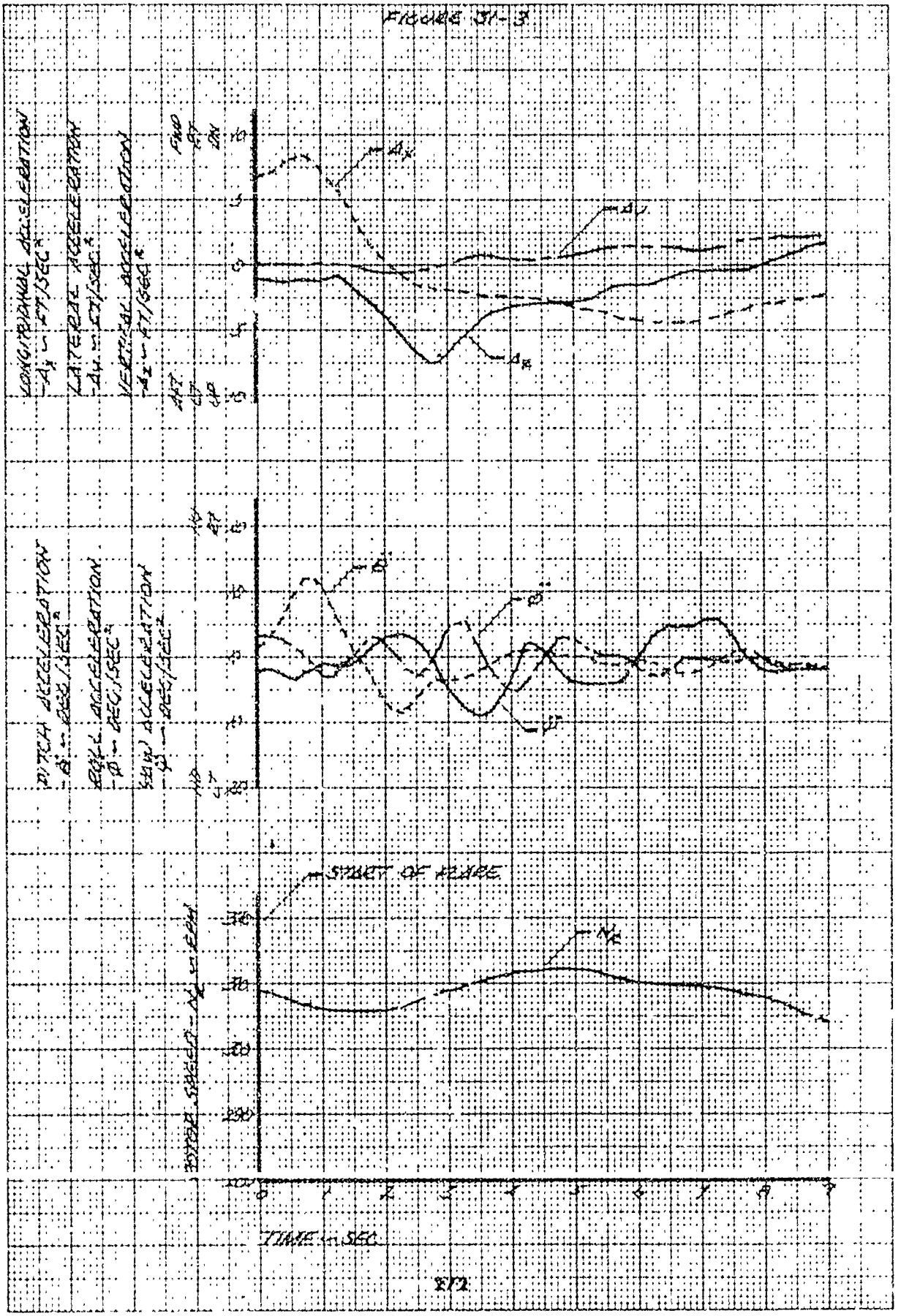
FIGURE 31-3
LONGITUDINAL ACCELERATION
A_x -- FT/SEC²
LATERAL ACCELERATION
A_y -- FT/SEC²
VERTICAL ACCELERATION
A_z -- FT/SEC²
PITCH ACCELERATION
$\dot{q}$ -- RAD/SEC²
ROLL ACCELERATION
$\dot{p}$ -- RAD/SEC²
YAW ACCELERATION
$\dot{r}$ -- RAD/SEC²
START OF FLARE
TIME -- SEC
271

FIGURE IV-4

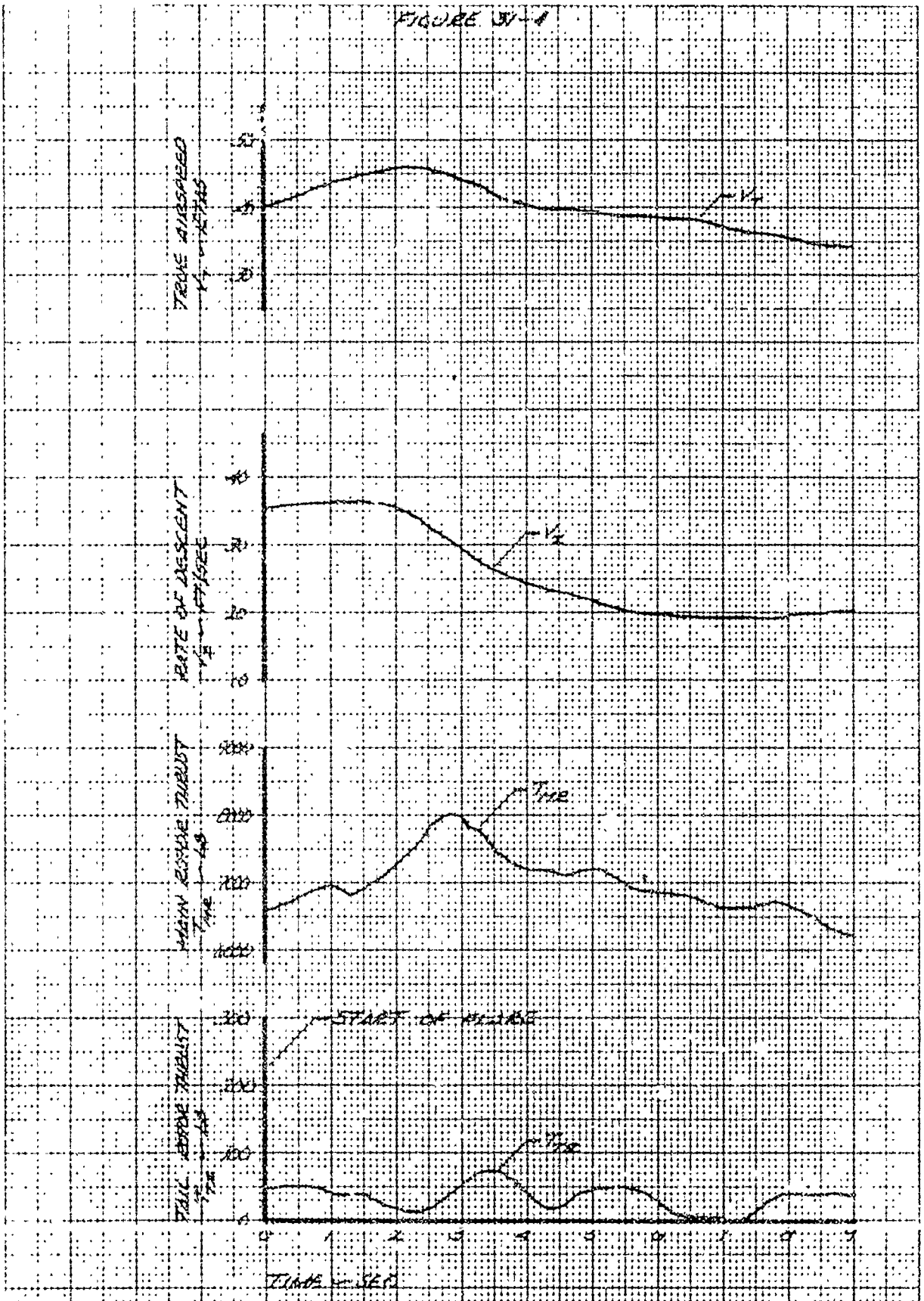
TRUE AIRSPEED
RATE OF DESCENT
MAIN ROTOR THRUST
TAIL ROTOR THRUST
START OF MANEUVER
TIME - SEC

FIGURE III-5
TIME - SEC
START OF FLARE

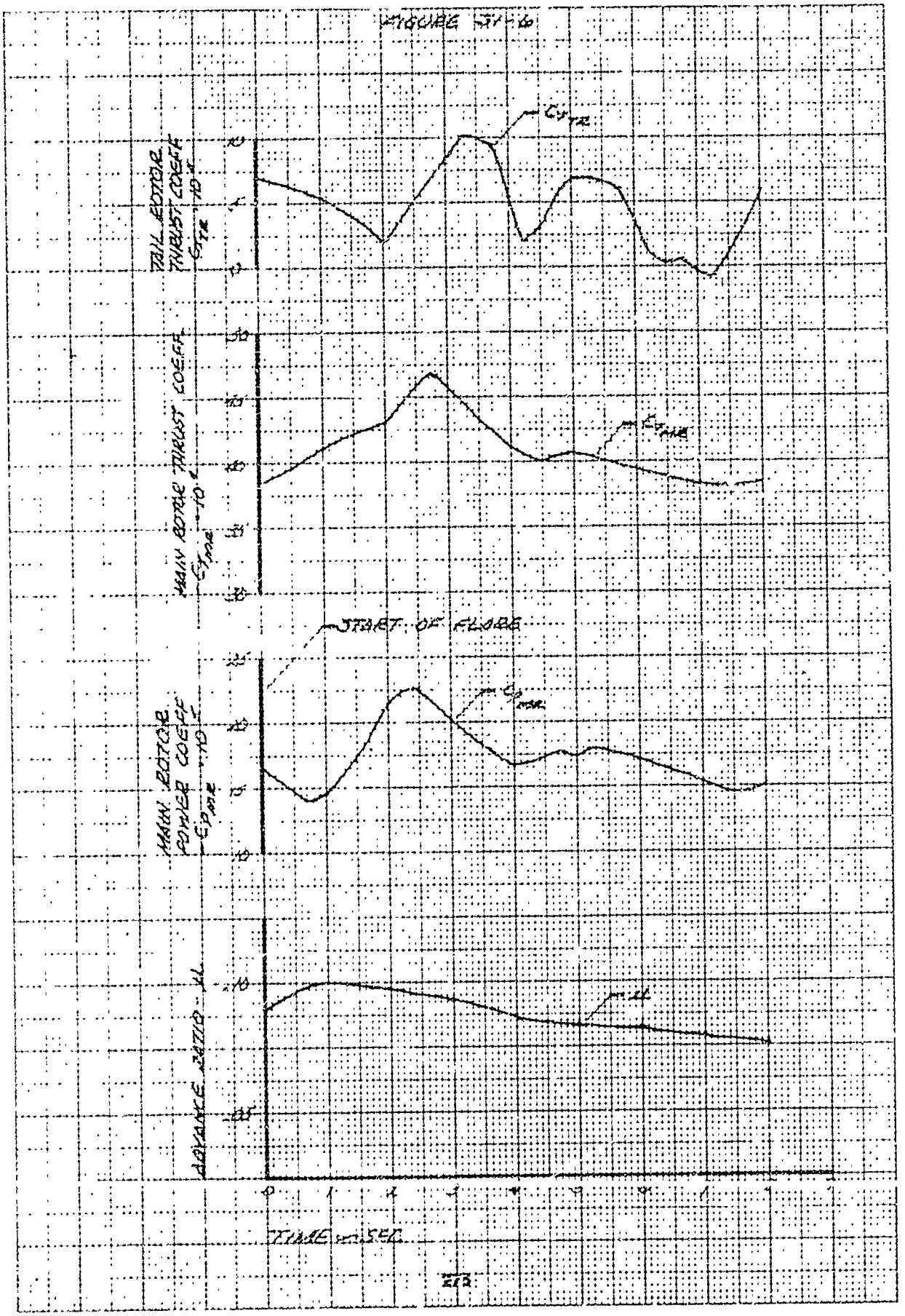
FIGURE 37-16
TAIL ROTOR THRUST COEFF
MAIN ROTOR THRUST COEFF
START OF FLARE
MAIN ROTOR POWER COEFF
ADVANCE RATIO - μ
TIME - SEC
213

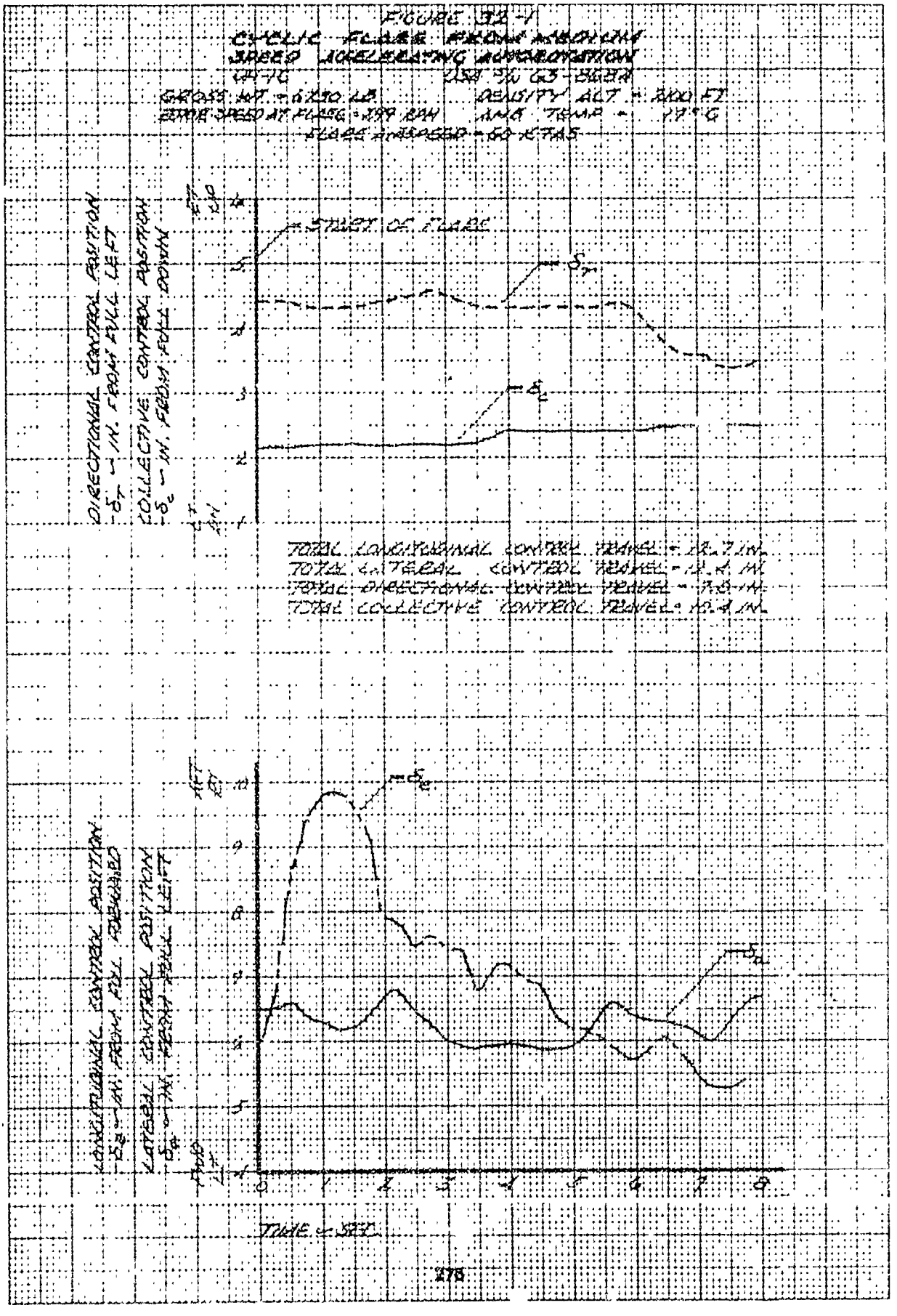
FIGURE 32-1
CYCLIC FLARE FROM MACH 2.4
SPEED DECELERATING ACCELERATION
USN 3% G3-BEAM
GROSS WT = 6250 LB
ZERO SPEED AT FLARE = 197 KIAS
FLARE ANGLE = 60 KIAS
DENSITY ALT = 2100 FT
OAT = 17°C
DIRECTIONAL CONTROL POSITION
-δr — IN. FROM FULL LEFT
COLLECTIVE CONTROL POSITION
-δc — IN. FROM FULL DOWN
δr
δc
TOTAL LONGITUDINAL CONTROL TRAVEL = 12.7 IN.
TOTAL LATERAL CONTROL TRAVEL = 12.4 IN.
TOTAL DIRECTIONAL CONTROL TRAVEL = 7.0 IN.
TOTAL COLLECTIVE CONTROL TRAVEL = 10.4 IN.
LONGITUDINAL CONTROL POSITION
-δe — IN. FROM FULL FORWARD
LATERAL CONTROL POSITION
-δa — IN. FROM FULL LEFT
δe
δa
TIME — SEC

FIGURE 32-12

ANGLE OF ATTACK OF WING REF.
ANGLE OF SIDESLIP - DEG
ANGLE OF BANK - DEG
BODY RATE - Q - RAD/SEC
BODY RATE - P - RAD/SEC
BODY RATE - R - RAD/SEC
START OF FLARE
TIME - SEC

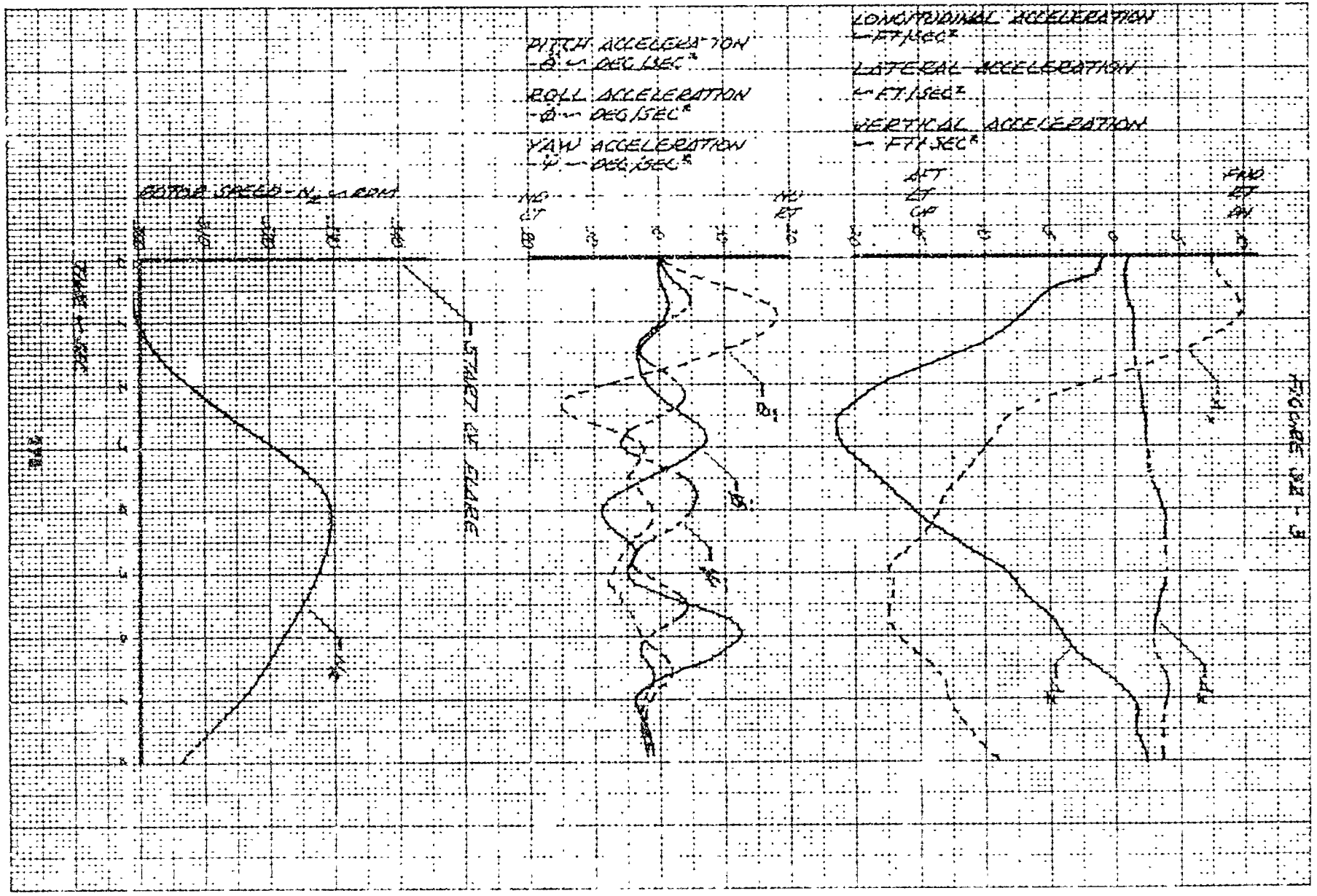
PITCH ACCELERATION
$\dot{Q}$ — DEG/SEC²
ROLL ACCELERATION
$\dot{\phi}$ — DEG/SEC²
YAW ACCELERATION
$\dot{\psi}$ — DEG/SEC²
LONGITUDINAL ACCELERATION
— FT/SEC²
LATERAL ACCELERATION
— FT/SEC²
VERTICAL ACCELERATION
— FT/SEC²
ROTOR SPEED - N_R — RPM
TIME — SEC
STALL ONSET FLARE
FIGURE 3.2.1 - 28

FIGURE 52-4

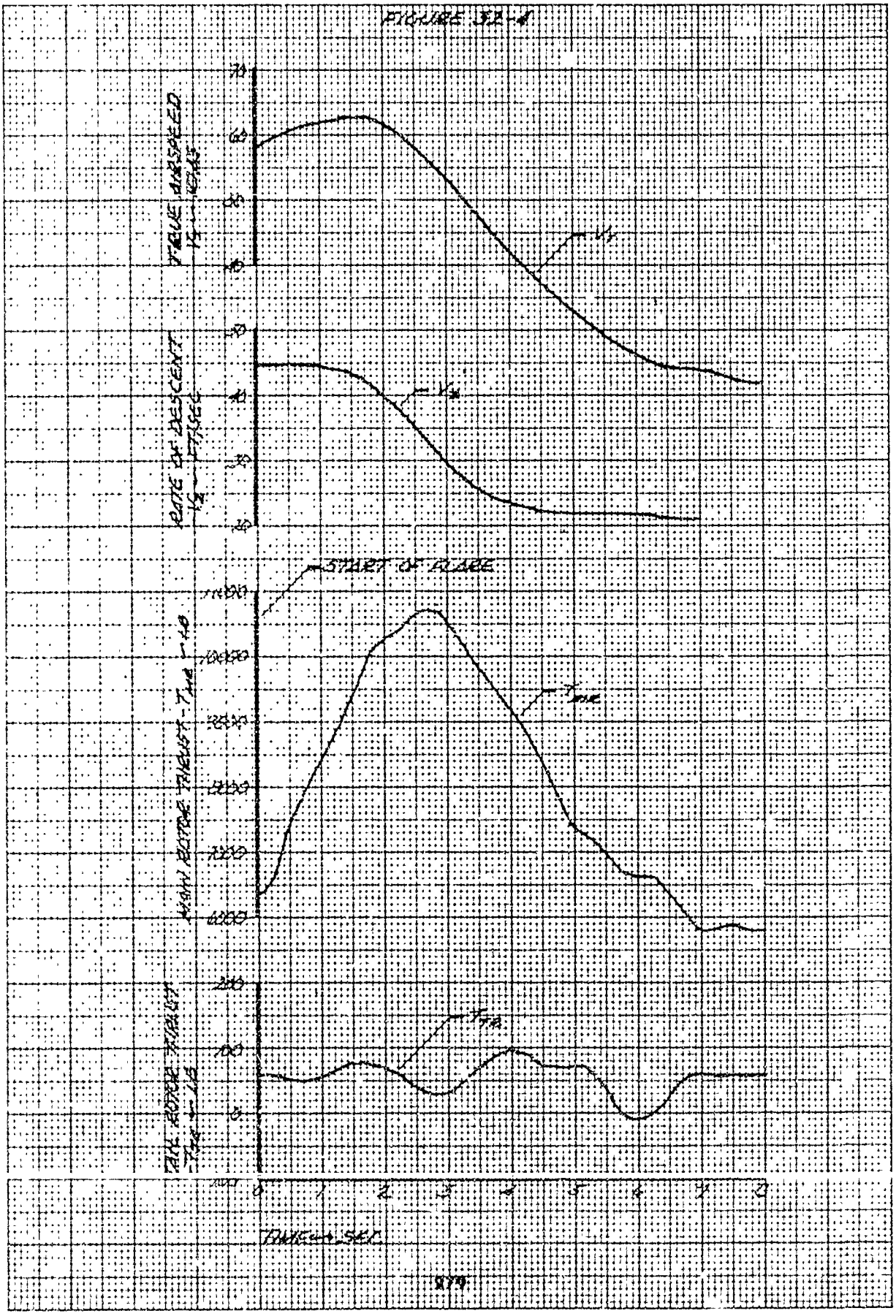
70
60
50
40
30
20
RATE OF DESCENT
Hz — FEET/SEC
TRUE AIRSPEED
Hz — KNOTS
START OF FLARE
H_{TA}
H_{RA}
H_{RC}
H_{RA}
0
1
2
3
4
5
6
7
8
TIME — SEC

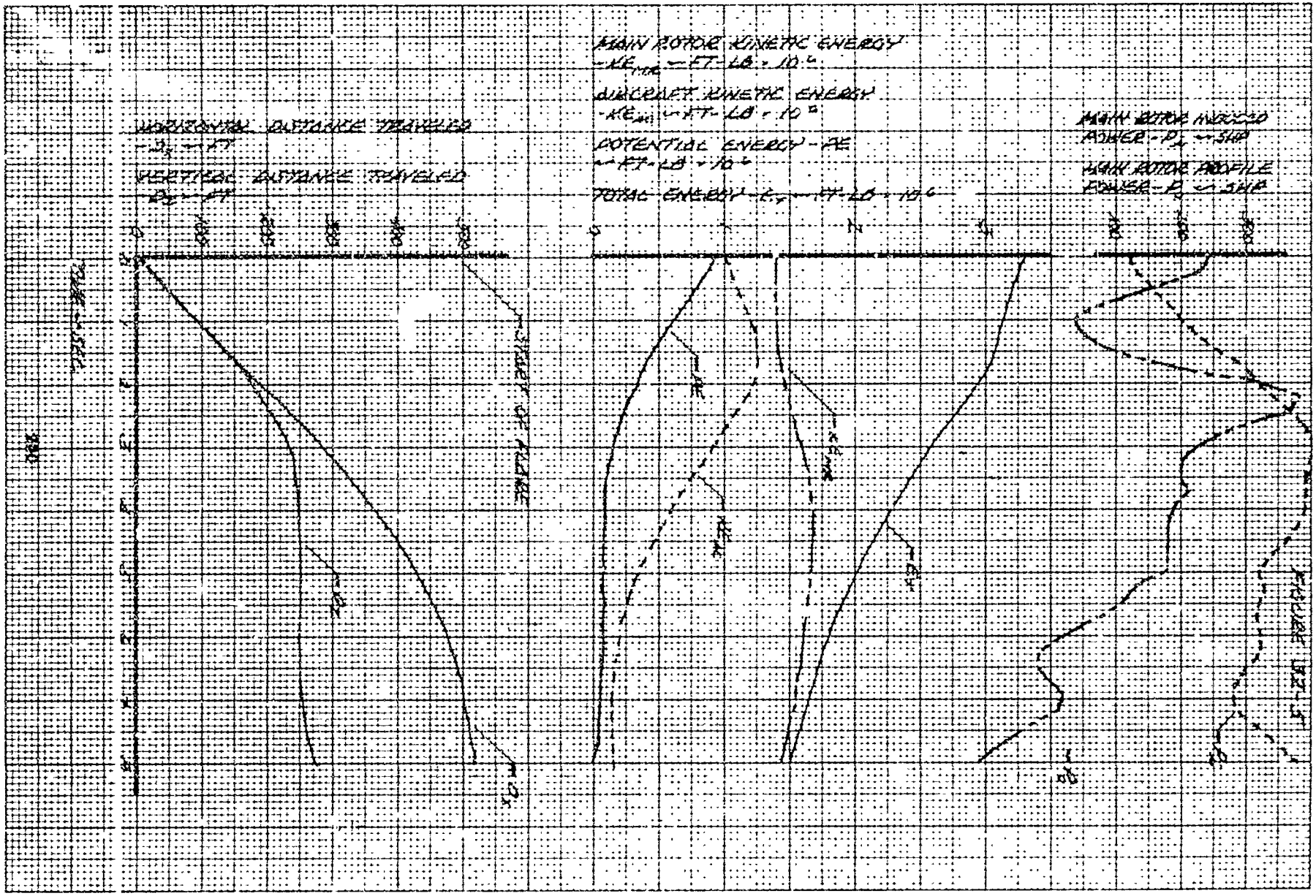
MAIN ROTOR KINETIC ENERGY
DUCTED FAN KINETIC ENERGY
POTENTIAL ENERGY - PE
TOTAL ENERGY
MAIN ROTOR INDUCED POWER
MAIN ROTOR PROFILE POWER
HORIZONTAL DISTANCE TRAVELED
VERTICAL DISTANCE TRAVELED
SPEED OF AIRCRAFT
FIGURE OF MERIT

FIGURE 32-16

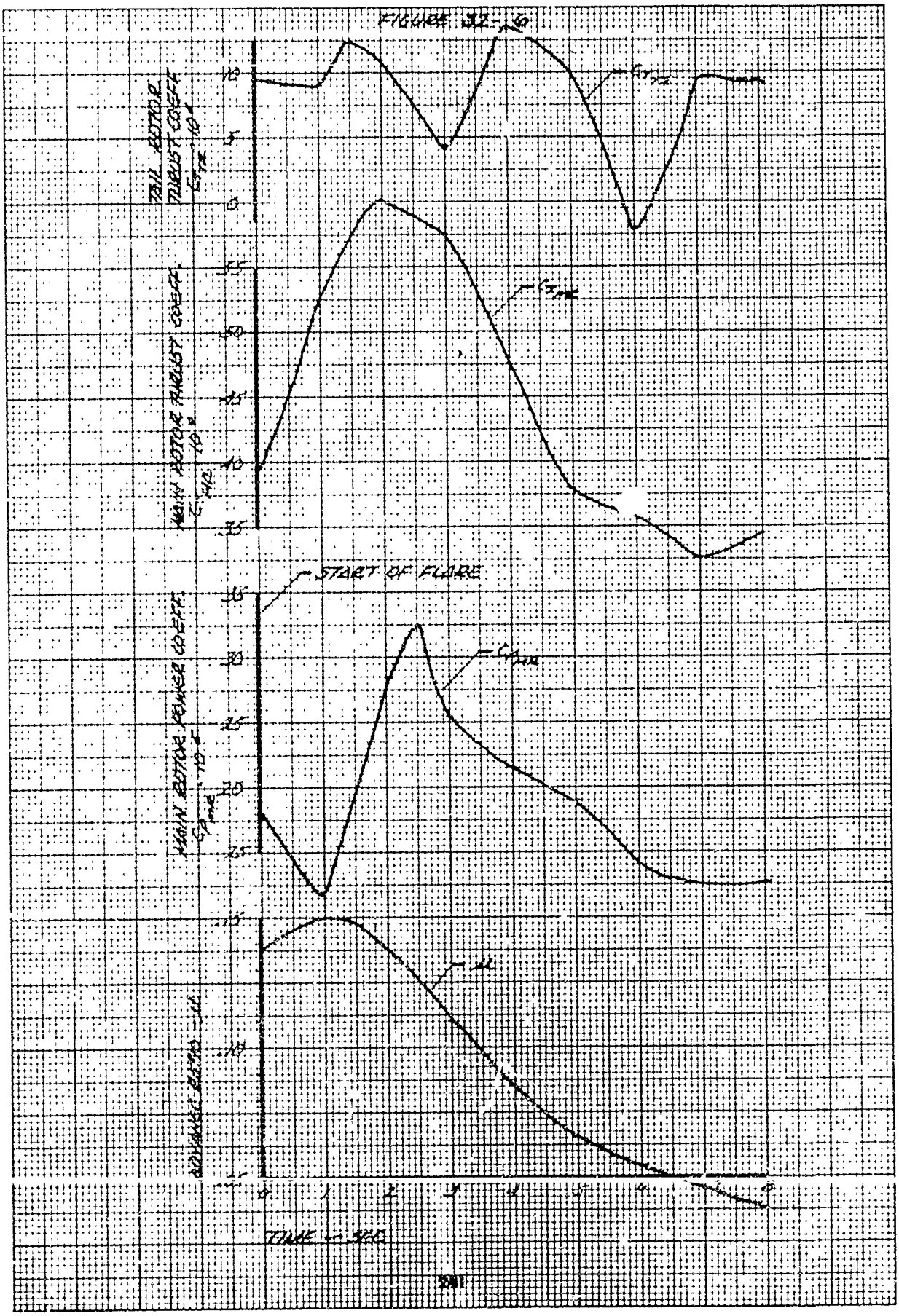
TAIL ROTOR THRUST COEFF. $C_{T_{TR}} \cdot 10^4$
MAIN ROTOR THRUST COEFF. $C_{T_{MR}} \cdot 10^4$
MAIN ROTOR POWER COEFF. $C_{P_{MR}} \cdot 10^4$
ADVANCE RATIO μ
$C_{T_{TR}}$
$C_{T_{MR}}$
START OF FLARE
$C_{P_{MR}}$
μ
TIME — SEC

FIGURE 33-1

COMPARISON OF CYCLIC FLARE PERFORMANCE WITH LONGITUDINAL CONTROL INPUT

CH-1C USA S/N 63-8684

GROSS WT = 6620 LB DENSITY ALT = 4400 FT

AMB TEMP = 25 °C

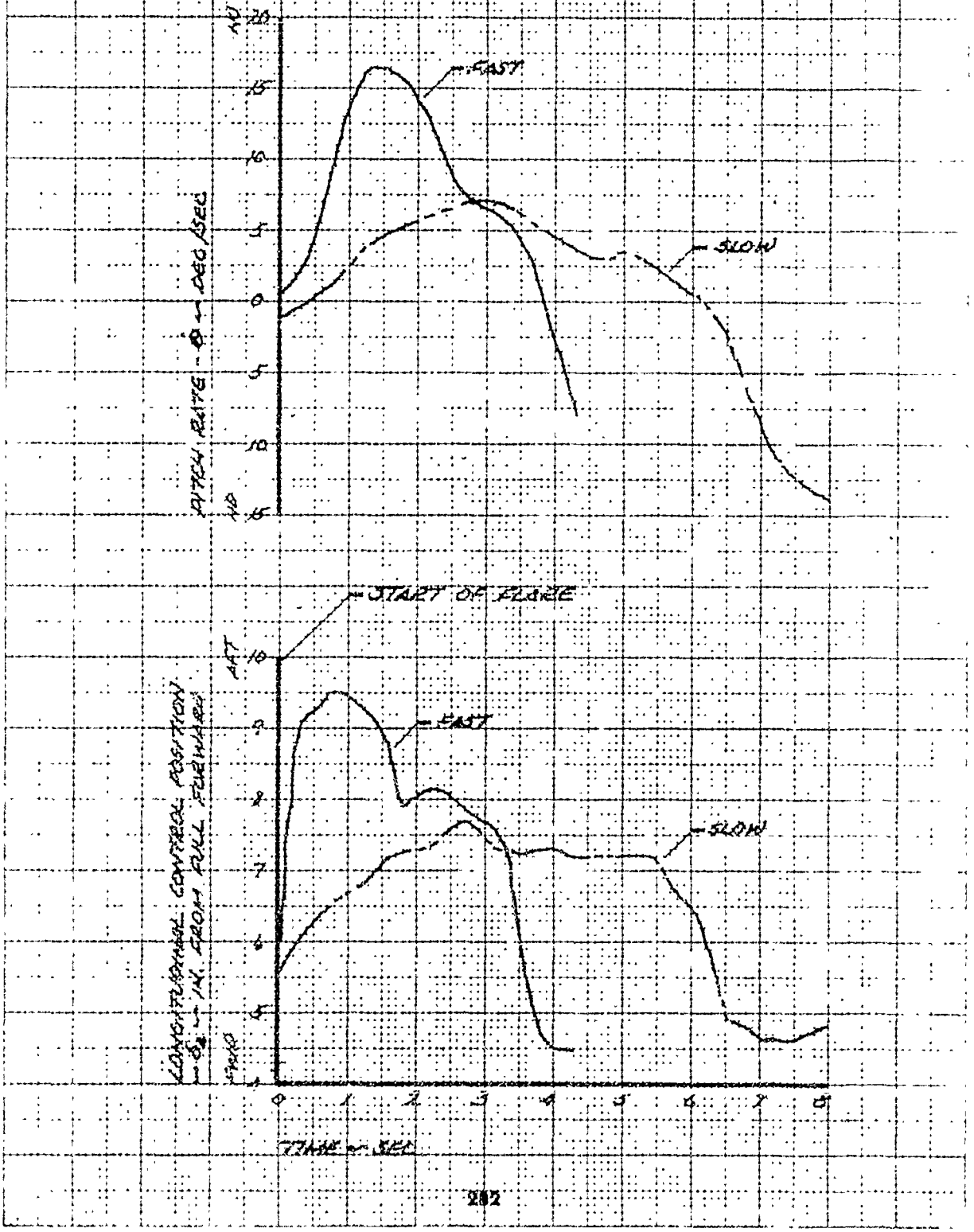

FIGURE 3.5-2

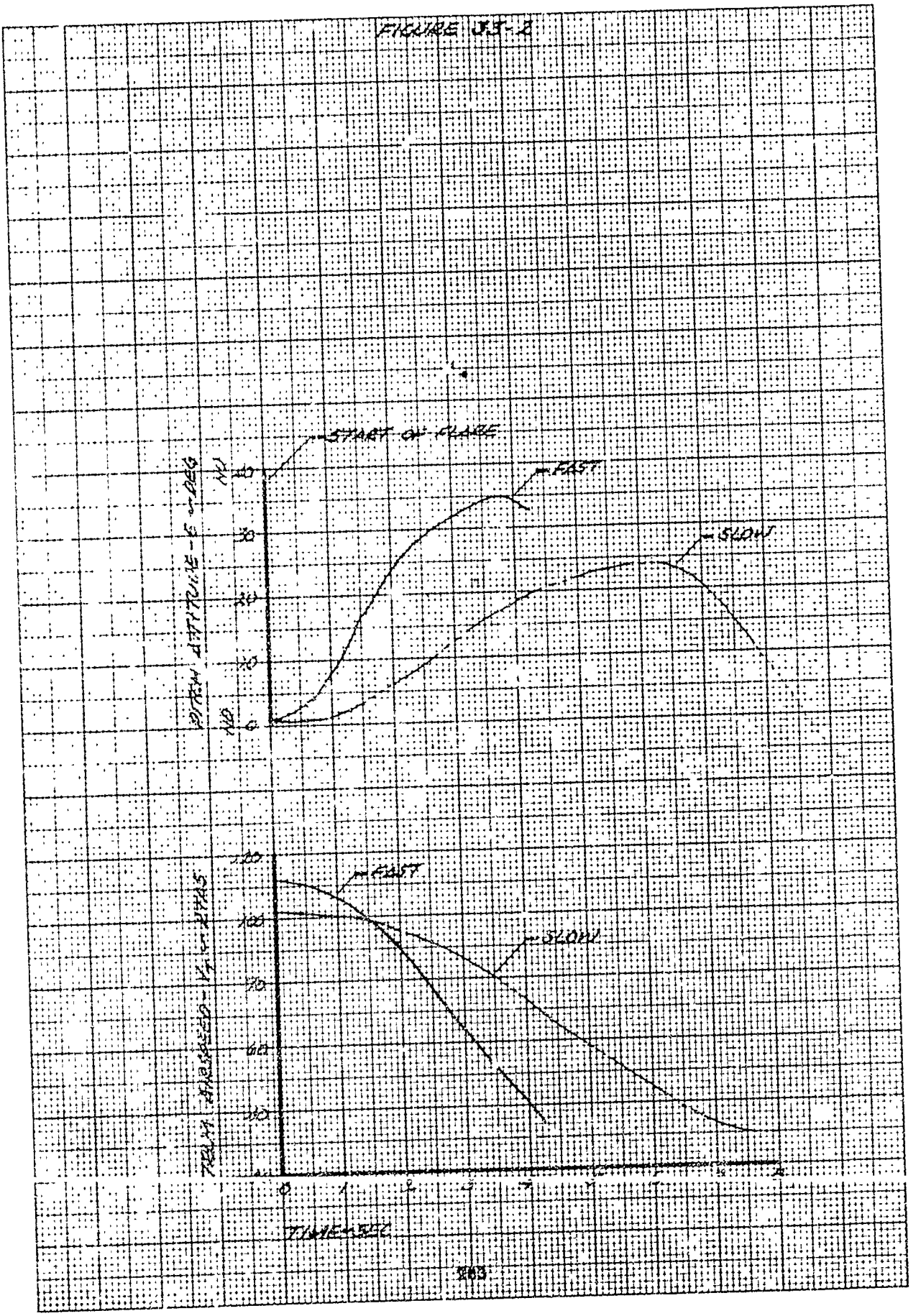

FIGURE 33-3

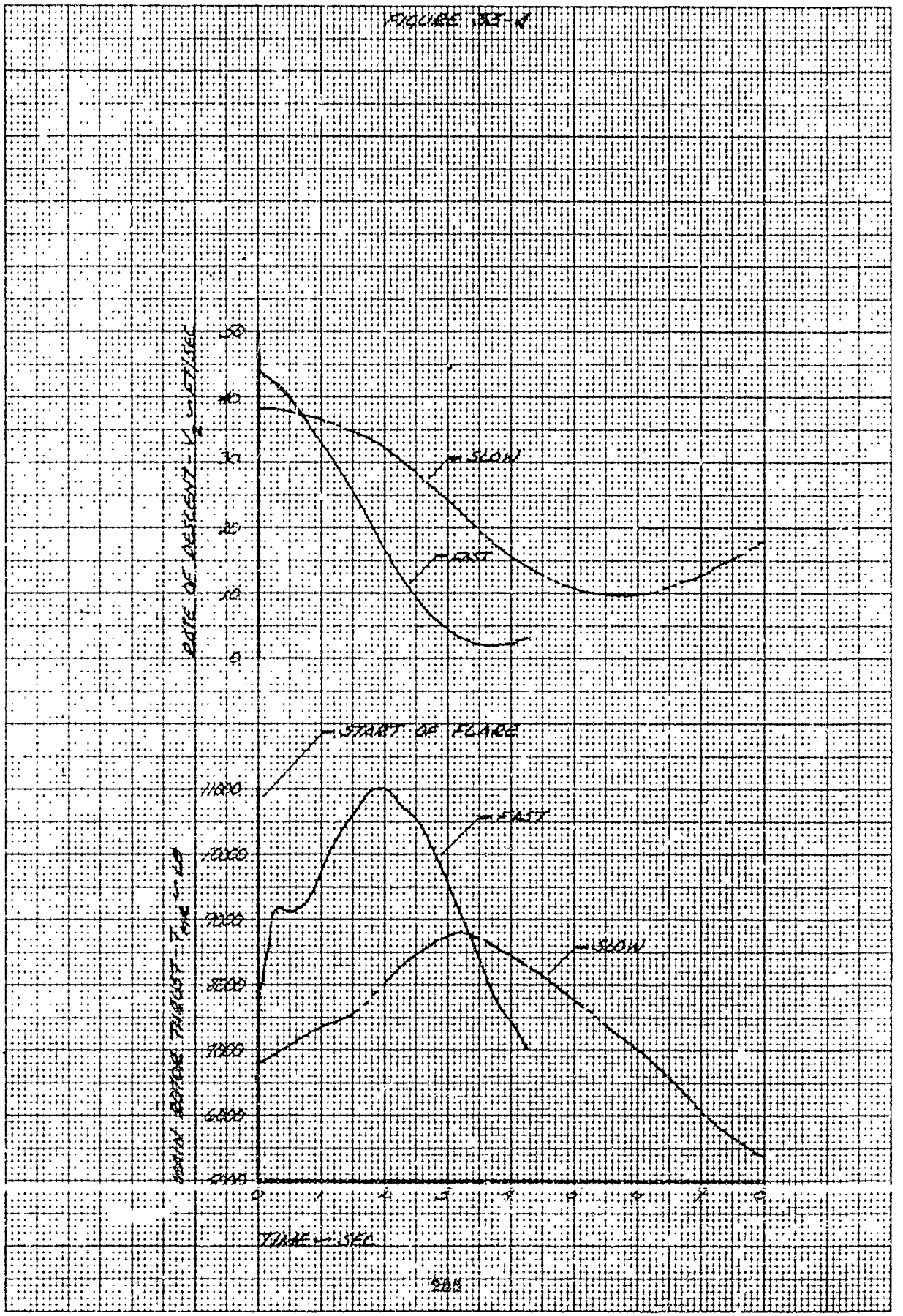
FIGURE XII-4
RATE OF DESCENT - FT/SEC
SLOW
FAST
START OF FLARE
FAST
SLOW
TIME - SEC

FIGURE X3-5

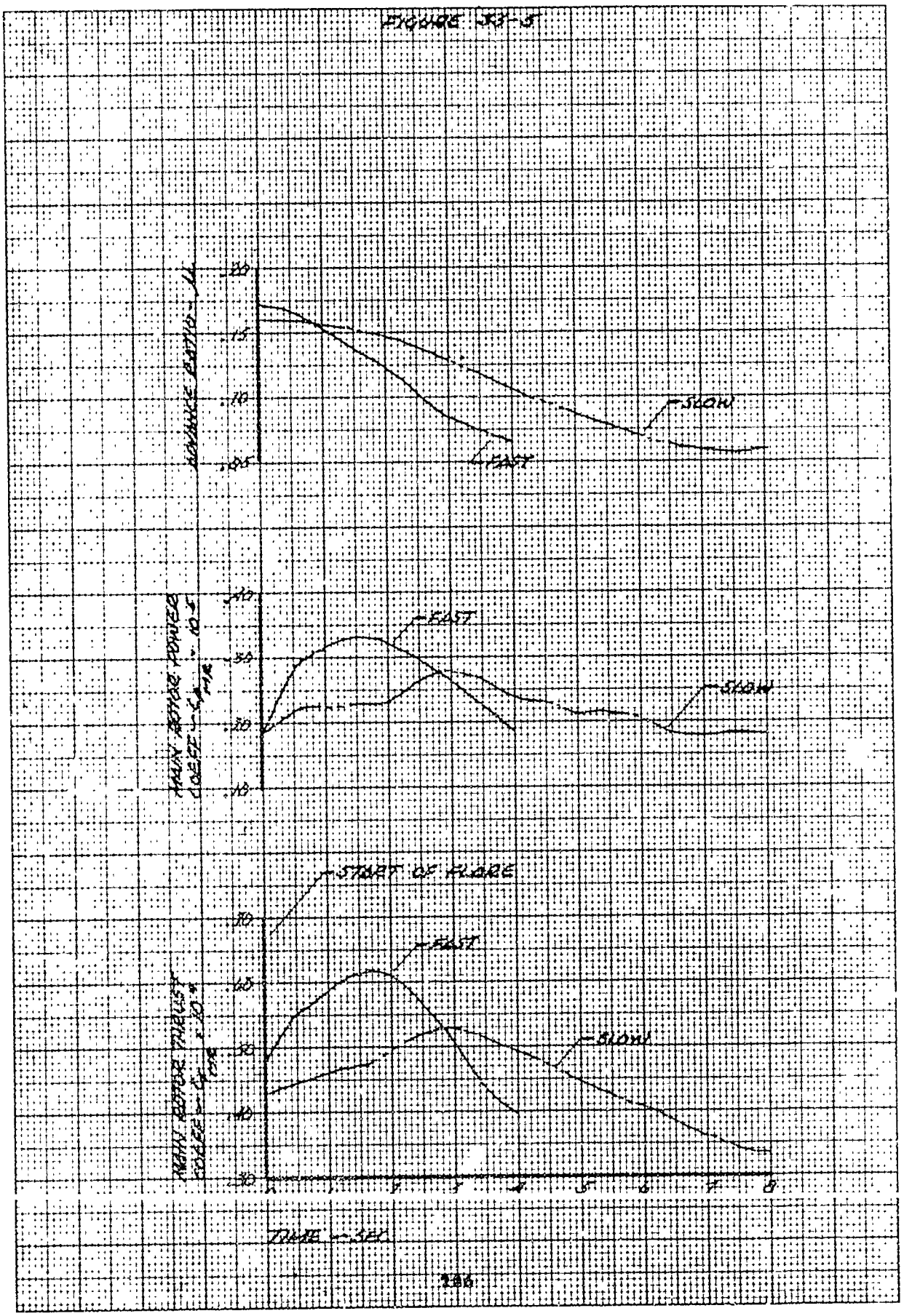
MAIN ENGINE POWER
CLOSE-UP
SLOW
FAST
FAST
SLOW
START OF FLARE
FAST
SLOW
TIME - SEC

FIGURE 54-1

PERFORMANCE FOR A COLLECTIVE CONTROL APPLICATION IN STEADY STATE DESCENT

CH-47C
GROSS WT - 7000 LB
AND TE 40 = 27 °C

USA Sv 63-8684
DENSITY ALT - 1000 FT

INITIAL RATE OF COLLECTIVE CONTROL INPUT - $\Delta\delta_c/\Delta T$ - IN/SEC

$\Delta\delta_c/\Delta T$

TOTAL COLLECTIVE CONTROL TRAVEL = 10.4 IN.

COLLECTIVE CONTROL INPUT - $\Delta\delta_c$ - IN.

$\Delta\delta_c$

TRUE AIRSPEED - KTAS

FIGURE XI-2
TRUE AIRSPEED — KTAS
MAXIMUM RATE OF ACCELERATION - Δθ — RADIANS/SEC²
MAXIMUM RATE PITCH RATE - θ̇ — DEG/SEC
MAXIMUM PITCH ATTITUDE - θ — DEGS
CHANGE IN PITCH ATTITUDE - Δθ — DEGS
DECREASE IN ANGLE OF ATTACK - Δα — DEGS
LEVEL
NU
TURN
Δθ
θ̇
θ
Δα

FIGURE 34-3

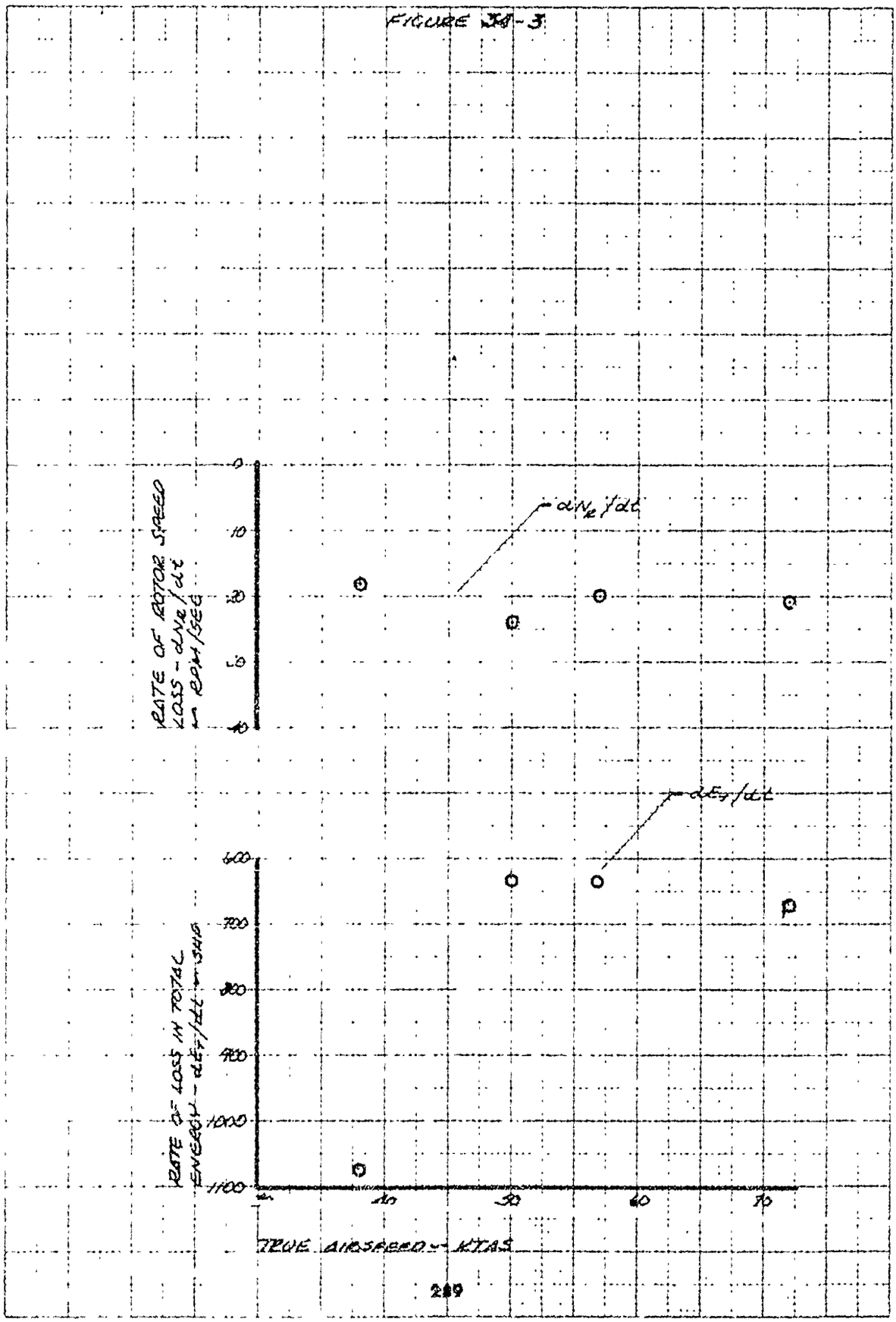
RATE OF ROTOR SPEED LOSS - dN_R/dt = RPM/SEC
0
10
20
30
40
$-dN_R/dt$
RATE OF LOSS IN TOTAL ENERGY - dE_T/dt = SHP
600
700
800
900
1000
1100
$-dE_T/dt$
10
20
30
40
50
TRUE AIRSPEED - KTAS

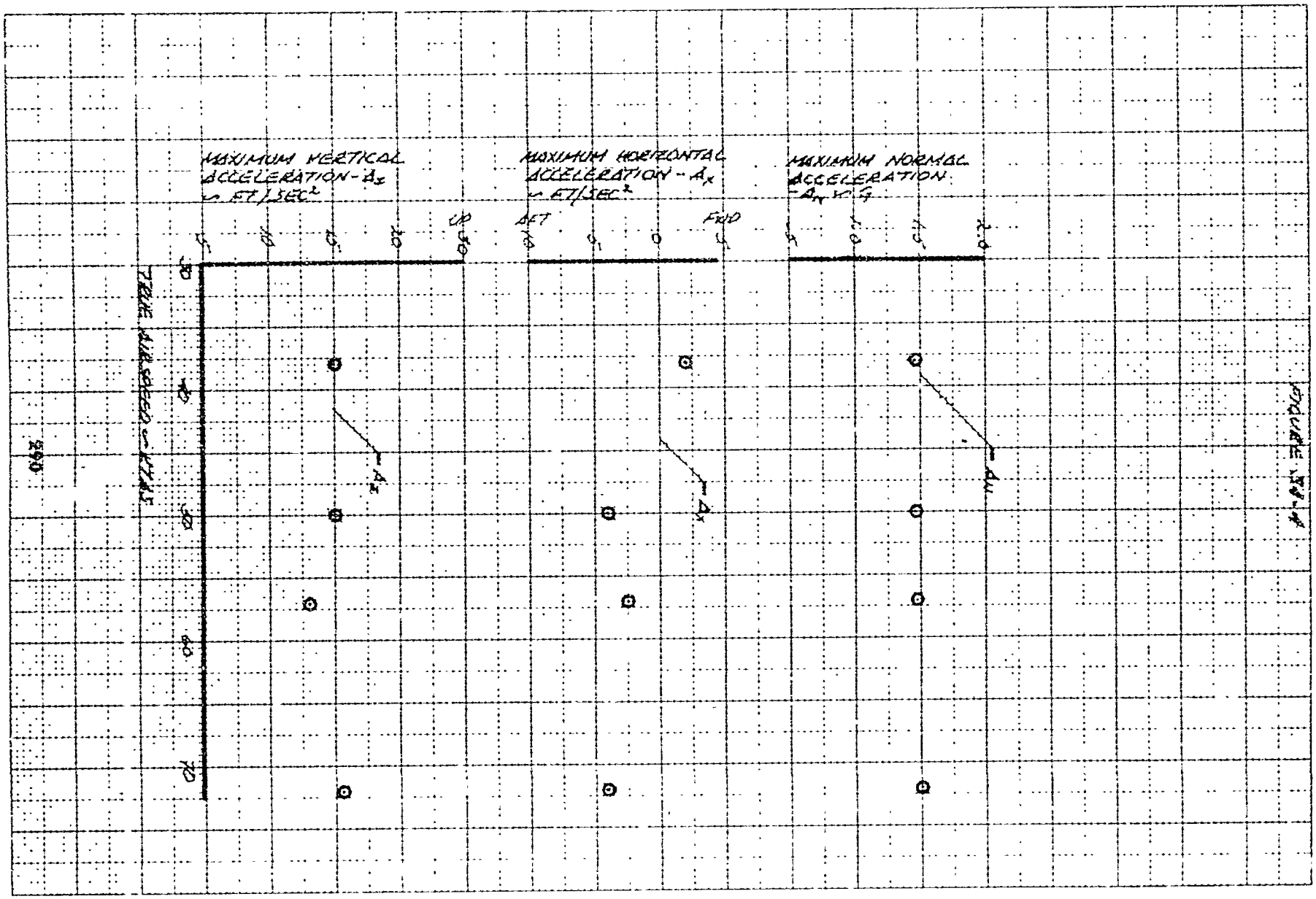
MAXIMUM VERTICAL ACCELERATION - A_z ~ FT/SEC²
MAXIMUM HORIZONTAL ACCELERATION - A_x ~ FT/SEC²
MAXIMUM NORMAL ACCELERATION - A_N IN g
UP
AFT
FWD
15
10
5
0
5
2.0
1.5
2.0
A_z
A_x
A_N
TRUE AIRSPEED ~ KNOTS
30
40
50
60
70
200

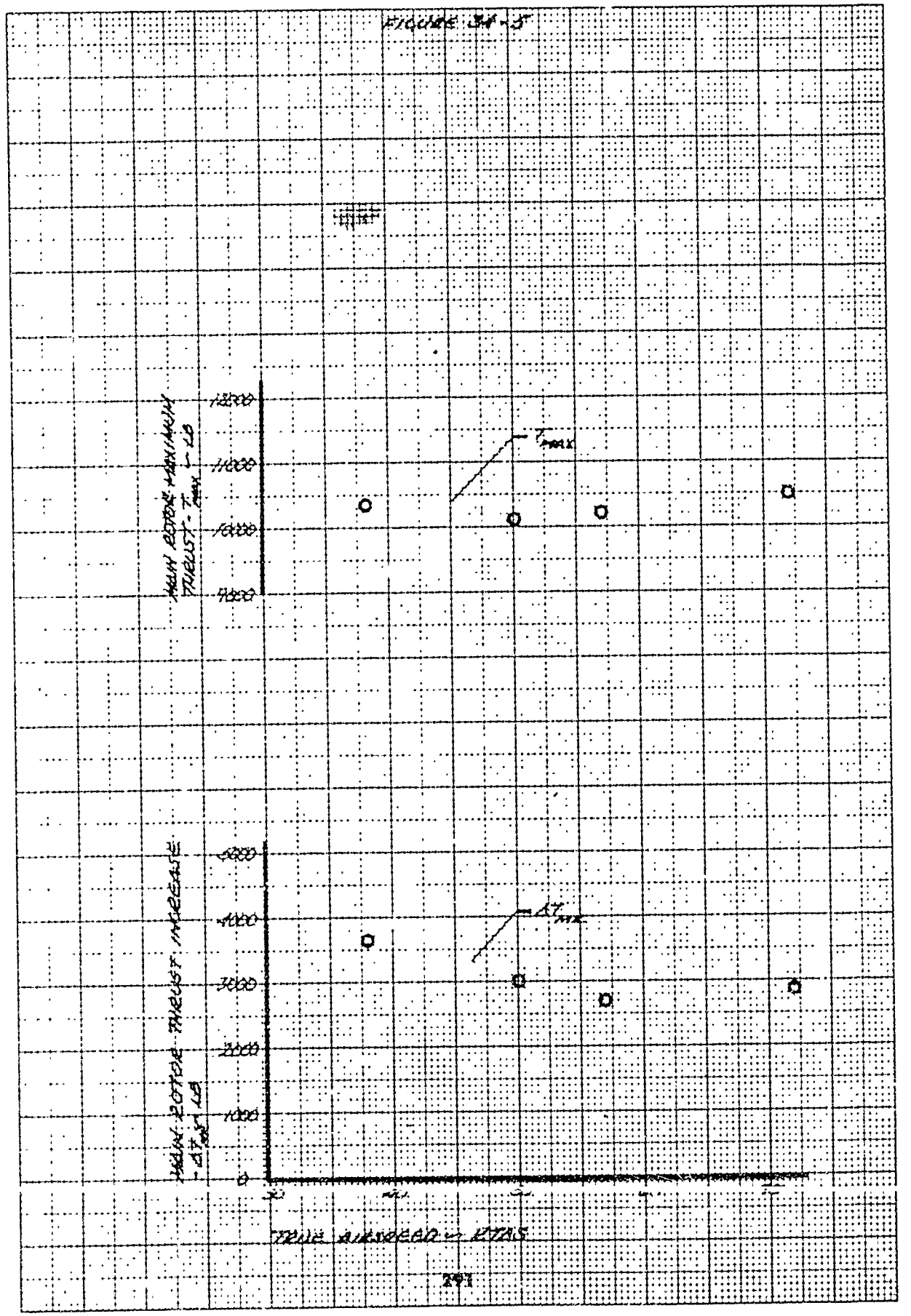
FIGURE 34-5
MAIN ROTOR MAXIMUM THRUST - T_{max} - LB
MAIN ROTOR THRUST INCREASE - ΔT_{max} LB
T_{max}
ΔT_{max}
TRUE AIRSPEED - KNOTS

FIGURE 3A-6

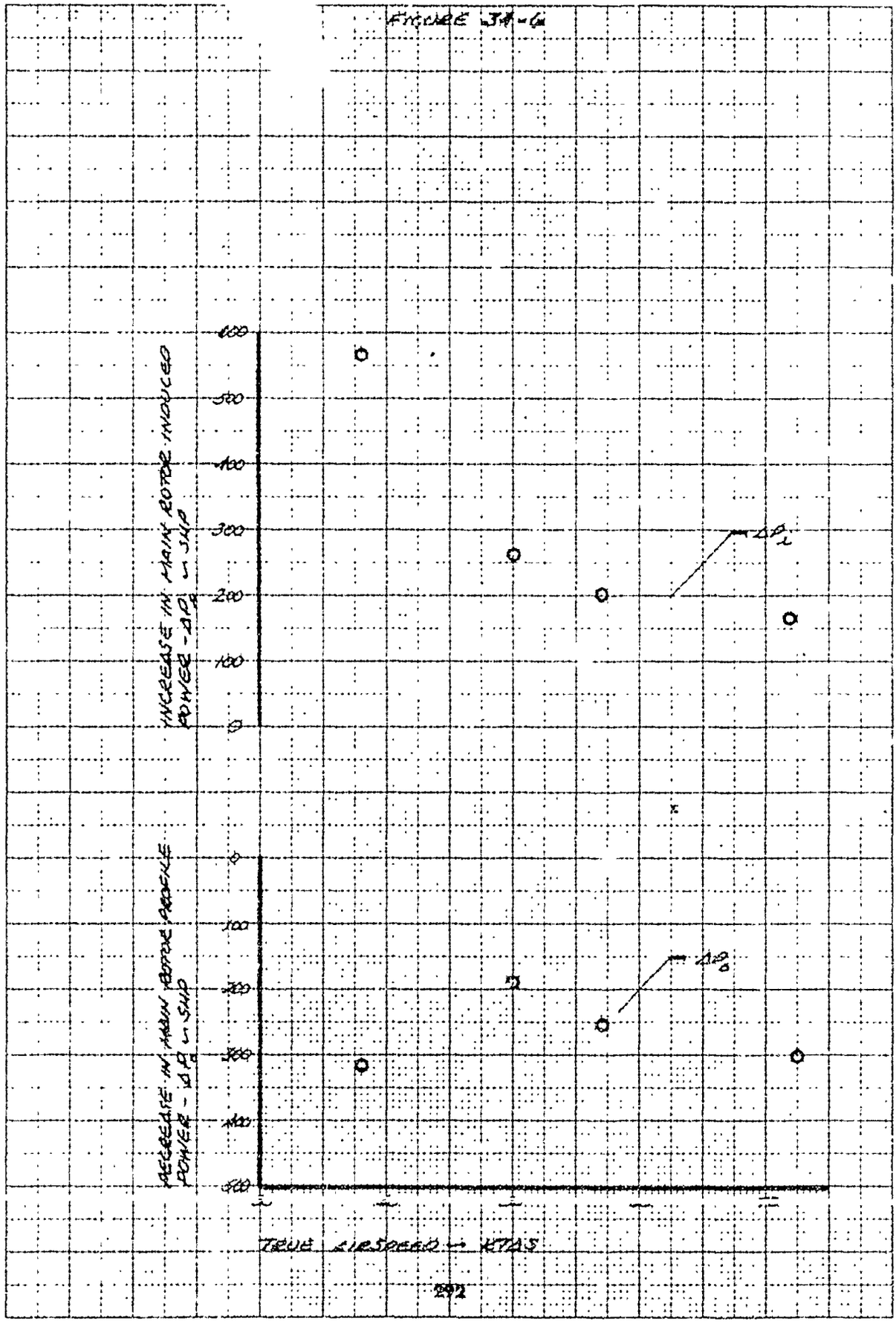
INCREASE IN MAIN ROTOR INDUCED POWER - ΔP_i — SHP
600
500
400
300
200
100
0
ΔP_i
DECREASE IN MAIN ROTOR PROFILE POWER - ΔP_o — SHP
0
100
200
300
400
500
ΔP_o
TRUE AIRSPEED — KTAS

FIGURE 34-7

DECREASE IN RATE OF DESCENT dV_z — FT/SEC
HEADSPEED CHANGE ΔV_x — KTS/SEC
GAIN
10
0
10
20
30
40
VERTICAL DISTANCE TRAVELED - D_z — FT
500
400
300
200
100
HORIZONTAL DISTANCE TRAVELED - D_x — FT
150
100
50
ΔV_z
ΔV_x
D_x
D_z
30
40
50
60
70
TRUE AIRSPEED — KTAS

FIGURE 33-1
COLLECTIVE APPLICATION IN LOW SPEED STEADY STATE AUTOROTATION
DENSITY ALT = 4500 FT
AMB. TEMP = 24 °C
TOTAL LONGITUDINAL CONTROL TRAVEL = 12.7 IN.
TOTAL LATERAL CONTROL TRAVEL = 12.4 IN.
TOTAL DIRECTIONAL CONTROL TRAVEL = 7.01 IN.
TOTAL COLLECTIVE CONTROL TRAVEL = 10.4 IN.
DIRECTIONAL CONTROL POSITION
δ_r — IN. FROM FULL LEFT
COLLECTIVE CONTROL POSITION
δ_c — IN. FROM FULL DOWN
δ_r
δ_c
START OF COLLECTIVE APPLICATION
LONGITUDINAL CONTROL POSITION
δ_e — IN. FROM FULL AFT
LATERAL CONTROL POSITION
δ_a — IN. FROM FULL LEFT
δ_e
δ_a
TIME — SEC

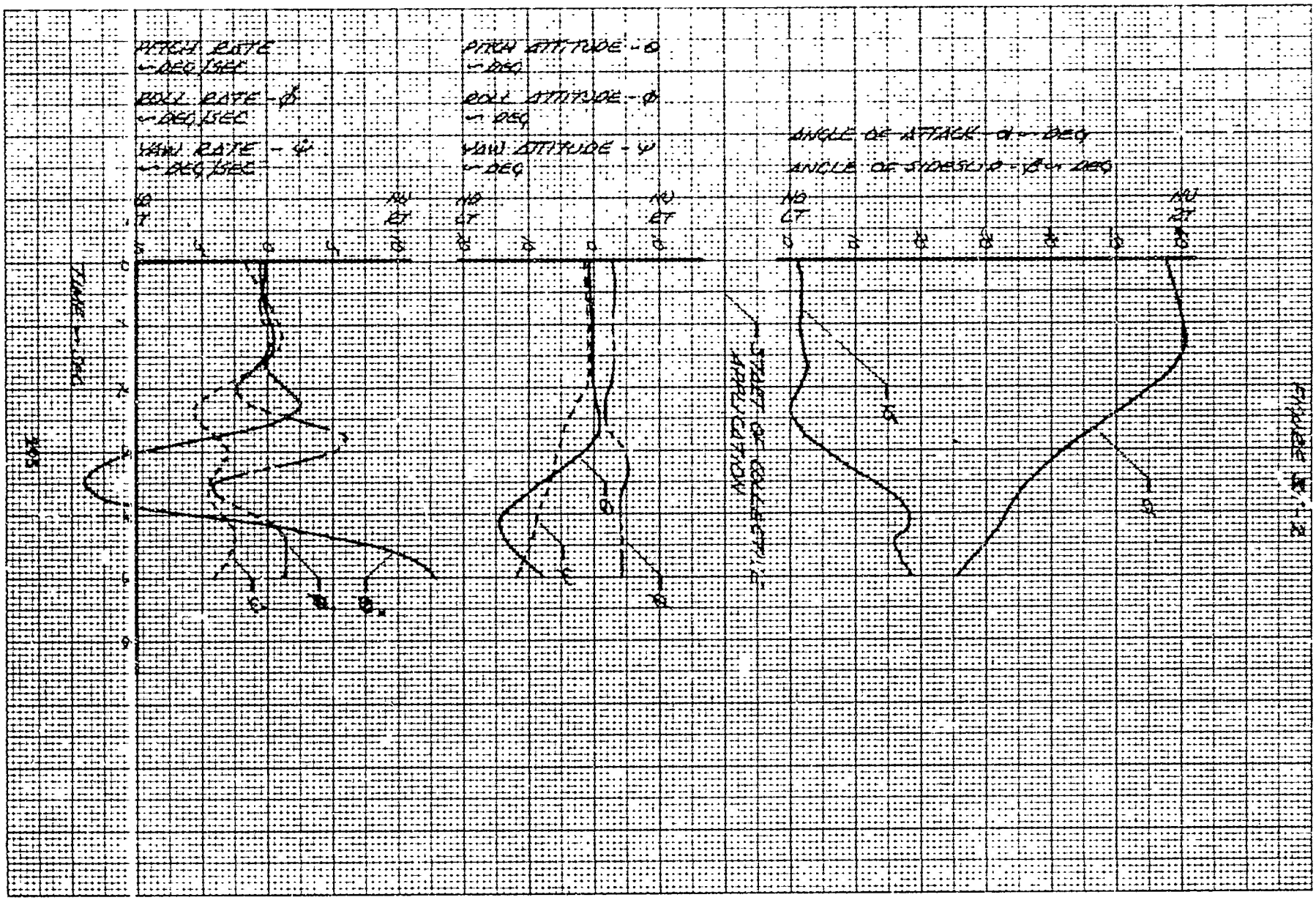
PITCH RATE
- DEG/SEC
ROLL RATE - $\dot{\phi}$
- DEG/SEC
YAW RATE - $\dot{\psi}$
- DEG/SEC
PITCH ATTITUDE - θ
- DEG
ROLL ATTITUDE - ϕ
- DEG
YAW ATTITUDE - ψ
- DEG
ANGLE OF ATTACK - α - DEG
ANGLE OF SIDESLIP - β - DEG
TIME - SEC
START OF COMPUTATION
FIGURE 4.1-12

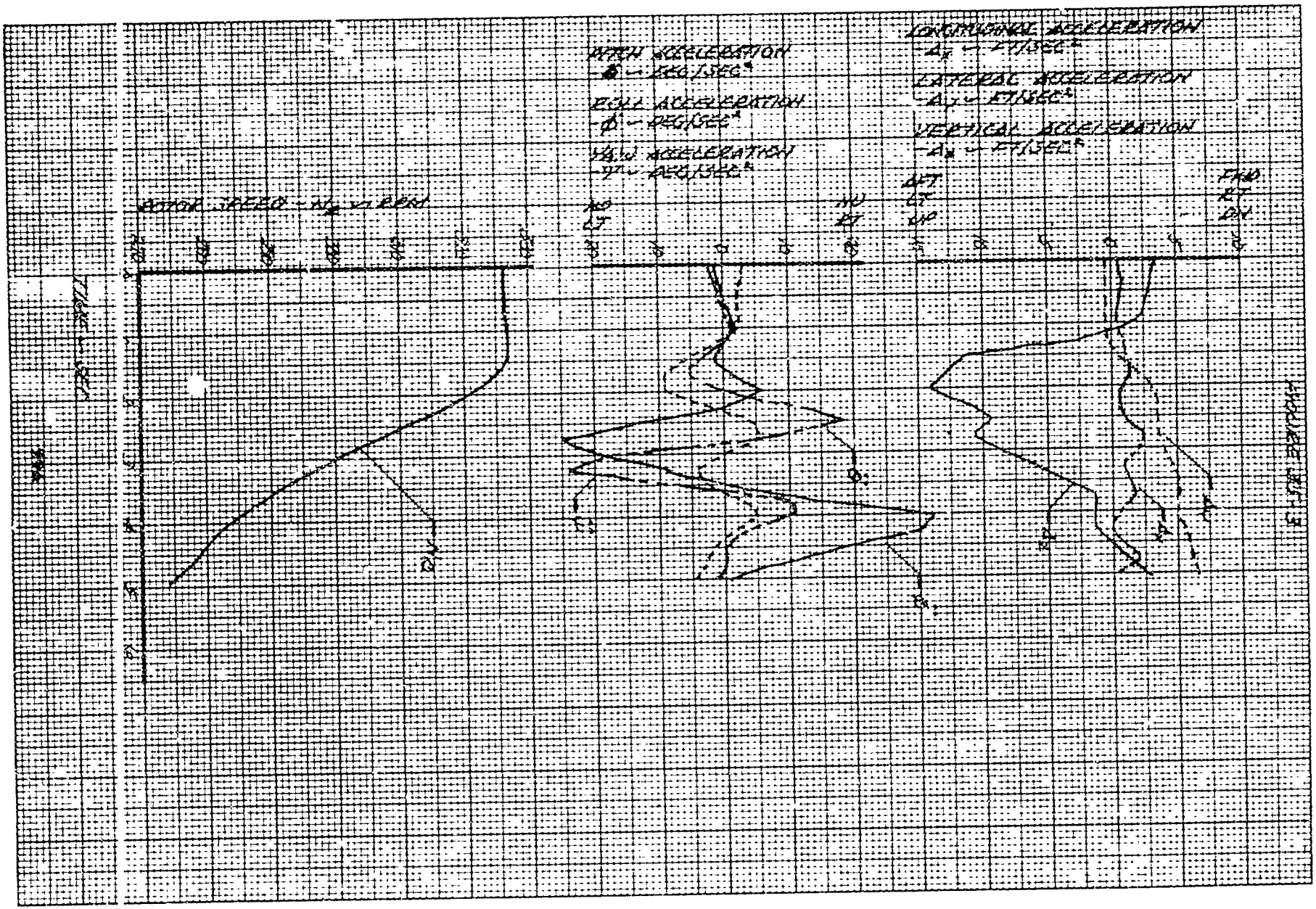
YAW ACCELERATION
ROLL ACCELERATION
LONGITUDINAL ACCELERATION
LATERAL ACCELERATION
VERTICAL ACCELERATION

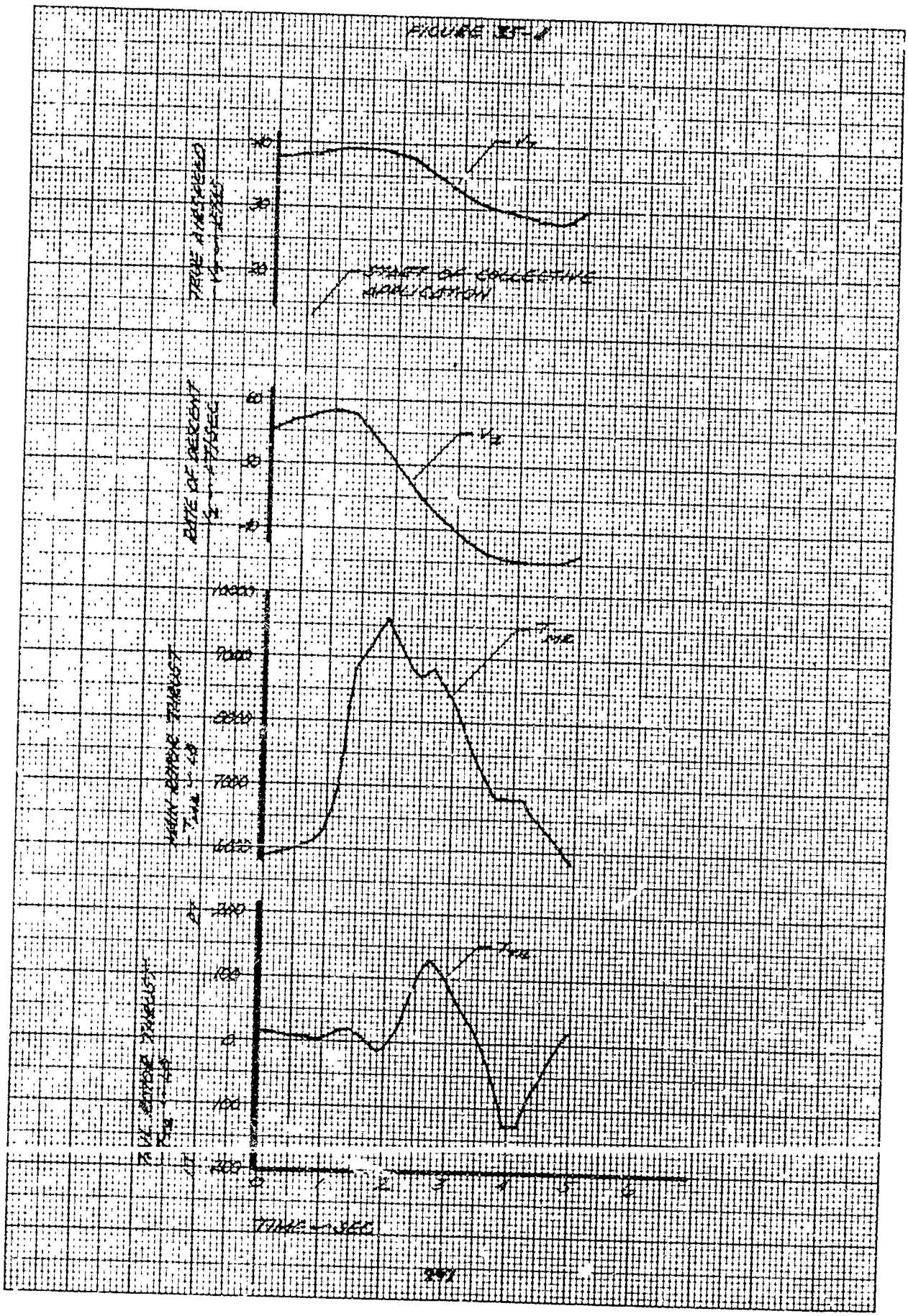
FIGURE 37-4
TRUE AIRSPEED
V
KNOTS
RATE OF DESCENT
h
FT/SEC
HEIGHT ABOVE THRUST
LINE
FT
TIME
SEC

FIGURE 35-5

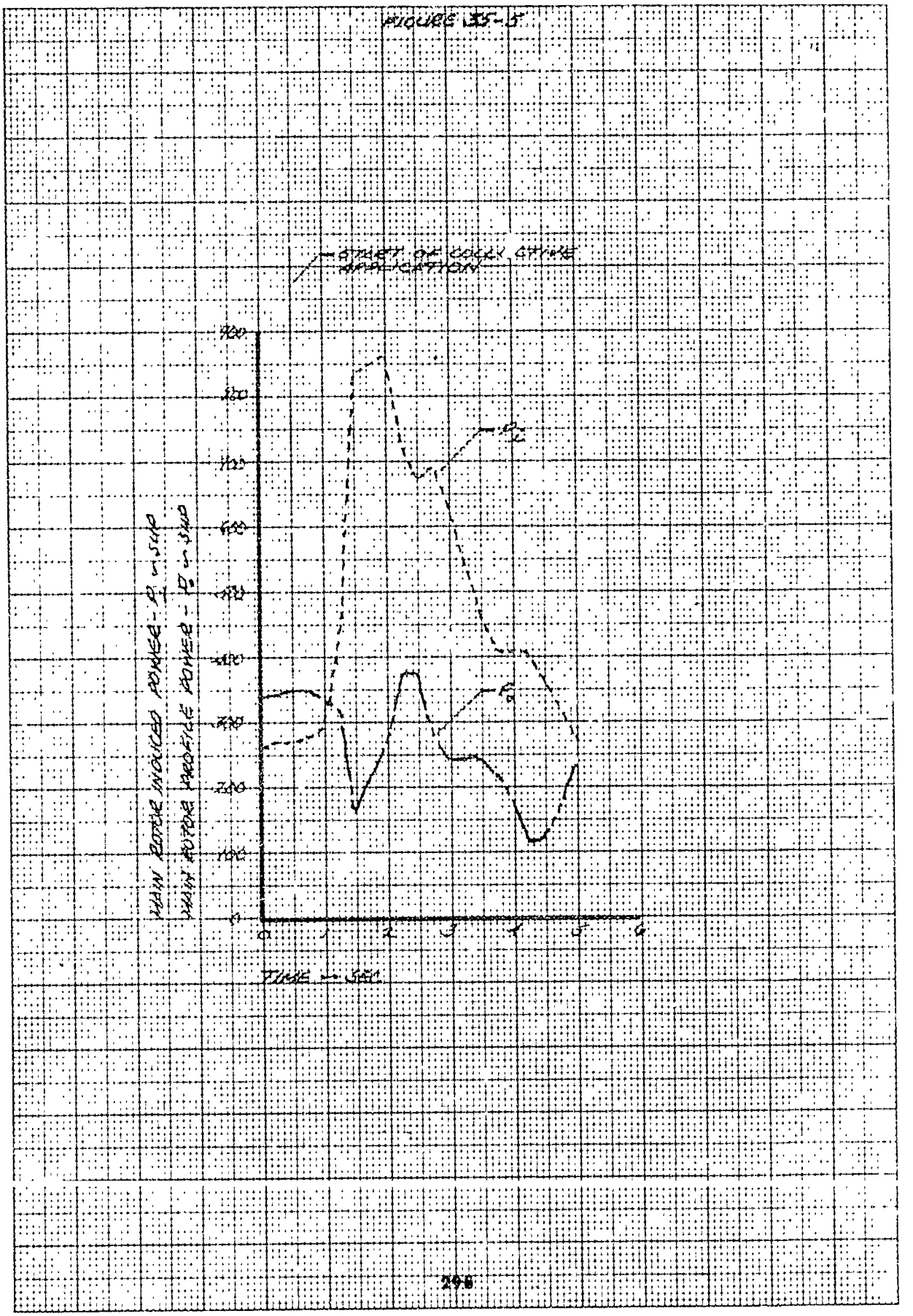
START OF COLD STROKE APPLICATION
MAIN BOOSTER INDUCED POWER - 50 WATTS
MAIN ROTOR INDUCED POWER - 20 WATTS
TIME - SEC.

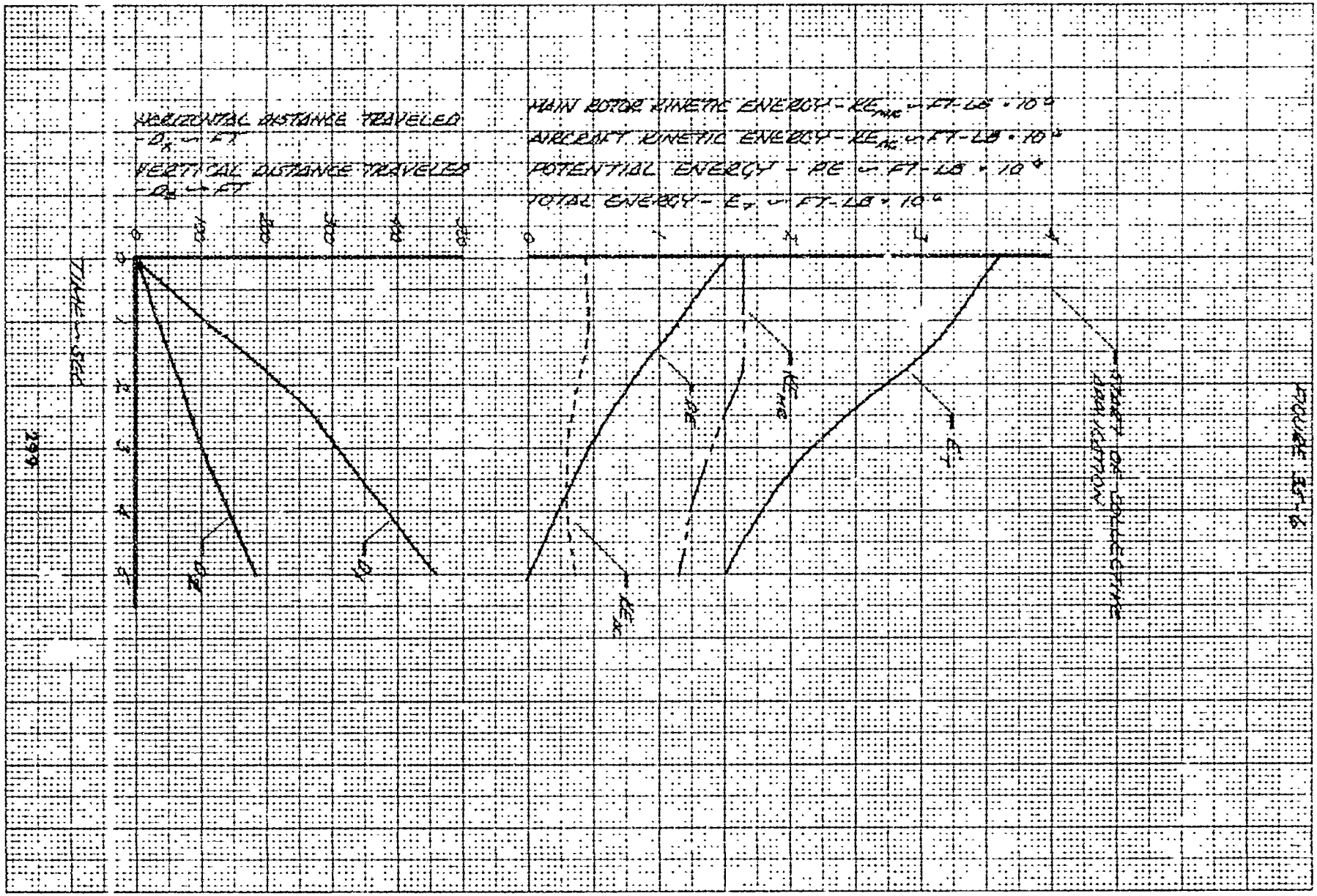
HORIZONTAL DISTANCE TRAVELED - D_x - FT
VERTICAL DISTANCE TRAVELED - D_z - FT
MAIN ROTOR KINETIC ENERGY - KE_{MR} - FT-LB · 10^4
AIRCRAFT KINETIC ENERGY - KE_{AC} - FT-LB · 10^4
POTENTIAL ENERGY - PE - FT-LB · 10^4
TOTAL ENERGY - E_T - FT-LB · 10^4
TIME - SEC
KE_{MR}
PE
KE_{AC}
E_T
TIME OF IGNITION
FIGURE EF-6

FIGURE 55-1

COLLECTIVE APPLICATION IN HELICOPTER
SPEED STABILITY STATE ACCELERATION

FIGURE 36-2

ANGLE OF ATTACK
α ~ DEG
ANGLE OF SIDESLIP
-β ~ DEG
START OF COLLECTIVE APPLICATION
PITCH ATTITUDE
-θ ~ DEG
ROLL ATTITUDE
-Φ ~ DEG.
YAW ATTITUDE
-ψ ~ DEG.
PITCH RATE -q
~DEG/SEC
ROLL RATE -p
~ DEG/SEC
YAW RATE -r
~DEG/SEC
TIME ~ SEC

FIGURE 36.5
LONGITUDINAL ACCELERATION
A_x — FT/SEC²
LATERAL ACCELERATION
A_y — FT/SEC²
VERTICAL ACCELERATION
$-A_z$ — FT/SEC²
ROLL ACCELERATION
$\dot{p}$ — RAD/SEC²
PITCH ACCELERATION
$\dot{q}$ — RAD/SEC²
YAW ACCELERATION
$\dot{r}$ — RAD/SEC²
FEET
METERS
START OF COLLECTIVE APPLICATION
TIME — SEC

FIGURE 36-2

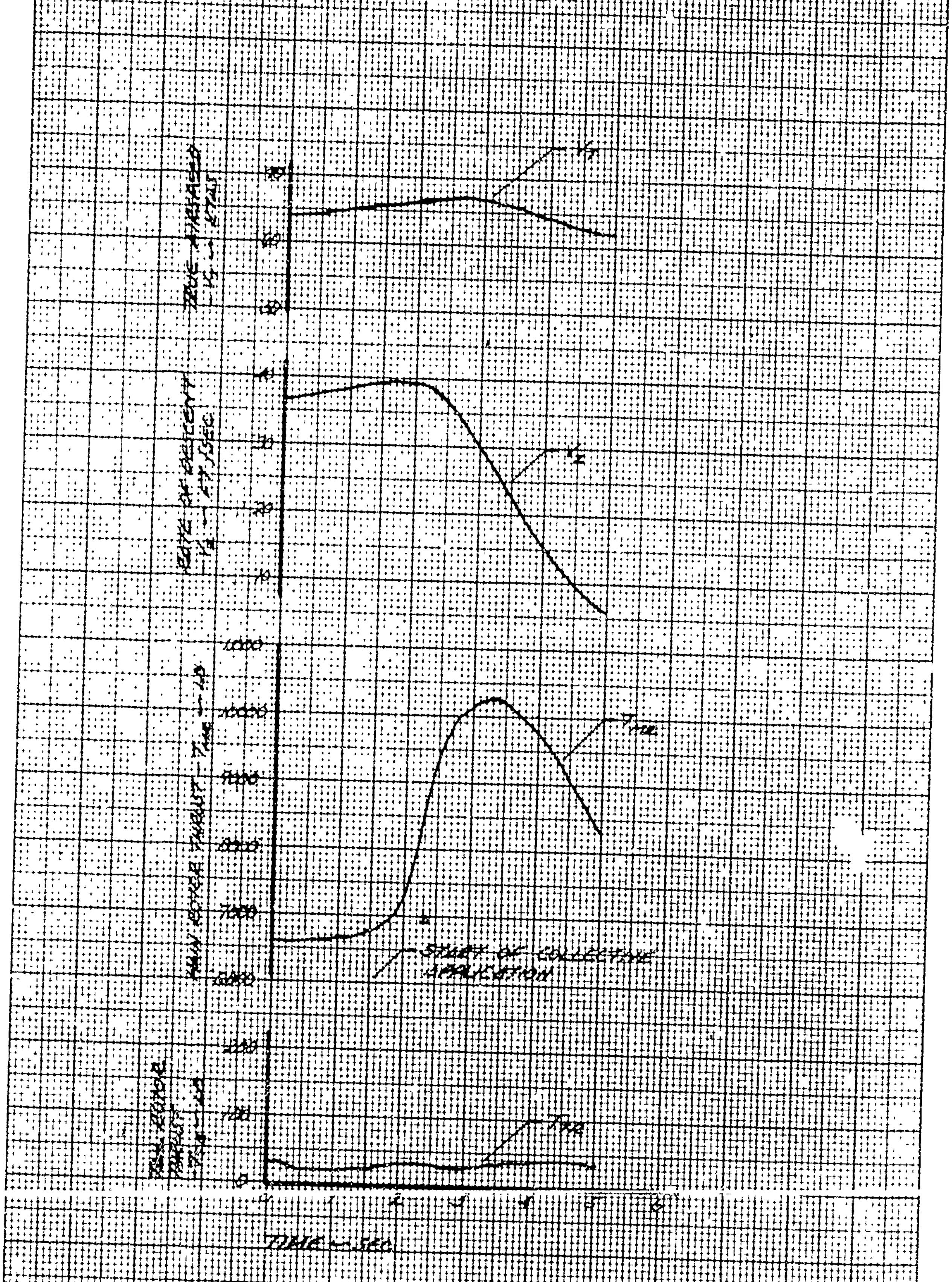
TRUE AIRSPEED
— VT — KTAS
RATE OF DESCENT
VZ — FT/SEC
MAIN ROTOR THRUST — TMR — LB
TAIL ROTOR
THRUST
TTR — LB
START OF COLLECTIVE
APPLICATION
TIME — SEC

FIGURE 3.2-5
TIME — SEC
START OF COLLECTIVE APPLICATION

FIGURE 37-J

LANDING FROM A HOVER

CH-1C USA S/N 63-8604

GROSS WT = 6800 LB DENSITY ALT = 3740 FT

SKID HEIGHT = 0" FT AMB. TEMP = 19 °C

TOTAL LONGITUDINAL CONTROL TRAVEL = 12.7 IN.

TOTAL LATERAL CONTROL TRAVEL = 12.4 IN.

TOTAL DIRECTIONAL CONTROL TRAVEL = 7.0 IN.

TOTAL COLLECTIVE CONTROL TRAVEL = 10.1 IN.

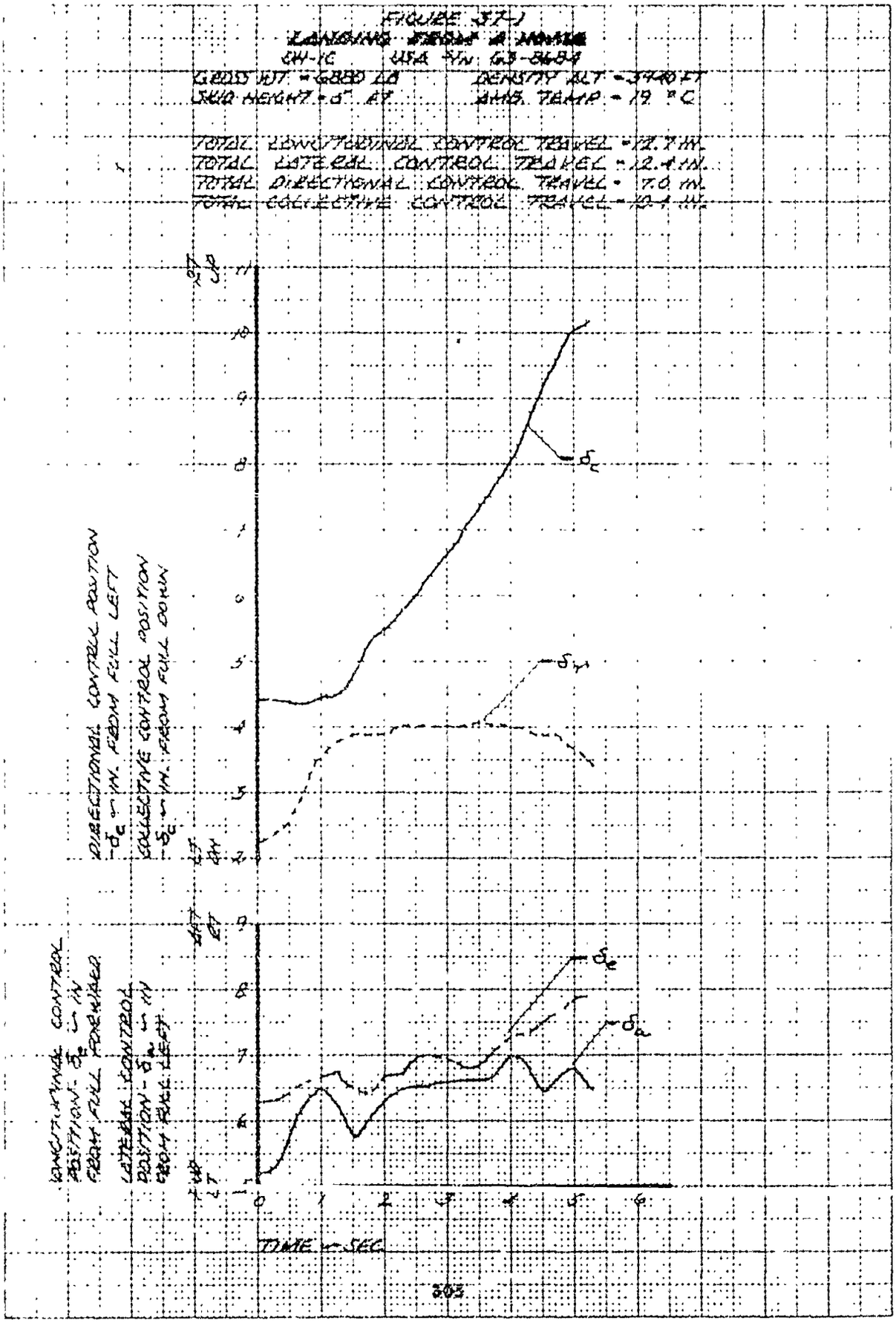

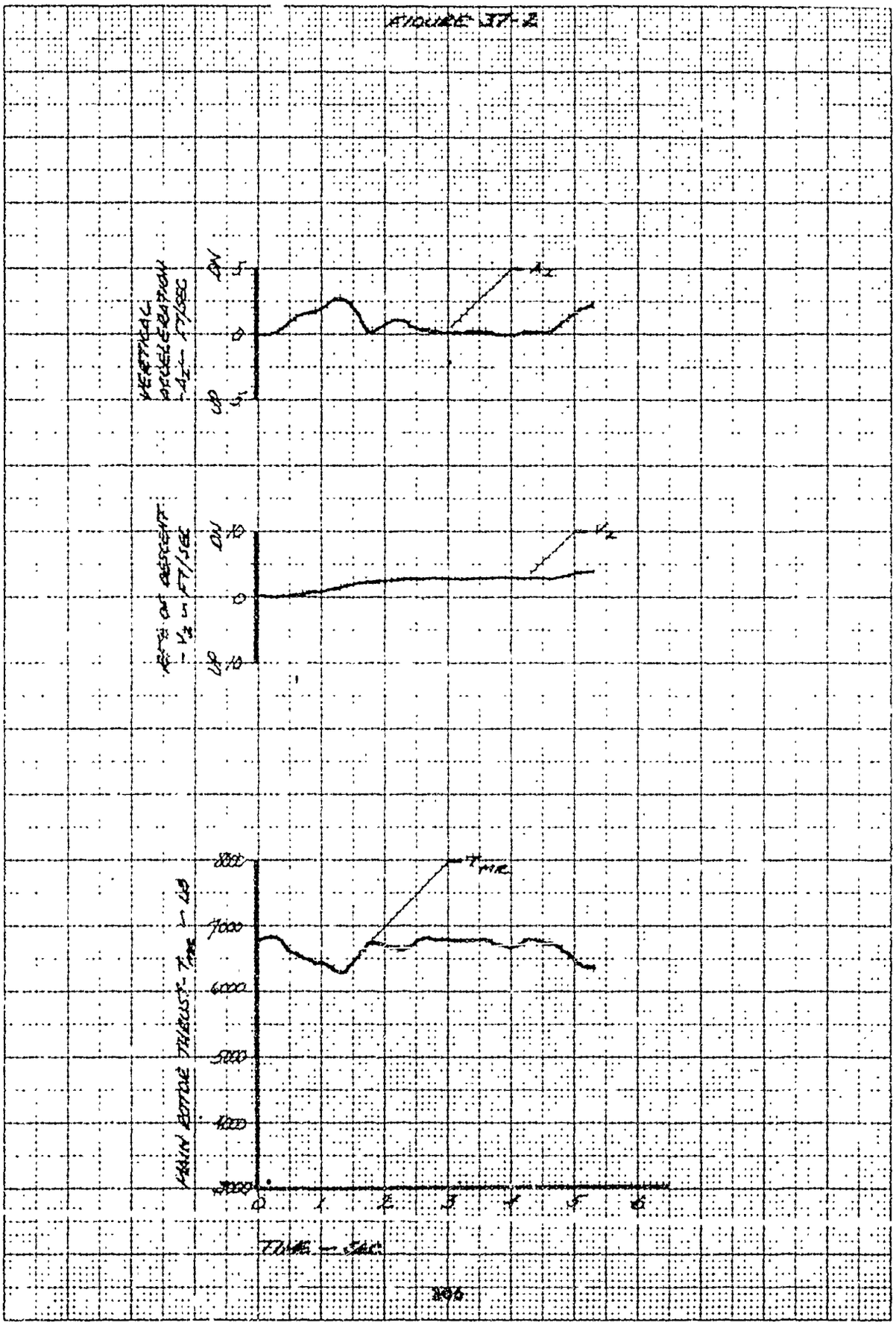
FIGURE 37-2
VERTICAL ACCELERATION
$-A_Z$ — FT/SEC²
UP
DOWN
RATE OF DESCENT
$-V_Z$ — FT/SEC
UP
DOWN
MAIN ENGINE THRUST - Thrust — LBS
8000
7000
6000
5000
4000
3000
TIME — SEC
0
1
2
3
4
5
6

FIGURE 37-3

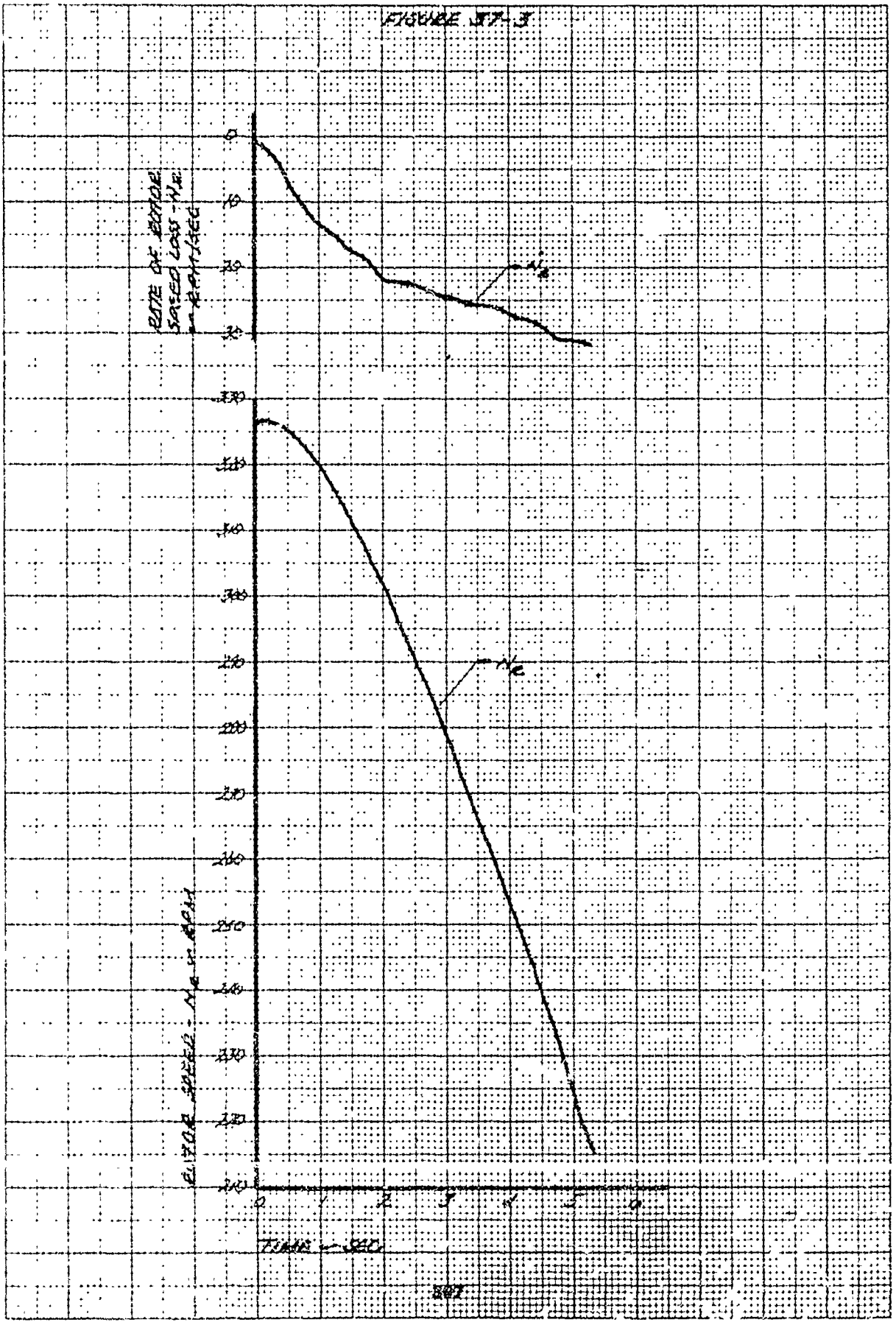
RATE OF ENGINE SPEED LOSS - N_E IN RPM/SEC
ENGINE SPEED - N_E IN RPM
TIME - SEC
0
10
20
30
0
1
2
3
4
5
6
N_E
N_E

FIGURE 38-1

LANDING FROM A HOVER

UH-1C USA 7th CAV-ABN

GROSS WT = 6000 LB DENSITY ALT = 3960 FT

SKID HEIGHT = 14 FT OAT TEMP = 19° C

TOTAL LONGITUDINAL CONTROL TRAVEL = 14.7 IN.

TOTAL LATERAL CONTROL TRAVEL = 12.4 IN.

TOTAL DIRECTIONAL CONTROL TRAVEL = 7.0 IN.

TOTAL COLLECTIVE CONTROL TRAVEL = 10.1 IN.

DIRECTIONAL CONTROL POSITION
$-\delta_r$ — IN. FROM FULL LEFT

COLLECTIVE CONTROL POSITION
$-\delta_c$ — IN. FROM FULL DOWN

LONGITUDINAL CONTROL POSITION
$-\delta_e$ — IN. FROM FULL FORWARD

LATERAL CONTROL POSITION
$-\delta_a$ — IN. FROM FULL LEFT

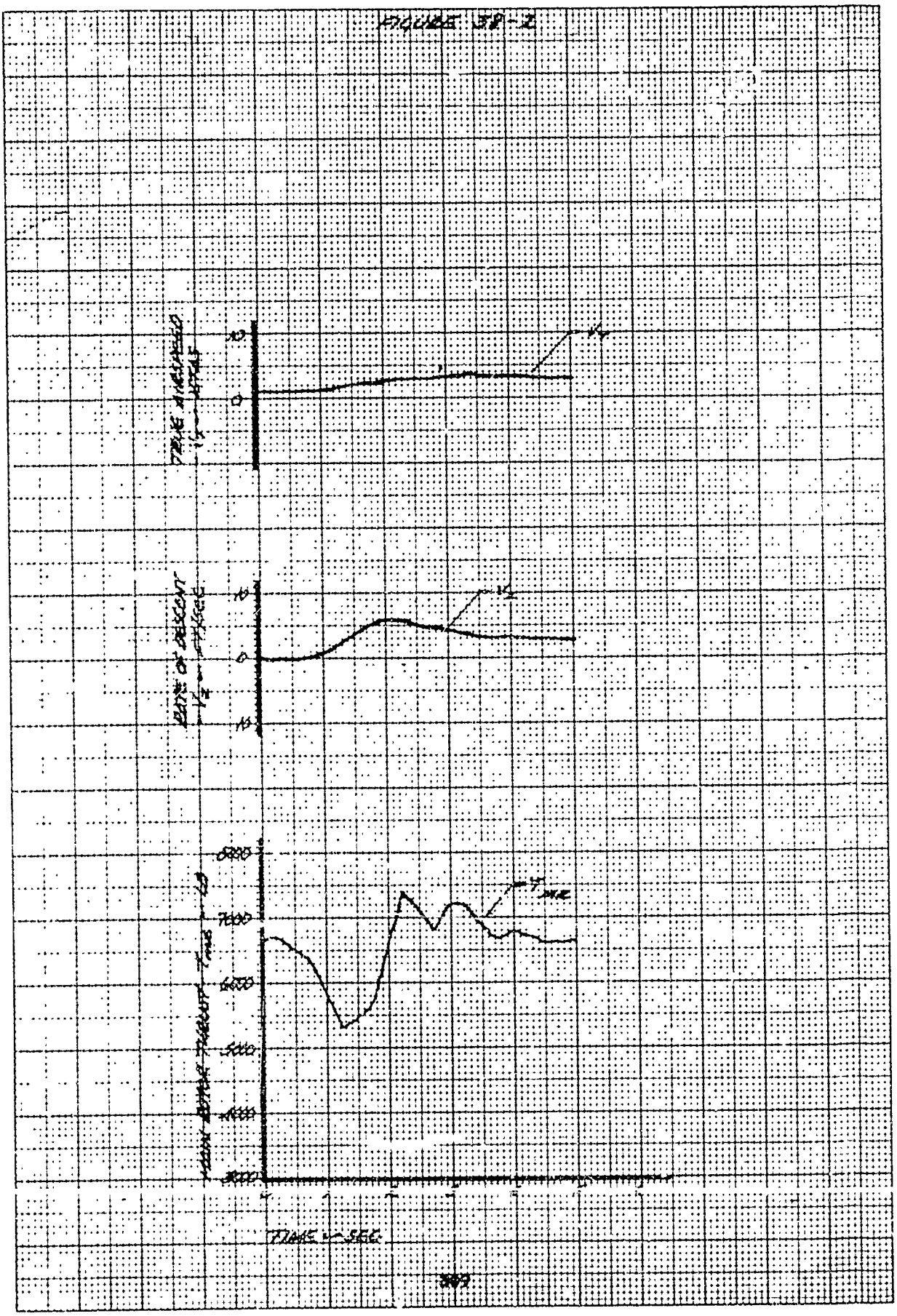
FIGURE 38-2
TIME ACCELERATED
RATE OF DESCENT
TIME - SEC

FIGURE 26-3
0
10
20
30
N_1
N_2
TIME - SEC
0
1
2
3
4
5
6

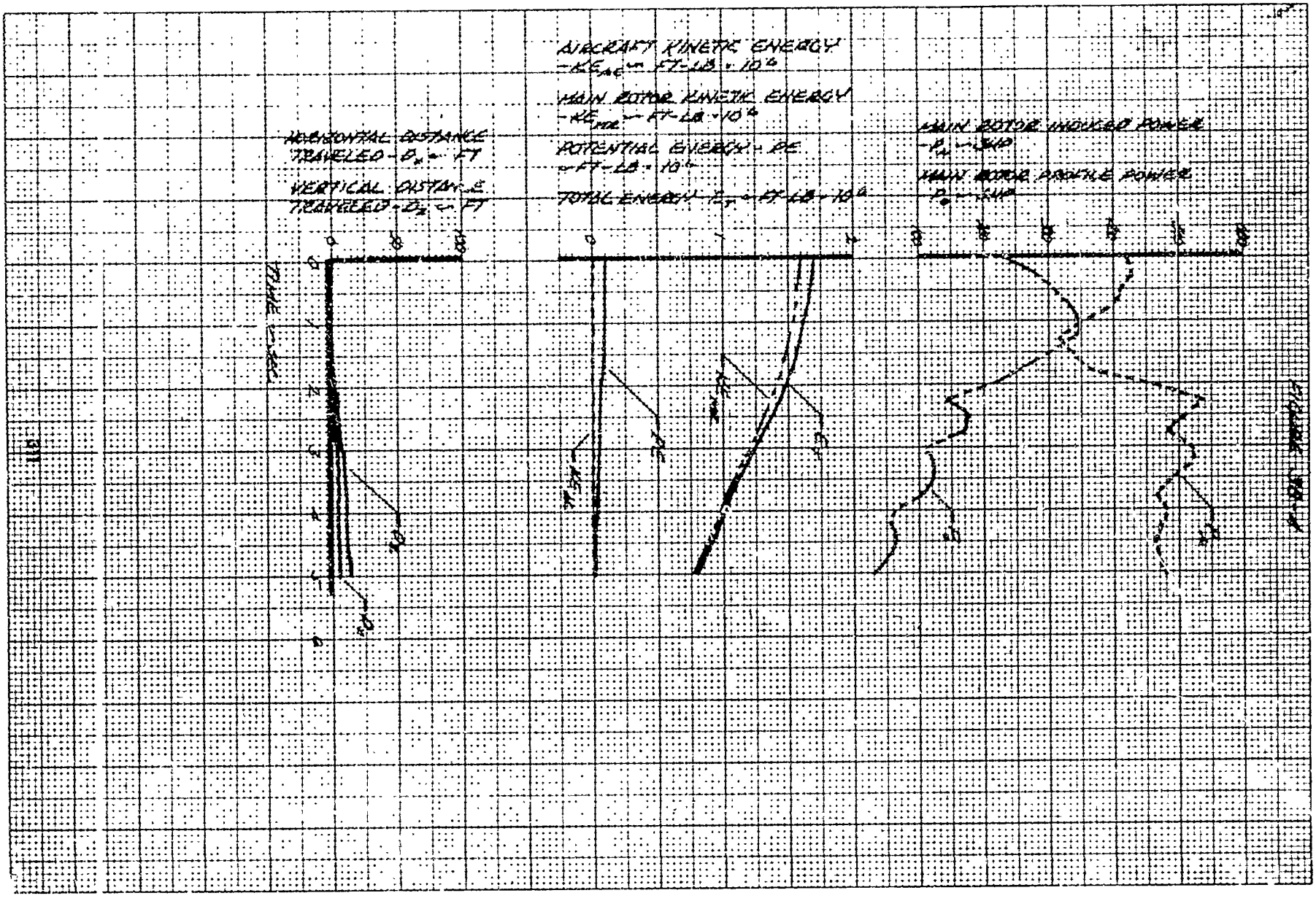
HORIZONTAL DISTANCE TRAVELED - D_x - FT
VERTICAL DISTANCE TRAVELED - D_z - FT
TIME - SEC
AIRCRAFT KINETIC ENERGY - KE_{AC} - FT-LB - 10^6
MAIN ROTOR KINETIC ENERGY - KE_{MR} - FT-LB - 10^6
POTENTIAL ENERGY - PE - FT-LB - 10^6
TOTAL ENERGY - E_T - FT-LB - 10^6
MAIN ROTOR INDUCED POWER - P_{MI} - HP
MAIN ROTOR PROFILE POWER - P_{MP} - HP

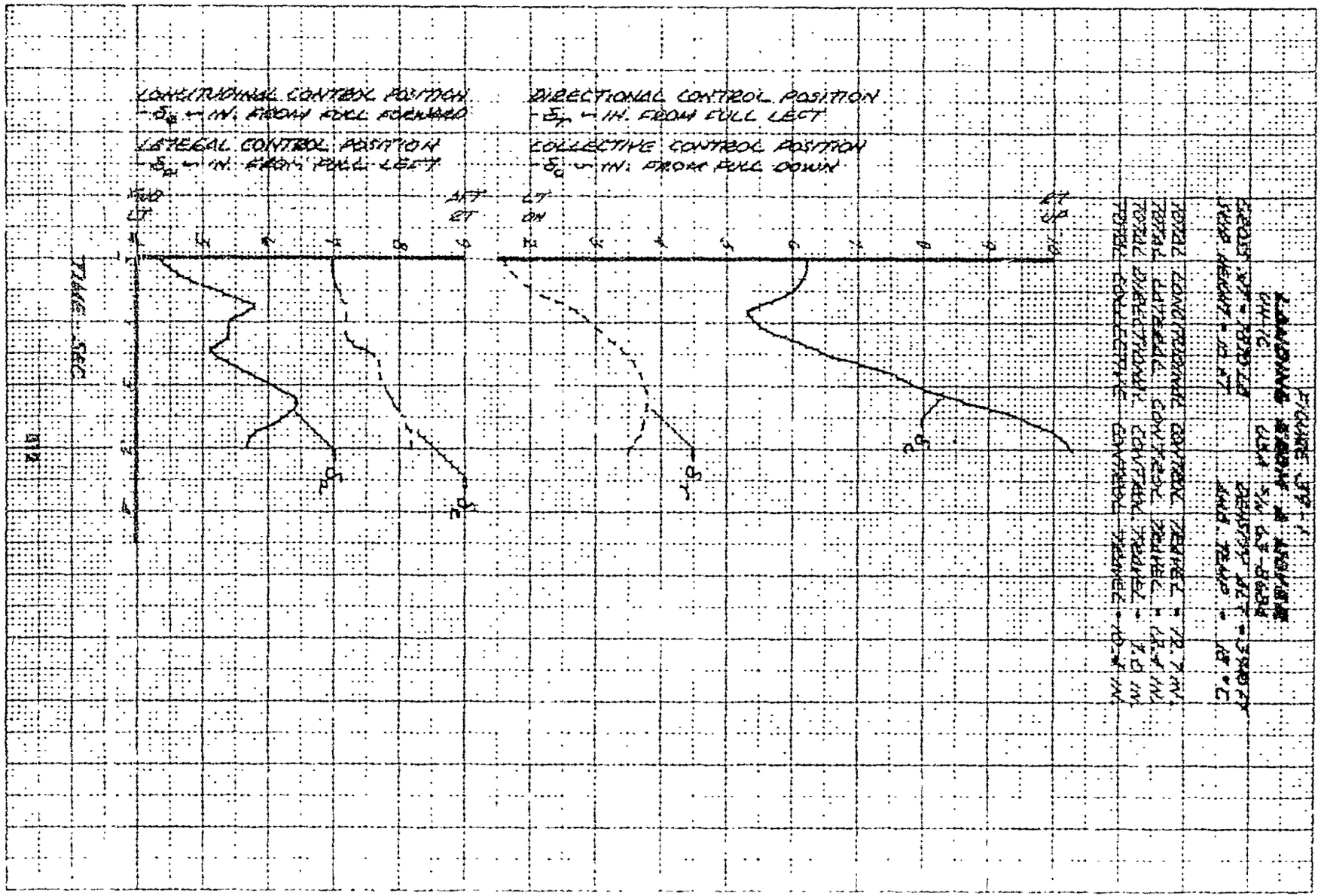
LONGITUDINAL CONTROL POSITION
$-\delta_B$ — IN. FROM FULL AGAINST
LATERAL CONTROL POSITION
$-\delta_{LT}$ — IN. FROM FULL LEFT
DIRECTIONAL CONTROL POSITION
$-\delta_R$ — IN. FROM FULL LEFT
COLLECTIVE CONTROL POSITION
$-\delta_C$ — IN. FROM FULL DOWN
TIME, SEC

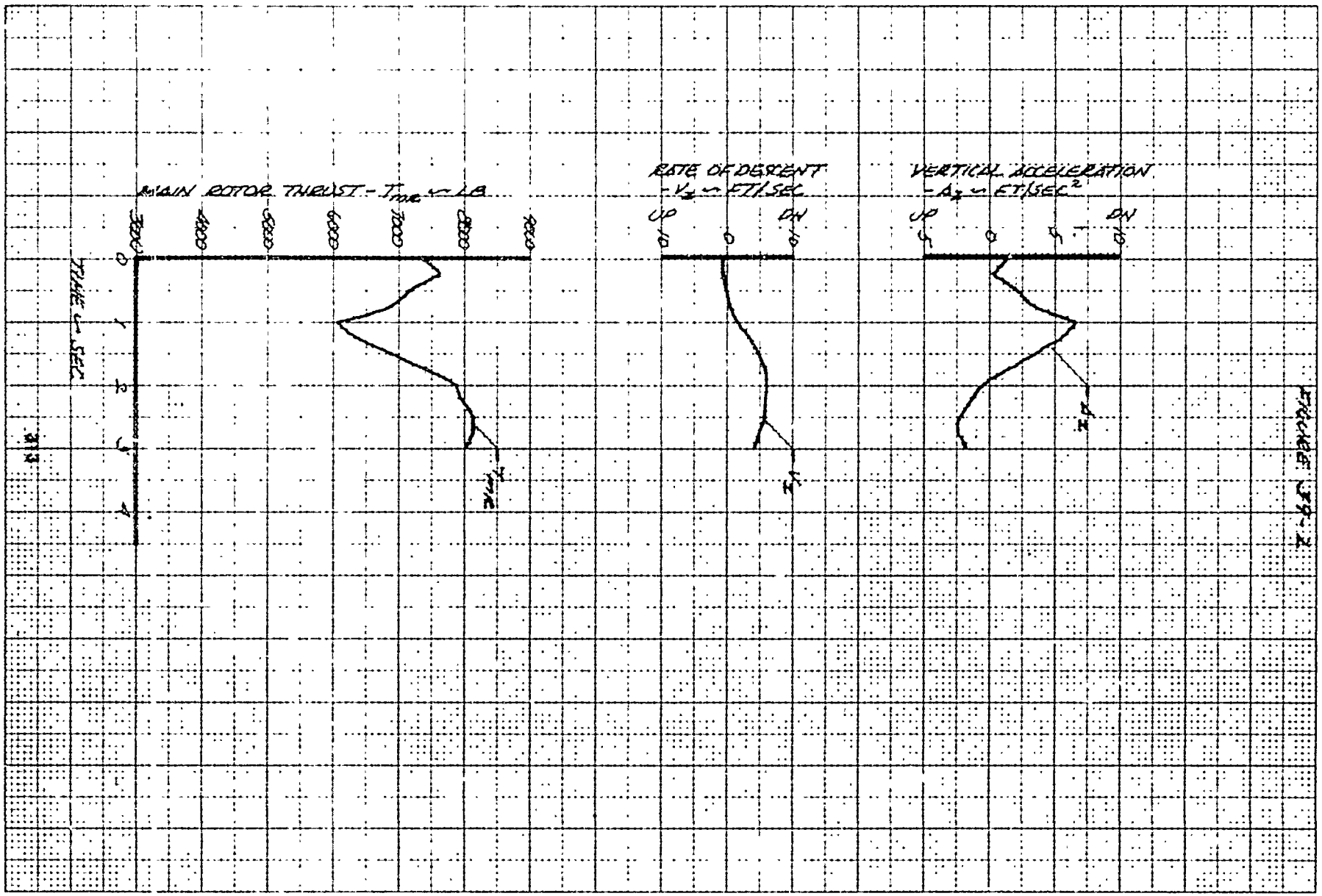
MAIN ROTOR THRUST - T_{MR} ~ LB
3000
4000
5000
6000
7000
8000
9000
TIME ~ SEC
0
1
2
3
4
T_{MR}
RATE OF DESCENT
$-V_z$ ~ FT/SEC
UP
10
0
DN
10
V_z
VERTICAL ACCELERATION
$-A_z$ ~ FT/SEC^2
UP
5
0
5
10
DN
A_z

FIGURE 5.9-2

FIGURE VP-3

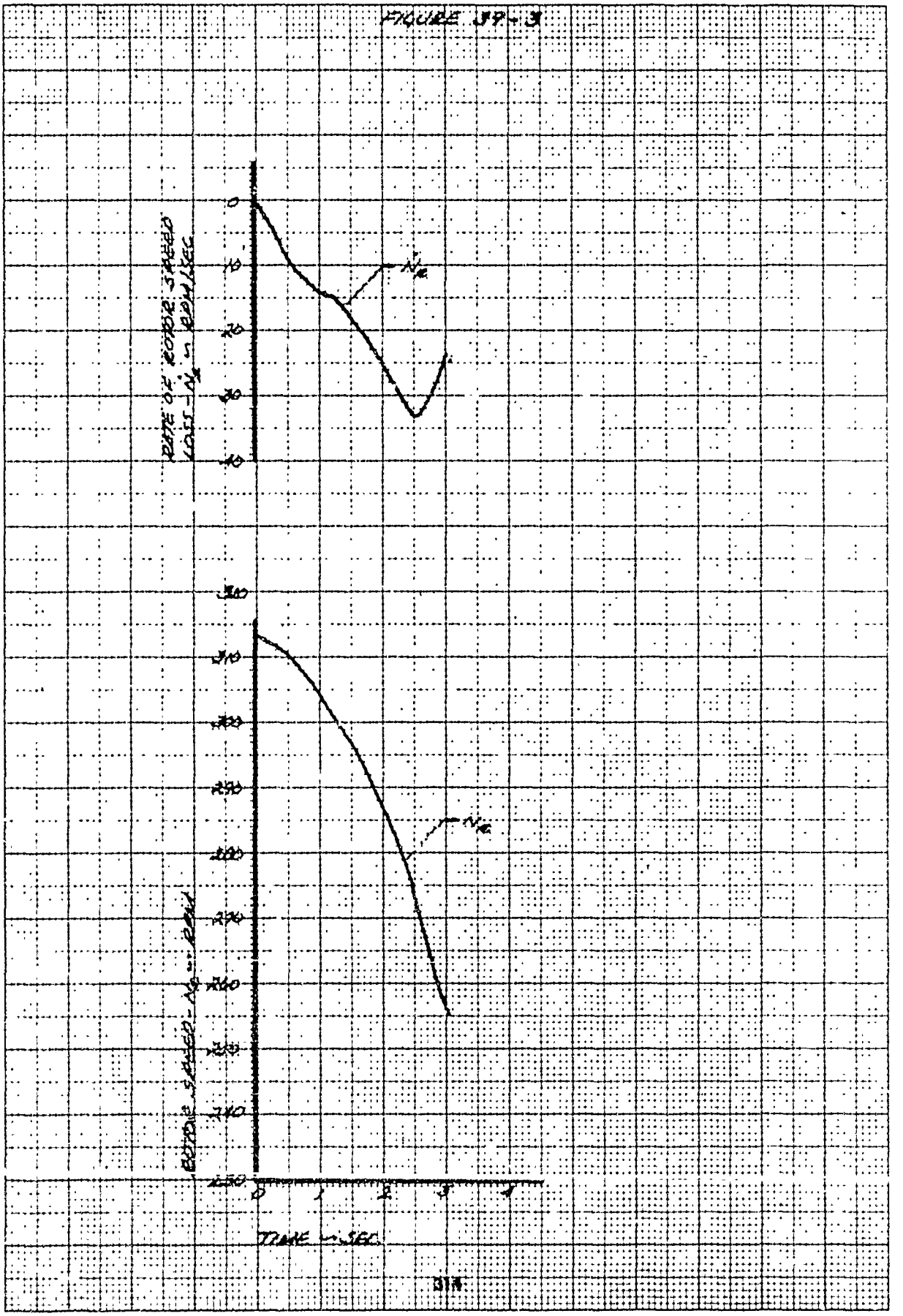
RATE OF BODY SPEED
0
-10
-20
-30
-40
$\dot{N}_{BE}$
BODY SPEED - N_B - KNOTS
300
250
200
150
100
50
0
N_{BE}
0
1
2
3
4
TIME - SEC

LONGITUDINAL CONTROL POSITION
δe — IN. FROM FULL FORWARD
LATERAL CONTROL POSITION
δa — IN. FROM FULL LEFT
DIRECTIONAL CONTROL POSITION
δr — IN. FROM FULL LEFT
COLLECTIVE CONTROL POSITION
δc — IN. FROM FULL DOWN
TIME — SEC

FIGURE 80-2

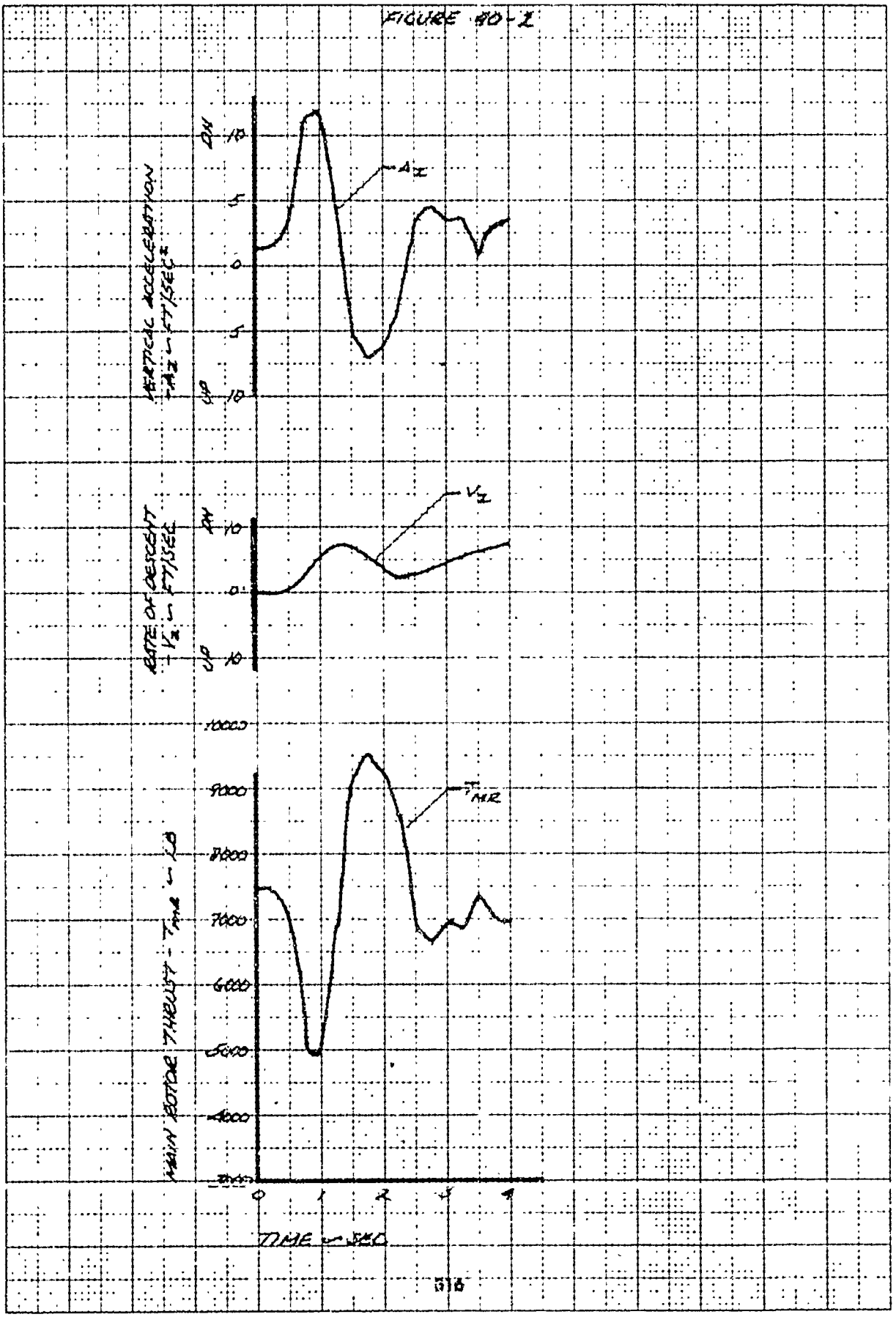
VERTICAL ACCELERATION
$+A_Z$ - FT/SEC²
DN
UP
10
5
0
5
10
A_Z
RATE OF DESCENT
$-V_Z$ - FT/SEC
DN
UP
10
0
10
V_Z
MAIN BOTTLE THRUST - T_{MB} - LB
10000
9000
8000
7000
6000
5000
4000
3000
T_{MB}
0
1
2
3
4
TIME - SEC

FIGURE 40-3

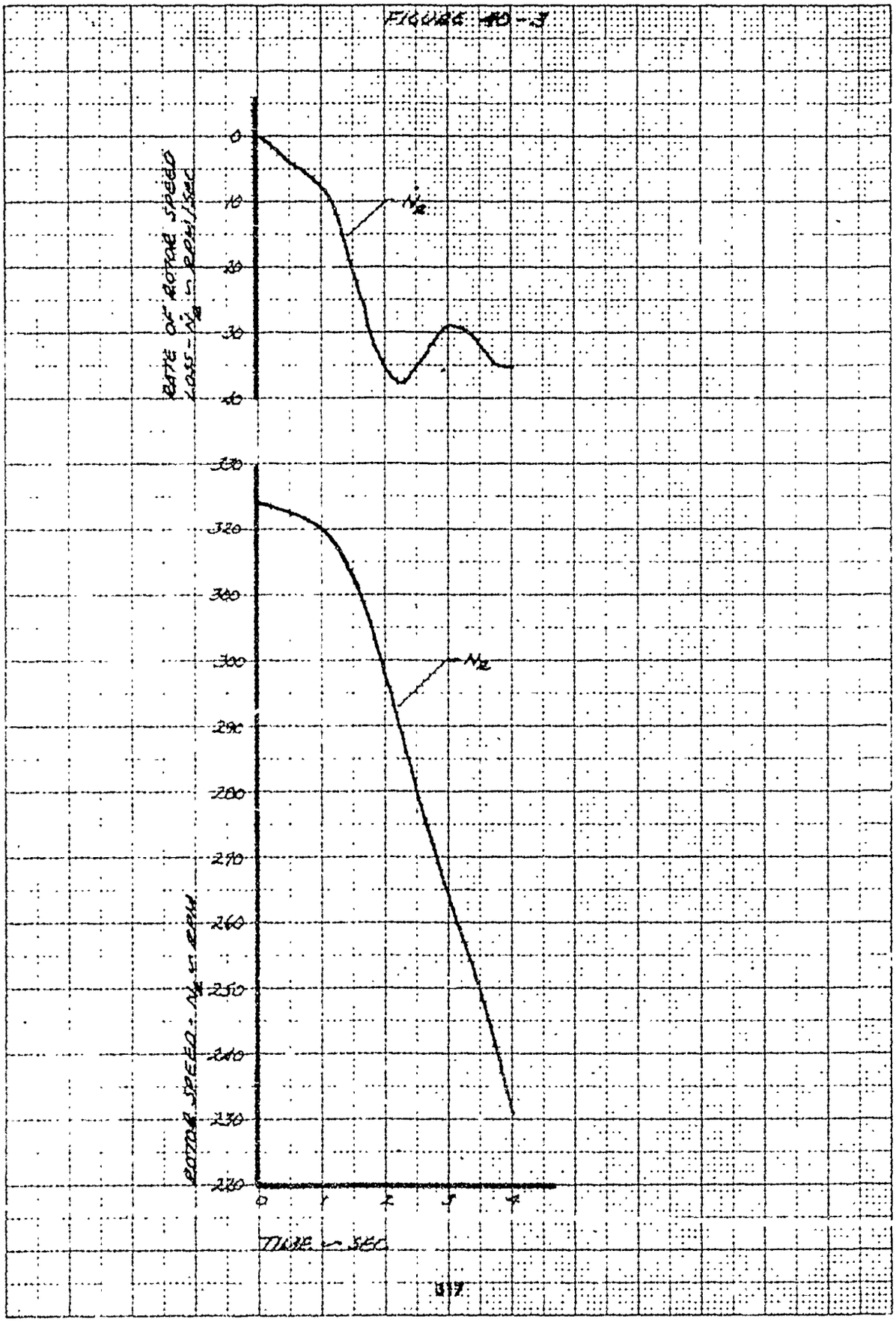
RATE OF ROTOR SPEED LOSS - $\dot{N}_2$ = RPM/SEC
0
10
20
30
40
320
300
280
260
240
220
N_2
N_2
ROTOR SPEED - N_2 = RPM
0
1
2
3
4
TIME - SEC

FIGURE A1-1

LANDING FROM LOW SPEED LEVEL FLIGHT ENTRY

CH-47C GW = 33,000 LB

GROSS WT = 47,000 LB DENSITY ALT = 11000 FT.

PRESS HEIGHT = 4.5 FT AMB. TEMP = 10 °C

ENTRY AIRSPEED = 10 KTAS

TOTAL LONGITUDINAL CONTROL TRAVEL = 12.7 IN.

TOTAL LATERAL CONTROL TRAVEL = 11.5 IN.

TOTAL DIRECTIONAL CONTROL TRAVEL = 7.0 IN.

TOTAL COLLECTIVE CONTROL TRAVEL = 10.4 IN.

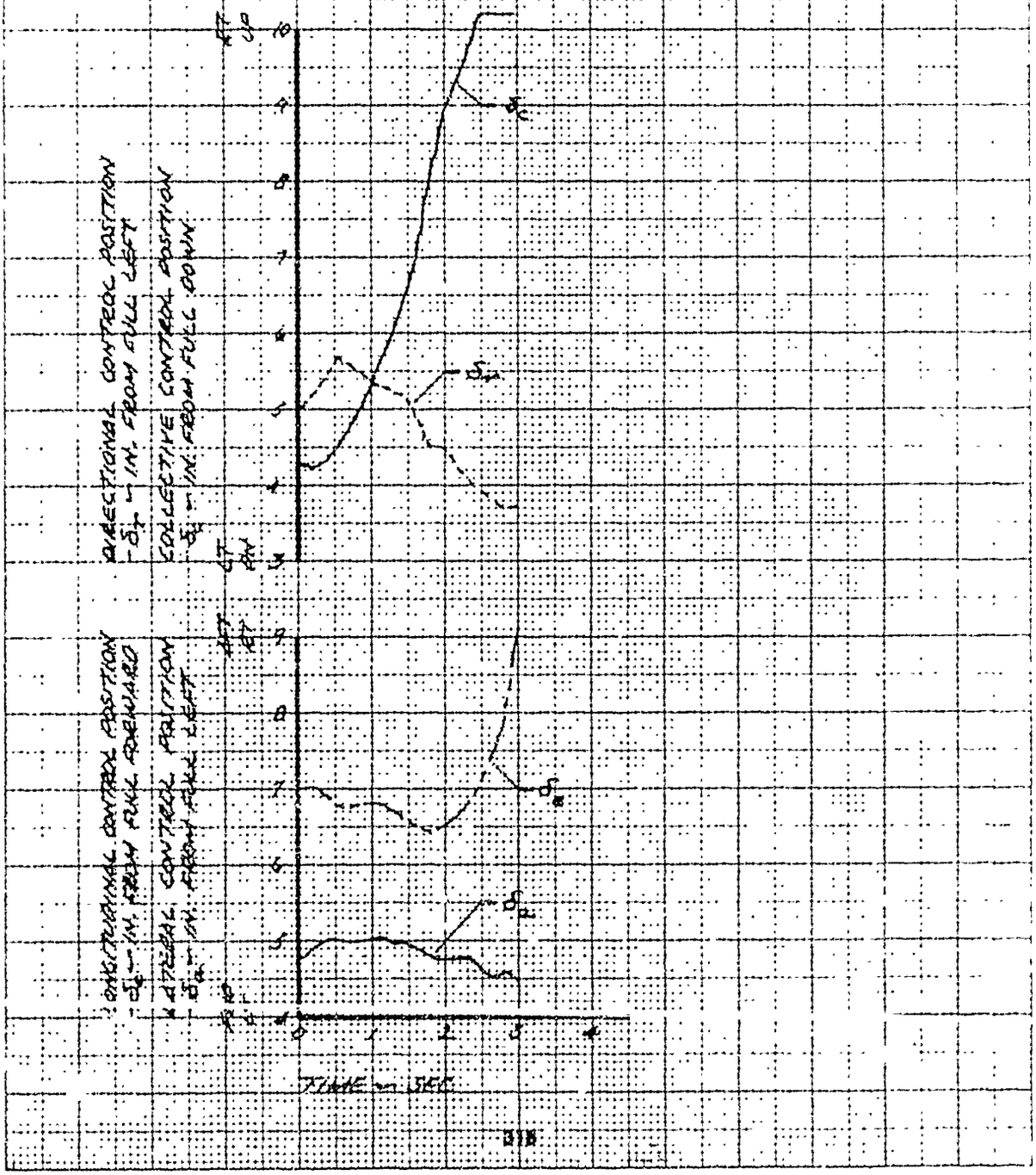

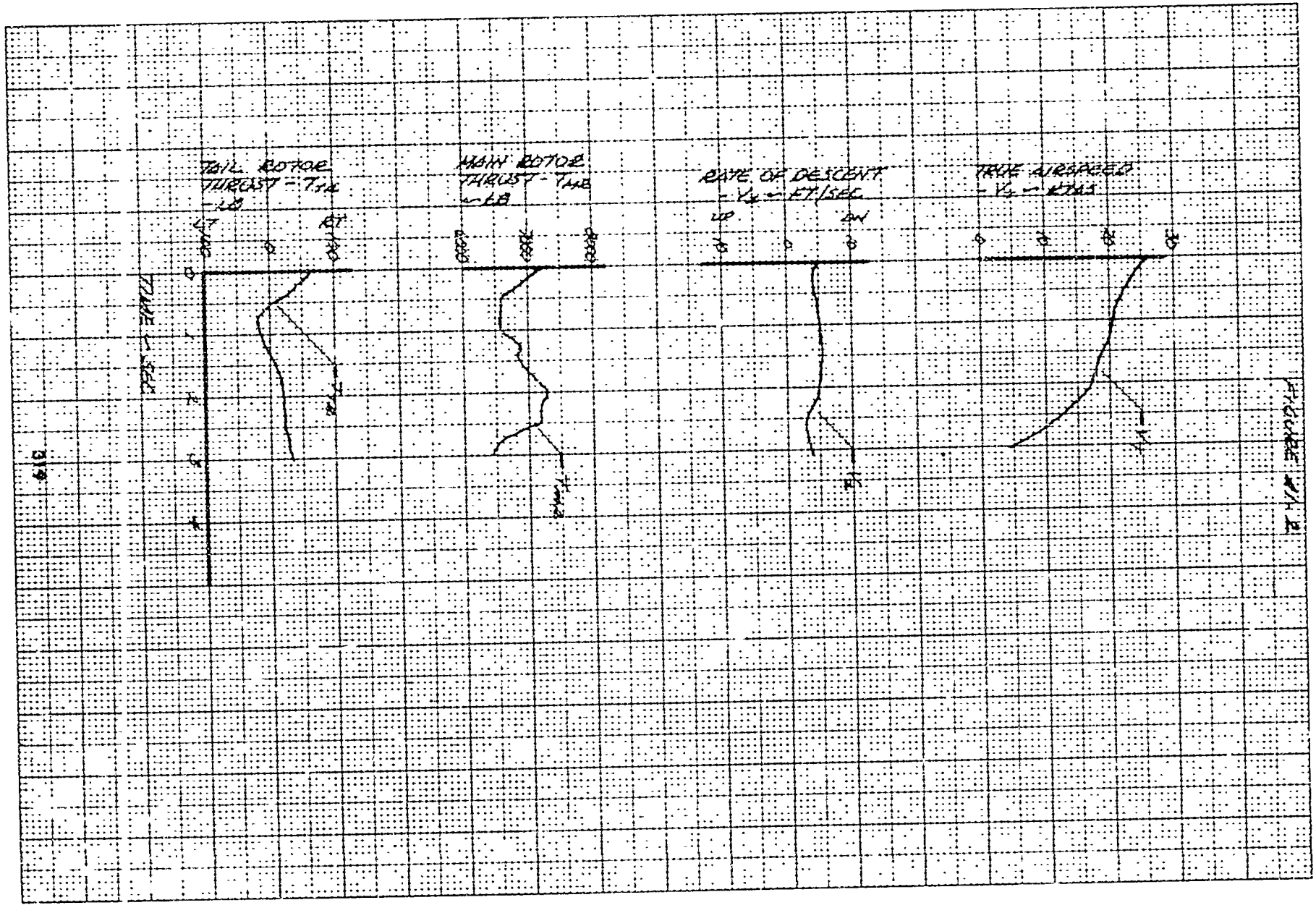
TAIL ROTOR THRUST - T_{TR} - LB
MAIN ROTOR THRUST - T_{MR} - LB
RATE OF DESCENT - V_R - FT/SEC
TRUE AIRSPEED - V_T - KNTS
TIME - SEC
UP
DN

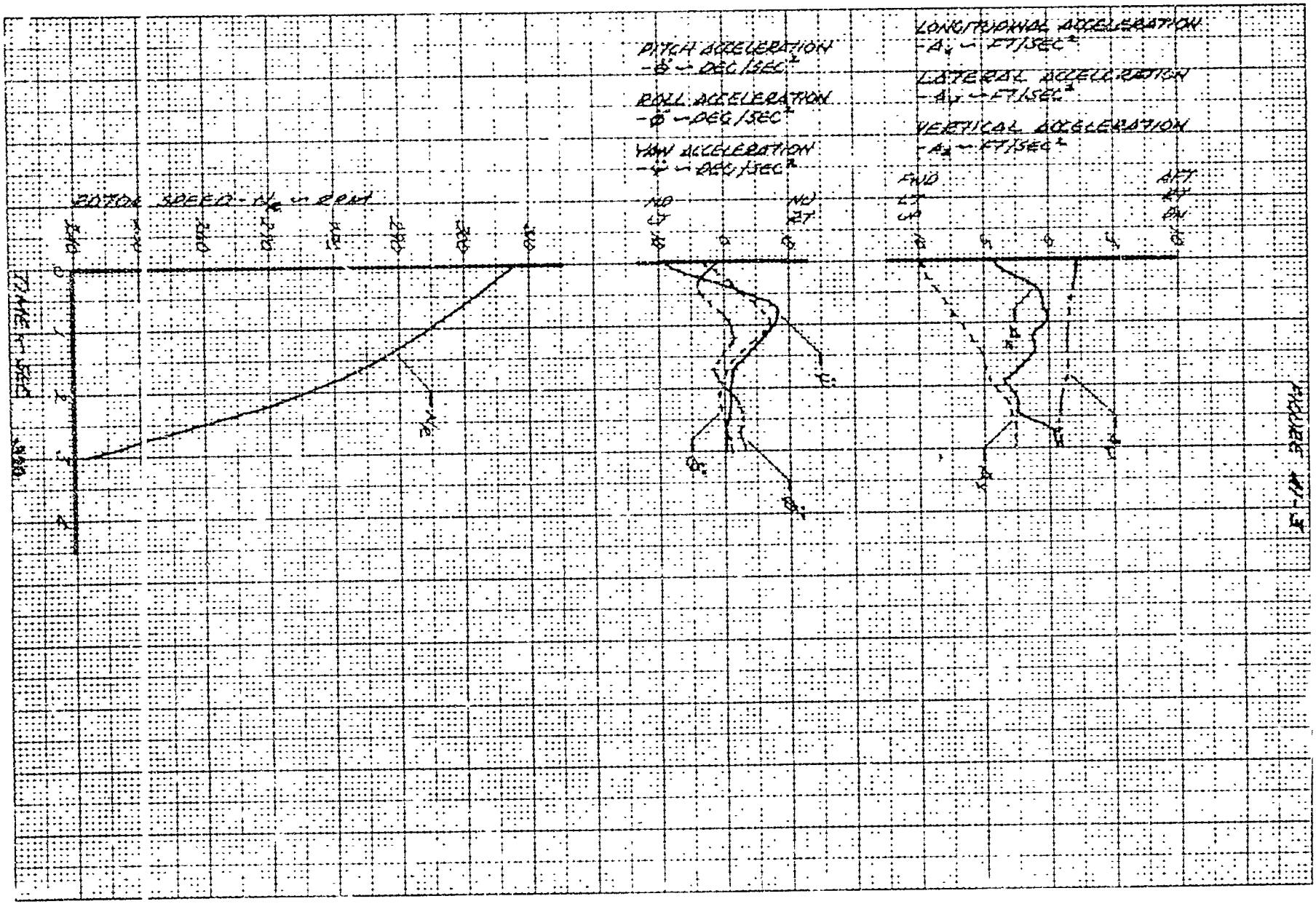
PITCH ACCELERATION
$-\ddot{\theta}$ – DEG/SEC^2
ROLL ACCELERATION
$-\ddot{\phi}$ – DEG/SEC^2
YAW ACCELERATION
$-\ddot{\psi}$ – DEG/SEC^2
LONGITUDINAL ACCELERATION
$-A_x$ – FT/SEC^2
LATERAL ACCELERATION
$-A_y$ – FT/SEC^2
VERTICAL ACCELERATION
$-A_z$ – FT/SEC^2
TIME FROM LIFT-OFF

TIME - SEC
0
1
2
3
4
30
20
10
0
10
15
20
A
B
C
D
E
F

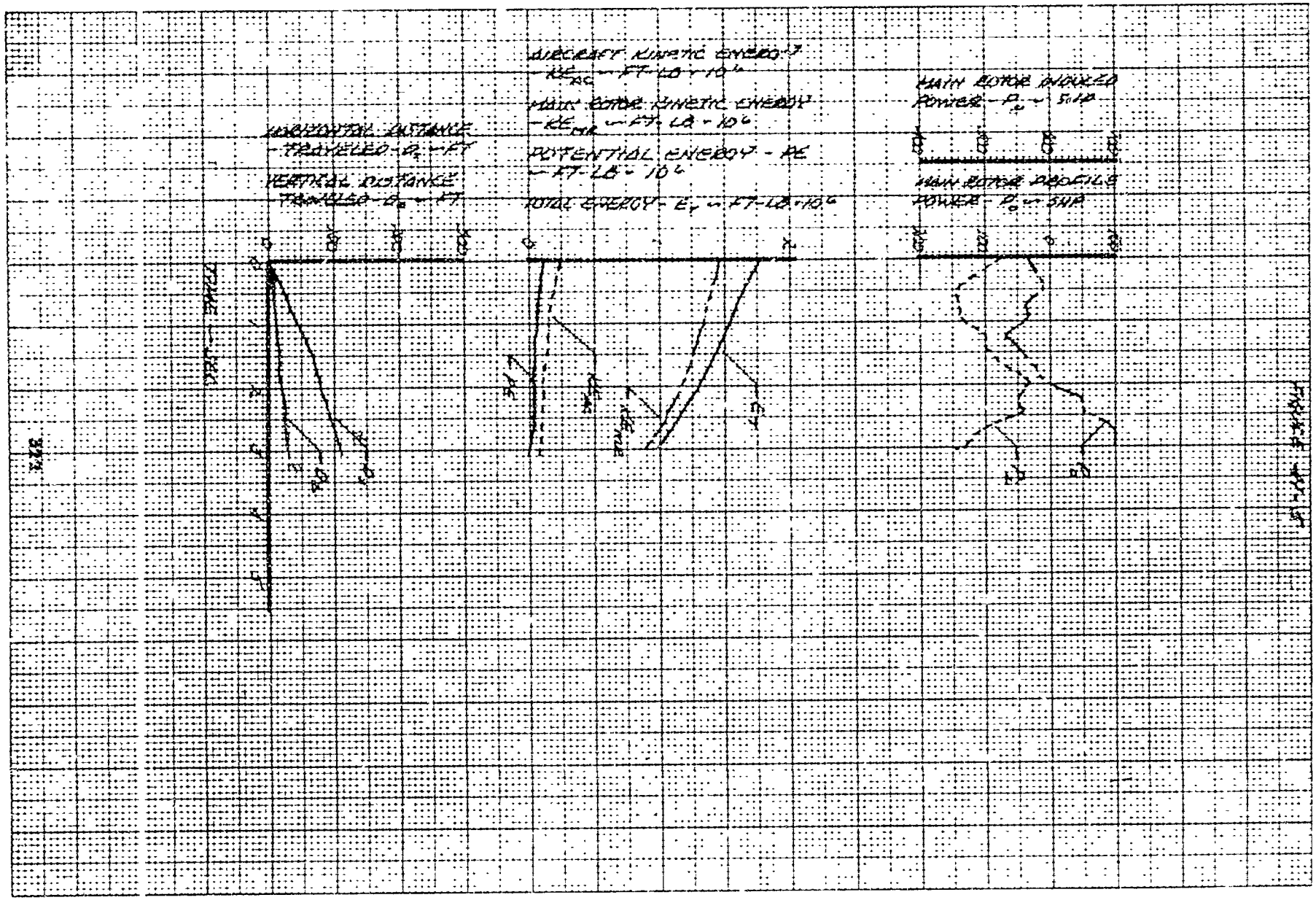
HORIZONTAL DISTANCE TRAVELED - D_x - FT
VERTICAL DISTANCE TRAVELED - D_y - FT
AIRCRAFT KINETIC ENERGY - KE_{AC} - FT-LB - 10^6
MAIN ROTOR KINETIC ENERGY - KE_{MR} - FT-LB - 10^6
POTENTIAL ENERGY - PE - FT-LB - 10^6
TOTAL ENERGY - E_T - FT-LB - 10^6
MAIN ROTOR INDUCED POWER - P_i - SHP
MAIN ROTOR PROFILE POWER - P_o - SHP
DRAG - LBS
ALTITUDE - FEET

FIGURE A.2 - 1

LANDING FROM A MEDIUM SPEED LEVEL FLIGHT ENTRY

UH-1C USA SN 63-8684

GROSS WT = 6720 LBS
SKID HEIGHT = 20 FT
ENTRY AIRSPEED = 36 KTAS

DENSITY ALT = 11000 FT
AMB. TEMP = 10 °C

TOTAL LONGITUDINAL CONTROL TRAVEL = 12.7 IN.
TOTAL LATERAL CONTROL TRAVEL = 12.1 IN.
TOTAL DIRECTIONAL CONTROL TRAVEL = 7.0 IN.
TOTAL COLLECTIVE CONTROL TRAVEL = 10.4 IN.

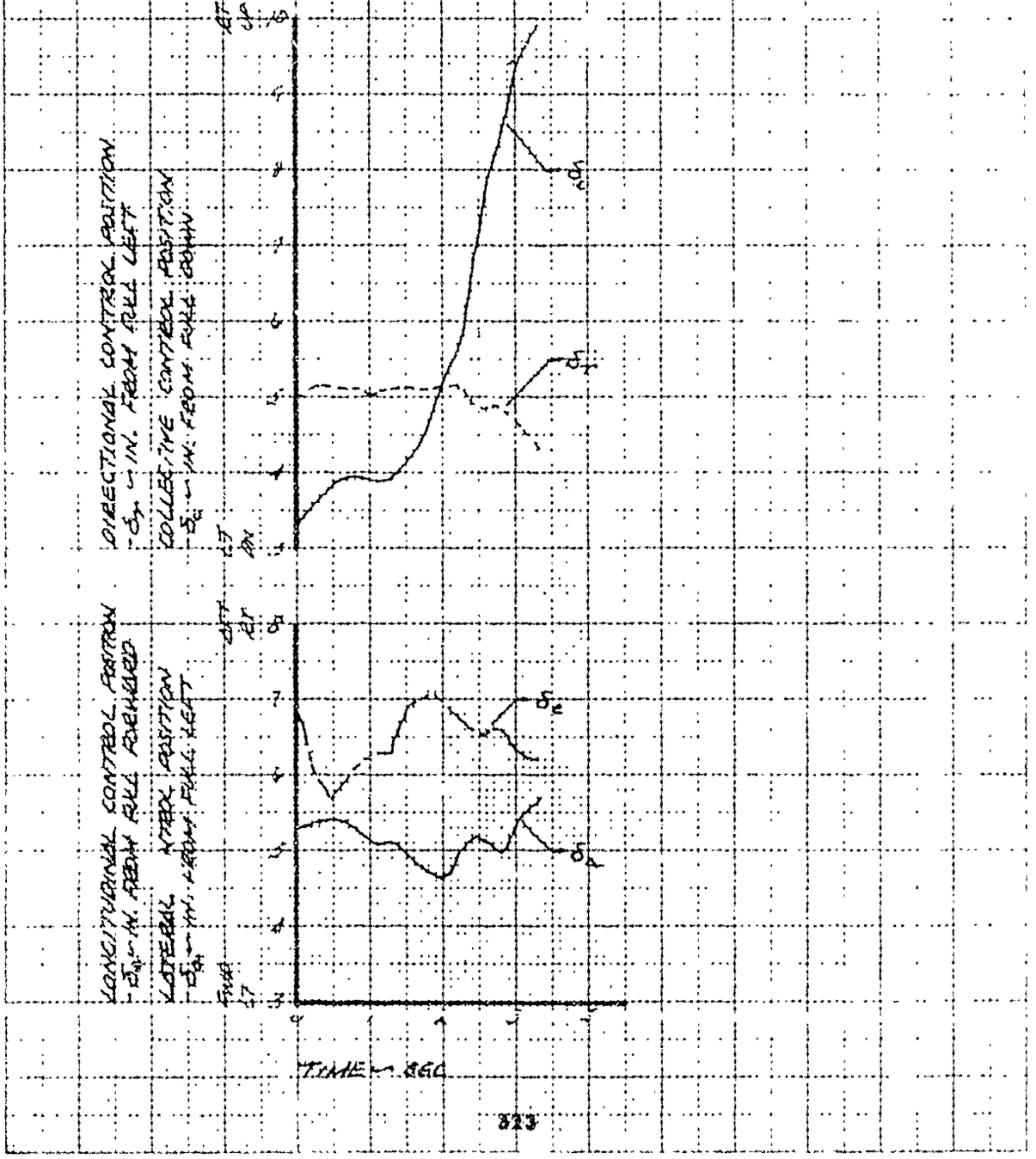

FIGURE 22-2.

TRUE AIRSPEED
RATE OF DESCENT
PRIMARY ERROR CURRENT
Time - SEC.

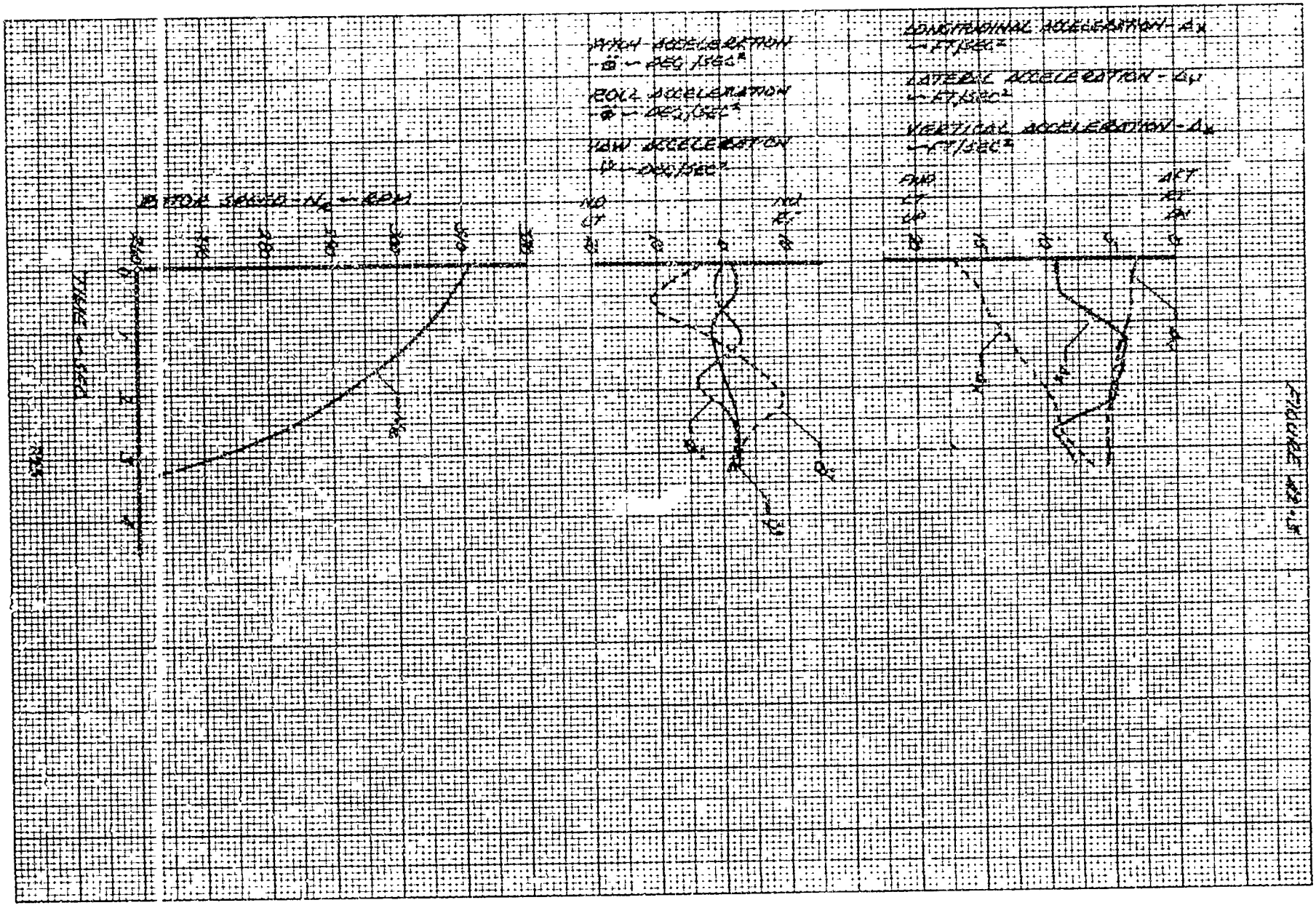

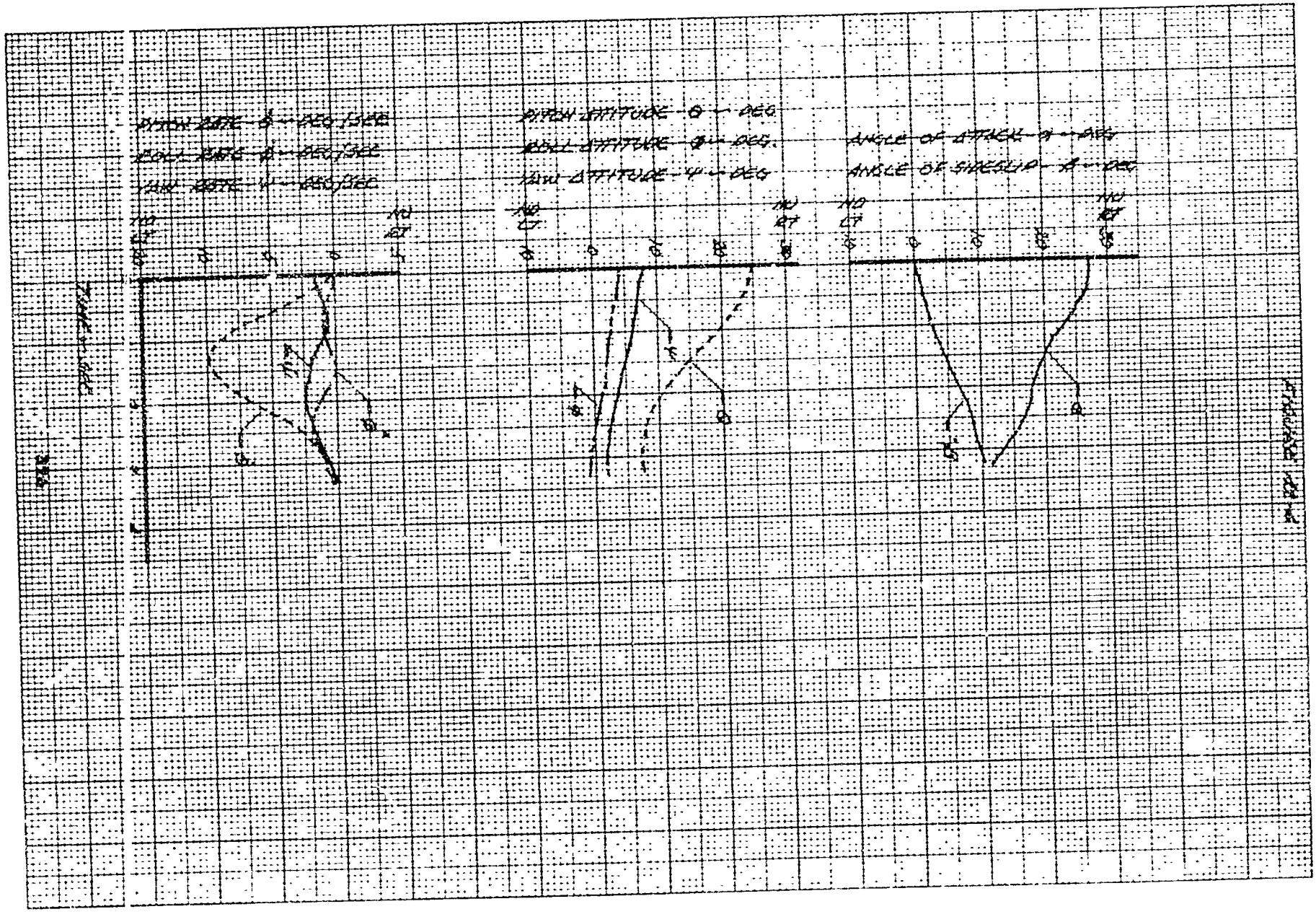
YAW RATE - r - DEG/SEC
ROLL RATE - p - DEG/SEC
PITCH RATE - q - DEG/SEC
YAW ATTITUDE - ψ - DEG
ROLL ATTITUDE - φ - DEG.
PITCH ATTITUDE - θ - DEG
ANGLE OF ATTACK - α - DEG
ANGLE OF SIDESLIP - β - DEG
NO. OF FLIGHTS

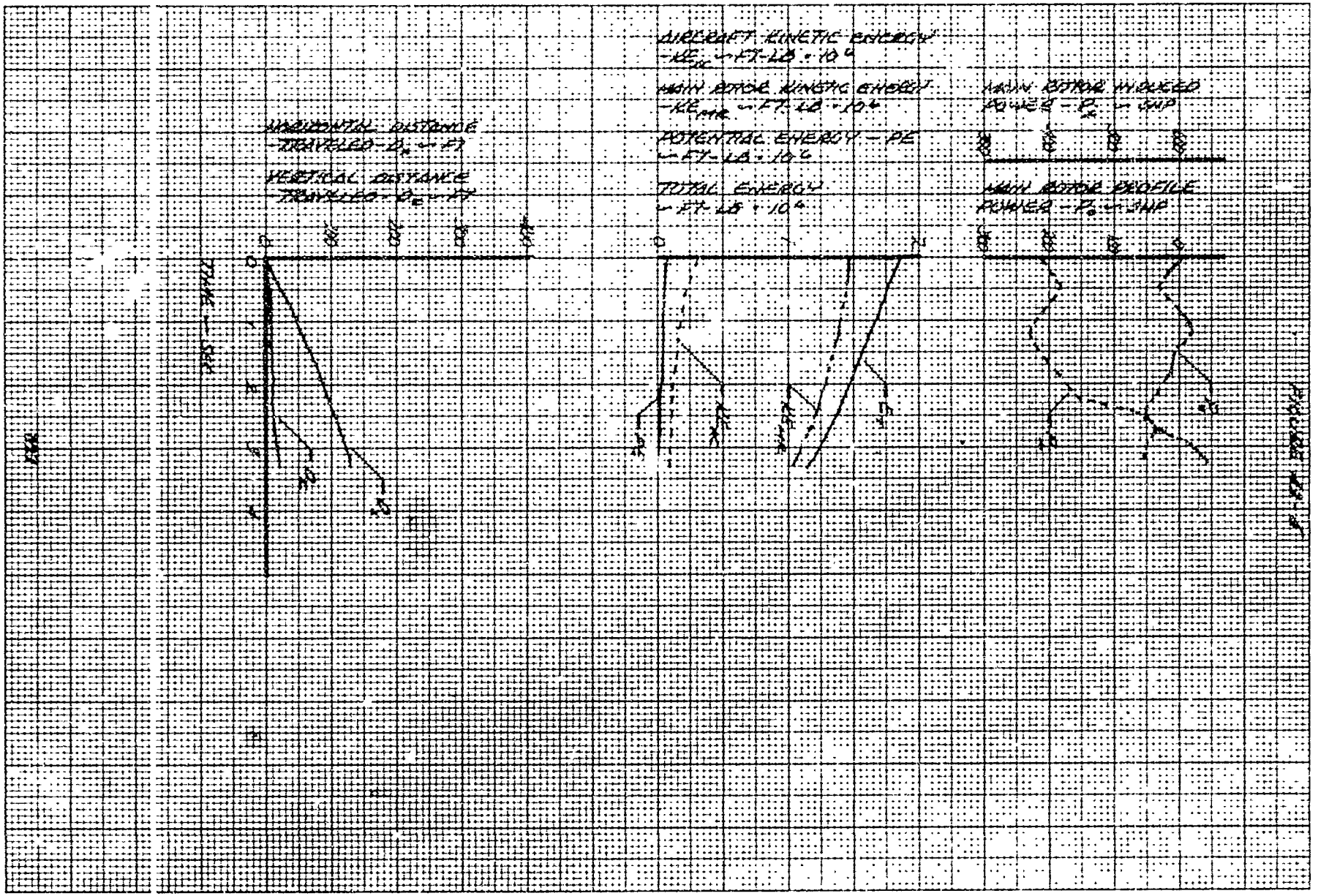
HORIZONTAL DISTANCE
TRAVELED - D_x - FT
VERTICAL DISTANCE
TRAVELED - D_z - FT
TIME - SEC
AIRCRAFT KINETIC ENERGY
- KE_{AC} - FT-LB · 10^4
MAIN ROTOR KINETIC ENERGY
- KE_{MR} - FT-LB · 10^4
POTENTIAL ENERGY - PE
- FT-LB · 10^4
TOTAL ENERGY
- FT-LB · 10^4
MAIN ROTOR INDUCED
POWER - P_i - HP
MAIN ROTOR PROFILE
POWER - P_o - HP

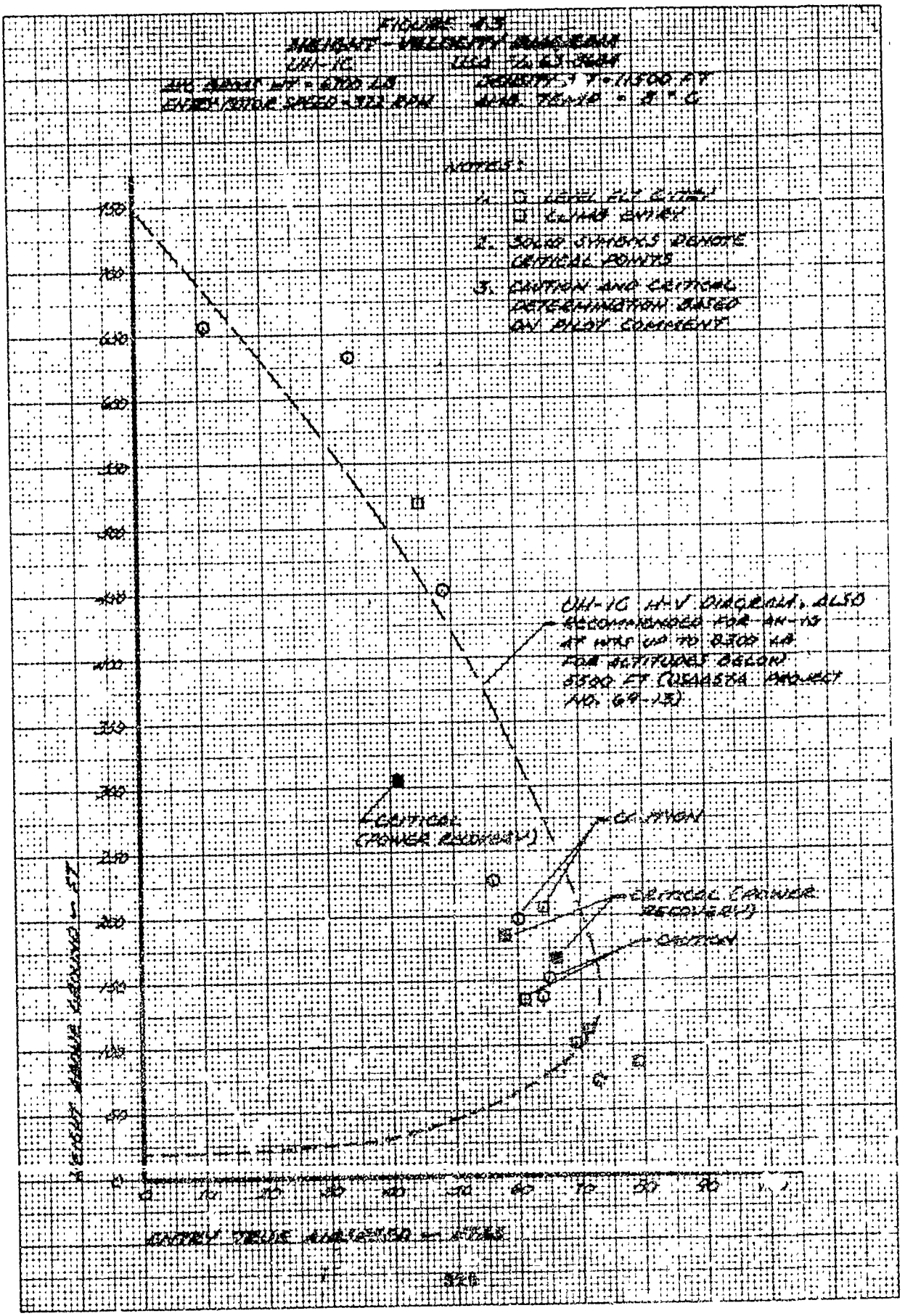
NOTES:
1. SOLID SYMBOLS DENOTE CRITICAL POINTS
3. CAUTION AND CRITICAL DETERMINATION BASED ON PILOT COMMENTS
CRITICAL CRUISE ALTITUDE
CRUISE
CRITICAL CRUISE RECOVERY
DESCENT
ENERGY HEIGHT, HUNDREDS OF FEET
AIRSPEED, KNOTS TRUE

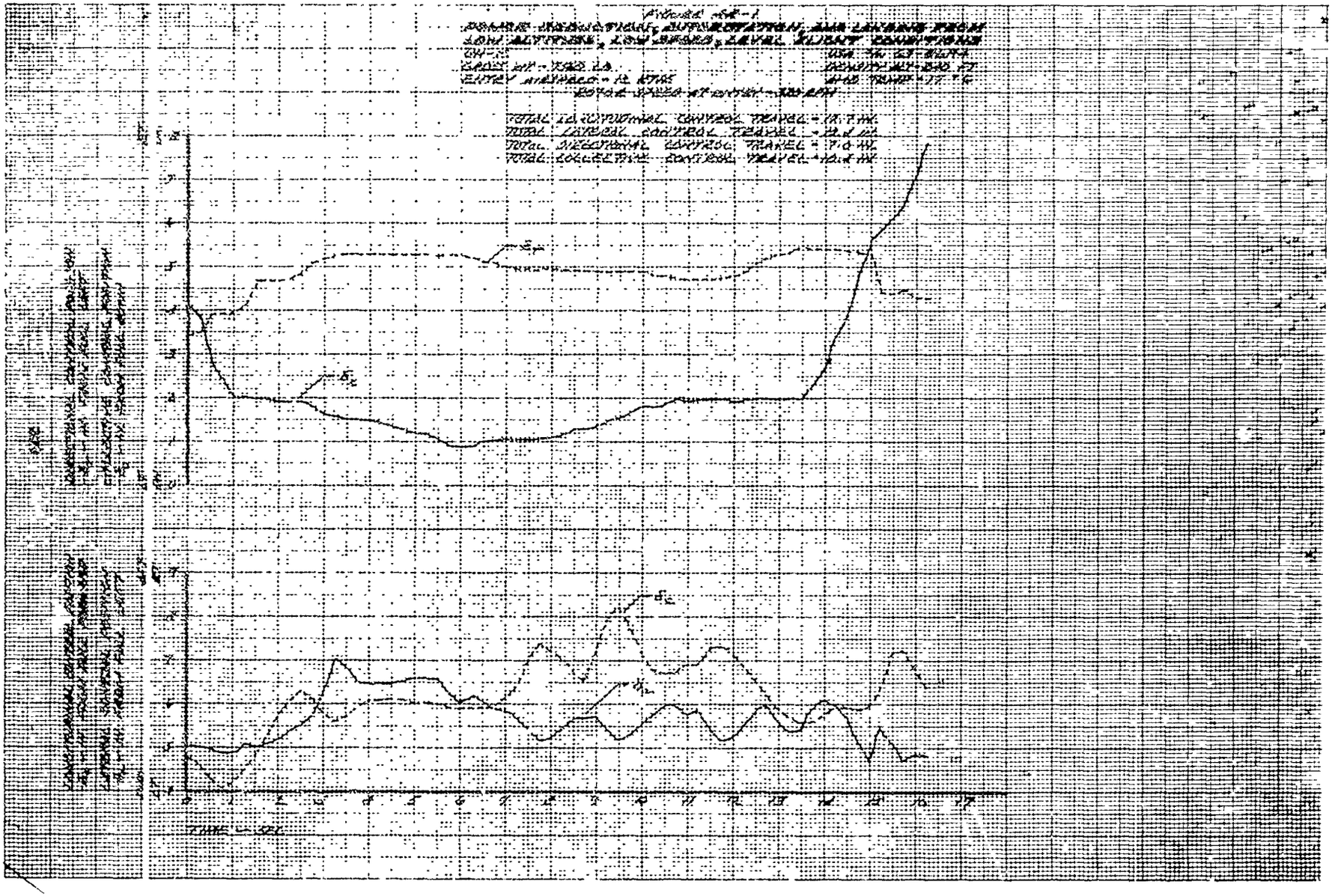

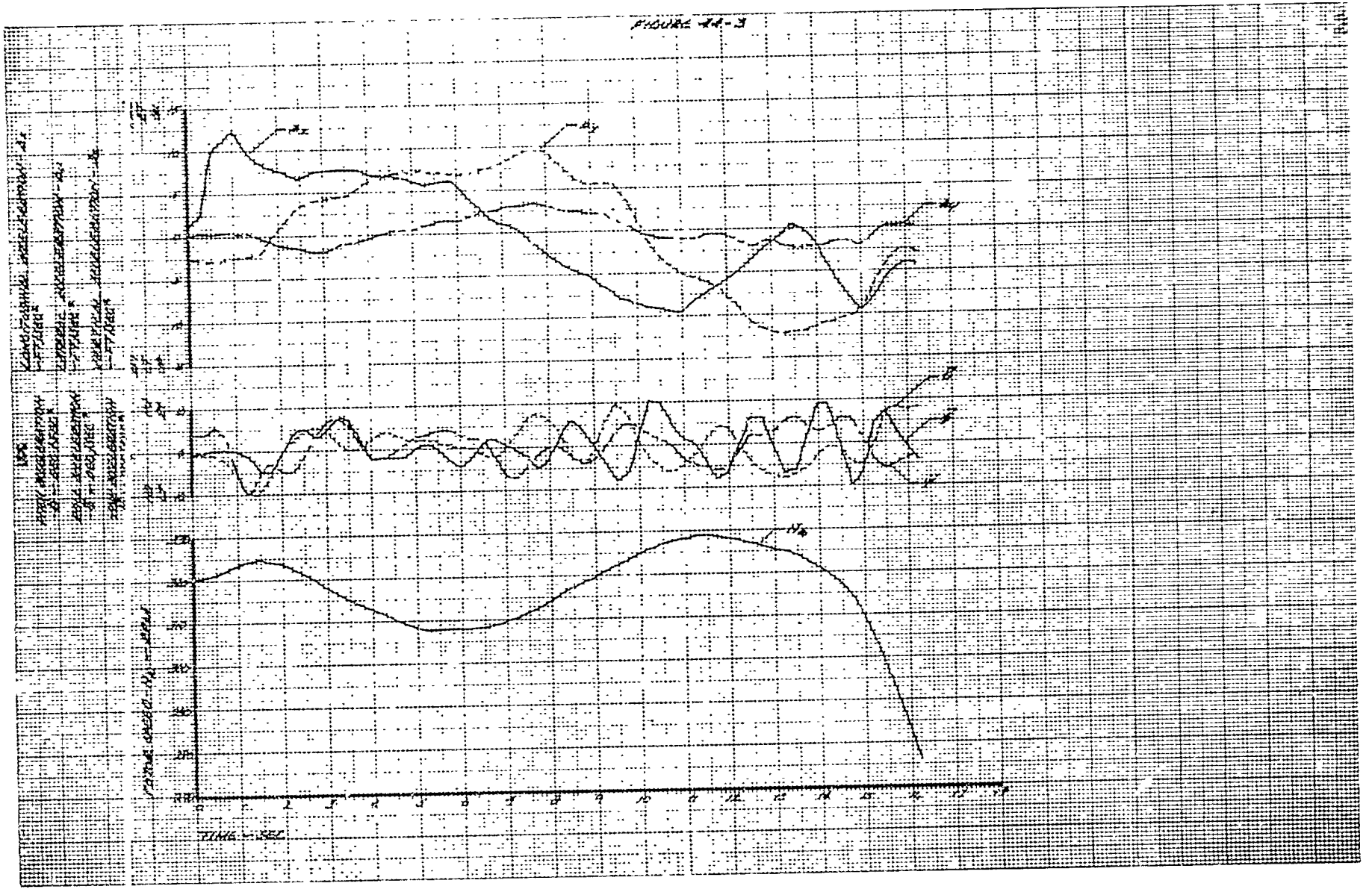
FIGURE 44-3
TIME - SEC

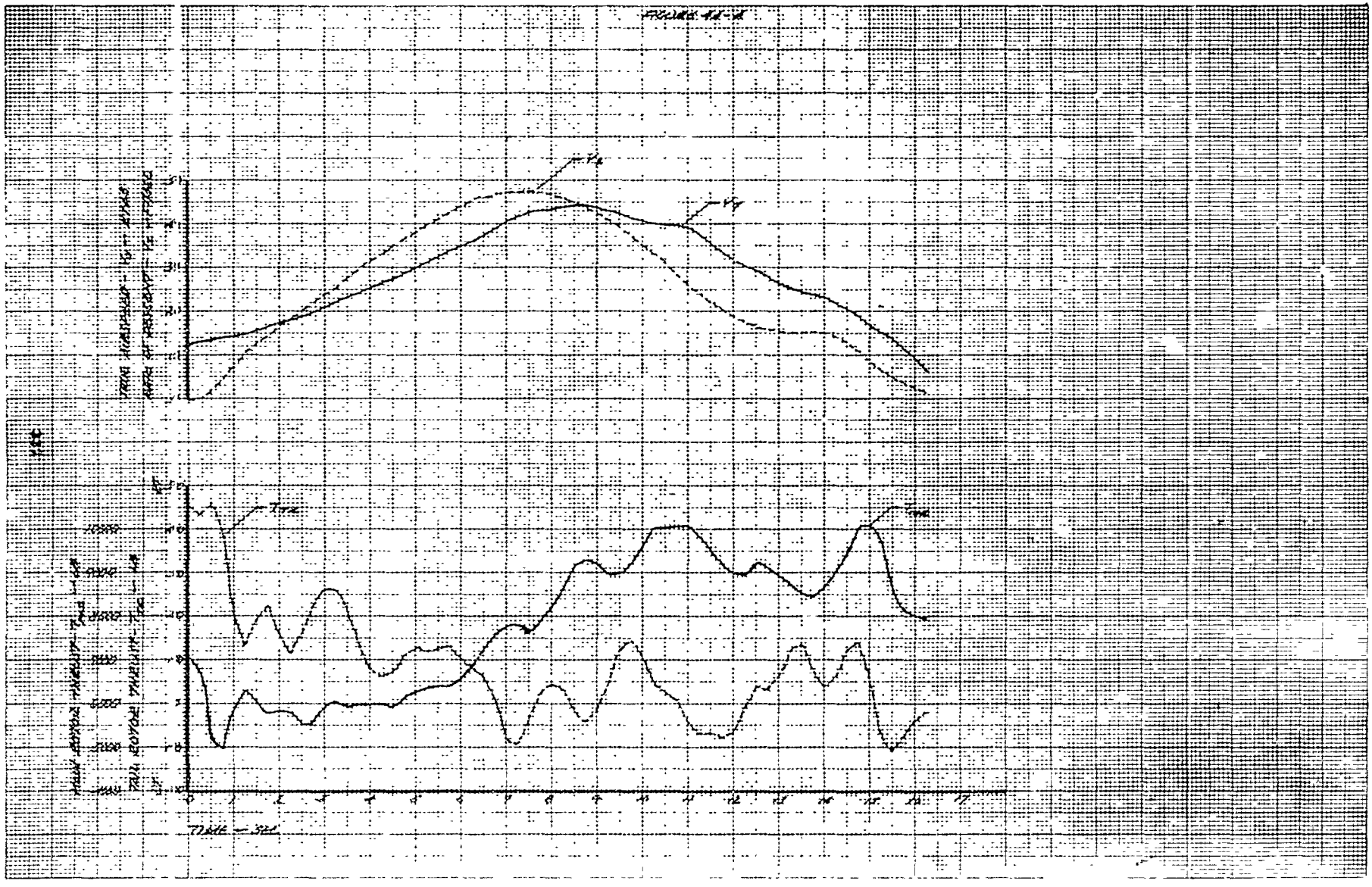
TIME — SEC

FIGURE A4-5

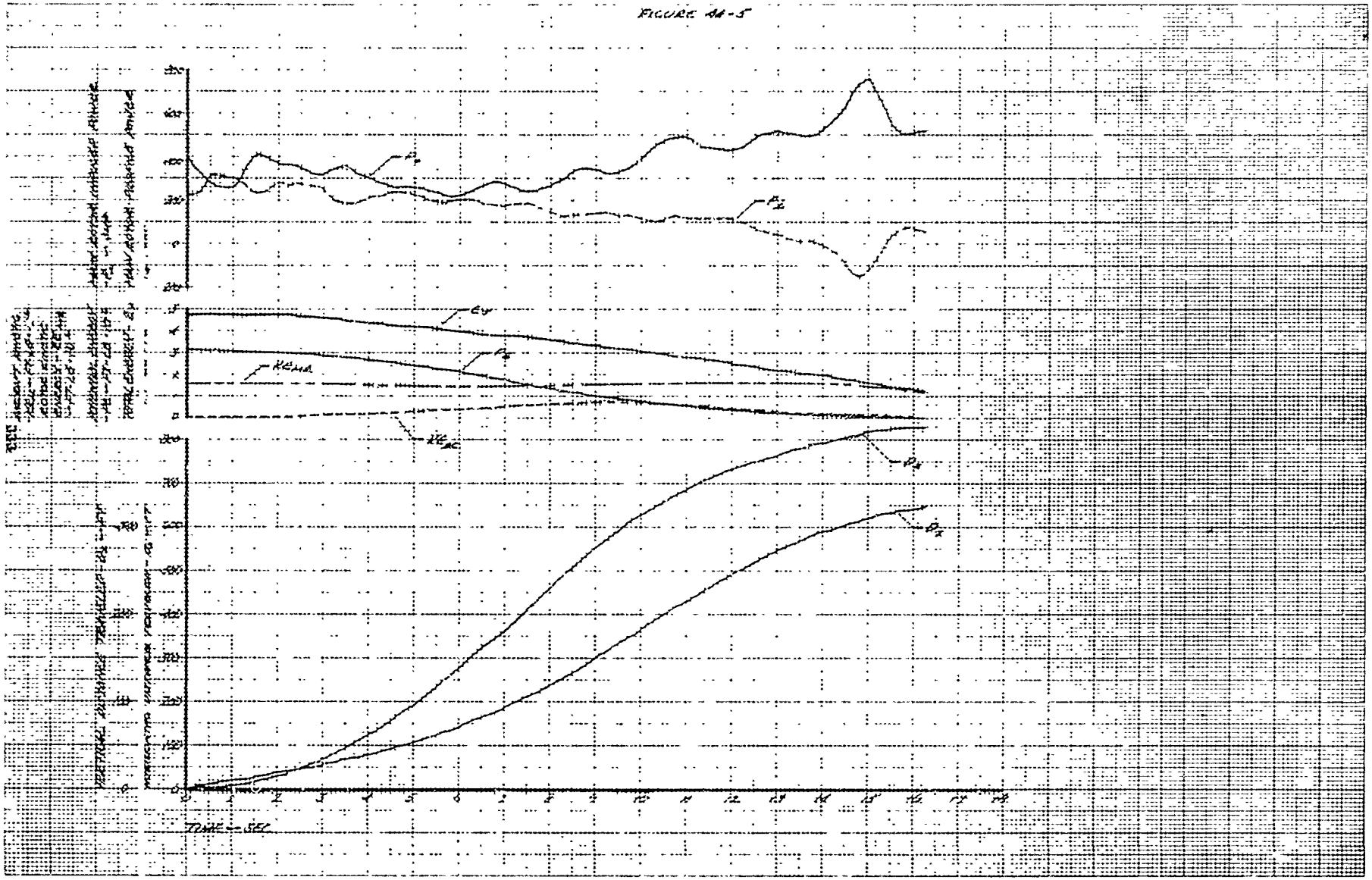

FIGURE 4.8-7

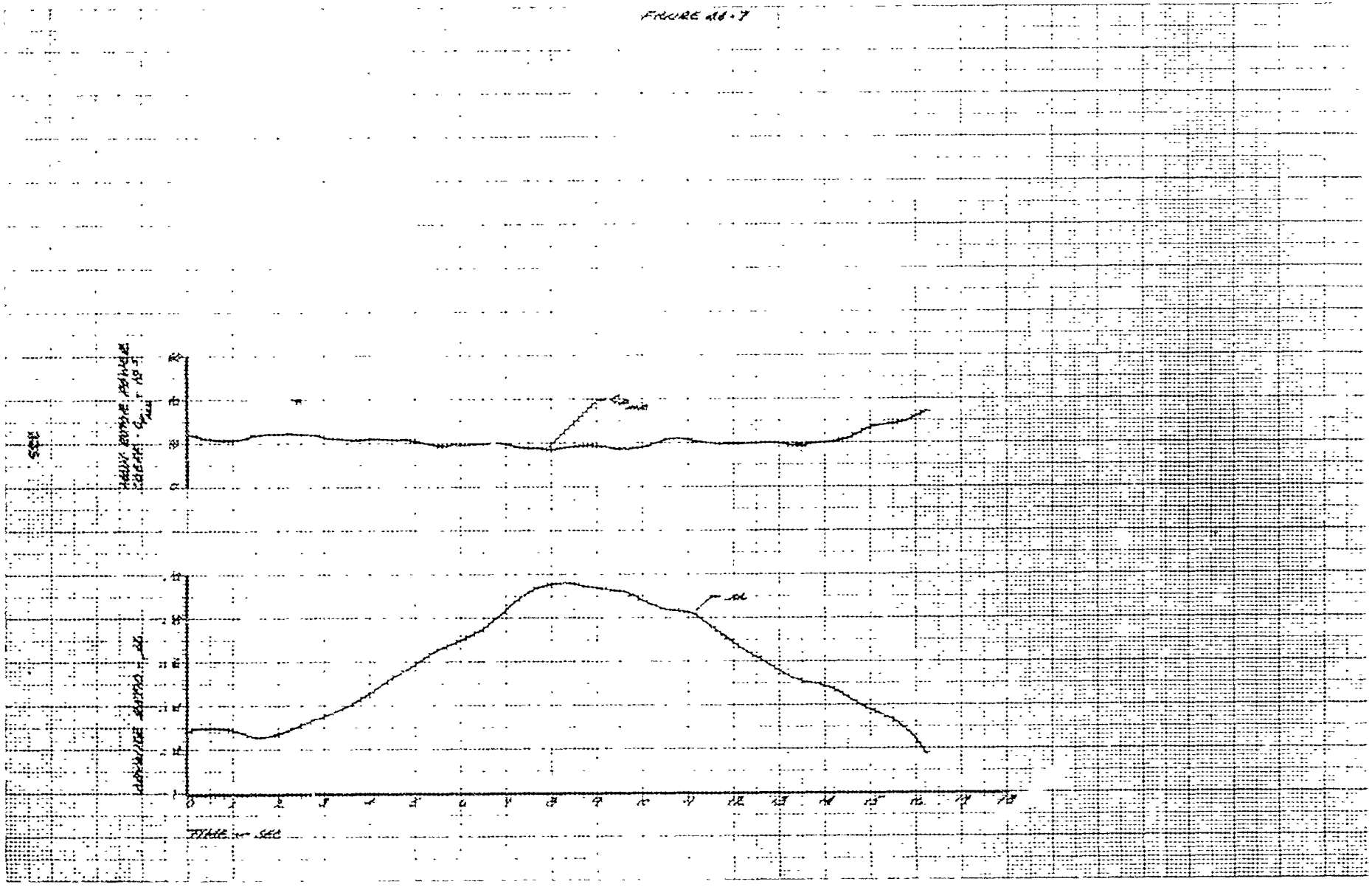

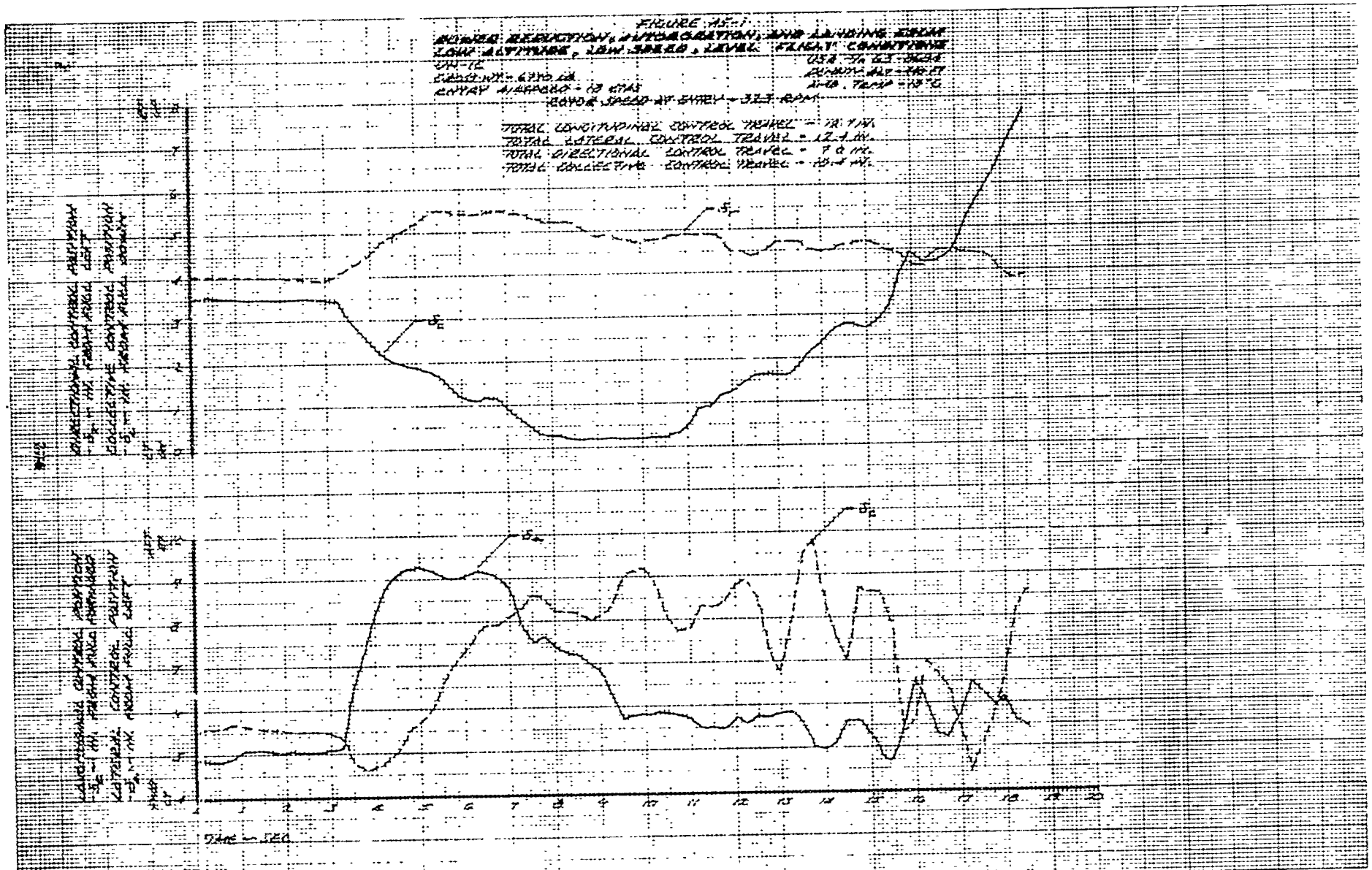
TIME — SEC

FIGURE 15-2

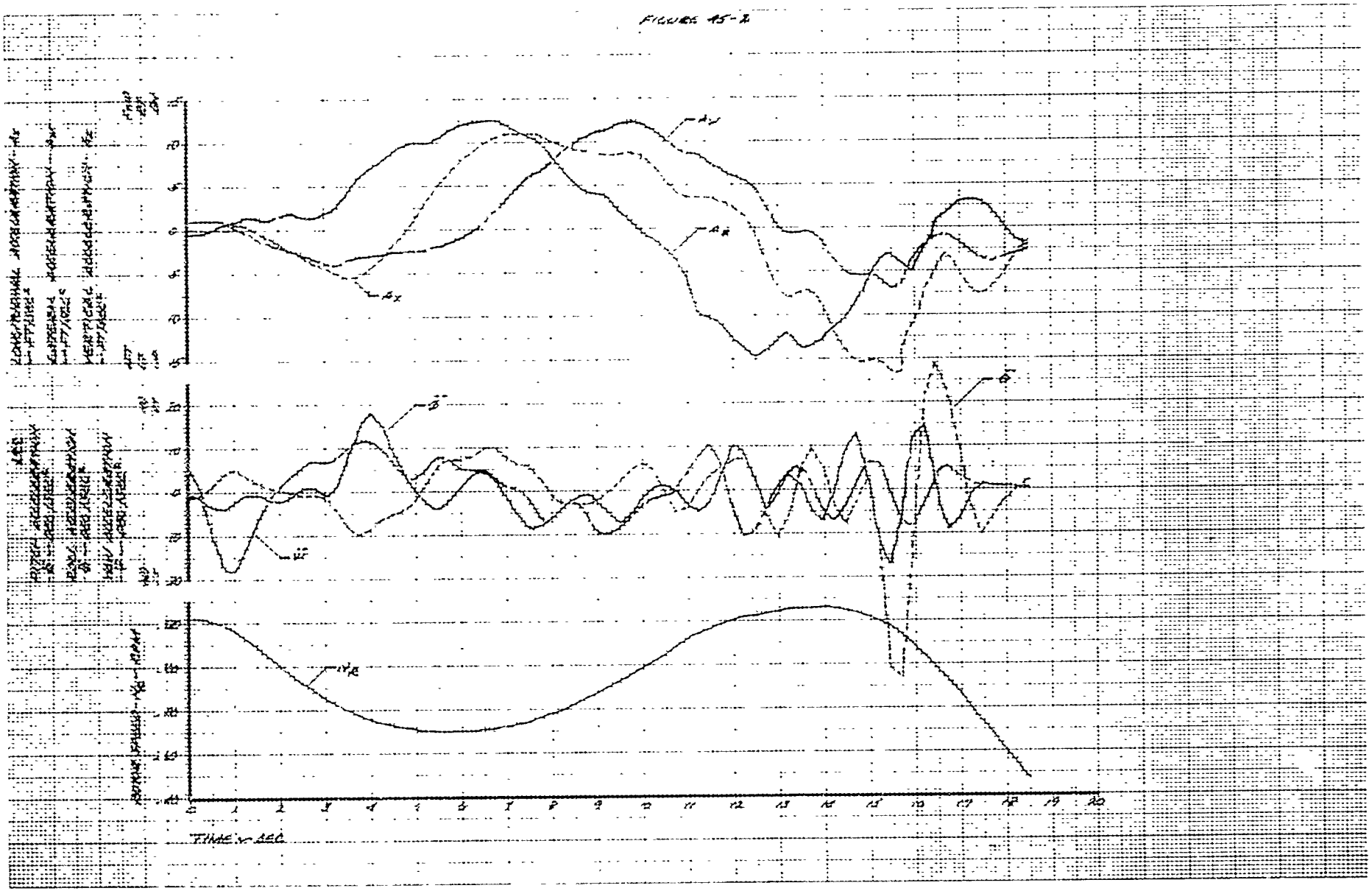

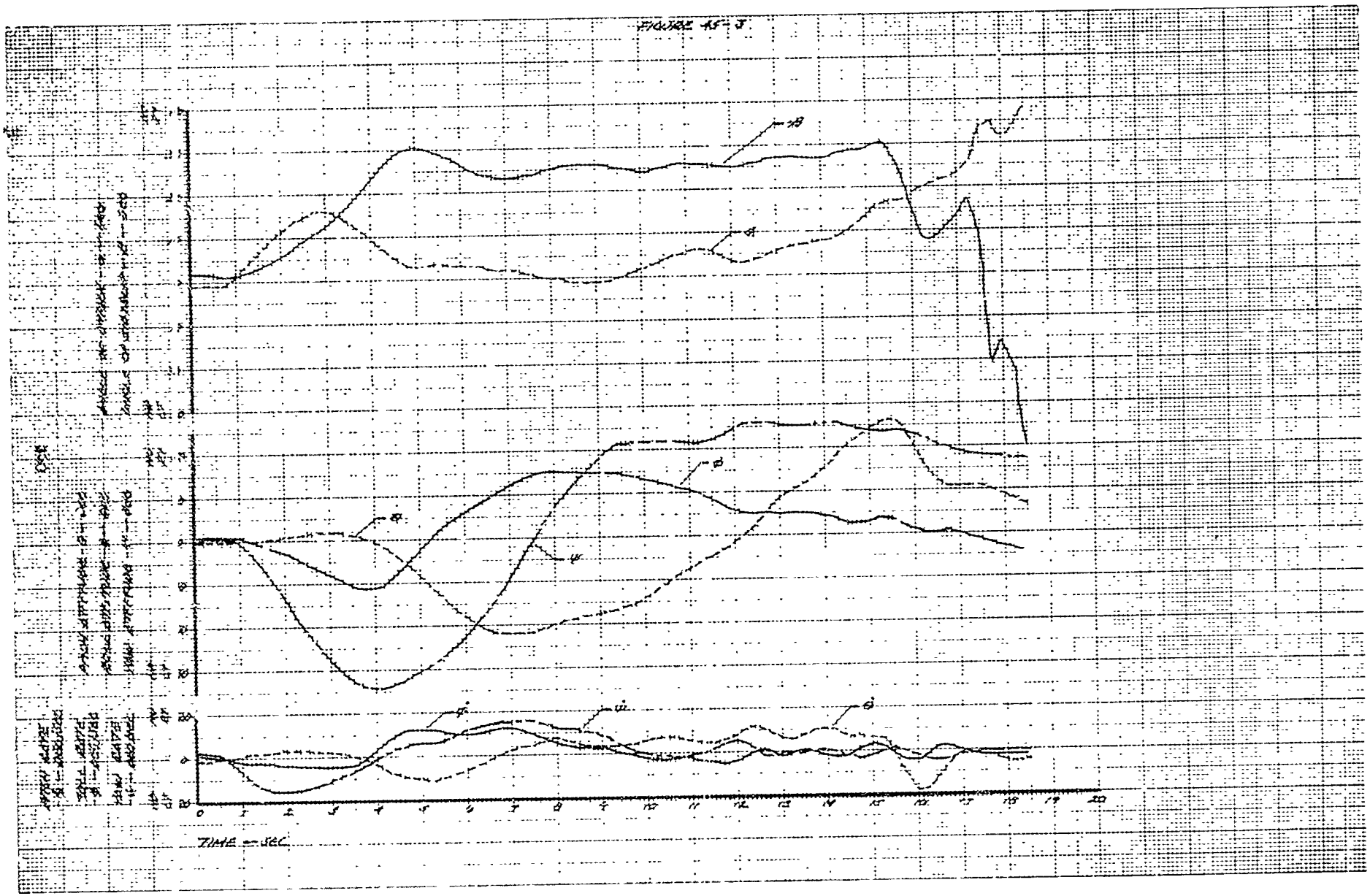
TIME — SEC

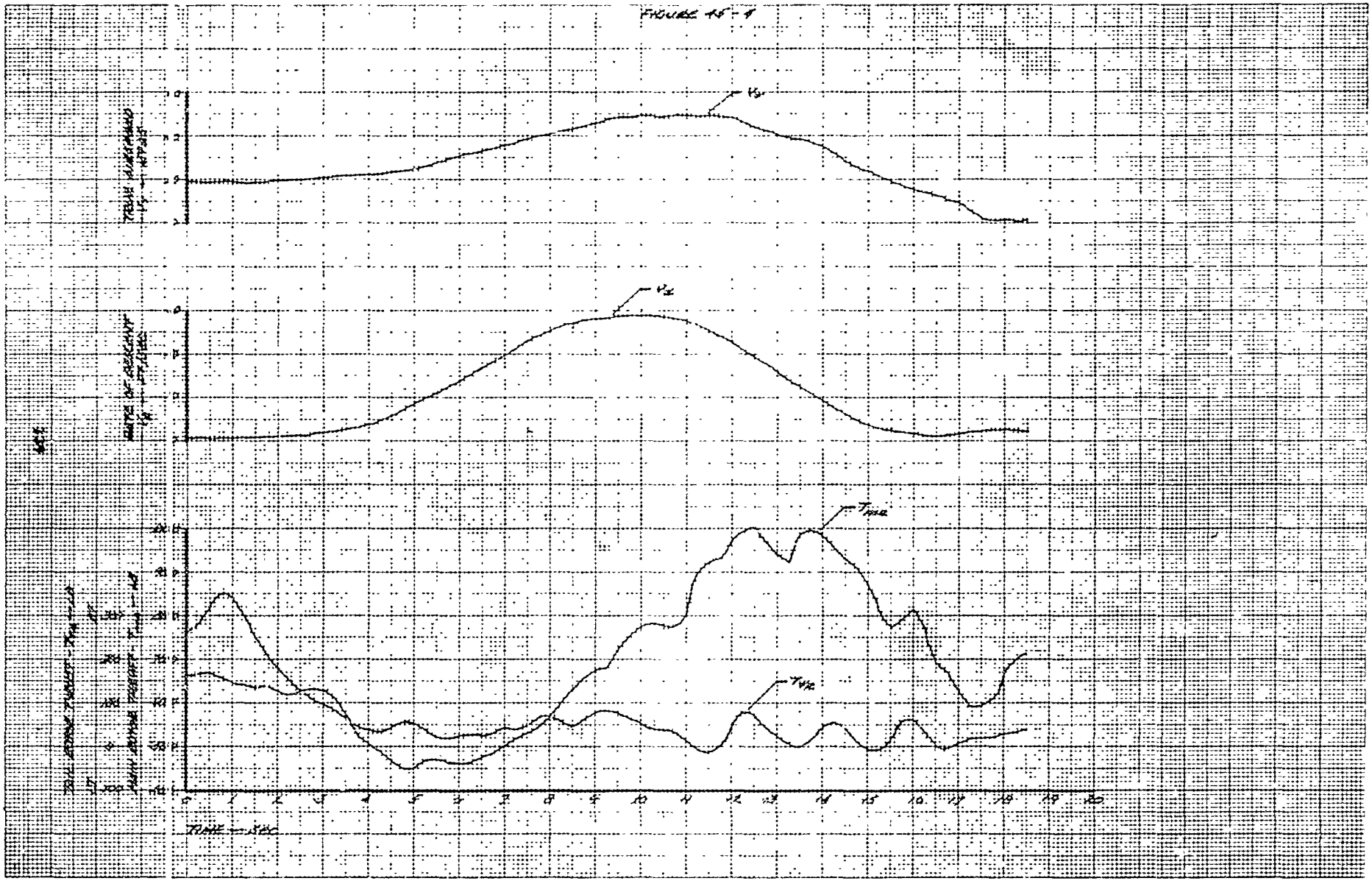
FIGURE 45-9
TIME — SEC

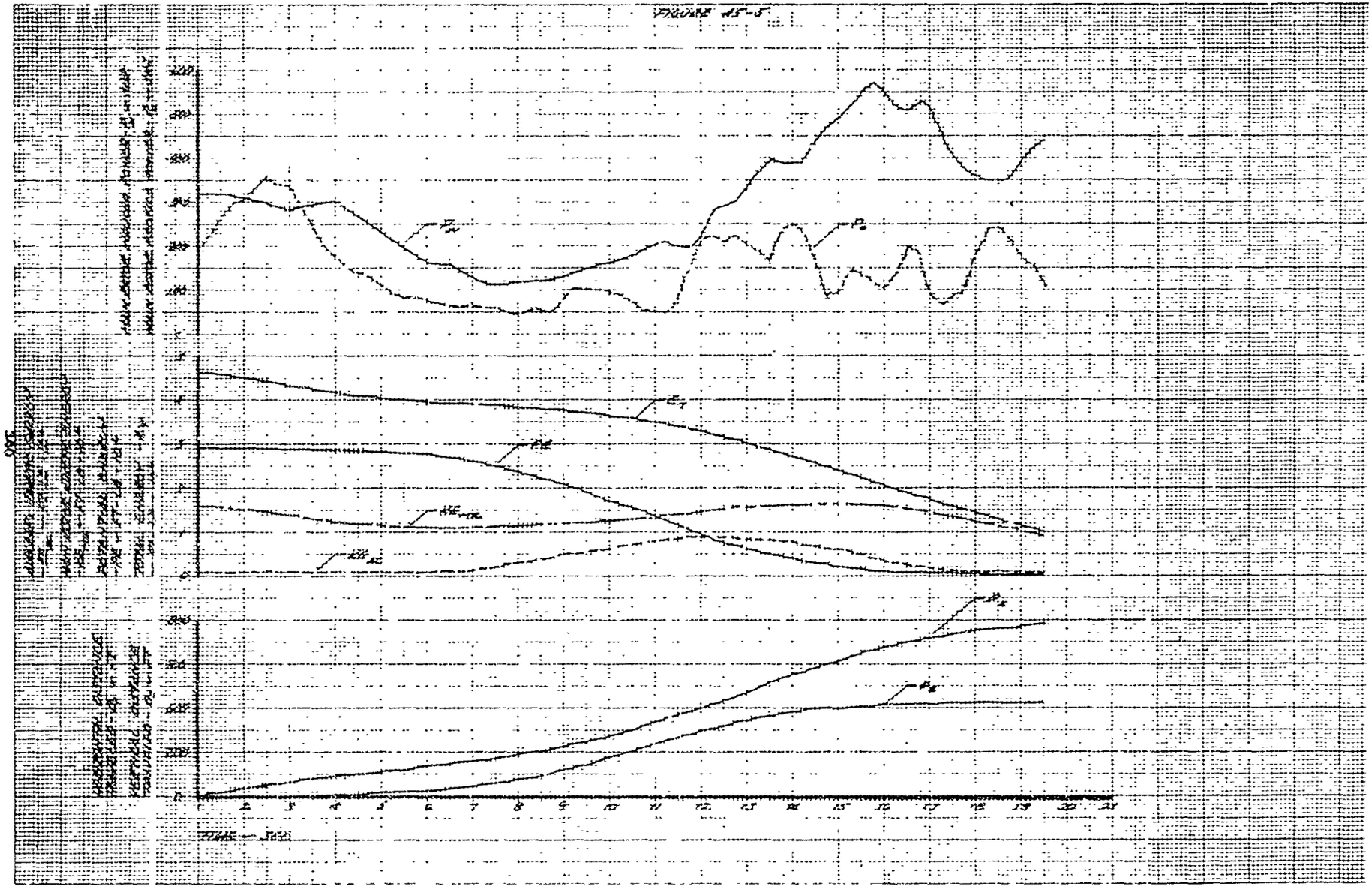

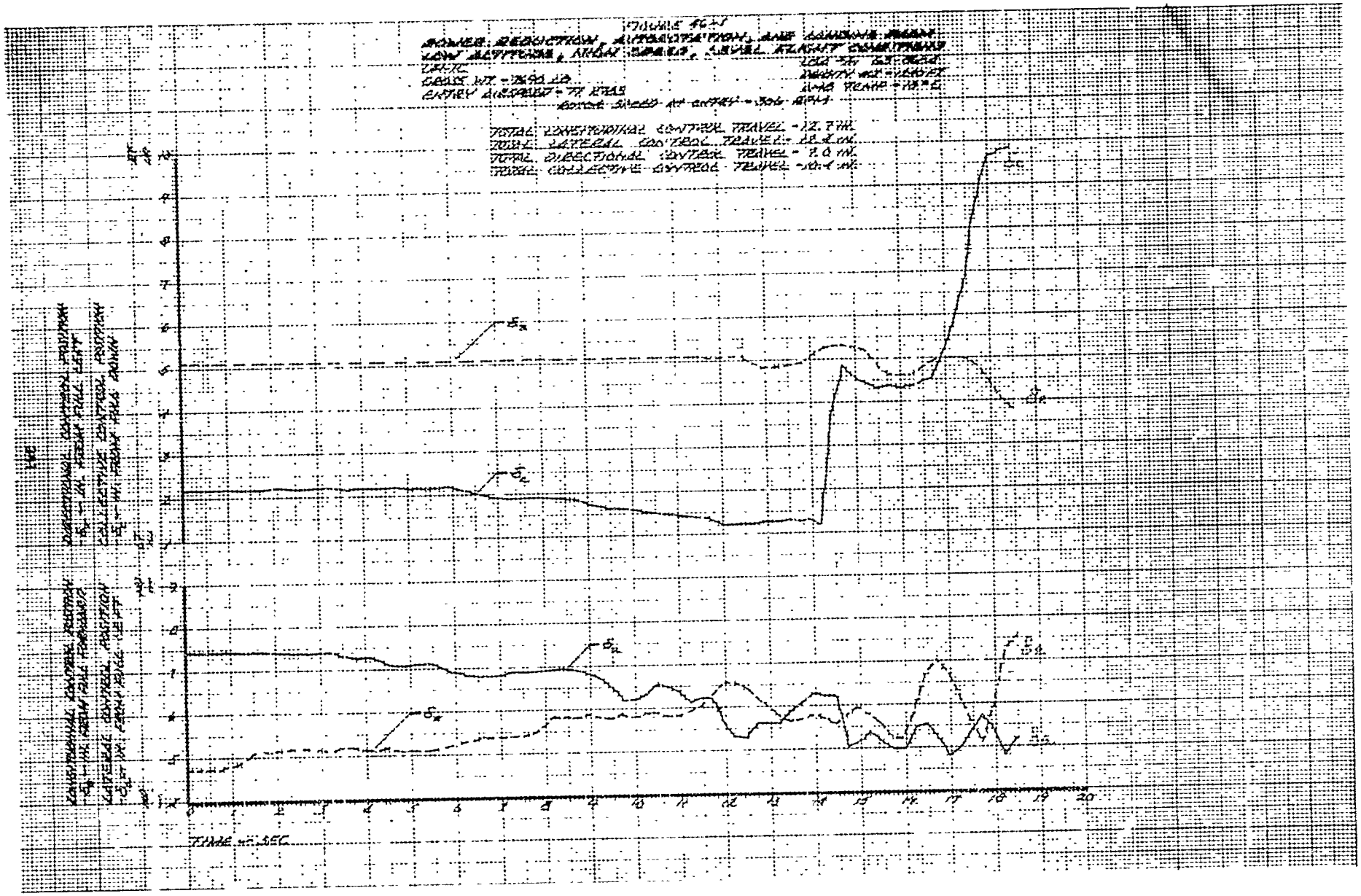
TIME - SEC

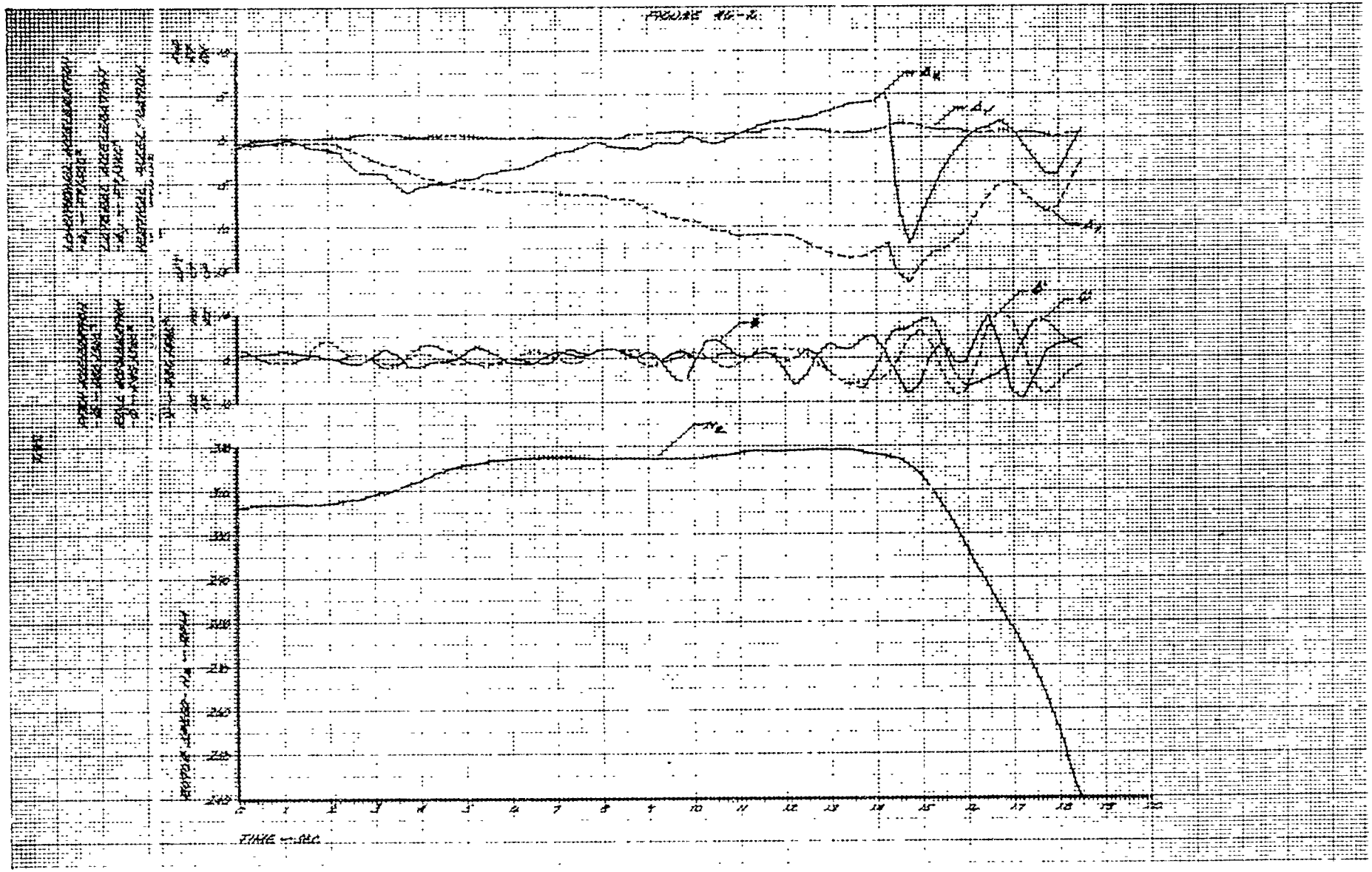
TIME - SEC

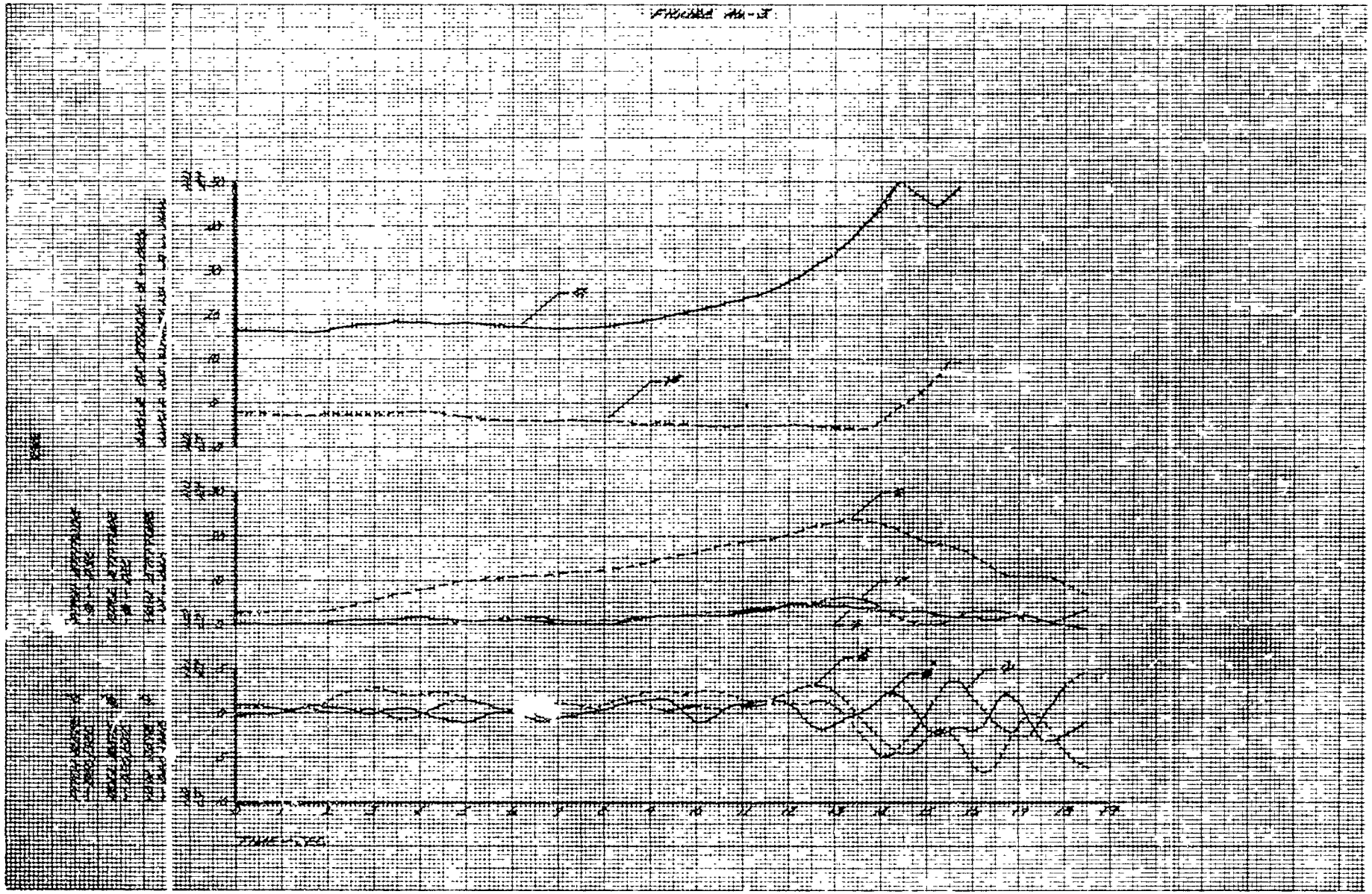

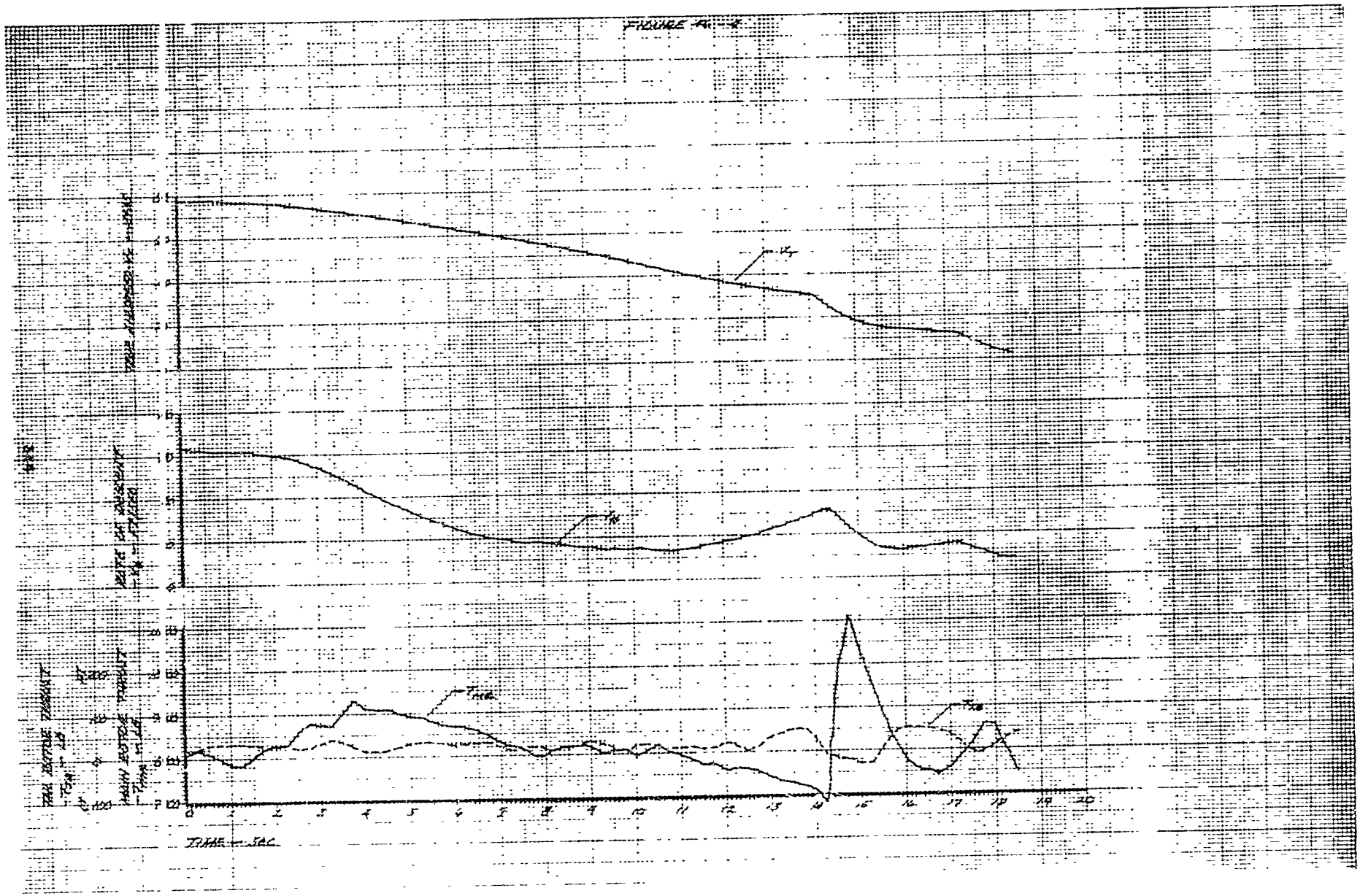
FIGURE A-1
TIME - SEC

FIGURE 16-6

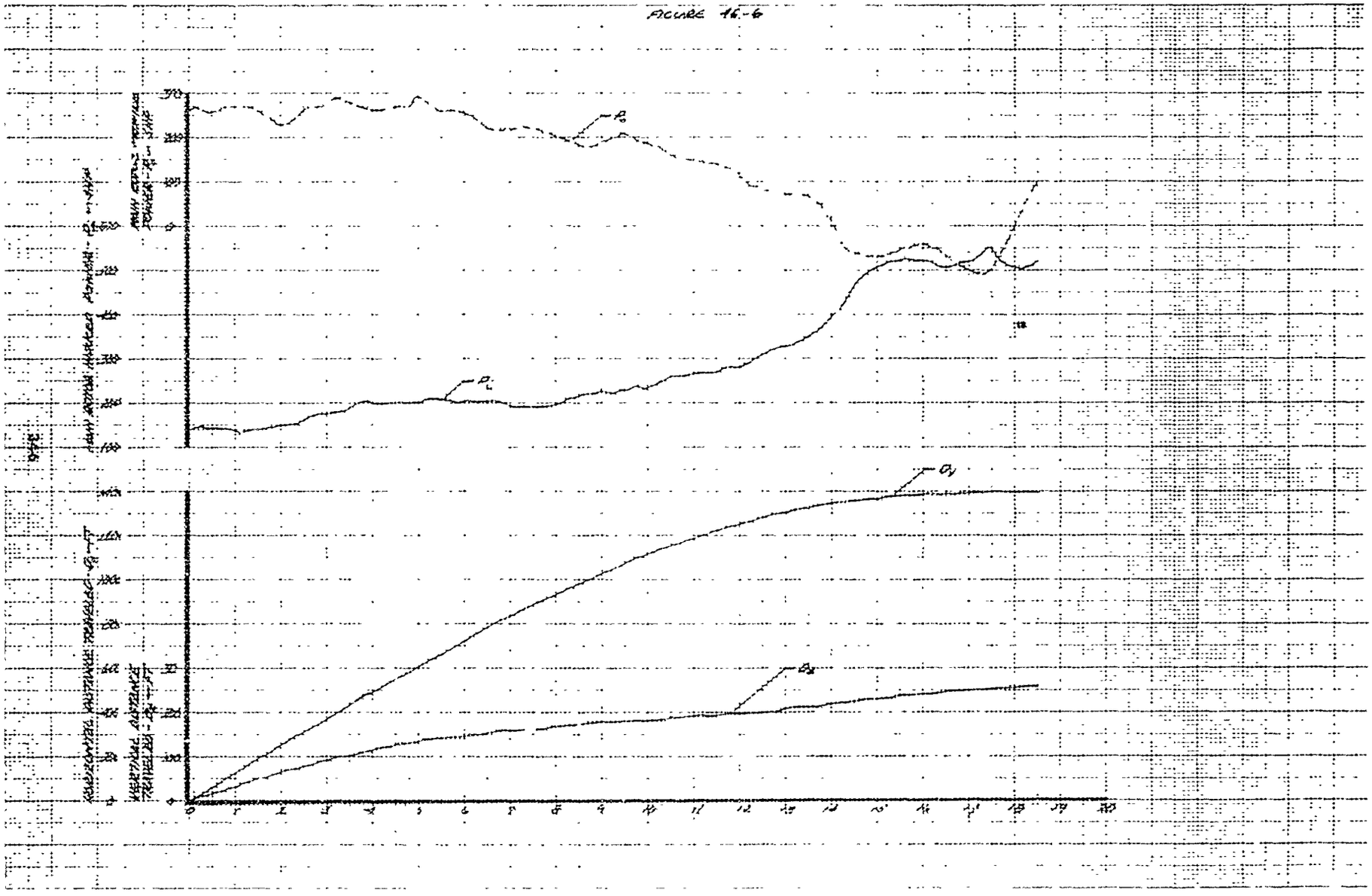

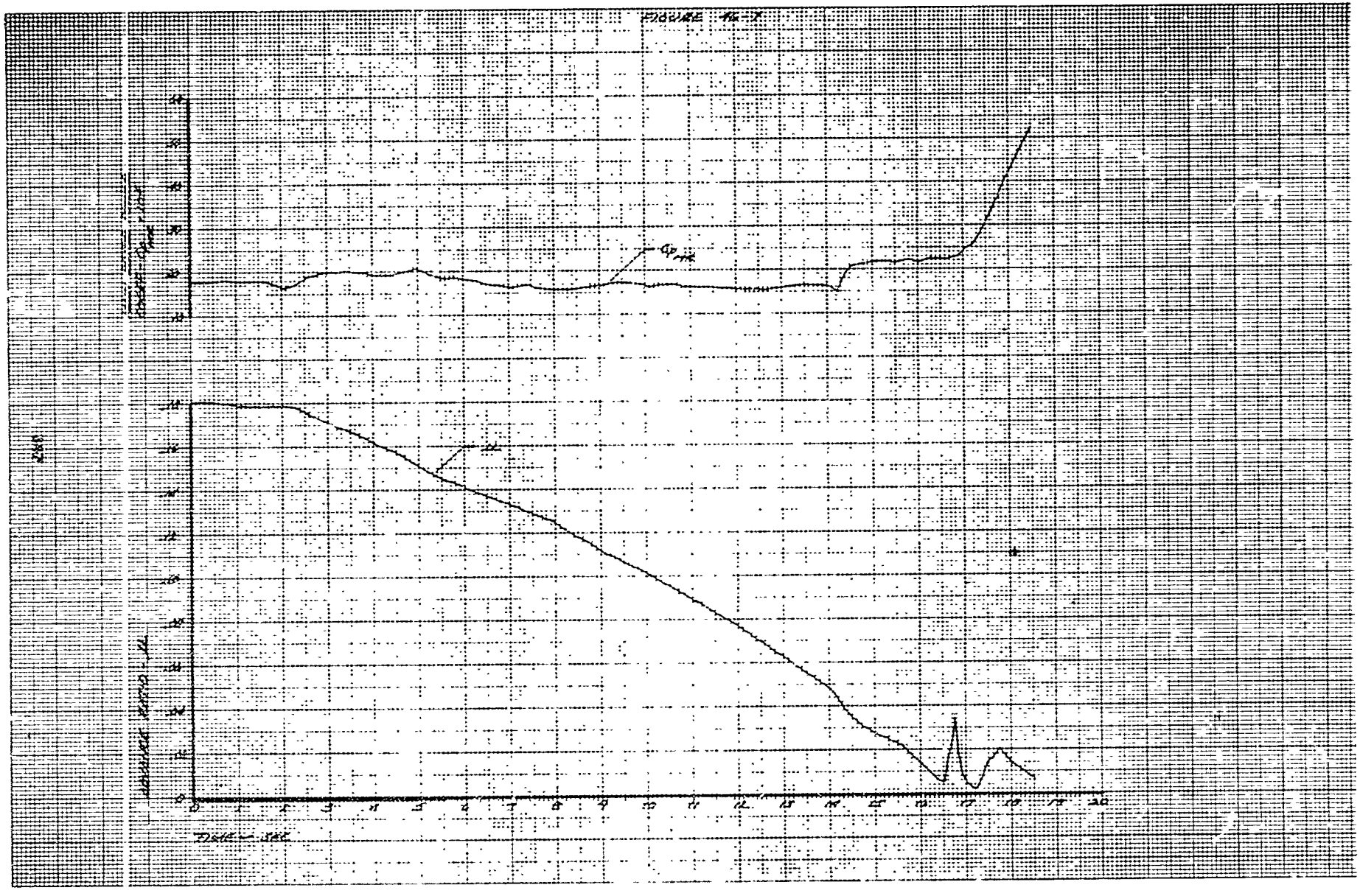

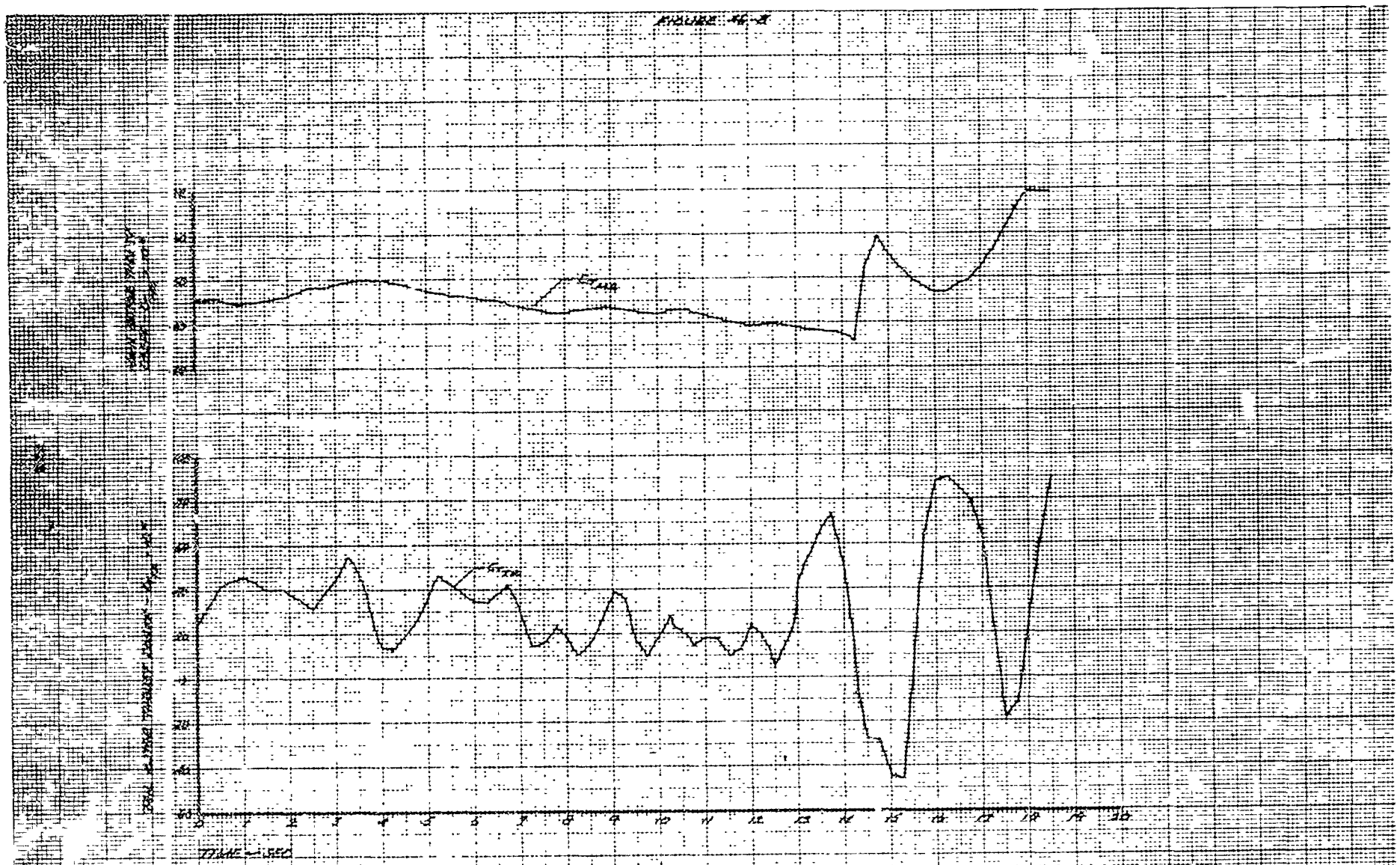

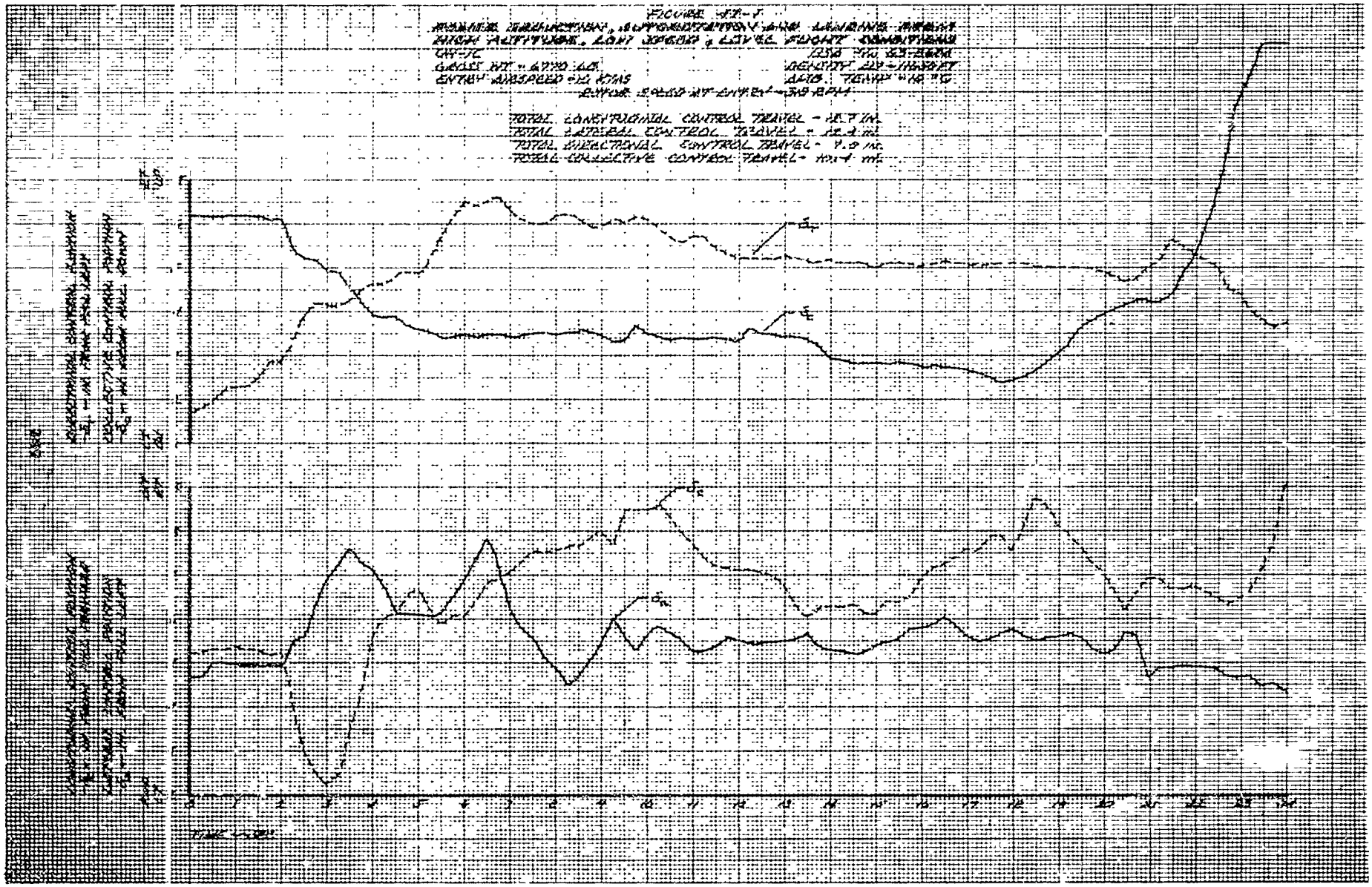

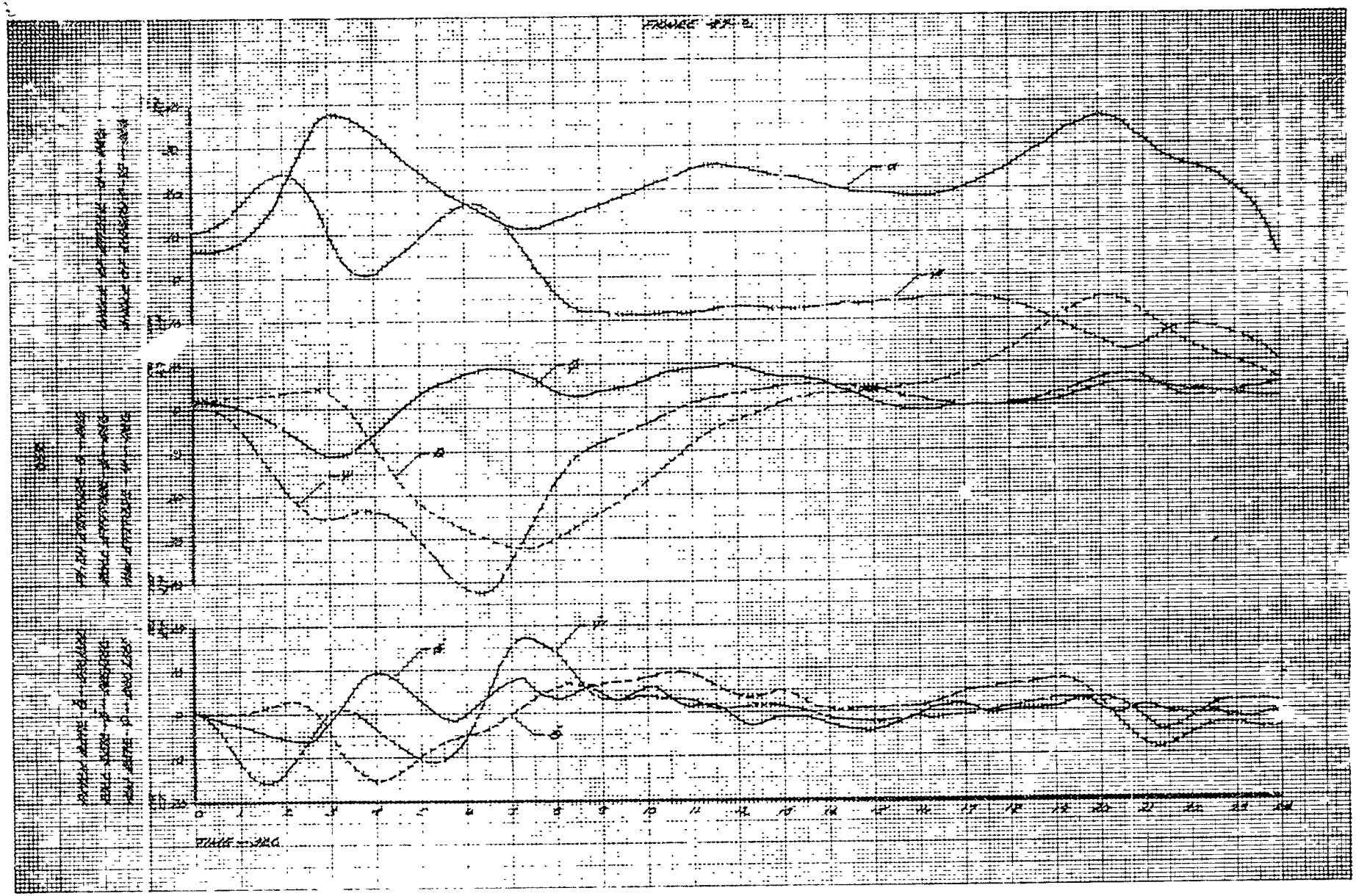

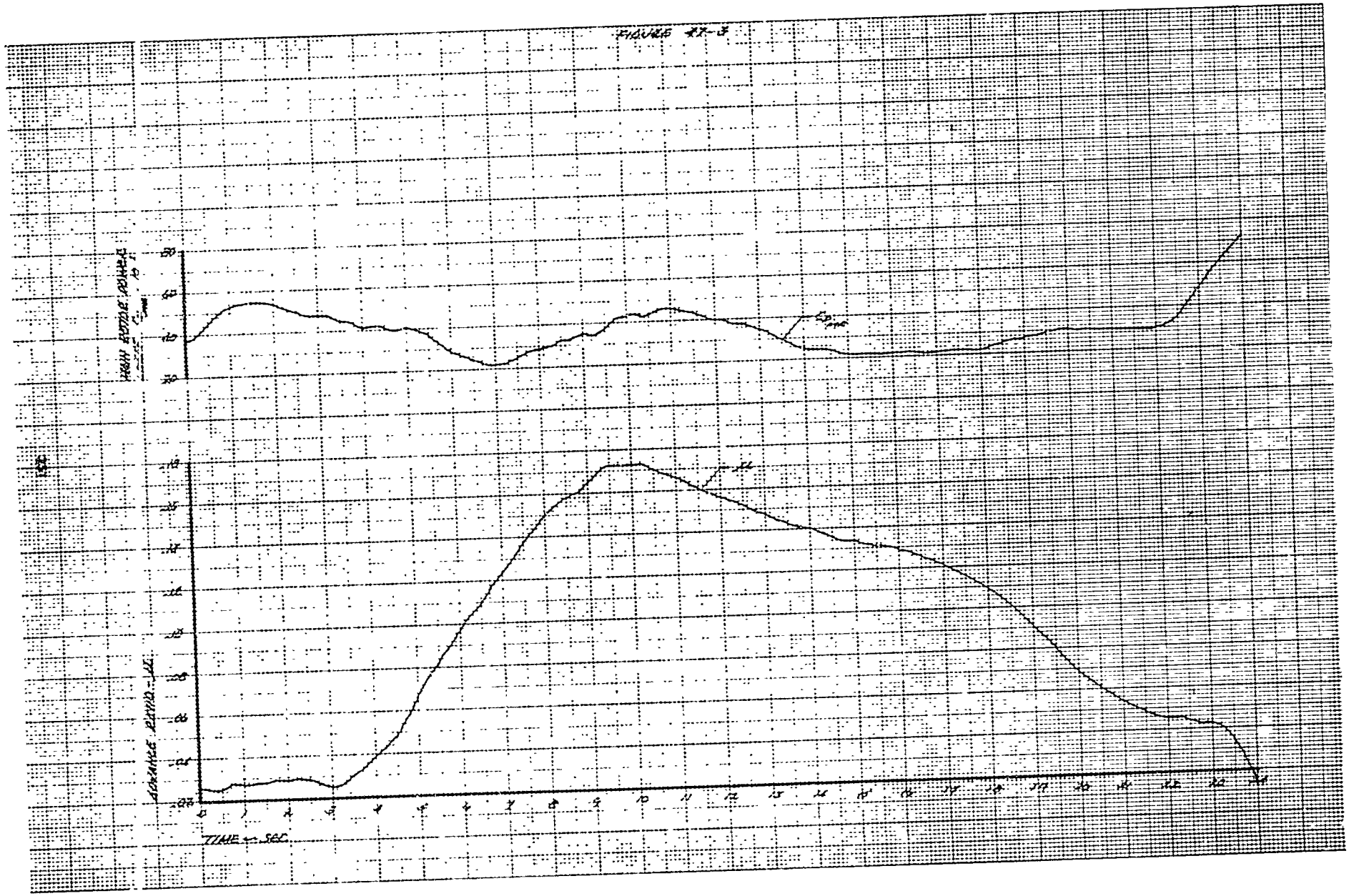
TIME — SEC.

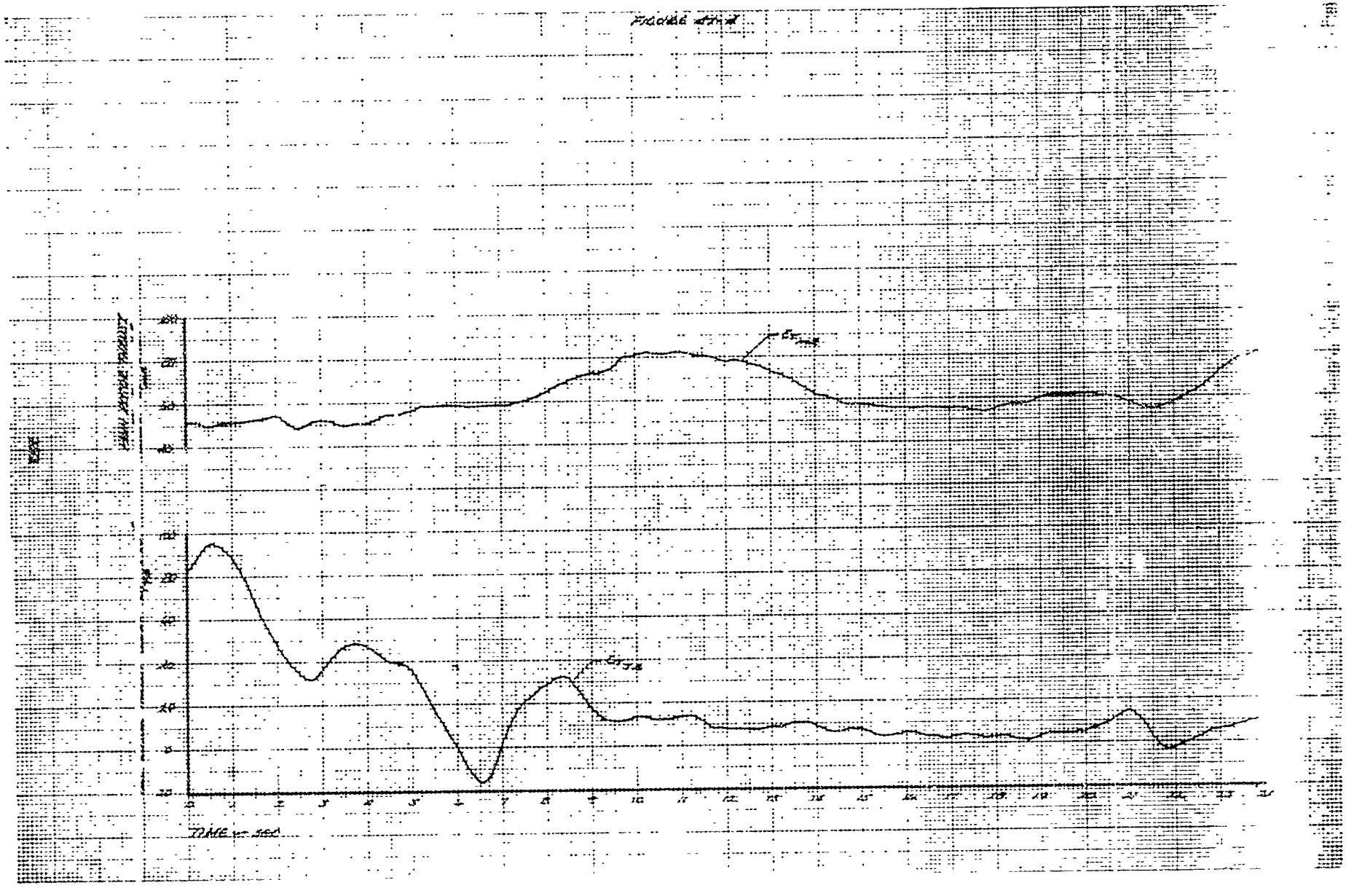
TIME in sec

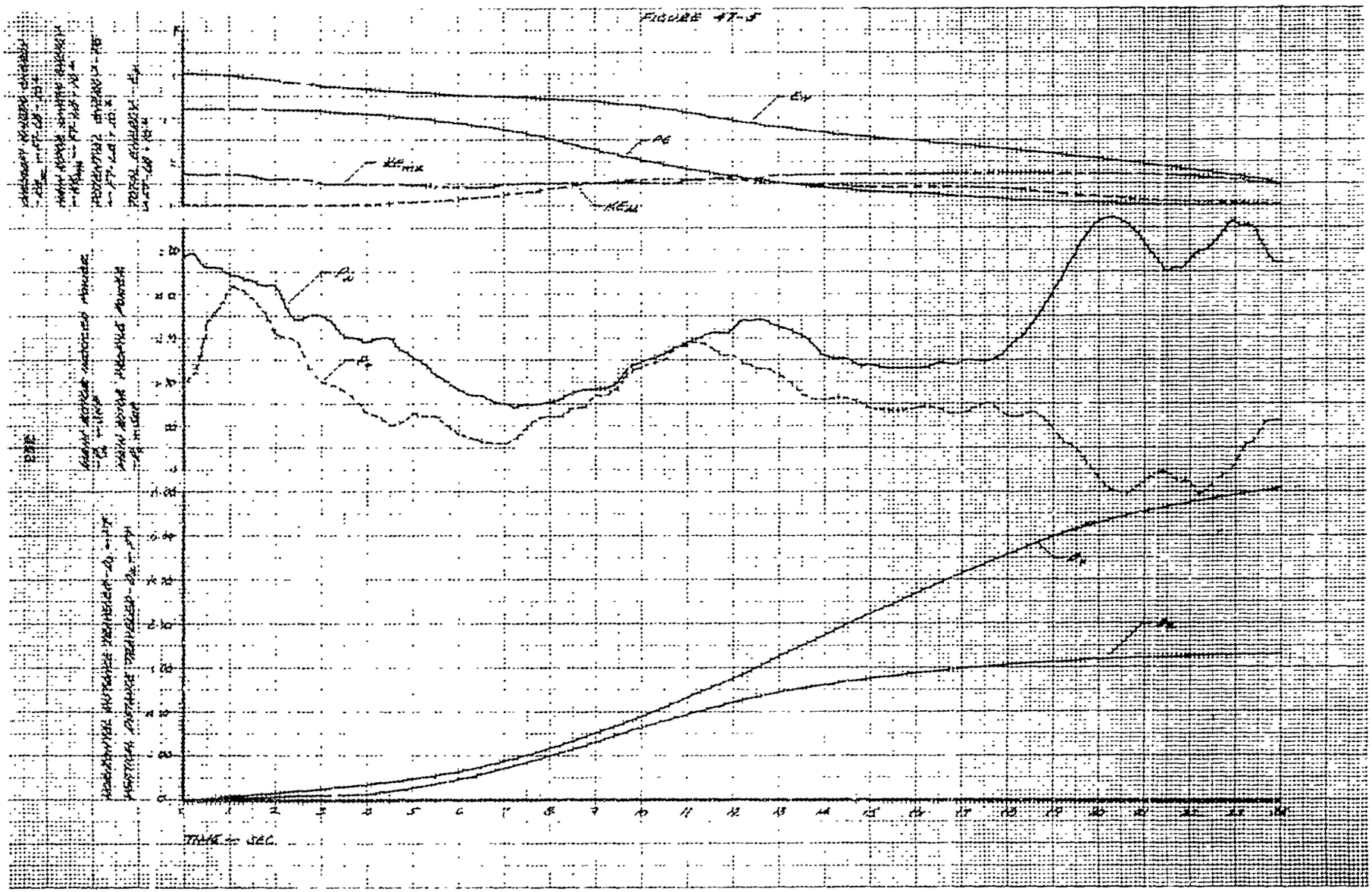
TIME - SEC.

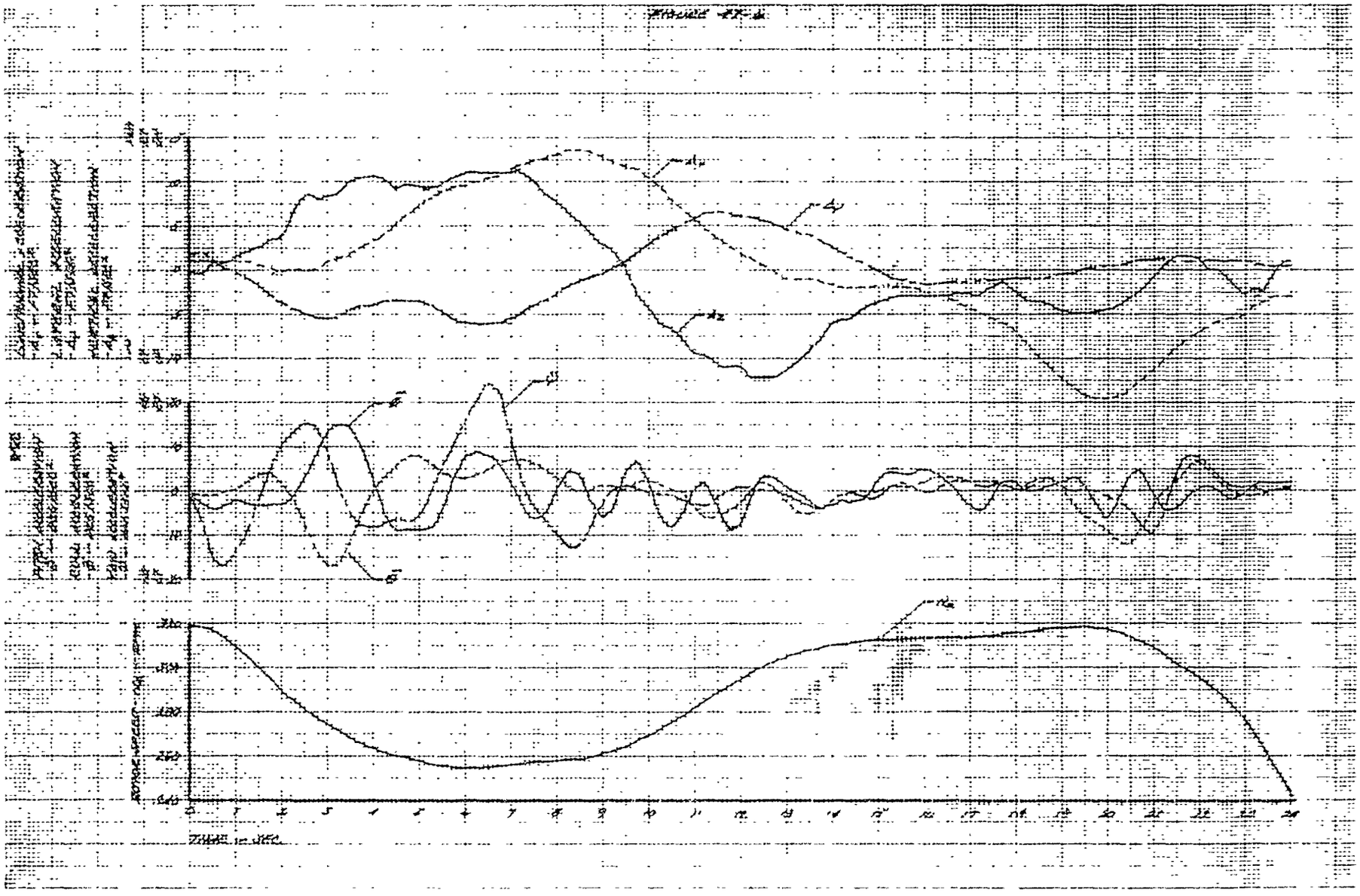

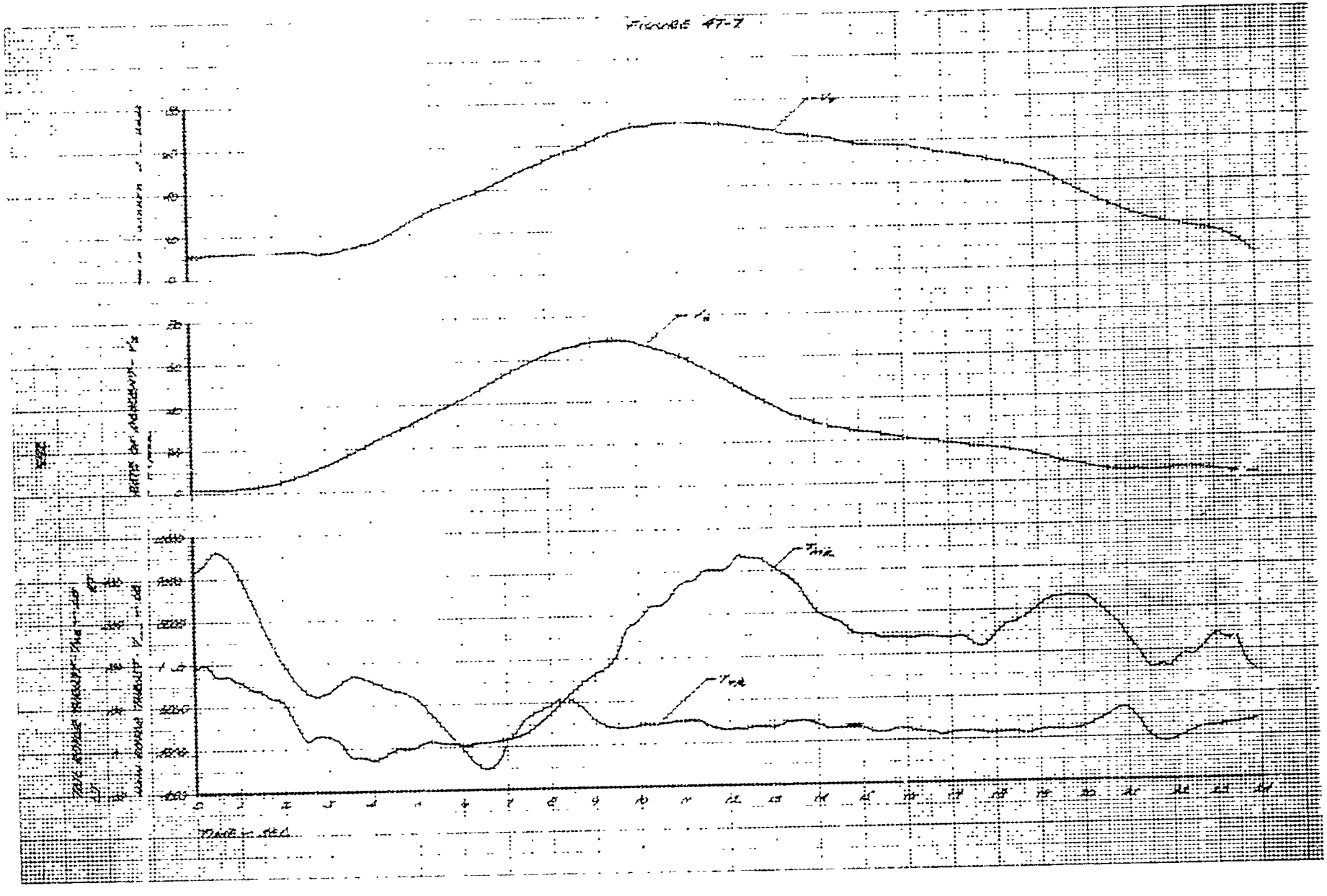
FIGURE 47-7

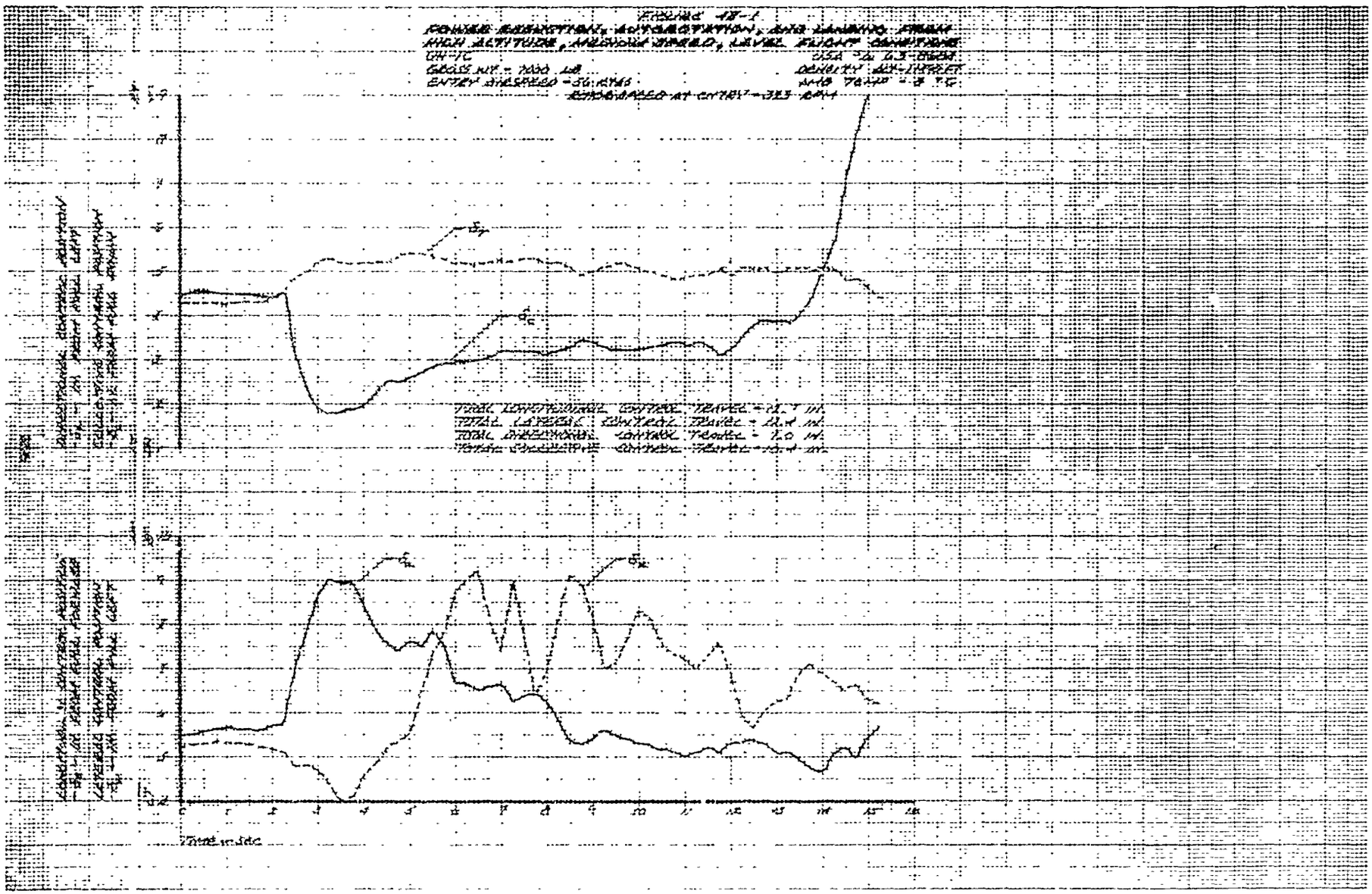

FIGURE 18-2

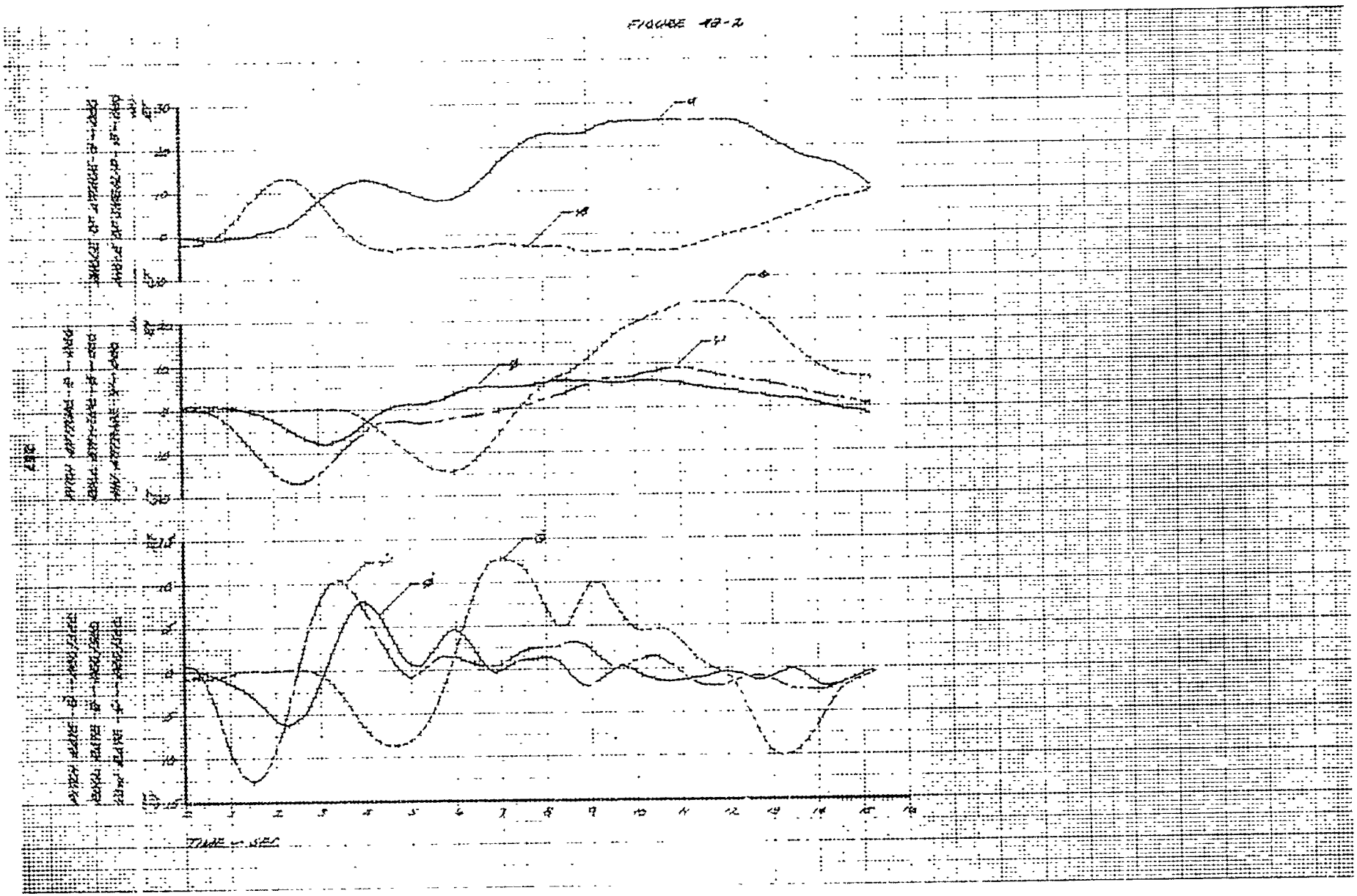

FIGURE 48-1

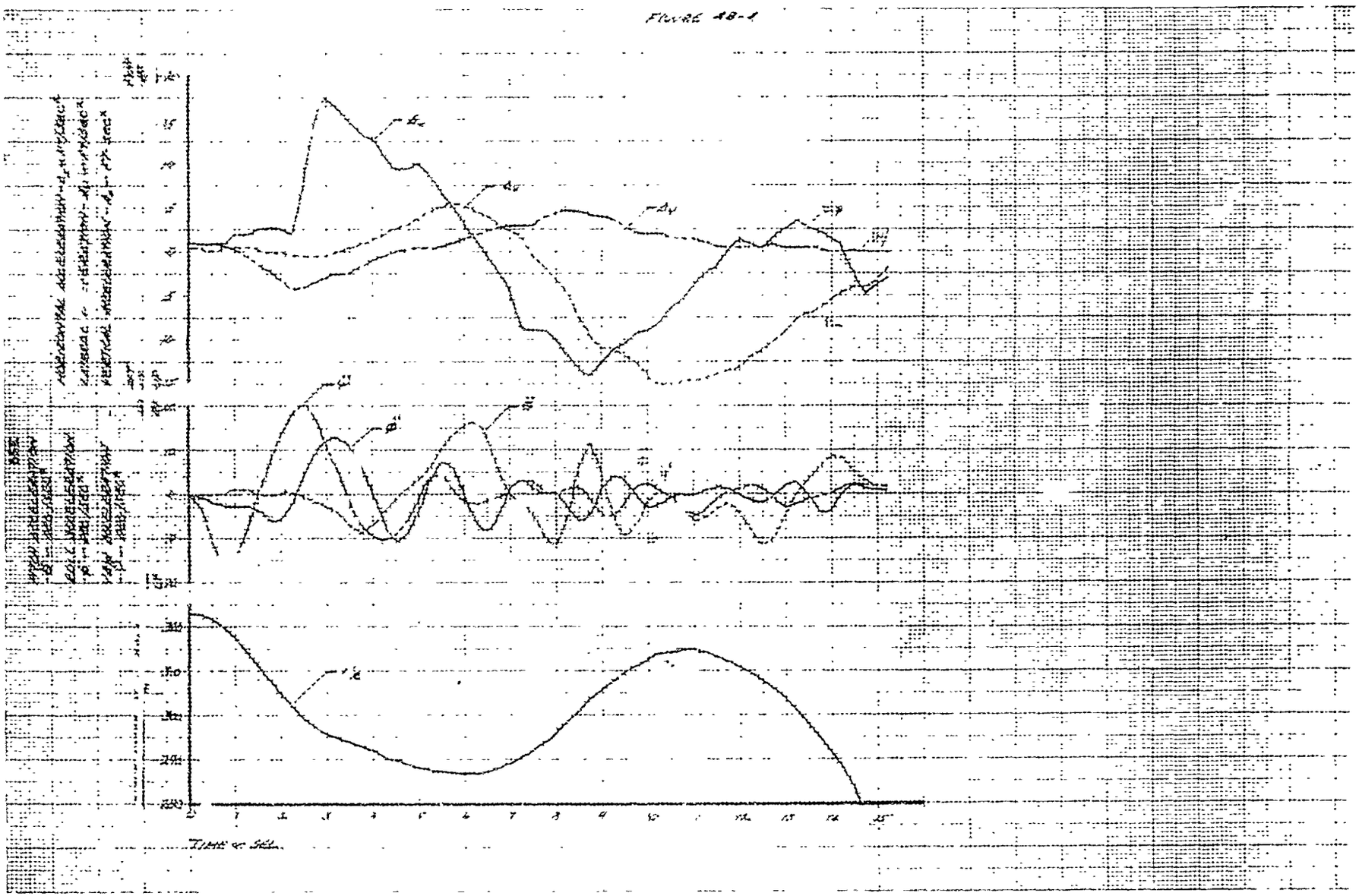

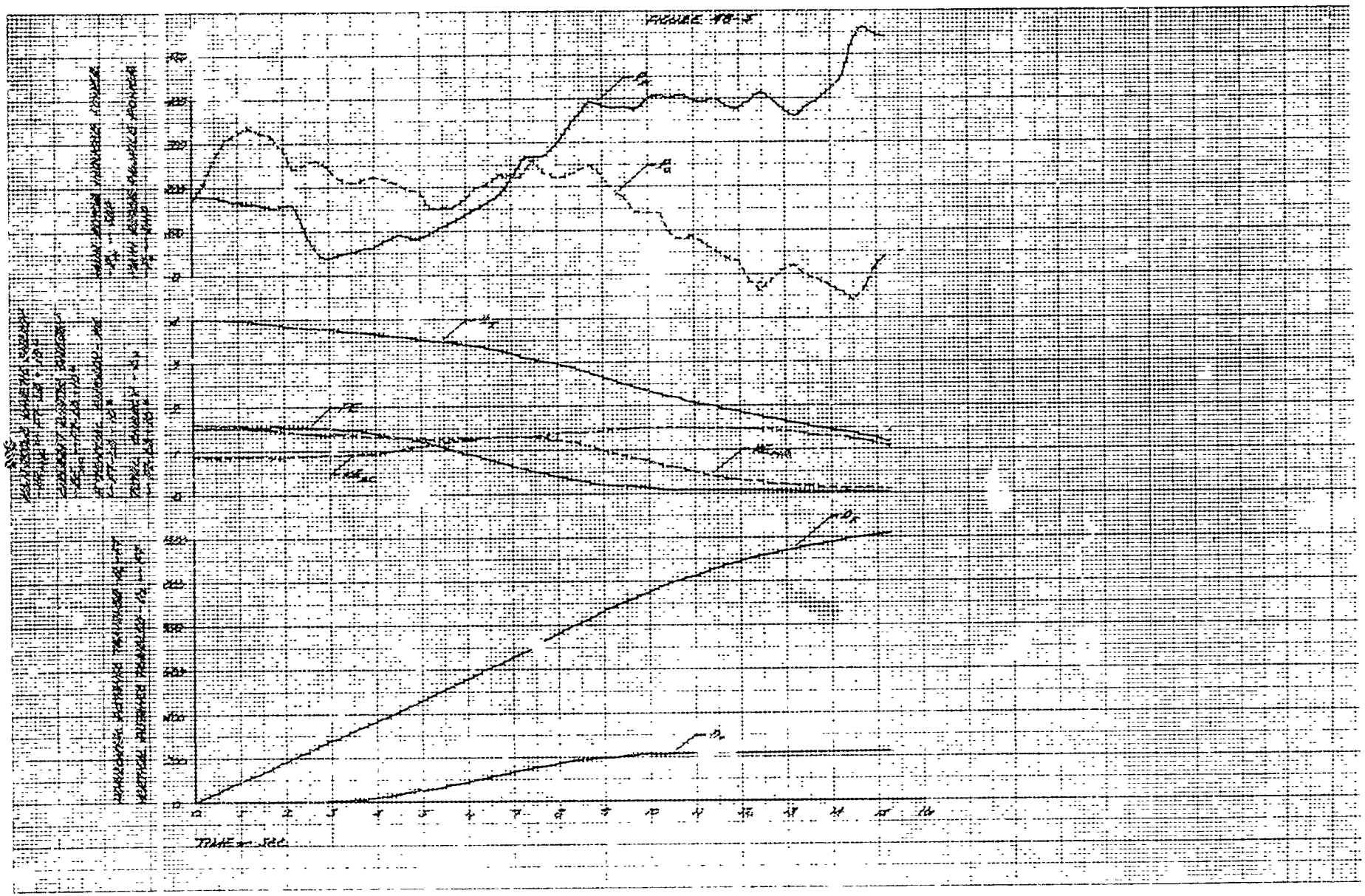
TIME - SEC.

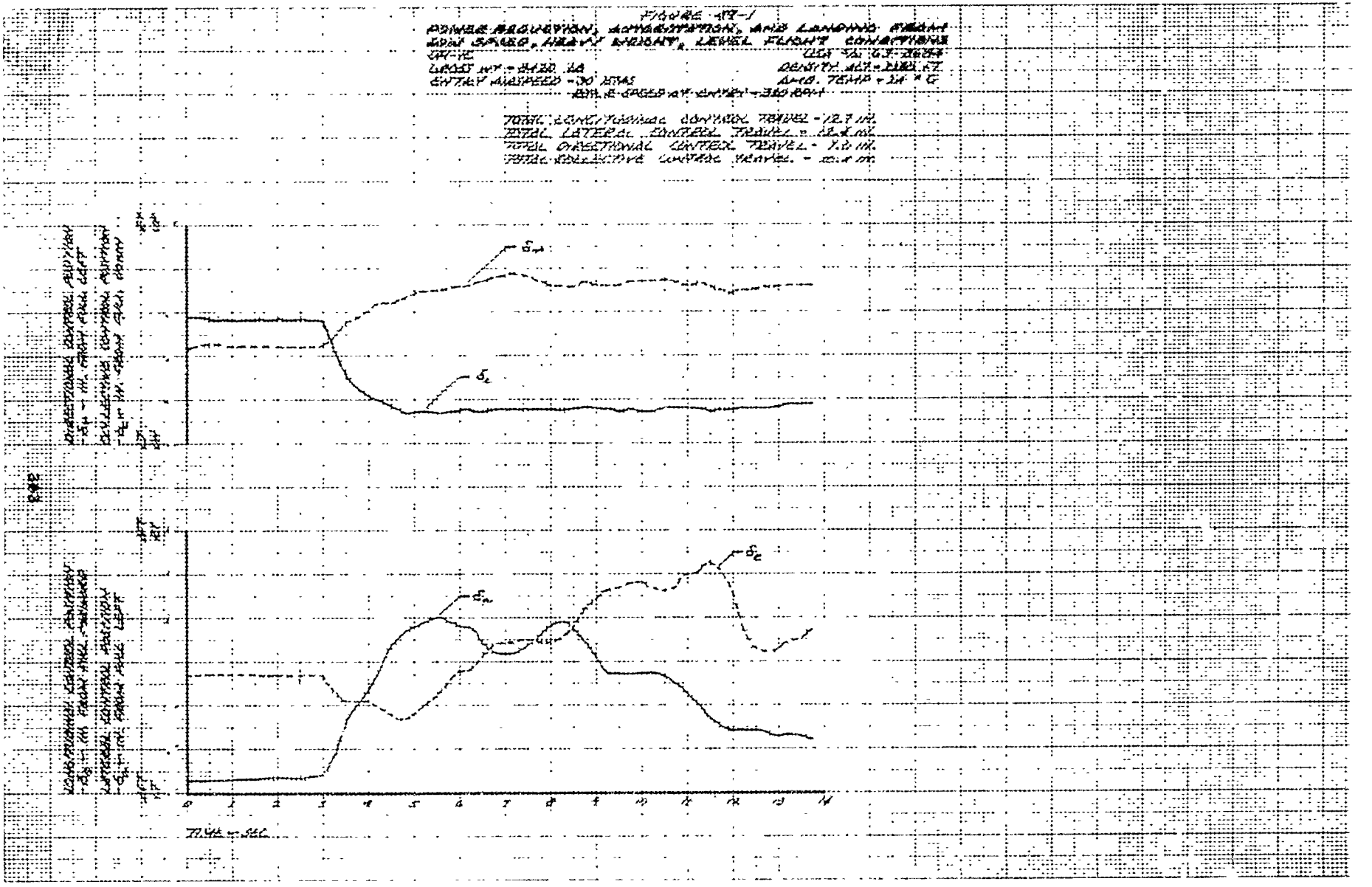
δ_{a_R}
δ_E
δ_E
δ_{a_R}
TIME - SEC

FIGURE 50

POWER REDUCTION, AUTOROTATION, AND LANDING FROM LOW ALTITUDE, LOW SPEED, LEVEL FLIGHT CONDITIONS

UH-1C — USAF/N 63-8684

GROSS WT - 8000 LB — DENSITY ALT - 490 FT

ENTRY AIRSPEED = 71 KIAS — AMB. TEMP = 17° C

ROTOR SPEED AT ENTRY = 324 RPM

ENTRY HEIGHT ABOVE GROUND - 600 FT

NOTE: DEMONSTRATION OF TECHNIQUE BY A TRANSITIONAL PILOT

TOTAL LONGITUDINAL CONTROL TRAVEL = 12.5 IN.

TOTAL COLLECTIVE CONTROL TRAVEL = 10.5 IN.

TOUCHDOWN

TIME — SEC.

FIGURE 51

POWER REDUCTION, CONFIGURATION, AND LONGITUDINAL TRIM FOR LOW ALTITUDE, LOW SPEED, LEVEL FLIGHT CONDITIONS

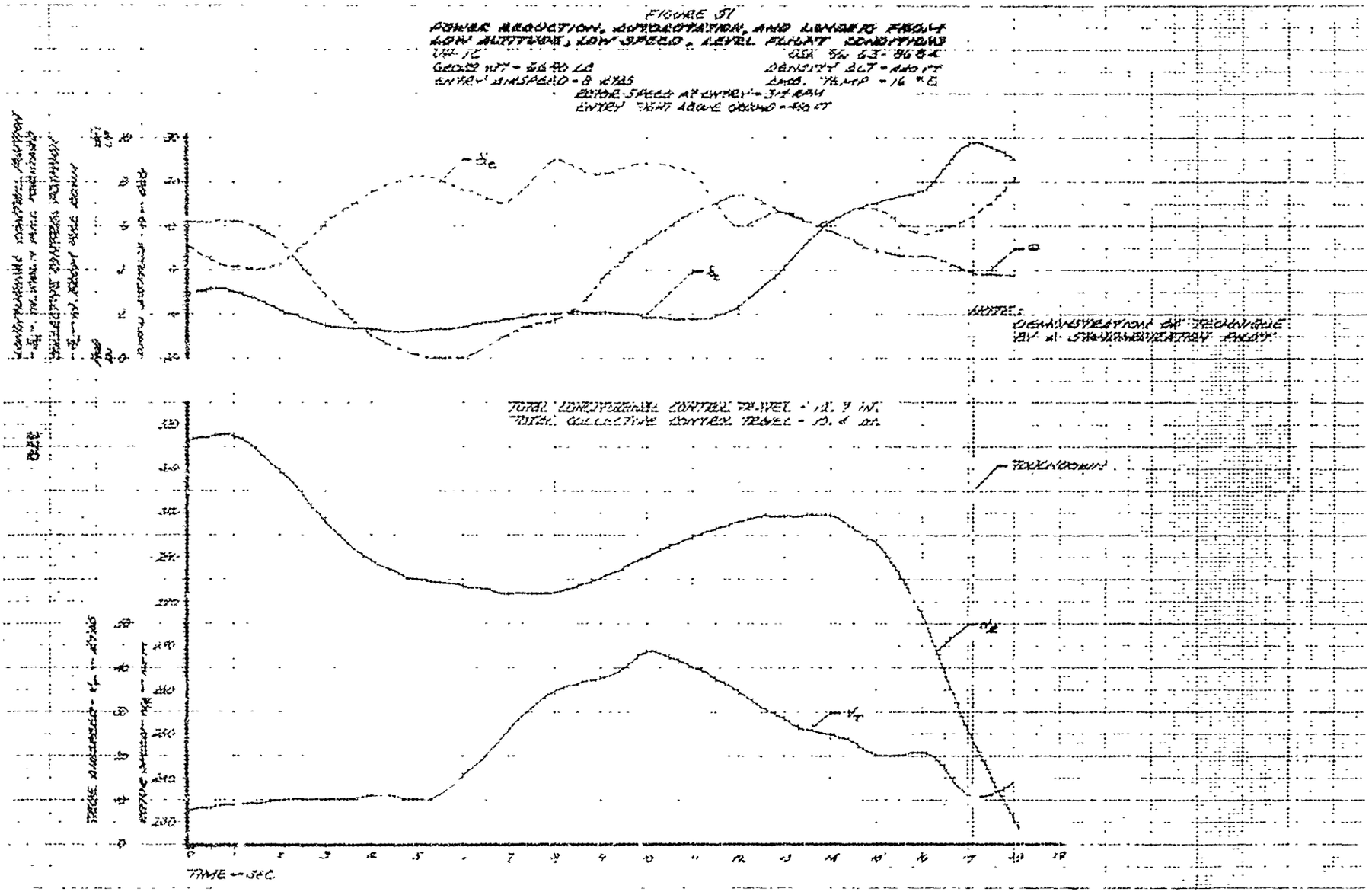

FIGURE 52

LONGITUDINAL CONTROL CHARACTERISTICS

DH-7C USA SN 63-8684

NOTE

DATA OBTAINED FROM REFERENCE 11, APPENDIX A.

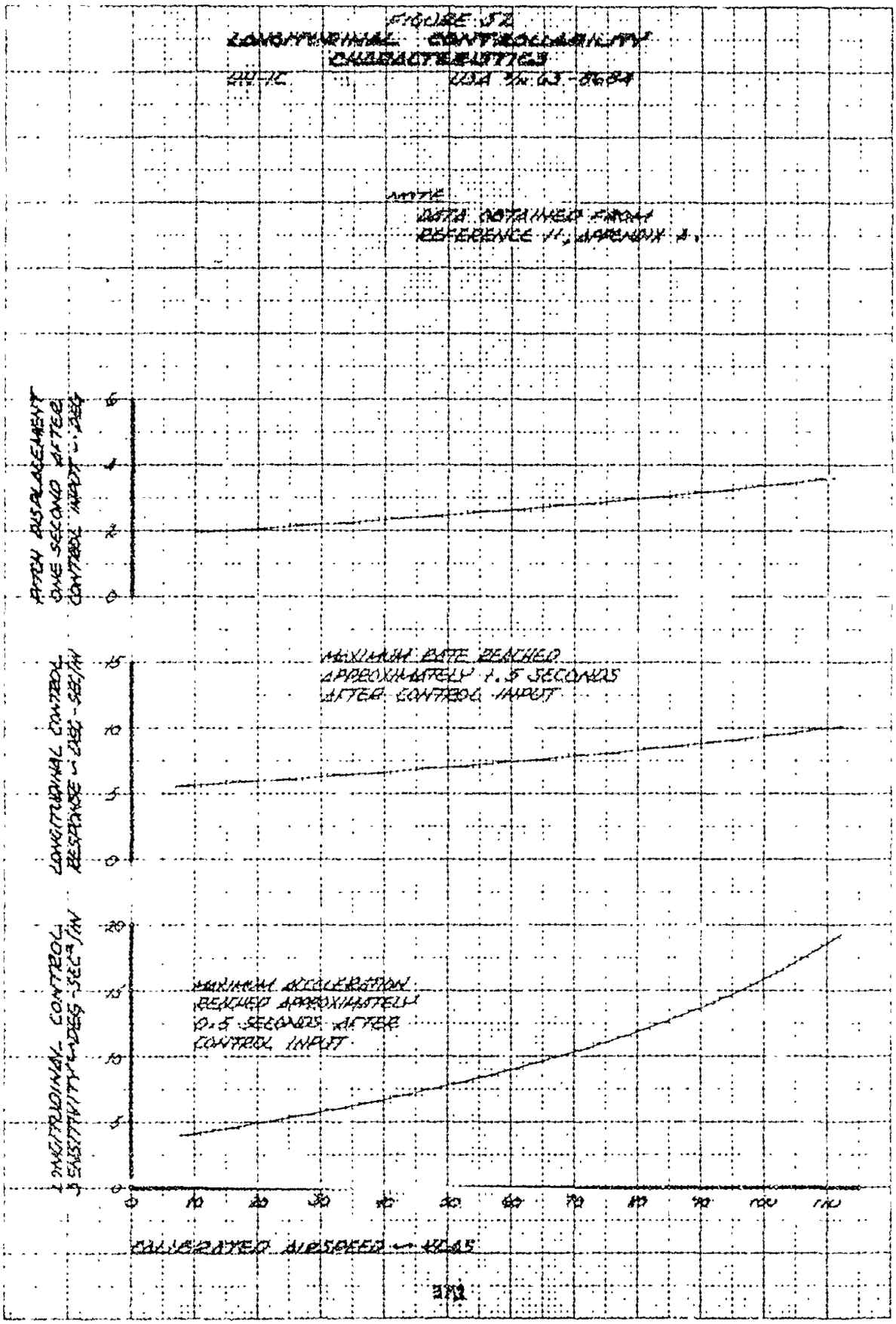

FIGURE XI

CONTROL TRIM CHANGE FROM LEVEL FLIGHT TO STEADY-STATE AUTOROTATION

CH-37C USA S/N 63-8684

NOTE

DATA OBTAINED FROM REFERENCE 11, APPENDIX A.

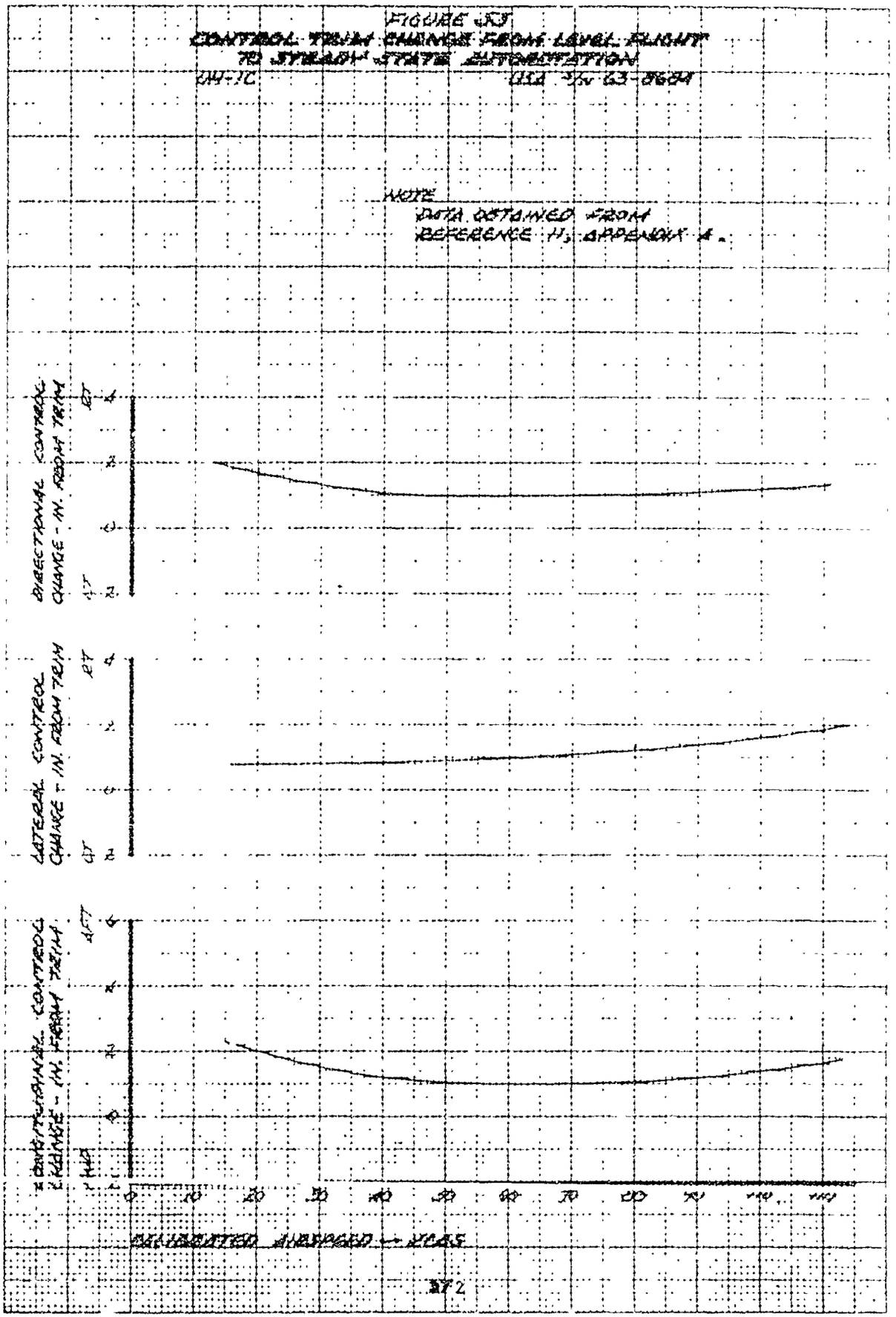

DISTRIBUTION

Director of Defense Research and Engineering	2
Deputy Director of Test and Evaluation, OSD (OAD(SSST&E))	1
Assistant Secretary of the Army (R&D), Deputy for Aviation	1
Deputy Chief of Staff for Research, Development, and Acquisition (DAMA-WSA, DAMA-RA, DAMA-PPM-T)	4
US Army Materiel Development and Readiness Command (DRCPM-BH, DRCPM-AAH-TM-T, DRCPM-CO, DRCPM-CH-47M, DRCDE-DW-A, DRCSF-A, DRCQA)	20
US Army Aviation Research and Development Command (DRDAV-EQ)	12
US Army Training and Doctrine Command (ATCD-CM-C)	1
US Army Materiel Systems Analysis Activity (DRXSY-CM, DRSXY-MP)	3
US Army Test and Evaluation Command (DRSTE-AV, USMC LnO)	3
US Army Electronics Research and Development Command (AMSEL-VL-D)	1
US Army Forces Command (AFOP-AV)	1
US Army Armament Command (SARRI-LW)	2
US Army Missile Command (DRSMI-QT)	1
Director, Research & Technology Laboratories/Ames	2
Research & Technology Laboratory/Aeromechanics	2
Research & Technology Laboratory/Propulsion	2
Research & Technology Laboratory/Structures	2
US Army Air Mobility Laboratory, Applied Technology Lab	1
US Army Human Engineering Laboratory (DRXHE-HE)	1
US Army Aeromedical Research Laboratory	1
US Army Infantry School (ATSH-TSM-BH)	1
US Army Aviation Center (ATZQ-D-MT)	3
US Army Aviation Test Board (ATZQ-OT-C)	2
US Army Aviation School (ATZQ-AS, ATST-CTD-DPS)	5
US Army Aircraft Development Test Activity (PROV) (STEBG-CO-T, STEBG-PO, STEBG-MT)	5
US Army Agency for Aviation Safety (IGAR-TA, IGAR-Library)	5
US Army Maintenance Management Center (DRXMD-EA)	1
US Army Transportation School (ATSP-CD-MS)	1

US Army Logistics Management Center	1
US Army Foreign Science and Technology Center (AMXST-WS4)	1
US Military Academy	3
US Marine Corps Development and Education Command	2
US Naval Air Test Center	1
US Air Force Aeronautical Division (ASD-ENFTA)	1
US Air Force Flight Dynamics Laboratory (TST/Library)	1
US Air Force Flight Test Center (SSD/Technical Library, DOEE)	3
US Air Force Electronic Warfare Center (SURP)	1
Department of Transportation Library	1
US Army Bell Plant Activity (DAVBE-ES)	5
US Army Boeing Vertol Plant Activity (DAVBV)	2
US Army Grumman Plant Activity	2
US Army Hughes Plant Activity	2
AVCO Lycoming Division	5
Beech Aircraft Corporation	5
Bell Helicopter Textron	5
Boeing Vertol Company	5
General Electric Company, Technical Information Center	2
Grumman Aerospace Corporation	1
Hughes Helicopter Company	5
Lockheed-California Company	1
Sikorsky Aircraft Division of United Technologies Corporation	5
Teledyne CAE	2
United Aircraft of Canada Ltd	5
Defense Documentation Center	12